THE
PHYSICAL REVIEW

A journal of experimental and theoretical physics established by E. L. Nichols in 1893

SECOND SERIES, VOL. 70, NOS. 11 AND 12 DECEMBER 1 AND 15, 1946

The Total Scattering Cross Sections of Deuterium and Oxygen for Fast Neutrons

RICHARD G. NUCKOLLS,* CARL L. BAILEY, WILLIAM E. BENNETT,* THOR BERGSTRALH,**
HUGH T. RICHARDS,*** AND JOHN H. WILLIAMS
University of Minnesota, Minneapolis, Minnesota

(Received September 20, 1946)

By observations of the transmission of H_2O and D_2O for neutrons of discrete energies between 0.35 and 6.0 Mev and from a knowledge of $\sigma_s(H)$[1], values of $\sigma_s(D)$ and $\sigma_s(O)$ are deduced as a function of neutron energy. $\sigma_s(D)$ is a monotonic function of neutron energy in this region but $\sigma_s(O)$ shows evidence for resonance phenomena.

INTRODUCTION

EXPERIMENTAL studies of the interaction of neutrons with light nuclei are of fundamental interest to nuclear theory. Neutron-proton scattering[1] and proton-proton scattering[2] have been studied and, in combination with a knowledge of the properties of the deuteron, serve as a basis for our theories of the interaction of these fundamental particles. The natural extension of neutron interaction studies is the scattering of neutrons by deuterons. To be complete such investigations should cover a neutron energy range sufficiently great to provide information on the interaction of these particles in higher states of angular momentum than $l=0$. The present study is limited to neutrons of energies up to 6 Mev and does not satisfy this criterion.

METHOD

The scattering measurements to be described in this paper were carried out under conditions of "good geometry" as described in a previous report on neutron-proton scattering.[1] The neutron sources were targets of lithium, carbon, and solid D_2O under ion bombardment. The reactions

$$Li^7+H^1\rightarrow Be^7+n^1, \quad (1)$$

$$C^{12}+D^2\rightarrow N^{13}+n^1, \quad (2)$$

$$D^2+D^2\rightarrow He^3+n^1, \quad (3)$$

provided neutrons in the energy regions 0.37 to 0.97 Mev, 1.0 to 2.0 Mev, and 2.0 to 6.0 Mev, respectively. The bombarding ions were accelerated by means of the Minnesota pressure insulated electrostatic generator.[3]

The technique of neutron energy definition, scattering geometry, neutron intensity monitoring, and detectors were similar to those previously described.[1] Corrections to the ob-

* Now at Illinois Institute of Technology, Chicago, Illinois.
** U.S.N.R.
*** Now at the University of Wisconsin, Madison, Wisconsin.

[1] C. L. Bailey, W. E. Bennett, T. Bergstralh, R. G. Nuckolls, H. T. Richards, and J. H. Williams, Phys. Rev. 70, 583 (1946).

[2] R. G. Herb, D. W. Kerst, D. B. Parkinson, and G. J. Plain, Phys. Rev. 55, 998 (1939). G. Breit, E. U. Condon, and R. D. Present, Phys. Rev. 50, 825 (1936). G. Breit, H. M. Thaxton, and L. Eisenbud, Phys. Rev. 55, 1018 (1939).

[3] J. H. Williams, L. H. Rumbaugh, and J. T. Tate, Rev. Sci. Inst. 13, 202 (1942).

TABLE I. Observations and calculations on the cross section as a function of neutron energy. Values for cross section are given in barns (10^{-24} cm^2).

E_n in Mev	$\sigma_s(H_2O)$	$\sigma_s(D_2O)$	$\sigma_s(H)-\sigma_s(D)$	$\sigma_s(H)$[a]	$\sigma_s(D)$	$\sigma_s(O)$
0.35	20.20±0.53	11.86±0.36	4.17±0.32	7.70	3.53±0.32	4.80±0.53
0.46	17.01±0.25	10.25±0.20	3.38±0.16	6.70	3.32±0.16	3.61±0.25
0.72	12.43±0.20	8.93±0.17	1.75±0.13	5.21	3.46±0.13	2.01±0.20
0.97	13.92±0.20	11.00±0.19	1.46±0.14	4.43	2.97±0.14	5.06±0.20
1.0±0.1	12.56±0.35	10.08±0.19	1.24±0.20	4.35	3.11±0.20	3.86±0.35
1.6	8.19±0.13	7.23±0.20	0.48±0.12	3.38	2.90±0.12	1.43±0.13
2.0	6.85±0.12	6.09±0.11	0.38±0.08	2.98	2.60±0.08	0.89±0.12
2.6	6.19±0.11	5.77±0.05	0.21±0.07	2.55	2.34±0.06	1.09±0.11
3.0	5.64±0.09	5.44±0.15	0.10±0.09	2.34	2.24±0.09	0.96±0.09
3.5	6.57±0.12	5.47±0.07	0.05±0.07	2.09	2.04±0.07	2.39±0.12
4.0	6.64±0.09	6.30±0.11	0.17±0.07	1.87	1.70±0.07	2.90±0.09
4.5	5.21±0.16	5.21±0.12	0.00±0.05	1.69	1.69±0.05	1.83±0.16
5.0	4.74±0.09	4.58±0.05	0.08±0.05	1.54	1.46±0.05	1.66±0.09
5.5	3.80±0.08	3.90±0.14	−0.10±0.08	1.42	1.52±0.08	0.96±0.08
6.0	3.66±0.08	3.64±0.11	0.01±0.07	1.31	1.30±0.07	1.04±0.08

[a] See references 1 and 4.

served transmission for finite scatterer size and source to detector distance were made by assuming that the scattering process was isotropic in the center of gravity system of coordinates. No corrections have been made for multiple scattering since such calculations are complicated and lead to negligible corrections in comparison with the accuracy of the experimental data.

OBSERVATIONS

Since the primary objective of these experiments was to determine the scattering cross section of the deuteron, we chose to use H_2O and D_2O as the scattering materials. This choice was determined by a previous knowledge[1] of $\sigma_s(H)$. Small brass containers (diameters 4 cm) containing either ordinary or heavy water were interposed midway between the neutron source and the detector. The transmissions of these scatterers were determined by comparing the neutron intensity, I, at the detector with the water-filled cans interposed to the intensity, I_0, when duplicate empty cans were interposed. Each observation was corrected by subtracting a background intensity measured with a long paraffin candle between the source and detector. This background intensity was in general less than two percent of the unscattered intensity.

Since it is known that the radiative capture cross section of hydrogen and deuterium is small, the reduction in intensity is attributed to the scattering of neutrons by the nuclei of H_2O and D_2O. The scattering cross sections were, therefore, calculated directly from the transmissions (corrected for single scattering geometry) by the following equation:

$$I/I_0=e^{-n\sigma_s x},$$

where n is the number of molecules per cm^3, σ_s is the total scattering cross section per molecule in units of cm^2, and x is the thickness of scatterer in cm. These observations and calculations consequently give $\sigma_s(H_2O)$ and $\sigma_s(D_2O)$. The results are listed as a function of neutron energy in the second and third columns of Table I. The probable errors shown in this listing are calculated from the deviations from the mean of several, usually ten, independent observations of the transmission.

By direct subtraction of $\sigma_s(D_2O)$ from $\sigma_s(H_2O)$ and division by two, one obtains the values of

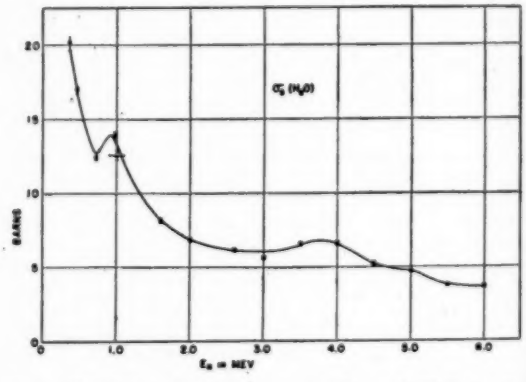

FIG. 1. Total scattering cross section of H_2O in barns (10^{-24} cm^2) as a function of neutron energy.

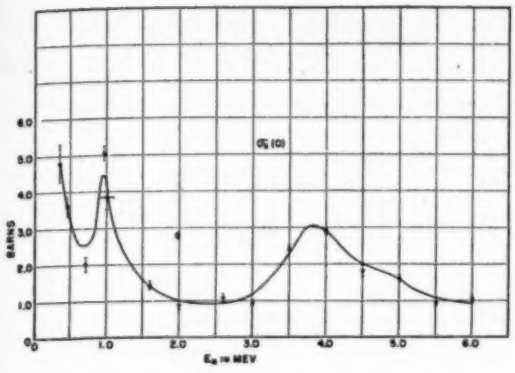

FIG. 2. Total scattering cross section of O in barns (10^{-24} cm^2) as a function of neutron energy.

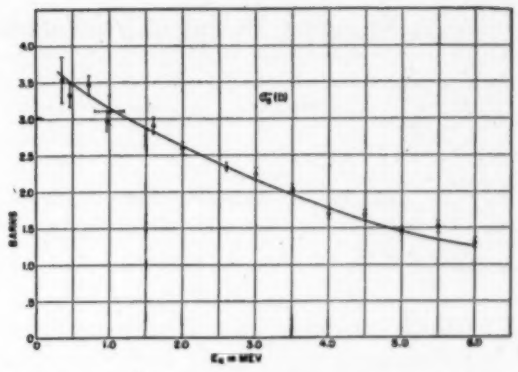

FIG. 3. Total scattering cross section of D in barns (10^{-24} cm^2) as a function of neutron energy.

σ_s(H)$-\sigma_s$(D) listed in the third column of Table I. Earlier measurements[1] and theoretical considerations[4] provide data on σ_s(H), which are listed in the fifth column and are thought to be trustworthy to five percent. By subtracting the figures of the fourth column from those of the fifth the results for σ_s(D) are obtained. The errors shown in this sixth column do not include any uncertainty in the values of σ_s(H) from which they are derived.

Similarly the values of σ_s(O) shown in the last column of Table I are obtained from the measured values of σ_s(H_2O) and the values of σ_s(H) listed in the fifth column.

The results of the observations on H_2O are shown graphically in Fig. 1. It is seen that the cross section is not a smooth function of neutron energy but presents evidence for resonances in the interaction of neutrons with either H or O nuclei. Since a similar curve is obtained for D_2O and σ_s(H) is a smooth function of energy, it is necessary to attribute these resonances to O. Obviously it would be more desirable to use almost any other scatterer than H_2O to investigate the behavior of the (n, O) cross section as a function of neutron energy since the variations of σ_s(O) are small compared to σ_s(H_2O).

The values of σ_s(O) listed in the last column of Table I are plotted as a function of neutron energy in Fig. 2.

The higher energy resonance occurring at neutron energies from 3.0 to 5.5 Mev is not resolved in this work. By analogy with the more accurate observations[1] on σ_s(C) in the same energy region, we are led to think that more detailed measurements of σ_s(O) between 3.0 and 6.0 Mev might resolve the assymetrical peak of Fig. 2 into a doublet.

Since the thermal neutron cross section of oxygen is known to be 4.0 barns, the variations of σ_s(O) with neutron energy less than 1.5 Mev indicate a doublet resonance in this region. This indication has been proven by later unpublished work of D. H. Frisch at Los Alamos. The present work should be considered only as a preliminary study of σ_s(O) and suffers severely from a choice of scatterers which was made to study σ_s(D) and not σ_s(O).

The results for σ_s(D) as a function of neutron energy are shown in Fig. 3. It is seen that the cross section decreases monotonically from the lowest measured neutron energy of 0.35 Mev to a value of 1.3 barns at 6.0 Mev. Over the energy interval from 4.5 to 6.0 Mev σ_s(D) is experimentally indistinguishable from σ_s(H).

The work reported in this paper was done as part of an O.S.R.D. contract with the University of Minnesota during the winter 1942–43.

[4] Bohn and Richman—forthcoming report.

PHYSICAL REVIEW VOLUME 70, NUMBERS 11 AND 12 DECEMBER 1 AND 15, 1946

Stopping Power of Various Substances for Fission Fragments†

E. SEGRÈ* AND C. WIEGAND*
University of California, Los Alamos Scientific Laboratory, Santa Fe, New Mexico
(Received August 9, 1946)

The relative stopping power of collodion, aluminum, copper silver, and gold for fission fragments has been measured. The results are similar to those for alpha-particles of 4.5 Mev.

SEVERAL investigations, both experimental and theoretical, concerned with the passage of uranium fission fragments through matter have been published in the past few years.[1] Although these studies cover the subject generally, they do not seem to have especially investigated the relative stopping powers of various substances for fission fragments. Relative stopping powers are often a matter of importance in experimental investigations, e.g., for determining thickness corrections. We have thought it worth while to make a special study of them.

CATCHER-FOIL ACTIVITY EXPERIMENT

Two types of experiments have been performed. In the first type a thin (0.085 mg/cm²) layer of U_3O_8 enriched in U^{235} and deposited on a platinum disk was covered with various thicknesses of aluminum foil. On top of the aluminum foil we placed a thick celluloid foil. The whole system was irradiated with neutrons and the activity due to the recoiling fission fragments collected in the celluloid foil was measured.

The decay curves of this activity do not show any significant variation in their form as a function of the thickness of aluminum interposed. The observations were always made nine hours after the end of the irradiation.

In Fig. 1 we show the result of these experiments.

If the fission fragments had all the same range one would expect that the curve of Fig. 1 would be a straight line. This is easily seen by considering the fission fragments emitted by an element of area dS in the active surface (Fig. 2). The end points of their trajectories in air lie with uniform density on the surface of a sphere of radius R (range of the fission fragments). By covering the source with a substance of thickness t such that, after traversing it normally, the residual range is reduced from R to $R-t$, the number of fission fragments emerging in air is also reduced in the same ratio and hence the activity collected is $A=b(R-t)$, where b is a coefficient depending upon the conditions of irradiation, etc.

The curve of Fig. 1 is not a straight line because the fission fragments do not have all the same range. Each range represented gives a straight line and what is observed is the composite curve. The large scattering of the fission fragments has also probably a considerable influence. From Fig. 1 one may try to determine a mean range and an extrapolated range in aluminum, these being, respectively, 2.2 and 3.7 mg/cm². It is, however, obvious that such a procedure is considerably arbitrary since the fission fragments do not have a uniform range.

IONIZATION-CHAMBER EXPERIMENT

In the second series of experiments the same thin foil of U_3O_8 was covered with the absorbers and introduced into an ionization chamber filled with nitrogen. The depth of the ionization chamber was 1.0 cm and electrons were collected. The ionization chamber was connected to a linear amplifier whose amplification and bias were kept constant.

The apparatus was tested with polonium covered with aluminum or gold foils and in Fig. 3 we show the results of these test runs. Because of the homogeneity in energy of the Po alphas, we should this time really expect that the number of pulses registered, N, varies according to $N=c(R-t)$, in which again c depends on the

† The report describing this work was filed on February 29, 1944.

* Present address: Physics Department, University of California, Berkeley, California.

[1] See, e.g., W. E. Lamb, Phys. Rev. 58, 696 (1940) which includes also a bibliography and J. Knipp and E. Teller, Phys. Rev. 59, 659 (1941).

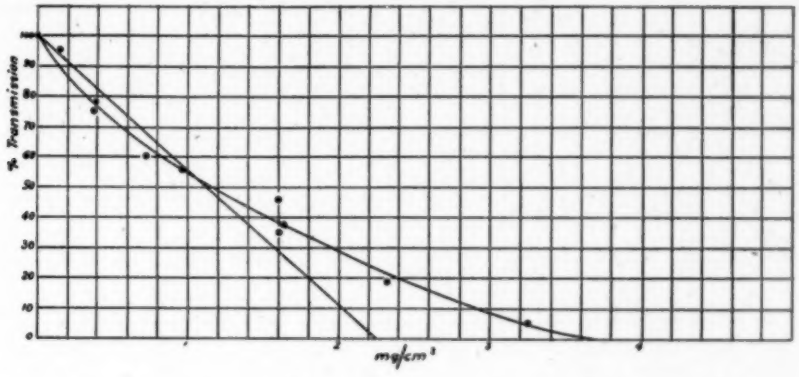

FIG. 1. Fragments through aluminum.

bias, strength of the source, etc. Figure 3 shows the linear dependence of N on t, and by comparing the slopes of the two curves, for aluminum and gold, we find that the relative mass stopping power is 2.45. This is in excellent agreement with the accepted value of 2.45.[2]

In the runs with uranium fission fragments we obtain the curves given in Fig. 4. Five types of absorbers were used: aluminum, copper, silver, gold, and also collodion (approximately $C_{12}H_{17}O_{16}N_3$), which should not differ very much in its stopping properties from air. In Table I we summarize the results. Of each pair of numbers in the table, the upper one is the thickness necessary to stop a certain fraction of the fission fragments and the lower one is its ratio to the thickness of aluminum having the same stopping power. These ratios do not vary much as a function of the thickness employed, and inasmuch as we are willing to consider them constant we may speak of a stopping power.

In Table II we report the mass stopping power and the atomic stopping power and for comparison the similar number for 4.66 Mev of α-particles.

It must be borne in mind that in this experi-

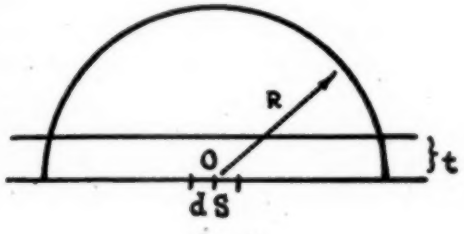

FIG. 2.

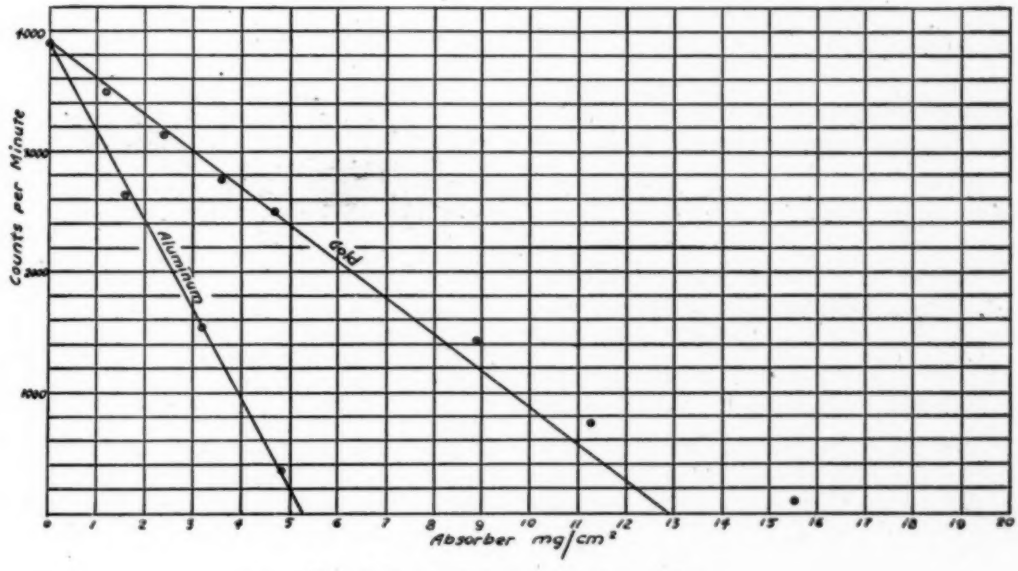

FIG. 3. Transmission of polonium alphas.

[2] See e.g., Livingston and Bethe, Rev. Mod. Phys. 9, 272 (1937).

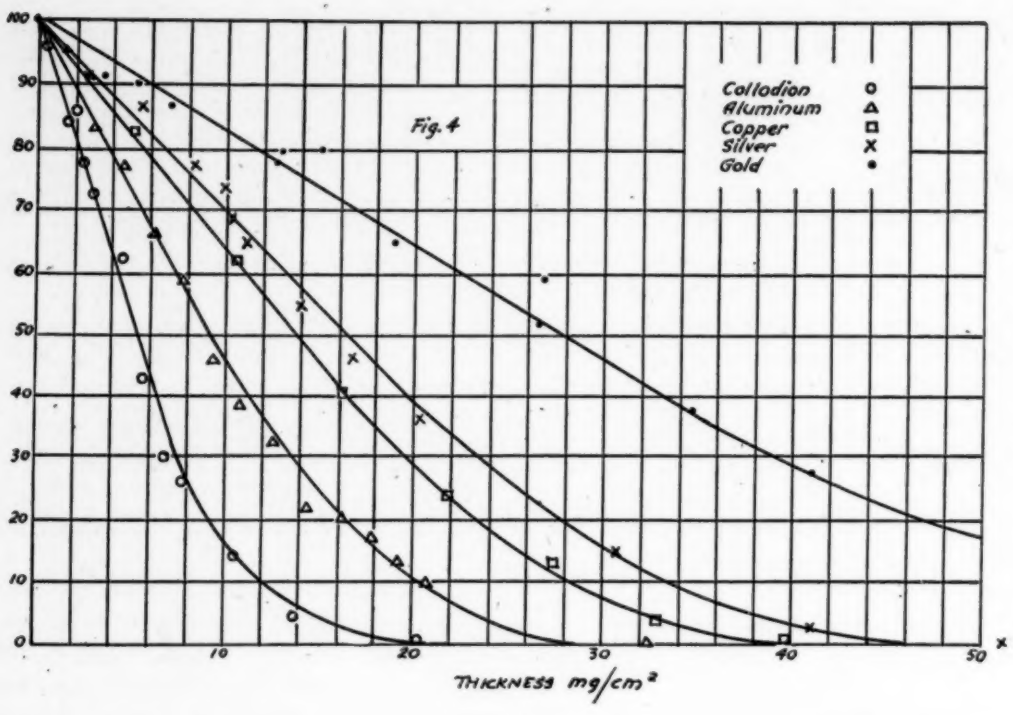

FIG. 4.

ment counts were registered only if the fission fragments spent enough residual range in the ionization chamber. We can have a rough estimate of this quantity by comparing the range in aluminum measured in the foil-activity experiment (3.7 mg/cm²) with that measured in the chamber experiments, approximately 2.9 mg/cm². It thus appears that the fission fragment has to spend approximately a residual range of 0.8 mg/cm² of aluminum in the chamber in order to be registered on our apparatus. If we increase the bias so as to count only larger pulses, the apparent stopping power of the various substances increases, as to be expected, but we have observed that the ratios between the stopping powers of various substances stay practically constant. To give at least a qualitative idea of the magnitude of this effect we point out that in taking the data of Fig. 4 a bias of 10 arbitrary units was used, whose position with respect to the plateau for fission fragments can be seen in Fig. 5. If we use a bias of 20 of the same arbitrary units, i.e., twice the previous one, we obtain a figure similar to Fig. 4 but with all the abscissae divided by approximately 2. The quantitative features of this effect are of course dependent upon the ion-

TABLE I. Stopping power of fission fragments in various substances.

Fraction of fission fragments absorbed in layer	Thickness of layer in mg/cm²				
	Collodion	Al	Cu	Ag	Au
0.0					
0.10	0.11	0.18	0.28	0.33	0.60
	1.6		0.64	0.55	0.30
0.20	0.22	0.36	0.56	0.68	1.16
	1.64		0.64	0.53	0.31
0.30	0.32	0.54	0.82	0.98	1.68
	1.69		0.66	0.55	0.32
0.40	0.42	0.72	1.10	1.30	2.20
	1.72		0.66	0.55	0.33
0.50	0.54	0.90	1.36	1.62	2.78
	1.67		0.66	0.55	0.34
0.60	0.64	1.10	1.66	1.96	3.34
	1.72		0.66	0.56	0.33
0.70	0.74	1.36	2.0	2.33	3.94
	1.84		0.68	0.58	0.35
0.80	0.91	1.63	2.34	2.75	4.65
	1.78		0.69	0.59	0.35
0.90	1.23	2.06	2.85	3.39	5.7
	1.67		0.72	0.61	0.36
1.00	(2.10)	(2.90)	(4.10)	(4.80)	(9.0)
	(1.38)		(0.71)	(0.60)	(0.42)

ization chamber construction, the absolute value of the bias, etc., and are not simple to analyze.

We can obtain the end points of the various absorption curves by adding to the last thickness of Table I the quantity 0.8 mg/cm² divided by the mass stopping power relative to aluminum. This gives:

Collodion	Al	Cu	Ag	Au	U	U_3O_8	
2.6	3.7	5.2	6.1	11.14	(12.6)	(10.0)	mg/cm²

These numbers are a little uncertain because both the apparent end points of Fig. 4 and the stopping power at the end of the range are not precisely known. We have given also the calculated values for uranium and U_3O_8 because they are particularly important.

The atomic stopping power S as a function of Z can roughly be represented by the formula[3]

$$S=aZ^{\frac{1}{2}}.$$

Silver and collodion depart from this formula considerably. The reason for collodion is most probably the presence of hydrogen which is expected to be anomalous, and the reason for silver is not known. It is quite possible that the different degree of homogeneity of the thickness of the foils affects the precision of the measurements.

TABLE II. Mass and atomic stopping power of various substances. For comparison the stopping power for 4.66 Mev, α-particles is shown.

	Mass stopping power		Atomic stopping power	
	α(4.66 Mev)	f	α(4.66 Mev)	f
Collodion	1.38	1.70	—	—
Aluminum	1	1	1	1
Copper	0.69	0.66	1.59	1.52
Silver	0.51	0.55	2.04	2.20
Gold	0.36	0.34	2.62	2.48

[3] Cf. Rutherford, Chadwick, and Ellis, *Radiations from Radioactive Substance* (Cambridge University Press, 1930), pp. 99 and following.

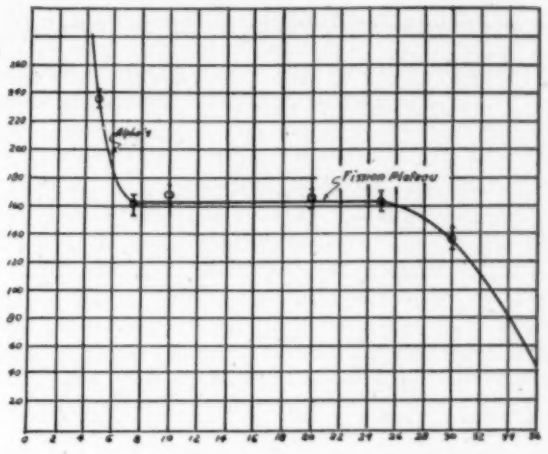

FIG. 5. Fission bias curve; thin uranium foil, no absorber. Ordinates are fissions per minute with a constant neutron source; abscissae, amplifier bias in arbitrary units.

A further check, of practical interest, on these measurements is afforded by the following experiment. A thick piece of uranium foil of 1 cm² surface is placed against a celluloid foil and exposed to neutrons. The recoil activity is then measured and compared to the recoil activity collected on celluloid from a mass m of uranium spread as thin foil, and exposed to the same neutron flux. We find by experiment that 1 cm² of thick uranium is equivalent to 4.7 mg of thin uranium.

This relation can be calculated also by multiplying the abscissae in Fig. 1 by the relative mass stopping power of aluminum with respect to uranium (3.4) and integrating the curve. In this way we find that 1 cm² of thick uranium should give as many active recoil atoms as 4.6 mg of thin uranium in agreement with the experiment quoted above.

ACKNOWLEDGMENT

This work was carried out under contract between the University of California and the Manhattan District, Corps of Engineers, War Department.

PHYSICAL REVIEW VOLUME 70, NUMBERS 11 AND 12 DECEMBER 1 AND 15, 1946

Radioactive Isotope of Gold, $_{79}Au^{198}$* and Low Energy Range of Its Spectrum

SWAMI JNANANANDA
The Harrison M. Randall Laboratory of Physics, University of Michigan, Ann Arbor, Michigan
(Received September 26, 1946)

The soft range of the energy spectrum of $_{79}Au^{198}$ was measured by means of a magnetic lens β-ray spectrometer. The part of the spectrogram so obtained shows a part of continuous β-spectrum and a broad line spectrum of secondary β-rays ejected from the L-level of gold by the softest component of non-corpuscular radiation first found by Richardson. The peak of the line spectrum at $H\rho = 837.5$ corresponds to the maximum energy of 58.4 kev of electrons ejected from L-group of gold. The energy of the radiation which might have given rise to these β-rays must be 70.3 kev with a wave-length $\lambda = 175.7$ x.u. This value of λ is practically identical with the estimated value of the wave-length of $K\alpha_1$ line of mercury. The breadth and the spread of the line towards the low energy side indicate that the spectrum of the L-group of electrons of gold, ejected by a 70.3-kev energy radiation partly overlaps another line spectrum of the same group of electrons ejected by a radiation, softer than 70.3 kev radiation by an energy of the order of only a few kev. This softer one could be identical with the K-radiation of $_{78}Pt^{198}$. The softest component of non-corpuscular radiation found in $_{79}Au^{198}$ is therefore very likely composed of the K-radiation of $_{78}Pt^{198}$, and the K-radiation of $_{80}Hg^{198}$. From the evidence, the radioactive isotope of gold $_{79}Au^{198}$ appears to have a dual transition, a transition to $_{80}Hg^{198}$ following β-decay and another to $_{78}Pt^{198}$, following K-capture as assumed by Sizoo and Eijkman.

1. INTRODUCTION

WHEN gold is bombarded with slow neutrons, a radioactive isotope $_{79}Au^{180}$ is produced.[1] Its half-life was measured electrochemically and is 2.7 days.[2] There have been other measurements[3] of its half-life, the latest value being 2.76 days.[4] This isotope emits β-rays with an upper limit of 0.78 Mev,[5] and also non-corpuscular radiation containing four components. Of these, three with energies of 70, 280, and 440 kev have first been observed and measured by Richardson[6] with the aid of an expansion chamber. Sizoo and Eijkman[7] have, in addition to these three, found a hard component with an energy of 2.5 Mev by absorption method. The last three components with energies of 0.28, 0.44, and 2.5 Mev were found to be γ-rays having their origin in nuclear transition. The soft component with an energy of 70 kev was assumed to be K-radiation of $_{80}Hg^{180}$ by its discoverer.[6] Sizoo and Eijkman, whose measured energy value of the component is 73 kev, however, have supposed that this soft component consists partly of the K-radiation of $_{78}Pt^{198}$ following the capture process and partly of the K-radiation of $_{80}Hg^{198}$, emitted after internal conversion of the nuclear γ-radiations.[7] To ascertain the validity of either of these assumptions, further evidence and a more exactly measured energy value of the soft component would be very valuable.

2. METHODS OF ENERGY MEASUREMENT

The energy of the soft components of this non-corpuscular radiation may be determined by measuring their wave-lengths with the method of analysis of crystal grating and photographic registration. It is, however, difficult to measure the wave-lengths of high energy components since the constant of the usually used crystal grating is too large for them. This method involves the use of strong sources and long exposures for photographic registration in order to obtain satisfactory results.

An important and very useful method which does not necessitate the use of very strong sources for determining the energies of the components of the non-corpuscular radiation consists of the measurement of the energies of electrons ejected by them from the electronic orbits.

* This research was conducted at George Holt Physics Laboratories, The University of Liverpool, England.

[1] E. Fermi, E. Amaldi, O. D'Agostino, F. Rasetti, and E. Segrè, Proc. Roy. Soc. **A146**, 483 (1934).

[2] E. Amaldi, O. D'Agostino, E. Fermi, B. Pontecorvo, F. Rasetti, and E. Segrè, Proc. Roy. Soc. **A149**, 522 (1935).

[3] E. McMillan, M. Kamen, and S. Ruben, Phys. Rev. **52**, 375 (1937).

[4] N. Feather, private communication to Sir J. Chadwick (1942).

[5] A. F. Clark, Phys. Rev. **61**, 242 (1942).

[6] J. R. Richardson, Phys. Rev. **53**, 942 (1938); **55**, 609 (1939).

[7] J. Sizoo and C. Eijkman, Physika **6**, 332 (1939).

These ejected electrons are called secondary β-rays and their energy values may be obtained either by determining the retarding electric field, just sufficient to drive them back to the radiator or by determining the coefficient of absorption of these β-rays in aluminum. The energy of these β-rays may also be calculated from the measurement of the curvature of their trajectories produced by a magnetic field obtained in an expansion chamber. A direct method of determining the energy of these β-rays is spectroscopic analysis which involves either semicircular focusing or lens selective focusing of these rays in a magnetic field and detecting the results by an electrical method.

3. EXPERIMENTAL ARRANGEMENT AND PROCEDURE

A foil of gold, irradiated with slow neutrons in the cyclotron, was used for the investigation of the low energy part of β-ray spectrum of $_{79}Au^{198}$. The foil, about 3 mm in diameter, is of multi atomic layers and is not only a source of nuclear β- and non-corpuscular radiations, but also serves as a radiator of electrons ejected by non-corpuscular radiations. The investigation was made with a thick magnetic lens spectrometer.[8]

The irradiated foil of gold was mounted on the holder of the source chamber and was placed so that its center lay on the axis at the entrance aperture of the spectrometer. The spectrometer and the source chamber were evacuated to a pressure of nearly 10^{-5} mm of mercury. Then the general effect on the electrical counter without magnetic field was carefully observed, and it was found that there was an effect of four counts due to scattered radiations in addition to the natural effect.

Magnetizing current, supplied from 110-volt accumulators was applied and was raised at regular intervals in small and precisely measured steps beginning from zero position on the ammeter scale up to 3.1 amp., the upper limit of the working range of the spectrometer. At the end of each one of these intervals, the counter impulse frequency, corresponding to the magnetizing current applied during that period, was carefully recorded. After taking the readings at each interval for the whole range, the magnetizing current was switched off, and the general effect on the electrical counter without magnetic field was noted.

[8] Swami Jnanananda, Phys. Rev. 69, 571–572 (1946).

4. LOW REGION OF NORMALIZED ENERGY SPECTRUM

Each one of the entire series of counter readings taken in this way was individually corrected for decay. From the values of the coil currents in terms of $H\rho$ obtained by an experimental determination of the magnetizing current corresponding to F-line of thorium B (Th B) at $H\rho=1385.6$[9] and the series of corrected counter frequency records, the $N/H\rho$ values for the entire measured range was obtained. A graphing of $N/H\rho$ values against their corresponding $H\rho$ gave the normalized β-ray spectrogram of $_{79}Au^{198}$ up to a range of $H\rho=1800$, shown in Fig. 1.

5. A SURVEY OF THE SPECTROGRAM

The spectrogram shows that from zero up to a range of about $H\rho=700$, an additional effect on the counter due to focused β-particles is not apparent. This absence of the additional effect on the counter in the range between $H\rho=0$ and $H\rho=700$ is very likely caused by the absorption of the low energy β-particles by the mica window of the counter. From the range of about $H\rho=750$, the curve starts rising, indicating the beginning of an increased effect on the counter due to

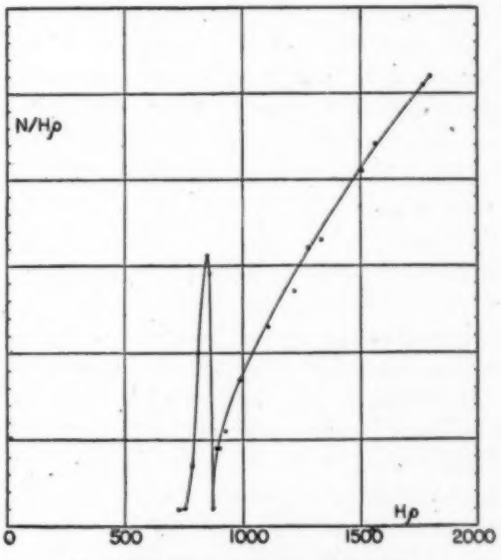

FIG. 1. Energy spectrum of $_{79}Au^{198}$.

[9] C. D. Ellis, Proc. Roy. Soc. A139, 659 (1933).

focused higher energy β-particles which penetrate the mica window and find access into the counter. Thereafter, the curve rises abruptly to a clear and distinct peak, falls down steeply to the basic position, and again rises continuously with the increasing value of $H\rho$. The emergent peak on the curve with its maximum at $H\rho=837.3$ indicates unmistakably a spectral line of β-particles with an energy of 58.4 kev. The rest of the spectrogram shows continuous and gradual increase in the value of $H\rho$ till the end of the working range of the spectrometer.

6. THE CONTINUOUS β-RAY SPECTRUM AND THE DISCRETE SPECTRUM OF SECONDARY β-RAYS

The spectrogram of $_{79}Au^{198}$ within the measured range, shown in Fig. 1, consists of a distinct β-line, impressed, as it were, on a continuous energy curve. In this spectrogram, the β-line is fairly broad, extending from $H\rho=810$ up to $H\rho=840$ nearly. From the peak, the descent towards the low energy side is less steep and abrupt than that towards the high energy side. This spectral line indicates that these β-rays are from one and the same extra nuclear group. The breadth of the line, however, suggests that the energy of this group of β-rays is not homogeneous but heterogeneous, indicating thereby that these β-rays are mainly from different energy sublevels of the same group ejected by more than one component of radiation each with a discrete energy according to the laws of the photoelectric effect. The breadth of the line is of such magnitude as to suggest that the L-group of electrons are ejected by two different radiations whose energy difference is of the order of about 3 kev.

It is very likely that the radiation with discrete energies emergent from the inner atomic layers of the source $_{79}Au^{180}$ ejects electrons of L-, etc. groups of the same isotopic atoms from the outer atomic layers of the foil. Thus the L-group electrons give rise to the β-line with β-particles from L_{III} spreading towards the higher energy side and those from L_{II} and L_I to the lower energy side of the line. The peak of the line, obviously, is inclined towards the higher energy side. Hence it is reasonable to assume that the β-particles corresponding to the peak of the line with $H\rho=837.3$ are electrons ejected from $_{79}Au\,L_{III}$.

Now the value $H\rho=837.3$ obviously corresponds to 58.4 kev energy of the β-particles, and the ν/R value for $_{79}Au^{180}$ level is 877.7,[10] which amounts to 11.9 kev energy. Then by the law of photoelectric effect, the energy of the radiation is

$$58.4 \text{ kev}+11.9 \text{ kev}=70.3 \text{ kev},$$

and its wave-length $\lambda=175.7$ x.u. which agrees with the expected value of the wave-length of $Hg\,K\alpha_1$.

The energy of the radiation which gives rise to the secondary β-rays with an energy of 58.4 kev is 70.3 kev, and this value agrees with the value of about 70 kev, obtained by Richardson. In this connection, it may be remarked that the β-line of the M-group, which is expected to be comparatively weaker than that of the L-group, is overlapped by the continuous β-ray spectrum.

7. THE DUAL TRANSITION OF $_{79}Au^{198}$

From the spectrogram shown in Fig. 1, the continuous energy curve indicates that the isotope of gold $_{79}Au^{198}$ is essentially a β-radioactive nucleus. It is very likely that, owing to the transition of $_{79}Au^{198}$, to the immediate next isobar $_{80}Hg^{198}$, the radiation with the energy of 70.3 kev could be the K-radiation of $_{80}Hg^{198}$ emitted after internal conversion of nuclear γ-radiation. The spread of the line towards the low energy side may also be due to electrons emitted from the same group but by a radiation whose energy is smaller than that of the K-radiation of $_{80}Hg^{198}$ probably by an energy of only a few kev. The latter could then be the K-radiation of $_{78}Pt^{198}$, following the capture process. In other words, the broad spectral line is the energy spectrum of electrons from the L-group of gold ejected partly by the K-radiation of $_{80}Hg^{198}$, and partly by the K-radiation of $_{78}Pt^{198}$. Therefore, the radioactive isotope of gold $_{79}Au^{198}$ appears to have a dual transition, a transition to $_{80}Hg^{198}$, following β-decay and another to $_{78}Pt^{198}$, following K-capture as assumed by Sizoo and Eijkman.[7]

It is a pleasure for the author to express his thanks to Sir James Chadwick for the kind interest taken in this work. The author also wishes to express his appreciation of the help by the Cyclotron Group in preparing the radioactive isotope of gold and of the technical assistance given by Mr. B. D. Aves.

[10] M. Siegbahn, *Spektroskopie der Roentgenstrahlen* (Verlagsbuchhandlung, Julius Springer, Berlin, 1931), second edition, p. 346.

Production of Low Energy Neutrons by Filtering through Graphite*

HERBERT L. ANDERSON, ENRICO FERMI, AND LEONA MARSHALL
Metallurgical Laboratory, University of Chicago, Chicago, Illinois

(Received September 19, 1946)

Neutrons of energy much lower than thermal were produced by filtering a beam of thermal neutrons through a block of graphite 23 cm long. In such a block, Bragg scattering removes the neutrons whose wave-length is less than the largest Bragg wave-length in graphite, 6.69 angstroms. Measurement of the boron absorption of the filtered neutrons showed that they had an effective wave-length of 7.15 angstroms which corresponds to neutron temperatures around 18° Kelvin. The cross section of graphite for the filtered neutrons is 0.70×10^{-24} cm². That a part of this is caused by the incoherence due to thermal agitation of the atoms of the crystal was demonstrated by heating the crystal and observing the increase in this cross section. The filtered neutrons were used to show interference effects in other substances such as Be, Bi, and S. In water a fourfold increase in the scattering cross section of hydrogen due to chemical binding was observed.

A SIMPLE method to produce a beam of neutrons having average energy much lower than that corresponding to room temperature is described in this paper. The method consists in filtering ordinary thermal neutrons through a long and narrow block of graphite which, as will be shown, scatters out of the beam all the neutrons except those of very low energy.

On top of the graphite chain reacting pile which was constructed at the Argonne Laboratories, a graphite column was constructed with base 5′×5′ and 7′ high. The column rose above the pile through a hole in the shield which covers the whole of the chain reacting pile. In such a column the fast neutrons emitted by the pile are slowed down in the lower part of the column so that predominantly only thermal neutrons diffuse upward in the column. Thermal neutrons purified to a high degree from higher energy neutrons are obtained in this way.

Attempts were made to measure the cross section of boron for neutrons emerging from the top of this column. We obtained 867×10^{-24} cm²/atom, a result considerably greater than the value 770×10^{-24} cm²/atom when a somewhat shorter column was used. These results indicated that lower energy neutrons penetrate more readily through large thicknesses of graphite than do the neutrons in the upper energy part of the Maxwell distribution.

In order to investigate this effect in a more systematic way a good beam geometry was set up as shown in Fig. 1. To increase the intensity and yet maintain good collimation, the neutrons used were those emitted from the lower part of a hole extending two feet down in the graphite filter (which was removable) and then through the sample whose transmission it was desired to measure and finally to a BF_3 proportional counter

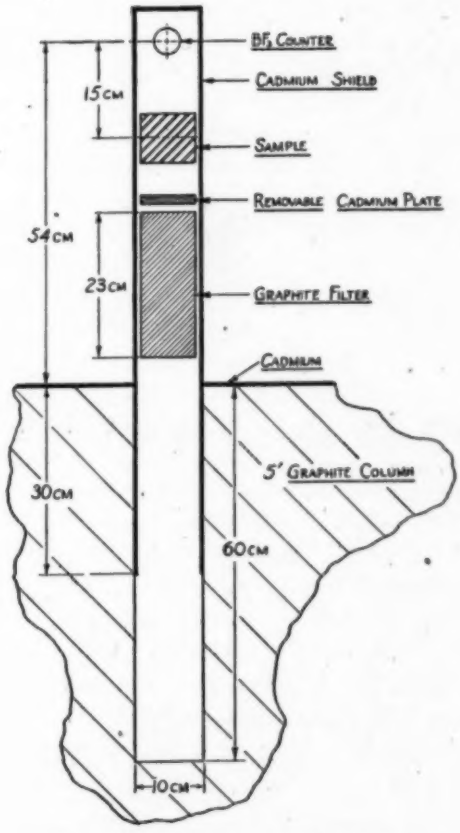

FIG. 1. Arrangement of apparatus.

* This paper is a result of work performed under contract W-7401-eng-37 with the Manhattan Project at the Metallurgical Laboratory, University of Chicago.

TABLE I. Transmission of filtered neutrons.

Substance	g/cm²	No filter Log transmission	No filter σ in 10^{-24} cm²/atom	23-cm graphite filter Log transmission	23-cm graphite filter σ in 10^{-24} cm²/atom
C (graphite)	12.96	2.639	4.05	0.453	0.70
Pyrex	0.241	0.437		1.537	
Be	4.52	0.977	3.25	0.219	0.73
Be	9.04	1.693	2.82	0.424	0.71
$\frac{1}{2}D_2O$	4.352	2.008	7.65	2.475	9.44
$\frac{1}{2}H_2O$	0.455			2.61	85.8
$\frac{1}{2}H_2O$	0.265			1.461	82.5
Bi	76.39	1.469	6.68	0.226	1.03
S crystalline	19.91	0.617	1.66	1.08	2.89
S amorphous	8.02	0.530	3.52	1.063	7.06
S amorphous (next day)	8.02			0.497	3.31

used as a detector. The whole assembly was isolated from stray thermal neutrons by the cadmium shield. A cadmium plate could be inserted above the graphite filter in order to measure the background. In all measurements the small background observed with this cadmium plate in place was always subtracted.

Measurements by the transmission method were made of the total cross sections of a number of substances with and without the 23-cm long graphite filter. The results are given in Table I.

The first column gives the sample, the second its thickness in grams/cm², the third and fourth columns give the logarithm of the transmission and the total cross section σ in units of 10^{-24} cm²/atom obtained without the filter, while the fifth and sixth columns give the same quantities for neutrons which were filtered through 23 cm of graphite.

The marked decrease in the scattering cross section of graphite from 4.05×10^{-24} cm²/atom to the value 0.70×10^{-24} cm²/atom is quite striking. With the filter the log of the transmission of the Pyrex plates (boron) increase by a factor of 3.5. This corresponds to a reduction of energy by a factor of more than 12 for the neutrons which emerge from the graphite filter.

Since graphite is a polycrystalline material, Bragg reflection scatters all neutrons whose wave-length is smaller than the two times the largest lattice spacing.[1] The low energy neutrons are transmitted through the filter because their wave-length is larger than the largest lattice spacing in graphite crystals. Interference takes place in all directions except the straight through direction for such neutrons.

A calibration of the Pyrex plates used in these experiments was carried out by E. Bragdon, E. Fermi, J. Marshall, and L. Marshall who determined their transmission as a function of neutron velocity, using a mechanical velocity selector. In order to obtain the average velocity of neutrons by a measurement of transmission in boron, some assumption has to be made about the velocity distribution of the neutrons, in order to take into account the hardening of the beam in its transmission through the Pyrex plate. For the neutrons emerging from the hole in the graphite column a Maxwell distribution may be assumed and the correction for hardening can be made using the Bethe[2] correction. In this way we found that the kT energy of the neutrons from the hole was 0.023 ev, about 10 percent less than what corresponds to room temperature. The difference being presumably caused by a partial filtering of the neutron coming from the hole.

For the neutrons which filtered through 23 cm of graphite the transmission data with the Pyrex plate gave an effective neutron velocity of 533 meters per second. This corresponds to an effective neutron wave-length of 7.15A. By effective wave-length we mean the wave-length we would measure if all the neutrons had the same velocity. For graphite the largest Bragg wave-length is 6.69A. Our result for the effective wave-length is higher than this because of the contribution of the low energy tail of the Maxwell distribution. With a longer filter we obtained an even larger effective wave-length which showed that for our 23-cm filter the filtering was not yet complete.

TABLE II. Temperature effect on the scattering of filtered neutrons by graphite.

Temp. of scatterer °C	Total cross section in 10^{-24} cm²/atom
20	0.71
69	0.84
117	0.97
254	1.33
370	1.92

[1] W. M. Elsasser, Comptes rendus **202**, 1029 (1936). G. C. Wick, Physik. Zeits. **38**, 403 (1937).

[2] H. A. Bethe, Rev. Mod. Phys. **9**, 136 (1937).

Similar crystal effects were observed in Be and also in Bi in spite of the fact that both atoms have a nuclear spin different from zero.

In the case of water a fourfold increase in the cross section over the value[3] 21×10^{-24} cm^2 measured at 1.44 ev (indium resonance) was observed as was to be expected from the effects of chemical binding.[4] The effect of chemical binding is presumably also responsible for the increase in the cross section of D_2O.

Sulphur proved interesting. Sulphur prepared in the amorphous state gave a cross section of 7.06×10^{-24} cm^2 for the filtered neutrons, a value twice as high as the value obtained for the same sample with the unfiltered thermal neutrons. This increase is believed caused by the cooperative scattering in aggregates of sulphur atoms with dimensions small compared to the neutron wave-length. In such aggregates of n atoms the scattering is proportional to n^2 rather than to n. The next day the same specimen, having partially crystallized, showed a smaller cross section.

To show the effects of the thermal motion of the atoms in a crystal on the interference conditions, the scattering cross section for 15.4 g/cm^3 of graphite was studied with filtered neutrons as a function of temperature of the scatterer. The scatterer was heated with an oxyacetylene torch and the temperature measured using a thermocouple. Temperature equilibrium was not perfectly established in these experiments but the effect is evident. The results are given in Table II. These experiments show clearly that the thermal motion of the crystal atoms tends to destroy the interference conditions.

[3] H. B. Hanstein, Phys. Rev. **59**, 489 (1941).
[4] E. Fermi, Ricerca Scient. **7**, 13 (1936). H. A. Bethe, Rev. Mod. Phys. **9**, 127 (1937).

PHYSICAL REVIEW VOLUME 70, NUMBERS 11 AND 12 DECEMBER 1 AND 15, 1946

Some Mesotron Observations by Simultaneous Registration at Two Stations

F. A. BENEDETTO*
Department of Physics, Fordham University, New York, New York
(Received September 9, 1946)

Two cosmic-ray telescopes were used in these investigations, each being screened against the softer vertical component by 20 cm of lead. One telescope, permanently located at the lower station 142 feet above sea level, served as a "control" with reference to which readings of the second telescope were corrected for fluctuations caused by variations in atmospheric temperature, barometric pressure, and magnetic effects. The second telescope, after having recorded intensities at the lower station, was moved to a platform atop the Empire State Building, 1125 feet above sea level. Intensities here were measured both with and without a compensating layer of lead equivalent to the 35-millibar pressure difference between stations. Estimated mean life range of the mesotron was 9.7 ± 3 km, accuracy being limited chiefly by the comparatively short differential in height between stations. In the second part of this paper a series of correlations of ground values of mesotron intensities with the height variations of the 1000-, 850-, 700-, 500-, 300-, 200-, and 100-millibar pressure levels of the atmosphere is described. From these observations the existence of two production levels for mesotrons is inferred from the position of two peaks in the value of the correlation coefficients, peak values being found for the 500- and 100-mb observations. Mesotron decay coefficients for these two levels were approximately the same and equal to -0.0705 km^{-1}, thus giving a mean life range of 14.2 ± 1.4 km consistent with an effective mesotron spectrum of 2.37×10^9 ev assuming the rest lifetime of the mesotron as 2×10^{-6} sec.

INTRODUCTION

THE determination of the mean life range of the mesotron by height differential compensating-mass-absorber methods has been made by several observers.[1,2] As a check on this decay phenomenon over a short interval near sea level, it was deemed advisable to repeat this type of

* Now at Loyola University, New Orleans, Louisiana.

[1] B. Rossi and D. B. Hall, Phys. Rev. **59**, 223 (1941).
[2] W. M. Nielsen, C. M. Ryerson, L. W. Nordheim, and K. Z. Morgan, Phys. Rev. **59**, 547 (1941).

experiment utilizing the moderate altitude afforded by the observation platform of the Empire State Building in New York City. Since the height differential effect caused by mesotron decay could easily be masked by other variations such as temperature, pressure, and magnetic effects, it was necessary to have a "control" station operating simultaneously with the upper station and in close enough proximity to it so that each station should be influenced equally by the same disturbing factors mentioned above. The control station was located at Fordham University on the roof of the physics building, 142 feet above sea level; the upper station was located on the roof of the Observation Platform of the ESB, 1125 feet above sea level. In previous experiments of this nature, observers utilizing the greater height differentials afforded by mountain ridges, approximately 2000 m, were able to accumulate sufficient data in a comparatively shorter time and consequently were able to measure without the need of a control station.

In addition to serving as a control station the Fordham apparatus was also used in conjunction with radiosonde data to study the effect of variations in height of certain pressure levels from 1000- to 100-mb on the intensity of mesotrons measured at sea level. This study was undertaken in the attempt to discover some level, or levels as results indicated, exerting greater influence on ground mesotron intensities. In the study of various cosmic-ray and mesotron experiments Rathgeber[3] concluded to the existence of two mesotron originating levels, one around the height of 6 km and the other above 17 km. Since the time of Blackett's paper on the temperature effect,[4] it has become customary to assume a single production level around 16 km. Correlation studies such as those described in this paper are expected to aid more directly in the solution of this problem.

APPARATUS

Two similar cosmic-ray telescopes were used in this investigation. The aperture of each was the same and was determined such that the one destined for use on the ESB would not be screened by the tower structure of that building. Each telescope consisted of three trays of argon-oxygen filled Geiger counters. Each tray had nine counters overlapping so as to form a continuously sensitive area 11 cm wide and 19.3 cm long; the distance between bottom and top trays was 62 cm. Trays were supported by sturdy steel frames and were screened against the softer component by 9.5 cm lead between the top and middle trays, and by 10.5 cm lead between the middle and bottom trays. The ESB telescope was also screened against possible side showers originating in the tower structure by a 10-cm iron screen arranged about the periphery of the lowest tray. High potential of -900 volts for the counters, and the power for the coincidence circuits were obtained from stabilized power packs which were fed from self-regulating transformers. Voltages were checked daily, no noticeable drift being observed during the course of the investigation. Each telescope and its associated equipment was housed in demountable thermostated huts. The original dual telescope from which these two separate telescopes were made is described in a previous paper.[5] No anticoincidence tubes were used in the present arrangement, and the original recorders were replaced by watch movement recorders driven by 6N7 multivibrators. Visual readings were taken every 24 hours.

METHOD OF OBSERVATIONS

The loss of mesotrons through decay $-dN$ over a path dh, representing the difference in altitude between two stations that are beneath the same total mass absorber equivalent, is given by

$$-(dN/N)=-(dh/L),$$

consequently

$$L=dh/\log\,(N_1/N_2),$$

where L = mean life range of mesotrons; N_1 = observed mesotron intensity at the higher station; and N_2 = observed mesotron intensity at the lower station.

The procedure thus resolved itself into measuring first the intensity (A) recorded by the ESB telescope while it was located at Fordham,

[3] H. D. Rathgeber, Phys. Rev. 61, 207 (1942).
[4] P. M. S. Blackett, Nature 142, 692 (1938).
[5] F. A. Benedetto, G. O. Altmann, and V. F. Hess, Phys. Rev. 61, 266 (1942).

then moving it to the higher location and measuring the intentisy (B) at that elevation. The ratio (B/A) gives the increase in intensity caused by the fact that less mass absorber is above the higher station and also caused by the shorter path for decay. (B/A) must be corrected however for variations in temperature, pressure, etc., that occurred during the measurements; during the same interval of time that (A) was being measured the control telescope recorded an intensity (A'), likewise the intensity (B') was measured simultaneously with the intensity (B). (B'/A') gave the decrease of intensity caused by the extraneous disturbances. Correction of (B/A) was made by dividing by (B'/A'), thus corrected this ratio is designated (I).

Layers of sheet lead were next placed above the ESB station to compensate for the difference in mass between this and the lower station. This layer was 35.49 g/cm² and approximated the average 35-mb difference in pressure between stations. Intensity as measured at the higher station and under the compensating absorber is designated (C). (B/C) corrected for extraneous disturbances by reference to the corresponding ratio (B'/C') gives the increase in intensity at the higher station that was attributable to the smaller mass above this station and is designated (II'). To convert the absorption in the lead absorber to the corresponding absorption in carbon the ratio (II') was multiplied by the factor 4.960/4.908 which was the rate ratio found by Rossi and collaborators[6] in lead and carbon, (II') corrected is designated (II). Intensities (B) and (C) as well as (B') and (C') were measured alternately and for a total of 13 and 10 days, respectively. Intensity measurements are given in Table I; the various rate ratios are given in Table II.

TABLE I. Mesotron intensities at both stations.

Minutes	Counts	Rate	Experimental condition	
29,890	160,278	5.362	ESB telescope at Fordham, no added lead.	(A)
29,700	162,688	5.478	Control telescope at Fordham.	(A')
18,950	104,294	5.501	ESB telescope at ESB, no added lead.	(B)
18,606	98,339	5.285	Control telescope at Fordham.	(B')
14,240	77,268	5.426	ESB telescope at ESB with added lead.	(C)
14,346	76,273	5.317	Control telescope at Fordham.	(C')

TABLE II. Uncorrected, and corrected, rate ratios for both stations.*

Increase due to less mass, and shorter decay path	1.026±0.004	(B/A)
Control decrease, due to extraneous variations	0.965±0.004	(B'/A')
Corrected value of (B/A)	1.063±0.006	(I)
Increase due to less mass	1.014±0.005	(B/C)
Control decrease, due to extraneous variations	0.994±0.005	(B'/C')
Corrected value of (B/C)	1.020±0.007	(II')
(II') corrected to carbon equivalent	1.031±0.008	(II)

* Errors indicated are the standard statistical fluctuations.

The ratio N_1/N_2 desired for the calculation of L is, therefore, effected by correcting (I) for the 3.1 percent increase indicated by (II), this value is

$$N_1/N_2 = 1.0314 \pm 0.01.$$

Since $dz = 983$ feet $= 0.2996$ km, the mean life range is given by

$$L = 0.2996 \text{ km}/\log 1.0314 = 9.7 \pm 3 \text{ km},$$

for mesotrons reaching sea level with sufficient momentum to penetrate 20 cm of lead. The statistical error is larger by a factor of two than that given by measurements taken over larger path differentials; for comparable accuracy an excessive amount of time would be required in using the short differential in height afforded for this experiment.

CORRELATIONS OF GROUND MESOTRON INTENSITIES WITH HEIGHT VARIATIONS OF ATMOSPHERIC PRESSURE LEVELS FROM 1000 TO 100 MILLIBARS

Data accumulated by the control telescope from February 19 through June 10, 1946 were used for these correlations with the upper air data obtained from the Buffalo, New York, radiosonde reports. Mesotron intensity readings were taken once per day and were averaged over the whole 24-hour period centered around 21:00 EST. For the most part air data were taken from the midnight balloon ascents; however missing data from the midnight reports were supplied for by taking the noon radiosonde data. In Table III the number of days is indicated for which the noon reports were used.

Barograph records for each day were averaged over the 24-hour interval centered about 21:00 EST; correlation of mesotron variations with barometric variations gave a coefficient of -1.24

[6] B. Rossi, N. Hilbury, and J. B. Hoag, Phys. Rev. 57, 461 (1940).

TABLE III. Correlations of mesotron intensities with height variations of various pressure levels of the atmosphere.

Pressure level (mb)	Total days	Noon raob days	Average height ($\bar{z}$) (feet)	Correlation coef. (r)	Decay coef. (β) (km^{-1})
1000	79	10	481.6	-0.014 ± 0.11	-0.008
850	100	10	4757.8	$-0.31\ \pm0.09$	-0.12
700	101	10	9821.2	$-0.26\ \pm0.09$	-0.068
500	97	13	18,252.6	$-0.62\ \pm0.06$	-0.0705
300	96	15	29,905.2	$-0.36\ \pm0.09$	-0.045
200	93	21	38,645.6	$-0.43\ \pm0.08$	-0.050
100	73	44	53,243.6	$-0.45\ \pm0.09$	-0.060
100	56	56	53,339.7	$-0.48\ \pm0.1$	-0.070

percent/in. Hg. Average barometric pressure for the entire period was 29.859 in. Hg, and the daily values of mesotron intensities were corrected to this pressure using the above coefficient.

The radiosonde reports gave directly the heights at which the 1000-, 850-, 700-, 500-, 300-, 200-, and 100-millibar levels occurred; accordingly, these were the barometric levels whose height variations were studied in this investigation. It has been pointed out[3,5] that the mean life range L can be determined from height variations of mesotron producing levels by the following relation

$$L=-1/[(1/N)(dN/dz)]=-1/\beta,$$

where N=mesotron intensity, z=height of mesotron producing layer, and β=decay coefficient.

In 1941 the author and collaborators[5] made a study similar to this in which only two levels were considered, *viz.*, the heights of the atmospheric "center of gravity" and the height of the 400-mb layer. It is believed that the present study is the first to comprise data extending over the much wider range here considered. The correlation coefficients (r), decay coefficients (β), average heights of pressure levels over the period investigated ($\bar{z}$), the numbers of days for which data were available, and the numbers of days for which noon raob were used, are tabulated in Table III.

DISCUSSION OF CORRELATION RESULTS

As is seen from Table III there is a sharp rise to a maximum value of $r=-0.62$ at the 500-mb level as one considers the various levels of progressively higher altitudes. Beyond the 500-mb level there is a diminution in r which however appears to tend towards a second maximum of -0.45 or -0.48 around the 100-mb level. This is taken as an indication that at least two production levels for mesotrons exist at the altitudes of approximately 5.5 km and 16 km, respectively. These two altitudes are in very good agreement with the altitudes of approximately 6 km and 17 km obtained by Rathgeber[3] by an altogether different approach.

Since the mean life range L can be determined by taking the reciprocal of the decay coefficient, the value $L=14.2\pm1.4$ km is estimated from the decay coefficient obtained from variations of the 500-mb level. Approximately the same value is obtained from the less accurate 100-mb measurements. Assuming the lifetime of the mesotron as 2×10^{-6} sec. the value of $L=14.2$ km is consistent with an effective mesotron spectrum of 2.37×10^{9} ev.

It is believed that this method of correlation analysis offers definite possibilities in the study of the complex phenomena of mesotron production and absorption in the atmosphere. Longer periods of observation should considerably improve the accuracy of the estimate of L, and should also help define more sharply the production levels for mesotrons.

In conclusion, the author wishes to express his appreciation to Professor V. F. Hess for many valuable suggestions and for his continued encouragement throughout this investigation; to Professor W. F. G. Swann for suggesting the first part of this experiment and for furnishing the facilities of the Bartol Research Foundation, Swarthmore, Pennsylvania, in the repair of counters. Space for the upper station was generously furnished through the courtesy of the Empire State, Inc., New York City, Mr. J. H. Tarry being most cooperative by granting much time and assistance in this regard. Radiosonde reports were furnished through the kindness of Mr. Garrett of the La Guardia Field Weather Bureau. Financial aid was granted through the Penrose Fund of the American Philosophical Society of Philadelphia, Pennsylvania.

PHYSICAL REVIEW VOLUME 70, NUMBERS 11 AND 12 DECEMBER 1 AND 15, 1946

Multiple Scattering and the Mass of the Meson

H. A. BETHE
Cornell University, Ithaca, New York, and General Electric Research Laboratory, Schenectady, New York
(Received September 20, 1946)

It is shown that multiple scattering by the atoms of the gas in a cloud chamber can cause large apparent curvature of tracks. This effect makes the measurement of curvature in a magnetic field meaningless if the energy of the particle is small and the magnetic field low. An analysis shows that *all* published meson tracks are compatible with a unique mass of about 200 electron masses.

1

IT has been attempted repeatedly to determine the mass of the meson in a cloud chamber,[1–4] by simultaneous measurement of the range of the particle in the gas, and of the curvature of the track in a magnetic field. It is the purpose of this note to point out that such measurements are subject to very large errors due to multiple scattering of the mesons in the coulomb fields of the gas atoms. When properly analyzed, all existing data are compatible with a unique mass of the meson, of about 200 electron masses.

The reason for the large effect of multiple scattering is the extremely low energy of any particle which can be stopped in the cloud chamber gas. The mean angle of deflection due to multiple scattering in a given thickness of material, is inversely proportional to the kinetic energy of the particle. The deflection due to a magnetic field is only inversely proportional to the momentum. Therefore, at sufficiently low velocities, the scattering effect will always be greater than the curvature in the magnetic field. This is especially true if a small magnetic field (1000 gauss) or a gas of high atomic number (argon) is used.

Multiple scattering was also responsible for the erroneous interpretation of some cloud-chamber pictures recently obtained with the betatron of the General Electric Research Laboratory. These pictures were believed[5,6] to show tracks of mesons which were therefore supposed to be produced by γ-rays of 100 Mev or less. More recent cloud-chamber studies[7] to investigate the influence of multiple scattering in air indicate that the tracks can be interpreted as due to protons.

Even the most "direct" method for measuring the meson mass, that of Leprince-Ringuet,[8] is affected by scattering. In this method, the momentum of a recoil electron is measured in a magnetic field. This momentum, combined with the angle between recoil electron and incident meson, gives the mass of the latter. Both the momentum and especially the angle measurement may be falsified by scattering.

2

The mean square average angle of scattering in a thickness x of a substance of atomic number Z is[9–11]

$$\theta_{sc\,pl}^2 = \frac{4\pi e^4 Z^2 N x}{p^2 v^2} \ln \frac{\theta_{\max}}{\theta_{\min}}, \qquad (1)$$

where N is the number of atoms per cm^3 in the substance, p the momentum, and v the velocity of the particle. The subscript pl indicates that the projection of the scattering on a *plane* is meant.

[1] D. J. Hughes, Phys. Rev. **69**, 371 (1946).
[2] Y. N. Nishina, M. Takeuchi, and T. Ichimiya, Phys. Rev. **55**, 585 (1939).
[3] A. J. Ruhlig and H. R. Crane, Phys. Rev. **53**, 266 (1938). In this paper, the change of curvature along the path was actually used, but the results can also be interpreted on the basis of curvature and range.
[4] Further literature in J. A. Wheeler and R. Ladenburg, Phys. Rev. **60**, 756 (1941).
[5] M. Schein and A. J. Hartzler, Phys. Rev. **69**, 248T (1946).
[6] M. Schein, A. J. Hartzler, and G. S. Klaiber, Phys. Rev. **70**, 435 (1946).
[7] G. S. Klaiber, A. E. Luebke, and G. C. Baldwin, Bull. Am. Phys. Soc. (September, 1946), Abstract C11.
[8] L. Leprince-Ringuet, S. Gorodetzky, E. Nageotte, and R. Richard-Foy, Phys. Rev. **59**, 460 (1941).
[9] E. J. Williams, Proc. Roy. Soc. **169**, 531 (1939).
[10] E. J. Williams, Phys. Rev. **58**, 292 (1940).
[11] B. Rossi and K. Greisen, Rev. Mod. Phys. **13**, 240 (1941).

The minimum scattering angle $\theta_{\min}$ in (1) is given by screening and is

$$\theta_{\min}=(mc/p)(Z^{\frac{1}{3}}/181) \tag{2}$$

with m the electron mass. The maximum angle, $\theta_{\max}$, should be taken for cloud-chamber tracks as that angle which can easily be recognized as single scattering (normally about 0.1 radian). (The finite size of the nucleus does not provide a limitation on $\theta_{\max}$ for the small momenta with which we are concerned.)

To obtain the apparent radius of curvature, let us consider the projection of a track on a plane (Fig. 1). Let M be the midpoint of the track, and $\mathbf{t}$ the tangent to the track at M. Let y_1 and y_2, respectively, be the distance of the end points, P_1 and P_2, of the track from the tangent $\mathbf{t}$, and x the distance from M to either end point (assumed to be large compared with y_1 and y_2). Then it is easily seen (e.g., reference 9, Eq. (1.68)) that

$$(y_1^2)_{Av}=(y_2^2)_{Av}=(\tfrac{1}{3})x^2\theta_{Av\,pl}^2. \tag{3}$$

The distance s of M from the straight line P_1P_2, i.e., the sagitta of the curve, is given by

$$s=(y_1+y_2)/2. \tag{4}$$

Since y_1 and y_2 are statistically independent, we have

$$s_{Av}^2=(y_1^2+y_2^2)_{Av}/4=x^2\theta_{Av\,pl}^2/6. \tag{5}$$

From s, we get the radius of the closest fitting circle,

$$\rho_s=x^2/2s, \tag{6}$$

or inserting (5),

$$\rho_s=(\tfrac{3}{2})^{\frac{1}{2}}\frac{x}{(\theta_{Av\,pl}^2)^{\frac{1}{2}}}. \tag{7}$$

If the gas contains PL nuclei per cm^3 where L is Loschmidt's number ($L=2.7\cdot10^{19}$, $P=2$ for air at NTP, $P=1$ for argon at NTP), the apparent radius of curvature becomes

$$\rho_s=103\frac{M\beta^2}{Z}\left(\frac{x}{BP}\right)^{\frac{1}{2}}. \tag{8}$$

Here M is the mass of the particle (including relativistic correction) in units of the electron rest mass, β is v/c, and B is a correction factor close to unity, *viz.*,

$$B=1+0.444\log_{10}\frac{p}{mc}\theta_{\max}Z^{-\frac{1}{3}}. \tag{9}$$

The apparent radius ρ_s is given in cm. If the velocity is non-relativistic and if E is the kinetic energy of the particle in Mev, (8) can be rewritten:

$$\rho_s=404\frac{E}{Z}\left(\frac{x}{BP}\right)^{\frac{1}{2}}. \tag{10}$$

The "scattering radius" (8) may be compared with the radius of curvature in a magnetic field,

$$\rho_H=1700M\beta/H, \tag{11}$$

and we obtain

$$\rho_H/\rho_s=\beta_0/\beta, \tag{12}$$

with

$$\beta_0=16.5\frac{Z}{H}\left(\frac{BP}{x}\right)^{\frac{1}{2}}. \tag{13}$$

Below the "critical velocity" β_0, the major contribution to the curvature arises from scattering which makes any calculation of the mass from the curvature meaningless.

Table I gives some results for β_0 for gases at NTP. (For the calculation of B, $\theta_{\max}$ was assumed equal to the deflection of the particle in

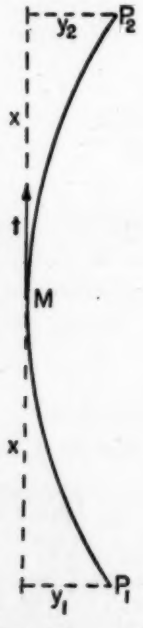

FIG. 1. Curvature of track due to scattering.

TABLE I. Values for the critical velocity, β_0.

Gas	$Hx^{\frac{1}{2}}\beta_0$	β_0 for $H=1000$, $x=10$	Corresponding proton energy (Mev)
H_2	25	0.008	0.03
He	35	0.011	0.06
Air	176	0.056	1.4$_5$
Ne	173	0.055	1.4
A	310	0.098	4.5

a magnetic field of 1000 gauss over a distance of 10 cm; the result is not sensitive to this assumption.) It is seen that for argon, with a field of 1000 gauss and a track length of $2x=20$ cm, the measurements become completely meaningless when $\beta \leq 0.1$, and even if the velocity is equal to that of light, the scattering introduces an error of 10 percent in $H\rho$.

The situation is even worse for particles close to the end of their range because then the available track length is often much shorter than the 20 cm assumed in Table I. Table II gives, for protons and for mesons of mass 200, the values of the kinetic energy at which the "scattering radius of curvature" ρ_s becomes equal to the radius in a magnetic field of 1000 gauss, assuming that the entire range of the particle is used for the curvature measurement.[12] For simplicity, the energy at the midpoint of the track was assumed to determine both ρ_H and ρ_s. The table shows clearly that in air, and even more in argon, magnetic curvature measurements on any track stopping in a cloud chamber are meaningless if the magnetic field is as low as 1000 gauss. Even at much higher fields, the errors are very large. Increase of pressure is only of little help because, although particles of higher energy can then be stopped in the chamber, the curvature due to scattering for a given energy increases.

TABLE II. Energies and ranges below which curvature measurements in a field of 1000 gauss become meaningless.

Gas (NTP)	Proton $\beta=v/c$	Proton Energy Mev	Proton Range cm	Meson ($\mu=200$) $\beta=v/c$	Meson ($\mu=200$) Energy Mev	Meson ($\mu=200$) Range cm
Hydrogen	0.032	0.47	2.2	0.047	0.112	0.96
Air	0.082	3.14	15.2	0.123	0.765	6.5
Argon	0.101	4.75	31	0.151	1.15	13.8

3

We have seen that the curvature of a short range track does not permit one to infer the mass of the particle. The best one can do is to investigate whether the observed "curvature" can reasonably be ascribed to scattering (plus possible magnetic deflection) for an *assumed* mass of the particle. Since scattering is a statistical phenomenon, a curvature $1/\rho_s$ of twice the expected value must be considered as quite likely and the assumed particle mass must in such a case not be ruled out.

This argument is strengthened by the fact that at the larger angles single scattering becomes important. The probability distribution for multiple scattering is, of course,

$$P(\theta)d\theta = \frac{d\theta}{(2\pi\theta_M^2)^{\frac{1}{2}}} \exp\left[-\theta^2/2\theta_M^2\right]. \quad (14)$$

The distribution for single scattering is

$$P(\theta)d\theta = \frac{\theta_M^2 d\theta}{\theta^3 \ln\left(\theta_{\max}/\theta_{\min}\right)}, \quad (15)$$

where $\theta_{\max}$ and $\theta_{\min}$ have the same meaning as in Eq. (1). This gives quite appreciable probabilities for deflections of several times θ_M.

One should further keep in mind that the observer is attracted to the unusual tracks showing large curvature while the normal, nearly straight tracks pass unnoticed. It should, therefore, not be surprising to find tracks whose statistical probability is of the order of one percent.

It is often objected that the scattering should cause an erratic path, rather than a smooth circular arc. This argument is fallacious because of the limited accuracy with which the track can be observed, especially if it is a thick and short track of a heavily ionizing particle near the end of its range. Consider again Fig. 1: It is equally probable that the points P_1 and P_2 lie on the *same* side of the tangent **t**, as that they lie on opposite sides. In the former case, we observe in first approximation a circular (*C*-type curve) arc, although closer examination might possibly reveal that most of the curvature is in one-half of the track. In the latter case, we get an S-

[12] Frequently, only the first half of the range is used. While this makes for better definition of the energy, it gives a smaller x and therefore no improvement in the ratio ρ_s/ρ_H.

shaped curve, but the expectation value of the sagitta of each half of this curve is smaller by a factor $2^{\frac{1}{2}}$ than the expectation value of the sagitta of the entire curve. This means that the deviation of the S-curve from a straight line can be observed only if the accuracy of measurement is quite high, whereas the curvature of a C-type track can be clearly recognized. In other words, "erratic" deviations of the track are much smaller and harder to recognize than its over-all curvature. However, photographs of proton tracks, taken by Klaiber, Luebke, and Baldwin[7] without a magnetic field, show S-type as well as C-type curves.

A further point which makes for apparently smooth curvature is the combination of magnetic and scattering curvature. Even if the scattering predominates, the magnetic field still gives some contribution and helps to make the curvature more uniform. However, cases may also occur in which the scattering "curvature" is opposite to the magnetic one, and predominates sufficiently to give seemingly the wrong sign of the electric charge. One such example was observed in the General Electric Research Laboratory, in which a proton showed a "negative" curvature.

The smoothness of a track is thus no argument against a major contribution of scattering. Nor is the variation of curvature along the track a valid criterion: If an (already short) track is broken into sections, the curvature in each section is relatively even more influenced by scattering than that of the entire track. The "right" law of increase of curvature (as expected in a magnetic field) is qualitatively also produced by scattering which also increases towards the end of a track.

4

The formulae developed in Section 2 may be compared with those of Williams.[9,10] In particular, Williams has given a very simple rough formula for the apparent radius of curvature due to scattering,* namely,

$$\rho_s/R=1.3(M/mZ)^{\frac{1}{2}}. \qquad (16)$$

Here R is the range of the particle and ρ_s is the mean curvature over the first half of the range. Therefore, if we wish to compare Williams' result with our Eq. (10), we must put in the latter $x=\frac{1}{4}R$ and E equal to the energy of a particle of range $\frac{3}{4}R$. The comparison of Eqs. (10) and (16) shows then considerable discrepancies; e.g., for protons of range between 2 and 20 cm in air, Eq. (10) gives a radius of curvature which is about 0.6 of that obtained from Williams' formula (16). Since Williams' formula has been widely used, it is necessary to explain this discrepancy.

The main part of the discrepancy is caused by a different definition of ρ_s. Williams uses the straight mean deflection, whereas we have used the mean square. This causes a factor $(2/\pi)^{\frac{1}{2}}$ which is about 0.8. There is, of course, no real difference between using the two different kinds of mean, but it must be remembered that when the straight mean is used, scattering may exceed this mean by a large factor. Curvatures of 3–4 times the straight mean are statistically quite probably.

The second difference is in the definition of the radius of curvature. Williams defines this by means of the change of direction of the track from the beginning to the end. It is experimentally not easy to determine the direction of a track at a given point with any accuracy. We, therefore, believe that our definition in terms of the sagitta of the curve is closer to actual experimental procedure such as fitting the best circle to a given curve. This difference in definition causes another factor $(3/4)^{\frac{1}{2}}$ which is 0.87, again in the direction of making our ρ_s smaller than that of Williams.

Finally there is some inaccuracy in the analytical range-energy relation used by Williams in deriving Eq. (16). This inaccuracy causes an error of about 10 percent, again in the same direction. The error is greater in the case of heavier elements; e.g., for argon the correction is about 20 percent. The results from Williams formula should, therefore, be multiplied by about 0.6 for air and about 0.52 for argon.

A further difference between Williams' paper and ours is the much more accurate way in which he treated the maximum scattering angle $\theta_{\max}$. Williams[9] wanted to give an *accurate* value for the average scattering angle and included a

* Reference 10, Eq. (21a).

detailed discussion of the large deflections. In this paper, we are concerned only with approximate values permitting some judgment as to the statistical probability of certain curvatures of cloud-chamber tracks. We were, therefore, satisfied with a much rougher treatment of θ_{max}, and we wished at the same time to determine θ_{max} in conformity with experimental procedures; i.e., as the angle which can be observed without difficulty as single scattering. The difference between the two determinations of θ_{max} corresponds to only a few percent in ρ_s is all particle cases.

In much of the literature great liberty is taken with the range-energy relation and particularly with the stopping power of argon and similar substances. Very frequently the stopping power is assumed to be proportional to the number of electrons in an atom which is reasonably accurate for very high energy particles but fails even in this case by 10–20 percent.[11] In the case of slow particles, with which we are here concerned, this assumption is entirely wrong; for instance, argon has a stopping power[13] of about 0.97 of that of air instead of 1.25 as would correspond to the number of electrons. The energy, and therefore the expected radius of curvature, of tracks in argon has, therefore, been grossly over-estimated in much of the literature.

5

We shall now analyze some of the tracks which have been reported.

1. The track of D. J. Hughes.† This track was interpreted by Hughes as caused by a particle of mass between 10 and 50 electron masses. We shall show, however, that the data are compatible with the "normal" meson mass of 200.

The track length (measured on photograph) is 2.5 cm in argon of NTP. At the low velocity of the particle concerned, the stopping power of argon is slightly less than that of air,[13] rather than 1.4 times as great (proportional to the density) as apparently assumed by Hughes. At the midpoint, the residual range is then 1.2 cm air (Hughes gives 1.8). The measured radius of curvature is 3.5 cm.

[13] M. S. Livingston and H. A. Bethe, Rev. Mod. Phys. 9, 261 ff. (1937) (Table 48, p. 272). The number given there (1.94) is for one argon *atom* as compared to one air "atom"; per molecule, the stopping power is then 0.97.

† Reference 1, Fig. 5.

A meson of mass 200 m and of range 1.2 cm air has an energy[13] of 280 kev. This gives the following results:

$H\rho = 2.5 \cdot 10^4$.

$\rho_H = 22$ cm (Since $H = 1165$ gauss).

Curvature attributable to scattering: $1/\rho = 1/3.5 - 1/22$, $\rho = 4.1_5$ cm.

$\rho_s = 7.5$ cm (calculated from Eq. (10), with $Z = 18$, $P = 1$, $B = 0.89$, $x = 1.25$).

The "observed" curvature is 1.8 ($=7.5/4.1_5$) times the standard scattering. This is quite probable: the statistical probability that the curvature is more than 1.8 times its average value is 7 percent. The track observed by Hughes, therefore, is no evidence for a meson mass different from the "normal" value of 200.

For all the remaining tracks reported by Hughes, the mass of 200 is included in the interval of probable error given by Hughes himself.

2. The track of Nishina and collaborators.[2] This track gave, in the analysis of the authors, a mass of 177 ± 8 electron masses (error due to measurement alone). This experiment was made under much more favorable conditions since the magnetic field was high (12,600 gauss) and the gas was air rather than argon. The data:

Range 6.15 cm at 1.2–1.3 atmosphere pressure, corresponding to 7.3–8.1 cm air at NTP.

Measured radius of curvature $\rho_m = 3.08$ cm.

Critical velocity from Eq. (13),

$$\beta_0 = 16.5 \frac{7.2 \cdot 1.02}{12{,}600} \left(\frac{2.5}{3.08}\right)^{\frac{1}{2}} = 0.0087.$$

Residual range at midpoint of track $= 3.8_5$ cm air at NTP, corresponding to an energy of 0.56 Mev for a meson of mass 200.

Therefore velocity $\beta = 0.105$.

Probable error of curvature due to scattering $\beta_0/\beta = 0.083$.

For $\mu = 200$ m we have $H\rho = 35{,}700$, $\rho_H = 2.83$ cm which differs from the observed radius of curvature, $\rho_m = 3.08$ cm, by 8 percent which is within the probable error due to scattering. A mass of 200 is easily compatible with this measurement.

3. The track of Ruhlig and Crane.[3] According to the analysis of the authors, this track gave a mass of 120 ± 30. Data:

Track length (measurable) 4.7 cm. (Actual range may be longer because track probably passes out of the field of illumination.)

Measured radius of curvature 9 cm.

At midpoint, residual range 2.3$_8$ cm (if 4.7 cm is the total range). If mass is assumed to be 200 m, the energy is 420 kev.

The calculated scattering radius is $\rho_s = 25.6$ cm ($Z = 7.2$, $B = 1.00$).

Calculated

$$H\rho = 30{,}500, \quad \rho_H = 10.7 \text{ cm} \quad (H = 2850).$$

A combination of magnetic and scattering curvature can easily explain the measured radius of curvature of 9 cm.

This track was the only one considered by Corson and Brode[14] to show a definite deviation from a mass of 200. Our analysis proves, however, that it is not in disagreement with such a mass.

4. One of the tracks observed with the betatron of the General Electric Research Laboratory[5,6] has the following characteristics:

Range 6.1 cm in argon of 80 cm pressure.

Curvature corresponding to a *negative* charge, observed radius of curvature 22 cm in field of $H = 800$ gauss.

This track was originally interpreted as caused by a meson, especially because of its apparent negative charge. However, it is quite compatible with a proton. Interpreting it in this way, we find for the midpoint of the track:

Residual range 3.1-cm air equivalent.
Proton energy 1.21 Mev.
$H\rho = 1.58 \cdot 10^8$, therefore calculated $\rho_H = 200$ cm.

To compensate for this magnetic curvature, and give the observed negative curvature, the scattering by itself must have had a radius of curvature $\rho = 20$ cm. The calculated $\rho_s = 43$ cm ($Z = 18$, $B = 1.23$). The actual scattering curvature is thus about twice the "average" value which is statistically sufficiently probable. The track is therefore compatible with a proton and cannot be used as evidence for production of a meson by the betatron. This conclusion must be reached in spite of the apparent negative curvature: If scattering predominates over magnetic deflection, the sign of the curvature clearly has no physical meaning.

Another track of range 5 cm showed a positive curvature of radius 27 cm. This is even closer to the theoretical curvature than the first example. In addition, there was definite evidence of single scattering in this track.

Tracks observed without a magnetic field in air[7] include one of 3.5-cm length and $\rho = 12$ cm and one of 13-cm length and 60-cm curvature. These are about three times the "expected" scattering for protons.

5. Another experiment which is affected by multiple scattering is the measurement by magnetic deflection of the energy of the proton arising from the photo-disintegration of the deuteron.[15] Fortunately, this experiment was done in deuterium gas at low pressure (8 cm Hg) and the main scattering is due to the water (D_2O) vapor in the cloud chamber whose partial pressure was probably about one-half of the total pressure. The magnetic field was also reasonably high (3762 gauss). The data:

Total range of protons (220 kev) in air 0.22 cm, in the cloud chamber about 3.2 cm (average of measurements).
At midpoint: residual range $x = 1.6$ cm.
Energy 110 kev.
Effective $Z\sqrt{P} = 1.9$.
Calculated from midpoint energy, $\rho_s = 46$ cm ($B = 1.02$), $\rho_H = 18$ cm.

This indicates a probable error of 40 percent in the determination of $H\rho$ which may be one cause of the large fluctuations in the measured energy release (although there are also other causes for such fluctuations).

6. We shall now discuss the method of Leprince-Ringuet and others[8,16] for the measurement of the mass of cosmic-ray particles. The method consists of measuring the momentum and direction of emission of a recoil electron, and the momentum of the primary particle which has produced the recoil electron. The method is very free of theoretical assumptions such as the ionization as a function of energy. However, even this method is subject to errors due to multiple scattering. These come in four places: (a) the measurement of the momentum of the primary particle, (b) the momentum of the electron, (c) the angle χ_1 between electron and primary particle in the plane perpendicular to the magnetic field, and (d) the angle χ_2

[14] D. R. Corson and R. B. Brode, Phys. Rev. **53**, 773 (1938).

[15] F. T. and M. M. Rogers, Phys. Rev. **55**, 263 (1939).

[16] L. Leprince-Ringuet and M. Lhéritier, J. de Phys. et rad. (8) **7**, 65 (1946).

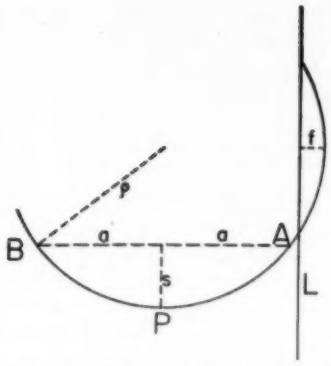

FIG. 2. Mass determination by the method of recoil electrons. APB is the measured section of the track of the electron, L represents the track of the primary.

between these particles in a plane parallel to the magnetic field.

The first of these is a standard curvature measurement to which our theory is directly applicable. The error is usually quite small because a long track is available for curvature measurements.

Errors B and C are related to each other. In order to determine the data on the recoil electron, one tries to fit a circle to the track of the electron as closely as possible. The fitting should be done over as large an arc as possible in order to make the radius of curvature as accurate as possible; on the other hand, multiple scattering will gradually make the track deviate from the circle so that the position of the center of the circle is shifted appreciably; for this reason, parts of the track too far from the point of emission should not be used. The practical compromise used by Leprince-Ringuet and coworkers is to make the fitting near the point at which the electron has been deflected through 90° by the magnetic field, and to use a track length of about a quarter circle. In effect then, the part of the electron track from $\theta=45°$ to $\theta=135°$ is used for fitting. (See Fig. 2.)

The error in the radius of curvature is slightly greater than that given by the theory of Section 2. The result in Eq. (13), for instance, should be multiplied by a factor

$$F(\alpha)=\alpha^2/2(1-\cos\alpha) \tag{17}$$

where 2α is the angle subtended by the measured track length, in our case 90°. To find the angle of emission we have to extrapolate the electron track back to the track of the primary particle. A convenient measure of χ_1 is the sagitta f between electron track and primary track, the latter being substantially straight for our purposes. The extrapolation is done by assuming a circular path defined as the closest approximation to the track between A and B (Fig. 2). The error in f due to multiple scattering is calculated in the Appendix; for our choice ($\alpha=45°$ and $\beta=45°$), the probable error in f is

$$\Delta f=0.722\ \Delta\rho \tag{18}$$

where $\Delta\rho$ is the probable error of the radius of curvature. Now f is related to the angle χ_1 by the equation

$$f=\rho(1-\cos\chi_1). \tag{19}$$

The mass M of the primary particle, neglecting the electron mass in comparison with it, is given by

$$Mc=p_0\left[\frac{E+mc^2}{E-mc^2}\cos^2\chi-1\right]^{\frac{1}{2}}, \tag{20}$$

where p_0 is the momentum of the primary, E is the energy of the electron including rest mass, and

$$\cos\chi=\cos\chi_1\cos\chi_2 \tag{21}$$

provided the primary particle path lies in the plane perpendicular to the magnetic field as it normally does. From Eqs. (17) and (20) we can deduce the uncertainty in M.

However, the error in the radius (and therefore in E) and that in the sagitta f (and therefore in χ_1) are related. If the actual radius in the magnetic field is greater than the apparent radius of the track between A and B, the true path will have a greater sagitta than f and therefore a smaller $\cos\chi_1$ than the extrapolated circle. This means that the energy E is greater than estimated and $\cos\chi_1$ smaller than estimated. Both errors tend in the same direction of making the actual mass of the primary less than the estimated one. The correlation between the errors in radius and in f is

$$(\Delta\rho\Delta f)_{Av}=0.570(\Delta\rho_1{}^2)_{Av}, \tag{22}$$

where $\Delta\rho_1$ is the error in ρ without the correction factor (17).

The measurement D is independent of B and C. The slope of the track in the direction of the magnetic field is measured approximately at the same point as the curvature; i.e., between points A and B when the track is approximately at right angles to the primary. Multiple scattering will cause a mean square deflection which is given by Eq. (1) with $x=\pi\rho/2$.

Two measurements by Leprince-Ringuet and co-workers are of special importance.

A. The meson track reported in reference 8 which gave a mass of 240 electron masses. The magnetic field was $H=2650$ gauss, the observed radius of curvature of the electron 1.07 cm and for the meson 117 cm. The errors according to the above formulae are as follows:

a. The meson momentum has a probable error of 3 percent.

b. The electron momentum has a probable error of 8.4 percent. This causes a probable error in the expression $(E+mc^2)/(E-mc^2)$ of 8.6 percent.

c. The error in f is 0.061ρ; therefore the error in $\cos\chi_1$ is 0.061. Including the correlation, the error in the meson mass due to causes b and c is 15 percent.

d. The probable angle of scattering is 4.6° leading to a probable error in $\cos\chi_2$ of 2.4 percent and in the meson mass of 3.6 percent.

Altogether the probable error of the meson mass (adding the squares of the individual errors) is 16 percent. The error due to the measurement itself was given by the authors as 10 percent. A mass of 200, which is 17 percent lower than the mass of 240 resulting from the experiment, is therefore within the probable error.

B. In reference 16 a track is reported which gives a mass for the primary particle of about 1000 electron masses. It can easily be seen that this primary cannot be a meson of mass 200. We shall show, however, that the measurements are compatible with a primary proton. The individual errors are as follows:

a. The measurement of the momentum of the primary particle has a probable error of 5 percent because of multiple scattering. Taking the upper limit of the measured radius of curvature, and adding the probable amount of scattering, we get a maximum probable momentum for the primary of 580 Mev/c. A proton of this momentum will emit recoil electrons of a momentum

$$p=\frac{2mv\cos\chi}{1-(v^2/c^2)\cos^2\chi}=(0.755-0.670\chi^2)\frac{\text{Mev}}{c}. \quad (23)$$

d. The measured angle χ_2 is 20° to 24°. If we assume an electron momentum of 0.75 Mev as given by Eq. (23), we find that the probable angle of scattering in a track length of a quarter circle is 7.5°. We, therefore, get a minimum probable value of $\chi_2=12.5°$. Using this angle in Eq. (23), we get

$$p=(0.723-0.670\chi_1^2)\ \text{Mev}/c. \quad (24)$$

c. The observed sagitta f is between 0 and 0.07 cm. Therefore, it is consistent with the experiments to assume $\chi_1=0$. This gives for the maximum probable value of the electron momentum

$$p_m=0.723\ \text{Mev}/c. \quad (25)$$

b. The measured value of the electron momentum is between 1.09 and 1.16 Mev/c. If we assume that the actual momentum is 0.72 Mev multiple scattering according to Eq. (13) will give a probable error for the radius of curvature of 14 percent. Since a 90° arc is used for determination of the radius of curvature, the error due to scattering should, according to Eq. (17), be increased by a factor 1.053 to 15 percent. The radius of curvature expected for an electron from a primary proton is 32 percent less than the observed radius of curvature. This difference is 2.1 times the probable error due to multiple scattering and is, therefore, statistically quite probable.

We see, therefore, that the observed track can be reconciled with the assumption that it is made by a primary proton. It is true that we had to assume all errors on the same side. However, the error in the radius of curvature of the electron was only 2.1 times the probable error due to multiple scattering. It is also true that a proton of a momentum of 580 Mev should ionize about twice as strongly as a particle at the minimum of the ionization curve, and the observed track appears not to have an ionization significantly above the minimum. But it is generally admitted that estimates of ionization without droplet counting are qualitative and often incorrect.

Even though considerable stretching of the probable errors was necessary, we still believe that this particle is most likely a proton. It seems to us that an entirely new particle could only be established by much more than one event and by measurements of much smaller probable error.

6

These examples show that multiple scattering disturbs very seriously all measurements on low energy particles in the cloud chamber. It leaves reasonably unaffected all measurements on par-

ticles of high velocity. The best methods to determine the meson mass by cloud-chamber techniques therefore seem to be:

a. Measurement of curvature and droplet counting for tracks of reasonably high velocity ($\beta \approx 0.5$).

b. Measurement of the change of magnetic curvature upon penetration of a (reasonably thick) solid plate, as discussed in detail by Wheeler and Ladenburg.[4]

c. Measurement of curvature, followed by measurement of the penetration through a set of thin solid plates. This method was used successfully by Baldwin and Klaiber[7] on the protons obtained by photo-disintegration of nuclei by γ-rays from the betatron, and by Fretter and Brode[17] on cosmic-ray mesons.

In all cases, the magnetic field should be high (at least 3000 gauss) and the cloud-chamber gas light (hydrogen or helium).

7

Our analysis of some of the direct measurements of the meson mass show that all those data which appear to give a very low mass are subject to error due to scattering. There is not a single measurement which cannot be reconciled with a unique mass in the neighborhood of 200 electron masses.

Indirect arguments[18] have also been given for the existence of mesons of low mass. These are mainly based on some evidence that there are very many low energy mesons in cosmic radiation at high elevations, and that very few mesons of high ionization appear in cloud-chamber photographs. However, the latter point is really quite understandable: In order to be easily recognized, a "heavy" track should have an ionization at least twice, and preferably four times, that of an "average" particle, i.e., of a high energy meson or of an electron of, say, 50 Mev. The ionization of the latter is about 30 percent higher than the minimum ionization.* A meson of twice this ionization must have a momentum $p < 0.65\mu c$ and a kinetic energy below $0.15\mu c^2$. With a mass of 200 electron masses, its range in air or A is less than 3 g/cm^2. Therefore only about one percent of all mesons of energy below $6 \cdot 10^8$ ev should have an ionization greater than twice that of a fast electron. If four times normal ionization is required for clear recognition, we must have $p < 0.40\mu c$, $E_{\text{kin}} < 0.08\mu c^2$, range < 0.6 g/cm^2, so that only 0.2 percent of all mesons below $6 \cdot 10^8$ ev will qualify.

As regards the number of slow mesons from counter experiments, this is very difficult to obtain below $3 \cdot 10^8$ ev. Undoubtedly, in some analyses[19] many electrons have been considered as slow mesons. There does not seem to be much experimental basis for the (frequently made) assumption that, at about 4000 meters elevation, the number of mesons per unit energy interval increases rapidly below $3 \cdot 10^8$ ev.

We, therefore, do not believe that there is any real evidence for an unexpectedly small number of mesons of observably high ionization. Even if there were, we should consider it more likely that this is caused by an unknown absorption of slow mesons (about whose properties, after all, we know very little) than to a spread in mass.

This brings us to a more philosophical point: All known fundamental particles have a definite rest mass. To discover a particle for which this is not the case would be a tremendous deviation from previous experience. For this reason the most unambiguous and accurate experimental evidence would have to be obtained before a non-unique rest mass could be accepted. It is obviously very easy to explain each new experiment by a new assumption, and this was done in the last few years in the case of the meson mass: It is much more difficult to explain all experiments by a minimum of assumptions, which was the way in which physics has progressed in the past. The burden of proof lies always with the discoverer of a *new* phenomenon, and must in this case lie with the advocates of the variable rest mass of the meson.

ACKNOWLEDGMENTS

It is a pleasure to thank Doctors L. Tonks, G. S. Klaiber, A. E. Luebke, and G. C. Baldwin as well as Professor Leprince-Ringuet for helpful discussions of experimental and theoretical aspects of this problem.

[17] W. B. Fretter and R. B. Brode, Bull. Am. Phys. Soc. (September, 1946), Abstract C17.

[18] M. Schein, Carnegie Inst. of Wash. Yearbook **43**, 61 (1944).

* For this and the following, see reference 11, Figs. 1 to 4.

[19] E.g., P. V. Auger, Phys. Rev. **61**, 684 (1942).

APPENDIX

Discussion of Tracks of Considerable Curvature

In connection with the experiments of Leprince-Ringuet (Section 5, subsection 6), the problem of measuring electron tracks of considerable curvature arises. We shall assume in close accordance with the measuring procedure that the "best circle" is fitted to a section AB of the track (see Fig. 2). This amounts essentially to measuring the distance $AB=2a$ and the length of the sagitta s of the curve AB. If AB were a circle, its radius would be

$$\rho=a^2/2s+s/2. \tag{51}$$

This equation will be used as the definition of the measured radius of the curve.

Let us assume that the magnetic field alone would deflect the electron by an angle 2α over the distance from B to A, and that the radius of curvature in the magnetic field alone is ρ_0. Then, the track length from the point P to either A or B will be nearly $\rho_0\alpha$. The actual deflection from P to A will be $\alpha+\theta_1$, where the probable value of θ_1 is calculated from Eq. (1) with $x=\rho_0\alpha$. The lateral displacement of the track with respect to the circle of radius ρ_0 and the point A is given by Eq. (3) with $x=\rho_0\alpha$.

Figure 3 illustrates the situation. BPA now represents the circle in the magnetic field alone. The lateral displacements at A and B are assumed to be y_1 and y_2, respectively. In order to have the same ordinates for the end points of the actual track, we increase the track length by z_1 and z_2, respectively, at its two ends giving the new end points A' and B' for the actual track. The vertical displacements of A' with respect to A and of B' with respect to B are then

$$\begin{aligned} V_1&=y_1\cos\alpha+z_1\sin\alpha,\\ V_2&=y_2\cos\alpha+z_2\sin\alpha. \end{aligned} \tag{52}$$

The condition that these be equal determines z_1-z_2; otherwise the z's are arbitrary. It is a welcome check on the calculations to ascertain at each stage that the significant results are independent of z_1+z_2.

The sagitta s of the "observed" track $B'PA'$ is now

$$s=\rho_0(1-\cos\alpha)+Y\cos\alpha+Z\sin\alpha, \tag{53}$$

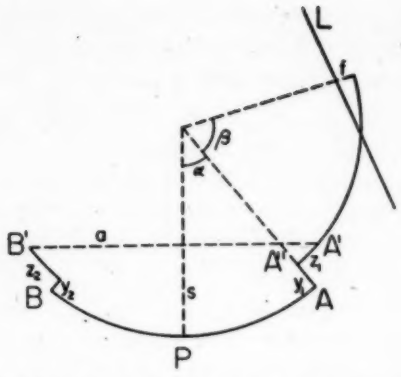

FIG. 3. Mass determination by the method of recoil electrons. BPA is a section of the circle which the particle would describe in the magnetic field alone. The actual path goes from B' *via* P to A'. Its continuation beyond A' is shown up to a point where the path is parallel to the straight line L which represents the path of the primary.

where

$$Y=\tfrac{1}{2}(y_1+y_2),\quad Z=\tfrac{1}{2}(z_1+z_2). \tag{54}$$

The cord $A'B'$ is

$$2a=2\rho_0\sin\alpha-2Y\sin\alpha+2Z\cos\alpha. \tag{55}$$

Using Eq. (51) we find for the radius, after some algebra

$$\rho=\rho_0-\frac{y_1+y_2}{2(1-\cos\alpha)}. \tag{56}$$

It will be noted that this result is independent of Z.

The error in the measured curvature is now

$$\Delta\left(\frac{1}{\rho}\right)=\frac{y_1+y_2}{2\rho_0^2(1-\cos\alpha)}, \tag{57}$$

whereas the simple formula (6) would give

$$\Delta\left(\frac{1}{\rho}\right)=\frac{y_1+y_2}{x^2}=\frac{y_1+y_2}{\rho_0^2\alpha^2}. \tag{58}$$

Equation (57) becomes identical with (58) in the limit of small α; in general the error given by the exact formula (57) is greater by a factor

$$F(\alpha)=\frac{\alpha^2}{2(1-\cos\alpha)}. \tag{59}$$

This result has been used in Eq. (17).

We shall now consider the error in the sagitta f between the continuation of the track $B'A'$ and a straight line L which makes an angle $\alpha+\beta$

with the cord $B'A'$. For this purpose we first calculate the direction of the track at A'. If we had no multiple scattering, we would have the circle BPA whose direction at A would be α (with respect to the tangent to the circle at P which is parallel to $B'A'$ by construction). Actually, because of multiple scattering, the direction of the actual track at A'' will be $\alpha+\theta_1$, where θ_1 is calculated from Eq. (1). Moreover, we have assumed that the length of the actual track is greater than that of the ideal circle by the amount z_1; this causes an additional deflection z_1/ρ_0. The actual direction of the track at A' is therefore $\alpha+\theta_1+(z_1/\rho_0)$. On the other hand, in the measurement it is assumed that $B'PA'$ is a circle. From the sagitta s and the cord $2a$ of this circle, one would conclude that the direction at A' is α' where

$$\tan\frac{\alpha'}{2}=\frac{s}{a}=\tan\frac{\alpha}{2}+\frac{Y}{\rho_0\sin\alpha}+\frac{Z}{\rho_0(1+\cos\alpha)}. \quad (60)$$

The actual curve deviates from the fitted circle in direction by the amount

$$\delta=\alpha+\theta_1+z_1/\rho_0-\alpha'$$
$$=\theta_1-\frac{y_2+y_1(1+2\cos\alpha)}{2\rho_0\sin\alpha}. \quad (61)$$

This expression is again independent of Z, Eq. (54).

We now proceed in two steps. First we consider a circle of the ideal radius ρ_0 which starts from A' in the actual direction of the path. Then the actual path will be displaced with respect to this "ideal circle" by a lateral displacement y_3 which can be calculated from Eqs. (1) and (3) with the track length $x=\rho_0\beta$. This displacement is statistically independent of the displacement between the "ideal circle" and the assumed circle which we shall now calculate.

The angle between these two circles is given by Eq. (61). The radius of the ideal circle is ρ_0, for the assumed circle ρ. A simple calculation shows that the distance between the two circles at an angle β from their common starting point A' is

$$\rho\delta\sin\beta+(\rho_0-\rho)(1-\cos\beta). \quad (62)$$

Inserting Eq. (56) for $\rho-\rho_0$ and (61) for δ, and adding y_3, we get for the change in the sagitta f (measured f minus true f)

$$\Delta f=\rho_0\theta_1\sin\beta$$
$$-y_1\left(\frac{1+2\cos\alpha}{2\sin\alpha}\sin\beta+\frac{1-\cos\beta}{2(1-\cos\alpha)}\right)$$
$$-y_2\left(\frac{\sin\beta}{2\sin\alpha}+\frac{1-\cos\beta}{2(1-\cos\alpha)}\right)+y_3. \quad (63)$$

In (63) the quantities y_1, y_2, and y_3 are statistically independent of each other but there is a correlation between y_1 and θ_1. According to a theory of Fermi (see reference 11, page 265), the correlation is given by

$$(y_1\theta_1)_{Av}=\tfrac{1}{2}x(\theta_1^2)_{Av}. \quad (64)$$

Using also Eq. (3), we can find the mean square error for the sagitta f.

The change of the sagitta and the change of the radius are correlated, cf. Eqs. (56), (63), (64).

For the actual evaluation we shall make the simplifying assumption that $\alpha=\beta=45°$. Then the factor (59) in the probable error for the radius is 1.053. The error in the sagitta becomes from (63)

$$\Delta f=\frac{4}{\pi\sqrt{2}}x\theta_1-\left(1+\frac{1}{\sqrt{2}}\right)y_1-y_2+y_3. \quad (65)$$

Evaluation gives

$$(\Delta f^2)_{Av}=2.735(y_1^2)_{Av}=0.520(\Delta\rho_1)^2_{Av}, \quad (66)$$

where $\Delta\rho_1$ is the error in radius calculated from Eq. (10). The correlation between ρ and f has the value

$$(\Delta f\Delta\rho)_{Av}=(\tfrac{3}{2}+\sqrt{2})(y_1^2)_{Av}-(\sqrt{2}+1)(y_1\rho_0\theta_1)_{Av}$$
$$+(1+1/\sqrt{2})(y_2^2)_{Av}=0.570(\Delta\rho_1)^2_{Av}. \quad (67)$$

Slow Neutron Resonances in Indium*

BOYCE D. MCDANIEL
Cornell University, Ithaca, New York

(Received September 21, 1946)

The neutron spectrometer previously described has been modified and improved to permit the use of 12 detector timing channels. It has been used to determine the neutron cross section for absorption in indium as a function of neutron energy in the range extending from 0.017 to 50 ev. Five absorber thicknesses were used in the measurements. These were 0.0227, 0.246, 0.907, 2.754, and 4.05 g/cm². The strong resonance previously observed was found to be located at 1.44 ev and two weaker resonances were found at about 3.7 and 9.0 ev. The resonance at 1.44 ev was carefully studied. An analysis was made to take into consideration the effective resolution and to determine the parameters of the Breit-Wigner one-level formula which best describe the resonance. The constants which provided the best fit with the data were $\sigma_0 = 26{,}400 \times 10^{-24}$ cm² and $\Gamma = 0.085$ ev. The resolution did not permit a similar analysis for the levels at higher energy and it was only possible to place rough lower limits for the values of the cross section at resonance.

THE strong resonance for neutron absorption in indium at about 1.4 ev has been examined by many different workers. It was first studied by boron absorption and self-absorption methods, while more recently the slow neutron velocity spectrometer, based upon the time of flight method, has been used in examining this resonance.[1-3]

A beta-activity, having a 54-minute period, is induced by the absorption of neutrons in In^{115}. This strong activity has permitted indium to be used extensively as a standard monitor of neutron intensity. Consequently an accurate knowledge of the variation of the cross section as a function of neutron energy is of considerable importance. In addition it is desirable to know if the Breit-Wigner one-level formula can be successfully used to describe the variation of the cross section in the region of the resonance.

At the time this work was begun, spectrometer apparatus and techniques had been developed to the extent that it was feasible to make measurements on indium with a resolution much better than any previously used. A study was made of the variation of the cross section over a wide range of neutron energy. In the region of the important resonance, sufficient accuracy and resolution were attained to permit the desired comparison of experimental results with the theory.

APPARATUS

The time of flight method and the equipment which was used have been described earlier.[1,2] The equipment has been modified to permit detection in 12 time of flight intervals; except for this it is essentially the same.

The available frequencies of arc modulation were 2500, 1000, 500, 200, 100 c.p.s. The available "on times" of modulation for both arc and detector ranged from 5 to 500 μsec. The standard of frequency was provided by a 100-kc crystal oscillator which was known to be accurate to at least 0.1 percent.

The detection system consisted of an ionization chamber filled with BF_3 gas, and a pulse amplifier employing cathode degeneration to provide gain stability. The "rise time" of the amplifier was about 2 μsec.

The beam collimation and shielding for the detector are shown in Fig. 1a. The collimation in front of the ionization chamber was in the form of a cylindrical shield of B_4C of density 1.0 g/cm². A similar shield was placed behind the chamber while immediately surrounding the chamber was a B_4C shield of about 0.5 g/cm. Except for 17.3 cm at the front end, the collimator was surrounded by at least 14 cm of paraffin. The absorber was placed at the front end of the collimator.

* This work was performed late in 1942 and was presented as a Ph.D. thesis in February, 1943 at Cornell University. It was withheld from publication as classifiable material for the duration of the war.

[1] R. F. Bacher, C. P. Baker, and B. D. McDaniel, Phys. Rev. 69, 443 (1946).

[2] C. P. Baker and R. F. Bacher, Phys. Rev. 59, 332 (1941).

[3] W. W. Havens, Jr. and James Rainwater, Phys. Rev. 70, 154 (1946).

For slowing down the neutrons, the Be target of the cyclotron was surrounded by a copper tank as illustrated in Fig. 1b. The tank was filled with water to its capacity of 11 liters. The face of the tank was in the direction of the detector. The arrangement of the equipment relative to the cyclotron room is shown in Fig. 1c.

PROCEDURE

In most respects the procedure for making the measurements of the transmission were similar to those used in experiments described in the references.[1,2]

The measurements which were made in the course of these experiments were taken with the detector at 2 meters and 3 meters from the source. In making the measurements on neutrons of energy 0.5 ev and greater, a thick layer of Cd was placed immediately in front of the detector to remove the slow, Cd absorbed neutrons from the beam to allow a higher repetition frequency to be used.

When measurements were made below 0.5 ev, they were taken with a source-detector distance of 2 meters. The source was then modified by adding 13.7 g/liter of borax ($Na_2B_4O_7 \cdot 10\ H_2O$) to the water in the tank. In addition, a 0.026 g/cm² B_4C filter was placed in the beam. In this manner the number of very low energy neutrons detected was reduced and the borax in the tank also reduced the mean life of thermal neutrons in the source. From previous measurements,[1] it was found that the mean life in the tank with this amount of boron, would be about 50 μsec. The resolution, as calculated from the assumed distribution of velocities,[4] was not greatly affected by the delayed emission from the source. Since the transmission of the absorber varied only slowly with the time of flight in this region, no correction was made for the effect of the mean life in the source on the resolution.

In performing the experiment it was necessary to consider the various sources of background and to make measurements for determining the magnitude of the corrections which should be applied. Two types of background exist. One of these is due to noise in the amplifier and pulses due to radioactive contamination. Since this background is proportional to the counting time, a correction is readily made. This correction, in individual channels, amounted in most cases to two percent or less of the incident beam intensity.

The other type of background is the fast neutron background which is proportional to the beam intensity and is due either to incomplete modulation of the cyclotron or to neutrons which have been scattered into the chamber without passing through the absorber, or else have passed through the absorber and have been delayed in arriving at the chamber and are recorded in the wrong time group.

This background was measured by interposing 2.0 g/cm² of B_4C and a 10-cm length of paraffin in the beam, with the boron closest to the detector, and observing the number of counts recorded in the timed channels as well as the total number of counts. From these measurements, the fraction of all counts which are due to this type of background may be computed. The background due to this cause was of the order of 3 percent.

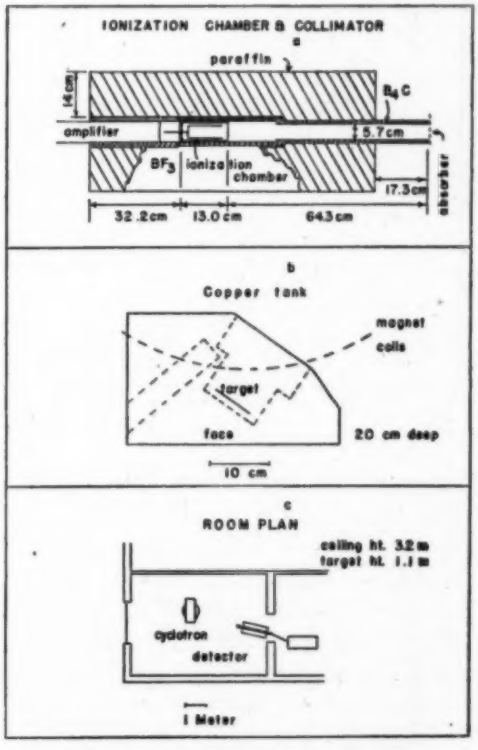

FIG. 1. Geometrical arrangements.

[4] C. P. Baker, B. D. McDaniel, and R. F. Bacher, "Velocity Distribution of Neutrons Emitted from a Slow Neutron Source," unpublished.

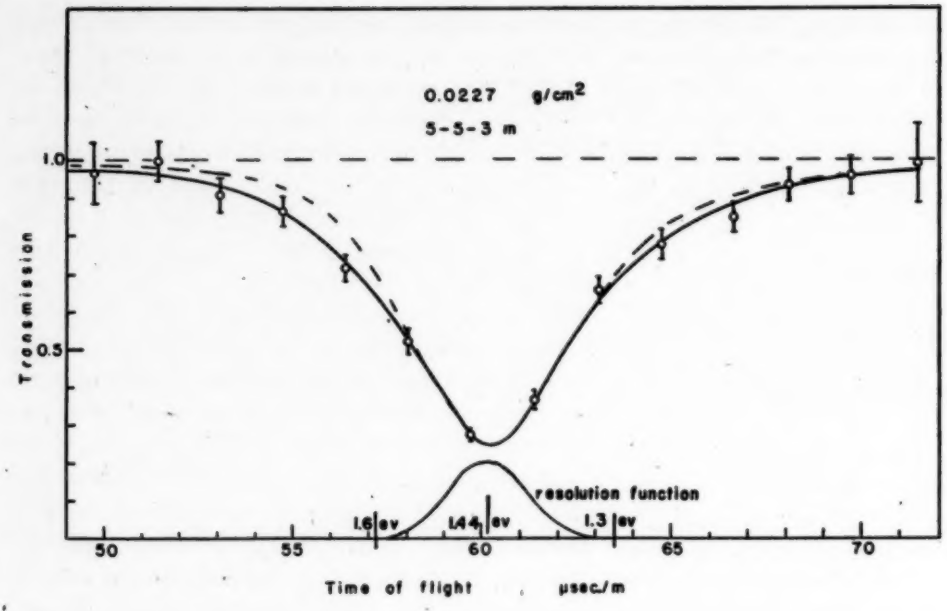

FIG. 2. Transmission of 0.0227 g/cm² of indium as a function of neutron time of flight.

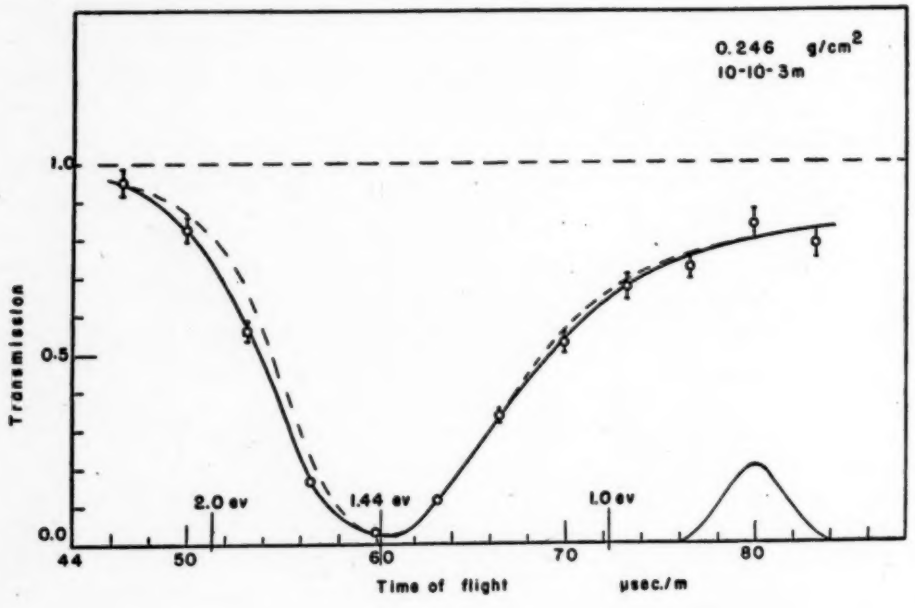

FIG. 3. Transmission of 0.246 g/cm² of indium as a function of neutron time of flight.

TABLE I. Experimental conditions.

Figure	On time μsec.	Distance meters	Rep. rate c.p.s.	Source	Filter g/cm²	Absorber thickness g/cm²	Time of flight μsec./m	Energy ev
2	5	3	2500	water only	0.45 Cd	0.0227	50–70	1.1 – 2.1
3	10	3	2500	water only	0.90 Cd	0.246	46–84	0.74 – 2.5
4	50	2	500	water and boron	0.026 B_4C	0.907	100–650	0.012– 0.52
4	20	2	500	water and boron	0.026 B_4C	0.907	50–175	0.17 – 2.1
5, 6	10	3	2500	water only	0.90 Cd	2.754	3.3–110	0.42 –480
5, 6	5	2	2500	water only	0.90 Cd	2.754	5–55	1.7 –210
7	10, 5	3	2500	water only	0.90 Cd	4.05	15–33	4.8 – 23

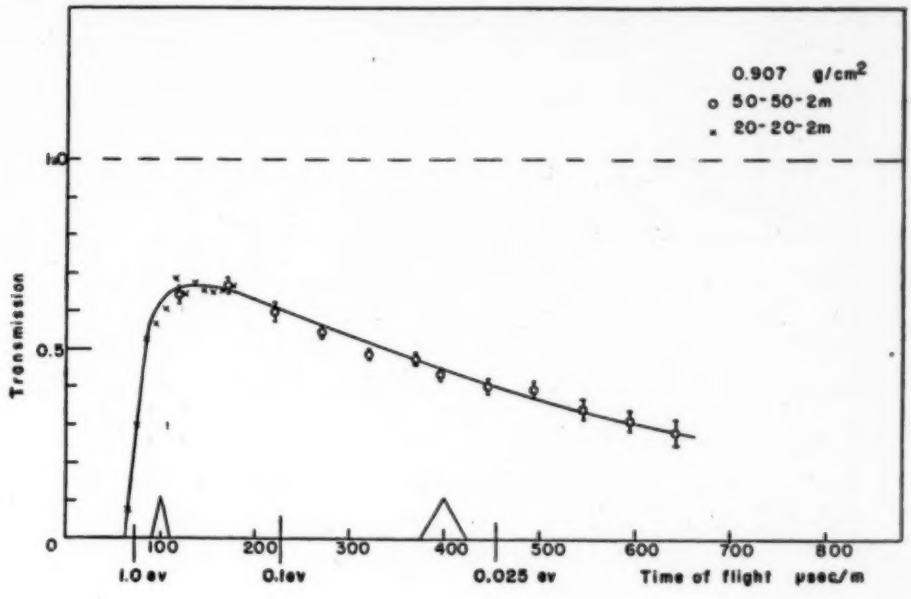

FIG. 4. Transmission of 0.907 g/cm² of indium as a function of neutron time of flight.

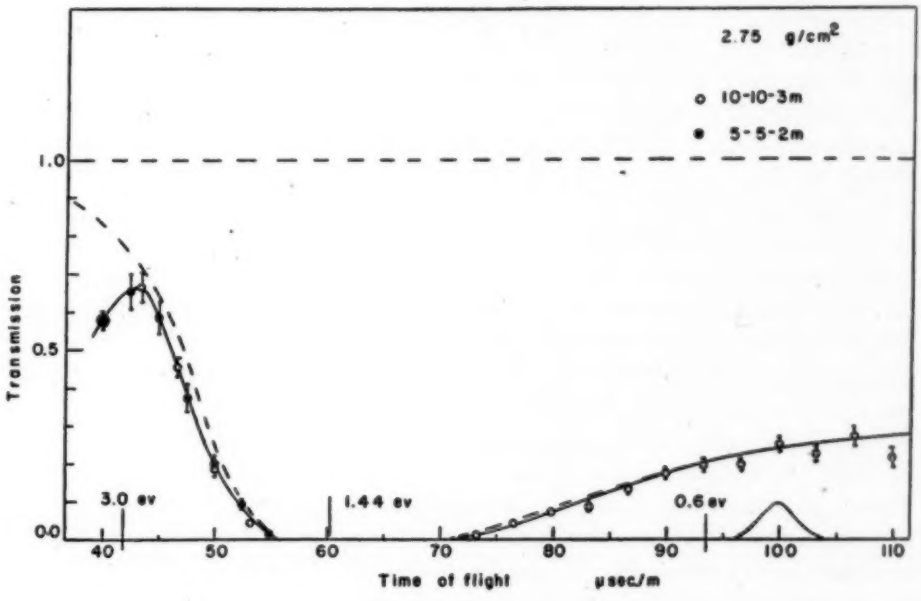

FIG. 5. Transmission of 2.75 g/cm² of indium as a function of neutron time of flight.

In the vicinity of the lowest and most important resonance, the background could also be measured by inserting an absorber of indium so thick that the transmission was known to be essentially zero over a long time of flight interval about the resonance. The number of counts recorded in the individual channels near exact resonance was found for a given number of total counts. Then by multiplying the ratio of these two numbers by the total transmission of the thick absorber, one finds the fraction of all neutrons in the incident beam which appear as background counts in the individual channels. The magnitude of the correction when measured in these two different ways agreed within the experimental error. However, it was felt that the latter method was best for determining the correction to be used in the vicinity of the resonance so that the value determined in this manner was used.

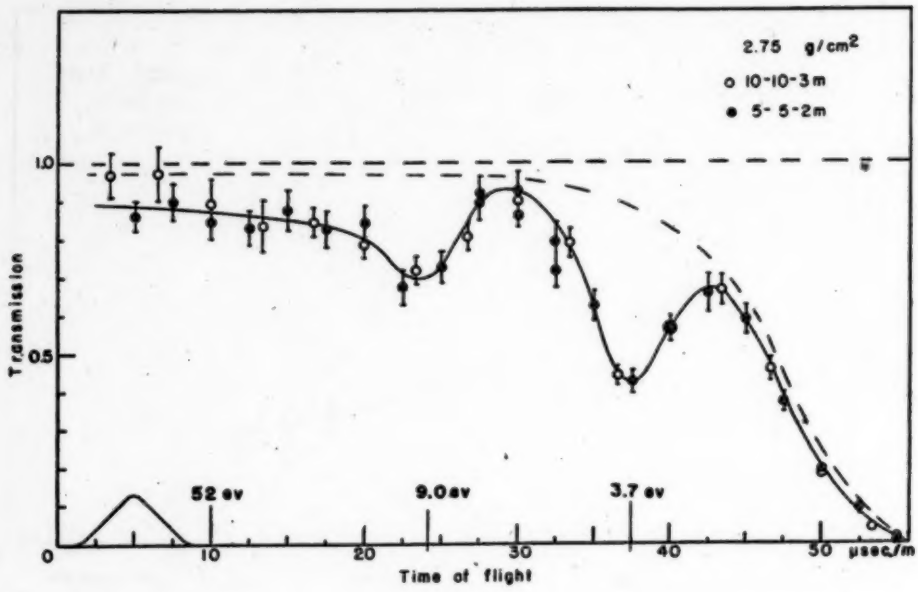

FIG. 6. Transmission of 2.75 g/cm² of indium as a function of neutron time of flight.

Several series of measurements of the time lag were made with different modulation schemes using a method similar to that described previously.[1] The values so determined were in good agreement with each other and gave an average of 10.5 μsec.

RESULTS

The transmissions of five indium absorbers were measured and the combined range of reliable measurements extended over a time of flight interval from 10 to 550 μsec./meter. This corresponds to an energy range from 0.017 to 50 ev. The main resonance was found at a time of flight of 60.2 μsec./meter (1.44 ev). A much weaker resonance was observed in the region of 37.5 μsec./meter (3.7 ev) and a still weaker one was detected at about 24 μsec./meter (9 ev).

The thicknesses of the absorbers were 0.0227, 0.246, 0.907, 2.754, and 4.05 g/cm². The uniformity of the various absorbers was measured. The thickest absorber was found to have a thickness constant to within one percent of the average thickness. The thinnest absorber, except for a few small pin holes in it, was uniform to within 10 percent of the average and calculations were made which indicated that for transmissions greater than 25 percent the error in transmission which would be made as a result would be less than one percent. The metal was analyzed and the analysis indicated that the total amount of impurity was less than 0.005 percent.

In Table I the experimental conditions are tabulated for the sets of measurements which were made. The results of these measurements are plotted in the Figs. 2, 3, 4, 5, and 6. The figure number corresponding to a given observation is given in the table. The results have been corrected for fast neutron background, noise, and chamber contamination. The solid lines have been drawn to fit the points. The statistical probable errors of the points are indicated by the lines extending above and below the points. The dotted curves, where they are shown are curves derived from theory and will be discussed later. The sequence of three numerals written above the graphs in the figures designate, respectively, the arc "on time," detector "on time" in microseconds, and distance of flight in meters The triangular shaped figures drawn along the horizontal axes are the resolution functions for the measurements given in the graphs. These functions are discussed in detail below.

In Figs. 2 and 3, the results taken with the two thinnest absorbers show the presence of the main resonance at 60.2 μsec./meter or 1.44 ev. Figure 4 shows the transmission of the 0.907 g/cm² sample in the energy region below the resonance extending through the thermal energy region.

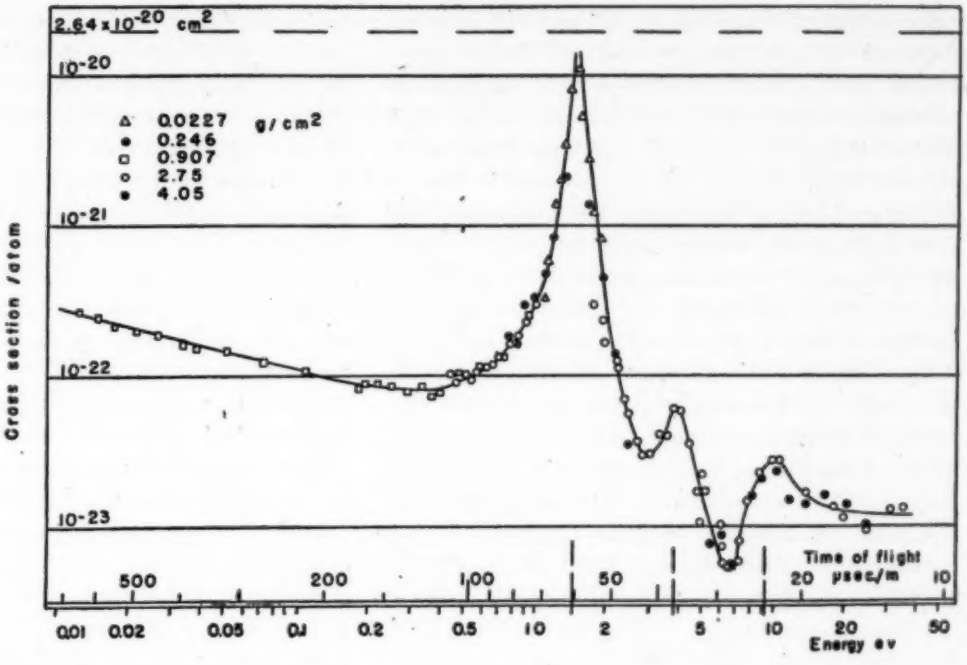

FIG. 7. Cross section of indium as a function of neutron energy. Logarithm of the cross section is plotted against the logarithm of the neutron energy. These data have not been corrected for the effect of finite resolution.

Figure 5 shows the results for the 2.75 g/cm² absorber in the vicinity of the main resonance while Fig. 6 is a plot presenting the results in the high energy region. In plotting the points for Fig. 5, the values for the corrected transmission in the region from 57 to 70 μsec./m time of flight were omitted since the points scattered on both sides of the axis because of statistical errors, and little significance could be placed upon these values.

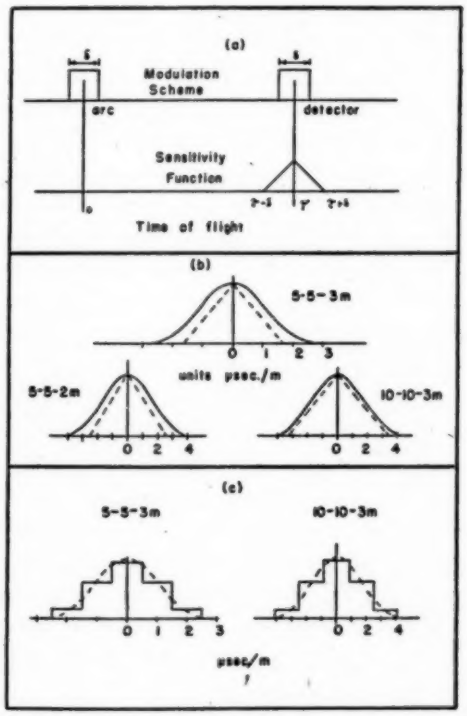

FIG. 8. Resolution functions: (a) ideal resolution, (b) experimental resolution, (c) step function approximation to the experimental resolution.

In Fig. 6, it is observed that in addition to the strong resonance at 1.44 ev there are two regions of strong absorption. These are at about 3.7 and 9 ev. While these resonances are much weaker and more poorly resolved, they are quite definite. Since there are only two known isotopes of indium, In^{113} and In^{115}, and since there are a total of three resonances, it is clear that at least two of these resonances occur in the same isotope. Even though the abundance of isotopes is about 21 to 1 for In^{115} and In^{113}, respectively, a definite isotopic assignment of the higher resonance is difficult. Since the lowest resonance is so much stronger than the others, and since thermal neutron bombardment strongly excites the 54 minute beta-period, it is reasonable to conclude that this resonance occurs in In^{115}.

To verify further the presence of the weak resonance near 9 ev, additional observations were made of the transmission of the 4.05 g/cm² absorber. The range of this set of measurements

only extended from 15 to 33 μsec./m time of flight so that the results were not plotted separately, but instead, the cross section values were calculated from the observed transmissions and plotted in Fig. 7 along with the cross sections calculated from each of the transmission measurements for the five absorbers. The horizontal axis is a logarithmic energy scale and the vertical axis a logarithmic cross-section scale. In addition, certain times of flight are marked along the horizontal axis to permit comparison.

In plotting this figure, no attempt was made to correct the cross sections for the effect of the finite resolving power of the apparatus. However, three of the points were omitted from the graph because the corrections which should have been made for resolution were obviously large, and as a result, the uncorrected values fell far off the curve.

DISCUSSION

It is first desired to obtain some idea of the probable effect which the resolution produced on the measurements. A rather complete discussion of the ideal case of equal "on time" for the arc and detector is given by Baker and Bacher.[2] For a given setting, the function which measures the sensitivity of one of the channels to neutrons of various times of flight is given in Fig. 8a. (τ) is the average time separation between the "on time" of the arc and the "on time" of the detector channel. (δ) is the length of the "on times." The sensitivity is zero for any neutron having a time of flight less than ($\tau-\delta$) or greater than ($\tau+\delta$). At these two times the sensitivity begins to rise linearly to a maximum at (τ).

However, several factors enter to distort this sensitivity function even at energies well above thermal energies. One is a straggling in the production of the slow neutrons. This straggling may arise in either the acceleration of the ions in the cyclotron or in the slowing down of the fast neutrons that are produced at the target. Probably neither of these effects is sufficiently large to be considered very seriously. The straggling in the acceleration of the ions in the cyclotron is less than a microsecond as was indicated by earlier measurements,[1] which were made with a fast neutron detector. In these earlier measurements the sensitive time of the detector was moved progressively over the "on time" of the arc. The shape of the resultant curve indicated no large straggling in the acceleration. As far as straggling is concerned in the slowing down of neutrons to the energy of 1 ev, it is not significant because the mean slowing down time is probably of the order of 1.5 μsec.

Another cause for distortion of the sensitivity function is improper settings of the timing equipment. Small errors in setting up the modulation system or drifts of the timing during observations would cause a distortion of the average sensitivity function. It is thought that the uncertainty in the modulation times from this source was limited to 0.5 μsec.

Probably the largest factor in distorting the ideal sensitivity function is the time required for the neutron to traverse the length of the ionization chamber. A neutron having an energy of 1.44 ev, the energy of the main indium resonance, has a time of flight through the effective length (11.0 cm) of the chamber of about 6.6 μsec. Since the neutron may produce a disintegration anywhere over the length of the chamber, this introduces an uncertainty in the distance traveled, or an equivalent uncertainty in the time of flight to associate with a given neutron. Although a similar uncertainty exists in determining the origin of the neutrons at the source, since the mean free path in the source is fairly short (1.0 cm) this effect is not important. In Fig. 8b is plotted the sensitivity function for 5 μsec. "on times" at both 2 and 3 meters as well as one for 10 μsec. at 3 meters. The functions have been corrected for the effect produced by the depth of the chamber and depth of the source. It is noted that the effective width of the sensitivity function is considerably increased for the case of 5 μsec. "on time" and is still significant for the 10 μsec. "on time." It is also seen that the function for 5 μsec. "on time" at 2 meters corresponds very closely to that of 10 μsec. "on time" at 3 meters, so that in treating the data taken with the 2.75 g/cm² absorber, the resolution was considered effectively the same for both sets of data.

As was pointed out by Baker and Bacher,[2] it is very difficult to proceed from the observed transmission curves to calculate the transmission

curves which would be expected if the resolution were infinitely sharp. Such a calculation is made especially difficult because of the statistical uncertainties associated with the observations. Because of this, it seemed more reasonable to determine from the experimental results the most probable values of the parameters of the Breit-Wigner one-level formula for neutron absorption when it is applied to the main resonance.

The Breit-Wigner one-level formula[5] is given by

$$\sigma(E)=\sigma_0\left(\frac{E_R}{E}\right)^{\frac{1}{2}}\frac{\Gamma^2}{\Gamma^2+4(E-E_R)^2},$$

$\sigma(E)$ = cross section for neutron of energy E,
σ_0 = cross section at exact resonance,
E_R = resonance nergy,
E = energy of incident neutron,
Γ = total width.

Because of the Doppler effect, the effective cross section will be given by the following expression

$$\sigma(E)=\frac{\sigma_0}{\pi^{\frac{1}{2}}\Delta}\int_0^\infty\left(\frac{E_R}{E'}\right)^{\frac{1}{2}}\frac{\exp\left[-(E-E'/\Delta)^2\right]}{1+(4/\Gamma^2)(E'-E_R)^2}dE',$$

Δ = Doppler width $=2(E_R E_{th} m/M)^{\frac{1}{2}}$,
m = neutron mass,
M = mass of target atom,
E_{th} = thermal energy.

The effective thermal energy was assumed to be $1.2\,kT$ rather than kT, to take into account the lattice binding. This is based on the calculations of Lamb.[6] With this value the Doppler width was found to be 0.039 ev.

The determination of the most probable value for the Breit-Wigner parameters is made in the following manner. The time of flight of neutrons at exact resonance was determined from the transmission curve for the 0.0227 g/cm² absorber. Reasonable estimates were made of the value for the constants σ_0 and Γ. By use of these values for the constants, and by making the correction for the Doppler effect, the corresponding effective cross section was calculated as a function of time of flight. From these, the transmissions were calculated for absorbers of the same thickness as those used in the experiments. It was next desired to see what transmissions one would expect to observe if absorbers having these calculated transmissions were to be measured by the apparatus. The resolution was assumed to be the same as that which was used in making the experimental determinations and step function approximations to the sensitivity curves were used to calculate the expected observed transmissions. The step functions are shown in Fig. 8c. The expected observed transmissions, hereafter described as "derived" transmission curves, were then compared with the experimental data. Successive choices of σ_0 and Γ were made to determine the set which yielded the best fit of the derived curves to the experimental curves. In determining the quality of the fit two regions were weighted heavily. One of these was at the maximum cross section and the other at the minimum in the cross section which occurs between exact resonance and zero energy (near 135 μsec./meter time of flight). The value of the scattering cross section was assumed to be 2×10^{-24} cm²/atom, and a correction was made.

The values which seemed to produce the best fit are given below. The probable errors listed were estimated and include consideration of statistical errors, lack of resolution, and other factors which are discussed below.

Resonance energy	1.44 ± 0.03 ev
Maximum cross section at resonance	$(26{,}400\pm6500)\times10^{-24}$ cm²/atom
Total width	0.085 ± 0.01 ev.

Because of the Doppler effect, the maximum cross section given by the Breit-Wigner formula is effectively lowered. For the parameters chosen, the effective maximum cross section was 32 percent less than the cross section uncorrected for the Doppler effect.

The derived curves may be directly compared to the experimentally determined curves. The comparison is made in the Figs. 2, 3, 5, and 6 which show the observed transmissions. The dotted lines are the derived curves. In Fig. 4 the curve which would be drawn to fit the points differed so slightly from the derived curve that only one curve was drawn and it was the derived curve.

[5] H. A. Bethe, Rev. Mod. Phys. 9, 116 (1937), Eq. (428).
[6] W. E. Lamb, Phys. Rev. 55, 190 (1939).

In general, the agreement between the experimental results and those predicted by theory is quite good. This is particularly true if one considers the great range in cross section and energy over which the measurements were made.

In Fig. 2, for the 0.0227 g/cm² absorber, it is seen that the experimental curve fits the derived curve moderately well except on the high energy side of the resonance. Though the probable errors are relatively large compared with the difference between the two curves it seems that there may be a real difference between these observed values and the expected values. The difference between the observed curve and the derived curve on the low energy side is not considered significant with the probable errors as shown.

To show the sensitivity of the shape of the transmission curve of this absorber to the value of the constants that were chosen, two other derived curves were calculated. One assumed a $\Gamma=0.094$, the other $\Gamma=0.075$ ev. In the region of greatest difference, the difference between the two curves was found to be about twice the probable error associated with the experimental points in the same region.

Both in Figs. 3 and 5, corresponding to 0.246 and 2.75 g/cm² absorbers, the observed curves and the derived curves fit well on the low energy side, but are in slight disagreement on the high energy side.

The agreement between the experimentally determined points and the derived curve for the 0.907 g/cm² absorber (Fig. 4) is excellent. This is to be expected for two reasons. One reason is that except at the very high energy, the transmission does not vary rapidly so that the effect of the resolution is not very pronounced. The other reason is that the point of maximum transmission was taken as one of the points at which the Breit-Wigner formula was adjusted to the experimental data. The points at still lower energy would be expected to agree well with the derived curve because the shape of the derived curve is not sensitive to the choice of the constants in this region, where the cross section dependence is proportional to the time of flight. The value of the total cross section at 0.025 ev is found to be 191×10^{-24} cm²/atom.

The differences between the experimental curves and the derived curves in the region just above the resonance may indicate that the one-level formula does not accurately describe the variation of the cross section. Because of the presence of higher levels, it would not be surprising if this were the case. However, it cannot be stated with any certainty that this is the explanation.

It is to be noted that a shift in the time axis of less than one microsecond per meter (3 microseconds at 3 meters) would greatly improve the agreement on the high energy side of the resonance, but this would be at the expense of the agreement on the low energy side. It does not seem that this could serve as a satisfactory explanation for the disagreement.

Because the resolution used was more likely to be poorer rather than better than the assumed resolution, it seems that if there is any large error in the values of Γ and σ_0, it is most probable that they should be smaller and larger, respectively.

The results of the self-absorption measurements of Hornbostel, Goldsmith, and Manley[7] give for the values of the constants:

$$E_R=1.0 \text{ ev},$$
$$\sigma_0=23{,}000\times10^{-24} \text{ cm}^2/\text{atom},$$
$$\Gamma=0.07 \text{ ev}.$$

In this early measurement the value of 1.0 ev for the resonance energy was determined by the boron method assuming a value of 0.025 ev for the average energy of neutrons emitted from a slow neutron paraffin source. The average energy from such a source is now known to be considerably higher.[1] Since their result for the values for σ_0 and Γ are dependent on the assumed resonance energy, correction of the calculation by using the correct resonance energy might give better agreement on the width and maximum cross section. The value of $E_R=1.44$ ev reported by Havens and Rainwater[3] is in agreement with that found here.

Relatively little may be learned from the measurements of the two weaker resonances because of insufficient information. The existence of both resonances seems to be established without doubt. It is not surprising that these reso-

[7] J. Hornbostel, H. H. Goldsmith, and J. H. Manley, Phys. Rev. **58**, 18 (1940).

nances were not observed earlier, since comparable resolution has not previously been used. Even the resolution used here is not sufficient to make it possible to determine the strengths of the resonances. However, minimum values may be ascribed to the cross section at resonance by taking into account the resolution. These values are about 220×10^{-24} and 67×10^{-24} cm²/atom for the 3.7 and 9 ev levels, respectively.

ACKNOWLEDGMENT

The author wishes to express his gratitude to Professor R. F. Bacher for his encouragement and guidance of the work, to Dr. C. P. Baker for much valuable assistance, and to Professor H. A. Bethe for his many helpful suggestions.

The indium metal used in these experiments was very kindly loaned by the Indium Corporation of America.

PHYSICAL REVIEW VOLUME 70, NUMBERS 11 AND 12 DECEMBER 1 AND 15, 1946

The Density Spectrum of the Extensive Cosmic-Ray Showers of the Air

G. Cocconi, A. Loverdo, and V. Tongiorgi
Institute of Physics, University of Milan, Milan, Italy

(Received May 4, 1945)

The paper describes measurements performed at 2200 meters above sea level for the purpose of studying the density of particles in the extensive air showers. From the results obtained, one finds that the dependence of the number of showers on the density can be expressed over a wide range by an exponential low.

1

THE so-called "extensive air showers" are produced by cosmic-ray particles which arrive at the top of the atmosphere with very high energies (10^{13}–10^{16} ev) and give rise to a large number of electrons and photons through a process of multiplication extending to the bottom of the atmosphere. The large number of particles observed indicates a large subdivision of the primary energy, while the length of the path between two successive elementary processes produces a considerable spread of the shower particles.

The problem of the spread of air shower has been fully investigated by Auger and co-workers with experiments carried out at different heights above sea level. These experiments led to the establishment of the well-known "decoherence curve" which relates the number of showers with their extension.[1]

The same experimenters,[2] as well as others, have also investigated the dependence of the number of air showers on their density, i.e., on the number of particles per m². The results, however, are uncertain and contradictory. Therefore new experiments were undertaken in order to contribute to the solution of this problem.

2

The experimental determination of the particle density in an air shower detected with a set of G-M counters is based upon a classical probability formula which was first applied to this specific problem by Auger, and was later used by other authors. This formula reduces the computation of the density to the determination of the relative number of coincidences, C_n and C_{n-1}, recorded in equal times with n and $n-1$ counter, respectively. The counters are arranged in a horizontal plane, over an area small compared with the spread of the shower.

Let $p(S, \Delta)$ be the probability that a counter of area S is *not* struck by a shower of average density Δ. If the area is increased by dS, this probability becomes

$$p(S+dS, \Delta)=p(S, \Delta)(1-\Delta\cdot dS),$$

[1] P. Auger, R. Maze, P. Ehrenfest, and A. Freon, J. de phys. et rad. **10**, 39 (1939).
[2] H. Geiger, Abhandl. Preuss. Akad. Wiss. **10** (1941). J. Daudin, University of Paris, Thesis, 1942. J. Clay, Physica **9**, 897 (1942).

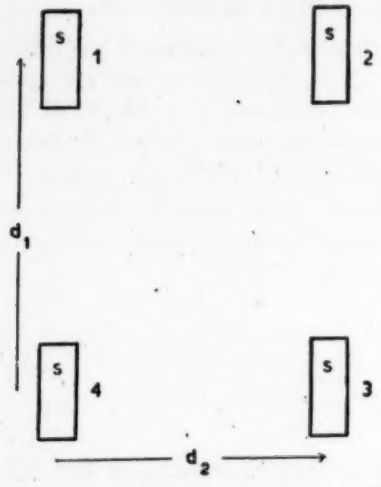

FIG. 1. Counter arrangement in the first series of measurements.

from which it follows:

$$p=e^{-S\Delta}.$$

Therefore, the probability for a counter to be struck is

$$P=1-p=1-e^{S\Delta},$$

and the probability per n counter, all with the same area S, to be struck is

$$P^n=(1-e^{-S\Delta})^n.$$

The ratio C_n/C_{n-1} of n-fold to $(n-1)$-fold coincidences is given by

$$C_n/C_{n-1}=(1-e^{-S\Delta})$$

from which it follows

$$\Delta=\frac{1}{S}\log\frac{1}{1-C_n/C_{n-1}}. \qquad (1)$$

3

All the experiments described in the present paper were performed in the periods July–October, 1942 and July–October, 1943 at Passo Sella (Bolzano), in a wide porch under a roof having a thickness 4 g/cm². The altitude was 2200 m above sea level and the average pressure 7.95 m H_2O.

The experiments consisted in recording threefold and fourfold coincidences between counters (or groups of counters in parallel) having different areas.

The first series of experiments (1942) was carried out with counters arranged as in Fig. 1; fourfold (1+2+3+4) and threefold (1+2+3) coincidences were recorded separately. Measurements were taken with counting units formed by one, two, or four individual counters, each of 30×4.3 cm$^2=0.0129$ m^2 sensitive area, so that the area of the unit was 0.0129, 0.0258, 0.0516 m², respectively. Different distances d_1 and d_2 between the counting units were used. Also a set of measurements was taken with $d_1=d_2=2$ m, using four counters of 10×2.4 cm$^2=0.0024$ m². The results are shown in columns 3 and 4 of Table I.

The second series of experiments (1943) was carried out with the counter arrangement shown in Fig. 2, by counting fourfold (1+2+3+4) and threefold (1+2+3) coincidences *simultaneously*, so as to minimize the statistical errors. The surface of each counting unit was varied between 0.0011 and 0.1032 m² by variously combining counters of three different sizes (4.5×2.4 cm², 11×2.4 cm², 30×4.3 cm²). The results are shown in Table II.

All the counters used had brass walls from 0.5 to 1 mm thick and were filled with a mixture of argon and alcohol. The threshold was approximately 1300 volts. During operation they were kept at a temperature of about 15°C by thermostatic control. The high voltage (1450–1500 volts) was supplied by an Evans model stabilizer. The recording was done with a conventional Rossi's coincidence circuit, having a resolving time $\tau=4\div5\times10^{-7}$ minutes. Chance coinci-

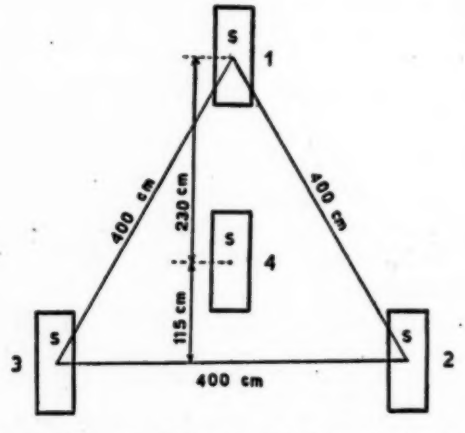

FIG. 2. Counter arrangement in the second series of measurements.

TABLE I. Distribution of shower density with counters arranged as in Fig. 1.

1 $d_1 \times d_2$	2 Area of the counter S (m^2)	3 Fourfold coincidence ($min.^{-1}$)	4 Threefold coincidence ($min.^{-1}$)	5 Density Δ (m^{-2})
	0.0024	204/34,565 =0.0059±0.0004	178/16,200 =0.0110±0.0008	325±85
	0.0129	386/4,799 =0.080±0.004	177/1,569 =0.113±0.008	96±36
2×2 m^2	0.0258	1,370/7,206 =0.190±0.005	590/1,887 =0.313±0.013	37± 8
	0.0516	1,074/2,065 =0.52±0.016	714/993 =0.726±0.027	24± 5
	0.0129	492/6,937 =0.071±0.003	294/2,560 =0.114±0.007	75±25
4×4 m^2	0.0258	462/2,875 =0.160±0.008	317/1,158 =0.270±0.016	35±10
	0.0516	1,005/2,132 =0.470±0.015	432/593 =0.730±0.035	20± 5
	0.0129	1,080/16,106 =0.067±0.002	729/6,919 =0.105±0.004	79±15
4×8 m^2	0.0258	1,243/6,647 =0.187±0.005	929/3,412 =0.273±0.009	45± 8
	0.0516	1,072/2,673 =0.402±0.013	1,239/1,743 =0.710±0.020	16± 3

dences were negligible in all measurements with fourfold coincidences and in most of the measurements with threefold coincidences. In the most unfavorable conditions (threefold coincidences with 8 counters in each unit, having a background of 3000÷3500 counts per minute) the number of chance coincidences was less than 2 percent of the number of true coincidences. The numbers given in the three last rows, column 4, of Table II have been corrected for chance coincidences.

The measurements were carried out uninterruptedly day and night. The operation of the counters and of the circuits was checked daily with a cathode-ray oscilloscope. Absence of electric pick-up was checked by verifying that no fourfold coincidences were recorded when the counter voltage was kept 50 to 100 volts below threshold. The errors due to the roof of the porch as well as the determination of the sensitive areas of the counters will be discussed below.

The first series of experiments was performed by A. Loverdo and V. Tongiorgi; the second by A. Loverdo.

4

By applying formula (1) to the results obtained, we have calculated the average densities of shower particles listed in Tables I and II. Examination of Table I shows that Δ varies considerably when the counting area S changes, while it is approximately independent of d_1 and d_2. The latter result indicates that shower particles are uniformly distributed over all areas investigated. Therefore in the second series of experiments the distances between the four groups of counters were kept unchanged. Moreover, the more symmetrical "triangular" arrangement was used.

The variation of Δ with S shown by Table I is confirmed beyond any doubt by the results contained in Table II, where Δ is seen to vary by a factor of about 100 when S is changed from 0.0011 to 0.1032 m^2.

The dependence of Δ on S can be explained in the following way. The showers striking the counters have different densities. This is so (a) because the number of particles in a shower depends on the energy of the primary particle by which the shower is produced and (b) because our counter array, whose dimensions are small compared with the dimension of the shower, may find itself either near the center of the

TABLE II. Distribution of shower density with counters arranged as in Fig. 2.

1 Area of counters S (m^2)	2 Minutes	3 Threefold coincidence (total)	4 Threefold coincidence ($min.^{-1}$)	5 Fourfold coincidence (total)	6 Fourfold coincidence ($min.^{-1}$)	7 Density Δ (m^{-2})
0.0011	77,070	179	0.0023±0.0002	112	0.00145±0.00014	890±145
0.0027	69,153	818	0.0118±0.0004	511	0.0074±0.0004	370±28
0.0054	37,006	1,167	0.0316±0.0010	732	0.0198±0.0008	183±12
0.0108	17,905	1,474	0.0824±0.0022	956	0.0534±0.0017	97±5.5
0.0129	18,825	2,380	0.126±0.003	1,515	0.0806±0.0021	79.2±3.5
0.0258	13,030	3,885	0.299±0.005	2,517	0.193±0.004	40.4±1.4
0.0516	10,063	7,671	0.76±0.01	5,087	0.507±0.007	21.7±0.6
0.0774	6,688	7,910	1.165±0.013	5,330	0.796±0.011	14.9±0.4
0.1032	3,545	6,466	1.79±0.023	4,529	1.28±0.02	12.2±0.4

shower, where the density is larger or near the edge, where the density is smaller.

With S constant, the probability of 3 (or 4) counters being struck by a shower varies considerably with Δ. In a rough approximation, we may assume that all showers with Δ larger than a certain value Δ_1 are recorded, while none of the showers with $\Delta<\Delta_1$ are recorded. Now Δ_1 changes with S and more precisely increases when S decreases. Hence, the average density of the showers recorded must vary when the counter area S is changed.

5

We shall now make our considerations more quantitative.

As explained in Section 1, the probability of a coincidence between n counters each of area S when a shower of density Δ falls upon them is given by

$$P^n=(1-e^{-S\Delta})^n=\varphi(S\Delta). \tag{2}$$

Let us now assume an exponential distribution for the density Δ; i.e., let us assume that the probability of a shower of density $(\Delta, d\Delta)$ striking the counters is given by:

$$\nu(\Delta)d\Delta=K\Delta^{-\gamma}d\Delta. \tag{3}$$

Then the probability for an n-fold coincidence is

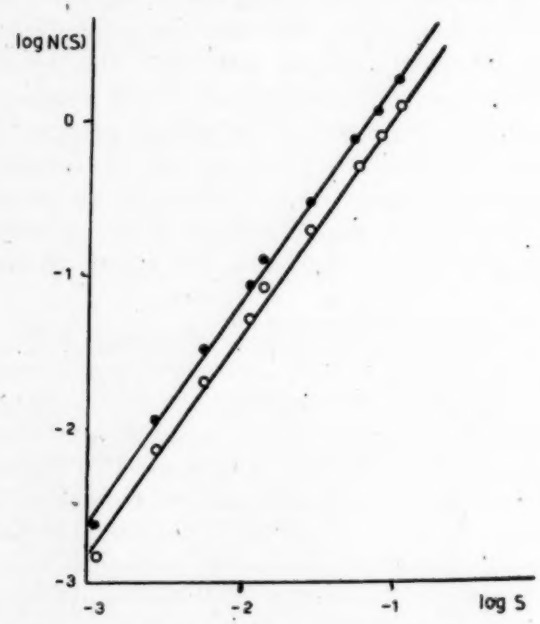

FIG. 3. Threefold and fourfold coincidences as a function of the counter area.

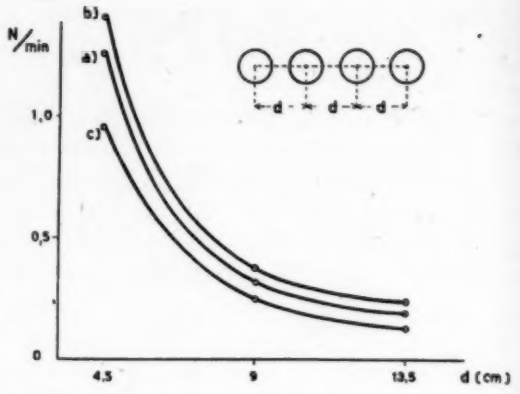

FIG. 4. Fourfold coincidences between counters: (a) immediately under the roof; (b) 2 meters from the roof; (c) in the open air.

represented by

$$N(S)=K\int_0^\infty \Delta^{-\gamma}\varphi(S\Delta)d\Delta \tag{4}$$

or, if we put $S\cdot\Delta=x$

$$N(S)=KS^{\gamma-1}\int_0^\infty x^{-\gamma}\varphi(x)dx. \tag{5}$$

Considering now two different values of S, we have:

$$N(S_1)/N(S_2)=(S_1/S_2)^{\gamma-1}. \tag{6}$$

All the quantities on the right side of Eq. (6) can be measured experimentally; hence γ can be determined.

In Fig. 3 the numbers N of threefold and fourfold coincidences listed in Table II are represented, on a double logarithmic plot, as a function of the corresponding area S. Within the statistical errors the experimental points lie on two straight lines with the same slope, thus confirming the dependence of N on S expressed by Eq. (6). From the value of this slope one obtains

$$\gamma=2.45.$$

The value of K can also be determined from the experimental results, using Eqs. (2) and (5). One obtains

$$K\approx 80.$$

Hence Eq. (3) can now be written as follows:

$$\nu(\Delta)=80\Delta^{-2.45}, \tag{3'}$$

where Δ is measured in m^{-2}.

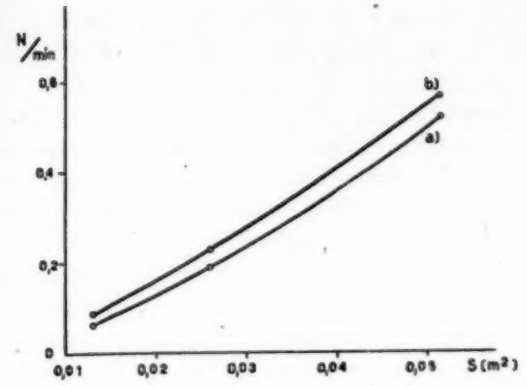

FIG. 5. Fourfold coincidences as a function of counter area. (a) Immediately under the roof; (b) 2 meters from roof.

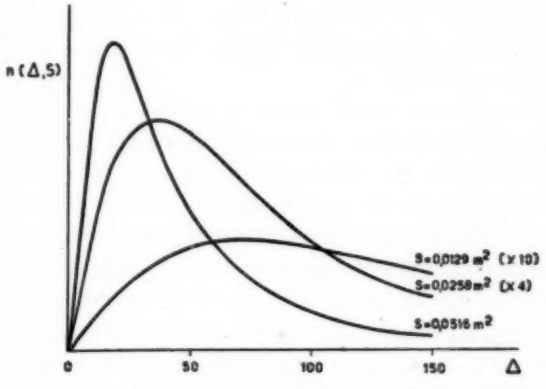

FIG. 6. Number of showers recorded with various fourfold coincidence arrangements as a function of shower density.

6

As already pointed out, our measurements were carried out under a light roof. It had been shown by Cosyns[3] that the effect of a roof on the multiplication process cannot be neglected, and experiments were performed to check this result. Coincidences were recorded between four counters in a horizontal plane placed (a) immediately under the roof, (b) 2 meters below the roof, and (c) in the open air. Measurements were taken with 4.3, 9, 13.5 cm between the axes of the counters, and the results are shown in Fig. 4. The three curves are similar, but definitely distinguishable from one another.

In order to study the effect of the roof with a counter arrangement similar to that used in the actual experiments, coincidences were recorded between four counting units placed at the four

[3] M. Cosyns, Nature **145**, 668 (1940).

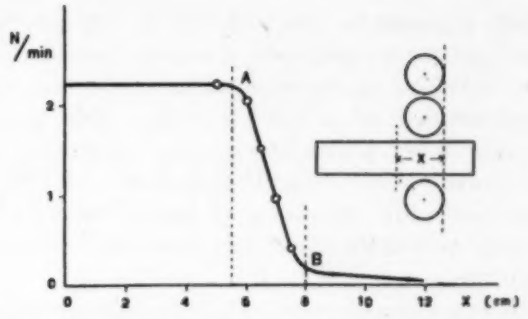

FIG. 7. Fourfold coincidence arrangement for the measurement of the sentitive area of a 2.4×11 cm² counter.

corners of a square of 2-m sides, first with the counters immediately under the roof, second with the counters 2 meters below the roof. For each position, one, two, and four counters, respectively, were used in each counting unit. The results are shown in Fig. 5.

In our experiments on the air showers,[4] the counters were placed immediately under the roof, in order to minimize the coherence effect produced by the roof. Just the same, as shown by Fig. 4, the effect of the roof is not negligible. This effect may be described as producing an increase of the effective area of the counters, increase which is relatively more pronounced for the smaller counters. As a consequence, the showers of greater density appear to be more abundant when the measurements are carried out under the roof than when they are carried out in the open air. Therefore, the value of γ as determined above is somewhat too large; we believe that its most likely value is:

$$\gamma = 2.6.$$

7

It is interesting to investigate the behavior of the function

$$n(S, \Delta)d\Delta = \Delta^{-2.6}(1-e^{-S\Delta})d\Delta,$$

which represents the probability of recording a shower with density between Δ and $\Delta+d\Delta$ with a given experimental arrangement. The curves in Fig. 6 give n as a function of Δ for $n=4$ and three different values for S, namely, 0.0129, 0.0258, 0.0516 m². Each of these curves exhibits a pronounced maximum for a value of the density

[4] G. Cocconi and V. Tongiorgi, Ricerca Scient. **10**, 566 (1939).

which depends on the value of S. This means that any given experimental arrangement favors the recording of showers with density in the neighborhood of a certain value. This is so because showers with low density are numerous but have a very small probability of being recorded, while showers with high density have a large probability of being recorded, but are very rare.

In other words, every experimental arrangement operates like a monochromator, selecting a given band of the density spectrum of air showers. Thus our results are explained and the disagreement between the conclusions of different authors becomes clearly understandable.*

8

In the evaluation of our experiments it is important to know the sensitive area of the counters exactly. As effective width, we have used the diameter of the brass tube. However, we have not deemed safe to take the effective length as equal to that of the wire because of possible end effects due to modifications of the electric field near the supports of the wire.

Therefore, the effective length was determined experimentally by placing the counter in question between three other counters of 2.4 $\times$11 cm^2, forming a vertical counter telescope (see Fig. 7). The axis of the counter to be examined was perpendicular to the axes of the other counters, and the number of fourfold coincidences was measured for different positions of the counter investigated. The results obtained with a counter of 2.4$\times$11 cm^2 are represented in Fig. 7. Similar curves were obtained with the other types of counters used. The effective lengths of the counters were taken as equal to twice the value of x corresponding to the point A in the diagram.

It may be noted that in all our experiments the distance AB over which the counting rate drops from its full value to practically zero is nearly equal to the diameter (2.4 cm) of the counters forming the vertical telescope. This means that the efficiency of the counter drops very abruptly from one to zero as one moves along the axis. No region of appreciable width seems to exist where the efficiency has an intermediate value.

* By the same token, the results obtained by Auger and collaborators [P. Auger, Robley, and Culvinage, Comptes rendus **209**, 536 (1939)] comparing the average density of air showers at two different altitudes are valueless because the measurements were performed with counters of different areas. The differences found are probably due to the different nature of the experimental arrangement used at the two elevations.

PHYSICAL REVIEW VOLUME 70, NUMBERS 11 AND 12 DECEMBER 1 AND 15, 1946

Experimental and Theoretical Evaluation of the Density Spectrum of Extensive Cosmic-Ray Showers

G. COCCONI, A. LOVERDO, AND V. TONGIORGI
Institute of Physics, University of Milan, Milan, Italy

(Received January 31, 1946)

Measurements are made of the density spectrum of extensive cosmic-ray showers at an altitude of 120 m above sea level. The results together with the measurements previously made at 2200 m confirm the electronic nature of the primary radiation which produces the extensive showers. It is estimated that the denser showers are generated by electrons of 10^{15} to 10^{16} ev, the less dense showers by electrons of energies 10^{13} ev.

IN a previous note[1] we gave the results on the density spectrum of extensive cosmic-ray showers at 2200 m above sea level (Passo Sella, atmospheric pressure 760 g/cm^2). We present here first the results of similar measurements carried out by two of us (A.L. and V.T.) at 120 m above sea level (Milan, 1000 g/cm^2). We then discuss the results obtained at the two stations in the light of the theory of cascade multiplication (G.C.).

[1] G. Cocconi. A. Loverdo, and V. Tongiorgi, Nuovo Cimento **2**, 14 (1944).

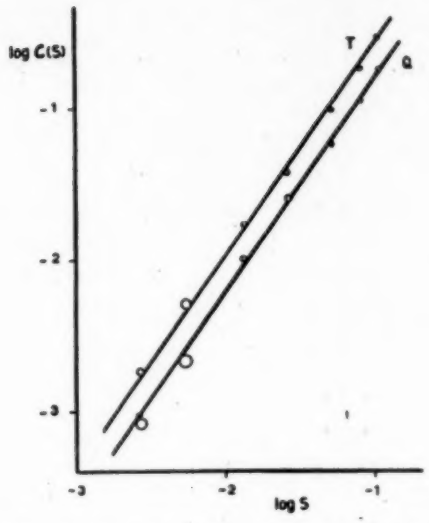

FIG. 1. Logarithms of triple and quadruple coincidences frequencies as function of counters' surfaces.

(1) The method of measurements at Milan was the same as that at the mountain station. The geometrical disposition, the details of counters, the apparatus used for coincidence counting are the same as previously described. The experiments continued without interruption from February to November 1944. They were carried out in the garden of the Physical Institute inside wooden huts with wall thickness not more than 1 g/cm² and kept at constant temperature. The experimental results are shown in Table I.

Shower densities are calculated as usual from the formula:

$$\Delta=\frac{1}{S}\log\frac{C_{III}}{C_{III}-C_{IV}},$$

where C_{III} and C_{IV} are the frequencies of triple and quadruple coincidences among counters (or groups of paralleling counters) whose surface is S.

In Fig. 1 is plotted the logarithm of the frequencies of triple and quadruple coincidences against the logarithm of the surfaces of the counters. As will be seen, the resultant curves are two parallel straight lines showing that even at 120 m above sea level the density spectrum of large showers is given by:

$$\nu(\Delta)d\Delta=K\Delta^{-\gamma}d\Delta.$$

As has been shown,[1] the value of γ may be calculated from the formula

$$\gamma=1+\log\frac{C(S_1)}{C(S_2)}\Big/\log\frac{S_1}{S_2},$$

and the value of K from

$$K=\frac{C_{IV}(S)}{S^{\gamma-1}}\Big/\int_0^\infty x^{-\gamma}(1-e^{-x})^4dx.$$

Since the slope of the straight lines in Fig. 1 is 1.46, it follows that $\gamma=2.46$. The value of $\int_0^\infty x^{-\gamma}(1-e^{-x})^4dx$ estimated by Simpson's method is 0.448 and therefore $K=10.85$.

From the differential spectrum it is immediately possible to deduce the integral spectrum, that is to say, the frequency of showers with density $\geqslant\Delta$:

$$H(\Delta)=0.124\left(\frac{10^{-4}\text{ cm}^{-2}}{\Delta}\right)^{1.46}\text{sec.}^{-1}. \quad (1)$$

At 2200 m above sea level the value obtained for this quantity was

$$H(\Delta)=0.92\left(\frac{10^{-4}\text{ cm}^{-2}}{\Delta}\right)^{1.46}\text{sec.}^{-1}.$$

However, the measurements at Passo Sella were carried out under a veranda whose roof had a thickness of about 4 g/cm². An estimate of the corrections to be made would increase the value of the exponent to about 1.55 and the value of the coefficient to about 1.0, hence, eliminating wall effects, we take as the value at 2200 m

$$H(\Delta)=1.0\left(\frac{10^{-4}\text{ cm}^{-2}}{\Delta}\right)^{1.55}\text{sec.}^{-1}. \quad (2)$$

(2) If it be assumed that extensive showers are caused by cascade multiplicative processes of very energetic electrons, it is possible to calculate

TABLE I. Shower density measurements.

Surface in m²	Minutes	Triple coinc. min.⁻¹	Quadruple coinc. min.⁻¹	Density Δ m⁻²
0.0027	213,262	0.00183	0.00082	220±46
0.0054	47,404	0.00517	0.00211	97±29
0.0129	110,661	0.0168	0.0102	73±4.6
0.0258	32,988	0.037	0.025	43.5±2.8
0.0516	29,193	0.0953	0.056	17.2±0.92
0.0774	23,328	0.179	0.110	12.3±0.54
0.1032	18,367	0.293	0.176	8.85±0.33

theoretically the spectrum of shower density at a fixed altitude. Moliére[2] has already shown that the cascade theory can account for Auger's results for the frequency variation of showers with the distance between counters. (Auger's measurements were made with counter distant 300 meters.) Following Moliére, it has been assumed that all extensive showers reach, in the lower atmosphere, a state of geometrically stationary development. Therefore, they are equal in transverse dimensions but differ from each other not in extension but only in density and, of course, in the total number of particles which are formed. This number depends upon the energy E of the primary electron and upon the distance l from the top of the atmosphere to the place of observation

$$N(E, l). \tag{3}$$

This number may be calculated from the formula of Heisenberg[3]

$$N(E, l) = (1.5s+0.5)\frac{1}{s(l)^{\frac{1}{2}}} \times \exp\left[-1+2(1-\alpha)^{\frac{1}{2}}(y-\beta)^{\frac{1}{2}}\right], \tag{4}$$

where l is measured in units of a characteristic length 33,000 cm of normal air or 42.6 g/cm² and $s=[(l-\alpha)/(y-\beta)]^{\frac{1}{2}}$; $y=\log E/E_j$; $E_j=1.13\times10^{8}$ ev; $\alpha=1.4$; $\beta=0.56$.

The distribution of the N particles in the shower which was used in our calculation is the one given in Fig. 1b of Moliére's note here reproduced as Fig. 2. In this figure the probability P that an electron of an extensive shower is at a distance from the shower's axis* between r and $r+dr$ (r is expressed in appropriate units r_1; in air under normal conditions $r_1=5950$ cm).

The probability density $W(r)$ that a particle of the shower fall on one cm² at distance r from the shower axis is

$$W(r)=P/2\pi r dr \text{ cm}^{-2}.$$

Therefore, the density δ of the particles as a function of the distance r from the shower axis is

$$\delta(r, N)=W(r)N \text{ cm}^{-2}.$$

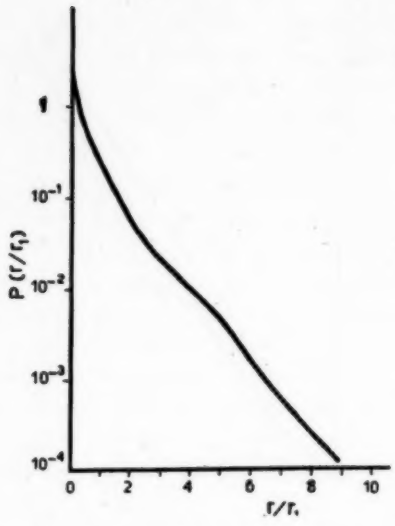

FIG. 2. Moliere's probability that an electron of an extensive shower be placed at a distance from the shower's axis included between r and $r+dr$.

If R is the value of r such that for $r\leqslant R$, $\delta\leqslant\Delta$, the surface S covered by the shower with $\delta\geqslant\Delta$ is $S=\pi R^2=S(N, \Delta)$.

From Eq. (3) this can be written

$$S=\Sigma(E, l, \Delta).$$

If the thickness l and the density Δ be fixed the area of the surface covered with density $\geqslant\Delta$ by a shower generated by a primary electron of energy E can be calculated. Let $\nu(E)dEd\omega$ cm^{-2} sec.$^{-1}$ be the number of primary electrons which in unit time are incident on unit surface at the top of the atmosphere with energy between E and $E+dE$ and in a direction included in the solid angle $d\omega$ (isotropy of the primary radiation is assumed). This number can be calculated from the integral spectrum given by Heisenberg[3]

$$H(E)=0.05(10^{10} \text{ ev}/E)^{1.8} \text{ cm}^{-2} \text{ sec.}^{-1},$$

which refers to primary electrons striking the top of the atmosphere with energy $\geqslant E$ and coming from all semi space.

We have

$$\nu(E)dEd\omega=(1/2\pi)9\times10^{-12}\times(10^{10} \text{ ev}/E)^{2.8}dEd\omega \text{ cm}^{-2} \text{ sec.}^{-1}.$$

It is sufficient to note the frequency with which a recording apparatus placed beneath a thickness l

[2] G. Moliére, *Vorträge über Kosmische Strahlung* (Berlin, 1943), p. 24.
[3] W. Heisenberg, *Vorträge über Kosmische Strahlung*, (Berlin, 1943), p. 10.
* The "shower axis" is defined as the direction of the primary electron of the shower.

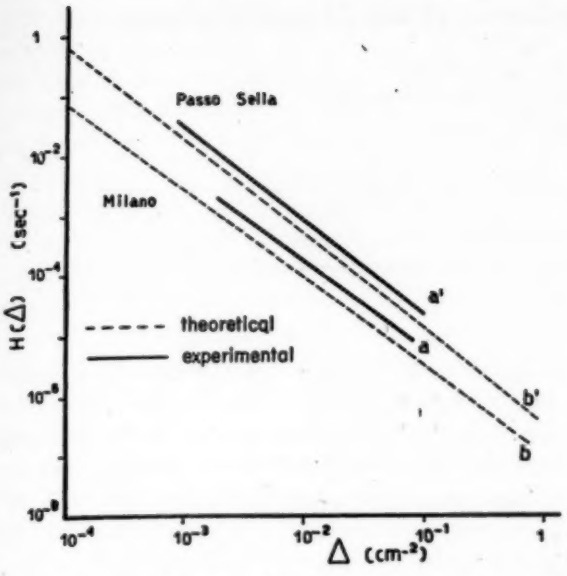

FIG. 3. Theoretical (a, b) and experimental (a′, b′) intensities $H(\Delta)$ of extensive showers as function of density Δ.

of air and having a surface small with respect to the surface covered by the shower (condition always satisfied in our experiments because the surface of showers is several thousands of m^2) gets struck with a rain of particles with density greater than Δ. This will be the frequency of the showers whose axis is distant from the apparatus less than R which fall at the top of the atmosphere on a surface S. Therefore, the frequency of showers which strike the apparatus due to primary particles in the energy band E to $E+dE$ and to the element of solid angle $d\omega$ is given by

$$\nu(E)dEd\omega \cdot \pi R^2 = f(E, l, \Delta)dEd\omega \text{ sec.}^{-1}.$$

The total frequency of the showers is given by integrating this expression over all energies and over all semi-space. If the vertical thickness of air above the recording apparatus is l_0, the thickness traversed by the shower generated by a particle whose direction forms an angle θ with the zenith is $l=l_0/\cos\theta$. The integral which gives the total frequency is

$$H(l_0, \Delta) = \int_0^\infty \int_0^{\pi/2} \int_0^{2\pi} f(E, \theta, l_0, \Delta)dEd\theta d\varphi.$$

This integral has been calculated graphically for Milan ($l_0=23.5$) and for Passo Sella ($l_0=18.5$) and for five values of Δ ($\Delta=10^{-4}$, 10^{-3}, 10^{-2}, 10^{-1}, cm^{-2}). The results are given in Fig. 3 (b and b′). They represent two spectra with densities varying exponentially, represented by equations:

$$H(\Delta) = 0.07\left(\frac{10^{-4}\text{ cm}^{-2}}{\Delta}\right)^{1.47} \text{ sec.}^{-1} \text{ (Milan)},$$

$$H(\Delta) = 0.63\left(\frac{10^{-4}\text{ cm}^{-2}}{\Delta}\right)^{1.57} \text{ sec.}^{-1} \text{ (Passo Sella)}.$$

In the figure are drawn also the two spectra (a and a′) from the experimental results at the two stations which are expressed by the two equations (1) and (2). The agreement between theory and experiment as regards the exponents and the relative frequencies at the two stations is excellent. In regard to the observed values of the frequencies the experimental values at Passo Sella and at Milan are greater by a factor of about 1.7 than the theoretical values. We believe, however, that the disagreement is within the error of approximation in Eq. (4). We believe that the results obtained for the density spectrum of extensive showers confirm the electronic nature of the primary radiation which produces them. It is true that from our experiments we cannot draw any conclusion about the nature of the effective primary particles, that is to say, of the radiation that, incident at the top of the atmosphere, generates the extensive showers. (It may be generated by electrons or by protons which are produced by electrons in the top layers of the atmosphere.) Nevertheless, the second hypothesis would lead to no different results.

Finally it is pointed out that the denser showers observed at Passo Sella ($\Delta=10^{-1}$ cm^{-2}) and in Milan are generated by electrons of 10^{15}–10^{16} ev and the correspondence between calculation and experiment lead us to believe that the spectrum of electronic radiation at the top of the atmosphere and, therefore, the spectrum of other possible primary radiations, reaches these high energies. The less dense showers observed by us ($\Delta=10^{-3}$ cm^{-2}) are generated by electrons of energies 10^{12} ev.

On the Fine Structure of Zenithal Curves of the Cosmic Radiation

G. COCCONI AND V. TONGIORGI
Institute of Physics, University of Milan, Milan, Italy
(Received January 31, 1946)

Differential measurements of the absorption in lead of the mesonic component of cosmic radiation at 2200 m above sea level and also measurements of the variation of the mesonic component with zenith angle do not confirm the existence of a fine structure in the intensity spectrum. With zenith angle the variation is perfectly regular and roughly follows the $\cos^2\theta$ law.

IT is known that the directional intensity of the cosmic radiation decreases as the inclination θ with respect to the zenith increases. This decrease may with good approximation be represented by the $\cos^2\theta$ law.

Schremp and Ribner,[1] Cooper,[2] and Schremp and Banos[3] have made measurements of the directional intensity as a function of the zenith angle at different azimuths and have observed a "fine structure" in the intensity curve. Schremp[4] inferred that a fine structure may be produced by the terrestrial magnetic field or by anomalies in the primary spectrum.

On the basis of the last hypothesis we performed an experiment during the period June–September, 1941 designed to show the possible band structure of the primary radiation by observing the spectrum of the mesonic component. It is assumed that the spectrum of mesons produced high in the atmosphere would correspond to the primary radiation which produced them and show the same irregularities.

With the apparatus indicated in Fig. 1 at 2200 m above sea level (Passo Sella, $H=7.9$ m, H_2O; geomagnetic latitude 49°N) we observed the triple coincidences among the counters A, B, C, and the quadruple coincidences $ABCD$ at the same time. Lead with thickness from 0 to 78 cm was placed at Σ_1 and Σ_2. From these observations the anticoincidences $ABC-D$ can be deduced.

The difference between the anticoincidences obtained with and without the 3 cm of lead placed at P gives the number of particles which after passing through the lead $\Sigma=\Sigma_1+\Sigma_2$ are stopped in P. This is the number of particles with energies between E and $E+\Delta E$ where E is the energy necessary to penetrate the atmosphere and the lead Σ and ΔE is the energy necessary to penetrate the 3 cm of lead at P. Thus the spectrum of the mesons with energy between 1.7 and 2.7×10^9 ev is determined directly.

Curve (a) in Fig. 1 represents the anticoincidences registered with 3 cm of Pb at P and curve (b) the anticoincidences without Pb at P. The curve a–b thus represents the spectrum in this energy range and it will be observed that no significant irregularities appear to exist.

A careful discussion of this experiment is given elsewhere.[5] It is concluded that the small oscillations shown on absorption curves and in the spectrum curve for 55–60 cm of Pb must be caused by spurious effects, particularly by the action of lateral showers the effects of which will not be the same with and without the 3 cm of Pb at P.

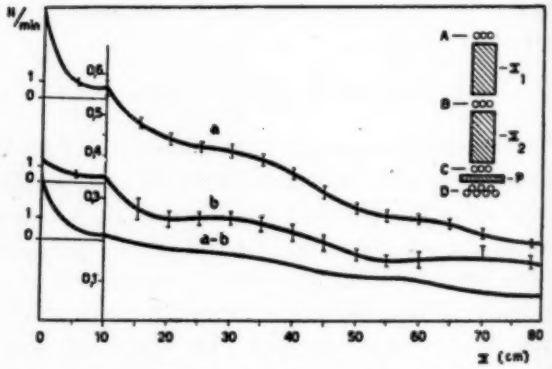

FIG. 1. Curve a: anticoincidences with 3 cm Pb in P; Curve b: anticoincidences without 3 cm Pb in P; Curve $(a-b)$: differential spectrum of vertical mesons, at 2200 m a.s.l.

[1] E. J. Schremp and H. S. Ribner, Rev. Mod. Phys. **11**, 149 (1939).
[2] D. Cooper, Phys. Rev. **58**, 288 (1940).
[3] E. J. Schremp and A. Banos, Phys. Rev. **58**, 662 (1940); **59**, 614 (1941).
[4] E. J. Schremp, Phys. Rev. **54**, 153 (1938).
[5] G. Cocconi and V. Tongiorgi, Ricerca Scient. **12**, 21 (1941).

The anomalies observed by Cooper for the zenithal angles, $\theta=7°$, 20°, and 35° should be represented in our experiments by anomalies corresponding to thickness of Pb of about 35, 40, and 65 cm. The amplitudes of the oscillations observed by Cooper are calculated as two percent of the total intensity. His apparatus had a resolving power ($\rho=E/\Delta E=\cot\theta/\Delta\theta$) as large as ours. Our measurements were made under more favorable conditions for in his measurements the intensity at inclinations to the zenith would be reduced by disintegrations of mesons in the atmosphere. In our experiments the effect of the decay of mesons is small because they were carried out at considerable altitude and because the absorption took place in dense materials instead of in air.

Since the anticoincidences ($ABC-D$) are just of the order of 2 percent of the coincidences ABC the suggested oscillations should be of the same order as the anticoincidences.

We conclude, therefore, that the direct determination of the energy spectrum of mesons excludes, at least in the range from 1.7 to 2.7×10^9 ev, the existence of anomalies which might cause a fine structure in the zenithal curves.

To aid in further clarifying these matters we decided to repeat the zenithal measurements of the authors mentioned above with an experimental arrangement equivalent to that used by one of them.[6] We felt it more desirable, however, to study the zenithal variation of only the mesonic component rather than of the total cosmic radiation. Since the soft components are in large part secondary to the hard component, particularly for directions more inclined to the zenith, it seemed desirable to make measurements only on the hard components. This has the further advantage of eliminating the effects of electronic radiations from material around the counters. These effects are difficult to check and can cause great trouble in the measurements of small intensities.

The measurements were carried out at Passo Sella continuously for 120 days during the period June–October, 1942. We used three counter telescopes, each one arranged as shown in Fig. 2 (solid angle of each telescope $5°\times16°$). Two of them were pointed SW, the third SE. The mesonic radiation was selected by 13 cm of lead. The inclination of the telescopes to the zenith were changed in steps of 5° from 0° to 60°, the inclinations being changed every five hours during the measurements. It was verified that the three telescopes in vertical orientation registered practically the same frequency of response. During the measurements, to avoid spurious effects the two telescopes in the same azimuthal orientation were kept at different zenithal inclinations. The intensity of the effect of lateral showers was determined by measuring the quadruple coincidences for each telescope when one set of counters was thrown out of alignment.

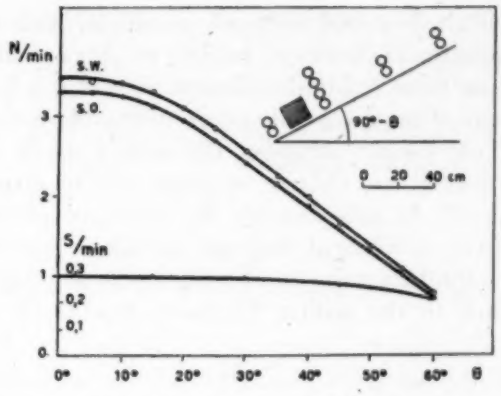

FIG. 2. Fourfold coincidences as function of zenith angle.

All counters (4.5×30 cm^2, filled with argon-alcohol, threshold 1300 volts, working voltage 1500 v) were electrically shielded, kept at constant temperature, and checked daily with an oscillograph.

Figure 2 shows the results of the zenithal measurements, corrected for lateral showers and the variation in intensity of the showers. It will be seen that the course of the zenithal curves is perfectly regular and follows roughly the $\cos^2\theta$ law although at large θ the intensity falls off more rapidly than would follow from this law. We conclude, therefore, that the mesonic component of the radiation shows no irregular variation with zenith angle.

From these measurements it would appear that the irregularities observed by the above authors must be attributed to the soft components which are not secondary to the mesons,

[6] V. Tongiorgi, Nuovo Cimento 1, 96 (1943).

viz., to the so-called electronic residuals. Such an explanation is, however, subject to grave doubt because these residual radiations form but a few percent of the total. The experiments referred to were carried out at about the same latitude as ours but at an altitude of about 200 m above sea level. At this altitude the intensity of the residuals in vertical direction is but 5 percent of the total intensity and is even less in directions inclined to the zenith. Furthermore, the effect observed did not change sensibly with change in altitude, i.e., with change in magnitude of the residual component. At 2500 m the above authors report a deviation from the $\cos^2\theta$ law of the same order as at 200 m.

In conclusion our measurement both with lead absorbers and with varying zenith angle on the intensity variation of the mesonic component of cosmic radiation does not confirm the existence of fine structure in the absorption curves.

PHYSICAL REVIEW VOLUME 70, NUMBERS 11 AND 12 DECEMBER 1 AND 15, 1946

Penetrating Particles in Air Showers

G. Cocconi, A. Loverdo, and V. Tongiorgi
Institute of Physics, University of Milan, Milan, Italy

(Received May 4, 1945)

The paper describes some experiments performed at 2200 meters above sea level for the purpose of investigating the nature of the particles which form the extensive cosmic-ray showers in air. The results show that these showers contain both electrons and mesons.

I

IN the study of extensive air showers the question of the role played by penetrating particles (mesons) is an important one.

Since air showers were first discovered, coincidences were observed with one of the G-M counters surrounded by lead shields of a thickness greater than an electron can penetrate.[1]

Later, experiments by Wataghin, De Souza, and Pompeia[2] revealed the existence of showers of considerable extent, containing at least two penetrating particles. These experiments were performed with G-M counters in coincidence, all appropriately shielded and placed in a horizontal plane, at distances varying from 35 to 120 cm.

However, the above experiments had only a qualitative value because the number of coincidences observed was of the same order as the number of chance coincidences. Moreover, they did not establish clearly the relation between penetrating showers and ordinary electron showers.

The existence of air showers containing several mesons, generated by a multiplication process closely related to that responsible for the production of ordinary air showers, was revealed by the writers in 1942.[3] Subsequently we were

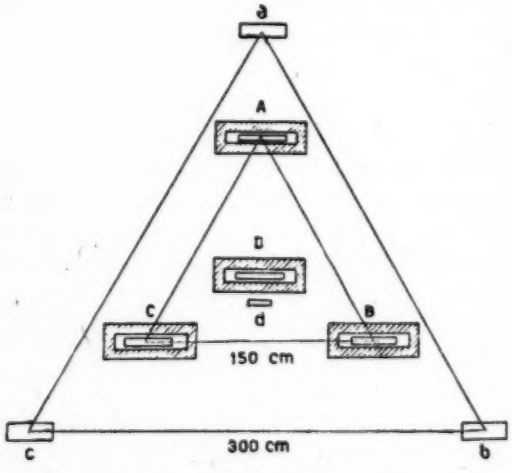

FIG. 1. Counter arrangement.

[1] P. Auger, R. Maze, P. Ehrenfest and A. Freon, J. de Phys. et Rad. 10, 39 (1939).
[2] G. Wataghin, N. D. De Souza Santos, and S. A. Pompeia, Phys. Rev. 57, 61 (1940); 59, 902 (1941).
[3] G. Cocconi, A. Loverdo and V. Tongiorgi, Naturwiss. 31, 135 (1943).

able to show that the majority of the meson showers are accompanied by electron showers containing a large number of particles.

2

Experiments on the meson showers were repeated in the summer of 1943 at Passo Sella (2200 m above sea level), with an experimental arrangement designed to furnish more detailed information on the phenomenon.

With two independent circuits, we recorded threefold ($T_h = A+B+C$) and fourfold ($Q_h = A+B+C+D$) coincidences between heavily shielded counters. These counters were placed at the vertices and at the center of an equilateral triangle of 150-cm sides (see Fig. 1). In this way one could be sure that the coincidences were produced by extensive showers, of 3 or 4 particles at least, capable of penetrating the absorber.

With another similar arrangement, we also recorded threefold ($T_s = a+b+c$) and fourfold ($Q_s = a+b+c+d$) coincidences between unshielded counters placed as indicated in Fig. 1, so as to detect ordinary electron showers.

Finally, with two circuits T_s+T_h and T_h+Q_s (see Fig. 2) we also recorded coincidences between showers of penetrating particles (T_h) and ordinary electron showers (T_s and Q_s).

From the numbers of coincidences T_h and Q_h we obtain information on the density Δ_h of penetrating particles (mesons); while from the numbers of coincidences T_h+Q_s and T_h+T_s we obtain information on the density of electrons Δ_{h+s} which accompany the meson showers.

To make sure that the observed particles were

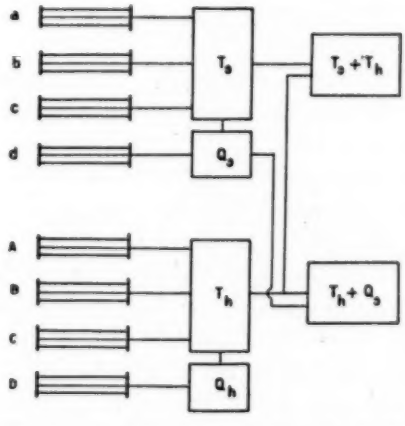

FIG. 2. Arrangement for the recording of coincidences.

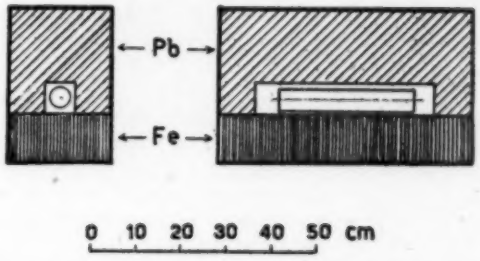

FIG. 3. Arrangement of the shield around the counters.

mesons, counters A, B, C, and D were shielded at the bottom by an iron plate 10 cm thick, at the top by a lead absorber not less than 16 cm thick, and on the sides by lead walls not less than 8 cm thick, as shown in Fig. 3.

Increasing the thickness of the upper absorber from 16 to 24 cm, and that of one of the side walls from 8 to 16 cm, failed to produce any appreciable variation in the number of coincidences per minute. This confirms the assumption that the observed particles are mesons.

The counters (a, b, c, and d) recording electron showers were placed immediately under the roof (which had a thickness of 4 g/cm²) in order to minimize the effect of multiplication in the material of the roof.[4] The shielded counters were placed on the floor.

All the counters had brass walls, were filled with an argon-alcohol mixture, and had a threshold of about 1300 volts. They were kept at a temperature of about 15°C by thermostatic control. The resolving time of the coincidence circuits was approximately 3×10^{-7} minutes. The number of threefold chance coincidences, in the most unfavorable conditions was less than 3 percent of the number of true coincidences and was, therefore, negligible.

The measurements were carried out uninterruptedly day and night for a period of 100 days The operation of the counters and of the circuits was checked daily. Special care was taken to guard against spurious counts by grounding the counters, the circuits, and the cables. The absence of disturbances was checked every 3 or 4 days by test runs with the counter voltage below threshold. These checks were particularly desirable on account of the very small number of true coincidences.

[4] G. Cocconi, A. Loverdo, and V. Tongiorgi, Nuovo Cimento 1, 314 (1943); Phys. Rev. 70, 841 (1946).

TABLE I. Summary of experimental results.

Counter area (m^2)	Minutes	T_4	Q_4	Δ_4 (m^{-2})	T_4+T_5	T_4+Q_5	Δ_{4+5} (m^{-2})
0.0129	66,016	$34=5.2\pm0.9\times10^{-4}$ min.$^{-1}$	$19=2.9\pm0.7\times10^{-4}$ min.$^{-1}$	64 ± 22	34	27	800 ± 400
0.0258	31,271	$32=10.2\pm1.8\times10^{-4}$ min.$^{-1}$	$23=7.4\pm1.5\times10^{-4}$ min.$^{-1}$	49 ± 21	32	23	600 ± 300

3

In order to obtain quantitative information on the density distribution of the meson showers, shielded counters with three different areas were used, namely $S_1=0.0258m^2$, $S_2=0.0129m^2$, $S_3=0.0027m^2$. As explained elsewhere,[4] by changing the sensitive area of the counters one explores different "bands" of the density spectrum of showers.

The arrangement for the detection of electron showers had to satisfy two conditions: (1) have a high efficiency, in order to detect most of the electron showers associated with meson showers and (2) furnish quantitative information on the density of showers with large numbers of particles.

The first purpose was achieved by using large counters ($S=0.0258m^2$) in the threefold coincidence arrangement ($T_5=a+b+c$). The second purpose was achieved by selecting as fourth counter in the fourfold coincidence arrangement ($Q_5=a+b+c+d$) one with small area ($S=0.0020m^2$).

The experimental results, which are summarized in Table I, confirm our previous conclusions. Out of a total of 74 meson showers recorded, only 8 were not accompanied by a coincidence in the counters detecting electron showers. In order to explain this result, one as to assume that the average density of particles in the electron showers associated with meson showers is larger than 150–200 m^{-2}.

The densities Δ were determined from the equation

$$\Delta=\frac{1}{S}\log\frac{T}{T-Q}.$$

It appears from the table that the density Δ_4 of meson showers is a function of S. The same has been shown to be true for electron showers.[4] It may be noted here that no counts were recorded in 20,000 minutes using shielded counters with sensitive areas $S=0.0027m^2$.

Comparison with previous results[4] shows that meson showers are about 300 times less frequent than electron showers of the same density; i.e., recorded with counters of the same area S. If this holds true for all values of S, it explains the failure of recording any count with shielded counters of $0.0027m^2$ area (the expected number of counts turns out to be one every 25,000 minutes!).

The average density Δ_{4+5} of electron showers associated with meson showers has also been determined and has a value between 600 and 800 particles/m^2.

The above results, although necessarily inaccurate, throw some light on the nature of extensive air showers. In fact, the number of meson showers of density $\Delta_4\approx50m^{-2}$ which give rise to threefold coincidences is 10^{-3} per minute. Since the efficiency of our experimental arrangement may be estimated to be about 0.4, the absolute number of the above showers turns out to be approximately 3×10^{-3} per minute.

From the distribution formula for electron showers established elsewhere[4]

$$\nu(\Delta)=80\Delta^{-2.6}\text{ min}^{-1},$$

one calculates a number of 2×10^{-3} showers per minute with $\Delta>600$ particles per m^2. Even considering the large statistical errors, one can hardly escape the conclusion that *the majority if not all of the electron showers are accompanied by meson showers.*

This conclusion, along with that reached previously, to the effect that all meson showers are accompanied by electron showers, shows in our opinion that *in the multiplication process which gives rise to large air showers, not only electrons, but also mesons are produced.*

We wish to thank the Comitato per la Geofisica e la Meteorologia del Consiglio Nazionale delle Ricerche and the Physical Institute of the University of Milan, for financial support of this work. We also thank Professor G. Polvani for lending us experimental equipment.

The Mean Lifetime of the Meson

G. COCCONI AND V. TONGIORGI
Institute of Physics, University of Milan, Milan, Italy

(Received January 31, 1946)

Measurements of the lifetime of mesons which have traversed varying distances in air have been made and show that the value of $\tau/\mu c^2$ is constant. The existence of a spectrum of lifetimes is therefore excluded. The most probable value of $\tau/\mu c^2$ from our measurements is $2.6 \pm 0.3 \times 10^{-14}$ sec./ev.

1

MEASUREMENTS during recent years have shown with certainty that the meson is unstable with a mean lifetime of 2 to 3 microseconds. Discussion now turns chiefly on questions of the exact value of the mean life and on whether it is the same for different mesons.

Recently Weisz[1] from an analysis of the results of various authors concluded that they could be brought into harmony by assuming that the value of $\tau/\mu c^2$ (τ, mean lifetime of meson at rest; μ, rest mass of meson) increases as the path traversed by the meson increases. This could be accounted for by assuming that in the upper reaches of the atmosphere not just one type of meson is generated but that the mesons produced have a spread either in mean lifetime, rest mass or both. If the mass is assumed constant, the mean lifetime would decrease with decreasing path traveled.

Because of the importance of this matter we maintain that before concluding that $\tau/\mu c^2$ varies with the path length of the meson in air, as previous measurements have somewhat indirectly indicated, measurements designed specifically to test this point should be carried out.

Juilfs' tested the variation of $\tau/\mu c^2$ by varying the zenith inclination and reported an increase in $\tau/\mu c^2$ with increasing θ. We have repeated Juilfs[2] calculations using careful zenith measurements at Passo Sella (2200 m above sea level) by one of us[3] and found no variation of $\tau/\mu c^2$.[4] This ratio remained constant within experimental error from $\theta = 0°$ to 60°.

In any case the values of $\tau/\mu c^2$ deduced from measurements of this type are uncertain, above all because of the uncertainty in our knowledge of the energy spectrum of the mesons. We have held it important therefore to do experiments from which it would be possible to deduce the

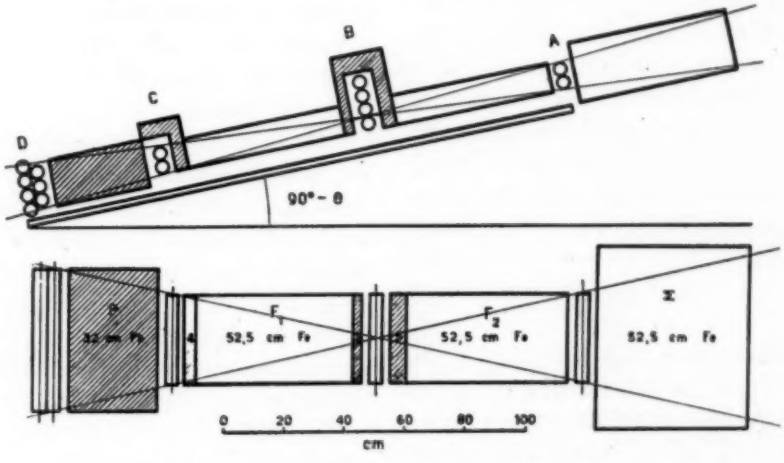

FIG. 1. Arrangement of counters and absorbers.

[1] P. Weisz, Phys. Rev. **59**, 845 (1941).
[2] J. Juilfs, Naturwiss. **30**, 584 (1942).
[3] V. Tongiorgi, Nuovo Cimento **1**, 96 (1943).
[4] G. Cocconi and V. Tongiorgi, Naturwiss. **31**, 108 (1943).

TABLE I. Essential data involved in the measurements.

1	2	3	4	5	6	7	8	9	10	11	12
Series	Type of mean.	θ	Absorb. $A+B$ g/cm²	g/cm² Pb in P	g/cm² Fe in F_1	g/cm² Fe in F_2	g/cm² Fe in Σ	$\frac{1020}{\cos\theta}$	E total ev	E mean ev	Km in air
I	20 *CP*	20° 00′	140	358	404	404	404	1085	5.25×10^9	4.97×10^9	18.6
	20 *SP*	20° 00′	140	0	404	404	404	1085	4.70×10^9		
	43 *CP*	43° 52′	140	358	404	404	0	1415	5.26×10^9	4.99×10^9	27.2
	43 *SP*	43° 52′	140	0	404	404	0	1415	4.72×10^9		
II	54 *CP*	54° 16′	140	358	0	0	404	1745	5.26×10^9	4.99×10^9	36.2
	54 *SP*	54° 16′	140	0	0	0	404	1745	4.72×10^9		
	60 *CP*	60° 32′	140	358	0	0	0	2075	5.29×10^9	5.01×10^9	45.4
	60 *SP*	60° 32′	140	0	0	0	0	2075	4.74×10^9		

value of $\tau/\mu c^2$ for mesons belonging to the same energy band but which have traveled over widely varying path lengths.

2

With the counter telescope illustrated in Fig. 1 we have registered the difference $D=T-Q$ between triple ($T=A+B+C$) and quadruple ($Q=A+B+C+D$) coincidences. The counters in groups A, B, C had brass walls 1 mm thick and had an effective area 4.3×30 cm². They were filled with argon and alcohol. The tubes of group D were similar to those of A, B, C but had an area 4.3×45 cm². The solid angle of the telescope was $8°\times27°$. As shown in Fig. 1 lead and iron absorbers could be placed between and in front of the counters. The absorbers (of Pb, 140 g/cm²) around the counters B and C were present in all measurements and served to protect the system in large part from the effect of lateral showers and to eliminate the electronic component in the absence of the other absorbers.

The counters and absorbers were mounted on a mobile support which could turn on a horizontal axis to give to the telescope different zenith inclinations.

All measurements were carried out at the Physical Institute of the University of Milan (average barometric pressure 1020 g/cm²) before a large window which left the solid angle of the telescope completely unobstructed in all positions used in the experiments.

The conditions of the series of measurements are given in Table I. In column 9 is shown the path length to the top of the atmosphere (measured in g/cm²). We assume that the mesons are not generated at the top of the atmosphere but only after the primary cosmic radiation which generates them has passed through a distance s in air about equal to 100 g/cm². We shall see later the importance of taking for the path length of the meson the value $(1020/\cos\theta-s)$. In column 10 are given the values of the energy which a meson must have to traverse the absorbing materials given in columns 4–9 and thus reach counters D. These values of meson energy are taken from the charts given by Wick.[5] Wick's calculations were made under the assumption that μc^2 for the meson is 10^8 ev but even assuming a variation of ±20 percent in the mass of the meson the values of the energy would not be seriously altered.

The first series of measurements was carried out in early 1942. The positions of absorbers and telescope were changed each day. A daily check was made of the operation of the counters and coincidence equipment. At each position of telescope and for each disposition of absorbers the difference between the triple and quadruple coincidence frequency was measured. The results are given in Table II.

The difference of the frequency differences 20 *CP*−20 *SP* is proportional to the frequency with which mesons in the energy range 4.70 to

[5] G. C. Wick, Nuovo Cimento 1, 302 (1943).

TABLE II. Differences between triple and quadruple coincidence.

I Series	20 *CP*	20 *SP*	43 *CP*	43 *SP*
$\frac{T-Q}{\text{min.}}$	$\frac{3283}{30844}=0.105\pm0.0019$	$\frac{512}{14186}=0.0361\pm0.0016$	$\frac{2825}{37897}=0.0746\pm0.0014$	$\frac{344}{13862}=0.0248\pm0.0014$
II Series	54 *CP*	54 *SP*	60 *CP*	60 *SP*
$\frac{T-Q}{\text{min.}}$	$\frac{885}{18369}=0.0481\pm0.0016$	$\frac{71}{5349}=0.0132\pm0.0015$	$\frac{627}{21227}=0.0295\pm0.0012$	$\frac{106}{8306}=0.0128\pm0.0013$
$\frac{T-Q}{\text{min.}}$	$\frac{2624}{45307}=0.0519\pm0.0012$	$\frac{231}{9777}=0.0236\pm0.0016$	$\frac{1901}{52903}=0.0359\pm0.0008$	$\frac{147}{7016}=0.0209\pm0.0017$

5.25×10^9 ev (average energy 4.97×10^9 ev) reach the telescope within its effective solid angle around its inclination to the zenith. Similarly for the difference 43 *CP*−43 *SP* except that the energy range is from 4.72 to 5.26×10^9 ev (average energy 4.99×10^9 ev). Aside, therefore, from the completely negligible energy difference and assuming the space isotropy of cosmic radiation the ratio

$$R_1=\frac{43\ CP-43\ SP}{20\ CP-20\ SP}$$

gives the relative probabilities that mesons of average energy 4.98×10^9 ev will reach sea level with the above inclinations.

As already stated the lead absorbers around counters *B* and *C* largely eliminated the effect of lateral showers. The residual effect of these have been observed by moving two counters out of alignment. It was found that their effect besides being small was equal in all dispositions of the telescope and absorbers used. They are therefore eliminated in taking differences *CP*−*SP*.

In column 12 of Table I are given the path lengths l of the trajectories of the mesons at the various inclinations to the zenith. In the calculation it is assumed that the mesons are generated after passing through a stratum of air of 100 g/cm². The values of l are calculated from the relation

$$l=\frac{17.0}{\cos\theta}\log\frac{10.2}{\cos\theta}\ \text{km}\quad\text{(isothermal atmosphere at }-20°\text{C)}.$$

From the first series of measurements the value of $\tau/\mu c^2$ can be calculated for mesons which have traversed in the mean about 23 km.

In the second series similar measurements were made at 54° 16′ and 60° 32′ inclination to the zenith. Here again the average energy of the mesons stopped in *P* is practically the same as in the first series (5×10^9 ev). The lateral showers were also constant for all arrangements. From the ratio

$$R_2=\frac{60\ CP-60\ SP}{54\ CP-54\ SP}$$

the value of $\tau/\mu c^2$ may be computed for mesons which have traversed not 23 km but 42 km.

Comparison of the values for $\tau/\mu c^2$ from R_1 and R_2 will therefore show whether or not this quantity varies with the path length. It is to be noted that by this method we are measuring the values of $\tau/\mu c^2$ for mesons of the same energy and energy spread and therefore the results are independent of any assumption of the shape of the primary spectrum. This is one of the principal causes of differences between measurements carried out by different experimenters under different conditions.

The only uncertain quantity introduced in our calculations is the value of s, the mean path length in air (in g/cm²) for the creation of mesons by the primary cosmic radiation. It will be seen, however, that our conclusions are not critically sensitive to the value assumed for s.

The second series of measurements was repeated twice, once during the spring of 1942 and once during the winter of 1943.

From Table II

$$R_1=\frac{0.0498}{0.0689}=0.724\pm0.039,$$

$$R_2=\frac{0.0167}{0.0349}=0.479\pm0.054,$$

$$R_3=\frac{0.0150}{0.0343}=0.439\pm0.062.$$

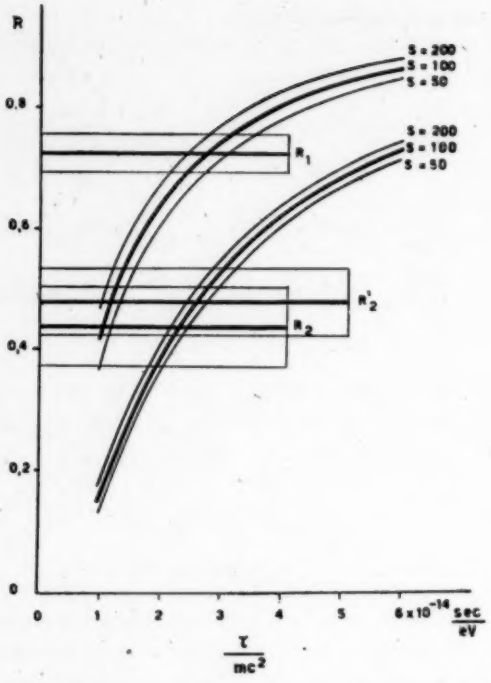

FIG. 2. Calculated relation between R and $\tau/\mu c^2$ together with the three measured values of R and their statistical errors.

If τ is the mean lifetime of the meson, μ its mass, the probability that it will disintegrate in a vertical distance dz is

$$-d\Pi=\frac{\mu c^2}{\tau c W\cos\theta}\frac{dz}{},$$

where W is the meson energy and θ is the inclination of the path of the meson to the zenith. This formula takes account of relativistic corrections and is a sufficiently close approximation for values of $W>10^8$ ev.

In terms of pressure change

$$dp=(p/p_0)\delta dz,$$

where δ is the density of normal air at p_0. Substitution gives

$$-d\Pi=\frac{\mu c^2}{\tau}\frac{p_0}{c\delta}\frac{dp}{pW\cos\theta}.$$

If we designate by $\Pi(p, W, \theta, s)$ the probability that a meson generated by a primary cosmic ray after passing through a stratum s of air will reach a level in the atmosphere of pressure p with energy W and inclination θ, Π will satisfy the differential equation

$$\frac{-d\Pi(p, W, \theta, s)}{dp}=\frac{\mu c^2}{\tau}\frac{p_0}{c\delta}\frac{\Pi(p, W, \theta, s)}{pW\cos\theta}.$$

We may calculate the energy W of the meson at the point where the pressure is p in terms of its energy W_0 at the point where it is created by assuming that it loses a quantity α of energy for each unit of mass/cm² crossed.

$$W=W_0-a(p/\cos\theta-s),$$
$$=\frac{(W_0+as)\cos\theta-\alpha p}{\cos\theta},$$
$$=\frac{E\cos\theta-\alpha p}{\cos\theta},$$

where $E=W_0+as$ is the virtual energy of the meson at the top of the atmosphere (the values listed in column 11 of Table I). Substituting and integrating we get

$$\log\Pi(p, E, \theta, s)$$
$$=A\frac{\mu c^2}{\tau}\frac{1}{E\cos\theta}\log\left(\frac{\alpha p-E\cos\theta}{\alpha p}\right)+\text{const.}$$

where $A=p_0/c\delta$. Assuming $\Pi=1$ for $p=s$ gives

$$\Pi(p, E, \theta, s)=\left[\frac{(E\cos\theta-\alpha p)s}{(E-as)p}\right]^{\frac{\mu c^2}{\tau}\frac{A}{E\cos\theta}}.$$

In calculating Π we assume $p_0=1033$ g/cm², $\delta=1.40\times10^{-3}$ g/cm²,* $c=3\times10^{10}$ cm/sec. From Wick's charts it is reasonable to assume that, for $E=5\times10^9$ ev, $\alpha=2.2\times10^6$ ev cm²/g.

We have calculated in this way the value of Π (1020, E, θ, s) for the various values of θ in Table I as a function of $\tau/\mu c^2$ and for three values of s ($s=50$, 100, 200 g/cm²). For each value of s we have obtained two curves which give as a function of $\tau/\mu c^2$ the values of the ratios

$$R_1=\frac{\Pi(1020; 4.98\times10^9; 45°52'; s)}{\Pi(1020; 4.98\times10^9; 20°00'; s)}$$

and

$$R_2=\frac{\Pi(1020; 5\times10^9; 60°32'; s)}{\Pi(1020; 5\times10^9; 54°16'; s)}.$$

* Mean temperature of air 20°C. It is to be noted that generally authors have assumed an isothermal atmosphere at 0°C. All the values of mean lifetime calculated on this basis are about 8 percent too low.

The six curves are shown in Fig. 2 together with the three experimental values and their statistical errors. An examination of the curves shows that the different values of s do not seriously affect the theoretical values of R_1 and R_2. Since s almost certainly lies between 50 and 200 g/cm², it seems reasonable to conclude that the assumption $s=100$ g/cm² will not cause an error in $\tau/\mu c^2$ greater than 10 percent. Since we are here primarily interested in relative values this uncertainty will not appear.

With $s=100$ g/cm² we get for the first series of measurements

$$\tau/\mu c^2=(2.8\pm0.5)\times10^{-14}\text{ sec./ev.}$$

For the second series the two values

$$\tau/\mu c^2=(2.6\pm0.4)\times10^{-14}$$

and

$$(2.3\pm0.4)\times10^{-14}\text{ sec./ev.}$$

We therefore conclude that the value of $\tau/\mu c^2$ does not increase when the path traversed is increased from 23 to 43 km. (If anything there is a slight decrease.) We believe, therefore, that these measurements confirm what we have already stated[4] that $\tau/\mu c^2$ is independent of path traversed, at least within the experimental errors of the measurements to date.

The three measurements together give a mean value for $\tau/\mu c^2$ of $(2.6\pm0.3)\times10^{-14}$ sec./ev. This value agrees within experimental errors with that given by Bernardini[6] from an extensive analysis of all measurements to date. It also agrees with the recent careful direct measurements of M. Conversi and O. Piccioni[7] which gave $\tau=(2.30\pm7\text{ percent})\times10^{-6}$ sec.

[6] G. Bernardini, Zeits. f. Physik **120**, 413 (1943).
[7] M. Conversi and O. Piccioni, Nuovo Cimento **11**, 71 (1944).

PHYSICAL REVIEW VOLUME 70, NUMBERS 11 AND 12 DECEMBER 1 AND 15, 1946

On the Mean Life of Slow Mesons

M. CONVERSI AND O. PICCIONI*
Institute of Physics, University of Rome, Rome, Italy
(Received February 10, 1945)**

A new investigation on the spontaneous decay of mesons is performed by counting delayed coincidences between the impinging low energy mesons and the decay electrons. Four points of the decay curve of mesons are obtained for relative delay times ranging between -0.91 and 2.43 μsec. The results give an exponential curve which is evidence of the decay process. For the mean life we find $\tau=2.33$ μsec. ±6.5 percent. The effect disappears completely by inverting the sign of the delay.

1. INTRODUCTION

ACCORDING to current ideas, the particles which make up the hard component of cosmic rays have properties very similar to those of the particles first postulated by Yukawa[1] to explain the nuclear forces. This particle (meson, positive, or negative) having a mass of about 200 electron masses, undergoes spontaneous disintegration producing—according to the scheme generally accepted—one electron and one neutrino. The instability of mesons was assumed in order to explain the anomalous absorption of the hard component, upon which are based all the measurements performed up to now of the ratio $\tau/\mu c^2$ of the mean life τ to the rest energy μc^2 of mesons.[2–14]

* At the present Visiting Research Associate at Massachusetts Institute of Technology.
** The manuscript of the present paper was prepared in 1944. At that time no information was available in Italy on the experiment on the disintegration of mesons carried out by N. Nereson and B. Rossi (Phys. Rev. **64**, 199 (1943)). On account of wartime conditions the manuscript did not reach the Editor of *The Physical Review* until February 10, 1945.
[1] Yukawa, Proc. Phys. Math. Soc. Japan **20**, 319 (1938).

[2] Johnson and Pomerantz, Phys. Rev. **55**, 104 (1940).
[3] Rossi, Hilberry, and Hoag, Phys. Rev. **57**, 461 (1940).
[4] Ageno, Bernardini, Cacciapuoti, Ferretti, and Wick, Phys. Rev. **57**, 945 (1940).
[5] Pomerantz, Phys. Rev. **57**, 2 (1940).
[6] Cocconi, Ricerca Scient. **11**, 50 (1940).
[7] Rossi and Hall, Phys. Rev. **59**, 223 (1941).

The most reliable value of this ratio seems to be 3.0 ± 0.3 sec./Mev.[14] One notes, however, that the results obtained by different authors do not agree very well, and that the deduction of the value of $\tau/\mu c^2$ from experimental measurements is based on special assumption about the generation of mesons. Moreover, a determination of τ based on the anomalous absorption is to be considered only an indirect proof of the assumption of the disintegration of mesons. Direct proofs of the instability of these particles have been supplied up to the present only by two cloud chambers photographs[15] and by two direct experiments, the first obtained by Rasetti[16] and the second attributed to Auger, Maze, and Chaminade,[17,18] which allow at the same time a direct measurement of the mean life of the decay process.

The first attempt at a direct measurement of τ is attributed to Montgomery Ramsey, Cowie, and Montgomery[19] who counted the delayed coincidences of two sets of G.M. counters between which could be inserted a lead plate 2 cm thick, where the slow mesons were stopped and in which they decayed. The mean life could be deduced by comparing the number of delayed coincidences with and without the lead absorber. These authors concluded that the experiment had given a strictly negative result; it is, however, to be noticed that they had evaluated the amount of the effect (to about ten times the experimental error) by taking into account only the geometrical condition under which the experiment was performed and overlooked the effect of the low value of the range of the decay electrons, which in their absorber of lead is 1.23 cm according to Bethe and Heitler.[20]

For this reason, and because of the uncertainties affecting measurements of absolute delay and the evaluation of the efficiency of delayed coincidences, the negative result of this experiment cannot be considered as definitive. In fact, as will be seen later, our experimental disposition gave a number of undelayed coincidences nearly equal to that of Montgomery and collaborators, and a slightly higher number of delayed coincidences. As an absorber, we used iron which is more convenient than lead for detecting the maximum number of decay electrons.

The second experiment of this type is attributed to Rasetti and was published in June, 1941.[16] Typical of this experiment was a very successful disposition of the counters: a fivefold coincidence set which by its geometry did not register particles following a straight line. In effect fivefold coincidences were simultaneously registered by means of three circuits having resolving times equal, respectively, to $t_2=15.0$; $t_3=1.95$; $t_4=0.95$ μsec.

Therefore the differences (with obvious correspondence in the labels) n_2-n_3 and n_2-n_4 gave the number of coincidences due to pulses separated one from the other by times ranging, respectively, between 1.95 and 15.0 μsec. and 0.95 and 15.0 μsec. The value of τ was determined by the ratio of these two differences not by their absolute values.

The result of this experiment was positive. In fact Rasetti found different values for the abovementioned differences as would be expected if the meson decays with electron emission.

The value of τ deduced from two series of measurements, one performed with an iron, the other with an aluminum absorber, was $\tau=1.5\pm0.3$ μsec.

As a qualitative proof of the reality of the effect, Rasetti showed that almost no effect was observed without an absorber.

This result was considered a rather good proof of the decay of mesons, the more so as the experimental value of the mean life was in reasonable agreement with the values deduced at that time by the anomalous absorption of mesons on the assumption of $\mu c^2=100$ Mev.[9]

However, it seems to us that in his deduction

[8] Cacciapuoti and Piccioni, Ricerca Scient. **12**, 874 (1941).
[9] Nielsen, Ryerson, Nordheim, and Morgan, Phys. Rev. **59**, 547 (1941).
[10] Bernardini, Cacciapuoti, Pancini, and Piccioni, Nuovo Cimento **19**, 69 (1941).
[11] Festa, Santangelo, and Scrocco, Nuovo Cimento **1**, 71 (1942).
[12] Bernardini and Festa, Atti d. R; Acc. d'Italia **7**, 4 (1943).
[13] Conversi and Scrocco, Nuovo Cimento **1**, 372 (1943).
[14] Bernardini, Zeits f. Physik **120**, 413 (1943).
[15] Williams and Roberts, Nature **145**, 102 (1940).
[16] Rasetti, Phys. Rev. **59**, 613 (1941); **60**, 198 (1941).
[17] Auger, Maze, and Chaminade, Comptes rendus **213**, 381 (1941).
[18] Maze and Chaminade, Comptes rendus **214**, 266 (1941).
[19] Montgomery, Ramsey, Cowie, and Montgomery, Phys. Rev. **51**, 635 (1939).
[20] Bethe and Heitler, Proc. Roy. Soc. **A146**, 83 (1934).

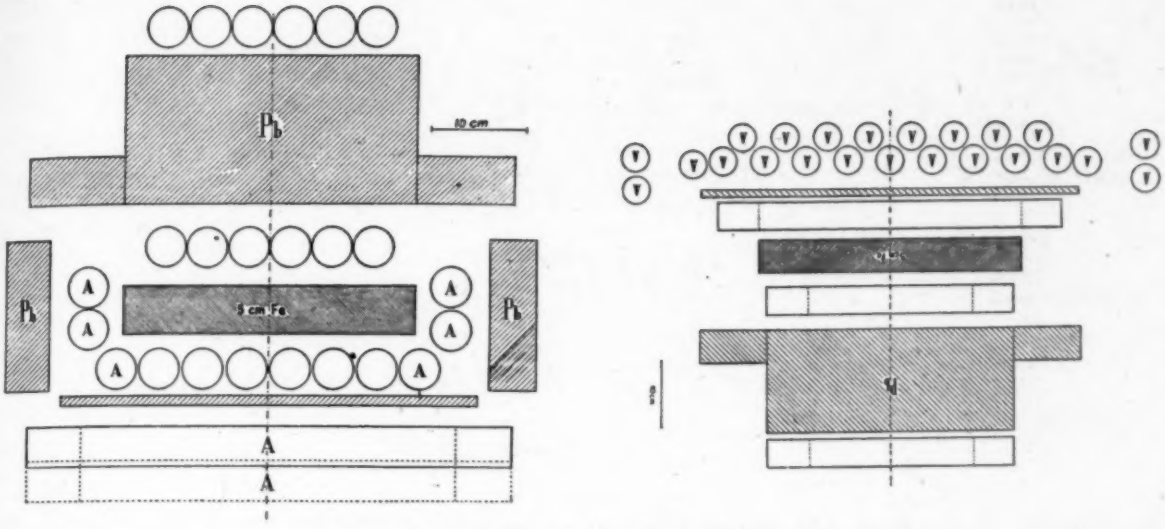

FIG. 1 (a) and (b). Vertical sections of the whole set of counters.

of the mean life of mesons, Rasetti makes the implicit assumption that, by using a circuit of resolving power θ, only the double coincidences due to pulses following one another by a time t smaller or equal to θ are registered.

On this point one can make the two following remarks: (a) Under the assumption that the two branches of the coincidence circuit give pulses of the same time length, Rasetti's procedure is correct only if the two branches introduce no delay or, at least, equal delays; otherwise t is larger than θ by the difference of the delays introduced by the amplifiers;

(b) Under the assumption that those delays are zero or equal, Rasetti's assumption is correct only if the effective coincidence-times θ_1 and θ_2 of the pulses in the two branches are strictly equal. In the general case, when θ_1 and θ_2 are not equal, a coincidence will be registered provided that the pulse of the second branch is delayed by no more than θ_1 over the pulse of the first branch, or the first pulse by no more than θ_2 over the second pulse. Calculating the resolving power from the number of random coincidences $N_c = N_1 N_2(\theta_1+\theta_2)$, ($N_1$, N_2 being the zero-effect of each branch) according to the usual formula $\theta = N_c/N_1N_2$ we get for θ the mean value of θ_1 and θ_2.

Such a difference between θ_1 and θ_2, actually occurs, when circuits with too large values of RC are used that may obviously introduce a considerable error in the value of τ; therefore, we thought it desirable to make a direct measurement of τ by using a registering set appropriate for very short pulses whose behavior could be checked frequently during the measurements by means of a suitable disposition of the tubes. At the same time we had the purpose of giving new evidence of the instability of mesons, besides that based on the comparison "with and without absorber": (a) by obtaining many points of the decay curve in order to show its exponential shape, (b) by comparing measurements (that we shall call *normal*) in which were registered the coincidences of a set of counters (set 3) delayed with respect to two other sets (sets 1, 2); and measurements (that we shall call *inverted*) in which were registered the delayed coincidences of the two sets 1, 2 with respect to the set 3.

While we were arranging our experiment, we heard about the results obtained by Auger, Maze, and Chaminade[17,18] who had found three points of the decay curve, with an arrangement similar to that of Rasetti, although independently. The points obtained by these authors in the above mentioned paper[18] are not sufficient to prove the exponential shape of the decay curve nor allow an exact determination of τ. In the paper available to us, the authors do not state that the measurements for the different delays were made alternatively; this point is very important since the experiment took a rather long time because of the

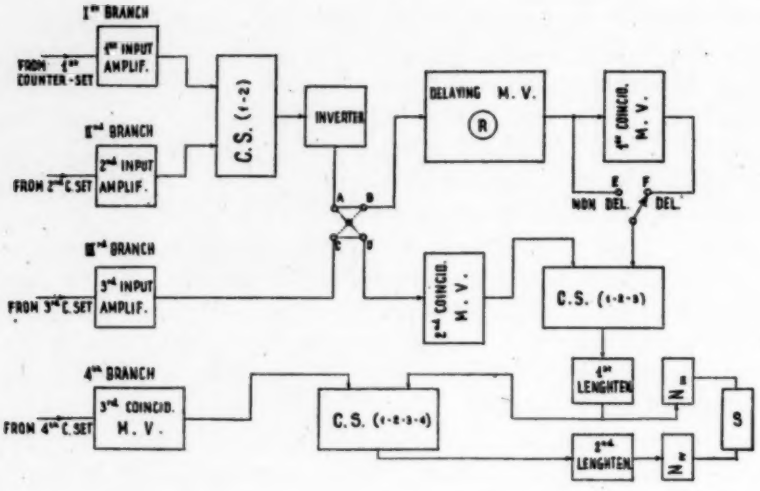

FIG. 2. Block diagram of the registering set.

low intensity of the effect. The authors claim to have found no effect for an inverted delay and give for τ the value (1.45 ± 0.44) μsec. We started to arrange our equipment in the autumn of 1941. The already considerable time, necessary to make and calibrate the above mentioned set, was much increased by the war conditions. The work was finished in February, 1943 and published in *Nuovo Cimento*.[21]

2. COUNTER SETS

Two vertical sections of the whole set of counters, lead plates, and iron absorber are shown in Figs. 1(a) and 1(b). Our arrangement is similar to that of Montgomery and collaborators from which it differs in the number of coincidence branches (3 instead of 2), and in the counter-set for anti-coincidence marked in Fig. 1 with a letter *A*. This set, which is formed by an unusual number of counters, is able to reach a rather large intensity (about 40 times greater than that of Rasetti).

The first and second set of counters define a solid angle to which belong all mesons stopped by the iron absorber in which they disintegrate. The third set detects the disintegration electrons, since its pulses are registered only if in delayed coincidence with the first two sets. Finally the fourth set of counters, i.e., the anti-coincidence, has as its purpose the cancellation of registration of the delayed coincidences between the first three sets of counters which are accompanied by a particle crossing the fourth set. Between the first and the second set of counters (each set consisting of 6 counters of 4×25 cm^2 area connected in parallel) were placed about 15 cm of lead in order both to absorb almost completely the soft component and to get the energy interval of mesons stopped in iron in a suitable region of the differential mesonic spectrum. In fact it is known that at the sea level the spectrum of the hard component, owing to the disintegration of mesons in air, has a very low intensity for the first few centimeters of lead.[22] To the 15 cm of Pb we had to add about 150 g/cm^2 because of the 3 floors above our equipment.

The third set of counters is composed of 6

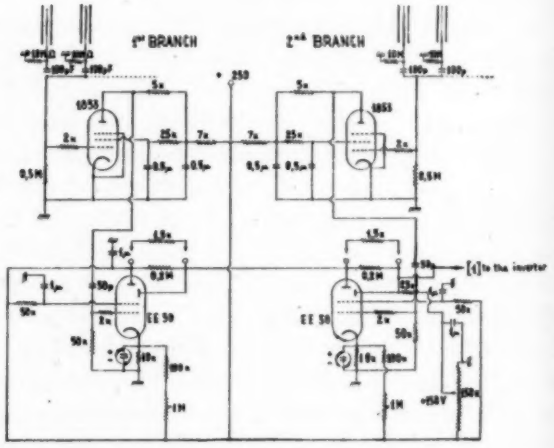

FIG. 3. Input amplifiers (first and second branches) and *CS* (1–2).

[21] M. Conversi and O. Piccioni, Nuovo Cimento **2**, 40 (1944).

[22] Bruins, Proc. Roy. Soc. Amsterdam **17**, 672 (1939); Cocconi, Ricerca Scient. **11**, 58 (1940).

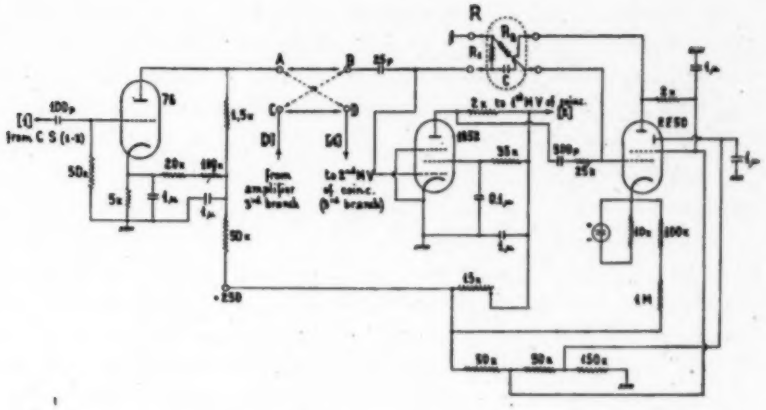

FIG. 4. Inverter and delaying multivibrator.

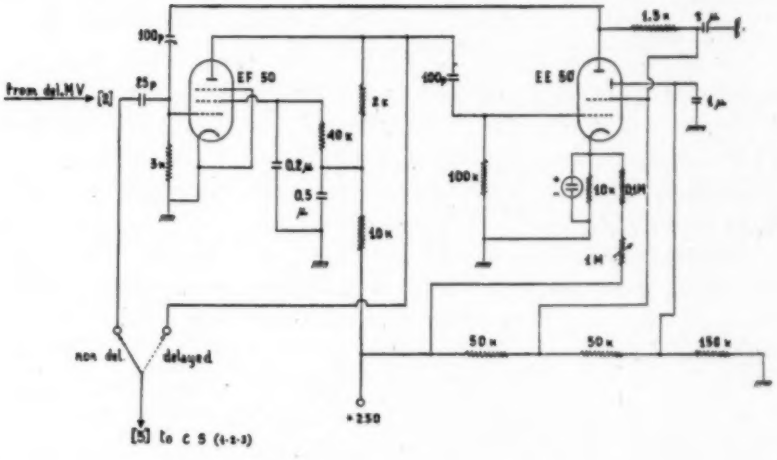

FIG. 5. First coincidence multivibrator.

counters of 4×40 cm^2 area. The absorber formed by an iron plate 5 cm thick could be inserted between the second and the third set of counters. The mesons stopped in iron decay giving electrons which, if emitted in proper direction, hit a counter of the third set.

All counters marked by *A* in Fig. 1(a) and (b) (29 counters 4×40 cm^2 area) belong to the fourth set, which we shall call *anti-coincidence*. Such a set, arranged to cover as completely as possible the solid angle defined by the first two sets of counters, was connected with the fourfold coincidence circuit; the intensity of the last, subtracted from the threefold coincidence intensity, allowed us to eliminate the spurious coincidences due to one or more particles of which one at least had crossed the fourth set and so reduced considerably the amount of spurious coincidences registered. Geometric reasons are mainly responsible for the anti-coincidence loss (see Section 5).

Just under the third set there is a lead plate 1 cm thick, where the decay electrons which have crossed the third set are stopped, so that they cannot reach the fourth set.

The lead plates placed on the sides of the second and the third set (Fig. 1(a), (b)) are 5 cm thick and protect these counters from the showers. For the same reason, the horizontal surface of the first lead plate 5 cm thick placed between the first and second set has been made about 45×45 cm^2 instead of 25×25 cm^2 as it was necessary to cover the solid angle formed by the first two sets of counters.

All counters are of metallic type filled with the Trost-mixture; the walls are of brass 1 mm thick. The counters of each set were connected as shown in Figs. 3, 6, and 8. This arrangement is particularly useful for sets of many counters, for it avoids in each counter all the voltage variations due to pulses in the other counters. Taking into account the time length ($\sim10^{-3}$ sec.) of each pulse and their large number, it is easy to recog-

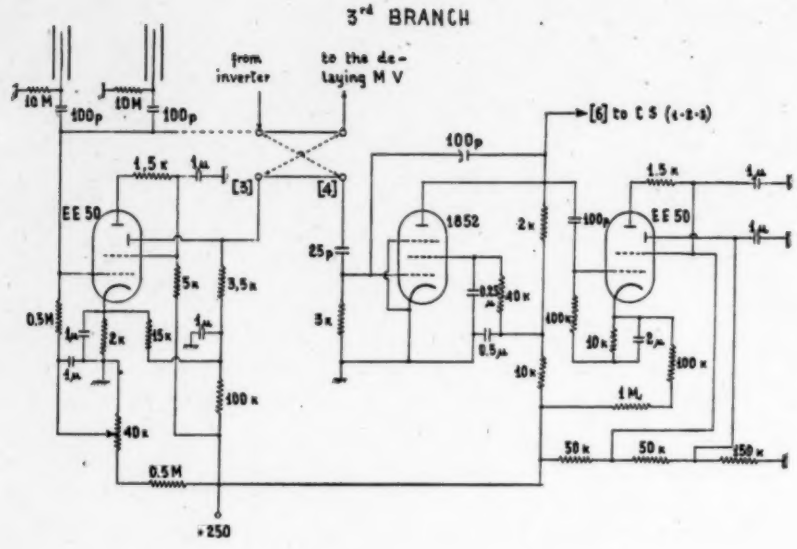

FIG. 6. Input amplifier (third branch) and second coincidence multivibrator.

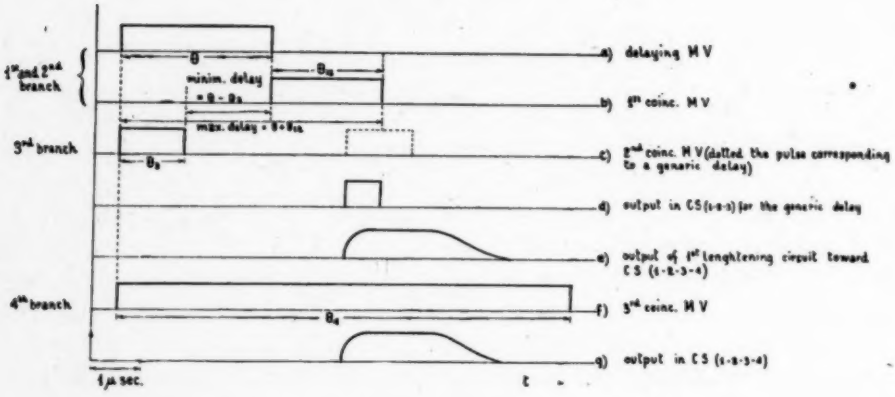
1st and 2nd branch
minim. delay
3rd branch
4th branch
a) delaying M V
b) 1st coinc. M V
c) 2nd coinc. M V (dotted the pulse corresponding to a generic delay)
d) output in CS (1-2-3) for the generic delay
e) output of 1st lengthening circuit toward CS (1-2-3-4)
f) 3rd coinc. M V
g) output in CS (1-2-3-4)
1 μ sec.
t

FIG. 7. Schematic diagram showing the time distribution of pulses.

nize that with a direct connection each counter would work for an appreciable fraction of time with a voltage lower than normal. The voltage on the counters was supplied by a vacuum tube stabilizer.

For the first three sets of counters a working voltage was chosen such that the sizes of the pulses was 25 volt ±10 percent. For the fourth set the size of the pulses was 35 volt ±10 percent. This has been done mainly to compensate for the reduction of the size of the pulses due to the remarkable capacity of the fourth set.

3. REGISTER SET

A block diagram of the registering set is given in Fig. 2. The more important circuit details are shown in Figs. 3–6 and 8.

The pulses of the first two branches, through an amplifying stage, enter *CS*(1–2) which is, as *CS*(1–2–3) and *CS*(1–2–3–4), a twofold coincidence circuit of the type "series" (see Fig. 3).[23] At the output of *CS* we have a positive pulse (we get it from the secondary emission electrode)

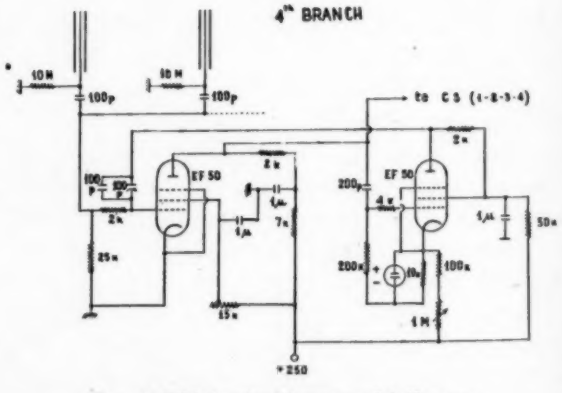

FIG. 8. Third coincidence multivibrator.

[23] Piccioni, Nuovo Cimento **1**, 56 (1943).

which has to be reversed before being sent, through the AB connection, to the delaying multivibrator (MV) or to the second coincidence MV if we connect A with D.

As is known, a multivibrator is a circuit of two tubes the plates of each of which are connected by capacity to the grid of the other tube. This circuit, with proper bias, gives relaxation oscillations. However, one may adjust the bias such that the MV does not oscillate permanently, but gives only an oscillation when excited by a driving pulse. We obtain in this way a driven multivibrator; the time length and the shape of its oscillations are independent, within wide limits, of the form of the driving pulse.[24]

When a negative pulse comes in B, the delaying circuit gives a positive pulse of rectangular shape, the time length θ[25] of which depends on the values of the resistences R_1, R_2 and of the capacity C (Fig. 4); R_1, R_2 and C form an easily interchangeable element R.

The first coincidence MV (Fig. 5) as for all our MV is sensitive only to negative pulses. The pulse of the delaying MV is positive and reaches the first coincidence MV by means of a low value RC coupling. Therefore, the first MV coincidence starts immediately at the sudden decrease of the delay $-MV$ pulse, i.e., at the end of its positive pulse. The coupling condenser between the grid of EF50 and the plate of EE50 is a variable one (of the type of compensating condenser used in the normal radio sets) and allows one to adjust the time length θ_{12} of the pulse of the MV coincidence.

The behavior of all these circuits was frequently checked during the experiments by observations performed with a synchronized oscillograph (see Section 4).

One of the two CS(1–2–3) tubes is connected with the output of the second coincidence MV; the other one can be connected either with the output E of the delaying MV (*non-delayed coincidences arrangement*) or with the output E of the first coincidence MV (*delayed coincidences arrangement*).

Thus at the first tube of CS(1–2–3) the θ pulse or the θ_{12} pulse arrives; while at the second tube of CS(1–2–3), the θ_3 pulse of the second coincidence MV arrives. This is for *normal delay*. For *inverted delays* connections are shown in Fig. 2.

In the amplifying stage of the third branch, we used a secondary emission tube (EE50) so that the output pulse at the secondary cathode (Fig. 6) has the same sign as the input pulse. This pulse can be sent either to the second coincidence MV connecting C with D (when A is connected with B) or to the delaying MV when C is connected with B. In the first case, the *delay* is *normal;* in the second, it is *inverted*. In both cases the pulse which reaches D drives the second coincidence MV, the pulse of which has the same shape as the one of the first MV and a time length θ_3.

The coincidence pulse at the CS(1–2–3) output has to be sent through a circuit (first lengthening-circuit, see Fig. 2) which may increase its time length to the counting circuit of the threefold coincidences and, at the same time, to CS(1–2–3–4). At the other, input of the last circuit is supplied the pulse of the third coincidence MV (4th branch); we shall call θ_4 the time length of this pulse; θ_4 is large enough (see Fig. 7) to assure that the pulses θ_{12}, θ_3 are in coincidence with θ_4 between large limits. This MV for simplicity is driven by the counters (Fig. 8). The fourfold coincidence pulse at the CS(1–2–3–4) output has to be sent to the circuit for fourfold coincidence numeration through a second lengthening circuit.

Figure 7 shows the mutual disposition, with respect to the time, of the pulses in the different circuit stage under the assumption of four contemporary pulses at the four branches input and considering the delays introduced by the branches themselves equal to zero or all equal.

In Fig. 7 it is clearly shown that the third branch-pulse must delay from a minimum of $\theta-\theta_3$ to a maximum of $\theta+\theta_{12}$ in order to give a threefold coincidence. Therefore, our set registers the portion of the decay-curve corresponding to a time interval of $\theta_{12}+\theta_3$, starting from the time $\theta-\theta_3$: we must expect that varying θ the number of the delayed coincidences due to delay electrons will follow an exponential curve.

The assumption in Fig. 7, that the delays introduced by the different branches are all equal, cannot be considered strictly true. In fact the delay introduced by one branch depends on several parameters (stray-capacity, inter-elec-

[24] Conversi and Piccioni, Nuovo Cimento 1, 279 (1943).
[25] In general, we mean by θ_i the time length of the pulse.

trode-capacity, sensitivity of the branch, size of the counter pulse). In order to avoid considerable errors introduced by the inequality of the delays (above all on account of possible variation during the long time necessary for the experiment) we proceeded as follows: (a) We arranged the registering set so that the above-mentioned delays were as small as possible. (b) We made the delay circuit so that the delays of the branches were constant for the different interchangeable elements R (Figs. 2 and 4). Thus the difference of the branches introduces a constant delay T (positive or negative) and, therefore, only a multiplying factor $e^{-T/\tau}$ of the intensity. Of course, this does not give any source of error in the value of τ deduced from the experimental curve.

In order to insure that the pulse at the output of a branch has the smallest delay with respect to the pulse of the counter, it is necessary to introduce between the counter and the grid of the coincidence tube an amplifying stage which increases the amplitude and shortens the time length of the pulses. Now the above-mentioned delays depend mainly on plate circuits of this amplifying stage. These circuits, in fact, consist of a load resistance R in parallel with a capacity C with respect to the ground given by the various electrodes and the connecting wires. The delay given by the circuit is of the order of RC, the time constant of the circuit. For a normal tube we cannot make R lower than 50 kΩ, and on the other hand, the internal resistance of the tube, in parallel with R, is much higher. Since the value of C can be evaluated to about 20 μf, the value of RC, and, therefore, also of the delay is of the order of 10^{-6} sec. For many stages the resultant delay is, of course, the sum of the delays of each stage. Such a delay is intolerable in measurements of the present type.

As the value of C cannot be reduced appreciably, it is necessary to lower R, and therefore, in order to obtain a properly high amplification SR, it is necessary to use tubes with a high grid-plate transconductance S. For this reason in our experiment, we used tubes such as 1852, EF50, EE50, which allow one to reach amplifications of 10 to 20 with plate resistances of 2 to 3 kΩ. Under these conditions the above-mentioned delays are reduced by more than a factor 10.

Another crucial point in this experiment is that the resolving time of the set must be constant and free from any critical behavior. For such a purpose it is necessary that the size of the circuit pulses be independent, as much as possible, of the amplitude of counter pulses and constant during the experiment. Such a condition is satisfied by using an equalizing circuit as those we made on the MV principle.[24]

In the MV which we place before the coincidence circuits and in the delaying MV (Figs. 4–6, 8), high transconductance tubes were used for obtaining pulses extending over times of the order of a few microseconds and of almost rectangular shape. In addition by using these tubes the delays given by the branches were greatly reduced as above mentioned.

The use of these MV's is necessary but not sufficient to obtain a set with pulses and resolving power exactly defined, as this last condition depends also on the properties of the coincidence circuits—namely, while a Rossi coincidence circuit does not fit the above-mentioned condition on account of his high load resistance, a coincidence circuit of the "series" type[23] does not introduce any undesired delay. This circuit (Fig. 3) is more convenient than the Rossi's type also because the tubes work normally at their cut-off, saving much plate current (which is very useful for a set with many tubes) and allowing the use of capacity-resistance filters in the plate and the screen-grid supply-circuits. In addition the high slope of the tubes (EE50) we used provides that the minimum pulse necessary for the complete control of the plate current is very low (~5 volt), while on account of the normal working condition at the cut-off, it is possible to make any desired "cut" of the driving pulses.

To obtain the zero effect of a branch at the output of the coincidence circuit, a resistance of 1.5 kΩ is introduced, as shown in Fig. 3, between the plate and the secondary electrode of the other tube.

All the insulators bearing wires subject to sharp voltage variations have been made with "frequenta" in order to reduce as much as possible the ground capacity.

The different delays necessary for obtaining the decay curve were introduced by changing the R_1, R_2, C elements (arranged on a "frequenta"

tube socket) forming the element R of the delaying MV (Fig. 4). The contemporary change of the values of both the resistances, and of the condenser C, allows one to keep constant the MV sensitivity and, therefore, to maintain unaltered the delays of the branches.

Low value resistances were introduced at the input of the branches in order to prevent self-oscillations which might appear as a consequence of the considerable amplification extending up to high frequencies. Low value resistances have been inserted also in the grid circuits in other parts of the set in order to reduce the corresponding currents and improve the pulse shape.

As can be seen from the diagrams, the plate feeding was unique; it was stabilized at 250 volts and could be regulated so as to compensate eventual slow variations of the stabilizer (with neon and iron-hydrogen tubes). On the other hand we have checked that variations of the plate potential of 10 percent do not affect in a noticeable way the behavior of the registering set. A small effect instead seems to take place for variations of the heating voltage of the tubes which was therefore stabilized.

In order to avoid the registration of interruptions or unexpected variations of the a.c. supply by the numerical counters, a thyratron "setting off" circuit S (Fig. 2) was introduced; this did not allow the numerator-circuits to act when the line voltage was lower than a fixed value. During the measurements taken throughout the night, a registering ammeter indicated the eventual periods of "set off" and a recording voltmeter registered the voltage variations, allowing in this way a check on the behavior of the "setting-off" circuit.

Using high transconductance amplifiers, multivibrators, and sets of "coincidences in series" we believe we have overcome all the technical difficulties inherent to the present problem.

The delays among the pulses produced by the same particle in different counters had also to be ascertained; more exactly, it was necessary to establish the frequency of these delays with respect to their value. Such delays were investigated by Montgomery and collaborators, who found that their counters (1×20 cm, filled with a mixture of argon 94 percent and oxygen 6 percent, pressure of 18 cm of Hg) had delays of about 2 μsec. with a frequency of 1.5 percent; for higher delays the frequency of the delays decreases reaching a value of about 0.5 percent for a delay of 5 μsec.

Rasetti, on the other hand, obtained full efficiency for twofold coincidences between two counters (one 2×22 cm^2 and the other 2×37 cm^2) in glass and filled with argon (5 cm Hg) and alcohol (1 cm Hg) at a resolving power of 0.5 μsec., which indicates that the above-mentioned delays are less than 0.5 μsec. For our counters (metallic type, 4×40 cm^2, filled with Trost's mixture) we found in a previous work[24] delays of 0.5 μsec. with a frequency of about 4.5 percent, and frequencies much less for delays near 1 μsec.

As it seems that such delays are mostly caused by differences in the steepness of different pulses, we have increased as much as possible the sensitivity of the registering set. The circuits we used kept a good sensitivity up to 10 MHz, so that shielding and, above all, grounding was rather difficult. The experimental conditions we finally attained were very satisfactory in this respect. We also took care to adjust each branch to the same sensitivity with respect to the counter pulses.

4. CALIBRATING SET

In order to have good accuracy in measuring the values of the delays corresponding to the different points of the decay curve, we thought that the best way was to get an oscillographic synchronized figure and to compare on the screen of the cathode-ray tube the unknown time interval with calibrating signal. The latter one was a sinusoidal signal of 1 MHz or 0.5 MHz. The distance between two consecutive crossings of the sinusoid with the zero axis gave therefore 0.5 μsec. and 1 μsec., respectively. The above-mentioned signal was obtained by means of a multiplication stage (checked on the oscillograph) and a quartz oscillator of 100 kHz (Fig. 9).

From the same oscillator, by means of a demultiplication stage, the horizontal deflecting signal was also driven, the frequency of which was 25 or 50 kHz. This signal, at first sinusoidal, was amplified through an aperiodic power stage (using a 6L6 tube) which cut on both sides the signal itself, while the central part was amplified

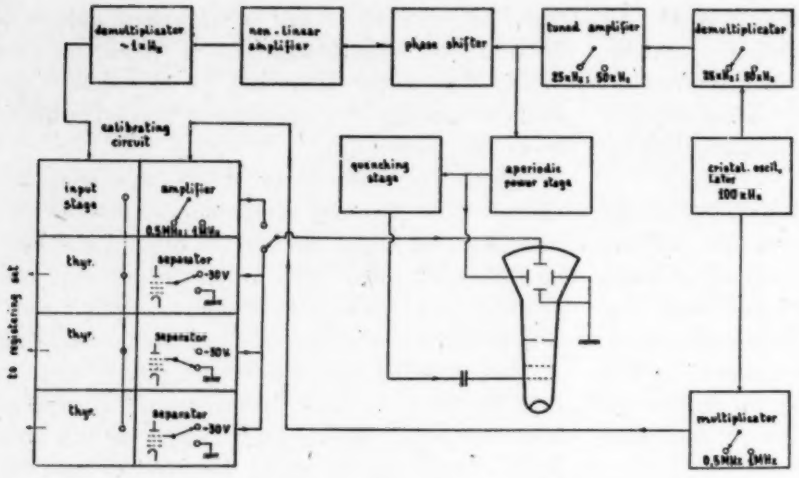

FIG. 9. Block diagram of calibrating set.

almost linearly. We could then obtain about 4 cm per μsec.

A quenching stage acted on the return. The calibration signal and the horizontal deflection, both coming from the same oscillator, were, of course, synchronized one with the other. A pulse generator which produced about 1000 pulses per second was also synchronized with the horizontal deflecting signal. Such a frequency was certainly much larger than the average number per second of the pulses, because of the zero effect of each branch, but since the registration was working with pulses of the order of 1 μsec. the overlapping of the pulses could be neglected. The only effect produced by the high frequency of the pulses was a change in the bias of those tubes which were working at cut-off with a resistance on the cathode. For the delaying MV such a variation was lower than 0.5 volt; but we have repeatedly verified the fact that a variation of 1 volt did not change at all the shape of the pulses.

In order to observe the pulses at the output of the calibrating set or at the registering stages, it is convenient to keep the pulse at the center of the oscillographic horizontal deflection. For such a purpose we used a circuit that we shall call "phase shifter," drawn from a plan given in the *Philips Technical Review*. It gave a phase-shift which could be regulated up to a maximum of about 180° with a rather constant amplitude.

The centered pulses, with a frequency of 1 MHz, were sent to a calibrating circuit consisting of three thyratrons (Fig. 10) which produced three pulses synchronized with the input pulse, but having a phase-shift among them which could be changed between 0 and 10 μsec.

The phase-shift was obtained by impressing on the grid of a 6J7 tube a pulse, driven by the above-mentioned generator, having a rising time of about 10 μsec. and by varying the thyratron bias. In this way the three pulses could be phase-shifted one with respect to the other by an amount less than 10 μsec. A minimum change of about 0.01 μsec. could be obtained.

The system has been so constructed that the ground capacity of the anode circuits of the thyratrons was as small as possible. In order to be certain that this capacity did not change during the oscillographic observations (the variation would have changed the pulse while observed) the plates of each thyratron were permanently connected through a small capacity to the grid of a 6J7 (acting then as separator tube) and the three plates of the 6J7 were connected together (Fig. 11). The passage from one to the other tube, necessary to observe one pulse or the other, was obtained by applying or not applying a high negative voltage (-30 volt) to the suppresser-grid of the 6J7's.

The calibrator allowed one to change the pulse amplitude by changing the thyratron anodic-voltage; by automatic adjustment of its cathode-bias at the same time, it was possible to maintain the pulse phase roughly constant.

The circuit proved good, especially for maintaining a constant phase of the thyratron pulses; as a matter of fact, no rippling appeared in a

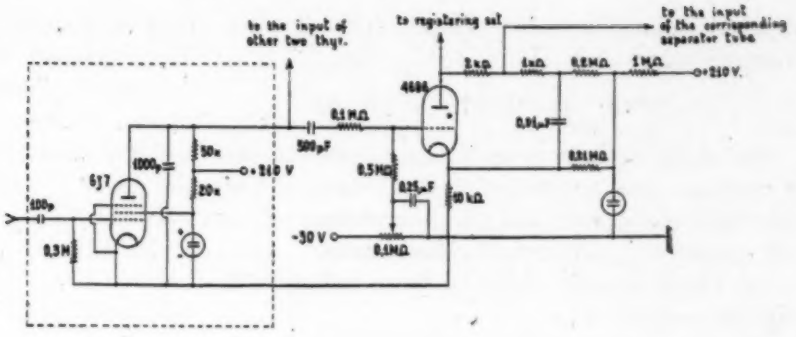

FIG. 10. Calibration circuit.

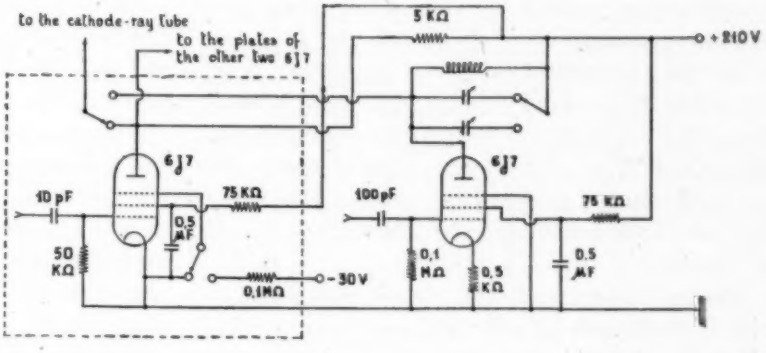

FIG. 11. Separator tube (three identical stages) and amplifier of the 0.5–1.0 MHz signal.

figure in which 1 μsec. corresponded to about 4 cm if a. c. supply did not change greatly.

The measurements of the various delays were made by marking successively over a Cellophane strip pressed against the oscillographic tube screen, the crossing points of the calibration sine wave with the zero axis and the starting point of the pulses. Normally only two branches of the calibrator were used: one connected with the first branch, the other with the third branch of the registering set, while the second and the fourth branches were short-circuited (see Section 3). Since the pulse given by a thyratron cannot be considered equal to that of a counter with respect to the steepness of the slope, the measurement did not give the absolute value of the delay but only the differences between the various delays. This is indeed what matters for the determination of the mean life.

5. CHECKS AND COMPUTATION OF RANDOM COINCIDENCES

On account of the low counting rate, it was necessary to check very frequently the proper behavior of the registering set. The more important measurements that we have repeated periodically are the following:

(a) Counting of the zero effects of the several counter sets. They were made (not very often) by means of a scale-of-16. The frequencies S^1, S^2, S^3, S^4 of the first, second, third, fourth set (pulses/min.) were as follows:

$$S^1=3300;\quad S^2=1540;\quad S^3=2350;\quad S^4=20{,}000.$$

For the fourth set the given value (obtained by means of two scales-of-16 in series) is approximate, because the first stage of the scale circuit missed some pulses.

(b) Check of transmission of a branch, i.e., it was ascertained that the counting rates at the input and output of each branch were equal one to the other.

(c) Measure of the twofold undelayed coincidences D_{12} between the first and the second set and of the threefold coincidences T_{123} among the first three sets. The average was:

$$D_{12}=7600/\text{hour};\quad T_{123}=5.000/\text{hour}.$$

(d) Measure of the efficiences:

$$\rho_1=Q/T_{123};\quad \rho_2=T_{124}/D_{12};\quad \rho_3=D_{34}/S_3,$$

where Q represents the intensity of the undelayed fourfold coincidences. Counting the un-

delayed coincidences we found the following average values:

$$\rho_1=0.948;\quad \rho_2=0.932;\quad \rho_3=0.240.$$

For these measurements we used two scale-of-8 counters, one connected to the output of the fourfold coincidences and the other connected to the output of the threefold coincidences.

(e) Oscillographic check of the amplitude of counter pulses.

(f) Measurements of the twofold delayed (with a great delay) coincidences C_d of one of the first two sets (connected with one of the first two registering branches) with the fourth set (connected with the third branch). The third branch, less sensitive than the fourth, transmitted only about the 75 percent of the pulses of the fourth set on account of the low peak value of the pulses, because of the great capacity (29 counters) of the set itself.

During these measurements we used to short-circuit the fourth branch: in this way we checked also the lengthening circuits, verifying the identity of the number of the pulses registered by the two numerator circuits.

The average was (with no great precision): $C_d=140$/hour.

(g) Determination (by means of the above-mentioned calibrator) of the times θ_{12}, θ_3, θ_4 of the three MV pulses; of the delays θ corresponding to the various elements R; and of the double of the resolving power of $CS(1\text{–}2\text{–}3)$. We found:

$$\theta_{12}=1.2\ \mu\text{sec.};\quad \theta_3=1.3\ \mu\text{sec.};\quad \theta_4=9.0\ \mu\text{sec.}$$

The double of the resolving time of $CS(1\text{–}2\text{–}3)$ was about 3 μsec.

(h) Check (made by taking away the voltage of the counters of one set) of the absence both of inductions among the registering branches and of external disturbances.

(i) Measurements of the intensity of the delayed coincidences with small delays. These coincidences are mainly caused by fluctuation in the steepness of the counter pulses (random delay coincidences): their intensity as a function of the delay time (that is, for the several values chosen for the elements R) is represented in Fig. 12, from which we can appreciate the variations of the absolute delay corresponding to a particular element, for instance R_{-1}, by the variation of the frequency registered with the same element R_{-1}. The variation of the absolute delay may be caused by a change in the amplitude of the pulses of the counters, as we have really verified by making measurements with different voltages on the third set of counters. The value of such variations was about 0.1 μsec. for a variation of about 30 percent in the pulse amplitude, while it became inappreciable for simultaneous voltage variation in all the counter sets. Though this shift had an equal repercussion on all the delays and did not alter the τ determination obtained by regularly alternated measurements, we checked, at least once a day, the delayed coincidence frequency with respect to the element R_{-1}.

This measurement was a critical check of the behavior of our registering set and in particular of the counters. The curve obtained with small delays is shown in Fig. 12; the small circles give counting rates corresponding to the different elements R. The curve was obtained several times during the experiment.

The threefold delayed coincidence frequency can be attributed not only to the disintegration electrons (the intensity of which we shall indicate with M) but also:

(1) To the random delay coincidences r due to the same particle which crosses the first three counter sets, giving three pulses conveniently shifted one with respect to the other. Part of them, $\rho_1 r$, are quadruple coincidences, where ρ_1 is the same efficiency Q/T_{123} which is measured for the undelayed coincidences.

(2) To the pure coincidences c due either to two particles one of which crosses the first two sets of counters and the other crosses the third with suitable disposition in time, or to three particles.

One can easily see that of the triple coincidences c, the fraction $(1-p_2p_3)c$ is caused by quadruple coincidences, where p_i are the losses corresponding to the efficiencies ρ_i, i.e.,

$$p_1=1-Q/T_{123};\quad p_2=1-T_{124}/D_{12};\quad p_3=1-D_{34}/S_3.$$

Considering that the lead plate 1 cm thick beneath the third counter set absorbs all the disintegration electrons (as can be seen from the identity of the quadruple intensity with and without absorber), we can write:

$$\text{III}=M+r+c;\quad \text{IV}=(1-p_1)r+(1-p_2p_3)c$$

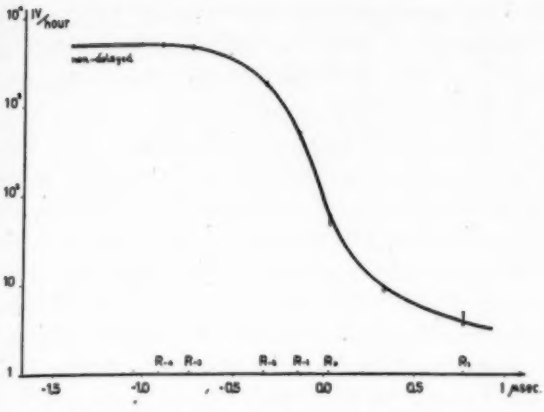

FIG. 12. Fourfold coincidence rates at small delays.

and since with our particular counter arrangement we found from the measurements: $p_1 \cong p_2 p_3 = 0.052$, we have

$$\Delta = \text{III} - \text{IV} = M + p_1(r+c) = M + \frac{p_1}{1-p_1}\text{IV}.$$

If, for convenience, we put $p = p_1/(1-p_1)$, we obtain: $M = \Delta - p\text{IV}$.

This evaluation of the random coincidences is to be preferred to that obtained from the measurements without iron, because of the smaller statistical error. In fact it should be noticed that p, which can be deduced from the measurements without delay, is known with a precision much greater than that corresponding to Δ and to IV, so that one can write

$$\pm(M)^{\frac{1}{2}} = \pm(\Delta)^{\frac{1}{2}} \pm p(\text{IV})^{\frac{1}{2}} = \pm(\Delta + p^2\text{IV})^{\frac{1}{2}},$$

but since $\Delta > p\text{IV}$ and $p = 0.055$, we can at once allow the error on M to be equal to the error on Δ.

Then

$$M = \Delta - p\text{IV} \pm (\Delta)^{\frac{1}{2}}.$$

6. DISCUSSION OF RESULTS

Figure 13 taken from the data given in the sixth columns of Tables I and III, shows the comparison between the results of the "normal" and the "inverted" measurements. The zeros of the time axis are not thought coincident for both curves, because the delays are presumed to vary from one to the other of the two groups of measurements.

However, such a variation is surely not greater than some tenths of μsec.

Figure 13 gives a rather reliable proof of the real existence of the disintegration of mesons.

The measurements for determining τ have been divided into five series corresponding to five successive periods[28] of work, during each of which the counter voltages had undergone negligible changes. The results are reproduced in Table II. Then the five series were put together, all referred to the delays of the third, i.e., introducing a correction in order to consider the small differences among the delays of the various series and those of the third. This has been evaluated by assuming an exponential decay of 2.2-μsec. mean life, as suggested by a first plot of the results.

We have considered also the small shift indicated by the intensities of the quadruple coincidences (IV) observed with R_{-1} element, which can be caused by small variations in the working conditions of the counters.

Both these intensities and the values of the losses p have been obtained as an average of the measurements made during each series.

The delay of the element R_2 has been assumed arbitrarily equal to zero, for its value—measured with the calibrating set—remained more constant than that of the other delaying-elements.

Also the R_{-1} delaying-element changed so little that we considered it as constant through all the series.

The errors in the delays have been evaluated both by considering the precision of the applied method and by repeating the measurements many times; the given values (Table II), 0.05 μsec. for the element R_1, R_2, R_3, and 0.1 μsec. for R_4, are mean square errors. They have been transformed into errors in M and combined with the statistical error always assuming an exponential slope with a mean life of 2.2 μsec. The corresponding variations of the delayed coincidence intensity is ± 2.3 percent for a change in the delay of ± 0.05 μsec.

A summary of the results of the five series of measurements is given in Table III and plotted in Fig. 14 on a semi-logarithmic scale.

The four points taken from the results of the

[28] At the end of the first series (September, 1943) we have been forced to stop our work for about two months. The consistency among the results of this and the successive series is however satisfactory. We want to thank Doctor C. Festa for the help she gave us in accomplishing the first series of measurements.

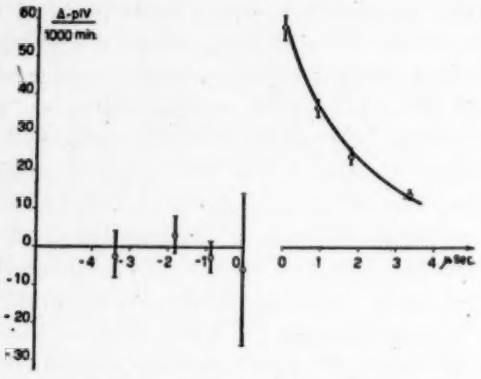

FIG. 13. Comparison between *normal* (right) and *inverted* (left) measurements (with absorber).

measurements made with the Fe absorber lie along a straight line proving in a satisfactory way the exponential shape of the decay-curve.

With the method of least squares we get for τ, using the measurements with iron absorber, a mean value 2.33 μsec. and the extreme values 2.19 and 2.50; therefore, we conclude

$$\tau = 2.33\ \mu\text{sec.} \pm 6.5\ \text{percent.}$$

Table III gives also the results of the measurements made without iron absorber, which also are plotted in Fig. 14. It is clear that also in these conditions a small fraction of the decay electrons is present. If one takes into account the considerable errors of the points corresponding to these measurements, we find the same decay coefficient as obtained in the measurements with absorber. Also for this reason we thought it more convenient to evaluate the random coincidences by the product pIV than by the measurements without absorber.

It should be noted however that even without any correction, the results of the measurements with Fe (normal delay) would have nearly the same shape as that shown in Fig. 14, since the corrections and the random coincidences amount to but a small fraction of the effect.

The decay electrons, which appear in the measurements without Fe, are probably generated in the counter walls of the second and third set, and in the lead between the third and the fourth set.

In this last case, however, a considerable geometric limitation is imposed by the presence of the lateral anti-coincidence counters and by the long recovery-time of counters (10^{-3} sec.) which requires that the decay electron hit a counter of the third set different from the one crossed by the primary meson.

A comparison between our results and the value of the ratio $\tau/\mu c^2$ obtained from the most recent differential experiments[2–14] on anomalous absorption is of interest.

Since there are reasons to think that the value given by Nielsen, Rierson, Nordheim, and Morgan is too small we shall consider only the results of Rossi and Hall[7] and those of Bernardini, Cacciapuoti, Pancini, and Piccioni.[10] According to these measurements, as pointed out by Bernardini,[14] the most reliable value of $\tau/\mu c^2$ is $3.0 \pm 0.3 \times 10^{-8}$ sec./Mev.

Referring to this value, our determination of τ gives for the rest-energy of mesons a value be-

TABLE I. Inverted measures.

	Delay (μsec.)	With absorber III	IV	Min.	Δ−pIV / 1000′	Without absorber III	IV	Min.	Δ−pIV / 1000′
R_1	0.00	1002	952	318	−6.0±20	245	232	120	8.5±30
R_2	−0.91	83	80	493	−3.0±4	24	22	170	5.0±8
R_3	−1.81	35	32	370	3.0±5	39	35	413	5.0±5
R_4	−3.34	26	266	510	−2.5±/	18	17	319	0.0±2

TABLE II. Data corresponding to the five series of normal measurements with absorber (5 cm Fe).

	Series	Delay* (μsec.)	III	IV	Min.	Reduc. min.	p(%)	(Δ−pIV)/60′
R_1	1	−1.00	273	179	1430	1468	4.9	3.47±0.4
	2(a)	−1.08	218	154	490	561	4.7	3.60±0.5
	2(b)				360	388		
	3	−0.91	156	104	840	840	6.1	3.34±0.5
	4	−0.90	195	122	1116	1080	5.8	3.65±0.5
	5	−0.82	367	279	1324	1240	5.7	3.49±0.55
R_2	1	0.00	100	30	1725	1700	4.9	2.42±0.3
	2(a)	0.00	44	14	715	755	4.7	2.08±0.4
	2(b)				90	90		
	3	0.00	68	31	1179	1179	6.1	1.80±0.3
	4	0.00	122	50	1846	1798	5.8	2.30±0.3
	5	0.00	130	50	1864	1815	5.7	2.55±0.3
R_3**	3	0.97	69	21	2240	2240	6.1	1.26±0.2
	4	0.98	147	37	4072	3940	5.8	1.64±0.15
	5	0.93	121	50	3015	2988	5.7	1.37±0.2
R_4	1	2.80	39	14	1933	1703	4.9	0.86±0.17
	2(a)	2.58	35	14	1002	990	4.7	0.79±0.18
	2(b)		89		550	550		
	3	2.43		34	3921	3921	6.1	0.82±0.12
	4	2.47	133	47	6777	6500	5.8	0.77±0.085
	5	2.51	203	85	7777	7316	5.7	0.93±0.10
R_{-1}	1	−1.70			578 IV/hour			
	2(a)	−1.73			1370 IV/hour			
	2(b)				735 IV/hour			
	3	−1.70			678 IV/hour			
	4	−1.73			473 IV/hour			
	5	−1.71			478 IV/hour			

* The delays of the first series have been obtained by means of an oscillographic method, less exact than the one described in this paper.
** The delay R_3 has been introduced at the end of the second series.

tween 60 and 90 Mev; i.e., the meson mass would be about 150 electronic masses, in agreement with the mean value of the more reliable direct measurements of the meson mass, as far as we know.[27] The value of the meson mass as calculated from a weighted average of results of various authors[28–35] is, in fact, 170±20. In addition the agreement between the values of $\tau/\mu c^2$ calculated (1) from our measure of τ and from those of mass as above mentioned and (2) from the differential experiments on anomalous absorption, would suggest that the assumption on which the $\tau/\mu c^2$ calculations are based in these last experiments are reliable. In particular it would result that the hard component of cosmic rays, as observed in the lowest part of the atmosphere, is mainly formed by mesons originating more than 4000 meters above sea level, and all unstable with the same mean life.

However, our results, considered alone, cannot eliminate the assumption, recently advanced,[36] of a complex nature of the hard component, since the decay curve which we have obtained (with iron and normal delay) does not exclude the existence of mesons having, for instance, two different mean lives mixed in a suitable percentage. However this assumption does not agree with results of other experiments.[13–37]

TABLE III. Definitive results of normal measures.

		With absorber				Without absorber			
	Delay (μsec.)	III	IV	Reduc. min.	$M/60'$	III	IV	Reduc. min.	$M/60'$
R_1	−0.91	1209	838	5577	3.50±0.22	588	529	2741	0.66±0.18
R_2	0.00	464	175	7337	2.22±0.15	98	74	3133	0.38±0.09
R_3	0.97	335	106	9346	1.43±0.10	20	12	1166	0.38±0.15
R_4	2.43	499	194	20980	0.84±0.06	37	27	3322	0.15±0.06

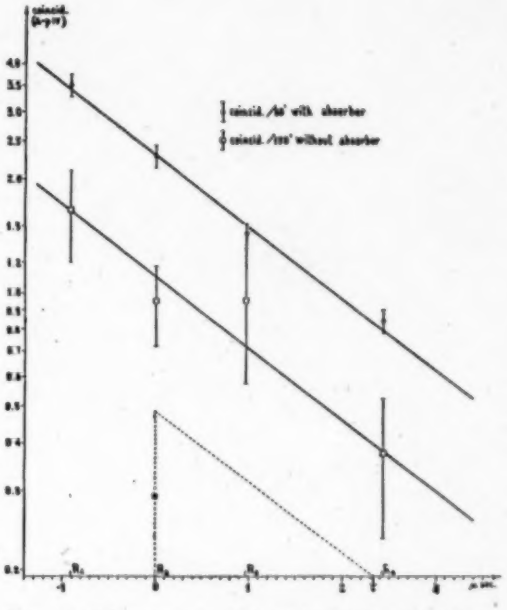

FIG. 14. Decay curve with and without absorber.

The authors take pleasure in thanking Professor G. Bernardini for many helpful discussions and Professors E. Amaldi and G. C. Wick for their advice and encouragement throughout the progress of this work. A fund for researches on nuclear physics was granted by the "Consiglio Nazionale delle Ricerche."

[27] We have not received foreign publications since 1940.
[28] Street and Stevenson, Phys. Rev. **52**, 1003 (1937).
[29] Nishina, Takeuchi, and Ichimiya, Phys. Rev. **52**, 1198 (1937).
[30] Merle A. Starr, Phys. Rev. **53**, 10 (1938).
[31] Ruhling and Crane, Phys. Rev. **53**, 266 (1938).
[32] Corson and Brode, Phys. Rev. **53**, 773 (1938).
[33] Williams and Pikup, Nature **141**, 684 (1938).
[34] J. G. Wilson, Proc. Roy. Soc. **172**, 522 (1939).
[35] Nishina, Phys. Rev. **55**, 585 (1939).
[36] Juilfs, Naturwiss. **30**, 584 (1942).
[37] Bernardini, Conversi, Pancini, Scrocco, and Wick, Phys. Rev. **68**, 109 (1945).

PHYSICAL REVIEW VOLUME 70, NUMBERS 11 AND 12 DECEMBER 1 AND 15, 1946

On the Disintegration of Slow Mesons

M. CONVERSI AND O. PICCIONI †
Istituto di Fisica della R. Università di Roma
Centro di Fisica Nucleare del Consiglio Nazionale delle Richerche, Italia
(Received October 15, 1945) *

With the same experimental device used in a previous work for a direct determination of the mean life of slow mesons, we have performed some measurements designed to give indications about the disintegration process of the mesons stopped in an iron plate. In agreement with the theoretical predictions of Tomonaga and Araki we found that only about one-half of the ionizing particles that compose the hard component of the cosmic rays and that are absorbed in an iron plate, undergo, in effect, the disintegration process. From the same experimental results, one deduces that the mean range of the decay-electrons is about 2.5 cm of iron, with a probable precision of 20 percent.

1. INTRODUCTION

IN a previous paper[1] we reported a direct measurement of the value of the mean life τ of the disintegration process of the mesons stopped in an iron plate, with the following result:

$$\tau = 2.33\ \mu\text{sec.} \pm 6.5 \text{ percent.}$$

Later we decided to perform some measurements with the same experimental arrangement in order to find out what percentage of the particles forming the hard component of the cosmic rays and absorbed by a plate of a heavy substance (iron) actually undergo the disintegration process. From Tomonaga and Araki's[2] calculations it follows that the probability that a meson interacts with the nuclei of the substance penetrated depends not only upon the thickness of the substance and upon the energy of the meson, but also upon the sign of its charge. In fact, on account of the Coulombian repulsion, positive mesons would have such a small probability of being captured by the nucleus that this could be neglected in comparison with the probability of decay. On the contrary for negative mesons of low energy the probability of capture would be much greater than that of decay. Consequently, among the mesons absorbed in a heavy substance, only the positive mesons could practically disintegrate, each producing one electron and one neutrino.

Measurements designed to check these theoretical conclusions have already been taken by Rasetti[3] and, independently, by Auger, Maze, and Chaminade,[4] who measured, by a different technique, the delayed coincidence in several groups of counters. The results obtained by these authors are contradictory: Rasetti found in agreement with Tomonaga and Araki's calculations that only about one-half of the stopped mesons disintegrate. Auger and collaborators, on the contrary, found that all the mesons undergo the disintegration process; unfortunately we have only a short report on the work of these last authors, which does not contain exact and sufficient details about the experimental method.[5] Moreover, Rasetti implicitly assumes in his work that the differences between the proper delays introduced by the various branches of the registering device can be neglected, while the error which is thus introduced cannot be neglected *a priori*, especially for a registering set which does not have small time constants. As a matter of fact, in order to determine the ratio $\eta = M/A$ between the number M of mesons which disintegrate and those A which are stopped in the absorber, it is necessary to know the

† At the present Visiting Research Associate at Massachusetts Institute of Technology, Cambridge, Massachusetts.

* The manuscript of the present paper was prepared in 1944. At that time no information was available in Italy on the experiment on the disintegration of mesons carried out by N. Nereson and B. Rossi (Phys. Rev. **64**, 199 (1943)). On account of wartime conditions the manuscript did not reach the Editor of *The Physical Review* until October 15, 1945.

[1] M. Conversi and O. Piccioni, Nuovo Cimento **II**, 40 (1944); M. Conversi and O. Piccioni, Phys. Rev. **70**, 859 (1946).

[2] S. Tomonaga and G. Araki, Phys. Rev. **58**, 90 (1940).

[3] F. Rasetti, Phys. Rev. **60**, 198 (1941).

[4] Auger, Maze, and Chaminade, Comptes rendus **213**, 381 (1941).

[5] Unfortunately in recent years we received only a few scientific papers.

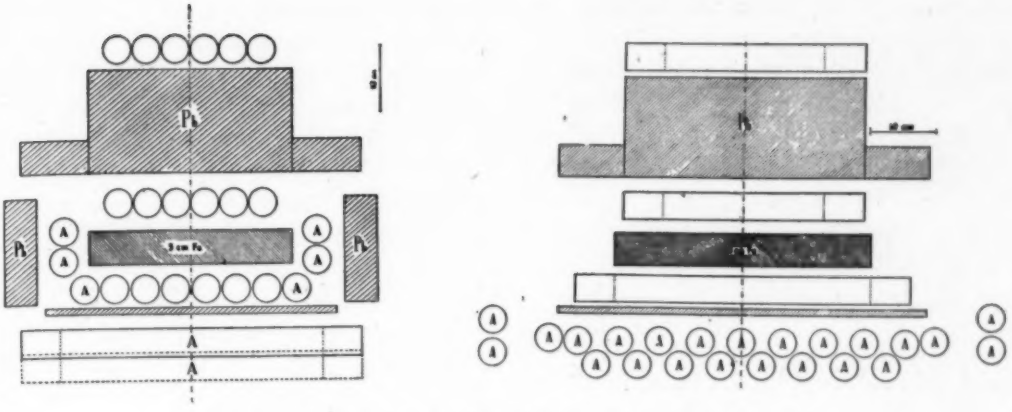

FIG. 1a and 1b. Vertical sections of the whole set of counters.

absolute delay, that is, the sum of the introduced delay and the algebraical difference between the proper delays of the branches of the registering set. In the present work, we have been able to evaluate the absolute delay (see Section 2) so that the error affecting the ratio depends essentially upon the statistical errors affecting M and A. Our measurements, moreover, allow one to obtain an indication about the value of the mean range of the disintegration electrons in the iron.

For a complete description of the experimental arrangement used in this work, we refer to the earlier work on the direct measurement of the mean life of the meson.[1] Here we give only a general description of the counter system and the registering apparatus. The experiment was carried out in Rome, in a classroom of the R. Liceo Virgilio.

2. THE EXPERIMENTAL ARRANGEMENT—EVALUATION OF ABSOLUTE DELAY

Figure 1 shows, in a vertical section, the disposition of the counters, the lead screens, and the iron absorber. The geometry of our arrangement is indicated by Fig. 1. The 15-cm thick lead layer, interposed between the first and second group of counters, absorbs practically all the soft component and allows at the same time the use of a convenient energy interval of the differential spectrum of mesons.[6,7] In addition to the 15-cm Pb, we must take into account about 150 g/cm of Ca, corresponding to the three floors of the building over the experimental device. The third group of counters reveals the disintegration electrons, since their pulses are normally registered only if they are in delayed coincidence with those of the two first groups. The fourth group of counters, covering as well as possible the solid angle defined by the two first sets, is connected to the circuit of the quadruple coincidences; subtracting the number of the quadruple coincidences from that of the triple coincidences, thus we eliminate the random coincidences due to one or more particles of which at least one crosses the fourth group of counters.

With such a procedure the number of the registered random coincidences is strongly reduced.

The counters of the fourth group are marked in Fig. 1, with the letter A. The Pb plate 1-cm thick, placed immediately underneath the third group, is designed to stop the disintegration electrons which have crossed one of the counters of the same group: a triple coincidence not followed by a quadruple one corresponds to the delayed emission of an electron.

The other lead blocks are designed to protect the counters from the showers. For a complete description of the registering device see our former paper[1]; here we give only the disposition of the different parts (Fig. 2) and a short description of their operation.

The pulses, at the input of the two first branches, amplified through the two input stages, coincide in CS (1–2), which like CS (1–2–3) and

[6] Bruins, Proc. Roy. Soc. Amsterdam **17**, 672 (1939).
[7] Cocconi, Ricerca Scient. **11**, 58 (1940).

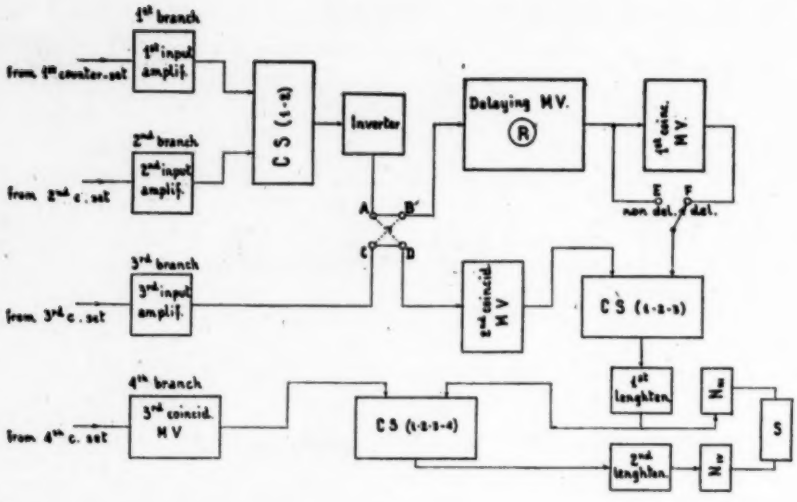

FIG. 2. Block diagram of registering set.

CS (1–2–3–4) is a system of double coincidences "in series."[8]

The positive coincidence pulse must be inverted before being sent through the connection *AB* to the delaying multivibrator. The latter, at the arrival of a negative pulse in *B*, produces a positive rectangular pulse, the duration of which is determined by the choice of certain elements of the circuit, forming together an interchangeable delaying group *R*.

The first coincidence multivibrator is sensitive only to negative pulses; it will work, then, only in the decreasing part, that is, at the end of the positive pulse of the delaying multivibrator and its pulse will be delayed by a time interval with respect to that of the double coincidence. One of the two tubes of *CS* (1–2–3) is permanently connected with the end of the second coincidence multivibrator. The other tube can be connected either with the end *E* of the delaying multivibrator (not delayed coincidences) or with the end *F* of the first coincidence multivibrator (delayed coincidences). In the second case, the coincidence occurs between the pulse θ_{12} of the first coincidence multivibrator and the pulse θ_3 of the second coincidence multivibrator and $T=\theta_{12}+\theta_3$ is the double of the resolving power of the system *CS* (1–2–3). In order to decrease the proper delay of the fourth branch, the third coincidence multivibrator has been connected directly with the fourth group of counters; the time length θ_4 of its pulse (~ 9 μsec.) is, moreover, much greater than the time lengths θ_{12}, θ_3. The working conditions of the experimental device have been checked by means of the same methods applied in the experiments for direct measurement of the mean life of mesons.[1] Among them, let us consider in some detail the curve of the counting rate of the quadruple coincidences as a function of the introduced delay "for short delays" which in the present case, has a particular importance. In fact, from this curve it is possible to evaluate the absolute delay in the following way. Let us suppose that the same particle crosses simlutaneously the four groups of counters; it will cause (a) a double coincidence between the first and the second branch, which will produce a delayed pulse θ_{12} of the first coincidence multivibrator; (b) a pulse θ_3 in the second coincidence multivibrator (third branch). Because of the fluctuations in the steepness of the counters-pulses both the pulses θ_{12}, θ_3 will not be produced after an exactly constant time interval evaluated from time zero (time when counters are crossed by the impinging particle).

Let us imagine that, for a certain delay θ of the delaying multivibrator, the most probable positions of the two pulses θ_{12}, θ_3 are that given in Fig. 3a. The time interval ϑ between the end of θ_3 and the beginning of θ_{12} is the absolute delay, since two independent particles, one of which crosses the first two groups of counters and the other the third one, would cause a coincidence only if the second (coincidence) is delayed at least for a time interval ϑ with respect

[8] O. Piccioni, Nuovo Cimento 1, 56 (1943).

to the first one, while, on the other hand, the coincidence produced by a single particle would be registered at the limit for $\vartheta=0$. The above-mentioned fluctuations of the counter pulses will cause fluctuations also in the positions of pulses θ_{12}, θ_3, which will be distributed in time as indicated by the differential curves $f_{12}(t)$, $f_3(t+\vartheta)$ of Fig. 3b. It may be seen that f_{12} is referred to the beginning of the pulse θ_{12} and f_3 to the end of θ_3, and that both are wider than θ_{12} and θ_3. Their shape has been drawn rather arbitrarily, but it is sufficient for our purpose to assume that they are symmetrical with respect to the maximum. Such an hypothesis cannot be considered strictly verified, especially for f_{12} which is the result of the coincidences between the first and the second branch. But the error introduced can be neglected in the determination of the ratio η (see Section 3). Since, for greater delays, the threefold coincidence counting rate III would be affected by the decay electrons, we preferred to put in Fig. 4 the fourfold coincidences counting into IV, keeping in mind that on account of the great width θ_4 of the third coincidence multivibrator, IV differ from III only by an efficiency factor independent of ϑ. Then, omitting a small constant part, because of the random coincidences of two or more particles, and putting briefly:

$$F_{12}=\int_{t-T}^{t} f_{12}(t)dt \quad [T=\theta_{12}+\theta_3],$$

we can practically write:

$$IV(\vartheta)=\int_{-\infty}^{+\infty} F_{12}(t)f_3(t+\vartheta)dt.$$

Differentiating with respect to ϑ, and integrating by parts successively and omitting the term $f_{12}(t-T)f_3(t+\vartheta)$ we obtain

$$\frac{d}{d\vartheta}IV(\vartheta)=\{F_{12}(t)f_3(t+\vartheta)\}_{-\infty}^{+\infty}-\int_{-\infty}^{+\infty} f_{12}(t)f_3(t+\vartheta)dt.$$

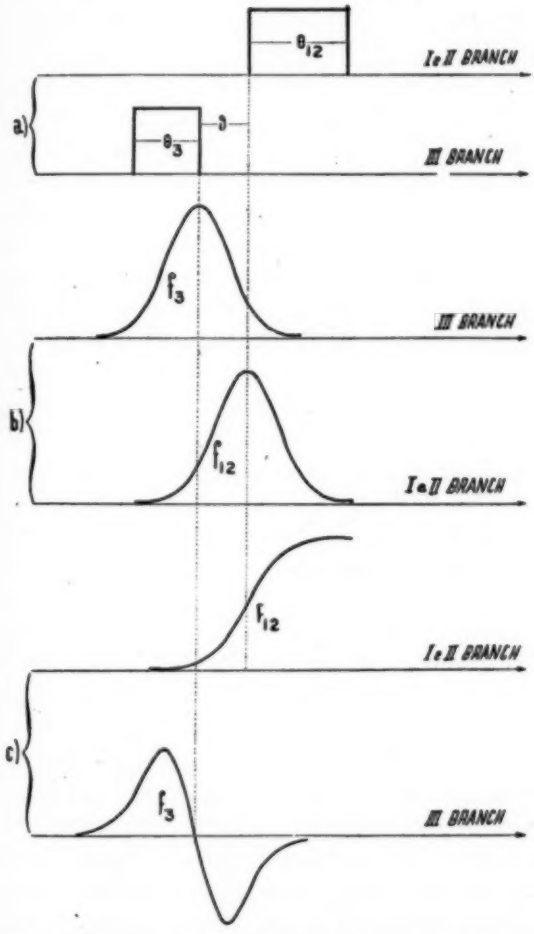

FIG. 3. Diagrams showing how the shape of IV (ϑ) curve is obtained. f_{12}, f_3 are differential distribution curves of pulses θ_{12}, θ_3.

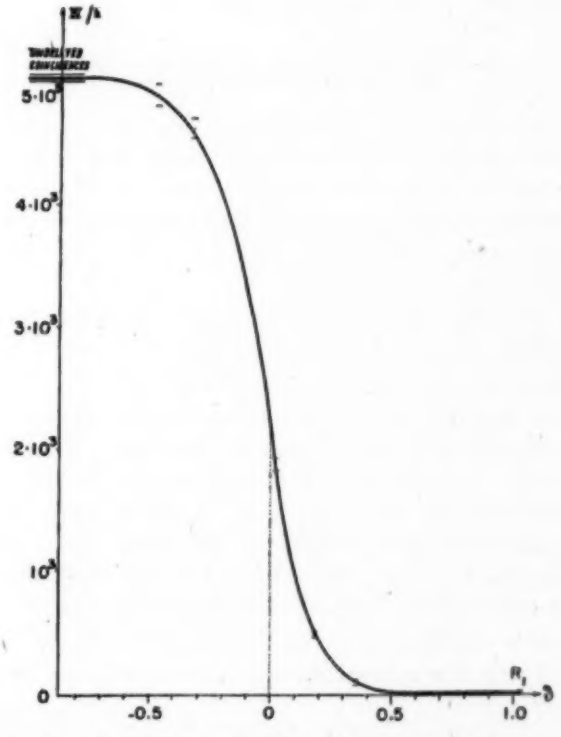

FIG. 4. Fourfold coincidence rates at small delay.

Since the first term on the right-hand side of this equation is obviously zero (Fig. 3b and 3c), we obtain

$$\frac{d^2}{d\vartheta^2}IV(\vartheta) = -\int_{-\infty}^{+\infty} f_{12}(t)\cdot f_3'(t+\vartheta)dt,$$

where $f_3' = df_3/d\vartheta = df_3/dt$ is plotted in Fig. 3. This integral is obviously zero for $\vartheta = 0$, on account of the symmetry of f_{12} and f_3. Thus the point of inflection of the curve IV (ϑ) corresponds to $\vartheta = 0$ and the distance of this point from the point R, corresponding to the introduced delay, gives the value of the absolute delay. A certain inaccuracy in the value of ϑ is connected with the errors affecting the measurements of the introduced delays, also with the statistical errors affecting the experimental points of the various curves IV (ϑ) and with the uncertainty of the determination of the point of inflection. This error however is certainly less than 0.2 μsec. as can be seen from Fig. 4. The delays corresponding to the points of the experimental curve of Fig. 4, as well as the pulse time-length of all multivibrators, were frequently checked during the experiment by means of the calibrating set described in our previous paper.

3. MEASUREMENTS, RESULTS, AND THEIR INTERPRETATION

Measurements of two types have been carried out alternatively in order to obtain the value of η.[9]

(a) Measurements of the delayed coincidences III and IV with absolute delay 1.025 μsec., have been taken with and without a 0.6-cm iron absorber.

(b) The undelayed coincidences between the double coincidences D_{12} (1st and 2nd group of counters) and the triple coincidences T_{124} (1st, 2nd, and 4th group) were measured alternatively with and without a 5-cm iron absorber.

The iron 0.6 cm thick, used in the measurements of the 1st type, was chosen in order to make them independent of the mean range of the disintegration electrons in the iron, the value of which is not known with sufficient accuracy but is certainly much greater than 0.6 cm.

From the measurements of the 1st type, the counting rate m of the mesons, stopped in the iron-plate and producing disintegration electrons which strike a counter of the third group, can be inferred as follows. If we put

$$\Delta_f = (\text{III}-\text{IV})_{\text{with Fe}};\quad \Delta_0 = (\text{III}-\text{IV})_{\text{without Fe}},$$

the counting rates m_f, m_0 of the mesons are given in the two cases by the equations

$$\begin{aligned} m_f &= \Delta_f - p(\text{IV})_f \pm (\Delta_f)^{\frac{1}{2}}, \\ m_0 &= \Delta_0 - p(\text{IV})_0 \pm (\Delta_0)^{\frac{1}{2}}, \end{aligned} \tag{1}$$

where

$$p = p_0/(1-p_0) \quad \text{and} \quad p_0 = 1 - QT_{123}. \tag{2}$$

Q is the undelayed quadruple coincidence and T_{123} the undelayed triple coincidence ($Q/T_{123} = \text{IV}/\text{III}$ for random coincidences). In deriving formula (1) it must be emphasized that, because of the little delay introduced, the random coincidences are essentially caused by the fluctuations in the steepness of the counter pulses (delay random coincidences RC). These RC rates would be the same in the two cases (with and without iron) if slight changes in the operating potentials of the counters did not occur during the measurements. In order to become independent of such variations we preferred to obtain separately the corrections $p(\text{IV})_f$, $p(\text{IV})_0$ instead of eliminating them as if they were equal. In order to obtain m, it is necessary to subtract integrally m_0 from m_f, the counting rate m_0 owing to the disintegration electron—(coming from the walls of the counters and from the 1 cm of lead beneath the third group)—which are still all present in the counting rate m_f measured with 0.6 cm of iron on account of their high penetrating power. In conclusion

$$m = m_f - m_0.$$

The results of this first kind of measurements are summarized in Table I. The measurements reported in Table I had been previously divided in partial series relating to successive periods of the experiment in which the counter potentials and the introduced delay had undergone slight variations. In putting together these partial series the necessary corrections have been introduced as described in our previous paper—as a correction to the sum of minutes. However, the value of m thus obtained and reported in the

[9] We thank L. Mezzetti for useful help in performing measurements.

TABLE I. Results of measurements with an absolute delay $\vartheta = 1.025$ μsec.

Absorber	III	IV	Corresponding minutes	Percentage	$\frac{\Delta - pIV}{\text{hour}}$	m/hour
0.6 cm iron	2.942	2.311	13.558	5.2	2.26±0.11	1.19±0.15
without iron	1.565	1.345	8.423	5.2	1.07±0.11	

TABLE II. Results of measurements without delay.

Absorber	D_{12}	T_{124}	Minutes	$(D_{12}-T_{124})$/hour	A_5/hour	A/hour
5-cm iron	143.520	132.120	1.105	619.0±5.8	129.1±7.8	15.5±0.94
without iron	139.632	130.912	1.068	489.9±5.3		

last column of Table I, is not sensibly different from that given by the simple formula $m = \Delta_f - \Delta_0$ without introducing any corrections.

The second type of measurements allows one to obtain the counting rate A_5 of the mesons stopped in 5-cm iron. We have, in fact (the meaning of the symbols is obvious): $A_5 = (D_{12} - T_{124})_f - (D_{12} - T_{124})_0$ while the number A of the mesons stopped in an iron plate 0.6 cm thick (during an hour) is given by $A = (0.6/5)A_5$. Table II contains the results of these measurements. The counting rate M of the mesons disintegrating in the 0.6-cm iron can be obtained from the equation

$$m = \bar{\alpha} e^{-\vartheta/\tau}[1 - e^{-T/\tau}]M \qquad (3)$$

where the ratio $\bar{\alpha} = \langle\Omega\rangle/4\pi$ between the mean solid angle permitted for the disintegration electrons and the total solid angle, has been calculated very carefully.[10] We take into account:

(a) The geometrical limitation due to the presence of the lateral counters of anticoincidence (Fig. 1a).

(b) The mean range (∼2.7 cm[11]) of the decay electrons in iron.

(c) The "weight" (incident intensity) relative to each point of the iron plate.

(d) That the hard component intensity varies almost as the square of the cosine of the zenith angle. We took into account this last circumstance only approximatively. We verified that the corresponding correction is very small (∼1.5 percent, while correction (c) is 4.5 percent). The result of our calculations was: $\langle\Omega\rangle = 3.98$. Using $\vartheta = 1.025$ μsec. and $T = 3.40$ μsec., formula (3) and the data contained in the last column of Tables I and II and taking $\tau = 2.3$ μsec., we obtain

$$\eta = M/A = 0.49 \pm 0.07.$$

Since during the measurements, the resolving power $T/2$ did not remain strictly constant—(the value $T = 3.4$ μsec. is a mean value)—and considering (see Section 2) that the measurement of the absolute delay is known with certain inaccuracies, it is useful to estimate an upper limit of the ratio η. Taking $\vartheta = 1.2$ μsec.; $T = 3.0$ μsec., we obtain

$$\eta = 0.56 \pm 0.08.$$

The value $T = 3.0$ μsec. is smaller than the minimum value obtained in the measurements, while the value $\vartheta = 1.20$ μsec. is certainly too high.

The agreement of the corresponding value of η with that obtained above shows that the errors affecting ϑ and T do not influence markedly the value of η.

4. MEAN RANGE OF THE DECAY-ELECTRONS

From our measurements an indication of the value of the mean range P of the disintegration electrons in iron can be obtained by comparing the results contained in Table I with those obtained with the same absolute delay 1.025 μsec. but with 5-cm iron instead of 0.6 cm. For such a purpose we point out that, if the third group of counters could be represented as an indefinite area, the permitted solid angle $\Omega(s)$ would be the same for all electrons produced at the same deepness s of the iron absorber and it would be given by the formula

$$\Omega = 2\pi(1 - x), \qquad (4)$$

where $x = s/P$.

This formula is correct for relatively great

[10] We thank C. Festa for useful help in performing calculations.

[11] This value is based on the calculation of H. Bethe and W. Heitler, Proc. Roy. Soc. **A146**, 83 (1934), about which some doubt can be raised: the work of these authors is antecedent to the theory of multiplicative processes and has been performed disregarding the electron scattering. However correction (b) is very small on account of the small thickness of the iron plate we have used and of the presence of the lateral anticoincidence counters. Moreover, as we shall see later, the experimental value that we found for the mean range of the decay electrons is in satisfactory agreement with the theoretical value of Bethe and Heitler.

values of the depth s and for the most of the points of the corresponding horizontal plane but it cannot be applied for the peripheric points; moreover, for small value of s the angle $\Omega(s)$ is essentially determined by the geometrical arrangement. The behavior of the function $\Omega(x)$ has been sketched in Fig. 5 (full curve) where the value $\langle\Omega\rangle$ of $\Omega(x)$ is that calculated in order to obtain the coefficient $\bar{a}$ (3) and $\bar{x}$ ($\cong 0.365$) has been derived from $\langle\Omega\rangle$ using (4). Assuming *a priori* $5/P>1$; $0.6/P=x<\bar{x}$ the ratio $\nu=m/m'$ between the effects m and m' observed, respectively with 0.6- and 5-cm iron, will be given by

$$\nu=\frac{\langle\Omega\rangle x'}{\langle\Omega\rangle\bar{x}+\frac{1}{2}(1-\bar{x})}=\frac{2x'}{1+\bar{x}};$$

by this equation we deduce:

$$x'=\tfrac{1}{2}\nu(1+\bar{x}). \qquad (5)$$

The m value can be derived from the experimental results, already published, obtained with the same absolute delay (corresponding to the delaying element R_1) and with (and without) 5 cm of iron. The corresponding counting rates m_f', m_0' are

$$m_f'=3.51\pm0.25; \quad m_0'=0.66\pm0.18.$$

In this case, we must not take for m' the difference $m_f'-m_0'$. In fact, as we already pointed out, the counting rate registered without iron is caused by the electrons produced in the walls of the counters and in the 1-cm lead plate beneath the third group of counters. Now, the electrons produced in the walls of the counters should not be subtracted from m_f', because the plate of iron, 5 cm thick, is sufficient to establish the equilibrium conditions between the electrons produced and those which are absorbed. The electrons produced in the 1 cm thick lead plate, should be subtracted but they form the smaller part of m_0' as can be easily recognized by considering the geometrical limitations due to the anticoincidences lateral counters and the fact that in order to be counted each decay-electron should strike a counter of the third set different from that crossed by the original meson (the reactivation period of a counter is $\sim 10^{-3}$ sec.). Omitting their contribution, we have

$$m'=m_f'=3.51\pm0.25;$$

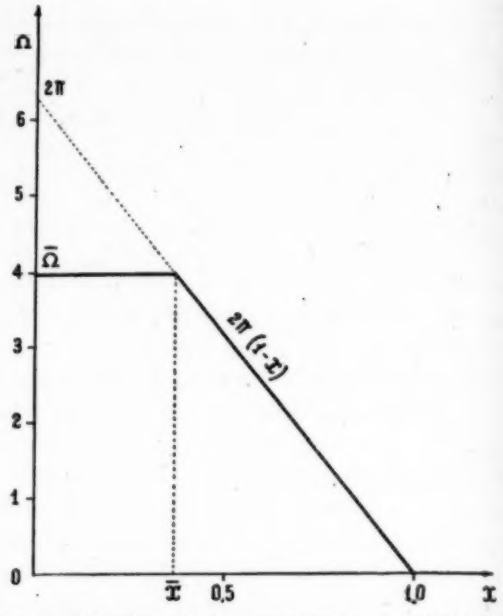

FIG. 5. Variation of the solid angle in which decay electrons are detected, with the thickness of the absorber, taking the range of decay electron = 1.

we find then

$$\nu=m/m'=0.339\pm0.005$$

and using (5)

$$P=0.6/x=2.60^{+0.43}_{-0.34}.$$

Assuming, on the contrary, that the electrons coming from the 1 cm plate of lead represent the 40 percent of m_0' (very likely an excessive value), we obtain

$$P=2.40^{+0.40}_{-0.32}.$$

5. DISCUSSION

The results of our measurements suggest that only a fraction of the mesons stopped in a heavy substance undergo the decay process. In fact the value $\eta=1$ seems to be decidedly out of range of the experimental errors. Moreover, the most probable value $\eta=0.49$ seems to indicate that about one-half of the slow mesons disintegrate; this conclusion is confirmed by the upper value $\eta=0.56$.

Our value of η agrees pretty well with Rasetti's result[3] ($=0.42\pm0.15$) but does not with that of Auger, Mase, and Chaminade[4]; moreover our

result seems to confirm Tomonaga and Araki's theoretical conclusions,[2] because the negative mesons captured by the nuclei would allow disintegration processes with a far too short mean life to be registered with our experimental device. It may be pointed out that, even taking into account the positive excess of the hard component (which amounts to about 20 percent),[12,13] the theoretical value of η would not rise to more than 0.6, which is in reasonable agreement with our result. Our result could be explained, also, by assuming that one-half of the hard component is formed by unstable particles having a mean life $\tau = 2.3$ μsec. and one-half by stable particles. This interpretation seems not to be correct on account of the relatively good agreement between the most probable value of $\tau/\mu c^2$ obtained from the experiments on the anomalous absorption and the value derived from direct measurements of τ and of the mass μ in the Wilson cloud chamber. If one-half of the particles of the hard component would be stable the observed value of the ratio $\tau/\mu c^2$ ought to be appreciably greater. This last circumstance would not occur according to Tomonaga and Araki's theory, because the capture process of the negative mesons suggested by the theory has a strong probability only at very low energies. Moreover, if one assumes that one-half of the hard component is formed by stable particles having the same sign, one would expect a variation of the positive excess with the total number, while direct experiments showed that such an excess keeps constant between 3500 m above the sea level and the sea level.[14]

In conclusion it seems that Tomonaga and Araki's suggestion represents the best explanation of the experimental result.

A few years ago Dr. E. Pancini suggested an experiment designed to give definitive answer about this point: it consists in measuring the delayed coincidences produced by the disintegration electrons concentrating alternatively the positive mesons and the negative ones by means of magnetized iron blocks. Experiments of this type are now in progress.

From the previous paragraph it follows that our experimental results allow the evaluation of the mean range P of the decay electrons in iron, with a probable error of about 20 percent. Although the experimental error is rather large, one could deduce from our value of P the rest energy of mesons, using the range-energy relation for electrons in iron. Unfortunately, we do not possess at present a reliable formula or experimental data of this type. Bethe and Heitler's calculations are antecedent to the theory of multiplicative processes and disregard the electrons scattering. However, with the help of the formula given by these authors, we find that the value $P = 2.5$ cm of iron obtained by us corresponds to an energy μc^2 of about 90 Mev.

This value of μ, even if it is to be considered only as an indication, gives a further and comfortable connection between the experiments of this kind, dealing with direct measurements on the disintegration process, and the other several experiments concerning the hard component of cosmic rays.

We thank Professor Gilberto Bernardini for his interest taken in our experiments. We thank also Professors A. Bandini, President of the Lyceum-Gymnasium Virgilio, and Professor L. Fagiolo, Vice-President, for their great interest and kindness. The present experiment has been carried out with equipment furnished by the Centro di Fisica Nucleare and the Istituto Nazionale di Geofisica of the Consiglio Nazionale delle Ricerche.

[12] H. Jones, Rev. Mod. Phys. **11**, 235 (1939); D. H. Hughes, Phys. Rev. **57**, 592 (1940).
[13] G. Bernardini, M. Conversi, E. Pancini, and G. C. Wick, Ricerca Scient. **12**, 1227 (1941); M. Conversi and E. Scrocco, Nuovo Cimento **I**, 372 (1943); G. Bernardini, M. Conversi, E. Pancini, E. Scrocco, and G. C. Wick, Phys. Rev. **68**, 109 (1945).
[14] G. Bernardini, M. Conversi, E. Pancini, and G. C. Wick, Ricerca Scient. **13**, 1227 (1941).

Resonances in the Disintegration of Fluorine by Protons

W. E. Bennett, T. W. Bonner, C. E. Mandeville, and B. E. Watt
Rice Institute, Houston, Texas

(Received October 1, 1946)

The voltage regulation of the Rice Institute pressure electrostatic generator has been improved by the use of a modulated electron current which proceeds up the vacuum tube in the opposite direction to the positive ions. The auxiliary apparatus is composed of a magnetic voltage analyzer and an electronic potential regulator. Calculations indicate that at 1 Mev the potential is controlled to ±150 volts. The resonances in the production of gamma-rays and soft radiation (pairs) when F^{19} is bombarded by protons have been studied with proton energies of from 800 to 1400 kev. Resonances for the emission of gamma-rays have been observed at 820, 862, 890, 927, 1076, 1107, 1122, 1161, 1274, 1335, and 1363 kev. The experimental half-widths of these resonance levels vary from 1.9 to 50 kev. Resonances for the production of soft radiation (pairs) have been observed at 832, 1100, 1220, and 1362 kev; the widths of these resonance levels vary from 28 to 85 kev. An explanation of the varying intensities and widths of the levels can be made on the basis that the protons which produce the disintegrations and the alpha-particles which result have several different values of angular momentum.

INTRODUCTION

THE transmutation of fluorine by protons has been the subject of extensive experimental and theoretical interest since the pioneer experiments of Cockcroft and Walton in 1932. Alpha-particles were the first products of the disintegration of fluorine which were detected.[1] These alpha-particles have been studied by Oliphant and Rutherford,[2] by Henderson, Livingston, and Lawrence,[3] and more recently by Burcham and Smith.[4] From these experiments it is known that the 5.9-cm alpha-particles come from the following reaction:

$$_9F^{19}+{}_1H^1\rightarrow{}^*{}_{10}Ne^{20}\rightarrow{}_8O^{16}+{}_2He^4+7.95\text{ Mev}. \quad (1)$$

The Q value of 7.95 Mev has been accurately determined by Burcham and Smith.[4] The early excitation curves for these alpha-particles gave a continuous increase in the yield in the proton energy range of from 700 to 1500 kev.[3] In 1939 Burcham and Devons[5] found resonances in the excitation curve at 720 and 830 kev. Streib, Fowler, and Lauritsen[6] extended these measurements to 1500 kev and found additional resonances at 1140 and 1350 kev.

Intense gamma-radiation was the next product of the disintegration of fluorine which was observed. These first experiments were carried out by McMillan[7] in 1934. A large amount of work has been done to determine the quantum energy of this radiation accurately.[8] The latest experiments with the cloud-chamber technique which have been carried out by Lauritsen, Lauritsen, and Fowler[9] give a value of 6.2 Mev for this energy, while the experiments of Dee, Curran, and Strothers[10] with a magnetic spectrograph give a value of 6.5 Mev.

Hafstad, Heydenburg, and Tuve[11] discovered pronounced resonances in the production of gamma-rays when fluorine is bombarded by protons. Later experiments[12–14] and especially

[1] J. D. Cockcroft and E. T. S. Walton, Proc. Roy. Soc. **A137**, 229 (1932).
[2] M. L. E. Oliphant and Lord Rutherford, Proc. Roy. Soc. **A141**, 259 (1933).
[3] M. C. Henderson, M. S. Livingston, and E. O. Lawrence, Phys. Rev. **46**, 38 (1934).
[4] W. E. Burcham and C. L. Smith, Proc. Roy. Soc. **A166**, 176 (1938).
[5] W. E. Burcham and S. Devons, Proc. Roy. Soc. **A173**, 555 (1939).
[6] J. F. Streib, W. A. Fowler, and C. C. Lauritsen, Phys. Rev. **59**, 253 (1941).
[7] E. McMillan, Phys. Rev. **46**, 325; 868 (1934).
[8] H. R. Crane, L. A. Delsasso, W. A. Fowler, and C. C. Lauritsen, Phys. Rev. **46**, 531 (1934); L. A. Delsasso, W. A. Fowler, and C. C. Lauritsen, Phys. Rev. **51**, 391; 527 (1937); E. R. Gaerttner and H. R. Crane, Phys. Rev. **52**, 582 (1937).
[9] T. Lauritsen, C. C. Lauritsen, and W. A. Fowler, Phys. Rev. **59**, 241 (1941).
[10] P. I. Dee, S. C. Curran, and J. E. Strothers, Nature **143**, 759 (1939).
[11] L. R. Hafstad, N. P. Heydenburg, and M. A. Tuve, Phys. Rev. **49**, 866 (1936); **50**, 504 (1936).
[12] R. G. Herb, D. W. Kerst, and J. L. McKibben, Phys. Rev. **51**, 691 (1937).
[13] S. C. Curran, P. I. Dee, and V. Petrzilka, Proc. Roy. Soc. **A169**, 269 (1938).
[14] E. J. Bernet, R. G. Herb, and D. B. Parkinson, Phys. Rev. **54**, 398 (1938).

those of Bernet, Herb, and Parkinson showed that the resonances were quite sharp. The experimental half-widths of the resonances were found by Bernet, Herb, and Parkinson to vary from 10 to 20 kev. Later, the low energy part of the excitation curve was investigated carefully by Burcham and Devons.[5] They were able to reduce the observed half-widths of the resonances at 330 and 670 kev to 6 kev. Bennett, Bonner, Hudspeth, and Watt[15] reduced the experimental half-widths of the resonances at 862 and 927 kev to 8 and 9 kev, respectively. These widths were in most cases believed to be experimental and not the natural widths of the resonance levels.

The nuclear reaction which was proposed originally to explain the origin of the gamma-radiation was the following:

$$ {}_9F^{19}+{}_1H^1\rightarrow{}^*{}_{10}Ne^{20}\rightarrow{}_{10}Ne^{20}+\gamma+13.1 \text{ Mev}. \quad (2) $$

For several years this reaction was believed to be the correct one, primarily because it was thought that sharp resonances would be observed only in the capture type disintegration of reaction (2). Since the quantum energy of the gamma-rays was known to be nearly half the Q value of reaction (2), it was generally believed that two gamma-rays were emitted in cascade from the excited ${}_{10}Ne^{20}$ nucleus. However in 1939 the experiments of Dee, Curran, and Strothers[10] to detect the simultaneous emission of two quanta showed that less than 1 percent of the gamma-rays were produced simultaneously. This showed that reaction (2) is not the source of the gamma-radiation which is observed.

The nuclear reaction, now generally accepted, which explains the origin of the gamma-rays is the following:

$$ \begin{aligned} {}_9F^{19}+{}_1H^1\rightarrow{}^*{}_{10}Ne^{20}\rightarrow{}^*{}_8O^{16}+{}_2He^4+Q_3, \\ {}^*{}_8O^{16}\rightarrow{}_8O^{16}+\gamma. \end{aligned} \quad (3) $$

According to this reaction the gamma-rays accompany the emission of a short range alpha-particle. These short range alpha-particles were first observed by McLean, Becker, Fowler, and Lauritsen[16] in 1939. From the 0.86-cm range of the alpha-particles they calculated that the Q value of reaction (3) is 1.74 Mev. They also showed that these short range alpha-particles displayed a resonance at 330 kev in the same manner as the gamma-rays. Burcham and Devons[5] have shown that the excitation curve of the short range alpha-particles is the same as that of the gamma-rays over a range of proton energies from 300 to 950 kev.

Electron pairs were the next product of the disintegration of fluorine which were observed. Fowler and Lauritsen[17] in 1939 found a soft radiation, in addition to the characteristic x-radiation, coming from the fluorine target. When they bombarded a fluorine target with 820- or 1130-kev protons they showed by absorption experiments that the radiation was composed of electrons and not gamma-rays. They substantiated these observations by cloud-chamber measurements with a bombarding energy of 820 kev. These cloud-chamber experiments showed that the radiation consisted of electron pairs with a total energy of 5.9 ± 0.5 Mev. Streib, Fowler, and Lauritsen[6] have observed the excitation curve for this soft radiation and have found no pairs below 650 kev. They discovered resonances for the soft radiation at 850, 1140, 1220, and 1350 kev; only at 820 and 1130 kev have they shown that this soft radiation is composed of electron pairs. The proton energies of the pair-resonances do not coincide with the gamma-ray resonances. The reaction to which the pairs are attributed is the following:

$$ \begin{aligned} {}_9F^{19}+{}_1H^1\rightarrow{}^*{}_{10}Ne^{20}\rightarrow{}^{\pi*}{}_8O^{16}+{}_2He^4+Q_4, \\ {}^{\pi*}{}_8O^{16}\rightarrow{}_8O^{16}+\pi+4.9 \text{ Mev}. \end{aligned} \quad (4) $$

The emission of pairs in place of gamma-rays is attributed to the fact that the ${}^{\pi*}{}_8O^{16}$ has a total angular momentum equal to zero and so the emission of a single gamma-ray is forbidden.[18]

The experiments to be described below were undertaken with the purpose of determining the widths of the resonances in the excitation curves of the gamma-rays and the pairs. With improved resolution it was expected that a number of new resonances would be resolved, and that the natural widths of the already known resonances would be determined.

[15] W. E. Bennett, T. W. Bonner, E. Hudspeth, H. T. Richards, and B. E. Watt, Phys. Rev. 59, 781 (1941).

[16] W. B. McLean, R. A. Becker, W. A. Fowler, and C. C. Lauritsen, Phys. Rev. 55, 796 (1939).

[17] W. A. Fowler and C. C. Lauritsen, Phys. Rev. 56, 835 (1940).

[18] J. R. Oppenheimer and J. S. Schwinger, Phys. Rev. 56, 1066 (1939).

EXPERIMENTAL ARRANGEMENTS AND PROCEDURES

The proton accelerator was the Rice Institute pressure Van de Graaff generator which had been used previously.[15] In the present experiments the generator was modified by the addition of an energy selector and a potential stabilizer.

Energy Selector

An annular ring type of magnet, similar in design to that used by Rutherford, Wynn-Williams, Lewis, and Bowden,[19] deflected the protons through 90° and resolved the molecular and atomic beams. It was simultaneously used to define the energy of the beam striking the target by the addition of a narrow slit at the line where the beam was focused after being bent through 90°. The arrangement is shown in Fig. 1.

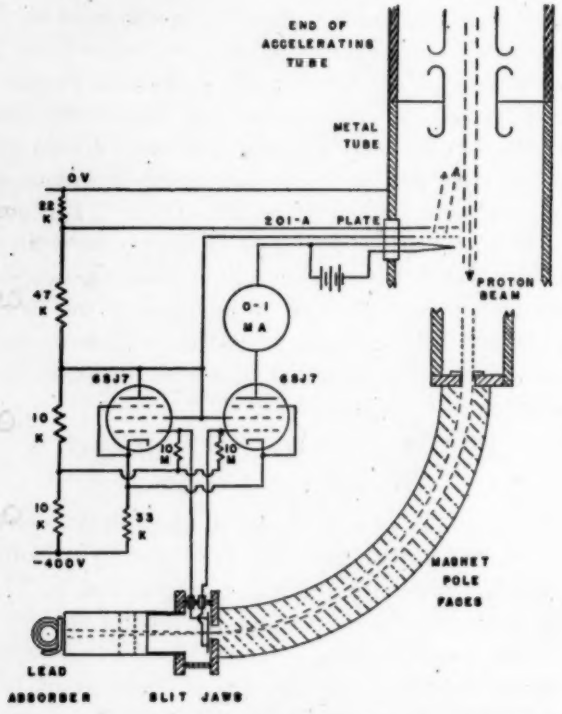

FIG. 1. Diagram of the experimental arrangement showing the magnetic energy selector and the electronic potential regulator. The proton-beam passes through the two insulated jaws of the narrow slit and proceeds to the target. The modulated electron current goes up the vacuum tube in the reverse direction to that of the positive ion-current. The 0–1 milliammeter measures the modulated electron current which leaves the electron gun; the current through this meter serves as an indicator of whether the stabilizer is centered within its limits of regulation.

[19] Lord Rutherford, C. E. Wynn-Williams, W. B. Lewis, and B. V. Bowden, Proc. Roy. Soc. A139, 617 (1933).

The radius of curvature of the beam of protons was 26 cm and the slit width was 0.015 cm. Observation of the focused beam of protons showed its width to be approximately 0.02 cm when the energy of the protons was 1 Mev. The expected width due to the finite size (1 cm) of the entrance aperature was 0.010 cm and the maximum energy spread possible because of voltages in the ion source was 1000 volts or 0.012 cm at the focal line. It is believed that the position spread due to aberrations in the focusing system was less than ± 0.05 percent, under the condition of maximum current through the slit.

Potential Stabilizer

To reduce the energy spread in the emerging proton beam and to maintain a steady current through the narrow slit, a stabilizer for the potential of the proton accelerator was constructed by insulating the jaws of the narrow slit and constructing an electronic circuit to alter the accelerating potential so as to maintain equal currents to the two jaws. The diagram of the potential stabilizer is shown in Fig. 1. The electron-gun sends electrons back up the vacuum tube to the ion source. The potential stabilizer works by modulating the electron current from the gun. Since the charging current on the belt of the electrostatic generator remains constant, a change in the electron current will produce a change in the potential of the generator. The circuit is made such that an increase in the current to the inner jaw will decrease the electron current up the vacuum tube, thus increasing the voltage so that the proton beam will be centered in the narrow slit. The time delay of this control system is extremely short since the electrons proceed up the vacuum tube at essentially the velocity of light. The total time delay around the circuit which includes the transit times of the protons down the vacuum tube, the electrons in the amplifier circuit, and the electrons up the vacuum tube is 2×10^{-6} sec. This time delay sets a lower limit to the theoretical potential stability which could be achieved with this circuit. An analysis of the circuit shows that the lower limit to the voltage fluctuations would be about 0.02 volt. However because the ion source had an internal accelerating voltage of 1000 volts, the protons would be expected to have a

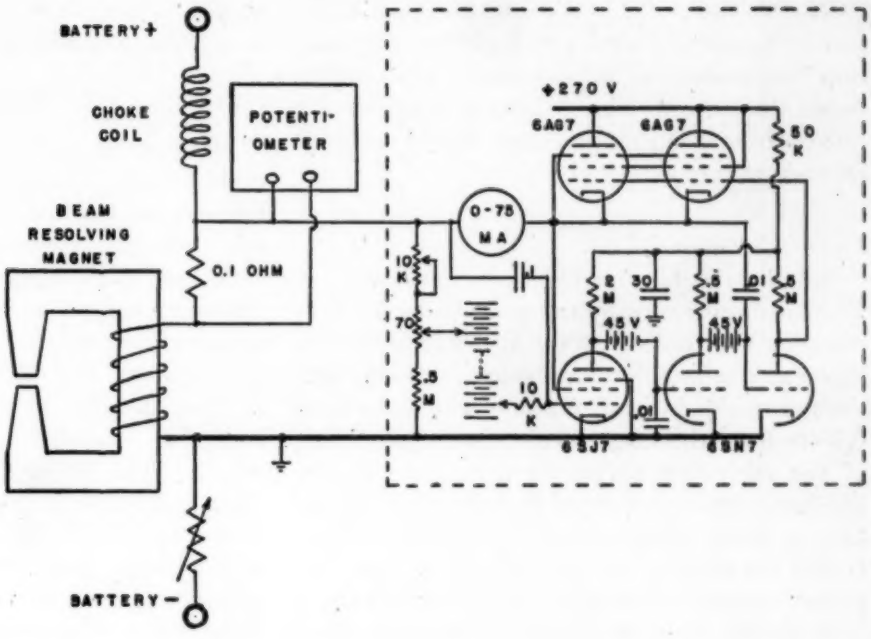

FIG. 2. Diagram of the electrical circuits which supply and measure the constant current to the magnetic analyzer.

spread in energy of several hundred volts and hence, it would not be useful to approach this theoretical limit with the present ion source. The calculated fluctuations in potential using the circuits of Fig. 1 are ±150 volts. This is somewhat smaller than the expected spread from the ion source and one-fourth the energy spread permitted by the narrow slit when operating at 1 Mev.

Current Regulator for Electromagnet

The current in the deflecting magnet was held constant by regulating the voltage which was applied to the coils. The diagram of the apparatus is shown in Fig. 2. The choke coil raises the impedance of the source for all the high frequency components of the supply voltage which was a 130-volt battery continuously charged by a generator. The potentiometer measured the total current through the coils by measuring the potential drop in the standard 0.1-ohm resistance and was capable of measuring the average current to 0.1 milliampere out of a total current of about 3 amperes. An oscillograph showed that the voltage across the coils of the magnet had no components in the frequency range 2 to 200,000 cycles per sec. of amplitude greater than 0.05 percent of the direct component, and the potentiometer showed no current fluctuations of lower frequency exceeding 0.01 percent. Owing to the large inductance of the magnet it is believed that the magnetic field was held constant to within 0.01 percent for the several minutes required to obtain one point on an excitation curve.

Because of the hysteresis in the iron, it took approximately 1.5 percent greater current to produce the same value of the magnetic field on increasing the field than when decreasing the field; so in running an excitation curve the convention of always increasing the current in the magnet was adopted. With this convention the displacements of excitation curves from day to day were less than 0.2 percent. Experience indicated that temperature variations in the air conditioned laboratory could explain most of the observed displacements.

Targets

The desired target thicknesses were in the range of from 500 to 2000 volts in stopping power. The thicker targets were used for survey experiments where it was expedient to take larger voltage intervals. All targets were prepared by evaporating a fluorine compound from a hot filament in a high vacuum onto a polished silver disk which was 3.2 cm in diameter. The compounds that were tried were CaF_2, MnF_2, and

ZnF_2. The ZnF_2 and MnF_2 were the most satisfactory because of their relatively low evaporation temperature. A micro-balance was used to weigh the deposit. The weights of the deposits ranged from 3 micrograms per square cm to 9 micrograms per square cm.

Detectors

Initially the detector for the gamma-rays was a bifilar electroscope in an iron cylinder 7 cm in diameter with walls 1 cm thick. It was filled with argon at 70 atmospheres pressure. Next, a Geiger counter shielded with 1.65 mm of lead was placed 0.7 cm from the target of fluorine. Comparison of the excitation curves in the region of the 862-kev resonance showed that the electroscope gave a larger background effect than did the Geiger counter, so it was decided to use the Geiger counter in the subsequent experiments.

To detect the softer radiation (electron pairs) a window was cut in the lead shield and the target holder made thin enough to admit electrons to the Geiger counter. The materials in the path of the electrons were 0.5 g/cm² of silver, 0.3 g/cm² of aluminum, 0.2 g/cm² of glass and 0.1 g/cm² of copper. The relative intensity of the soft radiation was determined by subtracting the yield observed with the lead absorber in place from the yield observed without the absorber. To compare the pair-yield with the gamma-ray yield corrections were made for the different probability of detection. Under the conditions of our experiments the gamma-rays were calculated to have approximately one-tenth the efficiency of counting as do pairs with a total kinetic energy of 4.9 Mev. In case some of the resonances are caused by pairs with a different energy or to soft radiation of another type, then the comparison factor between hard and soft radiation will be in error. The calculation of absolute yields of disintegrations has not been made, since Streib, Fowler, and Lauritsen[6] have determined the absolute values very accurately. With our experimental conditions the addition of the 0.165 cm of lead absorber increased the efficiency of counting 6-Mev gamma-rays by enough to compensate for the small absorption of the rays by this amount of lead. The sensitivity of the Geiger counter was checked frequently with a one milligram sample of radium at a standard position.

Procedure

After setting the current in the magnet to the desired value, the potential on the proton accelerator was adjusted to be within the range of the potential regulator. At each voltage, the time and total charge required to give several thousand counts in the Geiger detector were observed for the two conditions, lead absorber in position and out of position. The number of protons striking the target was determined by means of a current integrator described elsewhere.[20] The background count in the Geiger counter when the proton beam hit an iron shutter in place of the target was observed as a function of the x-ray intensity from the high voltage apparatus. Frequent readings of the x-ray intensity were made near the source of this radiation and these were used to compute the background. This was necessary since the x-ray intensity varied. In general this background was small in comparison to the effect due to gamma-rays at resonances, but was comparable to the gamma-ray effect in regions widely removed from resonances. A run with a blank silver target showed no increase over background within the experimental error. The voltage of each point on the excitation curve was obtained from a curve relating voltage as a function of magnet-current. The resonances at 927, 1335, and 1363 kev[14] were used to construct this curve.

RESULTS

The experimental results are shown in the graphs of Figs. 3–5. Five different targets were used to obtain these data. The precision in determining the yield of gamma-rays was considerably greater than that for pairs, since the yield of pairs is obtained by subtracting two measurements which sometimes were nearly equal. In order to improve the accuracy of the pair points, two or more neighboring points were averaged. Because of the necessity of this procedure and because of the reduced accuracy in determining pair points sharp pair resonances of weak intensity would have been missed.

[20] B. E. Watt, Rev. Sci. Inst. **17**, 334 (1946).

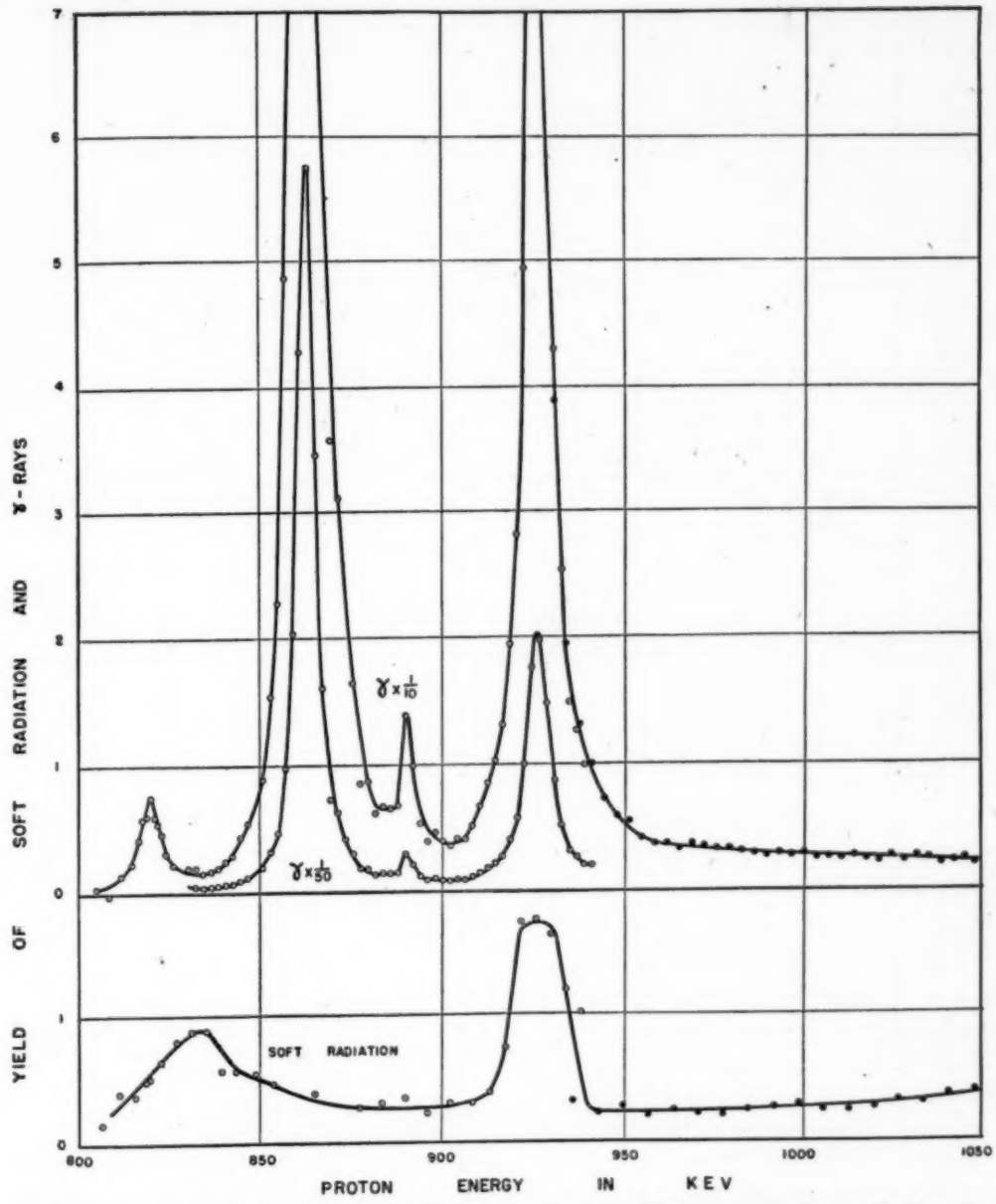

FIG. 3. The relative yield of gamma-rays and soft radiation (pairs) from 800 kev to 1050 kev. The data which is indicated by open circles was obtained with a 0.6-kev target of CaF_2, while that indicated by solid circles was obtained with a 1.8-kev target of ZnF_2.

The curves of Fig. 3 show sharp resonances for gamma-rays at 820 and 890 kev as well as the previously known resonances at 862 and 927 kev.[14] The curves for soft radiation (pairs) show broader resonances at 832 and 925 kev. The resonance at 832 kev is that discovered by Streib, Fowler, and Lauritsen[6] while the resonance at 925 kev was not observed by them. This resonance at 925 kev appeared relatively less intense when a thicker target of ZnF_2 was bombarded. Streib, Fowler, and Lauritsen also used thicker targets in their experiments. For this reason it appears likely that this resonance is not from F^{19} atoms but from some contaminant on the surface of the target, probably carbon or oxygen which are nearly always present in small quantities. Unfortunately no systematic study of the excitation curve of soft radiation from

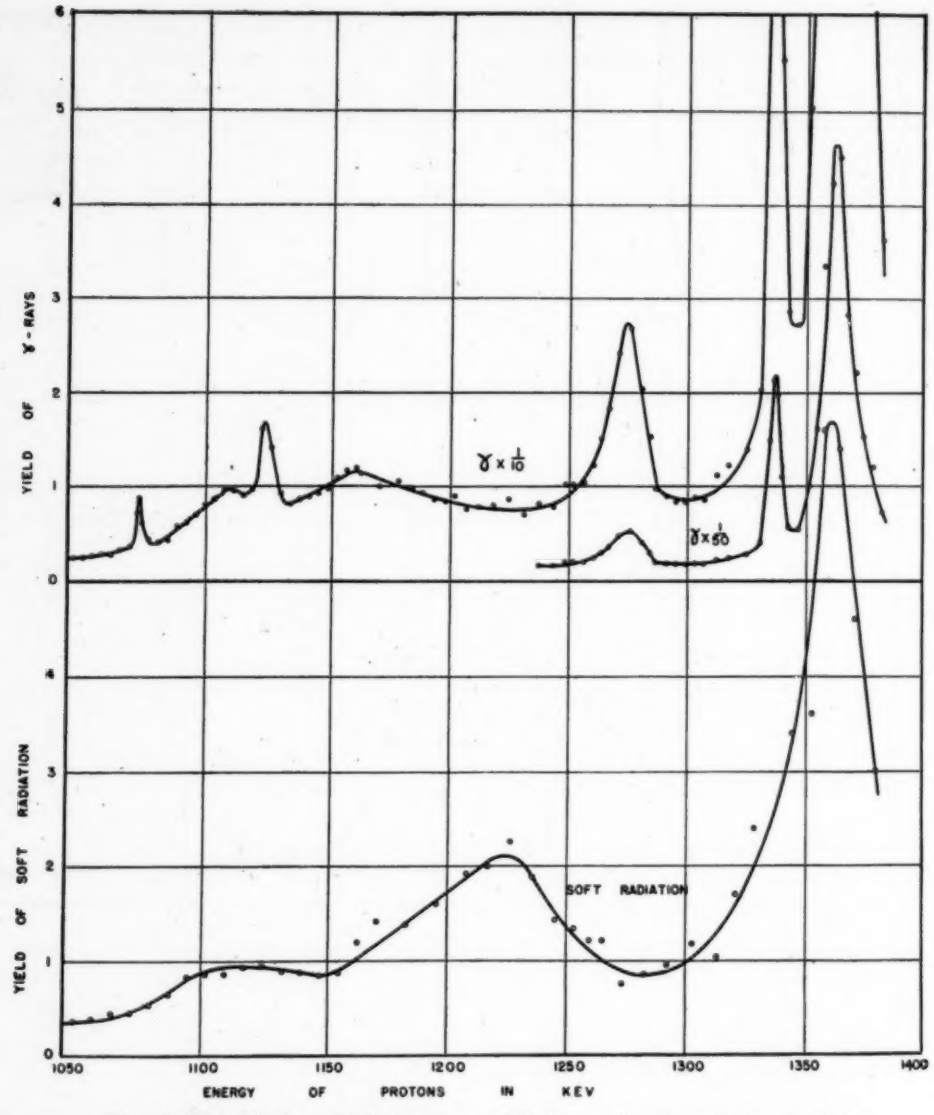

FIG. 4. The relative yield of gamma-radiation and soft radiation (pairs) from 1050 kev to 1400 kev. The data was taken with two different 1.8 kev targets of ZnF_2.

carbon or oxygen bombarded by protons has been obtained in the vicinity of 925 kev. This radiation may be a very low energy gamma-ray or more likely it is a beta-ray with an energy greater than 2 Mev. Radioactive $_9F^{17}$ has been formed at much higher energies by proton bombardment,[21] and it is quite possible that the effects observed are from radioactive $_9F^{17}$ which is made at a resonance in the capture reaction.

$$_8O^{16}+{}_1H^1\rightarrow{}_9F^{17}+\gamma+0.5 \text{ Mev.}$$
$$_9F^{17}\rightarrow{}_8O^{17}+e^{+}+2.1 \text{ Mev.} \quad (5)$$

[21] L. A. DuBridge, S. W. Barnes, and J. H. Buck, Phys. Rev. 51, 995 (1937).

In Fig. 4 the excitation curves of the hard and soft components of the radiation are extended up to 1400 kev. The excitation curve of gamma-rays exhibits sharp resonances at 1076 and 1122 kev as well as the previously known resonances at 1274, 1335, and 1363 kev. Two broader gamma-ray resonances were found at 1107 and 1161 kev. The excitation curve of the soft radiation (pairs) shows resonances at 1100, 1220, and 1363 kev.

The widths of the resonances in Fig. 3 and Fig. 4 vary over wide limits. The half-widths of resonances greater than 5 kev were determined from the curves of Figs. 3 and 4 when drawn to

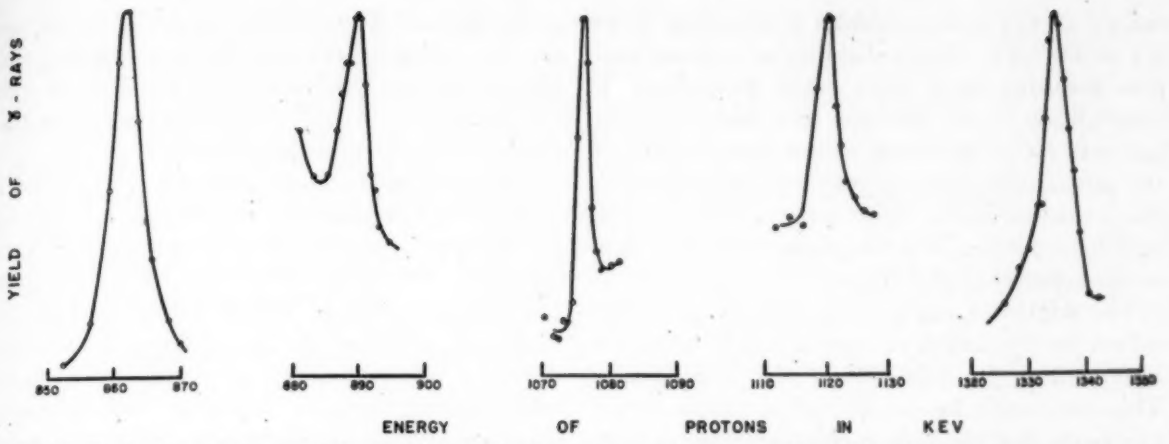

FIG. 5. Excitation curves to obtain the half-widths of the narrow resonances. The yields of the resonances have been normalized to the same value. The targets used were all 0.6 kev in equivalent thickness. CaF_2 was used to obtain the resonances at 862 and 890 kev; ZnF_2 was used in observing the resonances at 1076 and 1122 kev; and MnF_2 was used on the resonance at 1335 kev.

a large scale, and their values are given in Table I. In order to investigate the widths of the narrower resonances, excitation curves were carried out with targets whose equivalent thickness was only 0.6 kev. These excitation curves are shown in Fig. 5, and the half-widths are given in Table I. The narrowest experimental half-width is 1.9 kev for the resonance at 1076 kev. Since all the other half-widths are more than a factor of two larger than this, it can safely be said that they represent the natural widths of the resonance levels. The natural width of the level at 1076 kev must be less than 1.9 kev since the target alone had an average thickness of 0.6 kev and such a thin target may not have been uniform in thickness.

TABLE I. Data concerning resonances in the emission of gamma-rays and pairs.

Type of resonance (γ-ray or pair)	Proton energy at resonance kev.	Half-width kev.	Relative peak intensity	Relative intensity* (peak × width)
γ	820	7.6	0.8	6.1
π	832	28.	0.08	2.2
γ	862	5.2	29.	150.
γ	890	4.8	1.0	4.8
γ	927	8.0	10.	80.
γ	1076	<1.9	0.5	1.0
π	1100	$\approx 70.$	0.06	$\approx 4.$
γ	1107	$\approx 30.$	0.8	$\approx 24.$
γ	1122	4.1	0.9	3.7
γ	1161	$\approx 50.$	0.8	$\approx 40.$
π	1220	85.	0.2	17.
γ	1274	19.	2.2	42.
γ	1335	4.8	9.0	43.
π	1362	36.	0.6	22.
γ	1363	15.	22.	330.

* The relative intensities of pair as compared to γ resonances may be in error by as much as a factor of two or more, because of the unknown angular distribution of the pairs and because of errors in the relative efficiencies of counting pairs and gamma-rays.

The widths of all the gamma-ray resonances are less than previously observed. However, the widths of the resonances in pair formation are somewhat larger than the rough estimates of Streib, Fowler, and Lauritsen.[6]

INTENSITIES AND WIDTHS OF THE RESONANCE LEVELS

The height of the potential barrier of F^{19} for protons is 2.3 Mev and the barrier of O^{16} for alpha-particles coming out of the compound nucleus is 4.3 Mev.[22] Since the barrier heights are considerably greater than the particle energies, the intensities and widths of the resonance levels should be strongly influenced by the penetrabilities through the barrier. This is especially true of particles with large angular momentum. The penetrability of s-protons (angular momentum = 0) varies from 0.042 to 0.36 as their energy is increased from 800 to 1400 kev, while the penetrability of p and d protons (angular momenta = 1 and 2 units) will be less.[22] Thus the probability of a proton entering the F^{19} nucleus and forming a Ne^{20} nucleus in a highly excited state (≈ 14 Mev) will increase by about a factor of 8 as the proton energy is increased from 800 to 1400 kev. Similarly the penetrability of s-alpha-particles varies from 0.09 to 0.31 as the

[22] H. A. Bethe, Rev. Mod. Phys. 9, 166 (1937).

energy of the alpha-particles is increased from 2.5 to 3.0 Mev. The probability of a disintegration resulting in a short range alpha-particle which leads to the emission of a gamma-ray or pair will be proportional to the penetrability of the proton times the competition ratio between the emission of the short range alpha-particle and the emission of a long range alpha-particle or the reemission of a proton.

The widths of the resonance levels are determined by the length of time which it takes the intermediate nucleus ($^*Ne^{20}$) to disintegrate. This time may be considered as composed of two parts, first the time necessary to concentrate the appropriate energy on the particle concerned, and second the length of time it takes this charged particle to leak through the barrier. The relation between the width of the level and the lifetime of the intermediate nucleus is given by the uncertainty relation: $\Delta E \Delta T \approx \hbar$. The lifetimes of the excited states of $^*Ne^{20}$ given in Table I vary from 0.8×10^{-20} sec. for the wide level at 1220 kev to 4×10^{-19} sec. for the very narrow level at 1076 kev. Except for the level at 1161 kev, the only two modes of disintegration of the levels which give gamma-rays are into O^{16} and a short range alpha-particle or into F^{19} and a proton (elastic nuclear scattering). The 1161-kev level probably also disintegrates with the emission of long range alpha-particles.

If all the disintegrations are produced by *s*-protons which resulted in the emission of *s*-alpha-particles, both the intensity and widths of the resonances might be expected to increase smoothly when the proton energy is increased from 800 to 1400 kev. Quantitatively the increase in intensity expected would be about a factor of 8. The increased ratio of widths of the levels would be less than a factor of 8, depending on the relative times involved in concentrating the energy on the disintegration particle in the compound nucleus and the time required for the particle to leak through the barrier.

The general trend of the data of Table I indicates an increasing intensity and width of levels as the proton energy increases. However there are wide variations in intensity and width from level to level. These variations can be explained qualitatively by assuming that the different resonances are produced by protons with differing angular momenta and that the short range alpha-particles may also have several different values of angular momentum. The widths of the levels would decrease as the angular momenta of the protons and alpha-particles increases since the barrier penetrabilities decrease with higher angular momenta. The most intense levels would then correspond to particles with low angular momentum while the weak levels would correspond to particles with higher angular momenta. A complete theoretical interpretation of the problem has been given by Schiff,[23] and we are indebted to him for discussions on the interpretation of our results. He finds that the widths and intensities of the levels can be explained satisfactorily if protons with angular momentum 0, 1, 2, 3, and 4 produce disintegrations and short range alpha-particles with angular momenta of 0, 1, 2, and 3 units result in the disintegration. He concludes that the gamma-rays come from one level in $^*O^{16}$ with even parity and angular momentum $J=1$., and that the pairs come from a level in $^*O^{16}$ with even parity and zero angular momentum.

[23] L. I. Schiff, Phys. Rev. **70**, 891 (1946).

Discussion of the Fluorine-Proton Resonances

L. I. SCHIFF
Department of Physics, University of Pennsylvania, Philadelphia, Pennsylvania
(Received October 1, 1946)

The experimental data on the resonances observed in the production of gamma-rays and pairs during the bombardment of fluorine by protons, presented in the preceding paper, are analyzed with the object of making angular momentum and parity assignments to the excited states of Ne^{20} and O^{16}. The assignments made are of a tentative character, and suggest additional points that might be worthy of further experimental study. The best fit with the data appears to be obtained with a 1^+ oxygen level for the gamma-rays (which are then of magnetic dipole character), and a O^+ oxygen level for the pairs.

THE precise measurement of the excitation functions of the gamma-rays and pairs from the fluorine plus proton reactions by Bonner and his collaborators[1] makes it worth while to attempt a detailed interpretation of the observed resonances in terms of excited states of Ne^{20} and O^{16}. On the basis of the discussion given in the preceding paper, it seems likely that the gamma-rays and pairs arise from excited states of oxygen that are formed by emission of short range alpha-particles from intermediate compound states of neon. Since the resonances are well separated, we make use of the one-level dispersion formula,[2] which states that the thin target yield is proportional to $(2J+1)\Gamma_p\Gamma_\alpha/E[(E-E_0)^2+\frac{1}{4}\Gamma^2]$. Here, J is the total angular momentum quantum number of a particular compound state of Ne^{20}; Γ_p, Γ_α and Γ are, respectively, the proton, short range alpha-particle, and total breadths of this state; E is the bombarding proton energy; and E_0 is the proton energy at resonance. Γ is the sum of Γ_p, Γ_α, and the breadths caused by any other modes of disintegration of the compound state; we assume that the only other possible competing mode is long range alpha-particle emission that leaves the oxygen nucleus in its ground state.

The experimental results are conveniently tabulated in terms of corresponding values of E_0, Γ, and the yield at resonance, which is proportional to $(2J+1)\Gamma_p\Gamma_\alpha/E_0\Gamma^2$. Values for Γ_p and Γ_α are estimated by assuming a "breadth without barrier" and multiplying this by the penetrability of the Coulomb barrier. The latter can readily be calculated for various energies and angular momenta.[3] The breadth without barrier is assumed to have no trend with energy or angular momentum, but to be capable of some variation from the average in particular cases. The average breadth without barrier for the proton is taken to be 33 kev, which is about that obtained for the 440-kev lithium resonance if the observed breadth (11 kev) is not instrumental. Since the long range alphas, like the protons, leave the residual nucleus in its ground state, the same average breadth without barrier is used for them. The short range alphas, however, should have a greater breadth without barrier, since only about a quarter of the maximum alpha-particle energy need be concentrated on them; this breadth is assumed to be 100 kev. Angular momentum and parity are conserved throughout the reactions. The ground state of F^{19}, which has $J=\frac{1}{2}$, is assumed to have odd parity ($\frac{1}{2}^-$).

Several general observations can be made before going into detailed calculations of the type suggested by the above remarks. 1. The pair resonances are considerably broader than all but two of the gamma-ray resonances in the energy range covered (800 to 1400 kev). 2. Long range alpha-particles are found[4] to be in approximate coincidence (as to E_0 and Γ) with two of the four pair resonances (832 and 1362 kev), but with only one of the eleven gamma-ray reso-

[1] W. E. Bennett, T. W. Bonner, C. E. Mandeville, and B. E. Watt, Phys. Rev. **70**, 882 (1946). The writer is indebted to Dr. Bonner for communicating these results prior to publication.
[2] H. A. Bethe and G. Placzek, Phys. Rev. **51**, 450 (1937).
[3] H. A. Bethe, Rev. Mod. Phys. **9**, 166, 178 (1937).
[4] J. F. Streib, W. A. Fowler, and C. C. Lauritsen, Phys. Rev. **59**, 253 (1941).

nances (1161 kev). 3. The two pair resonances that are accompanied by long range alpha-resonances are narrower than the two that are not. 4. It is the broadest of the gamma-ray resonances that is accompanied by a long range alpha-resonance.

It is desirable to explain all of the pair resonances and all of the gamma-ray resonances each in terms of a single oxygen level, since the pairs can come only from a level with $J=0$ which has no non-zero levels below it, and the energy of a gamma-ray is very nearly independent of the resonance from which it arises.[5] Then point 2 above suggests that the oxygen pair level is reached in competition with long range alphas whereas the oxygen gamma-ray level (with perhaps one exception) is not. This is confirmed by point 1, since the long range alpha-competition would broaden the pair resonances in comparison with the gamma-ray resonances. Point 3 is in agreement with this, since the long range alpha-particle breadth is roughly independent of energy and angular momentum (being equal to the breadth without barrier), and so the pairs should be relatively stronger than the long range alphas for the resonances of greater total breadth. Also, point 4 suggests that if the 1161 kev gamma-ray resonance is not an unresolved doublet, the oxygen level is formed in this case from a neon state which can also give long range alphas, thus broadening this resonance. It should be noted in this connection that since the ground state of the oxygen nucleus is 0^+, a 0^+ pair level will always be in competition with long range alphas, whereas a 0^- pair level will never be; on the other hand, the oxygen gamma-ray level, which must have $J\neq 0$, may or may not be competed with by long range alpha-emission, depending on the character of the compound state of neon.

The above arguments lead to the conclusion that the oxygen pair level has even parity (0^+).[4] There is then no need to invoke a non-electromagnetic interaction to account for the production of the pairs.[6] In order to make assignments to the oxygen gamma-ray level and the various compound states of neon, the total breadths and resonance yields must be considered more quantitatively. This has been done with the help of estimates of the partial breadths made as outlined in the second paragraph. Best agreement is found when the oxygen gamma-ray level is 1^+; in this case, the gamma-radiation is of magnetic dipole character. The resulting assignments of the neon states and the angular momentum quantum numbers of the ingoing protons and outgoing alpha-particles are shown in Tables I and II. The total breadths and relative heights of the resonances computed in this way agree with observation within a factor of three in all cases, and within fifty percent in half the cases. Since the partial breadths can vary on account of factors that cannot now be estimated, this is considered satisfactory although not definitive agreement.

A few further points are worthy of mention. 1. The sharp 1076-kev gamma-ray resonance is expected to be considerably narrower and higher than observed. 2. The 1107- and 1161-kev gamma-ray resonances are broader than would be expected from the first assignments given in Table I; the second assignment for 1161 kev assumes long range alpha-competition. 3. As a whole,

TABLE I. Gamma-ray resonances.

E_0 (kev)	Experimental Breadth (kev)	Relative height	Theoretical l_p	Theoretical l_α	Neon state
820	7.6	0.8	2	1	2^-
862	5.2	29.	0	1	0^-
890	4.8	1.0	2	1	2^-
927	8.0	10.	0	1	0^-
1076	< 1.9	>0.5	4	3	4^-
1107	~30.	0.8	2	1	2^-
1122	4.1	0.9	3	2	3^+
1161	~50.	0.8	2 1	1 2	2^- 2^+
1274	19.	2.2	2	1	2^-
1335	4.8	9.0	3	2	3^+
1363	15.	22.	1	0	1^+

TABLE II. Pair resonances.

E_0 (kev)	Experimental Breadth (kev)	Relative height	Theoretical l_p	Theoretical l_α	Neon state
832	28	0.08	1	2	2^+
1100	~70	0.06	1	0	0^+
1220	85	0.2	1	0	0^+
1362	36	0.6	1	2	2^+

[5] P. I. Dee, S. C. Curran, and J. E. Strothers, Nature 143, 759 (1939); T. Lauritsen, C. C. Lauritsen, and W. A. Fowler, Phys. Rev. 59, 241 (1941).

[6] J. R. Oppenheimer and J. S. Schwinger, Phys. Rev. 56, 1066 (1939).

the pairs are somewhat less intense with respect to the gamma-rays than would be expected, by perhaps a factor of three. This may be due to experimental difficulties of calibration, or possibly to enhanced competition of two quantum emission with pair emission from the oxygen pair level produced by one or more fairly low lying 1^- levels of oxygen.[6] 4. In general, many fewer long range alpha-particles are observed than expected. This again may be due to calibration errors, or it may indicate an overestimate of the partial breadth for emission of long range alpha-particles. 5. The 832- and 1362-kev pair resonances should be accompanied by gamma-rays, since with the assignments given in Table II the 1^+ oxygen level can also be reached by alpha-particle emission in these cases. These would, however, be masked by the strong 862- and 1363-kev gamma-ray resonances, respectively. 6. A careful search should be made for the weaker long range alpha-particles that are expected to accompany the 1100- and 1220-kev pair resonances. 7. Measurement of the angular distribution of the long range alpha-particles at their resonances would provide an independent check on the assignments of those levels.

PHYSICAL REVIEW VOLUME 70, NUMBERS 11 AND 12 DECEMBER 1 AND 15, 1946

Experimental Yields with 14-Mev Deuterons*

E. T. CLARKE, *Department of Physics*

AND

JOHN W. IRVINE, JR., *Department of Chemistry*
Massachusetts Institute of Technology, Cambridge, Massachusetts

(Received September 16, 1946)

Thick target yields for the production of seventeen radioactive isotopes by deuteron bombardment are reported in terms of absolute disintegrations per second per microampere hour of 14-Mev deuterons.

TABLE I presents thick target yields obtained by bombarding various targets with the 14-Mev deuteron beam of the M.I.T. cyclotron. The deuteron energy was determined by range measurements in aluminum.[1] Yield data are given as absolute disintegration rates, in terms of 10^6 disintegrating atoms per second per microampere hour of deuterons. As recommended by the National Bureau of Standards and the National Research Council Committee on Standards of Radioactivity,[2] a disintegration rate of 10^6 disintegrations per second is called 1 rutherford (rd); if the millicurie (mC) is arbitrarily taken as 37×10^6 disintegrations per second, then 1 mC = 37 rd, or 1 rd = 0.027 mC = 27 μC. Absolute disintegration rates of gamma-ray emitters were determined on a calibrated gamma-ray counter,[3] while those of isotopes decaying only by beta-ray emission were found on a thin-window beta-ray counter[4] whose absolute efficiency was known.

The first four columns of the table list the characteristics of the processes: the isotope and its half-life,[5] its type of radiation, the target isotope, and the deuteron reaction producing it. The disintegration schemes upon which yield measurements were based are published in the references given in column V. Column VI gives the lower deuteron energy limit below which the reaction cannot be produced. Column VII contains the observed thick target yields which

* The research described in this article was supported in part by Contract N5ori-78, U. S. Navy Department.

[1] E. T. Clarke and J. W. Irvine, Jr., Phys. Rev. 66, 231 (1944).

[2] E. U. Condon and L. F. Curtiss, Phys. Rev. 69, 672 (1946).

[3] A. Roberts, L. G. Elliott, J. R. Downing, W. C. Peacock, and M. Deutsch, Phys. Rev. 64, 268 (1943).

[4] W. Good, A. Kip, and S. Brown, Rev. Sci. Inst. 17, 262 (1946).

[5] G. T. Seaborg, Rev. Mod. Phys. 16, 1 (1944).

TABLE I. Data on thick target yields.

I Isotope	II Half-life	III Radiation	IV Reaction	V Disint. scheme	VI Threshold Mev	VII Yield* rd/μah	VIII Practical target	IX Method of measurement
$_{11}Na^{22}$	3.0 yr.	β^+, γ	$Mg^{24}(d, \alpha)$	a	—	0.065	Mg=1	Ex. fn
$_{11}Na^{24}$	14.8 hr.	β^-, γ	$Na^{23}(d, p)$	b	—	410	Na=1	Ex. fn
$_{11}Na^{24}$	14.8 hr.	β^-, γ	$Mg^{26}(d, \alpha)$	b	—	8.70	Mg=1	Ex. fn
$_{11}Na^{24}$	14.8 hr.	β^-, γ	$Al^{27}(d; p, \alpha)$	b	10	1.66	Al=1	Ex. fn
$_{14}Si^{31}$	170. min.	β^-	$Si^{30}(d, p)$	c, d	—	37	SiO_2=0.47	Thick target
$_{15}P^{32}$	14.30 day	β^-	$P^{31}(d, p)$	c, e	—	8.5	P=1	Thick target
$_{17}Cl^{38}$	37. min.	β^-, γ	$Cl^{37}(d, p)$	f	—	1500	$CaCl_2$=0.64	Thick target
$_{19}K^{42}$	12.4 hr.	β^-	$K^{41}(d, p)$	c	—	8.3	K=1	Thick target
$_{25}Mn^{52}$	6.5 day	β^+, K, γ	$Cr^{52}(d, 2n)$	g	8	3	Cr=1	Thick target
$_{27}Co^{60}$	5.3 yr.	β^-, γ	$Co^{59}(d, p)$	h	—	0.040	Co=1	Ex. fn
$_{29}Cu^{64}$	12.8 hr.	β^-, β^+, K	$Cu^{63}(d, p)$	i	—	92	Cu=1	Ex. fn
$_{30}Zn^{63}$	38. min.	β^+	$Cu^{63}(d, 2n)$	j	6.5	1160	Cu=1	Ex. fn
$_{30}Zn^{65}$	250. day	K, γ	$Cu^{65}(d, 2n)$	k	4.6	0.126	Cu=1	Ex. fn
$_{35}Br^{82}$	34 hr.	β^-, γ	$Br^{81}(d, p)$	l	—	28.5	NaBr=0.80	Ex. fn
$_{36}Kr$	34 hr.	β^+, γ	$Br(d, 2n)$	—	5	190μg Ra	NaBr=0.80	Ex. fn
$_{38}Sr^{89}$	55 day	β^-	$Sr^{88}(d, p)$	m, n	—	1.3	$SrCO_3$=0.60	Thick target
$_{39}Y^{88}$	87 day	K, γ	$Sr^{88}(d, 2n)$	o	6	1.4	$SrCO_3$=0.60	Thick target
$_{53}I^{130}$	12.6 hr.	β^-, γ	$Te^{130}(d, 2n)$	p	?	32	Te=1	Thick target
$_{53}I^{131}$	8.0 day	β^-, γ	$Te^{130}(d, n)$	q	—	3.2	Te=1	Thick target

* 1 rd = 10^4 disintegrating atoms per second.
[a] W. M. Good, D. Peaslee, and M. Deutsch, Phys. Rev. **69**, 313 (1946).
[b] L. G. Elliott, M. Deutsch, and A. Roberts, Phys. Rev. **63**, 386 (1943).
[c] F. N. D. Kurie, J. R. Richardson, and H. C. Paxton, Phys. Rev. **49**, 368 (1936).
[d] H. W. Newson, Phys. Rev. **51**, 624 (1937).
[e] C. M. Witcher, Phys. Rev. **60**, 32 (1941).
[f] Watase, Proc. Phys. Math. Soc. Japan **23**, 618 (1941).
[g] W. C. Peacock and M. Deutsch, Phys. Rev. **69**, 306 (1946).
[h] M. Deutsch, L. G. Elliott, and A. Roberts, Phys. Rev. **68**, 193 (1945).
[i] Cu^{64}: β^+=21 percent, β^-=36 percent, K=43 percent, from S. N. Van Voorhis, Phys. Rev. **50**, 895 (1936), and W. M. Good, Thesis M.I.T. 1944.
[j] A. A. Townsend, Proc. Roy. Soc. **A177**, 357 (1941).
[k] W. M. Good and W. C. Peacock, Phys. Rev. **69**, 680 (1946).
[l] A. Roberts, J. R. Downing, and M. Deutsch, Phys. Rev. **60**, 544 (1941).
[m] E. Haggstrom, Phys. Rev. **62**, 144 (1942).
[n] D. W. Stewart, Phys. Rev. **56**, 629 (1939).
[o] J. R. Downing, M. Deutsch, and A. Roberts, Phys. Rev. **60**, 470 (1942).
[p] See reference 3 in text.
[q] J. R. Downing, M. Deutsch, and A. Roberts, Phys. Rev. **61**, 686 (1942).

would be obtained by bombardment of the pure element (natural isotopic mixture) given in column IV. Column VIII gives the target material generally used, together with the factor by which the given yield must be multiplied to obtain the practical yield.

The last column describes the method of measurement of the particular yield. Those obtained from excitation functions[1] are more accurate (probable error 10 percent) than those found by bombarding thick samples (probable error 20 percent) because the deuteron energy here could not be evaluated with as much certainty. This is particularly true of Mn^{52}, where the yield at 14 Mev is a rapidly varying function of energy.

Since the disintegration scheme for Kr is not known, the yield is given in micrograms radium gamma-ray equivalent, measured on a platinum screen wall gamma-ray counter shielded by 0.16-cm lead.

The Excitation-Function of the γ-Radiation Generated by Po-α Bombardment of Na

MAGDALENE KOVÁCS
Institute of Physics, University of Debrecen, Debrecen, Hungary
(Received June 13, 1946)

IN their early paper Bothe and Becker[1] referred to a weak γ-radiation hardly above the level of observability, when Na is bombarded by α-particles of Po. Their results were justified by Webster[2] and Savel.[3] Savel measured the intensity of the radiation at 5 different α-particle energies and found its energy by means of lead absorption measurements to be 1.7–1.9 Mev. The knowledge of the exact shape of the excitation-function might lead us to the explanation of the origin of this radiation. This excitation-function has been observed and is here reported.

Figure 1 shows the apparatus used. The Po source was situated in the middle of a glass bulb of 7-cm diameter. The Po was concentrated on the plain, highly polished surface of a Pt-Ir disk of 3-mm diameter by means of a volatilization method used at this Institute.[4] Its strength was 7 mC at the start of the measurements. As the source was not freshly prepared, the inhomogeneity of the α-rays was considerable with a spread of ±1.5 mm around the mean-range. The α-rays have been stopped in the usual way by a regulated CO_2 atmosphere. The γ-quanta were observed in a brass G-M counter, filled with argon and alcohol vapor and situated in a closed glass tube. The time-constant of the whole counting-equipment was about 0.003 sec. Pure metallic sodium was evaporated out of a very small electric furnace under vacuum into the inside of the cooled glass bulb. After several repeated vaporizations a sufficiently thick layer of pure metallic sodium condensed on the inside of the glass bulb.

Figure 2 shows the integral excitation-curve of the γ-radiation. The absolute yield of the γ-radiation is between 1 and 2 γ-quanta/10^6 α-particles at the maximum used range.

As for the discussion about the origin of the γ-radiation we must consider that when Na is bombarded by α-particles, the following processes may occur: (1) α-capture followed by a neutron emission; (2) α-capture followed by a proton emission; (3) excitation of the bombarded nucleus without capture of the α-particle (inelastic scattering).

Measurements of Savel and H. O. Brandt[5] show that neutron emission does not occur at such small α-energies. Investigations about the proton

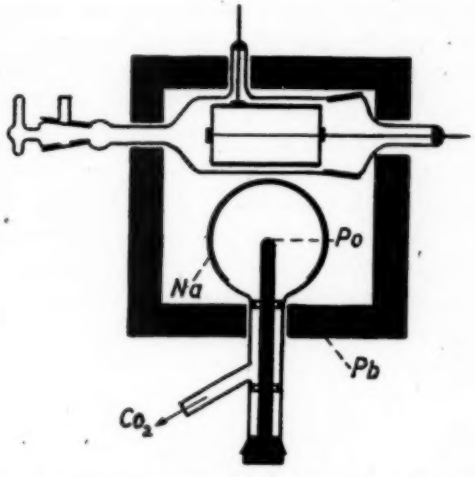

FIG. 1. Apparatus for the bombardment of Na by Po α-particles and observation of the γ-radiation.

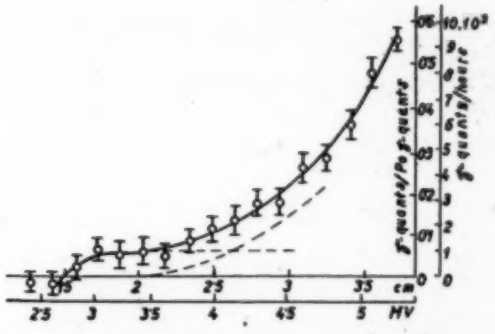

FIG. 2. Excitation-function of the γ-radiation excited, when Na is bombarded by α-particles. Abscissa: Range and energy of the α-particles, respectively; Ordinate: Left: number of excited γ-quanta in proportion of the γ-quanta of the bombarding Po source, Right: actual number of counted γ-quanta/hours.

[1] W. Bothe and H. Becker, Naturwiss. **18**, 705 (1930).
[2] H. C. Webster, Proc. Roy. Soc. London **A136**, 428 (1932).
[3] P. Savel, Ann. de physique **4**, 88 (1935).
[4] A. Szalay, Zeits. f. Physik **112**, 29 (1939).
[5] H. Brandt, Zeits. f. Physik **108**, 726 (1937).

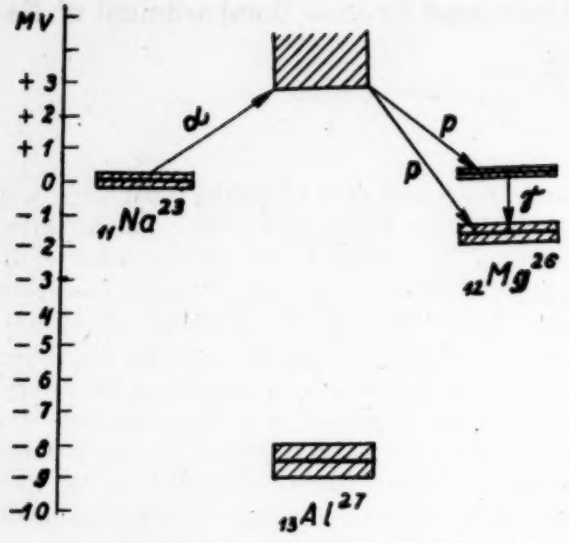

FIG. 3. Suggested term-scheme for the origin of the γ-radiation excited at the bombardment of Na by Po α-particles.

emission have been made by A. König,[6] May and Vaydianathan,[7] and Humphreys and Pollard.[8]

The excitation-curve of the radiation on Fig. 2 seems to consist of two parts. One of them starts at 2.7 ± 0.1 Mev α-energy and then keeps a small, but constant intensity level. In addition to this, there is a quick rise from 3.5 ± 0.1 Mev energy upwards, possibly originating from another component.

There are the following reasons to believe that this quickly rising γ-component must be in connection with the proton group C of 23-cm range observed by König:

1. König observed the minimum α-range needed for the emission of this proton group to be about 2 cm.

2. The energy difference between the proton groups D and C, as can be calculated from the measurements of König, is about 2 Mev and is herewith in accordance with the measurements of Savel for the energy of these γ-rays.

3. It has been shown by Humphreys and Pollard that the Mg^{26}-nucleus possesses an excitation level of 1.92 Mev.

4. The yields are in good accordance. The yield of the γ-radiation is about 1–2 γ-quanta/10^6 α-particles and the yield of the C proton group of 23-cm range is about 2 protons/10^6 α-particles for the same energy.

Considering the facts above, an explanation for the origin of the γ-radiation can be suggested according to the term-scheme on Fig. 3. The more intense part of the radiation finds its origin in the excitation level of the residual Mg^{26}-nucleus of the proton emission.

As for the less intense component of the γ-radiation starting at 2.7 Mev α-energy, it cannot be decided now whether it is a result of an excitation without capture (inelastic scattering) or whether it also corresponds to the proton emission as well, for the proton emission has not as yet been investigated with sufficient accuracy for such small α-energies.

I wish to express my best thanks to Professor A. Szalay, Director of the Institute, for his suggestions, kind help, and for having prepared the Po source.

These measurements were finished in June, 1943.

[6] A. König, Zeits. f. Physik **90**, 197 (1934).
[7] A. May and R. Vaydianathan, Proc. Roy. Soc. London **A155**, 531 (1936).
[8] R. F. Humphreys and E. Pollard, Phys. Rev. **59**, 942 (1941).

PHYSICAL REVIEW VOLUME 70, NUMBERS 11 AND 12 DECEMBER 1 AND 15, 1946

Angular Correlation of Gamma-Rays

G. GOERTZEL*
New York University, Washington Square, New York, New York
(Received August 23, 1946)

The calculation of the angular correlation of successive gamma-rays from an atomic nucleus, carried out by Hamilton, has been extended to take into account the effect of the magnetic field at the nucleus because of the extra-nuclear electrons. Results are given in a form valid for all multipole orders. In addition, it is shown that an external magnetic field may be used to reduce the effect of the extra-nuclear electrons on the angular correlation. A method of calculating the effect of an external magnetic field on the angular distribution of the successive gamma-rays is indicated.

INTRODUCTION

WHEN an atomic nucleus emits two gamma-rays in succession, one might expect from general considerations of radiation theory that the direction of emission of the second gamma-ray is related in some way to the direction of propagation of the first. This correlation is expected to depend on the electric or magnetic multipole nature of the radiation and on the angular momentum of the nuclear levels involved. Some light may be shed on these factors by a comparison of experimentally determined angular distributions with the theoretical expectations.

The pioneer investigations of Hamilton[1] into the theory of the angular distribution of successive gamma-rays emitted by a nucleus were made with the restriction that torques due to fields external to the nucleus be sufficiently small to have a negligible effect on the angular correlation. Inasmuch as fields external to the nucleus, arising from the spin and orbital angular moments of the extra-nuclear electrons, may produce appreciable torques, it seems desirable to investigate the quantitative effect of fields external to the nucleus and to determine their influence on the angular distribution of the successive gamma-rays.

THEORY

Consider an atom which is visualized as existing in any one of three gross energy levels, A', B', and C'. Each of the gross levels consists of several sublevels which arise through the coupling of one of the nuclear energy levels A, B, and C, with the external electronic structure of the atom. That is, each gross level is composed of a set of hyperfine structure sublevels with separations very small by comparison with the separation of the gross levels.

The sublevels of the gross energy levels A' are indicated by α, α', α'', $\cdots$; those of B' by β, β', β'', $\cdots$; and those of C' by γ, γ', γ'', $\cdots$. If the sequence of transitions

1. from a level α to a level β with the emission of a gamma-ray ρ of frequency ν_ρ,
2. from the level β to a level γ with the emission of a gamma-ray σ of frequency ν_σ,

is assumed, the equations for the probability amplitudes become[2]

$$-i\hbar\dot{a}_\alpha=\sum_{\beta,\rho}(\alpha|H_\rho|\beta)b_{\beta,\rho}+h\nu_\alpha a_\alpha, \tag{1a}$$

$$-i\hbar\dot{b}_{\beta,\rho}=\sum_\alpha(\alpha|H_\rho|\beta)^*a_\alpha+\sum_{\gamma,\sigma}(\beta|H_\sigma|\gamma)c_{\gamma,\rho,\sigma}+h(\nu_\rho+\nu_\beta)b_{\beta,\rho}, \tag{1b}$$

$$-i\hbar\dot{c}_{\gamma,\rho,\sigma}=\sum_\beta(\beta|H_\sigma|\gamma)^*b_{\beta,\rho}+h(\nu_\rho+\nu_\sigma+\nu_\gamma)c_{\gamma,\rho,\sigma}, \tag{1c}$$

where $E_\alpha=h\nu_\alpha$, etc., and the zero of energy is chosen at any convenient value.

The following solutions are assumed, subject to determination of the constants involved by substitution into Eq. (1).

$$a_\alpha=\delta_\alpha\exp(-2\pi\Gamma_\alpha t), \tag{2a}$$

* Now at Clinton Laboratories, Monsanto Chemical Company, Knoxville, Tennessee.

[1] D. R. Hamilton, Phys. Rev. **58**, 122 (1940).

[2] In setting up and solving Eq. (1), the procedure of reference 1 is followed closely. Cf. G. Breit, Rev. Mod. Phys. **5**, 91 (1933).

$$b_{\beta,\rho}=\sum_\alpha \zeta_{\alpha,\beta,\rho}\{\exp(-2\pi\Gamma_\alpha t)-\exp(-2\pi\Gamma_{\beta,\rho}t)\}, \quad (2b)$$

$$c_{\gamma,\rho,\sigma}=\sum_\alpha \epsilon_{\alpha,\gamma,\rho,\sigma}\{\exp(-2\pi\Gamma_\alpha t)-\exp(-2\pi\Gamma_{\gamma,\rho,\sigma}t)\}+\sum_\beta \eta_{\beta,\gamma,\rho,\sigma}\{\exp(-2\pi\Gamma_{\beta,\rho}t)-\exp(-2\pi\Gamma_{\gamma,\rho,\sigma}t)\}. \quad (2c)$$

Upon substitution of Eq. (2) into Eq. (1), one finds

$$\Gamma_\alpha=\gamma_A-i\nu_\alpha, \quad (3a)$$

$$\Gamma_{\beta,\rho}=\gamma_B-i(\nu_\rho+\nu_\beta), \quad (3b)$$

where

$$\Gamma_{\gamma,\rho,\sigma}=-i(\nu_\rho+\nu_\sigma+\nu_\gamma), \quad (3c)$$

$$h^2\gamma_A=\sum_{\beta,\rho}|(\alpha|H_\rho|\beta)|^2, \quad (4a)$$

$$h^2\gamma_B=\sum_{\gamma,\sigma}|(\beta|H_\sigma|\gamma)|^2. \quad (4b)$$

γ_A and γ_B are independent of the particular sublevels α or β of A' or B' from which they are computed. $\sum_{\beta,\rho}$ denotes the sum over all states β which can be reached by all perturbations H_ρ. One may deduce from Eqs. (2)–(4) that $4\pi\gamma_A$ is the total transition probability from any level α.

Also,

$$\lim_{t\to\infty} c_{\gamma,\rho,\sigma}=\sum_{\alpha,\beta}\frac{\delta_\alpha^*(\alpha|H_\rho|\beta)^*(\beta|H_\sigma|\gamma)^*\exp(i2\pi[\nu_\rho+\nu_\sigma-\nu_\alpha]t)}{(i\gamma_B+\nu_{\beta,\gamma}-\nu_\sigma)(i\gamma_A+\nu_{\alpha,\gamma}-\nu_\rho-\nu_\sigma)}, \quad (5)$$

where $\nu_{\alpha,\beta}=\nu_\alpha-\nu_\beta$, etc. δ_α expresses the arbitrariness of the phases of the wave functions of the initial states, so that

$$\langle\delta_\alpha^*\delta_{\alpha'}\rangle_{Av}=\delta_{\alpha,\alpha'}, \quad (6)$$

where $\delta_{\alpha,\alpha'}$ is the Kronecker delta-function and the angular brackets denote an average over all nuclei.

With the aid of Eq. (5), the angular correlation of the successive quanta may be obtained as follows. w, defined by

$$w=|\lim_{t\to\infty} c_{\gamma,\rho,\sigma}|^2, \quad (7)$$

may be interpreted as the probability that a given nucleus will be found in a final state γ and that quanta ρ and σ will have been emitted with definite directions, frequencies, and polarizations. The average of w over all nuclei, all gamma-ray energies,[3] both directions of polarization of each quantum, and all finall states γ of the system, gives the desired directional correlation of the successive gamma-rays:

$$W=\sum_{P,N}\int_0^\infty d\nu_\rho\int_0^\infty d\nu_\sigma\sum_\gamma w, \quad (8)$$

where $\sum_{P,N}$ denotes an average over all nuclei and all polarizations of the emitted quanta.

Using Eqs. (5)–(8), one obtains

$$W(\mathbf{k}_\rho,\mathbf{k}_\sigma)=\sum\{\alpha,\beta,\beta',\gamma,P_\rho,P_\sigma\}\frac{(\alpha|H(\mathbf{k}_\rho,P_\rho)|\beta)^*(\beta|H(\mathbf{k}_\sigma,P_\sigma)|\gamma)^*(\alpha|H(\mathbf{k}_\rho,P_\rho)|\beta')(\beta'|H(\mathbf{k}_\sigma,P_\sigma)|\gamma)}{1-i\nu_{\beta,\beta'}/2\gamma_B}. \quad (9)$$

In Eq. (9), $\mathbf{k}_\rho$ and $\mathbf{k}_\sigma$ are vectors indicating the directions of propagation of the quanta, whereas P_ρ and P_σ indicate the polarizations (it is convenient in the following to use circular polarization, so that the quantum number P has the values 1 and -1 corresponding to left- or right-handed circular polarization).

Each sublevel, α, β, or γ, is completely characterized by appropriate values of the quantum numbers I, J, F, and m[4]; I is the nuclear angular momentum quantum number, J the electronic angular momentum quantum number, F the resultant of I and J, and m the projection of F on the Z axis. One may therefore write (it is assumed that the emitted gamma-ray does not alter the configuration of the electronic state, so that J remains unaltered)

$$(\alpha|H(\mathbf{k}_\rho,P_\rho)|\beta)=(aF_\alpha m_\alpha|H(\mathbf{k}_\rho,P_\rho)|bF_\beta m_\beta). \quad (10)$$

Here, b represents the quantum numbers that

[3] The matrix elements in Eq. (5) are assumed to be effectively independent of frequency over a range of frequencies greater than both the radiation breadth of the nuclear levels and the hyperfine structure separation of the sublevels.

[4] It is assumed in the present calculation that J is a good quantum number.

are the same for all sublevels of B'; that is, b represents I_B, J, and any other quantum numbers necessary to describe the nuclear level B. Also, $\sum_\beta$ means $\sum\{F_\beta, m_\beta\}$, etc.

By using the well-known methods of transformation theory, the matrix elements in Eq. (10) may be written, in the first approximation,

$$\sum_{l, m_J, n} (I_A J F_\alpha m_\alpha | I_A J l m_J)(a l m_J | H(\mathbf{k}_\rho, P_\rho) | b n m_J) \times (I_B J n m_J | I_B J F_\beta m_\beta). \quad (11)$$

In Eq. (11), l is the component along the Z axis of I_A, n that of I_B, and m_J that of J. Similarly, in the following p will denote the component along the Z axis of I_C.

Since the matrix element

$$(a l m_J | H(\mathbf{k}_\rho, P_\rho) | b n m_J)$$

is independent of m_J, this quantum number will be omitted when writing the matrix element. The $(IJFm | IJm_I m_J)$ are the transformation coefficients for vector addition[5] and form a real and unitary matrix, so that

$$\sum_{F, M} (IJm_I m_J | IJFm)(IJFm | IJm_I' m_J') = \delta_{m_I, m_I'} \delta_{m_J, m_J'}, \quad (12)$$

$$\sum_{m_I, m_J} (IJFm | IJm_I m_J)(IJm_I m_J | IJF'm') = \delta_{F, F'} \delta_{m, m'}. \quad (13)$$

It is convenient to remember that

$$(IJm_I m_J | IJFm) = (IJFm | IJm_I m_J) = 0 \quad \text{unless } m = m_I + m_J. \quad (14)$$

Upon substituting of Eq. (10) and (11) and a corresponding set of relations for $(\beta | H(\mathbf{k}_\sigma, P_\sigma) | \gamma)$ into Eq. (9), one obtains, with the aid of Eqs. (12)–(14) and (17), for either $\mathbf{k}_\rho$ or $\mathbf{k}_\sigma$ along the Z axis,

$$W(\mathbf{k}_\rho, \mathbf{k}_\sigma) = \sum\{l, n, n', p, P_\rho, P_\sigma\} | (a l | H(\mathbf{k}_\rho, P_\rho) | b n) |^2 S_{n, n'} | (b n' | H(\mathbf{k}_\sigma, P_\sigma) | c p) |^2, \quad (15)$$

where

$$S_{n, n'} = \sum_{r, s, m, F, F', m'} \frac{(I_B J n r | I_B J F m)(I_B J F m | I_B J n' s)(I_B J n' s | I_B J F' m')(I_B J F' m' | I_B J n r)}{\{2J+1\}\{1+(\nu_{F, F'}/2\gamma_B)^2\}}. \quad (16)$$

The summation in Eq. (16) is over all values of r, s, m, F, and F' consistent with the definition of the transformation coefficients and the given values of I_B, J, n, and n'. $\nu_{F, F'}$ is the separation of the levels β and β' corresponding to F and F'. The factor of $2J+1$ in the denominator of Eq. (16) is merely inserted for convenience. The multiplication of W by any constant factor is permissible, since one is interested in the relative, not the absolute, value of W as a function of the angle between the successive quanta.

In the calculation of Eq. (15), use was made of the relation that, for $\mathbf{k}$ along the Z axis,

$$(a l | H(\mathbf{k}, P) | b n)^* (a l | H(\mathbf{k}, P) | b n') = 0 \quad \text{unless } n = n', \quad (17)$$

which follows from Eqs. (29)–(31), and (34) below.

Equations (15) and (16) are the formal results for the angular distribution of successive quanta emitted by a nucleus, including the effect of the magnetic moment of the extranuclear electrons. It is of interest to see how these reduce to Hamilton's[1] result. The criterion for this is that

$$(\nu_{F, F'}/2\gamma_B)^2 \ll 1, \quad (18)$$

so that, from Eq. (16),

$$S_{n, n'} = \delta_{n, n'}; \quad [(\nu_{F, F'}/2\gamma_B)^2 \ll 1]. \quad (19)$$

If Eq. (19) is substituted in Eq. (15), the following is obtained.

$$W(\mathbf{k}_\rho, \mathbf{k}_\sigma) = \sum\{l, n, p, P_\rho, P_\sigma\} \times | (a l | H(\mathbf{k}_\rho, P_\rho) | b n) |^2 \times | (b n | H(\mathbf{k}_\sigma, P_\sigma) | c p) |^2. \quad (20)$$

This is precisely the result of reference 1.

The criterion (18) is in agreement with the conclusion of Hamilton, who stated that the radiation width of the levels β must be much greater than the splitting of B' because of the magnetic field of the atomic electrons.

[5] E. U. Condon and G. H. Shortley, *Theory of Atomic Spectra* (Cambridge University Press, Cambridge, 1935), especially pages 73–78. See also reference 7.

Equation (18) may be put in a somewhat more instructive form. Writing

$$S_{n,n'}=\delta_{n,n'}-\alpha_{n,n'}, \tag{21}$$

one has from Eq. (16)

$$\alpha_{n,n'}=\sum_{F,F'}\left(\frac{[\nu_{F,F'}/2\gamma_B]^2}{1+[\nu_{F,F'}/2\gamma_B]^2}\right)\sum_{r,s,m,m'}\frac{(nr|Fm)(Fm|n's)(n's|F'm')(F'm'/nr)}{2J+1}, \tag{22}$$

$$|\alpha_{n,n'}|\leqslant(\Delta\nu/2\gamma_B)^2,$$

where $\Delta\nu$ is the largest value, for all F and F', of $\nu_{F,F'}$. If one assumes as the criterion that Eq. (20) be valid the relation $|\alpha_{n,n'}|\leqslant 0.01$, a sufficient condition for the validity of Eq. (20) is

$$|\Delta\nu/2\gamma_B|\leqslant 0.1. \tag{23}$$

In a slightly different form, one has

$$\tau_B=\frac{1}{4\pi\gamma_B}\leqslant\frac{1}{20\pi\Delta\nu} \tag{24}$$

as an upper limit to the lifetime of the intermediate nuclear state for the validity of the calculation of the angular correlation with the nelect of the interaction of the nuclear magnetic moment with that of the electrons. For a hyperfine structure splitting of 1 cm^{-1}, Eq. (24) yields as the upper limit to the lifetime of the intermediate state 0.5×10^{-12} sec. This estimate seems conservative.

The matrix elements in Eq. (15) may be evaluated in a general manner applicable to transitions of any multipole order by employing the expansion of the potential of a plane electromagnetic wave in terms of the spherical wave solutions of the radiation equations. A convenient form of this expansion is derived in Appendix 1 by group theoretical methods.

The matrix elements in Eq. (15) correspond to the emission from a nucleus of a plane wave in a given direction and with a specified polarization. A possible set of potentials to describe a plane electromagnetic wave is

$$\mathbf{A}(\mathbf{k},P)=2^{-\frac{1}{2}}(\mathbf{u}_1+iP\mathbf{u}_2)\exp i(\mathbf{k}\cdot\mathbf{r}-kct)+2^{-\frac{1}{2}}(\mathbf{u}_1-iP\mathbf{u}_2)\exp i(-\mathbf{k}\cdot\mathbf{r}+kct), \tag{25}$$

$$\varphi(\mathbf{k},P)=0,$$

where

$$\mathbf{k}\cdot\mathbf{k}=k^2;\quad \mathbf{k}=k\mathbf{u}_3;\quad P=\pm1,$$
$$\mathbf{u}_i\cdot\mathbf{u}_j=\delta_{i,j},\quad i,j=1,2,3;$$
$$\mathbf{u}_1\times\mathbf{u}_2=\mathbf{u}_3.$$

Equation (25) describes an electromagnetic plane wave of frequency $kc/2\pi$ propagated in direction $\mathbf{u}_3$. This wave is left- or right-handed circularly polarized, depending on whether P is 1 or -1, as may be verified by using

$$\mathbf{H}=\nabla\times\mathbf{A};\quad \mathbf{E}=-\frac{1}{c}\frac{\partial\mathbf{A}}{\partial t}$$

TABLE I. Spherical wave potentials for the electromagnetic field.* In the gauge where the scalar potential is zero, a complete set of potentials for the radiation field is given by the following electric and magnetic multipoles. The multipole order corresponding to a given L is 2^L, and there are $2(2L+1)$ solutions for each L, since M can take on any of the $2L+1$-values $-L,-(L-1),\cdots,(L-1),L$, and one can have either electric or magnetic radiation. All potentials are normalized to $(\pi^2\hbar k)^{-1}$ quanta/sec.

Magnetic multipoles, $\mathbf{A}_0(LM)$

$$2^{-\frac{1}{2}}(A_{0x}+iA_{0y})=B_1f_L(kr)\,Y_L^{M+1}\exp-ikct$$
$$A_{0z}=B_0f_L(kr)\,Y_L^{M}\exp-ikct$$
$$-2^{-\frac{1}{2}}(A_{0x}-iA_{0y})=B_{-1}f_L(kr)\,Y_L^{M-1}\exp-ikct,$$

where

$$B_\sigma=(L\;1LM|L\;1M+\sigma\;-\sigma),$$
$$\sigma=\pm1,0.$$

Electric multipoles, $\mathbf{A}_e(LM)$

$$2^{-\frac{1}{2}}(A_{ex}+iA_{ey})=\{C_1f_{L+1}(kr)\,Y_{L+1}^{M+1}+D_1f_{L-1}(kr)\,Y_{L-1}^{M+1}\}\exp-ikct$$
$$A_{ez}=\{C_0f_{L+1}(kr)\,Y_{L+1}^{M}+D_0f_{L-1}(kr)\,Y_{L-1}^{M}\}\exp-ikct$$
$$-2^{-\frac{1}{2}}(A_{ex}-iA_{ey})=\{C_{-1}f_{L+1}(kr)\,Y_{L+1}^{M-1}+D_{-1}f_{L-1}(kr)\,Y_{L-1}^{M-1}\}\exp-ikct,$$

where

$$C_\sigma=-\left(\frac{L}{2L+1}\right)^{\frac{1}{2}}(L+1\;1LM|L+1\;1\;M+\sigma\;-\sigma)$$
$$D_\sigma=+\left(\frac{L+1}{2L+1}\right)^{\frac{1}{2}}(L-1\;1LM|L-1\;1\;M+\sigma\;-\sigma)$$
$$\sigma=\pm1,0.$$

* See references 6 and 16 in text.

to obtain

$$\mathbf{E}\cdot\mathbf{u}_1=-2^{\frac{1}{2}}k\sin(\mathbf{k}\cdot\mathbf{r}-kct),$$
$$\mathbf{E}\cdot\mathbf{u}_2=P2^{\frac{1}{2}}k\cos(\mathbf{k}\cdot\mathbf{r}-kct),$$
$$\mathbf{E}\cdot\mathbf{u}_3=0,$$
$$\mathbf{H}\cdot\mathbf{u}_1=-P2^{\frac{1}{2}}k\cos(\mathbf{k}\cdot\mathbf{r}-kct),$$
$$\mathbf{H}\cdot\mathbf{u}_2=-2^{\frac{1}{2}}k\sin(\mathbf{k}\cdot\mathbf{r}-kct),$$
$$\mathbf{H}\cdot\mathbf{u}_3=0.$$

Only the term in Eq. (25) containing the factor $\exp(-ickt)$ contributes to the emission of radiation, so that only this term need be considered further. The following expansion is derived in Appendix (1):

$$2^{-\frac{1}{2}}(\mathbf{u}_1+iP\mathbf{u}_2)\exp i(\mathbf{k}\cdot\mathbf{r}-kct)$$
$$=\pi\sum_{L=1}^{\infty}\sum_{M=-L}^{L}i^L(2L+1)^{\frac{1}{2}}\mathbf{D}^{(L)}(\varphi,\vartheta,0)_{M,P}$$
$$\times[\mathbf{A}_0(LM)+iP\mathbf{A}_e(LM)]. \quad (26)$$

Here, $\mathbf{A}_e(LM)$ and $\mathbf{A}_0(LM)$ are the various spherical eigenwave solutions of Maxwell's equations, as derived by Heitler[6] and as listed in Table I. The $\mathbf{D}^{(L)}(\varphi,\vartheta,0)_{M,P}$ are known functions of ϑ and φ, some of whose properties are briefly discussed in Appendix (2).[7] ϑ and φ are the polar coordinates specifying the direction of the propogation vector $\mathbf{k}$, so that

$$k_x=k\sin\vartheta\cos\varphi;\quad k_y=k\sin\vartheta\sin\varphi;$$
$$k_z=k\cos\vartheta.$$

Since, in the gauge where $\varphi=0$,

$$H(\mathbf{k},P)=\mathbf{p}\cdot\mathbf{A}(\mathbf{k},P) \quad \text{(non-relativistic)} \quad (27a)$$
$$H(\mathbf{k},P)=\boldsymbol{\alpha}\cdot\mathbf{A}(\mathbf{k},P) \quad \text{(relativistic)} \quad (27b)$$

($\mathbf{p}$ is the linear momentum operator of the radiating particle and $\boldsymbol{\alpha}$ is the Dirac vector matrix), one finds with the aid of Eq. (25) and (26)

$$(bn|H(\mathbf{k},P)|cp)=\pi\sum_{L,M}i^L(2L+1)^{\frac{1}{2}}\mathbf{D}^{(L)}(\varphi,\vartheta,0)_{M,P}$$
$$\times(bn|\tfrac{\mathbf{p}}{\alpha}\cdot[\mathbf{A}_0(LM)+iP\mathbf{A}_e(LM)]|cp). \quad (28)$$

The assumption is now made that the nuclear transition corresponds to the emission of light of some definite multipole order.[8] Then, all the matrix elements in Eq. (28) vanish except those corresponding to, say, 2^L-pole radiation, so that

$$(bn|H(\mathbf{k},P)|cp)$$
$$=\pi i^L(2L+1)^{\frac{1}{2}}\sum_M\mathbf{D}^{(L)}(\varphi,\vartheta,0)_{M,P}$$
$$\times(bn|\tfrac{\mathbf{p}}{\alpha}\cdot[\mathbf{A}_0(LM)+iP\mathbf{A}_e(LM)]|cp). \quad (29)$$

From Appendix (3),

$$(bn|\tfrac{\mathbf{p}}{\alpha}\cdot[\mathbf{A}_0(LM)+iP\mathbf{A}_e(LM)]|cp)$$
$$=C(I_Bn|Y_L{}^M|I_Cp)=C'(I_CLpM|I_CLI_Bn), \quad (30)$$

where C and C' are independent of n, p, or M. Also,

$$(In|Y_L{}^M|I'p)=0 \quad \text{unless } n=M+p \quad (31)$$

(cf. Eq. (14)). Upon substituting Eq. (30) and (29) into Eq. (15) and using Eq. (31) (ϑ is written for the angle between $\mathbf{k}_p$ and $\mathbf{k}_e$), one finds

$$W(\vartheta)=\sum_{M,M',n,n'}|(I_An+M'|Y_{L'}{}^{M'}|I_Bn)|^2$$
$$\times S_{n,n'}|(I_Bn'|Y_L{}^M|I_Cn'-M)|^2f_{LM}(\vartheta), \quad (32)$$
$$M'=\pm1,$$

where $S_{n,n'}$ is defined by Eq. (16) and

$$f_{LM}(\vartheta)=\sum_{P=\pm1}|\mathbf{D}^{(L)}(\varphi,\vartheta,0)_{M,P}|^2. \quad (33)$$

In obtaining Eq. (32), $\mathbf{k}_p$ was taken along the Z axis and use was made of the result from Appendix (2) that

$$\mathbf{D}^{(L)}(0,0,0)_{M',P}=\delta_{M',P}. \quad (34)$$

If $\mathbf{k}_e$ is taken along the Z axis rather than $\mathbf{k}_p$, the

[6] W. Heitler, Proc. Camb. Phil. Soc. **32**, 112 (1936). An independent solution has been given by W. W. Hansen, Phys. Rev. **47**, 139 (1935).

[7] For a more complete discussion, see Eugen Wigner, *Gruppentheorie* (Friedrich Vieweg und Sohn Akt.-Ges., Braunschweig, 1931), Chapters 14 and 15.

[8] Magnetic and electric multipole radiation of the same order cannot occur in the same transition, since one or the other will be forbidden by the parity selection rules. However, a mixing of radiations of different multipole orders, such as magnetic dipole and electric quadrupole, might occur. (Cf. A. C. Helmholz, Phys. Rev. **60**, 415 (1941) and S. M. Dancoff and P. Morrison, Phys. Rev. **55**, 122 (1939)). In this case, it is necessary, to determine the angular correlation, to know the relative values of the constant C in Eq. (30) for the two types of radiation. Our knowledge of nuclear structure is insufficient to enable the determination of the complex constant C.

following apparently different result is found

$$W(\vartheta)=\sum_{M,M',n,n'}|(I_An+M'|Y_{L'}{}^{M'}|I_Bn)|^2 \times S_{n,n'}|(I_Bn'|Y_L{}^M|I_Cn'-M)|^2 f_{L'M'}(\vartheta), \quad (32')$$
$$M=\pm 1.$$

Since the angular correlation is independent of the choice of coordinate axis, Eqs. (32) and (32′) should give the same result for $W(\vartheta)$. The appropriate transformation of coordinates, when applied to Eq. (32), can be shown to convert Eq. (32) into Eq. (32′). This equivalence of Eqs. (32) and (32′) is a useful check in specific calculations.

Equation (32) may be transformed so as to verify a conjecture of Hamilton.[1] $W(\vartheta)$ is a polynomial of degree k in $\cos^2\vartheta$, where k is an integer such that[9]

$$k\leqslant L; \quad k\leqslant L'.$$

Hamilton conjectured that also

$$k\leqslant I_B.$$

To show this, note that

$$\sum_M|(I_Bn'|Y_L{}^M|I_Cn'-M)|^2 f_{LM}(\vartheta) = \sum_{p,\,(P=\pm 1)}(I_Bn'|\sum_M \mathbf{D}^{(L)}(R)_{M,P}Y_L{}^M|I_Cp) \times(I_Bn'|\sum_{M'}\mathbf{D}^{(L)}(R)_{M',P}Y_L{}^{M'}|I_Cp)^*, \quad (35)$$

where R denotes the rotation of coordinates that would bring the original Z axis (along $\mathbf{k}_p$) into coincidence with $\mathbf{k}_\sigma$. Upon applying the rotation of coordinates R to Eq. (35) and using the results of Appendix (2), one obtains

$$W(\vartheta)=\sum_{M,M',n,n',n''}|(I_An+M'|Y_{L'}{}^{M'}|I_Bn)|^2 \times S_{n,n'}|\mathbf{D}^{(I_B)}(R^{-1})_{n'',n'}|^2 \times|(I_Bn''|Y_L{}^M|I_Cn''-M)|^2, \quad (32'')$$
$$M=\pm 1; \quad M'=\pm 1.$$

From Eq. (32″) it is seen that the highest power of $\cos\vartheta$ that appears in $W(\vartheta)$ is not greater than $2I_B$.[10] Hence, $k\leqslant I_B$.

[9] One may verify from Eq. (33) and reference 7, page 180, Eq. (27), that $f_{LM}(\theta)$ is a polynomial of degree L in $\cos^2\vartheta$. From Eq. (32) one sees that $k\leqslant L$. Likewise, from Eq. (32′), $k\leqslant L'$.

[10] This again follows from reference 7, page 180, Eq. (27).

TABLE II. The following values are obtained by the use of Eq. (33) in conjunction with Eq. (A19).

L	$\lvert M\rvert$	$2f_{LM}(\theta)$
1	0	$2-2\cos^2\vartheta$
1	1	$1+\cos^2\vartheta$
2	0	$6\cos^2\vartheta-6\cos^4\vartheta$
2	1	$1-3\cos^2\vartheta+4\cos^4\vartheta$
2	2	$1-\cos^4\vartheta$

Values of the matrix elements $(In|Y_L{}^M|I'p)$ are given in many places,[11] while the $f_{LM}(\vartheta)$ are listed in Table II. A comparison of Eq. (32) with the corresponding result of reference 1 shows that whenever Eq. (19) is satisfied, the present results are identical with those of reference 1 for dipole and quadrupole radiation. Higher multipoles are not considered in detail in reference 1.

To summarize, the angular correlation of gamma-rays emitted in successive nuclear transitions is given by either Eq. (32) or Eq. (32′) in conjunction with Eqs. (16) and (33). If the lifetime of the nucleus in its intermediate state satisfies Eq. (18), then $S_{n,n'}$ may be replaced by $\delta_{n,n'}$. This case may be indicated by saying that the probability of reorientation of the nuclear angular momentum while the nucleus is in its intermediate state is negligible. In fact, it is clear from Eq. (15) that $S_{n,n'}$ may be interpreted as the probability that, if the nucleus has a component n of angular momentum along the Z axis immediately after the first gamma-ray is emitted, it will have a component n' just before the second gamma-ray is emitted.

EFFECT OF AN EXTERNAL MAGNETIC FIELD

Inasmuch as the projection along the field of the angular momentum of a system in a steady magnetic field is a constant of the motion, one might expect that the reorientation probability could be reduced by the application of a sufficiently strong field along the Z axis. (Note that the direction of the Z axis has been previously defined by the statement that one of the emitted gamma-rays is collected along the Z axis. Hence, the magnetic field must be applied so that it coincides in direction with the line from the radioactive source to one of the gamma-ray detectors.) That this expectation is justified is

[11] For example, references 5 and 7 (use is made of Eq. (30)).

shown below and an estimate of the strength of the necessary magnetic field is obtained.

To calculate the angular correlation of the successive gamma-rays in the presence of an external magnetic field in the direction specified above, the derivation of Eqs. (15) and (16) is repeated, taking into account the presence of the external field. This field alters the zero-order wave functions to be used in describing the states of the system.

In the derivation of Eqs. (15) and (16) the wave functions of the radiating system were taken in the form

$$\psi(IJFm)=\sum\{m_I, m_J\}\psi_N(Im_I) \times\psi_B(Jm_J)(IJm_Im_J|IJFm),$$

where the transformation coefficients are so defined that the wave functions $\psi(IJFm)$ diagonalized the hyperfine structure operator

$$H_0=f(r)\mathbf{I}\cdot\mathbf{J}. \quad (36)$$

If a magnetic field is present, the operator defined in Eq. (36) is replaced by

$$H_1=f(r)\mathbf{I}\cdot\mathbf{J}+H_z(\mu_II_z+\mu_JJ_z), \quad (37)$$

where H_z is the applied field. The eigenfunctions which diagonalize H_1 may be written as

$$\psi(IJM_IM_J)=\sum\{m_I, m_J\}\psi_N(Im_I) \times\psi_B(Jm_J)(m_Im_J|M_IM_J), \quad (38)$$

where M_I and M_J represent the eigenvalues of a complete set of operators which characterize the levels of the system when the effect of H_1 is taken into account and which, in the limit of vanishing hyperfine structure separation or large external field, become identical with m_I and m_J.

It is assumed for simplicity that J remains a good quantum number for all magnetic fields considered. This assumption will not affect the validity of the conclusions to be obtained, which depend primarily on the strength of the applied field being sufficiently great to decouple the nuclear spin from all other angular momenta that may be present.

In terms of the wave functions of Eq. (38), one obtains in place of Eqs. (15) and (16) an equation identical to Eq. (15) and the following in place of Eq. (16):

$$S_{n,n'}(H_z)=\sum\{r, s, M_I, M_J, M_I', M_J'\}\frac{(nr|M_IM_J)(M_IM_J|n's)(n's|M_I'M_J')(M_I'M_J'|nr)}{(2J+1)\{1+[(\nu_{M_IM_J}-\nu_{M_I'M_J'})/2\gamma_B]^2\}}. \quad (39)$$

It is apparent from the foregoing that Eq. (39) will reduce to Eq. (16) (although the use of the quantum numbers M_I and M_J is not convenient in this limit) for $H_z=0$.

The transformation coefficients $(m_Im_J|M_IM_J)$ may be evaluated by the usual perturbation theory for a degenerate state. From the condition that $\psi(IJM_IM_J)$ diagonalizes H_1, one obtains

$$\sum\{m_I, m_J\}(m_I'm_J'|H_1|m_Im_J)(m_Im_J|M_IM_J) =E_{M_IM_J}(m_I'm_J'|M_IM_J), \quad (40)$$

from which

$$|(m_I'm_J'|H_1|m_Im_J)-\lambda\delta_{m_I, m_I'}\delta_{m_J, m_J'}|=0, \quad (41)$$

where λ denotes any $E_{M_IM_J}$.

Now, from Eq. (37) using transformation theory and the results of the theory of hyperfine structure, one obtains

$$\begin{aligned}(m_I'm_J'|H_1|m_Im_J)&=H_z(\mu_Im_I+\mu_Jm_J)\delta_{m_I, m_I'}\delta_{m_J, m_J'} \\ &\quad+\sum_{F, F', m, m'}(m_I'm_J'|F'm')(F'm'|f(r)\mathbf{I}\cdot\mathbf{J}|Fm)(Fm|m_Im_J) \\ &=\{H_z(\mu_Im_I+\mu_Jm_J)\delta_{m_I, m_I'}+\sum_{F, m}(m_I'm_J'|Fm)h\nu_F(Fm|m_Im_J)\}\delta_{m_I+m_J, m_I'+m_J'}, \quad (42)\end{aligned}$$

where the ν_F are defined by

$$h\nu_F=C_{IJ}[F(F+1)-I(I+1)-J(J+1)] \quad (43)$$

and C_{IJ} is independent of F and m. That is, ν_F is the displacement from some zero position of the various levels in the hyperfine structure multiplet.

One may now substitute Eq. (42) into Eq. (41) to find $E_{M_IM_J}$ and then use Eq. (40) to determine

the $(m_I m_J | M_I M_J)$. But such a specific result is not required. Noting that

$$|\sum_{F,m} (m_I' m_J' | Fm) v_F (Fm | m_I m_J)| \leqslant \tfrac{1}{2}\Delta\nu, \quad (44)$$

where $\Delta\nu$ is the greatest value (for all F and F') of $\nu_F - \nu_{F'}$, and assuming that

$$h\Delta\nu \ll H_s\mu_J, \quad (45)$$

one finds

$$E_{M_I M_J} = (m_I m_J | H_1 | m_I m_J) + \text{terms of order } H_s\mu_J (h\Delta\nu/H_s\mu_J)^2, \quad (46)$$

with $M_I = m_I$; $M_J = m_J$; also,

$$(m_I m_J | M_I M_J) = \delta_{m_I+m_J,\, M_I+M_J} \times \{\delta_{m_I,\, M_I} + \text{terms of order } (h\Delta\nu/H_s\mu_J)\}. \quad (47)$$

Substituting Eq. (47) into Eq. (39), one finds

$$S_{n,n'}(H_s) = \delta_{n,n'} - \text{terms of order } (h\Delta\nu/H_s\mu_J)^2. \quad (48)$$

Thus, the probability of reorientation is negligible if the Zeeman splitting of the electronic levels because of an external magnetic field is several times as great as the hyperfine structure splitting of the same levels.

It has been shown that with magnetic fields obtainable in the laboratory it is possible to reduce the reorientation probability to a negligible amount, provided the magnetic field is oriented in a direction defined by the gamma-ray emitter and one of the detectors. The field need merely be large enough to give rise to a Zeeman effect of the atomic levels several times larger than the expected hyperfine structure splitting of the intermediate state.[12]

An interesting experimental possibility might be to measure the angular correlation as a function of the strength of the magnetic field. If one can infer the spins and multipole nature of the radiations for the nuclear transitions involved from the available evidence as to angular correlation with a strong magnetic field and from measured internal conversion coefficients, one might then use these values to deduce from the preceding theory the angular correlation at intermediate fields. A comparison between theory and experiment would check the assignment of spin values and radiation multipolarity and might also enable an estimate of the hyperfine structure splitting of the intermediate state.

[12] The criterion of Eq. (45) may be written

$$H_s^2 \gg (2\times 10^4 \Delta\nu)^2$$

where H_s is in gauss and $\Delta\nu$ in cm^{-1}. For bismuth ($\Delta\nu \sim 3\ \text{cm}^{-1}$), the Paschen-Back effect of the hyperfine structure is almost complete at 43,000 gauss. For most atoms, $\Delta\nu$ will be much less, so that smaller magnetic fields will suffice.

SUMMARY

It has been demonstrated above that the angular correlation of successive nuclear gamma-rays emitted by an isolated atomic system is given by either Eq. (32) or Eq. (32′), with $S_{n,n'}$ and $f_{LM}(\vartheta)$ defined by Eqs. (16) and (33), respectively In Eqs. (16), (32), (32′), and (33) the following notation is used:

ϑ	the angle between the successive gamma-rays,
$W(\vartheta)$	the relative probability of a given value of ϑ,
L'	the first nuclear transition gives rise to a $2^{L'}$-pole quantum,
L	the second nuclear transition gives rise to a 2^L-pole quantum,
M, M'	summation indices such that $-L \leqslant M \leqslant L$; $-L' \leqslant M' \leqslant L'$, unless otherwise noted,
n, n'	summation indices such that $-I_B \leqslant n, n' \leqslant I_B$,
I_A, I_B, I_C	spins of the initial, intermediate, and final states of the nucleus, respectively,
J	angular momentum of extra-nuclear electrons,
r, s	summation indices such that $-J \leqslant r, s \leqslant J$,
F, F'	summation indices such that $\lvert I_B - J\rvert \leqslant F$, $F' \leqslant I_B + J$,
m, m'	summation indices such that $-F' \leqslant m' \leqslant F'$; $-F \leqslant m \leqslant F$,
$1/(4\pi\gamma_B)$	lifetime of intermediate nuclear state,
$\nu_{FF'}$	hyperfine structure splitting of sublevels F and F' of the intermediate state,
$(I_B J n r \mid I_B J F m)$	transformation amplitude for vector addition (cf. reference 5),
$(I_A n+M' \mid Y_{L'}^{M'} \mid I_B n)$	matrix element of the spherical harmonics (cf. reference 11),
$\mathbf{D}^{(L)}(\varphi, \vartheta, 0)_{M,\pm 1}$	$2L+1$ dimensional representation of the three-dimensional rotation group (cf. Appendix 2, especially Eq. (A19), and reference 7).

If the intermediate state is sufficiently short lived, one may write

$$S_{n,n'} = \delta_{n,n'}. \quad (19)$$

The criterion for this is given by either Eq. (18) or Eq. (23). When Eq. (19) is used in place of

TABLE III. $S_{n,n'}$ for $J=\frac{1}{2}$ (cf. Eq. (16)).

$$S_{n,n}=1-2T\frac{I_B(I_B+1)-n^2}{(2I_B+1)^2}$$

$$S_{n,n\pm1}=T\frac{I_B(I_B+1)-n(n\pm1)}{(2I_B+1)^2},$$

where

$$T=(\nu_B/2\gamma_B)^2/[1+(\nu_B/2\gamma_B)^2]$$

and ν_B is the hyperfine structure separation of the two sublevels of the intermediate state.

Eq. (16) one obtains Hamilton's results for the angular correlations.

Even when the hyperfine structure separation is appreciable, the validity of the approximate Eq. (19) may be secured by the application of an external magnetic field in the direction of propagation of one of the collected gamma-rays. For an indication of the necessary field strength, see the discussion following Eq. (48).

DISCUSSION

It is clear from Eqs. (15) and (32) and from the subsequent discussion that the hyperfine structure interaction of nuclear and electronic magnetic moments will reduce the angular correlation between the successive quanta over that which would obtain for an isolated nucleus. The shorter the lifetime of the intermediate state, the less important is the effect of the external electrons. As an example, one may consider a specific application of the formula. For $J=1/2$, $I_A=I_B=I_C=I$, both transition dipole ($L=L'=1$), one finds for the angular correlation

$$W(\theta)=1+A\cos^2\theta,$$

where

$$A=\frac{(2I-1)(2I+3)-6T(2I-1)(2I+3)/(2I+1)^2}{12I^2+12I+1+2T(2I-1)(2I+3)/(2I+1)^2},$$

and (see Table III)

$$T=(\nu_B/2\gamma_B)^2/[1+(\nu_B/2\gamma_B)^2].$$

ν_B is the hyperfine structure separation of the two levels of the intermediate state. For $I=\frac{1}{2}$, the distribution is isotropic and independent of the hyperfine structure separation ν_B. For $I>\frac{1}{2}$, A is a monotonically decreasing function of ν_B, as is to be expected.

The above discussed decrease in predicted angular correlation may, as was previously pointed out,[13] be in part responsible for the small angular correlations observed experimentally.

It is clear that the preceding calculations will not apply in the event that there exist reorienting torques on the atom other than those arising from a uniform magnetic field. Thus, in the case of a solid, the electric fields of adjoining atoms will probably result in torques which reorient the atoms, so that the angular correlation of successive gamma-rays is not correctly given by the foregoing formalism unless the lifetime in the intermediate state of the nucleus is so short that reorientation may be neglected. On the other hand, there is no doubt as to the applicability of the above results to a monatomic gas or vapor at sufficiently low pressure.

Another limitation on the applicability of this work is the possibility that the nuclear transition gives rise to mixed radiations.[8] In such a case, the angular correlations calculated above will not apply.

In conclusion, I wish to express my gratitude to Professor I. S. Lowen for suggesting this problem and for continued valuable suggestions and discussions throughout the work. In addition, I thank the Radio Receptor Company wholeheartedly for the grant of a research fellowship which made this work possible.

APPENDIX 1. EXPANSION OF A PLANE ELECTROMAGNETIC WAVE IN TERMS OF SPHERICAL WAVES[14]

One may expand the potential

$$\mathbf{A}(\mathbf{k},P)=2^{-\frac{1}{2}}(\mathbf{u}_1+iP\mathbf{u}_2)\exp i(\mathbf{k}\cdot\mathbf{r}-kct) \qquad \text{(A1)}$$

in terms of the spherical potentials of Table I. The symbols in Eq. (A1) have the meanings given them after Eq. (25).

[13] A preliminary report on some aspects of the present work has been previously published (G. Goertzel and I. S. Lowen, Phys. Rev. 69, 533 (1946)).

[14] See also Hansen, reference 7.

The following expansion is given in many places:[15]

$$\exp i\mathbf{k}\cdot\mathbf{r}=\pi 2^{\frac{1}{2}}\sum_{l=0}^{\infty} i^l(2l+1)^{\frac{1}{2}}f_l(kr)\,Y_l^0(\vartheta,\varphi) \tag{A2}$$

where $\cos\vartheta=\mathbf{u}_3\cdot\mathbf{r}/r$. Substituting Eq. (A2) in Eq. (A1), one obtains

$$\mathbf{A}(\mathbf{k},P)=\pi(\mathbf{u}_1+iP\mathbf{u}_2)\exp -ikct\sum_{l=0}^{\infty} i^l(2l+1)^{\frac{1}{2}}f_l(kr)\,Y_l^0(\vartheta,\varphi). \tag{A3}$$

Equation (A3) is the expansion of a plane wave in terms of spherical waves in a coordinate system in which the plane wave is propagated along the $\mathbf{u}_3$ axis. It is desirable to obtain this expansion in terms of any arbitrary axis system.

A new axis system defined by unit vectors $\mathbf{v}_1$, $\mathbf{v}_2$, $\mathbf{v}_3$ is set up relative to the $\mathbf{u}_1$, $\mathbf{u}_2$, $\mathbf{u}_3$ system by the transformation:

$$\begin{aligned}
\mathbf{u}_1&=(\cos\alpha\cos\beta\cos\gamma-\sin\alpha\sin\gamma)\mathbf{v}_1+(\sin\alpha\cos\beta\cos\gamma+\cos\alpha\sin\gamma)\mathbf{v}_2-\sin\beta\cos\gamma\,\mathbf{v}_3;\\
\mathbf{u}_2&=-(\cos\alpha\cos\beta\sin\gamma+\sin\alpha\cos\gamma)\mathbf{v}_1-(\sin\alpha\cos\beta\sin\gamma-\cos\alpha\cos\gamma)\mathbf{v}_2+\sin\beta\sin\gamma\,\mathbf{v}_3;\\
\mathbf{u}_3&=\cos\alpha\sin\beta\,\mathbf{v}_1+\sin\alpha\sin\beta\,\mathbf{v}_2+\cos\beta\,\mathbf{v}_3.
\end{aligned} \tag{A4}$$

Define r, ϑ, φ as the spherical coordinates of a point relative to the $\mathbf{u}_1$, $\mathbf{u}_2$, $\mathbf{u}_3$, system and r, Θ, and Φ as the coordinates of the same point relative to the $\mathbf{v}_1$, $\mathbf{v}_2$, $\mathbf{v}_3$ coordinate system.

The factors $(\mathbf{u}_1+iP\mathbf{u}_2)$ and $Y_l^0(\vartheta,\varphi)$ on the right side of Eq. (A3) may be expressed in the $\mathbf{v}_1$, $\mathbf{v}_2$, $\mathbf{v}_3$ coordinate system as

$$-2^{-\frac{1}{2}}P(\mathbf{u}_1+iP\mathbf{u}_2)\doteq\sum_{\sigma=0,\pm1}\mathbf{D}^{(1)}(\alpha,\beta,\gamma)_{\sigma,P}\mathbf{w}_\sigma, \tag{A5}$$

$$Y_l^0(\vartheta,\varphi)=\textstyle\sum_m \mathbf{D}^{(l)}(\alpha,\beta,\gamma)_{m,0}Y_l^m(\Theta,\Phi), \tag{A6}$$

where

$$\mathbf{w}_{-1}=2^{-\frac{1}{2}}(\mathbf{v}_1-i\mathbf{v}_2);\quad \mathbf{w}_0=\mathbf{v}_3;\quad \mathbf{w}_1=-2^{-\frac{1}{2}}(\mathbf{v}_1+i\mathbf{v}_2)$$

and the $\mathbf{D}^{(L)}$ are the $2L+1$ dimensioned representations of the three-dimensional rotation group. Substituting Eqs. (A5) and (A6) in Eq. (A3) and using the formula

$$\mathbf{D}^{(1)}(\alpha,\beta,\gamma)_{\rho,P}\mathbf{D}^{(l)}(\alpha,\beta,\gamma)_{m,0}=\sum_{L=l-1}^{l+1}(l1m\rho\,|\,l1Lm+\rho)\mathbf{D}^{(L)}(\alpha,\beta,\gamma)_{m+\rho,P}(l1LP\,|\,l10P), \tag{A7}$$

which is a special case of Eq. (A18) below, one obtains

$$\begin{aligned}
\mathbf{A}(\mathbf{k},P)=-2^{\frac{1}{2}}\pi P\sum_{\rho,m,l,L} i^l(2l+1)^{\frac{1}{2}}(l1m\rho\,|\,lL1m+\rho)\mathbf{D}^{(L)}(\alpha,\beta,\gamma)_{m+\rho,P}\\
\times(l1LP\,|\,l10P)f_l(kr)\,Y_l^m(\Theta,\Phi)\mathbf{w}_\rho\exp -ikct.
\end{aligned} \tag{A8}$$

But, for $P=\pm1$

$$\begin{aligned}
2^{\frac{1}{2}}(2l+1)^{\frac{1}{2}}(l1LP\,|\,l10P)&=(2L+1)^{\frac{1}{2}}\left(\frac{L+1}{2L+1}\right)^{\frac{1}{2}}\quad\text{for } L=l+1,\\
&=(2L+1)^{\frac{1}{2}}\left(\frac{L}{2L+1}\right)^{\frac{1}{2}}\quad\text{for } L=l-1,\\
&=-(2L+1)^{\frac{1}{2}}P\quad\text{for } L=l,
\end{aligned} \tag{A9}$$

[15] For example, E. T. Whittaker and G. N. Watson, *Modern Analysis* (The Macmillan Company, New York, 1944), American edition, p. 401, exercise 9.

so that

$$\mathbf{A}(\mathbf{k}, P)=\pi \sum_{L, M, \rho} i^L(2L+1)^{\frac{1}{2}}\mathbf{D}^{(L)}(\alpha, \beta, \gamma)_{M, P}\mathbf{w}_{-\rho} \exp -ikct$$
$$\times\Big\{-iP\Big[(L+1\ 1M+\rho\ -\rho|L+1\ 1LM)\Big(\frac{L}{2L+1}\Big)^{\frac{1}{2}} Y_{L+1}{}^{M+\rho}(\Theta, \Phi)f_{L+1}(kr)$$
$$-(L-1\ 1M+\rho\ -\rho|L-1\ 1LM)\Big(\frac{L+1}{2L+1}\Big)^{\frac{1}{2}} Y_{L-1}{}^{M+\rho}(\Theta, \Phi)f_{L-1}(kr)\Big]$$
$$+(L1\ M+\rho\ -\rho|L1LM)\,Y_L{}^{M+\rho}(\Theta, \Phi)f_L(kr)\Big\}. \quad \text{(A10)}$$

Noting that

$$\mathbf{A}=2^{-\frac{1}{2}}(A_x+iA_y)\mathbf{w}_{-1}-2^{-\frac{1}{2}}(A_x-iA_y)\mathbf{w}_1+A_z\mathbf{w}_0 \quad \text{(A11)}$$

and comparing Eq. (A10) with Table I, one obtains

$$\mathbf{A}(\mathbf{k}, P)=\pi \sum_{L=1}^{\infty}\sum_{M=-L}^{L} i^L(2L+1)^{\frac{1}{2}}\mathbf{D}^{(L)}(\alpha, \beta, \gamma)_{M, P}\{\mathbf{A}_0(LM)+iP\mathbf{A}_e(LM)\} \quad \text{(A12)}$$

where $\mathbf{A}_0$ and $\mathbf{A}_e$ are given in Table I,

$$\mathbf{k}=k\mathbf{u}_3=k(\mathbf{v}_1\cos\alpha\sin\beta+\mathbf{v}_2\sin\alpha\sin\beta+\mathbf{v}_3\cos\beta),$$

and the $\mathbf{A}(LM)$ are evaluated in the $\mathbf{v}_1$, $\mathbf{v}_2$, $\mathbf{v}_3$ coordinate system.

APPENDIX 2. ROTATION OF COORDINATES AND SOME PROPERTIES OF THE REPRESENTATION OF THE THREE-DIMENSIONAL ROTATION GROUP.[7]

Consider two sets of coordinate axes specified by the unit vectors $\mathbf{u}_1$, $\mathbf{u}_2$, $\mathbf{u}_3$ and $\mathbf{v}_1$, $\mathbf{v}_2$, $\mathbf{v}_3$, respectively, where the relation between the $\mathbf{u}_1$, $\mathbf{u}_2$, $\mathbf{u}_3$, and the $\mathbf{v}_1$, $\mathbf{v}_2$, $\mathbf{v}_3$ is given by Eq. (A4). Let x_1, x_2, x_3 and r, ϑ, φ be rectangular and polar coordinates of an arbitrary point in the $\mathbf{u}_1$, $\mathbf{u}_2$, $\mathbf{u}_3$ set of coordinates and let X_1, X_2, X_3 and r, Θ, Φ be the coordinates of the same point in the v_1, v_2, v_3 system. It is a well-known principle of quantum theory that any wave function $\psi_{Jm}(x)$ of a system in free space may be expressed as a linear combination of the wave functions $\psi_{JM}(X)$ for the same system. Here, J is the total angular momentum of the system and m, M are the components of J along $\mathbf{u}_3$ and $\mathbf{v}_3$, respectively. Therefore, one may write

$$\psi_{Jm}(x)=\textstyle\sum_M \psi_{JM}(X)\mathbf{D}^{(J)}(\alpha, \beta, \gamma)_{M, m}, \quad \text{(A13)}$$

which specifies the $\mathbf{D}^{(J)}$ completely, if the phases of the ψ's are specified. A specialization of Eq. (A13) of particular interest is[16]

$$Y_L{}^m(\vartheta, \varphi)=\textstyle\sum_M Y_L{}^M(\Theta, \Phi)\mathbf{D}^{(L)}(\alpha, \beta, \gamma)_{M, m}. \quad \text{(A14)}$$

From Eq. (A13) it is immediately apparent that

$$\mathbf{D}^{(J)}(0, 0, 0)_{M, m}=\delta_{M, m}. \quad \text{(A15)}$$

Also, a comparison of Eq. (A14) with the spherical harmonic addition theorem

$$Y_L{}^0(\vartheta, \varphi)=\Big(\frac{4\pi}{2L+1}\Big)^{\frac{1}{2}}\textstyle\sum_M Y_L{}^M(\beta, \alpha)^* Y_L{}^M(\Theta, \Phi)$$

[16] We use Condon and Shortley's (reference 5, page 52) choice of phases for the associated Legendre polynomials.

shows that

$$\mathbf{D}^{(L)}(\alpha,\beta,\gamma)_{M,0}=\left(\frac{4\pi}{2L+1}\right)^{\frac{1}{2}}Y_L{}^M(\beta,\alpha)^*. \tag{A16}$$

Since

$$(4\pi/3)^{\frac{1}{2}}rY_1{}^1(\vartheta,\varphi)=-2^{\frac{1}{2}}(x_1+ix_2);\quad (4\pi/3)^{\frac{1}{2}}rY_1{}^0(\vartheta,\varphi)=x_3;\quad (4\pi/3)^{\frac{1}{2}}rY_1{}^{-1}(\vartheta,\varphi)=2^{\frac{1}{2}}(x_1-ix_2),$$

it is apparent that $-2^{-\frac{1}{2}}(x_1+ix_2)$, x_3, $2^{-\frac{1}{2}}(x_1-ix_2)$ and $-2^{-\frac{1}{2}}(\mathbf{u}_1+i\mathbf{u}_2)$, $\mathbf{u}_3$, $2^{-\frac{1}{2}}(\mathbf{u}_1-i\mathbf{u}_2)$ transform as $Y_1{}^1(\vartheta,\varphi)$, $Y_1{}^0(\vartheta,\varphi)$, $Y_1{}^{-1}(\vartheta,\varphi)$. Hence, one finds with the aid of Eq. (A4) the following values of $\mathbf{D}^{(1)}(\alpha,\beta,\gamma)_{i,j}$.[17]

i \ j	-1	0	1
-1	$e^{i\alpha}\frac{1+\cos\beta}{2}e^{i\gamma}$	$e^{i\alpha}\frac{\sin\beta}{\sqrt{2}}$	$e^{i\alpha}\frac{1-\cos\beta}{2}e^{-i\gamma}$
0	$-\frac{\sin\beta}{\sqrt{2}}e^{i\gamma}$	$\cos\beta$	$\frac{\sin\beta}{\sqrt{2}}e^{-i\gamma}$
1	$e^{-i\alpha}\frac{1-\cos\beta}{2}e^{i\gamma}$	$-e^{-i\alpha}\frac{\sin\beta}{\sqrt{2}}$	$e^{-i\alpha}\frac{1+\cos\beta}{2}e^{-i\gamma}$

(A17)

A relation of particular interest to us is derived in group theory:[18]

$$\mathbf{D}^{(J)}(\alpha,\beta,\gamma)_{M,N}\mathbf{D}^{(j)}(\alpha,\beta,\gamma)_{m,n}=\sum_{F=|J-j|}^{J+j}(jJmM\,|\,jJF\,m+M)\mathbf{D}^{(F)}(\alpha,\beta,\gamma)_{M+m,N+n}(jJF\,n+N\,|\,jJnN). \tag{A18}$$

Upon setting $N=0$, $j=1$ in Eq. (A18) and using Eqs. (A16) and (A17), one obtains

$$\begin{aligned}\mathbf{D}^{(L)}(\alpha,\beta,\gamma)_{M,1}=-\left[\left(\frac{4\pi}{2L+1}\right)\frac{1}{L(L+1)}\right]^{\frac{1}{2}}\Big\{&MY_L{}^M(\beta,\alpha)^*\sin\beta e^{-i\gamma}\\&+(L+1+M)^{\frac{1}{2}}(L-M)^{\frac{1}{2}}Y_L{}^{M+1}(\beta,\alpha)^*e^{i\alpha}\frac{1-\cos\beta}{2}e^{-i\gamma}\\&-(L+1-M)^{\frac{1}{2}}(L+M)^{\frac{1}{2}}Y_L{}^{M-1}(\beta,\alpha)^*e^{-i\alpha}\frac{1+\cos\beta}{2}e^{-i\gamma}\Big\}.\end{aligned} \tag{A19}$$

Also,

$$\mathbf{D}^{(L)}(\alpha,\beta,\gamma)_{M,-1}=(-)^{M+1}\mathbf{D}^{(L)}(\alpha,\beta,\gamma)_{-M,1}{}^*.$$

APPENDIX 3. EVALUATION OF A CLASS OF MATRIX ELEMENTS

It may be shown by group theoretical methods that if an operator transforms under change of coordinates according to the relation

$$H(L,M;\vartheta,\varphi)=\textstyle\sum_{M'}H(L,M';\Theta,\Phi)\mathbf{D}^{(L)}(\alpha,\beta,\gamma)_{M',M}, \tag{A20}$$

the matrix elements of the operator are given by

$$(Jm\,|\,H(LM)\,|\,J'm')=C(J'LJm\,|\,J'Lm'M)=C'(Jm\,|\,Y_L{}^M\,|\,J'm'), \tag{A21}$$

where C and C' are independent of m, m', and M.[19]

[17] See also reference 7, page 182.
[18] Reference 7, page 204, Eq. (16b).
[19] Reference 7, page 264, Eq. (19).

The operators

$$H_1(LM)=\mathbf{p}\cdot\mathbf{A}_0(LM);\quad H_2(LM)=\mathbf{p}\cdot\mathbf{A}_e(LM), \tag{A22}$$

where $\mathbf{p}$ is any vector and $\mathbf{A}_0$ and $\mathbf{A}_e$ are the potentials of a spherical electromagnetic wave as given in Table I, satisfy Eq. (A20). To show this, one proceeds as follows.

Let

$$p_1=-2^{-\frac{1}{2}}(p_x+ip_y);\quad p_0=p_z;\quad p_{-1}=2^{-\frac{1}{2}}(p_x-ip_y),$$
$$A_1=2^{-\frac{1}{2}}(A_x+iA_y);\quad A_0\doteq A_z;\quad A_{-1}=-2^{-\frac{1}{2}}(A_x-iA_y).$$

Then

$$H_1(L,M;\vartheta,\varphi)=\sum_{\sigma=\pm1,0}p_\sigma(\vartheta,\varphi)A_{0,-\sigma}(L,M;\vartheta,\varphi)$$

$$=\sum_{\sigma=\pm1,0}p_\sigma(\vartheta,\varphi)(L1LM|L1\ M-\sigma\ \sigma)f_L(kr)Y_L{}^{M-\sigma}(\vartheta,\varphi)\exp-ikct$$

$$=\sum_{\sigma,\sigma',M'}\mathbf{D}^{(1)}(\alpha,\beta,\gamma)_{\sigma',\sigma}\mathbf{D}^{(L)}(\alpha,\beta,\gamma)_{M',M-\sigma}p_{\sigma'}(\Theta,\Phi)(L1LM|L1\ M-\sigma\ \sigma)$$
$$\times f_L(kr)Y_L{}^{M'}(\Theta,\Phi)\exp-ikct$$

$$=\sum_{\sigma,\sigma',M',L'}(L1M'\sigma'|L1L'\ M'+\sigma')\mathbf{D}^{(L')}(\alpha,\beta,\gamma)_{M'+\sigma',M}(L1L'M|L1\ M-\sigma\ \sigma)$$
$$\times p_{\sigma'}(\Theta,\Phi)(L1LM|L1\ M-\sigma\ \sigma)f_L(kr)Y_L{}^{M'}(\Theta,\Phi)\exp-ikct$$

$$=\sum_{\sigma,M'}(L1LM'|L1\ M'-\sigma\ \sigma)\mathbf{D}^{(L)}(\alpha,\beta,\gamma)_{M',M}f_L(kr)Y_L{}^{M'-\sigma}(\Theta,\Phi)p_\sigma(\Theta,\Phi)\exp-ikct$$

$$=\textstyle\sum_{M'}\mathbf{D}^{(L)}(\alpha,\beta,\gamma)_{M',M}H_1(L,M;\Theta,\Phi).$$

A similar demonstration gives the corresponding result for $H_2(LM)$. It has therefore been shown that the matrix elements of the operators of Eq. (A22) are given by Eq. (A21).

Errata: A New Method of Measuring the Electric Dipole Moment and Moment of Inertia of Diatomic Polar Molecules

[Phys. Rev. **70**, 570 (1946)]

HAROLD KENNETH HUGHES
Socony-Vacuum Laboratories, Brooklyn, New York and Pupin Physics Laboratories, Columbia University, New York, New York

THERE are typographical errors in Eqs. (1) and (4). These should read as follows:

$$f=\frac{6\mu^2IE^2}{20(9)10^4hh^2}=4.529\times10^{75}\mu^2IE^2. \tag{1}$$

$$I=(\beta/\alpha^2)(1.97\times10^{-28}),\ \text{g cm}^2. \tag{4}$$

PHYSICAL REVIEW VOLUME 70, NUMBERS 11 AND 12 DECEMBER 1 AND 15, 1946

Production of Hg^{198} as a Possible Source of an Improved Wave-Length Standard*

JACOB H. WIENS
Department of Physics, University of California, Berkeley, California
(Received September 26, 1946)

The green line 5461A from any of the even isotopes of mercury is superior, in many respects, to the red line 6438A of cadmium for a primary standard of wave-length. The mercury isotope of mass 198 was produced by utilizing the nuclear transformation

$$_{79}Au^{197}+_{0}n^{1}\rightarrow{}_{80}Hg^{198}+{}_{-1}\beta^{0}.$$

One ounce of pure gold was sealed in a quartz tube and a section of 5-mm inside diameter quartz tube was sealed on the quartz-gold tube. The system was outgassed and 4-mm Hg pressure of spectroscopically pure argon was admitted and the tube was sealed. The gold was exposed to stray neutrons near the sixty-inch cyclotron for ten months. The gold was then heated and the mercury was condensed in the 5-mm quartz tube. The mercury vapor in the presence of argon gas was excited by means of a 100-megacycle oscillator and the spectrum was observed. The lines produced by the discharge were mercury lines, and the position of the lines of a Fabry-Perot etalon spectrogram agree with the position assigned by Schüler and Jones to the mercury isotope of mass 198. Larger quantities of gold exposed to known superior sources of neutrons will produce an adequate supply of the isotope for scientific purposes.

INTRODUCTION

FOR several decades the red cadmium line has been used as the primary standard of wave-length. A specially constructed cadmium lamp is used in conjunction with a Fabry-Pérot etalon to accurately compare the wave-lengths of the secondary standards with that of the red cadmium line. The lamp is also conveniently applied to measurement of standard scales of length, and to the testing of high quality optical parts and instruments, using various forms of the Michelson interferometer.

The accuracy with which these measurements and tests can be made depends upon the sharpness of the spectral line used for the standard. The ease with which some of the tests can be made depends upon the visual intensity of the standard. In recent years it has been recognized that while the cadmium lines are sufficiently sharp to produce adequate interference fringes for some purposes, a source giving rise to sharper lines is an urgent necessity for work of the highest precision.

Michelson and Benoit, in 1893, first selected the red cadmium line for the standard of wave-length, and it was adopted as such by the International Union for Cooperation in Solar Research in a resolution passed in 1907.[1] The present accepted value of 6438.4693A is the mean of seven intercomparisons of the wave-length with the meter made during the period from 1893 to 1936.[2]

Meggers,[3] in a study of the characteristics of a lamp suitable for use as a primary standard of wave-length, specified that the lamp should avoid or minimize the Doppler-Fizeau effect, hyperfine structure, self-reversal, and pressure effect. The Michelson H-type lamp as specified[4] has a number of disadvantages,[5] the most serious of which concern Meggers' first two specifications. Since the Doppler width is proportional to $\lambda(T/M)^{\frac{1}{2}}$, where λ is the wave-length, T the absolute temperature, and M the atomic weight, it is clear that the lamp should operate at as low a temperature as possible and should have as large an atomic weight as possible.

The sharpness of a spectral line may be specified by the maximum order of interference obtainable with it, which should theoretically be[6]

$$N=1.22(10)^{6}(M/T)^{\frac{1}{2}}.$$

For the standard cadmium lamp, with the gas in the lamp at 320°C, the computed value of N for 6438A is 530,000. For a mercury lamp, operating at a temperature of 40°C, the value for 5461A is 965,000.

* Submitted in partial satisfaction of the requirements for the degree of Doctor of Philosophy in Physics in the Graduate Division of the University of California.

[1] Trans. I.U.C.S.R. 2, 20 (1907).

[2] J. E. Sears, Sci. Prog. 31, 209 (1936).

[3] W. F. Meggers, Rev. Mod. Phys. 14, 2-3, 59 (1942).

[4] Procès-Verbaux Comité Int. Poids et Mes. 2, 17, 91 (1935).

[5] C.-W. Hsueh, J. Op. Soc. Am. 36, 160 (1946).

[6] H. Buisson and Ch. Fabry, J. de physique 5, 2, 442 (1912).

The ideal lamp should be capable of operating with very low currents and ion densities in order to prevent broadening due to the Stark effect. The pressure in the lamp should remain reasonably constant during operation so as not to cause a shift in the line due to the pressure effect. The influence of pressure on the wave-length can be further minimized by the correct choice of the line used as the standard. In general, the wave-lengths due to the triplet $P-S$ transitions are less susceptible to pressure than the $P-D$ transitions. The pressure effect, furthermore, always increases for lines where one of the levels involved is near the ionization limit. Self-reversal is most apt to occur where the ground state or low metastable states are concerned. The choice for a line, therefore, resolves itself into selecting a transition in the middle of the atomic energy diagram. Such a compromise is represented by the $^1P_1-{}^1D_2$, 6438A of cadmium and $^3P_2-{}^3S_1$, 5461A of mercury. Thus the most suitable cadmium line is in the red region, which results in low visual intensity. In order to increase the intensity for spectrographic work, the lamp must be viewed end-on and this reduces the field of view. Lastly, the red cadmium line possesses a hyperfine structure which, although it has never been resolved[7-9] increases the width of the fringes obtained with it.

Mercury has most of the properties that would make it a good choice for the standard. The green line has a very high visual intensity, is easily excited, and satisfies the conditions as to self-reversal and pressure effect as well as does the red cadmium line. The only difficulty is that the lines of mercury all show hyperfine structure as well as isotope shift.[10] Seven isotopes are present but since the isotope of mass 202 is the most plentiful, one might be inclined to try to use the mass spectrograph for separating this isotope from ordinary mercury. This and all other methods for separating the mercury isotopes in quantities large enough to produce a strong light source have until now been unsuccessful.

[7] A. Ferchmin, M. Romanowa, C. R. de l'Académie des Sciences de l'U.R.S.S., No. 2 (1933).
[8] H. Westmeyer, Zeits. f. Physik **94**, 590 (1935).
[9] Nagaoka and Sugiura, Sci. Pap. Inst. Phys. Chem. Res., Tokyo **10**, 263 (1929).
[10] H. Schüler and J. E. Keyston, Zeits. f. Physik **72**, 430 (1931).

In 1939, W. E. Williams[11] suggested the utilization of the known nuclear reaction[12]

$$_{79}Au^{197}+{}_0n^1\rightarrow{}_{79}Au^{198}$$
$$_{79}Au^{198}\rightarrow{}_{80}Hg^{198}+{}_{-1}\beta^0$$

for the production of the mercury isotope of mass 198, using neutrons from the cyclotron. Schüler and Keyston[10] had shown that the even isotopes of mercury have no hyperfine structure and hence that any of the even isotopes of mercury would be suitable for use in a lamp designed to furnish the primary standard of wave-length.

Fermi and his associates had used as their source of neutrons a mixture of beryllium powder and radon, a source which produced approximately 800,000 neutrons per second. When the present experiment was started in 1939, a much more copious source of neutrons was available in the cyclotron, neutrons being the by-product of almost every nuclear reaction produced by it. The manufacture of the mercury isotope of mass 198 therefore was accomplished by utilizing the stray neutrons existing near the cyclotron as a result of other bombardments.

OBJECTIVES

The purposes of this experiment were:

1. To verify, by spectrographic methods, the nuclear transformation $_{79}Au^{197}+{}_0n^1\rightarrow{}_{80}Hg^{198}+{}_{-1}\beta^0$. This was to be done by observing the spectrum of the product of the reaction.

2. To show that the resulting mercury isotope is the isotope of mass 198. Inasmuch as the odd isotopes are responsible for the hyperfine structure and the even isotopes yield simple spectral lines, this had to be accomplished by observing the lines with a Fabry-Pérot etalon. The lines should be simple lines and should coincide with the lines in ordinary mercury which had previously been assigned[13] to the isotope of mass 198.

3. To produce a sufficient amount of the single isotope of mercury to show that it is feasible to develop a lamp for use as a primary standard of wave-length.

[11] This suggestion was made in the course of an address to the Physics Department meeting at the University of California.
[12] E. Fermi, E. Amaldi, O. D'Agostino, F. Rasetti, and E. Segrè, Proc. Roy. Soc. **146A**, 484 (1934).
[13] H. C. Burger and P. H. Van Cittert, Physica **5**, 177 (1938).

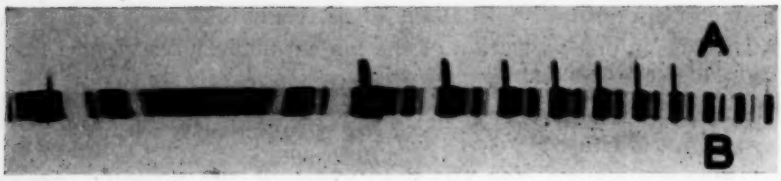

FIG. 1. Fabry-Pérot etalon spectrogram of 5461A. *A*, mercury 198. *B*, ordinary mercury. Etalon separation, 9.015 mm.

PRELIMINARY CALCULATIONS AND EXPERIMENTS

In order to determine the feasibility of the nuclear transformation of gold into the mercury isotope of mass 198, one ounce of gold was exposed to neutrons in the vicinity of the 37-inch cyclotron. After four days the gold was found to have an activity of 2.4 millicuries. From this and the mean life of radioactive gold, a simple calculation indicated that the sample of gold would produce 3.45×10^{13} atoms of mercury in equilibrium, and that this amount of mercury would yield a pressure of 3.16×10^{-3} mm Hg in a tube having a volume of 0.3 cm³.

Williams[11] reported that in his experiments he had obtained an electrodeless discharge in tubes containing mercury vapor at a pressure of 10^{-4} to 10^{-5} mm Hg, provided that an oscillator having a frequency of approximately 50 megacycles was used. Extensive experiments showed that, while this was true, a much higher vapor pressure is necessary if the tube is to be sealed off, due to the adsorption of mercury on the walls of the tube. An initial vapor pressure of the order of 10^{-2} was found satisfactory for a discharge tube of the size and type used in this experiment.

When the vapor pressure of the mercury is between 10^{-2} and 10^{-5} mm, the addition of a small quantity of argon increases the intensity of the discharge by a factor of at least 10. The first excitation potential of mercury is lower than the metastable state of argon. The argon atoms yield the energy of their metastable states to the mercury atoms in inelastic collisions, thus facilitating the excitation of mercury. An argon pressure of the order of 4 mm was found to be satisfactory, and very little difference was noted between the effects with 2 mm and 6 mm.

In order to determine if it would be feasible to separate completely any mercury produced from the parent gold, and to find whether it would be possible to completely purify the gold from any mercury contamination that might occur during processing, a drop of mercury was placed on a piece of gold foil. The gold was then sealed in a quartz tube attached to a vacuum system and the gold was heated in an electric furnace to about 900°C, very near to its melting point. Enough mercury vapor was found in the glass tubing between the gold and the first liquid air trap to be excited by means of a leak-tester. Heating the glass walls of the tube with a gas-oxygen torch did not satisfactorily remove the mercury.

An oscillator having a frequency of 100 megacycles was then attached to the glass tubing by wrapping the radiofrequency output leads around the tubing at points about a foot apart. A discharge formed along the length of the tubing, and enough high frequency energy was supplied to heat the glass close to its softening point. The heating effect was greatly increased by the addition of pure argon at a pressure of about 5 mm. The outgassing cycle consisted of admitting argon, operating the oscillator for five minutes, and then pumping out the gases while the oscillator was still operating. Fifteen to twenty such cycles were sufficient to outgas the system so completely that no trace of mercury could be found. Heating the glass walls by means of a gas-oxygen torch did not release any further mercury or other foreign gases.

EXPERIMENTAL PROCEDURE

A one-ounce sheet of pure gold foil 0.1 mm thick was chemically treated to remove surface contamination, sealed into a glass tube, and attached to the vacuum system. The gold was then placed in an electric furnace and heated to approximately 200°C to remove all traces of water and other easily volatile substances. The temperature of the furnace was then raised to about 450°C, or to a point where the glass showed a dull red in total darkness, and during the pumping process the outgassing oscillator was

operated so that a discharge appeared in the entire region between the gold and the first liquid air trap. Twelve to twenty hours of pumping were required to outgas the system so completely that the pressure remained at 10^{-5} mm of Hg for an hour after the system was isolated from the pumps.

The gold was then transferred to a quartz tube in order to heat it to just below its melting point. The outgassing oscillator and argon were used as before until the pressure remained at 10^{-6} mm of Hg for an hour after the system was shut off. At this time a 15-cm section of 4-mm i.d. quartz tubing was sealed to the far end of the large quartz tube containing the gold. Since the mercury produced by the reaction is to be distilled into this tube, sealing it on at this time prevents impurities from distilling into the section during the outgassing period.

After the complete system had been outgassed, a pressure of 4 mm of spectroscopically pure argon was admitted and the unit was sealed off. The complete assembly was placed in a suitable box and embedded in paraffin before being placed near the 60-inch Crocker cyclotron. The paraffin served to slow down the fast neutrons as well as to cushion the quartz tube during handling.

When the run was completed, the quartz tube was removed and the gold was again heated to just below the melting point while the far end of the 4-mm i.d. quartz tube was cooled to liquid air temperature by means of a specially constructed Dewar flask. After two to three hours, a 6-cm section was sealed off and this contained, besides argon, most of the mercury that had been produced. The mercury in this tube was then excited by means of the 100-megacycle oscillator, with the power adjusted so that a satisfactory intensity was obtained.

EXPERIMENTAL RESULTS

The first successful experiment was the result of exposing the one-ounce sample of gold to neutrons in the vicinity of the 60-inch cyclotron for one week. The discharge in the tube was examined with a constant deviation spectrometer and mercury lines were found. After about one minute the discharge decreased in intensity and soon disappeared.

The next tube was the result of one month's exposure to the same neutron source. Enough mercury was obtained from this bombardment to make it possible to photograph a Fabry-Pérot etalon spectrogram.[14] The mercury lines were found to be simple lines, and the absence of hyperfine components showed that the mercury is actually a transmutation product. This source operated successfully for about five minutes.

The gold was then left near the cyclotron for ten months, during which time the cyclotron was operated almost continuously. The mercury produced by this neutron bombardment was sufficient so that the discharge tube could be run for thirty minutes with no loss in intensity.[15] During this thirty minutes of operation, the spectrograms in Figs. 1–3, as well as some ten others not given here, were taken. The intensity of the discharge was so large that fifteen to thirty seconds were sufficient for a normal exposure.

ANALYSIS OF THE SPECTROGRAMS

The spectrograph used in this experiment had two large flint glass prisms, and the quartz Fabry-Pérot etalon was placed between the collimator lens and the prisms. The jaws of the slit were controlled by screws mounted horizontally on each side of the slit. This made it possible to close the slit from one side after one exposure and to open the slit again from the other side for the second exposure. The two spectrograms are then side by side and no adjustment has been made that would affect the position of the interference patterns on the photographic plate. In all cases, the center of the interference rings was so aligned that it fell on the line between the two spectrograms, since this arrangement is best for comparing two spectrograms.

The line 5461 was studied, as it is the one most suitable for a primary standard of wavelength. Figure 1 shows the etalon spectrogram of Hg^{198} and of ordinary mercury, the latter having been excited in an air-cooled d.c. arc. The positions of all the lines appearing in the spectrogram of ordinary mercury were measured on the original plates by means of a com-

[14] J. H. Wiens and L. W. Alvarez, Phys. Rev. 58, 11, 1005 (1940).
[15] J. H. Wiens, Phys. Rev. 65, 58 (1944).

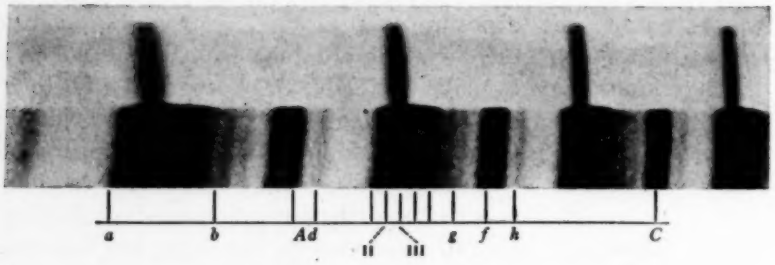

FIG. 2. Resolution of 5461A with designations as given by Schüler.

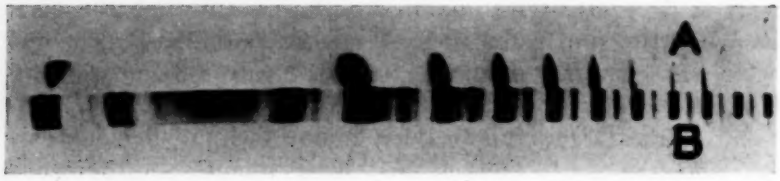

FIG. 3. Same as Fig. 1, except that *A* is more heavily exposed.

parator. From these measurements the wave-number separations were calculated, and by comparing them with the separations given by Burger,[13] assignments were made according to the notation originally given by Schüler and Keyston.[10] Figure 2 is an enlargement of Fig. 1 and these assignments are indicated.

The position of the line due to Hg^{198} was computed from the measurements, and the average of several values gave its position as -33×10^{-3} cm^{-1}. The wave number separation of line III due to Hg^{200} and line II due to Hg^{198} is given[13] as -29×10^{-3}cm^{-1}. Because of the large experimental error in determining the center of the broad component, which contains the five main lines, this difference is within the experimental error. Thus the line 5471A obtained from mercury that is produced by the nuclear transformation of gold coincides, within the experimental error, with the line due to Hg^{198} as assigned by Schüler and other observers. This also verifies the correctness of the mass number of the stable daughter element of radioactive gold as predicted from the observed β-emission of the parent substance. Figure 3 is similar to Fig. 1 except that the spectrogram due to Hg^{198} has been greatly overexposed in an effort to find any other weak lines. No additional lines could be observed in any of the spectrograms.

DISCUSSION OF RESULTS

The results obtained in this experiment indicate that it is both possible and feasible to use the nuclear transmutation of gold to mercury to produce sufficient mercury for use in developing a better primary standard of wave-length. The quantity of mercury can obviously be greatly increased by the use of a larger mass of gold, and since the reaction utilizes stray neutrons produced by the reactions in the cyclotron, no special operation of the cyclotron is required. With the development of other neutron sources many times stronger than the cyclotron, it should very soon be possible to produce enough mercury to make the more standard types of d.c. arcs. The ease of excitation, low operating temperature, high visual intensity, and inherently sharper line produced by the mercury lamp should be adequate reasons for seriously considering the green line from Hg^{198} as a new primary standard of wave-length.

ACKNOWLEDGMENTS

I wish to thank Professor L. W. Alvarez who first saw the feasibility of this problem and encouraged me to start the experiment. Furthermore, I am grateful for the suggestions and help that Professor F. A. Jenkins gave me during the course of the experiment. I wish to thank Professor H. E. White, under whose supervision this problem was completed, for his guidance and encouragement. Lastly, I wish especially to thank the Radiation Laboratory and the operators of the cyclotron for making it possible to bombard the gold samples during the four years occupied by these experiments.

PHYSICAL REVIEW VOLUME 70, NUMBERS 11 AND 12 DECEMBER 1 AND 15, 1946

On the Elastic Properties of Lattices

PAUL S. EPSTEIN
California Institute of Technology, Pasadena, California
(Received August 13, 1946)

The potential energy of a deformed lattice can be written in the form

$$V = V_0 + V_1 + V_2,$$

where V_0 is a constant (the energy of the undeformed lattice), V_1 the part linear in the displacements of the lattice points from their normal positions, V_2 the part quadratic in the displacements. The terms of higher order are neglected. In view of the requirement that the normal position of each lattice point be a position of equilibrium the linear part vanishes ($V_1=0$) so that the energy is simply equal to V_2 (apart from the constant V_0). As the energy must be invariant with respect to rotations of the system, W. Voigt postulated the invariance of V_2 and derived from this assumption the so-called *Cauchy relations* between the elastic coefficients. A closer analysis shows that this conclusion is open to objection. The term V_2 represents the energy only because of the subsidiary condition $V_1=0$ which, upon investigation, turns out to be not invariant with respect to rotations. Hence, V_2 is not invariant either: a fact which removes the theoretical basis of the Cauchy relations.

1. INTRODUCTION

IN recent years the problem of elastic oscillations of crystalline solids (conceived as atomic lattices) was the subject of papers by Blackman,[1] Kellermann,[2] Fine,[3] Montroll,[4] and others. Considerable progress has been achieved by these authors in the study of these oscillations and in devising numerical methods for calculating the frequency distribution. It seems, nevertheless, that some of the more fundamental questions are not yet very well understood and need further elucidation. We refer, in particular, to the relations between the coefficients of the quadratic form representing the potential energy of the lattice, on one hand, and the measurable coefficients of elasticity, on the other.

It is usually stated that, in the case of central forces between the atoms of the lattice, the symmetry of the lattice coefficients is such that it involves the so-called *Cauchy relations* between the coefficients of elasticity. In mentioning the Cauchy relations all modern writers on the subject refer to W. Voigt.[5] Although these relations are admittedly in contradiction to observed facts, nobody seems to have thoroughly reexamined their derivation or the conditions under which they are supposed to be valid. We shall show in this paper that Voigt's proof contains a serious flaw which invalidates his results: *as far as measurable elasticity coefficients are concerned, no relations of the Cauchy type exist between them, even in the case of central forces.*

This fact is not only of theoretical interest but has also some bearing on practical problems. Indeed, in some of the above mentioned papers, the Cauchy relations were used as a means for determining the numerical values of the lattice coefficients. In the light of our results these numerical estimates are no longer reliable and will have to be revised.

2. EXPRESSION FOR THE POTENTIAL ENERGY

Let an atom (or point) of the lattice be labeled by the Greek index μ, and let the three cartesian coordinates of its normal position be denoted by $x_{\mu i}$ ($i=1, 2, 3$), so that the latin subscript i refers to the three orthogonal directions of space. When the lattice is deformed, all the points get slightly displaced, and their coordinates assume the new values $x_{\mu i}+s_{\mu i}$, where $s_{\mu i}$ is called the i-component of the displacement of the point μ.

As our primary purpose is to investigate the validity of the Cauchy relations, which are

[1] M. Blackman, Proc. Roy. Soc. **A148**, 384 (1935); **149**, 126 (1935); **159**, 416 (1937); **164**, 62 (1938).
[2] E. W. Kellermann, Phil. Trans. **238**, 519 (1940).
[3] P. Chs. Fine, Phys. Rev. **56**, 355 (1939).
[4] E. W. Montroll *et al.*, J. Chem. Phys. **10**, 218 (1942); **11**, 481 (1943); **12**, 98 (1944).
[5] W. Voigt, *Lehrbuch der Kristallphysik* (Leipzig, 1910), Sections 297, 298.

claimed only for central forces between the atoms, it will save space if we restrict ourselves to the case of such forces. We assume, therefore, that the mutual energy of the pair of lattice points μ and ν is given by the function

$$\Phi(\bar{r}_{\mu\nu}),$$

symmetric in the pair of indices μ, ν.

$$\bar{r}_{\mu\nu}^2=(a_{\mu\nu 1}+s_{\mu 1}-s_{\nu 1})^2 + (a_{\mu\nu 2}+s_{\mu 2}-s_{\nu 2})^2+(a_{\mu\nu 3}+s_{\mu 3}-s_{\nu 3})^2,$$

where $a_{\mu\nu i}=-a_{\nu\mu i}=x_{\mu i}-x_{\nu i}$ is the i-component of the distance between the points μ and ν. Hence, the normal distance between these points is $r_{\mu\nu}$,

$$r_{\mu\nu}^2=a_{\mu\nu 1}^2+a_{\mu\nu 2}^2+a_{\mu\nu 3}^2.$$

Thus the total potential energy of the lattice can be written in the form

$$V=\tfrac{1}{2}\sum_{\mu\nu}\Phi_{\mu\nu}(\bar{r}_{\mu\nu})_0 \qquad (1)$$

where the factor $\frac{1}{2}$ insures that each term $\Phi_{\mu\nu}$ occurs in the expression only once.

Expanding the expression with respect to the small differences $s_{\mu i}-s_{\nu i}$ up to terms of the second order, we obtain

$$V=V_0+V_1+V_2, \qquad (2)$$

where V_0 is the energy of the undeformed lattice, while the terms of first and second order can be written as follows, using Einstein's convention with respect to the latin indices:

$$V_1=\sum_{\mu\nu}A_{\mu\nu}a_{\mu\nu j}(s_{\mu j}-s_{\nu j}), \qquad (3)$$

$$V_2=\sum_{\mu\nu}[(B_{\mu\nu j}-C_{\mu\nu}a_{\mu\nu j}^2)(s_{\mu j}-s_{\nu j})^2 + C_{\mu\nu}a_{\mu\nu i}a_{\mu\nu j}(s_{\mu i}-s_{\nu i})(s_{\mu j}-s_{\nu j})]. \qquad (4)$$

In introducing these notations we anticipate to some extent the results of Section 5 where it will be shown that the meaning of the coefficients is as follows:

$$\left.\begin{aligned} A_{\mu\nu}a_{\mu\nu j}&=\tfrac{1}{2}(\partial\Phi_{\mu\nu}/\partial a_{\mu\nu j})_0,\\ B_{\mu\nu j}&=\tfrac{1}{2}(\partial^2\Phi_{\mu\nu}/\partial a_{\mu\nu j}^2)_0,\\ C_{\mu\nu}a_{\mu\nu i}a_{\mu\nu j}&=\tfrac{1}{2}(\partial^2\Phi_{\mu\nu}/\partial a_{\mu\nu i}\partial a_{\mu\nu j})_0,\\ &\text{for } i\neq j.\end{aligned}\right\} \qquad (5)$$

The notations are chosen so as to bring out the symmetry character in the subscripts μ and ν since it can be inferred from the Eqs. (5) that $A_{\mu\nu}$, $B_{\mu\nu j}$, $C_{\mu\nu}$ are all symmetric in μ, ν.

However, for the present, we shall not make use of the relations (5) and shall regard the coefficients simply as empirically given constants whose dependence on i, j, and symmetry character in μ, ν could be established in a different way. Indeed, it is possible to proceed as follows. Instead of introducing explicitly Eq. (1), the theory can be built up on the following two postulates:

(1) The potential energy can be represented as the sum of mutual potential energies of pairs of points (without introducing from the start the dependence on $\bar{r}_{\mu\nu}$).

(2) The potential energy is invariant with respect to translations and rotations (law of action and reaction).

The dependence on the differences $s_{\mu i}-s_{\nu i}$, only, is then obtained from the invariance with respect to translations, the symmetry character of the coefficients from the invariance with respect to rotations. In particular we wish to underline that the independence of the coefficients $A_{\mu\nu}$ and $C_{\mu\nu}$ of the directional subscripts i, j, is a necessary consequence of the rotational invariance. We shall briefly return to this question in Section 4.

3. TRANSFORMATION TO STRAIN COMPONENTS

We shall define the first-order strain components as the matrix

$$e_{ij}^{(0)}=\frac{1}{2}\left(\frac{\partial s_j}{\partial x_i}+\frac{\partial s_i}{\partial x_j}\right), \quad (i,j=1,2,3). \qquad (6)$$

It should be noted that this definition is slightly different from that used in some textbooks in that the element off the diagonal ($i\neq j$) is supplied with a factor $\frac{1}{2}$. In addition we shall need the components of the rotations in their usual expression

$$\omega_{ij}=\frac{1}{2}\left(\frac{\partial s_j}{\partial x_i}-\frac{\partial s_i}{\partial x_j}\right). \qquad (7)$$

Adding the two formulas

$$\partial s_j/\partial x_i=e_{ij}^{(0)}+\omega_{ij}. \qquad (8)$$

Integrating this over a region in which $e_{ij}^{(0)}$ and ω_{ij} are uniform, s_j is obtained as a linear function in $e_{ij}^{(0)}$. The substitution into the energy expressions (3), (4) gives the energy as a function of the strain components. There is, however, one difficulty: the significant terms are those of second order in the strain components; these are incomplete as calculated by the above formulas, because $e_{ij}^{(0)}$ is only an approximate expression neglecting second order terms. It is sufficient for substitution into V_2 where the lowest terms are of the second order, but it is not sufficient to be used in V_1 since the error introduced by this approximation is of the same order as V_2 itself. It is therefore necessary to express the displacement of s_j as a function of the strain components up to terms of the second order. This fact was overlooked by Voigt who uses only the linear approximation. This is the point from which our theory begins to differ from his.

I do not know whether the creators of the theory of elasticity were familiar with the more accurate expression of the strain tensor. The earliest reference which is at my disposal is in the third volume of P. Appell's treatise on mechanics.[6] The formula is in our notations as follows:

$$e_{ij}=\frac{1}{2}\left(\frac{\partial s_j}{\partial x_i}+\frac{\partial s_i}{\partial x_j}\right)+\frac{1}{2}\frac{\partial s_k}{\partial x_i}\frac{\partial s_k}{\partial x_j}, \tag{9}$$

where Einstein's convention applies to the index k appearing twice. As we are interested only in terms of first and second order, it is permissible to substitute into those of the second order the first approximation (8) and even to omit in this approximation the superscript 0 (i.e., replace in these terms $e_{ij}^{(0)}$ by e_{ij}). Hence,

$$\frac{1}{2}\left(\frac{\partial s_j}{\partial x_i}+\frac{\partial s_i}{\partial x_j}\right)=e_{ij}-\tfrac{1}{2}(e_{ik}+\omega_{ik})(e_{jk}+\omega_{jk}). \tag{10}$$

It is useful to abbreviate the writing by introducing the symbol

$$f_{ij}=e_{ij}+\omega_{ij}; \tag{11}$$

this symbol is, however, non-symmetric ($f_{ij}\neq f_{ji}$) because e_{ij} is symmetric and ω_{ij} antisymmetric.

$$e_{ij}=e_{ji},\quad \omega_{ij}=-\omega_{ji}. \tag{12}$$

Adding ω_{ij} to the Eq. (10), we find

$$\partial s_j/\partial s_i=f_{ij}-\tfrac{1}{2}f_{ik}f_{jk}. \tag{13}$$

This can be readily integrated over a region where f_{ij} can be considered as constant, with the result

$$s_j=f_{lk}x_l-\tfrac{1}{2}f_{lk}f_{jk}x_l. \tag{14}$$

Actually, the expression could be written in a slightly more general form by adding a constant of integration $s_j^{(0)}$ which represents the possible translation. However, the invariance of our energy expressions with respect to translations is a matter of course so that we simplify the case by putting $s_j^{(0)}=0$.

We need to substitute into Eq. (4) only the first term of the formula (14). On the other hand, the second-order part of Eq. (3) entirely depends on the second term of (14). Indeed, it is easy to see that the part of second order of $V_1=V_1'+V_2''$ takes the form

$$V_1''=-\tfrac{1}{2}\sum_{\mu\nu}A_{\mu\nu}f_{jk}f_{lk}a_{\mu\nu j}a_{\mu\nu l},$$

which can be also written as

$$V_1''=-\tfrac{1}{2}\sum_{\mu\nu}A_{\mu\nu}f_{kj}f_{lj}a_{\mu\nu k}a_{\mu\nu l}. \tag{15}$$

On the other hand, the function V_2 becomes

$$V_2=\tfrac{1}{2}\sum_{\mu\nu}\{(B_{\mu\nu j}-C_{\mu\nu}a_{\mu\nu j}^2)f_{kj}f_{lj} + C_{\mu\nu}a_{\mu\nu i}a_{\mu\nu j}f_{ki}f_{lj}\}a_{\mu\nu k}a_{\mu\nu l}. \tag{16}$$

The complete second-order part of the energy is thus

$$V_1''+V_2=\tfrac{1}{2}\sum_{\mu\nu}\{(B_{\mu\nu j}-C_{\mu\nu}a_{\mu\nu j}^2-A_{\mu\nu})f_{kj}f_{lj} \times C_{\mu\nu}a_{\mu\nu i}a_{\mu\nu j}f_{ki}f_{lj}\}a_{\mu\nu k}a_{\mu\nu l}. \tag{17}$$

The writing of the last two equations is not quite orthodox with respect to Einstein's convention. What is meant here is that the summation over an index is implied if the index occurs in the term *two or more times*. (According to the strict Einstein rule it must occur just *two* times.)

[6] Paul Appell, "Traité de Mécanique Rationelle" (Gautier-Villars, Paris, 1901), Vol. 3, p. 243.

4. RELATIONS BETWEEN COEFFICIENTS

Since the energy V is invariant with respect to rotations all coefficients of the expansion of V with respect to the powers and products of ω_{ij} must vanish. The first-order part V_1' contains only linear terms, while $V_1''+V_2$ contains either terms of second order in ω_{ij} or terms in which components of ω_{ij} are multiplied by components of e_{ij}. As the rotations are independent of the strain, the two functions V_1' and $V_1''+V_2$ must be invariant each for itself. This involves certain relations between the coefficients $A_{\mu\nu}$, $B_{\mu\nu j}$, and $C_{\mu\nu}$. It will be necessary to write out our quadratic form explicitly:

$$\begin{aligned}V_1''+V_2=\tfrac{1}{2}\sum_{\mu\nu}\{&(B_{\mu\nu1}-A_{\mu\nu})a_{\mu\nu1}{}^2f_{11}{}^2+[(B_{\mu\nu3}-A_{\mu\nu})a_{\mu\nu2}{}^2f_{23}{}^2+(B_{\mu\nu2}-A_{\mu\nu})a_{\mu\nu3}{}^2f_{32}{}^2+2C_{\mu\nu}a_{\mu\nu2}{}^2a_{\mu\nu3}{}^2f_{23}f_{32}]\\&+2C_{\mu\nu}a_{\mu\nu2}{}^2a_{\mu\nu3}{}^2f_{22}f_{33}+2C_{\mu\nu}a_{\mu\nu1}{}^2a_{\mu\nu2}a_{\mu\nu3}(f_{23}+f_{32})f_{11}\\&+2[(B_{\mu\nu1}-A_{\mu\nu})f_{31}+C_{\mu\nu}a_{\mu\nu1}{}^2f_{13}]f_{11}a_{\mu\nu1}a_{\mu\nu3}+2[(B_{\mu\nu1}-A_{\mu\nu})f_{21}+C_{\mu\nu}a_{\mu\nu1}{}^2f_{12}]f_{11}a_{\mu\nu1}a_{\mu\nu2}\\&+2[(B_{\mu\nu1}-A_{\mu\nu})f_{21}f_{31}+C_{\mu\nu}(f_{12}f_{13}+f_{13}f_{21}+f_{31}f_{12})a_{\mu\nu1}{}^2]a_{\mu\nu2}a_{\mu\nu3}+\text{etc.}\}.\end{aligned}\tag{18}$$

By "etc." are meant additional terms which result from those written out by cyclic substitution of the indices (other than μ, ν). If we replace the symbols f_{ij} by their definitions (11), the invariance with respect to rotations requires the vanishing of all terms containing components ω_{ij} or their squares and products. This affects only the components ω_{ij} with $i\neq j$ because ω_{ii} is identically zero. The square and product terms entail the following relations,

$$\left.\begin{aligned}\sum_{\mu\nu}[(B_{\mu\nu3}-A_{\mu\nu})a_{\mu\nu2}{}^2+(B_{\mu\nu2}-A_{\mu\nu})a_{\mu\nu3}{}^2-C_{\mu\nu}a_{\mu\nu2}{}^2a_{\mu\nu3}{}^2]=0,\\ \sum_{\mu\nu}(B_{\mu\nu1}-A_{\mu\nu}-C_{\mu\nu}a_{\mu\nu1}{}^2)a_{\mu\nu2}a_{\mu\nu3}=0,\end{aligned}\right\}\tag{19}$$

while the linear terms lead to

$$\left.\begin{aligned}\sum_{\mu\nu}[(B_{\mu\nu3}-A_{\mu\nu})a_{\mu\nu2}{}^2-(B_{\mu\nu2}-A_{\mu\nu})a_{\mu\nu3}{}^2]=0,\\ \sum_{\mu\nu}(B_{\mu\nu1}-A_{\mu\nu}-C_{\mu\nu}a_{\mu\nu1}{}^2)a_{\mu\nu3}a_{\mu\nu1}=0,\\ \sum_{\mu\nu}(B_{\mu\nu1}-A_{\mu\nu}-C_{\mu\nu}a_{\mu\nu1}{}^2)a_{\mu\nu1}a_{\mu\nu2}=0,\end{aligned}\right\}\tag{19'}$$

and again to another relation already listed. Further, the relations must be added which result from these by cyclic substitution.

These relations can be used to reduce to a simpler form the remaining terms, which depend only on e_{ij}, namely,

$$\begin{aligned}V_1''+V_2=\tfrac{1}{2}\sum_{\mu\nu}\{&(B_{\mu\nu1}-A_{\mu\nu})a_{\mu\nu1}{}^2e_{11}{}^2+2C_{\mu\nu}a_{\mu\nu2}{}^2a_{\mu\nu3}{}^2(2e_{23}{}^2+e_{22}e_{33})\\&+4C_{\mu\nu}a_{\mu\nu1}{}^2(a_{\mu\nu2}e_{12}+a_{\mu\nu3}e_{13})e_{11}+4C_{\mu\nu}a_{\mu\nu1}{}^2a_{\mu\nu2}a_{\mu\nu3}(e_{11}e_{23}+2e_{12}e_{13})+\text{etc.}\}.\end{aligned}\tag{20}$$

Returning to the remark about the symmetry of the coefficients made at the end of Section 2, we may make here the following statement. If we had not postulated in Eqs. (5) the independence of $A_{\mu\nu}$ and $C_{\mu\nu}$ on the directions but had written more generally $A_{\mu\nu j}$, $C_{\mu\nu ij}$, then the requirement of rotational invariance would have given us a much larger number of conditions than the set (19), (19′). The burden of those additional conditions is precisely that $A_{\mu\nu j}$, $C_{\mu\nu ij}$ are the same for all subscripts i, j. Thus our assumptions (5) do not represent a loss of generality but only a more concise way of writing.

5. ANALOGS TO THE CAUCHY RELATIONS

Owing to Voigt's influence it has become customary to write quadratic forms of the type (20) in a manner which with our definition of e_{ij} is as follows

$$V_1''+V_2=\{\tfrac{1}{2}b_{11}e_{11}^2+2b_{44}e_{23}^2+b_{23}e_{22}e_{33}+2(b_{14}e_{23}+b_{15}e_{31}+b_{16}e_{12})e_{11}+4b_{56}e_{12}e_{13}+\text{etc.}\}. \quad (21)$$

All the coefficients b_{ij} are symmetric in i, j. By "etc.," again, are meant terms which result by cyclic substitution from those written out. In these permutations the subscripts 1, 2, 3 and 4, 5, 6 form two separate permutation groups: for instance, the term derived from $4b_{56}e_{12}e_{13}$ is $4b_{64}e_{23}e_{21}$.

By comparing with the form (20) it will be seen that taking care of the rotational invariance leads to the following symmetry relations:

$$b_{23}=b_{44}, \quad b_{14}=b_{56}, \quad (22)$$

to which must be added those following by cyclic permutation,

$$\left.\begin{aligned} b_{31}&=b_{55}, \quad b_{25}=b_{64},\\ b_{12}&=b_{66}, \quad b_{36}=b_{45}.\end{aligned}\right\} \quad (22')$$

These relations form the analogs to Voigt's Cauchy relations and we shall refer to them by that name. We shall first show that these relations are indeed identically satisfied when we have central forces. Carrying out the differentiations indicated in the Eqs. (5) we easily find

$$\left.\begin{aligned} A_{\mu\nu}&=\Phi_{\mu\nu}'/2r_{\mu\nu},\\ B_{\mu\nu j}&=\tfrac{1}{2}(a_{\mu\nu j}/r_{\mu\nu})^2\Phi_{\mu\nu}''+[1-(a_{\mu\nu j}/r_{\mu\nu})^2]\Phi_{\mu\nu}'/2r_{\mu\nu},\\ C_{\mu\nu}&=[\Phi_{\mu\nu}''-\Phi_{\mu\nu}'/r_{\mu\nu}]/2r_{\mu\nu}^2.\end{aligned}\right\} \quad (23)$$

The accent and double accent denote here, respectively, the first and second derivatives of $\Phi_{\mu\nu}(r_{\mu\nu})$ with respect to the argument $r_{\mu\nu}$.

We have seen that the Cauchy relations (22), (22′) are an immediate consequence of the conditions (19), (19′) and of their cyclic permutations. It is, however, obvious that all these conditions can be satisfied by the single relation

$$B_{\mu\nu j}-A_{\mu\nu}=C_{\mu\nu}a_{\mu\nu j}^2, \quad (24)$$

holding not only for the double sum but for each term separately. Now we find, indeed, from the Eqs. (23)

$$B_{\mu\nu j}-A_{\mu\nu}=\tfrac{1}{2}(a_{\mu\nu j}/r_{\mu\nu})^2[\Phi''-\Phi'/r_{\mu\nu}]=C_{\mu\nu}a_{\mu\nu j}^2. \quad (25)$$

We shall now go back to Voigt's work and see in what it differs from ours. It was mentioned in Section 3 that Voigt overlooked the second order terms (in e_{ij}) contained in V_1 of Eq. (3); this led him to attribute rotational invariance to the energy term V_2 alone. Such a contention is clearly untenable. Indeed, Voigt's theory differs from our formulas of Section 4 only in one point: the terms with $A_{\mu\nu}$ are left out in all the equations. Thus Voigt arrives at conditions equivalent to our conditions (19), (19′) with the $A_{\mu\nu}$ terms crossed off. For instance, the first condition is, according to him,

$$\sum_{\mu\nu}[B_{\mu\nu 3}a_{\mu\nu 2}^2+B_{\mu\nu 2}a_{\mu\nu 3}^2-C_{\mu\nu}a_{\mu\nu 2}^2a_{\mu\nu 3}^2]=0. \quad (26)$$

However, we have just verified that in the case of central forces the condition is satisfied in our form. Hence, the left side of Voigt's Eq. (26) is not equal to zero but to the negative of the missing terms, namely, to

$$\sum_{\mu\nu}A_{\mu\nu}(a_{\mu\nu 2}^2+a_{\mu\nu 3}^2).$$

This expression does not, in general, vanish but is often of the same order magnitude as the other sums entering into the Eqs. (19). In fact, it is possible to supply examples of lattices in which it can be explicitly calculated. However, it is well to remember that the simplest possible model in which each atom interacts only with its nearest neighbors is not suitable for the purpose, since in such models $A_{\mu\nu}=0$. Thus the deviations from the Cauchy relations are caused by interactions between points which are not nearest neighbors.

Voigt wrote the quadratic form V_2 in the form (21) with the only difference that he designated the coefficients by c_{ij} (instead of b_{ij} in our form $V_1''+V_2$). He claimed for them the Cauchy relations

$$c_{23}=c_{44}, \quad c_{14}=c_{56}, \quad \text{etc.} \quad (27)$$

It follows from our discussion that this claim was unfounded. If Voigt or the many authors

who repeated his claim had gone to the trouble to substitute into his relations of the type (26) the actual values of $B_{\mu\nu j}$ and $C_{\mu\nu}$, as they result from the assumption of central forces, they would have noticed that these relations are not satisfied. Some authors seem to regard the Cauchy relations as additional restrictive conditions imposed upon the coefficients $A_{\mu\nu}$, $B_{\mu\nu j}$, $C_{\mu\nu}$. This is, however, a misconception. In quadratic forms which are invariant with respect to rotations these conditions are merely a manifestation of the symmetry inherent in this invariance, they are satisfied identically and do not impose any further restrictions. In quadratic forms which are not rotationally invariant the Cauchy relations are not satisfied.

6. MEASUREMENT OF STRAINS

So far our discussion has been purely mathematical. We have now to tackle the physical question whether the actually measured elasticity coefficients are of the type satisfying the Cauchy relations. It is shown in the theory of elasticity that the deformation energy of an elastic body can be represented as a quadratic form in the strains e_{ij}. This quadratic form may be written out in the manner of formula (21). Following the customary notations, we shall designate the coefficients by c_{kl}, and we shall restrict ourselves in what follows to crystals and lattices of orthorhombic symmetry. This is done exclusively for the purpose of making the writing less cumbersome: all the arguments and conclusions apply just as well to the general case. The orthorombic symmetry requires the vanishing of all the terms which are linear or bilinear in e_{23}, e_{31}, e_{12}. Thus the energy expression becomes,

$$V=[\tfrac{1}{2}c_{11}e_{11}^2+2c_{44}e_{23}^2+c_{23}e_{22}e_{33}+\text{etc.}]. \quad (28)$$

If this energy is referred to a crystal cube of the volume 1 cm³, the components of the stresses can be obtained from it by differentiation,

$$\begin{aligned} p_{11}&=\partial V/\partial e_{11}=c_{11}e_{11}+c_{12}e_{22}+c_{13}e_{33}, \\ p_{23}&=\tfrac{1}{2}\partial V/\partial e_{23}=c_{44}e_{23}, \end{aligned} \quad (29)$$

and so on, by cyclic permutation. As the components of the deformation e_{ij} and the stress components p_{ij} are both observable, it is possible to infer from direct measurements the coefficients of elasticity c_{kl} by means of the Eqs. (29). The question which we have to answer is as follows: with which of the two quadratic forms of the lattice must the form V be identified?

In going back to the expressions (2)–(4) of the lattice energy in terms of the displacements, it is important to point out that $V_1=0$. In fact, the j-component of the force acting on the point ν is given by $-\partial V/\partial s_{\nu j}$. For the undistorted lattice we get thus

$$\textstyle\sum_\mu A_{\mu\nu}a_{\mu\nu j}=0,$$

because in the undeformed lattice every point is in an equilibrium position, so that the force on it vanishes. Multiplying this by $s_{\nu j}$ and summing with respect to ν, we find that the second term with $s_{\nu j}$ in the expression (3) vanishes. This implies, however, that the term with $s_{\mu j}$ also vanishes because it is equal to the other term, $A_{\mu\nu}$ being symmetric and $a_{\mu\nu}$ antisymmetric in μ, ν. Consequently, $V_1=0$; from the mathematical point of view it is important that this is not an identical relation but an additional condition imposed on the variables of the system. At any event, there follows,

$$V=V_2. \quad (30)$$

Therefore, the two quadratic forms in e_{ij} discussed in the preceding section have the following properties. (1) The form V_2 represents the energy of the lattice, but it is not invariant with respect to rotations and does not satisfy the Cauchy relations. (2) The form $V_1''+V_2$ is rotationally invariant and satisfied Cauchy's relations, but it is not equal to the energy. The mathematical reason for this behavior lies in the fact that the Eq. (30) results from the subsidiary condition $V_1=0$ which is not invariant with respect to rotations. Thus it comes about that the physical requirement of the invariance of the energy with respect to rotations is mathematically satisfied only when the energy is represented by the sums of a linear and a quadratic form and not by a quadratic form alone.

Since the function V which is used in the Eqs. (28) and (29) for the determination of the coefficients of elasticity must represent the energy, it is obvious that it must be identified with the form V_2. Hence, *the coefficients of elasticity do not satisfy the Cauchy relations.*

Since the whole burden of our argument hinges on this identification, it will not be amiss if we make it more cogent by calculating the stresses in a quite different way. This method has the further advantage that it works with linear relations only and is, therefore, independent of the second-order corrections to the strain expressions (as far as the stress-strain relations are concerned). Since the choice is only between the forms V_2 and $V_1''+V_2$, one single experimentum crucis is sufficient to decide the question: we need only to calculate one stress component in one particular kind of lattice.

Let us consider an orthorombic lattice whose principal directions coincide with the coordinate axes $j=1, 2, 3$. Let it have the shape of a prism with a square cross section of 1 cm² area and with its axis in the direction $j=1$. We imagine the prism divided into two halves by an ideal plane normal to the axis and lying between two lattice-net planes. We wish to calculate the forces exerted in the axial direction by one half of the prism upon the other half.

For this purpose we shall use the representation of the lattice energy by the sums (3) and (4) in which each term refers to the mutual energy of two lattice points labelled μ and ν, respectively. The force on the point ν exerted by the point μ in the axial direction is equal to the negative derivative with respect to $s_{\nu 1}$ of their mutual energy, namely, to

$$A_{\mu\nu}a_{\mu\nu 1}+2(B_{\mu\nu 1}-C_{\mu\nu}a_{\mu\nu 1}^2)(s_{\mu 1}-s_{\nu 1}) +2C_{\mu\nu}a_{\mu\nu 1}a_{\mu\nu k}(s_{\mu k}-s_{\nu k}).$$

Let now the points in the positive half be denoted by μ and those in the negative half by ν. The force of interaction of the two halves is then obtained by taking the double sum of the expression, where μ is extended over the positive half and ν over the negative half. We see that the first term of the double sum is a constant and independent of the displacements: it represents the force holding together the two halves of the undeformed crystal, and it is of no interest to us. The second and third terms of the double sums are the force due to the existing deformation, in other words, they represent the normal stress

$$p_{11}=2\sum_{\mu_1+\nu_1-}\{(B_{\mu\nu 1}-C_{\mu\nu}a_{\mu\nu 1}^2)(s_{\mu 1}-s_{\nu 1}) +C_{\mu\nu}a_{\mu\nu 1}a_{\mu\nu k}(s_{\mu k}-s_{\nu k})\}.$$

To explain the symbols at the sign of the sum we must make the following remark. The subscripts μ and ν are abbreviations each for three indices μ_1, μ_2, μ_3 and ν_1, ν_2, ν_3 labeling the coordinates of the points. Thus the sum is actually sixfold. We do not bring in evidence the summations with respect to $\mu_2, \mu_3, \nu_2, \nu_3$ because they extend over the complete cross dimensions of the lattice. But it is necessary to keep in mind that μ_1 extends over the positive half and ν_1 over the negative half in the axial direction.

We make now the transition to strain components by means of the relation (14). As we need only linear terms and as rotations are inessential to us, this relation simplifies into

$$s_j=e_{ij}x_i.$$

After substituting this into our sums, all the terms with odd powers of $a_{\mu\nu 2}$ or $a_{\mu\nu 3}$ will disappear because the summations in the 2,3 directions extend over the whole crystal whose dimensions are supposed to be extremely large compared with the lattice constant. The result is

$$p_{11}=\sum_{\mu_1+\nu_1-}[B_{\mu\nu 1}e_{11}+C_{\mu\nu}(a_{\mu\nu 2}^2e_{22}+a_{\mu\nu 3}^2e_{33})]a_{\mu\nu 1}. \tag{31}$$

It is possible to get rid of the summation with respect to ν_1 in a way which we shall carry through in detail only for the case of a simple orthorhombic lattice with only one point in every fundamental region. Let us consider all the points of the ν half which lie in a straight line parallel to the axis and are, therefore, characterized by the same fixed parameters ν_2, ν_3. All these points are acted on by forces originating in points of the μ-half. In particular let us consider their interactions with the points lying in a straight line parallel to the axis in the μ-half and labeled by the common fixed parameters μ_2, μ_3. With respect to the paramaters μ_1 and ν_1 (which change along the two straight lines) we can divide all these interacting pairs of points into groups such that the axial component of the mutual distance $a_{\mu\nu 1}$ of two points is constant within a group and equal to a, $2a$, $3a$, $\cdots$, respectively, in the different groups (where a is the lattice constant in the axial direction). The number of point pairs in the group $a_{\mu\nu 1}=na$ can be readily inferred from the fact that the coordinate ν_1 can assume the values $-\delta$, $-\delta-a$, $\cdots$

$-\delta-(n-1)a$, where δ is a fraction of a. These are, altogether, n different values, whence the number of pairs within a group is also $n=a_{\mu\nu 1}/a$. Now in the sums (31) the terms relating to point pairs of the same group are all identical, because $B_{\mu\nu 1}$, $C_{\mu\nu}$, $a_{\mu\nu 1}$ are all the same within the group. Hence, we can omit the summation with respect to ν_1 if, instead, we multiply each term of the sum by $a_{\mu\nu 1}/a$. Thus we find

$$p_{11}=(2/a)\sum_{\mu_1+}[B_{\mu\nu 1}e_{11}+C_{\mu\nu}(a_{\mu\nu 2}{}^2e_{22}+a_{\mu\nu 3}{}^2e_{33})]a_{\mu\nu 1}{}^2.$$

In this sum ν_1 has a constant value. Since all terms are symmetric in μ, ν (including symmetry in μ_1, ν_1) the summation could be extended, instead, over the negative half of the crystal (μ_1–) without changing p_{11}. Hence, it can be also extended over the whole crystal, provided that the sum is supplied with the factor $\frac{1}{2}$. In practice the coefficients $B_{\mu\nu 1}$, $C_{\mu\nu}$ decrease very rapidly with the distance between μ and ν. Hence, very few net planes of the lattice to both sides of the plane ν_1 appreciably contribute to the sum. Therefore, the plane ν_1 can be taken anywhere, within the crystal with the exception of two negligible layers at the borders. As the sum is independent of the choice of ν_1, we may sum with respect to ν_1 over the whole crystal and at the same time divide by the number N of values which ν_1 assumes within it, i.e., by the number of net planes in the direction $j=1$. To make the case comparable with that treated above, we must have a cubical crystal of 1-cm edge. Hence its length in the direction 1 is 1 cm, and the number of the net planes is $N=1/a$. Therefore, we arrive at

$$p_{11}=\sum_{\mu\nu}[B_{\mu\nu 1}e_{11}+C_{\mu\nu}(a_{\mu\nu 2}{}^2e_{22}+a_{\mu\nu 3}{}^2e_{33})]a_{\mu\nu 1}{}^2, \quad (32)$$

where the summation symbol denotes the ordinary double sum over the whole crystal.

Although the special case of the simple lattice is entirely sufficient for our purpose, we remark that this method of calculating the normal stress can be applied (with but slight changes) also to the general case when each fundamental region contains several points, possibly, of different physical properties. The result is identical with (32) in the general case also. On the other hand, the method must be modified to a greater degree in calculating the shearing stresses, because then not only the magnitudes of the individual interaction forces are significant, but also their points of attack.

Let us now see what form our general expression (18) of $V_1''+V_2$ assumes in the special case of orthorhombic symmetry. Because of the relation $a_{\mu\nu j}=-a_{\nu\mu j}$ all the terms disappear which contain odd powers of one of these parameters. Using the notation of the coefficients given by the formula (21), we find for $V_1''+V_2$

$$\left.\begin{aligned} b_{11}&=\sum_{\mu\nu}(B_{\mu\nu 1}-A_{\mu\nu})a_{\mu\nu 1}{}^2,\\ b_{44}&=\tfrac{1}{4}\sum_{\mu\nu}[(B_{\mu\nu 3}-A_{\mu\nu})a_{\mu\nu 2}{}^2\\ &\qquad+(B_{\mu\nu 2}-A_{\mu\nu})a_{\mu\nu 3}{}^2+2C_{\mu\nu}a_{\mu\nu 2}{}^2a_{\mu\nu 3}{}^2],\\ b_{23}&=\sum_{\mu\nu}C_{\mu\nu}a_{\mu\nu 2}{}^2a_{\mu\nu 3}{}^2. \end{aligned}\right\}(33)$$

On the other hand, the quadratic form V_2 differs from this only in that the quantities $A_{\mu\nu}$ are left out. In particular, we shall write out explicitly the following coefficients

$$\left.\begin{aligned} c_{11}&=\sum_{\mu\nu}B_{\mu\nu\cdot\mu\nu 1}{}^2, \quad c_{12}=\sum_{\mu\nu}C_{\mu\nu}a_{\mu\nu 1}{}^2a_{\mu\nu 2}{}^2,\\ c_{13}&=\sum_{\mu\nu}C_{\mu\nu}a_{\mu\nu 1}{}^2a_{\mu\nu 3}{}^2. \end{aligned}\right\}(34)$$

From these results it is clear that we obtain the Eq. (32) only when we substitute $V=V_2$ into the first relation (29), while the assumption $V=V_1''+V_2$ lead to an entirely incorrect result. Hence, we obtain another confirmation that the quadratic form (28) fundamental in elasticity must be identified with the function V_2 which is not invariant with respect to rotations and which does not satisfy the Cauchy relations.

PHYSICAL REVIEW VOLUME 70, NUMBERS 11 AND 12 DECEMBER 1 AND 15, 1946

Magnetoresistance and Domain Theory of Iron-Nickel Alloys

R. M. BOZORTH
Bell Telephone Laboratories, Murray Hill, New Jersey
(Received September 19, 1946)

Measurements of change of electrical resistivity with magnetization and with tension are reported for iron-nickel alloys containing 40 to 100 percent nickel. When the magnetostriction is negative (81 to 100 percent nickel), tension (σ) decreases resistivity, and magnetic field (H) increases it. Domain theory predicts the ratio σ/H at which the resistivity is equal to that of the unmagnetized specimen, and the theory is accurately confirmed. Measurements are made in transverse as well as longitudinal magnetic fields, and the difference between the resistances so measured is shown to be independent of the distribution of domains in the unmagnetized state; the erratic results reported in the literature are thus explained and avoided. When magnetostriction is positive, the limiting changes of resistivity with field and tension are sometimes found to be different; this is shown to be caused by the variation of magnetostriction with crystallographic direction.

INTRODUCTION

IT has been known for almost 100 years that the electrical resistivities of iron and nickel are increased when these materials are magnetized. It is now known that almost all ferromagnetic materials show this increase, which under certain conditions may amount to 15 percent or more. Closely associated with the change in resistivity due to magnetization is a change—an increase or a decrease—effected by tension within the elastic limit of the material. McKeehan[1] has studied both of these effects—called by him *magnetoresistance* and *elastoresistance*—in the face-centered iron-nickel alloys, and has pointed out the close relation that exists between elastoresistance and magnetostriction. More recently others[2] have discussed the domain theory of these phenomena.

The purpose of the present work has been (1) to extend the application of domain theory to these alloys, pointing out that certain new results can be accounted for quantitatively by theory, and (2) to measure the magnetoresistances of the iron-nickel alloys (40 to 100 percent nickel) and express them in such a way that the irregularities previously observed tend to disappear. The latter is accomplished by measuring the change in resistance when a specimen is placed first in a longitudinal field (field, H, parallel to electric current, i) and then in a transverse field ($H \perp i$); the difference between the resistivities is plotted against the percent of nickel.

The mechanism by which the change in resistance is produced is not well understood, and will not be discussed here.

METHOD OF MEASUREMENT

The alloys studied were of high commercial purity, and contained in addition to iron and nickel about 0.5 percent manganese, 0.4 percent cobalt, 0.02 percent carbon, and smaller amounts of sulfur and phosphorus. Specimens were thin tapes about 0.006×0.125 inch in section. They were straightened by stretching after a preliminary annealing, and were then annealed on a flat surface at 1050° to 1150°C in a hydrogen atmosphere. They cooled through 500°C at about 25°C/minute. Some of the alloys were subsequently held for 24 hours at 425°C to increase the amount of atomic ordering.

When tension was to be applied, specimens 60 cm in length were placed in a vertical position next to a heavy permalloy yoke used to reduce the demagnetizing factor. The magnetizing coil was placed around the middle 48 cm of the specimen, inside the yoke; and a search coil for ballistic measurements extended over the middle 15 cm. The specimen was held at its upper end by clamping it between the upper jaws of the yoke, and tension was applied to the specimen by hanging a weight on its lower end. A clearance

[1] L. W. McKeehan, Phys. Rev. **36**, 948–77 (1930). See also the earlier reports by H. D. Arnold and L. W. McKeehan, Phys. Rev. **23**, 114 (1924) and by L. W. McKeehan, J. Frank. Inst. **202**, 737–73 (1926).

[2] E. Englert, Ann. d. Physik **14**, 589–612 (1932); W. Döring, Ann. d. Physik **32**, 259–76 (1938); R. Becker and W. Döring, *Ferromagnetismus* (Verlagsbuchhandlung Julius Springer, Berlin, 1939).

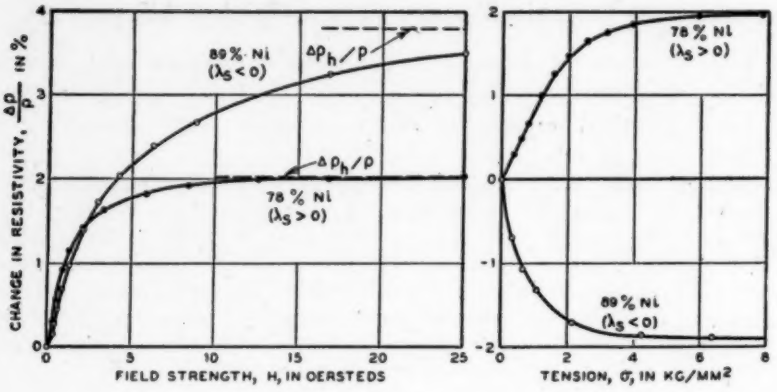

FIG. 1. A magnetic field usually causes an increase in resistivity. Tension increases resistivity of material when magnetostriction, λ_s, is positive, decreases it when magnetostriction is negative.

of a few tenths of a mm was left between the specimen and the lower jaws of the yoke to eliminate friction. Potential leads of fine wire were placed 40 cm apart.

When measuring transverse and longitudinal changes in resistance, with no tension applied, the specimen was 30 cm long, and was wrapped in paper and placed in a channel milled in a piece of brass ½ inch wide. Pressing against the brass were the pole pieces of a large electromagnet* capable of delivering much more than the 20,000 oersteds actually used in the ½-inch gap for measuring the transverse effect. The pole pieces extended over 15 cm of the specimen, and potential leads were symmetrically placed 10 cm apart. The demagnetizing factor for transverse magnetization was assumed to be equal to that for an ellipsoid having axes in the ratio 6:125:∞; with the field applied, as it was, parallel to the axis of intermediate length, $N/4\pi$ is 0.047.

After measuring the resistance as a function of the transverse field, it was desirable to measure it immediately in a longitudinal field; consequently the brass holder containing the specimen, and its associated leads, were immediately lifted onto heavy upright pieces of iron placed 22 cm apart on the tops of the pole pieces of the magnet. Although the longitudinal field was now relatively small, measurements were made to about 2000 oersteds, more than sufficient to obtain the maximum increase in resistance.

The currents traversing the specimen varied up to 100 milliamperes. When necessary the current was reduced to successively lower values and the resistivity for zero current obtained by extrapolation. Potentials were read on a Leeds and Northrup Type K potentiometer. Experience showed that no special precautions were necessary for controlling the temperature of the specimen.

* Designed by Mr. P. P. Cioffi, to whom the author is indebted for its use.

QUALITATIVE DOMAIN THEORY

The effects of field (H) and tension (σ) are illustrated by new data shown in Fig. 1. Here 78 and 89 Permalloy are used as examples of materials of positive and negative magnetostriction, respectively. The increase in resistivity due to H approaches a limiting value designated $\Delta\rho_h$. The change of ρ with σ is an increase if the magnetostrictive fractional change in length at

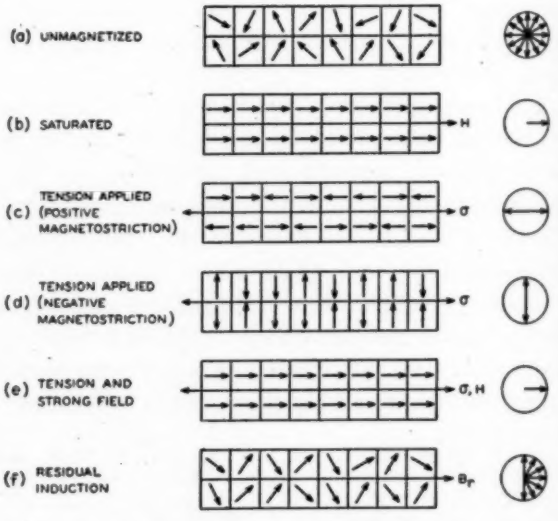

FIG. 2. Qualitative domain interpretation of effects of field and tension. Distribution of domains in various directions is represented by vectors in squares. In diagrams at right vectors have been moved to common origin.

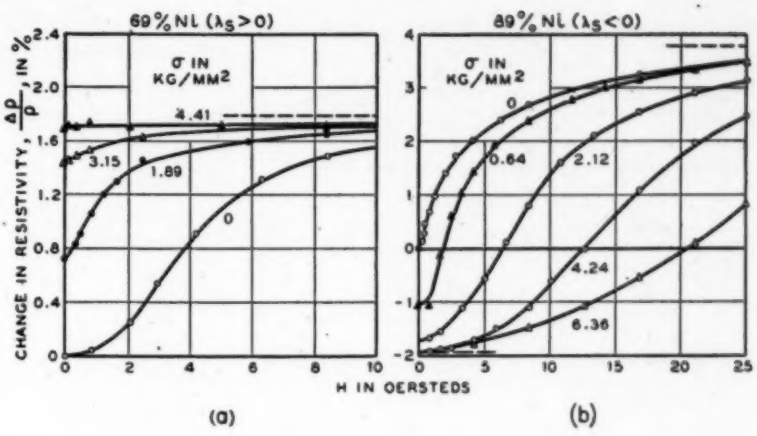

FIG. 3. Effect of magnetic field on resistivity of 69 and 89 Permalloys to which various tensions have been applied.

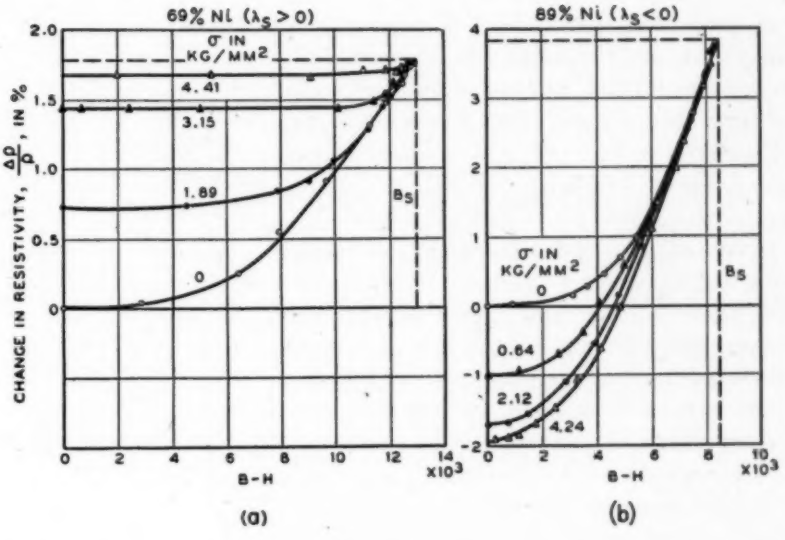

FIG. 4. Data like those of Fig. 3, plotted against $(B-H)$ instead of H.

saturation, λ_s, is positive, and a decrease if it is negative. A definite limit, $\Delta\rho_\sigma$, is observed for most of these alloys.

The domain interpretation of these results may be stated with the aid of Fig. 2. In the unmagnetized state the domains are oriented in many directions (*a*). A field aligns them so that their moments are parallel to the field—the "parallel" position (*b*). Tension causes the domains to take the two oppositely directed positions (*c*), parallel to the line of tension, if λ_s is positive, and positions perpendicular to the tension (*d*) if λ_s is negative. If the specimen is unmagnetized, the domains in a material with positive magnetostriction are aligned by tension so that there are equal numbers in the two opposite directions. Application of a strong field then reverses half of the domains. If tension is applied to a material with negative λ_s, subsequent application of a field will cause the domains to rotate continuously into the parallel position as the field is increased in strength to a high value.

The data of Figs. 3 and 4 can be interpreted in the manner just described. In 69 Permalloy ρ is increased by both H and σ, and the limit of ρ attained with H alone is the same as that with σ alone. When σ is applied first, and then H, Figs. 3(a) and 4(a) show that the magnetization increases for some time without change in ρ. As σ is increased the horizontal portion of the $\Delta\rho$ *vs.* $B-H$ curve increases in length until, in the limit, it constitutes the whole curve. Thus the 180° reversals, which do not alter the resistivity, become increasingly important and finally account for the whole change in magnetization.

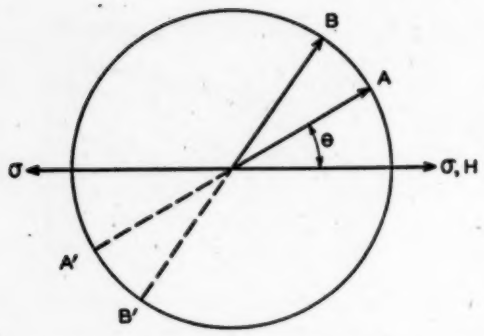

FIG. 5. Diagram showing how domain is rotated from initial position A to position B by tension σ, and rotated back to A by field H_0.

In 89 Permalloy ($\lambda_s<0$), σ and H oppose each other in their action; the effect of tension is to decrease, and magnetization to increase, the resistivity. The limiting change in resistivity due to σ is very close to $-\frac{1}{2}$ times that due to the field. That is,

$$\Delta\rho_\sigma/\rho \doteqdot -\tfrac{1}{2}\Delta\rho_h/\rho.$$

The curves of Fig. 4(b) have no horizontal portions, and this shows that at no stage in the magnetization is the 180° reversal the sole process occurring. On the contrary, evidence will be given below to show that under strong tension the whole change in magnetization is caused by domain rotation.

It will be noted that 89 Permalloy, when subjected to certain values of σ and H, has the same resistivity as in the initial demagnetized state. For this situation certain quantitative considerations are appropriate.

QUANTITATIVE RELATIONS

In materials with negative magnetostriction the effects of tension and longitudinal magnetic field are in opposite directions. It is possible to derive a relationship between values of tension and field strength which exactly compensate. This can be derived from Fig. 5. Here A shows the orientation of a domain in an unmagnetized, unstrained material. When a definite value of the tension, σ_0, is applied as indicated, the orientation will change to that indicated at B. Superposition of a field will then rotate the domain toward its original orientation, which it will attain at some specific value of the field-strength, H_0. Domains oriented originally at A' will be rotated by σ_0 to B', and when H_0 is applied they will presumably rotate suddenly by 180° (i.e., invert) and occupy the same final position A. In this final position it will be subject to the same balanced forces of crystal anisotropy and internal strain as existed in the demagnetized state, that is, the resultant of these forces will be zero. The relationship between these compensating values of σ_0 and H_0 should then be amenable to calculation by domain theory without having to take into account the complicating influences of crystal anisotropy and internal strain.

The domain energy associated with σ and H is given[3] by the relation

$$E=-\tfrac{3}{2}\lambda_s\sigma\cos^2\theta-HI_s\cos\theta,$$

in which θ is the angle between the local magnetization, I_s, and the common axis of σ and H. The equilibrium will occur when the energy is a minimum given by

$$dE/d\theta=0;$$

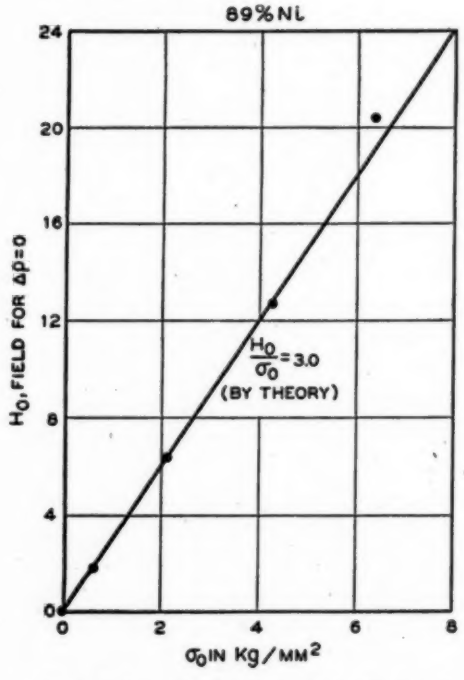

FIG. 6. Comparison of theory (straight line) and experiment (points). Application of tension, σ_0, decreases resistivity, ρ; H_0 is field strength necessary to bring ρ back to original value.

[3] Becker and Döring, reference 2.

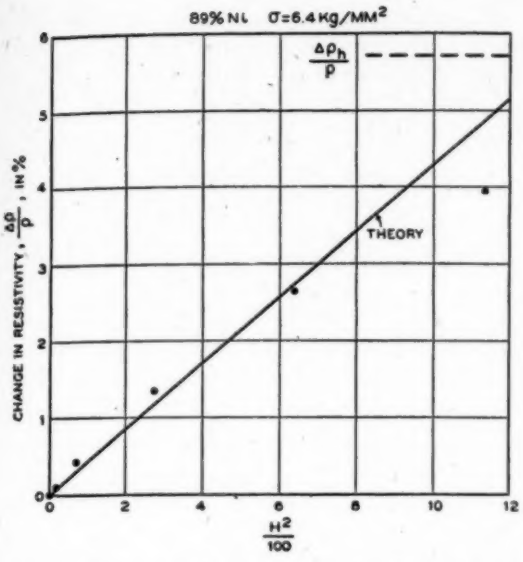

FIG. 7. Change of ρ with H when specimen is subject to high tension. Systematic departure from straight line is caused by forces not taken into account by theory.

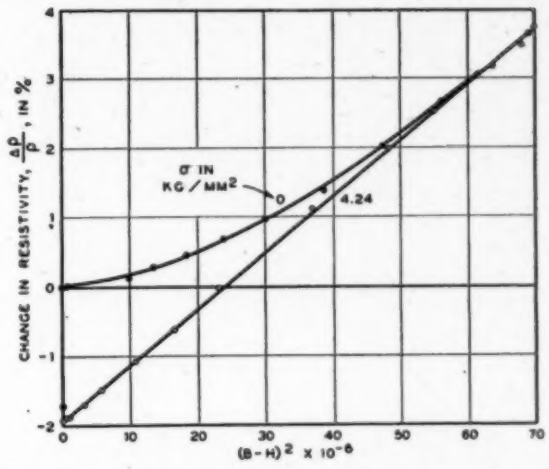

FIG. 8. In specimen under tension, $\Delta\rho$ increases linearly with square of magnetization (rotation process).

hence H_0 must be related to σ_0 as follows:

$$H_0/\sigma_0 = -3(\lambda_s/I_s)\cos\theta,$$

For 89 Permalloy the values of the constants λ_s and I_s are known to be -13×10^{-6} and $8300/(4\pi)$, respectively. For domains orientated uniformly over a hemisphere $\langle\cos\theta\rangle_{Av}=\frac{1}{2}$. If σ_0 is now expressed in kg/mm² and H_0 in oersteds, this relation reduces to

$$H_0/\sigma = 3.0 \text{ oersteds mm}^2/\text{kg}.$$

The corresponding line is drawn in Fig. 6. There the circles represent the values of H_0 and σ_0 corresponding to the intercepts on the H axis of the curves of Fig. 3(b). The agreement is well within the combined limits of accuracy of the data of the experiment and the numerical values of the constants of the equations.

Domain theory may also be applied, with some approximations, to the experiment in which σ is large enough to cause $\Delta\rho$ to attain its limit $\Delta\rho_\sigma$. Then θ is 90° for all the domains, and the disturbing effects of crystal anisotropy and internal stress are small, and can be neglected in comparison with the externally applied stress. It is known that changes in resistivity due to domain orientation are proportional to $\cos^2\theta$, a relation necessitated by the observation that when a material is saturated the change in resistivity, $\Delta\rho_h$, is the same whether the electric current used for measurement of ρ is parallel or antiparallel to H. If the zero of change of resistivity is chosen when σ is already applied and H not yet applied, the relation

$$\Delta\rho = \Delta\rho_1\cos^2\theta$$

therefore holds. This may be combined with the previously used expression containing $\cos\theta$ to give

$$\Delta\rho = \Delta\rho_1 I_s^2 H^2/(9\lambda_s^2\sigma^2).$$

Using the constants for 89 Permalloy this reduces to

$$\Delta\rho/\rho = 43\times10^{-6}H^2,$$

for the conditions of the experiment, in which $\sigma=6.36$ kg/mm². Since $\Delta\rho/\rho$ for large values of H approaches a definite limit, this relation applies only to values of $\Delta\rho/\rho$ that are well below this limit.

This equation is compared with the data in Fig. 7. The discrepancies are in the expected direction. In low fields, before the domains have been turned by the field from the transverse position ($\theta=90°$) to the equilibrium position occupied in the unmagnetized state, the forces due to internal strains and crystal anisotropy will tend to turn the domains from their 90° positions and so aid the field and cause $\Delta\rho$ to be higher than the theoretical value. After the domain has passed through this equilibrium orientation, which it possessed when the field

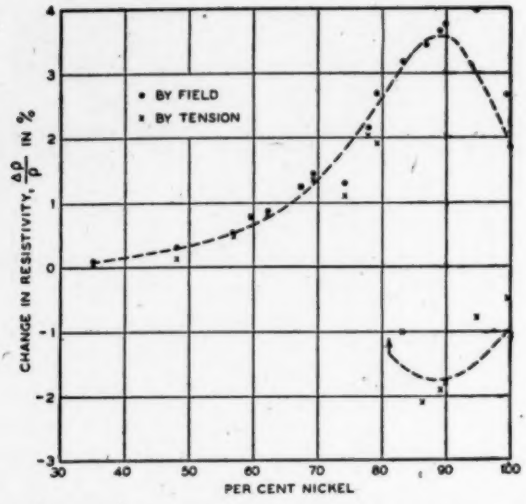

FIG. 9. Limiting effects of field and tension on various Permalloys, according to Shirakawa, Yamanaka, and the author. Broken line shows changes expected on simple theory.

strength had the value given by H_0 above, the internal strain and crystal anisotropy should cause $\Delta\rho$ to fall below the theoretical value, as the data of Fig. 7 show that they do. These forces cause $\Delta\rho$ to approach its limiting value $\Delta\rho_1$ asymptotically.

According to this view of the mechanism of change of magnetization and its effect on resistivity, the domains should assume the orientations they possessed when the specimen was unmagnetized (e.g., A in Fig. 5), or at an orientation 180° therefrom (A instead of A'), when the material as a whole is magnetized to just half of saturation. That is, it should be observed that $I/I_s=0.5$ when $\Delta\rho=0$. Actually I/I_s is somewhat greater than 0.5, almost 0.6. This difference could be caused by a non-random distribution of domain orientations in the unmagnetized condition, due to preferred orientation of crystals or internal strains.

When a sufficient tension is applied to a material with negative magnetostriction the domains are aligned transversely, and subsequent magnetization is accomplished by domain rotation. The induction is then proportional to cos θ,

$$B-H=B_s\cos\theta.$$

Since the change in resistivity is proportional to $\cos^2\theta$, it is, therefore, proportional to $(B-H)^2$. This is confirmed by experiment, as shown in Fig. 8; and such a linear relation may be interpreted, as previously pointed out by Gerlach[4] as evidence that the magnetization proceeds by a purely rotational process. It also shows that the $\cos^2\theta$ term is sufficient to describe the change of resistivity of a domain with orientation, and that no term of higher power is necessary.

IRON-NICKEL SERIES

The maximum changes in resistivity due to magnetization and to tension, as observed by many experimenters, have varied considerably from specimen to specimen. Data obtained by Shirakawa,[5] Yamanaka,[6] and the author, plotted in Fig. 9, show the wide range of values obtained, and similar variations were observed by McKeehan[1] in unsaturated alloys. It was believed that the non-uniformity of the results was caused by the differences in the initial condition of the specimens, resulting mainly from differences in crystal orientation and internal strain. Therefore, it seemed appropriate to measure a given specimen first in a longitudinal and then in a transverse field and plot the difference of the resistivities, $\rho_l-\rho_t$. This should be of rather fundamental importance because it represents the maximum change in resistivity that can result from domain orientation, and is independent of the initial condition of the particular specimen used. It would not be expected to vary with heat treatment unless phase transformations or atomic ordering occur.

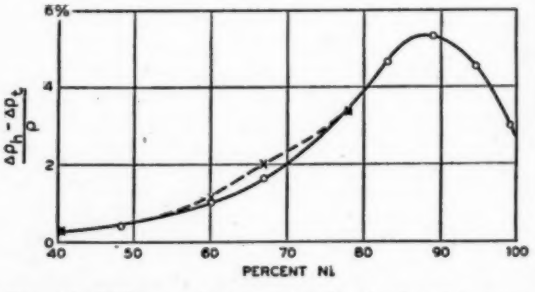

FIG. 10. Difference between longitudinal and transverse changes in resistivity. Solid line is for alloys cooled in normal way, broken line for alloys cooled very slowly to develop superstructure.

[4] W. Gerlach, Ann. d. Physik **12**, 849–64 (1932).
[5] Y. Shirakawa, Sci. Rep., Tohoku Imp. Univ. **27**, 485–531 (1939).
[6] N. Yamanaka, Sci. Rep., Tohoku Imp. Univ. **29**, 36–68 (1940).

Results of these measurements are given in Fig. 10, and lie on a relatively smooth curve. The maximum of over 5 percent occurs near 90 percent nickel, and the effect is relatively small in the low nickel alloys. The change in resistivity in alloys near $FeNi_3$ is increased by the ordering resulting from heating for 24 hours at 425°C.

Two-thirds of $\rho_h - \rho_t$ is shown (in percent) by the broken line of Fig. 9. This represents the value of $\Delta\rho_h$, to be expected only when the domains are distributed at random in the unmagnetized state and when there is negligible dependence of resistivity on the orientation of the domain with respect to the crystal axes. In that case the following relations hold[7]

$$\Delta\rho = \tfrac{3}{2}\Delta\rho_h(\cos^2\theta - \tfrac{1}{3}),$$

$$\Delta\rho_t = -\tfrac{1}{2}\Delta\rho_h,$$

$$\Delta\rho h = \tfrac{2}{3}(\rho_h - \rho_t),$$

$$\Delta\rho_\sigma = \Delta\rho_h \quad (\lambda_s > 0),$$

$$\Delta\rho_\sigma = \Delta\rho_t = -1/2\Delta\rho_h \quad (\lambda_s < 0).$$

The broken line in the lower part of Fig. 9, extending from 81 to 100 percent nickel, shows the values of $\Delta\rho_\sigma$ expected according to the last relation. In the alloys containing 69 and 89 nickel there is little if any departure from these ideal conditions, as shown by the data of Figs. 9 and 10. Substantial departures, however, have been observed[8] for the alloys containing low nickel (e.g., 50 percent) and high nickel (near 100 percent) and for those lying near the zero-magnetostriction point (81 percent). The high nickel anomaly, with $\Delta\rho_\sigma \neq -\frac{1}{2}\Delta\rho_h$, has been shown by Döring[9] to be caused by crystal anisotropy. In many other alloys, having $\lambda_s > 0$, it is found that $\Delta\rho_\sigma \neq \Delta\rho_h$, a fact to be discussed in the next section.

NON-EQUIVALENCE OF FIELD AND TENSION

As remarked above, the magnetoresistance and elastoresistance do not always approach the same limits, $\Delta\rho_h$ and $\Delta\rho_\sigma$, as simple theory indicates that they should when the magnetostriction is positive. This cannot be attributed to a non-random distribution of domains in the unmagnetized conditions, and it now appears that it is to be expected when the magnetostriction varies with crystallographic direction, as it does in these alloys. Lichtenberger's measurements[10] show that between 35 and 45 percent nickel the magnetostriction (λ_s) is positive in the [111] direction ($\lambda_{111} > 0$) and negative in the [100] direction ($\lambda_{100} < 0$). In a polycrystalline specimen tension will, therefore, increase the resistivity of those crystals that have [111] directions lying near the axis of tension, and decrease it in those having [100] near the axis. The resultant $\Delta\rho_\sigma$ will thus be less than $\Delta\rho_h$. Similarly Lichtenberger's curves show that λ_{111} and λ_{100} are opposite in sign between about 80 and 85 percent nickel; and this range may be expected to vary with heat treatment, which affects the amount of atomic order. In other alloys, except those near 60 and 85 percent nickel, λ_{111} and λ_{100} have the same sign but are substantially different in magnitude, and this difference prevents σ from causing complete alignment of all the domains by tension.

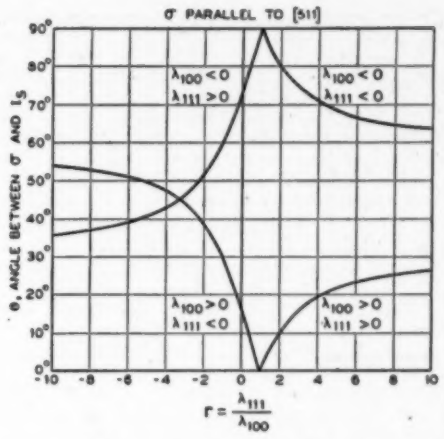

FIG. 11. Angle θ between directions of magnetization (I_s) and tension (σ) when tension is applied parallel to a [511] crystallographic direction. Theoretical.

In a quantitative evaluation of the effect of anisotropic magnetostriction we start with the expression for the magnetic strain energy of a domain, as given by Becker and Döring.[2] Let α_1, α_2, α_3 be the direction cosines of the magnetization (I_s) of the domain, and γ_1, γ_2, γ_3 the direction cosines of the stress (σ) with respect to the

[7] Englert, and Becker and Döring, reference 2.
[8] Yamanaka, reference 6, and the author.
[9] Döring, reference 2.

[10] F. Lichtenberger, Ann. d. Physik 15, 45–71 (1932).

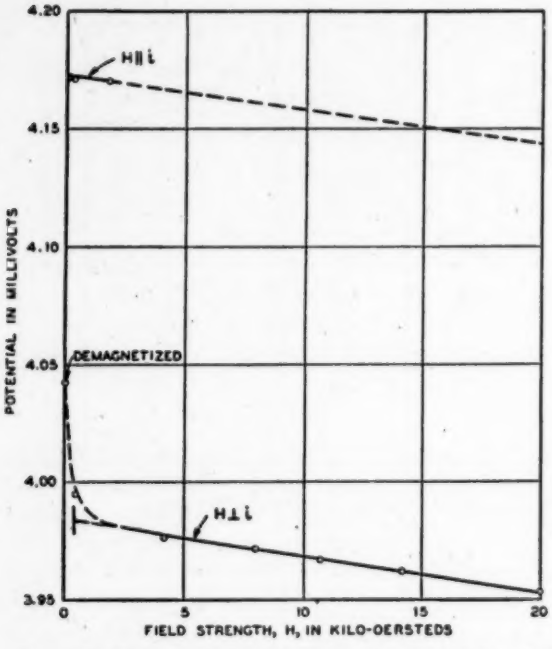

FIG. 12. Data from which changes in resistivity of 83 Permalloy, in longitudinal and transverse fields, are determined. Ordinate shows direct reading on potentiometer, current through specimen being held constant. Change in spontaneous magnetization causes the linear part of the decrease in ρ.

crystal axes. Then the energy is

$$F_\sigma = -\frac{3\sigma}{2}[\lambda_{100}(\alpha_1^2\gamma_1^2+\alpha_2^2\gamma_2^2+\alpha_3^2\gamma_3^2) +2\lambda_{111}(\alpha_1\alpha_2\gamma_1\gamma_2+\alpha_2\alpha_3\gamma_2\gamma_3+\alpha_3\alpha_1\gamma_3\gamma_1)].$$

The problem is first to find the angle, θ, between I_s and σ for any given set of values of λ_{100}, λ_{111}, and the γ's, and the corresponding α's which make F_σ a minimum. Then it is desired to evaluate $\cos^2\theta$ for these conditions and find its average value for all possible values of the γ's. This makes it possible to calculate the ratio, $\Delta\rho_\sigma/\Delta\rho_h$, for a polycrystalline wire having crystals oriented at random, when σ and H are applied separately along the wire axis.

The determinations of the α's which minimize F_σ for a given set of values of λ_{100} and λ_{111} and the γ's, can be accomplished as follows: For convenience set $r=\lambda_{111}/\lambda_{100}$ and $Q=-2F_\sigma/3\sigma$. Then it is well known that the quadratic form in the α's,

$$Q=\lambda_{100}[\alpha_1^2\gamma_1^2+\alpha_2^2\gamma_2^2+\alpha_3^2\gamma_3^2 +2r(\alpha_1\alpha_2\gamma_1\gamma_2+\alpha_1\alpha_3\gamma_1\gamma_3+\alpha_2\alpha_3\gamma_2\gamma_3)],$$

subject to the condition $\sum\alpha_i^2=1$, can be reduced, for any r, to the form

$$Q_1=\lambda_{100}(\sum\lambda_i y_i^2)$$

by means of the real orthogonal transformation

$$\alpha_i=\sum b_{ij}y_j.$$

The numbers λ_i are all real and are roots of the secular determinant

$$|Q-\lambda I|=0$$

or

$$\begin{vmatrix}\gamma_1^2-\lambda & r\gamma_1\gamma_2 & r\gamma_1\gamma_3\\ r\gamma_1\gamma_2 & \gamma_2^2-\lambda & r\gamma_2\gamma_3\\ r\gamma_1\gamma_3 & r\gamma_2\gamma_3 & \gamma_3^2-\lambda\end{vmatrix}=0.$$

The energy and direction of magnetization will be given by the largest eigenvalue if $\lambda_{100}>0$ (and the smallest if $\lambda_{100}<0$) and the corresponding eigenvector.[11]

The solution can be seen from inspection when the stress is parallel to any of the principal crystallographic directions [100], [110], and [111]; for these $\theta=0$ or 90° for all values of λ_{100} and λ_{111}. As an example of the effect expected in other directions, θ is plotted in Fig. 11 for the [511] direction for various ratios, $r=\lambda_{111}/\lambda_{100}$, and for positive and negative values of λ_{100}.

Lichtenberger's data show that $\lambda_{100}>0$, $r=10$, for some composition in the neighborhood of 75 to 80 percent nickel, the exact composition depending on the rate of cooling of the alloy after annealing.[12] Under these conditions the value of $\cos^2\theta$ averaged over the unit sphere (by a graphical method) is about 0.93, and this means that tension should effect a change of resistivity $\Delta\rho_\sigma=(3/2)(0.93-1/3)\Delta\rho_h=0.89\,\Delta\rho_h$. This ratio 0.89 is not far from the ratio 0.85 observed by Yamanaka[6] for 74 percent nickel (see Fig. 9); a definite comparison for an alloy of given composition is not possible in view of the uncertainty in the values of λ_{111} and λ_{100} for a given specimen.

A somewhat better comparison between theory and experiment may be made for the 35 percent nickel alloy. Here $\lambda_{100}<0$, $r\doteqdot-4$, according to Lichtenberger's data. The calculated value of $\langle\cos^2\theta\rangle_h$ is 0.8, from which can be derived the

[11] R. Courant and D. Hilbert, *Methoden der Mathematischen Physik* (Verlagsbuchhandlung Julius Springer, Berlin, 1924), Vol. 1, p. 20.

[12] E. M. Grabbe, Phys. Rev. **57**, 728–34 (1940).

ratio $\Delta\rho_\sigma/\Delta\rho_\lambda=0.7$, whereas the observed[6] ratio is 0.5.

Although the agreement between these values, and between observed and calculated values considered above, is not as good as might be desired, it appears to be adequate to establish the explanation here proposed.

UNANNEALED SPECIMENS

Measurements of magnetoresistance were made on two specimens of unannealed material, severely cold rolled, containing 67 and 89 percent nickel. The purpose was to find out whether or not $\Delta\rho_\lambda$ and $\Delta\rho_\lambda-\Delta\rho_t$ were the same as in the annealed material. The results are given in Table I.

It is apparent that the severe cold rolling of the material has not changed the total magnetoresistance, equal to the difference between the longitudinal and transverse effects. However, the effect of cold rolling on the longitudinal effect, $\Delta\rho_\lambda$, is substantial and shows that in the demagnetized state the domains are not oriented at random. The low value of $\Delta\rho_\lambda$ indicates that there is a preponderance of domains oriented nearly parallel to the axis.

A similar effect of cold working on lowering the *magnetostriction* of nickel[13] and of 68 Permalloy[14] has been observed, and the cold rolling of iron[15] has been found to increase its (positive) magnetostriction. In the almost identical 67 and 68 Permalloys the effect of the working is the same —a reduction of about 50 percent—in both magnetostriction and magnetoresistance. This is to be expected in view of the close relation between these properties.

The non-random distributions of domain orientations in all of these materials are consistent with the data[16] on the directions of easy magnetization in rolled sheets. These directions are parallel to the direction of rolling in nickel and 78 Permalloy, and at 45° from this direction in the plane of the sheet, in iron. In unmagnetized nickel, therefore, the domains tend to be oriented parallel to the direction of easy magnetization, and when a field is applied they first change orientation by 180°, without affecting magnetostriction or resistivity. In higher fields they rotate into more exact alignment with the field and so exhibit a limited magnetostriction and magnetoresistance. A similar consideration of iron shows that an increased positive magnetostriction is to be expected.

TABLE I. Longitudinal magnetoresistance, $\Delta\rho_\lambda$ (demagnetized state to saturation), and total magnetoresistance, $\Delta\rho_\lambda-\Delta\rho_t$ (transverse to longitudinal) of unannealed and annealed material.

Percent nickel	Treatment	$\Delta\rho_\lambda$	$\Delta\rho_\lambda-\Delta\rho_t$
67	Unannealed	0.5%	1.9%
67	Annealed	1.2	1.9
89	Unannealed	2.4	5.3
89	Annealed	3.7	5.3

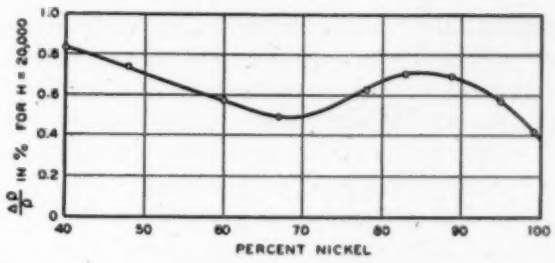

FIG. 13. Change in resistivity due to change in spontaneous magnetization in field of 20,000 oersteds.

Little is known of the distribution of stresses or crystal orientations that could cause the direction of rolling to be a direction of easy magnetization in these alloys. The effect of crystal orientation is very weak in 67 Permalloy, and the sign of the magnetostriction is opposite in 67 Permalloy and in 89 Permalloy (or nickel), so that neither crystal orientations nor internal strains appear to give an appropriate explanation. The same problem has been discussed by Conradt and Sixtus.[17]

HIGH FIELDS

The measurements in transverse fields were carried to $H=20{,}000$ oersteds. It has already been shown by Gerlach[18] that an increase in spontaneous magnetization will cause a decrease in resistivity. Since the fields used in these experiments are large enough to produce at room temperature a definite change in spontaneous

[13] A. Schulze, Ann. d. Physik 11, 937–48 (1931).
[14] H. J. Williams, R. M. Bozorth, and H. Christensen, Phys. Rev. 59, 1005–12 (1941).
[15] W. F. Brown, Jr., Phys. Rev. 50, 1165–72 (1936).
[16] R. M. Bozorth, J. App. Phys. 8, 575–88 (1937).
[17] H. W. Conradt and K. J. Sixtus, Zeits. f. tech. Physik 23, 39–49 (1942).
[18] W. Gerlach, Zeits. f. Physik 59, 847–849 (1930).

magnetization, and, therefore, in resistivity, it was necessary to separate this effect from the change in restivity due to domain orientation. The separation was made by the method used by Englert,[19] by extrapolating the ρ *vs.* H curve, as illustrated in Fig. 12 for 83 percent nickel. The points for transverse magnetization lie on a straight line permitting easy extrapolation to the demagnetizing field corresponding to saturation; for the specimen of tape used this was small, $(N/4\pi)B_s=0.047\times9800=450$. The same slope of ρ *vs.* H curve was used to extrapolate the longitudinal measurements to $H=0$.

The slope of the ρ *vs.* H line for nickel was nearly the same as that reported by Englert. The slopes for the other specimens are recorded in Fig. 13, as percent change in ρ for $H=20{,}000$ oersteds. The results are probably not accurate to less than 0.1 percent, but appear to lie on a smooth curve. The explanation of the shape of the curve is not apparent. On the one hand one might expect the effect to be large when the curie point is low, as it is at each end of the range of alloys studied, because there the change in spontaneous magnetization with field is relatively large. On the other hand, near 70 to 75 percent nickel the crystal anisotropy is zero, and order-disorder phenomena are observed, and there may be some connection, not now established, between these and the effect of spontaneous magnetization on resistivity.

I am indebted to Dr. C. L. Dolph and Miss C. L. Froelich for assistance with the mathematics and computations involved in the solution of the energy equation.

[19] E. Englert, Ann. d. Physik **14**, 589–612 (1932).

PHYSICAL REVIEW VOLUME 70, NUMBERS 11 AND 12 DECEMBER 1 AND 15, 1946

The Velocity of Sound in Hydrogen when Rotational Degrees of Freedom Fail to Be Excited

J. ELMER RHODES, JR.*
Rowland Physical Laboratory, The Johns Hopkins University, Baltimore, Maryland
(Received August 21, 1946)

The velocity of sound in parahydrogen, normal hydrogen, and 50 percent para-50 percent orthohydrogen mixtures has been observed at several temperatures, and over a range of frequency to pressure ratio from one to 60 megacycles per atmosphere. Dispersion attributed to failure of the rotational degrees of freedom to follow the temperature associated with the translational degrees of freedom has been observed with all mixtures and at every temperature at which observations were made. Measurements at two different frequencies for similar samples at the same temperature indicate that frequency and pressure affect the velocity of sound only as the quotient, frequency/pressure, with the exception of small corrections that must be applied because hydrogen is not a perfect gas. Experiments indicate that the dispersion occupies a greater range of frequency to pressure than would be expected if the rotational specific heat behaved as a simple relaxation phenomenon. It is shown that a simple relaxation phenomenon is not to be expected, and that the dispersion in parahydrogen can be characterized, approximately, by two relaxation frequency to pressure ratios, one for the rotational transition 0–2, and another for the transition 2–4. An expression for these relaxation frequency to pressure ratios, that roughly fits the observations, is derived on the basis of some assumptions about the collision process.

CHANGES of sound velocity in some gases with variation of the frequency to pressure ratio have been known for a number of years. These have been attributed to failure of the internal degrees of freedom of the molecules to follow temperature changes in the sound wave. The first phenomenon of this type to be observed was associated with vibrational degrees of freedom. In this respect carbon dioxide has been extensively investigated.[1]

Recently in this laboratory E. S. Stewart[2] observed a similar phenomenon associated with

* Now at Georgia School of Technology, Atlanta, Georgia.

[1] W. T. Richards, Rev. Mod. Phys. **11**, 59 (1939).
[2] E. S. Stewart, Phys. Rev. **69**, 632 (1946). See also, E. S. Stewart, J. L. Stewart, and J. C. Hubbard, Phys. Rev. **68**, 231 (1945).

the rotational degrees of freedom of hydrogen. This had been sought for by others,[3] but their work was not done at a sufficiently high ratio of frequency to pressure.

MEASUREMENTS AND APPARATUS

Measurements of sound velocity in parahydrogen and in mixtures of ortho- and parahydrogen were made at different frequency to pressure ratios. The results of the measurements are recorded in the curves of Fig. 1.

The velocity measurement was made by measuring the wave-length with a sonic interferometer and at the same time measuring the frequency. The interferometer was the one described by J. L. Stewart[4]; however, the electrical circuits were different. No separate oscillator was used to drive the quartz crystal of the interferometer; rather, the crystal was employed as one of the tuned circuits in the oscillator. Resonance of the gas column was indicated by a sensitive vacuum tube voltmeter that indicated change of the radiofrequency voltage across the quartz crystal.

The interferometer was inverted in a large Dewar flask which contained a liquid bath to maintain constant temperature. Water and ice were used for measurements near zero degrees Centigrade; dry ice and alcohol, near 200 degrees absolute; and water, near room temperature. The temperature of the bath was measured with a calibrated thermocouple.

The hydrogen was purified by slowly passing it through a trap surrounded by liquid hydrogen. Parahydrogen (99.8 percent) and 50 percent para-50 percent orthohydrogen were prepared at the temperatures of liquid hydrogen and of liquid air, respectively, by adsorbing hydrogen onto activated charcoal.[5]

RELATION BETWEEN THE VELOCITY OF SOUND AND THE RATE OF ROTATIONAL TRANSITIONS

If the effects depending upon the first and third derivatives of the displacement of an element of mass (heat conduction and viscosity) are neglected, Newton's laws of motion and the principle of conservation of mass yield for the velocity of plane waves of sound in a homogeneous isotropic medium:

$$V=\left[\left(\frac{\partial p}{\partial \rho}\right)_T+\frac{MT}{C\rho^2}\left(\frac{\partial p}{\partial T}\right)_\rho^2\right]^{\frac{1}{2}}, \qquad (1)$$

where M is the molecular weight of the material; ρ, the density; T, the absolute temperature; C, the specific heat per mole at constant volume;

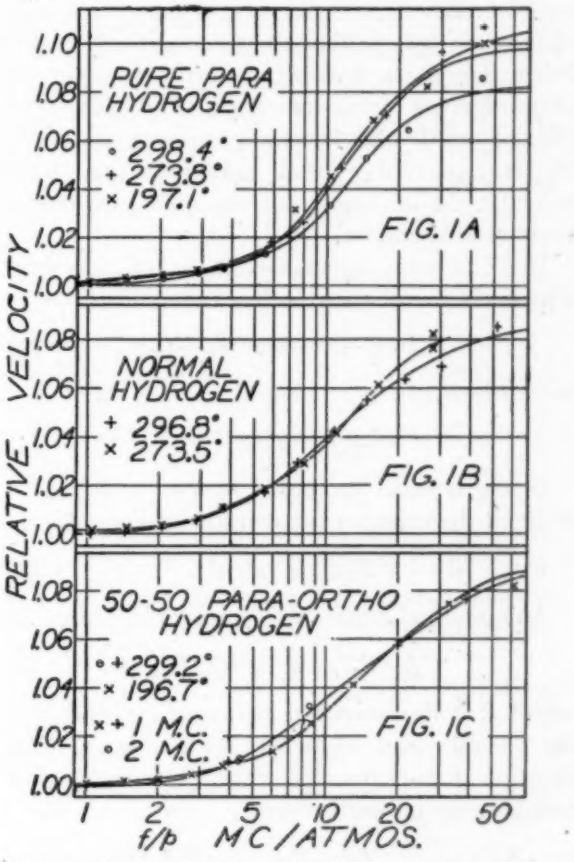

FIG. 1. The velocity of sound in hydrogen as a function of f/p, the frequency to pressure ratio; f/p is on a logarithmic scale. Velocity is shown in units equal to the calculated low frequency velocity for the temperature indicated. Figure 1A is for pure parahydrogen; 1B for normal (25 percent para-, 75 percent ortho-) hydrogen, and 1C is for a 50 percent para-, 50 percent orthohydrogen mixture. All experimental points were observed at a frequency of one megacycle except those in 1C indicated by o's, which were observed at a frequency of two megacycles. That both one and two megacycle observations lie on the same curve indicates that frequency and pressure affect the velocity only through the quotient, f/p, except for small correction terms that depend upon the second virial coefficient. The experimental errors are greater the greater the value of f/p.

[3] A. S. Roy and M. E. Rose, Proc. Roy. Soc. London **A149**, 511 (1935).
[4] J. L. Stewart, Rev. Sci. Inst. **17**, 59 (1946).
[5] A. Farkas and H. W. Melville, *Experimental Methods in Gas Reactions* (The Macmillan and Company, Limited, London, 1939), p. 154.

p, the pressure; and V, the complex velocity of sound.

In (1) M is constant; T and ρ are average temperature and density and are considered constant. Both partial derivatives are associated with the translational degrees of freedom. Consequently, they should be real in a sound wave whose period is long compared to the relaxation time for translational motion. All sound waves to be considered here have periods far longer than the relaxation time for translational motion. Only C is associated with internal degrees of freedom. When excitation of any internal degree of freedom lags behind the temperature change in the sound wave associated with the translational degrees of freedom, then C becomes complex. Then V also becomes complex, and it is the real part of V that represents the phase velocity, the quantity that one measures with a sonic interferometer.

If V^2 is expressed as $\alpha+i\beta$ and V as $v+iu$, where v is the phase velocity, then,

$$V^2=v^2-u^2+2iuv=\alpha+i\beta; \tag{2}$$

from which,

$$v^2=\tfrac{1}{2}\alpha[1+(\beta^2/\alpha^2+1)^{\frac{1}{2}}]. \tag{3}$$

If β/α is small compared to one, as it proves to be in the experiments considered here, then,

$$v^2\cong\alpha[1+\tfrac{1}{4}\beta^2/\alpha^2]. \tag{4}$$

An empirical equation of state for hydrogen is[6]

$$p=RT\rho/M+\rho^2B/M^2, \tag{5}$$

where R is the universal gas constant, and B is the second virial coefficient for hydrogen. This function for p inserted into (1) gives, after dropping second-order terms,

$$V^2=\frac{RT}{M}\left\{1+2pB\frac{T_0^2}{T^2}+\frac{R}{C}\left(1+2p\frac{T_0^2}{T}\frac{dB}{dT}\right)\right\}. \tag{6}$$

T_0 is 273.1 degrees absolute.

The theory of the effective specific heat for a two level gas has been carried through in great detail by Rutgers[7] for the case when the levels are associated with molecular vibrations. His approach applied to molecular rotations follows:

[6] E. H. Kennard, *Kinetic Theory of Gases* (McGraw-Hill Book Company, Inc., New York, 1939), pp. 221–223.
[7] A. J. Rutgers, Ann. d. Physik 16, 350 (1933).

Consider a gas transmitting a sound wave of angular frequency ω. Suppose some internal degree of freedom has only two levels, a and b, with energy difference ΔE between them. Let n be the number of molecules per mole, n_a the number in state a, and n_b the number in state b. Then $n_a+n_b=n$, and $dn_a=-dn_b$. The reaction equation is,

$$dn_b/dt=k_{ab}n_a-k_{ba}n_b, \tag{7}$$

where k_{ab} and k_{ba} are probabilities per second per molecule of the transitions $a-b$ and $b-a$, respectively. At equilibrium $dn_b/dt=0$, so,

$$k_{ba}=k_{ab}n_a/n_b. \tag{8}$$

For a rotator

$$\frac{n_a}{n_b}=\frac{2J_a+1}{2J_b+1}e^{\Delta E/kT}, \tag{9}$$

where

$$\Delta E/kT=\sigma[J_b(J_b+1)-J_a(J_a+1)]; \qquad \sigma=h^2/8\pi^2IkT; \tag{10}$$

J is the rotational quantum number; k is Boltzmann's constant; I is the moment of inertia of the molecule. Suppose T varies periodically so that $T=T_0+\Delta Te^{i\omega t}$, and suppose $n_b=n_b^0+\Delta n_be^{i\omega t}$. Then $n_a=n_a^0-\Delta n_be^{i\omega t}$. After dropping second-order terms, so long as $\Delta n_a\ll n_a$, $\Delta n_b\ll n_b$, $\Delta T\ll T$, these suppositions lead to,

$$i\omega\Delta n_b=-k_{ab}\Delta n_b-k_{ba}\Delta n_b+(n_a^0\Delta k_{ab}-n_2^0\Delta k_{ba}). \tag{11}$$

$$(n_a^0\Delta k_{ab}-n_2^0\Delta k_{ba})=\Delta k_{ab}n_a^0-n_b^0\left(\Delta k_{ab}\frac{n_a^0}{n_b^0}-k_{ab}\frac{2J_a+1}{2J_b+1}e^{\Delta E/kT}\Delta T\right),$$

$$\frac{\Delta E\Delta n_b}{\Delta T}=k_{ab}\frac{n_a^0}{n_b^0}\frac{(\Delta E)^2}{kT^2}\Big/(i\omega+k_{ab}+k_{ba}). \tag{12}$$

The term on the left is the effective rotational specific heat, and the expression on the right reduces to the statistical mechanical equation for the specific heat of a rotator with two levels if ω is set equal to zero. The general statistical mechanical equation for the specific heat of a rotator is Eq. (21) below. Thus the effective specific heat associated with levels a and b is

$$C_R'=\frac{C_R}{1+i\omega/\omega_0}, \tag{13}$$

where

$$\omega_0 = k_{ab} + k_{ba} = k_{ab}\left(1 + \frac{2J_a+1}{2J_b+1} e^{\Delta E/kT}\right), \quad (14)$$

and where C_R is the rotational specific heat when $\omega=0$. For a non-radiating rotator, rotational transitions are effected only by molecular collisions. The rate of collisions is proportional to the pressure, p. Thus, k_{ab} contains p as a factor, and (13) and (14) may be written,

$$C_R' = C_R \Big/ \left(1 + i\frac{f/p}{(f/p)_0}\right); \quad (15)$$

$$(f/p)_0 = \frac{k_{ab}}{2\pi p}\left(1 + \frac{2J_a+1}{2J_b+1} e^{\Delta E/kT}\right). \quad (16)$$

If the specific heat obeys (15), it is said to exhibit simple relaxation phenomena.

That frequency and pressure enter the dispersion only as f/p is shown by Fig. 1c. The ratio $(f/p)_0$ will be referred to as the relaxation frequency to pressure ratio.

To analyze such phenomena in a three level gas, one must solve three differential equations simultaneously. If n_a, n_b, n_c are the numbers of molecules per mole in levels a, b, and c, then $n=n_a+n_b+n_c$, and the three equations are

$$\begin{aligned} dn_a/dt &= -k_{ab}n_a + k_{ba}n_b; \\ dn_b/dt &= -\frac{dn_a}{dt} - \frac{dn_c}{dt}; \\ dn_c/dt &= k_{bc}n_b - k_{cb}n_c. \end{aligned} \quad (17)$$

This development neglects the possibility of transitions $a-c$ and $c-a$. As before, $k_{ba}=k_{ab}(n_a/n_b)$; $k_{cb}=k_{bc}(n_b/n_c)$. The assumption of harmonic variation of n_a, n_b, n_c, and T gives, after dropping second-order terms,

$$\begin{aligned} i\omega\Delta n_a &= -k_{ab}\Delta n_a + k_{ab}(n_a^0/n_b^0)\Delta n_b + P_1\Delta T; \\ \Delta n_b &= -\Delta n_a - \Delta n_c; \\ i\omega\Delta n_c &= k_{bc}\Delta n_b - k_{bc}(n_b^0/n_c^0)\Delta n_c + P_2\Delta T; \end{aligned} \quad (18)$$

where the P's contain n's and k's as in Eq. (11). Elimination of Δn_b in (18) leaves,

$$\begin{aligned} i\omega\Delta n_a &= -k_{ab}[\Delta n_a + (n_a^0/n_b^0)(\Delta n_a + \Delta n_c)] + P_1\Delta T; \\ i\omega\Delta n_c &= -k_{bc}[(\Delta n_a + \Delta n_c) + (n_b^0/n_c^0)\Delta n_c] + P_2\Delta T. \end{aligned} \quad (19)$$

If there were some simple relation between k_{ab} and k_{bc}, then (19) might be reduced to the form of (15), with the specific heat exhibiting a simple relaxation frequency to pressure ratio. With the help of some plausible assumptions, such a relation has been found for a vibrating molecule with many levels.[8] A simplifying factor in the case of a vibrator is the fact that energy levels are equally spaced. This is not the case with a rotator. If there are appreciable numbers of molecules in more than two levels, there is no simple relaxation frequency to pressure ratio for rotational specific heat.

Parahydrogen at room temperature is essentially a three level gas with most of its molecules in rotational levels with $J=0$, 2, and 4. One may associate 0, 2, and 4 with a, b, and c in (19). The $0-2$ transition fails to follow the sound wave at a lower f/p than the $2-4$ transition. Most of the rotational specific heat is associated with the $0-2$ transitions; thus Δn_a is much greater than Δn_c at low f/p. As f/p increases, (19) describes Δn_a and Δn_c. To a good approximation, at low f/p, Δn_c may be neglected in the first equation of (19). Then (19) becomes identical with (11). As f/p continues to increase Δn_a becomes smaller, and the approximation ceases to be valid. At sufficiently high f/p, Δn_a becomes small enough to be neglected when compared to Δn_c. Then the second equation of (19) becomes equivalent to (11). Thus at sufficiently high and at sufficiently low f/p hydrogen may be treated as a two level gas.

The total effective specific heat for a two level gas is,

$$C_E = C_\infty + (C_0 - C_\infty) \Big/ \left(1 + i\frac{f/p}{(f/p)_0}\right), \quad (20)$$

where the second term is obtained from (15). C_0 is the specific heat when transitions between the two levels concerned follow the sound wave and C_∞ is the specific heat when no transitions between these levels occur. The rotational specific heat can be calculated by the methods of statistical mechanics for any number of levels. Its value is[9]

[8] L. Landau and E. Teller, Physik. Zeits. Sowjetunion 10, 34 (1936).

[9] J. E. Mayer and M. G. Mayer, *Statistical Mechanics* (John Wiley and Sons, New York, 1940), Chap. 6.

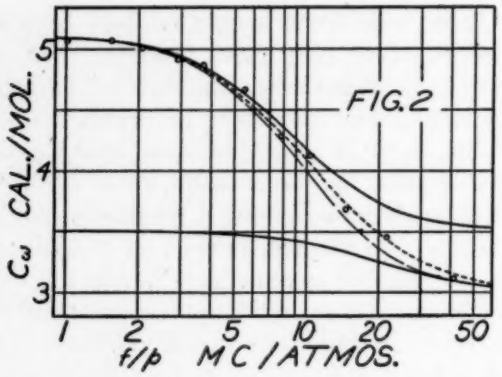

FIG. 2. The solid curves show C_ω calculated from Eq. (24). The upper curve has $(f/p)_0=7.2$ megacycles per atmosphere; the lower one, 20 megacycles per atmosphere. The asymtotic values for these curves, C_0 and C_∞, were calculated by Eq. (21). The dotted curve is the resultant of the two solid curves, and the o's are experimental points calculated by Eq. (23) from velocity measurements. The dashed curve shows what would be expected if the whole rotational specific heat showed a simple relaxation frequency to pressure ratio. The value of $(f/p)_0$ for the dashed curve was chosen to be 7.3 megacycles per atmosphere. The experimental points occupy a greater range of f/p than this curve, indicating that the rotational specific heat does not exhibit simple relaxation phenomena.

$$C_R=\frac{R}{Q}\left\{\sum_J (2J+1)[\sigma J(J+1)]^2 e^{-\sigma J(J+1)} - \frac{1}{Q}[\sum_J (2J+1)\sigma J(J+1)e^{-\sigma J(J+1)}]^2\right\}, \quad (21)$$

where Q is the partition function for a rotator,

$$Q=\sum_J (2J+1)e^{-\sigma J(J+1)}. \quad (22)$$

If some rotational transitions are considered as not occurring, the levels from which no molecules enter or leave are omitted from the sums in (21) and (22). The total specific heat is the effective rotational specific heat plus the translational specific heat which is $3R/2$.

Equations (20) and (6) substituted into (4) give

$$v^2=\frac{RT}{M}\left\{1+2pB\frac{T_0^2}{T^2}+\frac{R}{C_\omega}\left[1+2p\frac{T_0^2}{T}\frac{dB}{dT}\right]\right\} \times\left\{1+\frac{1}{4}\frac{\beta^2}{\alpha^2}\right\}, \quad (23)$$

where

$$C_\omega=\left(C_0^2+C_\infty^2\frac{(f/p)^2}{(f/p)_0^2}\right)\Big/\left(C_0+C_\infty\frac{(f/p)^2}{(f/p)_0^2}\right) \quad (24)$$

and

$$\frac{\beta}{\alpha}=\frac{R(C_0-C_\infty)\dfrac{f/p}{(f/p)_0}}{R\left[C_0+C_\infty\dfrac{(f/p)^2}{(f/p)_0^2}\right]+C_0^2+C_\infty^2\dfrac{(f/p)^2}{(f/p)_0^2}}. \quad (25)$$

Relaxation frequency to pressure ratios were obtained for the 0−2 and 2−4 transitions of parahydrogen at 298.4 degrees absolute. For the 0−2 transition, which has the lower $(f/p)_0$, observed values of v were put into (23). The last factor of (23) was first treated as one, and first approximations for C_ω were obtained. The value of $(f/p)_0$ that made (24) best fit these values was then obtained by trial. This approximation to $(f/p)_0$ was used in (25) to obtain β/α, which was subsequently used in (23) to obtain final values for C_ω. (These values for β/α were all less than 0.08, and the corrections on C_ω were less than 0.02 percent.) A final value of $(f/p)_0$ was obtained to make (24) best fit the final experimental values of C_ω for low values of f/p. The value of σT used in all of these calculations was 82.6 degrees.[10]

For the 2−4 transition the same procedure was carried out: (24) was made to fit the experimental C_ω's at high values of f/p rather than at low ones.

Figure 2 shows how (24) for the final $(f/p)_0$'s chosen fits the experimental points.

At lower temperatures parahydrogen is so nearly a two level gas that no reliable figures could be obtained for the 2−4 transition. The $(f/p)_0$'s for the 0−2 transition were obtained. Results are tabulated in Table I.

CALCULATION OF k_{ab}

After an inelastic collision in which masses M and m collide with relative velocity v_r, some of

TABLE I. Relaxation frequency to pressure ratios for parahydrogen.

Transition between rotational levels:	Temperature (deg. abs.)	Relaxation frequency to pressure ratio, $(f/p)_0$ (m.c./atmos.) Observed	Calculated
0–2	197.7	6.6±0.3	6.13
0–2	273.8	6.9±0.3	6.98
0–2	298.4	7.2±0.3	
2–4	298.4	20. ±5.	22.0

[10] P. S. Epstein, *Textbook of Thermodynamics* (John Wiley and Sons, New York, 1937), p. 305.

the energy of their relative motion appears as a subsequent relative velocity, and the rest goes into the internal energy of the colliding bodies. Momentum and energy are conserved. In order to conserve energy and the component of momentum in the direction of v_r, the maximum energy of relative translational motion that can go into internal energy is

$$E_{\max}=\frac{1}{2}\frac{mM}{m+M}v_r^2. \tag{26}$$

If the colliding bodies are two hydrogen molecules, then $M=m$, and $E_{\max}=\frac{1}{2}(\frac{1}{2}mv_r^2)=\frac{1}{2}E_r$, or half the kinetic energy of their relative motion.

In considering the probability that a molecule in rotational level a will be left in level b after collision with another molecule, one need consider only those collisions for which

$$E_{\max}+\Delta E_2 \gtrless \Delta E_{ab}, \tag{27}$$

where ΔE_{ab} is the energy required for the transition $a-b$, and ΔE_2 is the amount of internal (rotational) energy the colliding molecule might possibly lose. In the calculations that follow ΔE_2 is taken as the energy given up by the colliding molecule in undergoing a transition from its initial rotational level to its next lower allowed level. When the colliding molecule is initially in its lowest level, ΔE_2 is zero.

The number of collisions per second per molecule in a gas with magnitude of initial relative velocity between v_r and (v_r+dv_r) is[11]

$$dz=\tfrac{1}{2}\pi^{\frac{1}{2}}D^2N(m/kT)^{\frac{1}{2}}v_r^3 \times\exp\left[-mv_r^2/4kT\right]dv_r, \tag{28}$$

where N is the molecular density, D the collision diameter of the molecule.

If (28) is integrated over all relative velocities, one obtains the rate of occurrence of collisions. Consider one molecule in rotational level a that collides with a second molecule with an initial relative velocity, v_r. Let W be the probability that the first molecule will undergo a transition during the collision to its next higher allowed level b. W multiplied by (28), and then integrated gives k_{ab}, the rate per molecule in state a of the transition $a-b$. Thus:

$$k_{ab}=\int_{v_r=0}^{\infty} W dz. \tag{29}$$

Calculation of W requires the evaluation of the expression for such a probability:

$$W=\left[\frac{2\pi}{h}\int\int \Psi_b^* V_e \Psi_a dx dt\right]^2. \tag{30}$$

Ψ_a and Ψ_b are the rotational wave functions of the molecule: Ψ_a in rotational level a, and Ψ_b in level b. All coordinates of the rotator are included in x; t is time. V_e is the potential energy of the rotator resulting from the presence of the colliding molecule. In classical mechanics one can express any impulse on a rigid body by an equivalent impulse applied to the center of mass of the body plus an equivalent impulsive torque. V_e corresponds to the potential energy associated with this impulsive torque during the collision. Necessary information about the molecular forces during the collision for obtaining V_e as a function of the coordinates of the rotator and time are lacking so (30) cannot be evaluated.

Some properties of W are available. Unless condition (27) is satisfied, W is certainly zero. One would expect that as the left side of (27) becomes larger compared to the right side, W would increase. An attempt was made to express W as a function of $(E_{\max}+\Delta E_2-\Delta E_{ab})$, for positive values of this quantity. Several simple functions were tried, and it was found that

$$W\propto E_{\max}+\Delta E_2-\Delta E_{ab} \tag{31}$$

best fitted observations. It is possible that W can be accurately represented by a rapidly converging power series in $(E_{\max}+\Delta E_2-\Delta E_{ab})$.

To calculate k_{ab} on the basis of this assumption, one puts (31) and (28) into (29). Since W is zero for negative values of $(E_{\max}+\Delta E_2-\Delta E_{ab})=(\frac{1}{2}mv_r^2+\Delta E_2-\Delta E_{ab})$, the integration is carried out only from $v_r^2=(4/m)(\Delta E_{ab}-\Delta E_2)$ to ∞, when this lower limit is greater than zero. If $\Delta E_2>\Delta E_{ab}$, then the integration is carried out from zero to ∞. The result is

$$\begin{aligned} k_{ab}'&=\lambda p' T^{\frac{1}{2}}(X+2)e^{-X}, \quad X\geqq 0;\\ k_{ab}'&=\lambda p' T^{\frac{1}{2}}(-X+2), \quad X\leqq 0, \end{aligned} \tag{32}$$

where $X=(\Delta E_{ab}-\Delta E_2)/kT$. In obtaining (32), the molecular density, N, has been given its

[11] R. B. Lindsay, *Physical Statistics* (John Wiley and Sons, New York, 1941), pp. 87–88.

value for a perfect gas, $N=p'/kT$, where p' is the partial pressure of the molecules in the level that corresponds to ΔE_2. All multiplying constants, including the proportionality constant for W, are included in λ. In calculating k_{ab} by (32), one must calculate a term for the fraction of the molecules in each rotational level, as ΔE_2 is different for each level. Thus the final k_{ab} is a sum of terms like (32).

From k_{ab}, the relaxation frequency to pressure ratio, $(f/p)_0$, is determined by (16). The observed $(f/p)_0$ for the $0-2$ transition in parahydrogen at 298.4 degrees absolute was used in (16) and (32) to find λ. Values for the other $(f/p)_0$'s calculated from this λ are in the last column of Table I.

Properly chosen assumptions about the quantities in (30) can lead to (31). One such set includes the assumption that the collision occupies only a small region of the coordinates, so that the product of the Ψ's can be replaced by an average value; (30) then takes the form:

$$W=\left[\frac{2\pi}{h}\langle\Psi_b^*\Psi_a\delta x\rangle_{Av}\int V_e dt\right]^2,$$

or $W\propto[\int V_e dt]^2$. If V_e is assumed to have a maximum value proportional to $(E_{max}+\Delta E_2-\Delta E_{ab})$; if a coordinate ξ is zero just as the molecules "contact" and increases as they move closer together; and if the molecular force associated with V_e is a rapidly increasing function of the positive values of ξ, $e^{a\xi}$ or ξ^n, with n large, for example, then (31) results.

CONCLUSION

Dispersion of the velocity of sound in hydrogen has been observed at several temperatures; the frequency to pressure ratio at which the dispersion occurs shows no strong temperature dependence.

The excitation of rotational degrees of freedom in hydrogen is shown to have no simple relaxation frequency to pressure ratio; however, each rotational transition can be assigned a ratio that approximates a true relaxation frequency to pressure ratio. The range of frequency to pressure ratio over which the velocity of sound changes is greater for hydrogen than that called for by the law for a simple relaxation.

PHYSICAL REVIEW VOLUME 70, NUMBERS 11 AND 12 DECEMBER 1 AND 15, 1946

Frequency Dependence of the Properties of Sea Echo*

HERBERT GOLDSTEIN
Department of Physics, Harvard University, Cambridge, Massachusetts
(Received September 3, 1946)

The properties of sea echo—a radar echo associated with surface of the sea—have been measured at wave-lengths of 9.2, 3.2, and 1.25 cm, for grazing angles of incidence about 1° and over a wide range of sea states. The measurements, which are given in terms of a suitably defined cross section per unit area of the sea, were obtained with three experimental truck-borne systems. Details of these systems, and of the measuring techniques, are described. The troublesome rapid fluctuations of the sea echo signals were eliminated by an electrical averaging scheme. A discussion of the possible errors in the determination of the absolute cross sections leads to an estimated uncertainty of ±2 db on 9.2 and 3.2 cm and ±4 db on 1.25 cm. The results have been interpreted in the light of possible theories of the scattering mechanism responsible for the echo. Assuming the scatterers to be spray drops small compared to λ, the wave-length dependence of the cross section should be between λ^{-4} and λ^{-6} whereas the observed variation is between λ^0 and λ^{-4}. While these results are in better accord with the hypothesis of scattering from irregularities on the surface, the observed large changes of the cross section with polarization seem explainable only by some form of the drop theory. A modification of the drop theory is proposed, which assumes the presence of drops of diameter of the order of λ. The consequences of such a theory are examined and found to be in rough agreement with experiment.

INTRODUCTION

AT certain times, depending upon the state of the sea, microwave radar systems will receive echoes associated with the sea surface and commonly known as "sea echo." Large areas on the indicators are often covered by the echo, seriously interfering with the usefulness of airborne radar systems. The fundamental scattering

* This paper is based on work done while at the Radiation Laboratory, M.I.T.

mechanism responsible for the echo has not yet been established, although a number of theories have been proposed. One that has found considerable support ascribes sea echo to back scattering from small spray drops suspended above the sea surface. According to a second hypothesis diffraction, and possibly specular reflection, by the waves and ripples on the sea surface is the principal source of the echo.

It has been pointed out that these two theories yield radically different predictions as to the frequency dependence of the received power. The scattered intensity from drops of circumference small compared to the wave-length follows the familiar Rayleigh scattering formula, varying as λ^{-4}. An additional possible source of frequency dependence is furnished by the interference lobes in the field above the sea due to reflection from the surface.[1] If the sea is sufficiently smooth and the drops are close to the surface, the variation caused by this is also λ^{-4} but diminishes as the surface becomes rougher and the spray drops over several lobes. The total received intensity should therefore vary between λ^{-4} and λ^{-6}, according to the spray theory. On the other hand, scattering from surfaces large compared to the wave-length might even decrease with frequency (as in specular reflection where the returned beam covers the area of the antenna) or at worst vary as λ^{-2}. An experimental determination of the frequency dependence should thus provide a means for distinguishing between the two theories. A number of experiments have been performed at the Radiation Laboratory, M.I.T. for this purpose.

The measurements indicate a variation with wave-length between λ^{0} and λ^{-4} depending on the state of the sea. These values are almost all far below the predictions of the spray theory. On the other hand, it was found that the sea echo depends markedly on the direction of polarization, in contradiction to any surface scattering theory. A modification of the spray theory, involving suspended bodies of water too large to follow the Rayleigh scattering law, is therefore proposed. These results are presented in detail in Section III and discussed in Section IV. The first two sections deal with the method of specifying the intensity of sea echo in a fashion independent of the particular radar set used (Section I), and with the measurement techniques and sources of error (Section II).

[1] D. E. Kerr and P. J. Rubenstein, "An Introduction to Microwave Propagation," Radiation Laboratory Report 406, Sept. 16, 1943.

I. THE PHENOMONOLOGY OF SEA ECHO

It has been shown[2] that the probability distribution for the instantaneous sea echo power follows the simple exponential law characteristic of the "random walk" problem.[3] Therefore, at least several, and probably many, targets contribute to the echo received at one given range, and the relative phases of these component echoes are random. The average power received at one given range (averaged over many sweeps) is then just the sum of the power scattered by each individual target, namely:

$$\bar{P}_r=\frac{P_t G^2\lambda^2}{(4\pi)^3 R^4}\sum_j \sigma_j, \tag{1}$$

where P_t is the peak transmitted power, G the antenna gain, R the range, σ_j the radar cross section of the jth scatterer. This cross section is here defined so as to include the effect of any possible lobe structure of the incident field caused by reflection from the sea surface. Since the scatterers are undoubtedly point targets in comparison with the lobe dimensions, this procedure is allowable, though it may result in σ being a function of the target height above the surface. The summation in Eq. (1) is to be extended over all scatterers lying in a region such that echoes can be received at a time t equal to $2R/c$. The area of this region is roughly $R\phi\tau c/2$, for low grazing angles, where ϕ is the azimuth beam width and τ is the duration of the pulse. If the scatterers are distributed uniformly over the surface of the sea, then the summation is proportional to this area, with a constant of proportionality denoted by σ°. The equation for the received power can then be written

$$\bar{P}_r=\frac{P_t G^2\lambda^2}{(4\pi R)^3}\frac{\tau c}{2}\phi\sigma^{\circ}. \tag{2}$$

[2] H. Goldstein, "Preliminary Report on the Fluctuations of Radar Echoes," Radiation Laboratory Report 569, April 1944.

[3] Cf. S. Chandrasekhar, Rev. Mod. Phys. 15, 1 (1943).

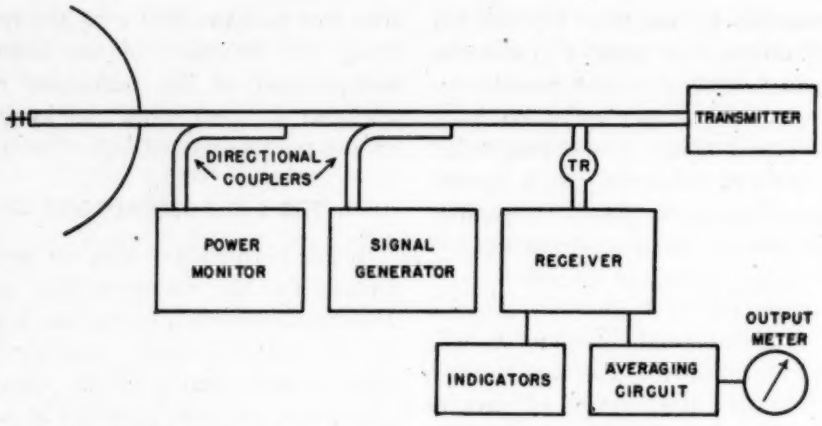

FIG. 1. Block diagram of radar system and associated measuring equipment.

Since one usually measures the average, and not peak transmitted power, it is convenient to replace the product $P_t\tau$ by p_t/ω, where p_t is the average transmitted power and ω is the pulse recurrence rate. With this substitution, Eq. (2) has the form

$$\bar{P}_r=\frac{p_tG^2\lambda^2}{(4\pi R)^3}\phi\frac{c}{2\omega}\sigma^\circ. \tag{3}$$

The quantity σ° may be termed the "sea echo cross section per unit area of the sea surface." It is dimensionless and will often be given in decibel notation. The general form of Eqs. (2) and (3) is substantially independent of the nature of the scatterers, the only important assumptions being incoherent scattering, and uniform spatial distribution of the scatterers. However, the values of σ° will depend upon external parameters such as wave-length, polarization, grazing angle, roughness of the sea, etc. Equations (2) and (3) say nothing about the form of the dependency; detailed hypotheses about the scatterers would be necessary for this purpose. The predictions of two such theories as to the frequency dependence of σ° has already been given in the introduction.

II. APPARATUS AND TECHNIQUES

A. The Radar Systems

Most of the measurements described here were performed with two truck-borne experimental radar systems, operating on wave-lengths of 9.2 and 3.2 cm, that had been developed in the Propagation Group, M.I.T. Radiation Laboratory specifically for accurate absolute measurements of echo intensity. In addition a few results were obtained on a similar system, operating at $\lambda=1.25$ cm. The characteristics of all three are summarized in Table I, but some details deserve separate comment. Both horizontal and vertical polarizations were available. The r-f system in the 9.2-cm set was of coaxial line so that rotation of the direction of polarization was simply achieved by rotating the dipole feed. On the 3.2-cm system which used wave guide, a section of flexible wave guide was inserted in the antenna feed which could be twisted 90° without appreciable effect on the standing wave ratio in the guide. An entirely different method was necessary for the 1.25-cm system. Here a metal-strip[4] half-wave plate could be placed in front of the entire antenna, rotating the polarization of the transmitted wave from horizontal to vertical and rotating that of the received field back to horizontal.

If the sea echo scatterers are not uniformly distributed over the surface the whole concept of a cross section per unit area breaks down. Therefore, as a precaution against the possible

TABLE I. Specifications of the radar systems.

Wave-length	Antenna size	Beam widths E plane degrees	Beam widths H plane degrees	Pulse lengths available, microseconds	Recurrence frequency	Approximate peak power
9.2 cm	48″ paraboloid	6.8°	5.9°	2, 1, 0.5	1000 c.p.s.	35 kw
3.2	48″ paraboloid	1.9°	1.9°	1.0, 0.33, 0.15	1000	20
	18″ paraboloid	4.8°	4.8°			
1.25	48″×6″ parabolic cylinder	0.8°	6.1°	0.75, 0.35, 0.15	800	10

[4] W. E. Kock, Bell Lab. Record 24, 193 (1946).

failure of this assumption, an attempt was made to keep the illuminated area roughly the same on all systems. Thus, most of the measurements on $\lambda = 3.2$ cm were made with an 18″ paraboloidal antenna so that the beam width was comparable to that for the 9.2-cm system. The pulse lengths used were also approximately equal, being 1.0 μsec. on both 9.2 and 3.2 cm and 0.75 μsec. on 1.25 cm.

The methods of measuring the transmitted and received power are schematically illustrated in Fig. 1. A known small fraction of transmitted pulse is obtained from the main line by a directional coupler and the average power measured by a temperature compensated thermistor bridge.[5] For the measurement of received power an r-f pulsed signal generator was used, coupled into the main line through a calibrated attenuator and directional coupler. Knowing the signal generator output and the line losses the equivalent power of this "artificial echo," referred back to the antenna input, can be calculated. By matching the heights of the generator pulse and echo pulse on the A-scope, the received power can be obtained, providing the echo does not fluctuate rapidly. In the case of sea echo, where the fluctuations are extremely rapid, special means must be devised for averaging the received echo intensity and comparing it with the signal generator pulse.

B. Method of Measuring Average Intensity

The electrical circuit used to obtain the average signal is shown schematically in Fig. 2. A "gating" pulse, initiated at some chosen time after the transmitted pulse, is used to select a small section of the video voltage corresponding to the given range. This "gate" causes a pentode tube to be cut off except during a small inverval, t_1, which is small compared to the pulse length. During this interval the video voltage charges up the condenser C through the pentode. (The second pentode is used in a balancing circuit to eliminate the effect of the charging of the condenser by the gate pulse.) Between these intervals the condenser discharges through the resistor R. In an analysis of the behavior of this circuit L. J. Neelands has shown that, when equilibrium is reached, the voltage across the condenser is proportional to the time average of the video voltage during the selected intervals. The time constant determining the rate at which equilibrium is approached is approximately RC; more accurately

$$\frac{RC}{1+Rg_m t_1/t_2},$$

where g_m is the mutual conductance of the tube, t_1 the duration of the gate pulse, and t_2 the interval between successive gate pulses (equal to $1/\omega$). By a single stage inverse feedback d.c. amplifier, the equilibrium voltage can be amplified sufficiently to be read on an output milliammeter.

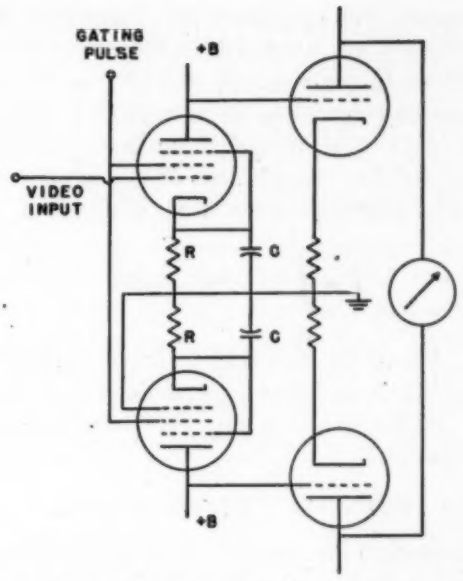

FIG. 2. Schematic diagram of averaging circuit.

In use, the gate is first moved to the range at which it is desired to measure the sea echo intensity, and the output meter read after equilibrium is reached. Without changing the receiver gain, the gate is then moved on to a signal generator pulse, and the calibrated attenuator is adjusted until the output meter reaches the same reading, thus giving the r-f level corresponding to the average video voltage.

It should be noted that the average video voltage does not necessarily correspond to the

[5] These devices are described in detail in *Technique of Microwave Measurements*, edited by C. G. Montgomery, Vol. 11, of the Radiation Laboratory Series (McGraw-Hill Book Company, Inc., New York, to be published).

average r-f voltage due to the distortion of the distribution of echo amplitudes by the non-linearities of the receiver. If $V(P_r)$ is the video voltage corresponding to an input r-f power P_r (with $P_r(V)$ the inverse function), and $W(P_r)$ the probability distribution of the input echoes, then the average video voltage is given by

$$\bar{V} = \int V(P_r) W(P_r) dP_r. \qquad (4)$$

The form of the function $V(P_r)$ is easily measured, and from other experiments[1] it is known that $W(P_r)$ is given by the "random walk" distribution:

$$W(P_r) = (1/\bar{P}_r) \exp [-P_r/\bar{P}_r]. \qquad (5)$$

By numerical integration, the correction ratio

$$\bar{P}_r/P_r(\bar{V})$$

could therefore be calculated as a function of $\bar{V}$, and it was found that by keeping $\bar{V}$ less than three-tenths of the saturation voltage, the correction was less than 1 db. This practice was followed throughout, even though the correction was applied, to ensure that the maximum possible error due to the effect would be small compared to other errors.

The time constant of the integrating circuit should be longer than the longest fluctuation period. It was found that the fluctuation spectrum for sea echo extended as high as 100 c.p.s. (on 3.2 cm) but that considerable energy was present at periods as long as 20 seconds. The time constant was therefore set at around 30 sec.

C. Estimated Errors in the Measurement of σ°

Possible errors in the determination of σ° may be both systematic, arising from the inaccurate system calibration, and random, because of the intrinsic variability of sea echo intensity. It is important that the range be the same on all systems to insure that the same patch of sea is being studied. Hence, in a comparison between two wave-lengths the range drops out and does not influence the accuracy of the result. The pulse recurrence frequency was crystal controlled, and therefore was known to within negligible error. The wave-length, too, was easily measured with great accuracy. The main sources of error, therefore, are the calibrations involved in the measurement of received and transmitted power, and the antenna gain and beam width.

Two independent methods were available for calibrating the arrangements for measuring received power. In the first, the output of the signal generator, the transmission loss of the directional coupler, and the line attenuation to the antenna were measured separately by conventional test-bench procedures. The individual values were then combined to give the total calibration. The second method, developed by J. L. Lawson, compared the signal generator pulse with the output of a second, c-w, signal generator matched into the line in place of the transmitting dipole. Pulses of random amplitude are produced by the beating of the c-w signal with the output of the pulsed signal generator. When these irregular pulses appear to fill up the signal generator pulse, the amplitude of the c-w oscillations is just one-half the peak amplitude of the r-f oscillations within the pulse. By this means the several elements entering into the measurement of received power are calibrated together, the accuracy depending only on the errors in the attenuators and the measurement of a c-w power.

On the 9- and 3-cm systems, both methods were used at frequent intervals with results generally agreeing to within 0.5 db, which is taken as the probable systematic error for the received power. Only the first method could be used with the 1.25-cm system and it is estimated that the systematic error was about 1 db.

The thermistor bridge used in the measurement of transmitted power was compared with a laboratory standard and found to have a negligible error. The losses in the r-f components (directional coupler, main r-f line) were measured both by the first method and by an obvious modification of the second method. From the spread of the results the systematic errors in the measurement of transmitted power were estimated to be 0.5 db for the 9- and 3-cm systems and 1 db for the 1.25-cm system.

The antenna gains were measured by repeated comparison with the primary gain standards of the Antenna Group, M.I.T. Radiation Laboratory, with estimated errors of 0.4 db on 9.2 and 3.2 cm, and 1.0 on 1.25 cm. It should be noted

that the square of the gain enters into the calculation of σ°. Beam widths (between half-power points) were measured, independently of the gains, from the measured antenna patterns. The uncertainties were ± 8 percent on 9.2 and 3.2 cm, but were much larger on 1.25 cm, ± 25 percent, due to the narrow beam width.

In addition to these main sources of systematic error, other errors were occasionally of importance. When the range was short, corrections of uncertain magnitude were required because of imperfect recovery of the TR tube,[6] and when the antenna beam was horizontal, for the vertical antenna pattern. A particularly troublesome source of error was attenuation in the radome[7] when wet, which occasionally required crudely estimated corrections of about 1 db. No radome was used on the 1.25-cm system, but attenuation due to water vapor and rain was often not negligible and corrections of 1 or 2 db were estimated at times.[8]

Combining the various possible errors, it is believed that the probable systematic error in the values of σ° is around 2 db on 9.2 and 3.2 cm, and about 4 db on 1.25 cm. If rain was falling, or the range was less than 2000 yards, about 1 db should be added to these figures.

The average intensity is not strictly constant but always shows a random scatter arising from changes in the sea surface with time. Some of this variation is eliminated in the averaging process, but successive measurements of the received power, at intervals of one minute, always showed a scatter, usually about 1–2 db, occasionally much larger. When the magnitude of the scatter was large, the echoes on two wavelengths varied in roughly the same way with time. Often, however, there was little correlation between the variations, perhaps indicating that the systems were not looking at exactly the same patch of sea. A random error is thus inevitably present in all measurements of σ°, independent of the accuracy of the measuring instruments. Usually, the random error could be reduced to less than 1 db by averaging three readings taken in rapid succession.

[6] A device in which a gas discharge is used to protect the receiver from the transmitted pulse.

[7] The plastic dome protecting the radar antenna.

[8] The attenuation due to water vapor was calculated on the basis of 0.04 db/na. mile/g/m^3 (S. H. Autler, G. E. Becker, and J. M. B. Kellogg, Phys. Rev. **69**, 694A (1946)), using the measured relative humidity. The attenuation due to rain was estimated from the recorded rate of rainfall with the figure of 0.3 db/mi./mm/hr. (S. D. Robertson and A. P. King, Proc. I.R.E. **34**, 178P (1946)). This procedure is admittedly rough but was justified by the smallness of the correction.

D. Range of External Parameters

Observations were made at a number of locations on the New England coast, at elevations ranging from 70 to 120 feet above mean sea level. At these relatively low elevations 2° represents the maximum depression angle that can be reached without serious difficulties due to TR recovery. To avoid the conditions peculiar to the shallow water near shore, it was usually necessary to further limit the depression angle to less than 1.3°. On the other hand, except in the roughest weather, the intensity of the sea echo was negligible for depression angles below 0.5°, although a few measurements were made as low as 0.3°.

The experiments cover a wide range of sea states from slight chop to the very rough seas with 14-ft. waves encountered in "northeasters." No objective measurements of sea roughness or wave height were feasible. However, rough values of the sea state were assigned on the Douglas scale,[9] on the basis of visual observations and wave heights expected from the observed surface wind velocities.[10]

III. RESULTS

A. Frequency Dependence of σ°

Only a few measurements were made on $\lambda = 1.25$ cm and attention will therefore be directed chiefly to comparison of the results on 9.2 and 3.2 cm. The ratio of σ° on 3.2 cm to the simultaneous value on 9.2 cm will be expressed in db and denoted by η. The 110-odd observations of η cover a wide range of sea states and depression angles and include both horizontal and vertical polarizations. To exhibit clearly the possible dependence of η on these external parameters, the data were treated in the following manner. After separating the two polarizations, the values were divided into three

[9] *Instructions to Marine Meteorological Observers* (Weather Bureau Circular M, 1941), seventh edition, p. 54.

[10] "Wind Waves and Swell, Principles in Forecasting," Hydrographic Office Miscellaneous Publication 11,275.

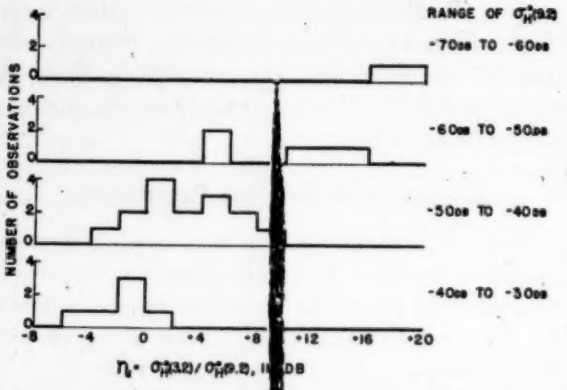

FIG. 3. Observed probability histograms for the ratio of the cross sections at 3.2 and 9.2 cm, for depression angles between 0.65 and 1.0.

rather broad classes according to the depression angle. As has been stated before, no objective scale for sea roughness is available. However, the cross section per unit area for constant wave-length, polarization, and depression angle should depend only on the state of the sea. Any correlation between η and the sea roughness should also appear between η and some suitably chosen cross section. Within each class the values of η were therefore grouped according to the value of σ° at $\lambda=9.2$ cm on horizontal polarization (denoted by $\sigma_H^\circ(9.2)$). In Fig. 3, the probability distributions for η are plotted in the form of histograms for the middle angle class on horizontal polarization for 10-db intervals of $\sigma_H^\circ(9.2)$. Although the range of η in each interval is fairly wide, it is clear that a correlation does exist between η and the sea roughness.

Table II lists the average value of η in each interval of $\sigma_H^\circ(9.2)$ according to polarization and angle group, along with the number of observations in each interval. For the middle angle group an attempt has been made to give the sea state description corresponding roughly to the intervals of $\sigma_H^\circ(9.2)$. This correspondence cannot necessarily be carried over to the other angle groups because σ° varies with depression angle in a way that is not well known and that probably varies with sea state. All the values of η are far below the 36-db figure corresponding to a frequency variation as λ^{-3}, and the large majority are significantly less than 18 db, which would be predicted by a λ^{-4} variation. It will be noted that the ratio is consistently smaller on vertical than on horizontal polarization.

Measurements on the 1.25-cm wave-length were too few to permit any detailed analysis. For the most part they were made with moderate seas on horizontal polarization with depression angles between 0.45 and 0.90 degrees. The average ratio, $\sigma^\circ(1.25)/\sigma^\circ(3.2)$ was found to be about +5 db under these conditions, to be compared to +16.5 db which would correspond to a λ^{-4} variation.

B. Polarization Dependence of σ°

The data on frequency dependence also yield information on the change of the cross section with polarization. The polarization ratio, defined as the ratio of σ° on vertical polarization to that on horizontal polarization, was found to vary from −8 db to +22 db depending upon circumstances, a range of 1000! On both 9.2 and 3.2 cm the ratio is largest for calm seas but steadily decreases as the sea becomes rougher. As might be expected from this statement, a good correlation exists between the simultaneous values of the ratio on two wave-lengths. Figure 4 is a correlation diagram in which the polarization ratio on 9.2 cm is plotted on the ordinate, while that on 3.2 cm is plotted on the abscissa. All the experimental points for depression angles between 0.65° and 1.30° are represented by the circles. Although the scatter of the points is

TABLE II. Average values of $\eta=\sigma^\circ(3.2)/\sigma^\circ(9.2)$.

	$\theta\geq 1.0°$			
Interval of $\sigma_H^\circ(9.2)$ in db	No. in interval Hor.	Vert.	η in db Hor.	Vert.
−40 to −50	2	0	+ 8.5 db	—
−50 to −60	0	0	—	—
−60 to −70	5	4	+13	+ 2
−70 to −80	1	2	+18	+11

	$0.65°\leq\theta<1.0°$				
Interval of $\sigma_H^\circ(9.2)$, in db	No. in interval Hor.	Vert.	η in db Hor.	Vert.	Approx. state sea
−30 to −40 db	6	4	− 2	−5	Rough
−40 to −50	15	11	+ 3	−1	Moderate
−50 to −60	5	7	+ 9	+3	Slight
−60 to −70	2	0	+18	—	Smooth

	$\theta<0.65°$			
Interval of $\sigma_H^\circ(9.2)$ in db	Number in interval Hor.	Vert.	η in db Hor.	Vert.
−30 to −40 db	6	6	0.0	−5
−40 to −50	11	11	+4	0.0
−50 to −60	5	4	+6	+3

considerable, the existence of a correlation is clear. It should be noted that the values of the polarization ratio are practically free from systematic error, since absolute calibration of the system is not required, and the only sources of error are in the attenuator calibrations and change in antenna characteristics when the polarization is rotated. The errors from both these sources should be negligible. However, the random errors are even greater than for the data on frequency dependence. The polarization ratio requires two measurements of sea echo intensity necessarily separated by several minutes in time. During this time there may be considerable change in the number and size of the scatterers. It is believed that this random error is largely responsible for the scatter of the points in Fig. 4.

The few observations on the polarization dependence at $\lambda = 1.25$ cm indicate that the echo is about equally intense on both polarizations with a scatter of ± 3 db.

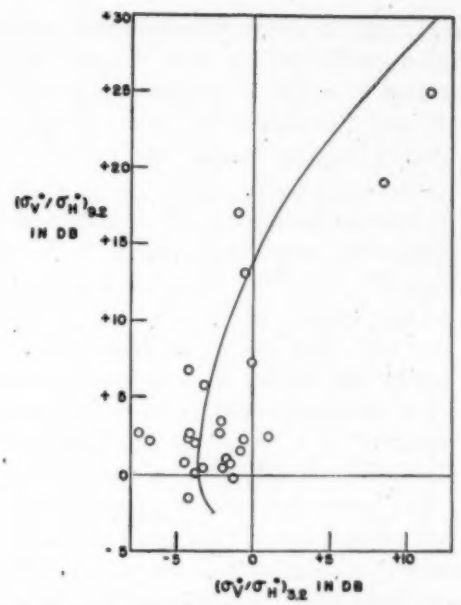

FIG. 4. Plot showing the correlation between the polarization ratio on 9.2 and 3.2 cm. The circles are experimental points, the smooth curve is predicted by the droplet theory with smooth sea.

IV. DISCUSSION

It is clear from the results obtained on the frequency dependence of σ° that the scatterers responsible for sea echo cannot in the main be drops sufficiently small to follow Rayleigh's law. On the other hand the theories of scattering from a corrugated surface, at least in their present form, seem incapable of explaining the striking polarization dependence. It can be shown that if the currents on the scattering surface correspond to the incident field, as is customarily assumed, then there should be no difference between vertical and horizontal polarization for back scattering aside from slight differences in the reflection coefficient. More rigorous calculations may possibly introduce some polarization dependence, but it is significant that in the "exact" Sommerfeld solution for the half-plane the back scattered field is also independent of polarization.

The drop theory, though apparently failing to account for the frequency dependence, does however afford a qualitative explanation for the changes with polarization. On the horizontal polarization the reflection coefficient for a smooth sea is almost exactly -1, but is sensibly less on vertical polarization even at grazing angles of the order of a degree. Consequently, drops just above the sea surface are located in an incident field, composed of direct and reflected components, which is practically negligible on horizontal polarization but quite appreciable for vertical polarization. Hence, the polarization ratio tends to be large for calm seas. When the sea becomes rougher, the drops are thrown higher covering a larger fraction of the first interference lobe. Also, the roughness tends to destroy the interference pattern, especially filling in the minima. Both effects should lead to a decrease in the polarization ratio, as is observed. If the spray drops cover several lobes, the average field on horizontal polarization is somewhat greater than on vertical polarization due to the difference in the magnitude of the reflection coefficient. (The magnitude of the difference, though, may be lessened by the effect of the sea roughness.) Hence, the polarization ratio may become less than unity. It is also understandable why the polarization ratio is always less on 3.2 cm than on 9.2 cm, since for constant angle the interference lobes are more finely spaced on the shorter wave-length.

To show these conclusions in some detail, calculations have been carried through for a conveniently simple, but quite artificial, model.

A perfectly smooth sea surface was assumed with a reflection coefficient on both 9.2 and 3.2 cm as calculated from the constants of sea water at 10 cm. It was also assumed that the drops were distributed in height according to a formula analogous to the barometric rule, i.e., exp $(-h/h_0)$, where h_0 is an adjustable parameter. The polarization ratio was then computed on both wavelengths at 1°, as a function of average drop height. The results are plotted as a smooth curve on the correlation diagram in Fig. 4. Quantitative agreement with the experimental data is not to be expected in any case, because of the inherent scatter of the measured points, and of the oversimplification of the theoretical model. The general qualitative agreement between the two is however quite satisfactory.

In order to reconcile the drop theory with the observed frequency dependence, it must be assumed that the cross sections of the individual drops are roughly independent of wave-length. This condition would require the drops to correspond roughly in size to the first maximum in the curve of back scattering *versus* diameter, e.g., drops of diameter in the neighborhood of 1.5 cm. The observed frequency dependence of σ° would then result solely from the effects of the interference pattern. At calm seas, if the height of the drops is less than the first maximum, the variation with wave-length should then go as λ^{-4}, as is roughly observed, and should then decrease as the sea becomes rougher and the drops cover larger portions of the lobe, again in agreement with observation. Since the minima of the interference pattern are less deep on vertical polarization, the observed frequency dependence should be less than for horizontal polarization, with calm seas. However, it might be expected that this difference would disappear as the seas become rough. Actually, the difference appears to persist even at the roughest sea state.

It is also possible to calculate the dependence of σ° on grazing angle assuming the drop theory. The results can be satisfactorily fitted to rough experimental data obtained by other workers[11] with assumed average drop heights ranging from 2 cm in calm seas to 30 cm for rough weather. The drop concentrations required to account for the absolute magnitudes of σ° as given in Table II range from 1 to 1000 drops per ten square meters, which do not seem unlikely *a priori*.

On the basis of the present sketchy experimental knowledge it thus seems that of all the proposed hypotheses, the drop theory most satisfactorily accounts for the sea echo phenomena. There are, however, a number of difficulties with the theory in its present form. To what extent the interference pattern is obliterated by the roughness of the sea is at present uncertain. The existence of such large "blobs" of water above the sea surface in calm weather in the apparent absence of whitecaps is also questionable. Finally, such drops should rapidly break up, and it is possible their lifetime would be too short to be of significance.

It should also be mentioned that the previous discussion has neglected multiple scattering and attenuation. If there were dense layers of small drops present, these mechanisms could possibly account for the observed frequency dependence without the necessity of assuming drops of large diameter. Further investigations along these lines, as well as more detailed experimental data about σ° appear necessary before the origins of sea echo can be said to be satisfactorily understood.

ACKNOWLEDGMENT

The author wishes to acknowledge gratefully the essential aid and cooperation of many members of the Propagation Group, Radiation Laboratory, M.I.T., especially Mr. Donald E. Kerr, Group Leader, for his continued support and encouragement; and Dr. L. J. Neelands, who developed the averaging circuit and supervised the system calibrations; and Frank Clelland, N. W. Hancock, M. C. Myers, Jr., W. H. Paulsen, and A. B. Vane, who kept the radar systems in operating order and took part in the measurements.

[11] Unpublished data obtained at the Radiation Laboratory, M.I.T.

PHYSICAL REVIEW VOLUME 70, NUMBERS 11 AND 12 DECEMBER 1 AND 15, 1946

Special Relativistic Field Theories in Five Dimensions

H. C. CORBEN*
University of Melbourne, Melbourne, Australia
(Received August 23, 1946)

In view of the current use of a five-dimensional manifold for the development of general relativistic unified field theories, special relativistic theories of pure fields are here expressed in terms of an extra dimension. According to these theories the rest mass of a particle is not an arbitrary parameter, constant under all conditions. It appears in the equations as an operator, although no clue would be expected from a special theory of the eigenvalues of this operator when the particle is moving freely. The Lagrangian densities and equations of motion assume a simpler form than in the usual treatment and the extra elements of the energy tensor which appear may be given a consistent physical significance. The unified vector-pseudo-scalar theory of mesons is a particular case of the fields here considered. The preliminary equations for the description of a pseudo-scalar-vector electromagnetic field are also written down. The pseudo-scalar part cannot be used in general to describe gravitational interaction approximately in special relativity theory.

INTRODUCTION

THE formal use of a fifth coordinate in theoretical physics has been familiar to workers in the field of general relativity theory since the publication of Kaluza's unified theory of gravitation and electromagnetism.[1] Indeed, the development of Kaluza's ideas by Klein, Pauli, Einstein, Flint, and others[2] makes it difficult to see how a satisfactory unified theory could be developed without the introduction of an extra coordinate.

Within the framework of the special theory of relativity the same device was used by Nordström[3] to obtain a unification of his scalar gravitational theory with Maxwell electrodynamics, by Wilson and Cattermole[4] in an attempt to explain classically the magnetic moment of the electron, and by Møller[5] to derive a unified vector-pseudo-scalar theory of mesons.

The fact that we interpret events in terms of a framework of (3+1) dimensions appears to lend to these theories a highly artificial character. The possible alternatives are

(a) none of these theories is valid,
(b) the use of the fifth coordinate is purely a mathematical trick,
(c) there is some deep significance in the extra space dimension, the awareness of which is denied to us because of our evolutionary background (e.g., predominance of gravitational forces over electromagnetic in determining the motion of macroscopic objects in our environment), and
(d) the extra coordinate is related to the proper time.

In this paper it is not our purpose to distinguish between alternatives (b) and (c), while in the light of researches on the general theory of relativity alternative (a) appears unlikely at present. It seems of interest, then, to investigate, at first within the framework of the special theory of relativity, the general Lagrangian field theories which arise by extension to five dimensions of the present theories. This generalization is not direct, but is modified by the explicit exclusion from the Lagrangians of all arbitrary constants denoting the rest masses of the particles associated with the fields. This postulate leads us to favor alternative (d) above.

In this paper we are concerned solely with pure fields, leaving out of account at present all interactions between fields of different character. We formulate the general five-dimensional theory for such fields, attach physical significance to the extra quantities introduced, and outline the possible application to particles of spin 0, ½, and 1.

* Now at Carnegie Institute of Technology, Pittsburgh, Pennsylvania.

[1] Th. Kaluza, Sitz. d. preuss. Akad. d. Wiss. 966 (1921).

[2] O. Klein, Zeits. f. Physik **37**, 895 (1926). O. Veblen and B. Hoffmann, *Projektive Relativitätstheorie* (Verlagsbuchhandlung Julius Springer, Berlin, 1933). A. Einstein and W. Mayer, Sitz. d. preuss. Akad. d. Wiss. 130 (1932). A. Einstein and P. Bergmann, Ann. Math. **39**, 683 (1938). W. Pauli, Ann. d. Physik **18**, 305 (1933). H. T. Flint, Phil. Mag. [7] **29**, 330, 417 (1940); Proc. Roy Soc. **A185**, 14 (1946).

[3] G. Nordström, Physik. Zeits. **15**, 504 (1914). H. C. Corben, Phys. Rev. **69**, 225 (1946).

[4] W. Wilson, and J. Cattermole, Phil. Mag. [7] **17**, 84 (1939).

[5] C. Møller, Kgl. Danske Vid. Sels. Math.-Fys. Medd. **18**, 6 (1941).

We assume throughout that the five-dimensional continuum is flat, and, in common with the theories mentioned above, postulate that the fifth coordinate is space-like. The complete exclusion from the theories of this paper of the metric of general relativity imposes an essential limitation, but the corresponding simplicity of treatment which ensues facilitates the quantization of the theories by standard methods.

I. GENERAL THEORY

For convenience we adopt the units and notation of Pauli,[6] reducing all quantities to the dimensions of a power of length by appropriate multiplication by powers of $\hbar$ and c. Latin suffixes assume throughout the values 1, 2, 3, 4; Greek suffixes run from 1 up to 5. We assume that the fifth dimension is space-like, and write $x_4=ix_0=it$; $x_5=t'$.

The canonical energy-momentum tensor and the current vector are defined as usual

$$T_{\mu\nu}=\sum_r[U_\mu^{*(r)}(\partial L/\partial U_\nu^{*(r)})+(\partial L/\partial U_\nu^{(r)})U_\mu^{(r)}+(\partial L/\partial V_\nu^{(r)})V_\mu^{(r)}]-L\delta_{\mu\nu}, \quad (1.1)$$

$$s_\mu=ei\sum[(\partial L/\partial U_\mu^{(r)})U^{(r)}-U^{*(r)}(\partial L/\partial U_\nu^{*(r)})], \quad (1.2)$$

with

$$U_\mu^{(r)}=\partial_\mu U^{(r)}, \quad U_\mu^{*(r)}=\partial_\mu U^{*(r)}. \quad (1.3)$$

It follows that

$$\partial_\mu s_\mu=0; \quad \partial_\nu T_{\mu\nu}=0. \quad (1.4)$$

The energy-momentum tensor may be considered as symmetrized by familiar processes.

These equations introduce extra densities $T_{\mu 5}$, s_5. We write

$$\left.\begin{aligned} -iT_{\mu 4}&=(\mathfrak{G}, iW, W_0),\\ T_{\mu 5}&=(\mathfrak{G}_0, iW_0, W_{00}),\\ \mathcal{T}_{\mu 4}&=\int T_{\mu 4}dV=i(\mathbf{G}, iE, E_0),\\ \mathcal{T}_{\mu 5}&=\int T_{\mu 5}dV=(\mathbf{G}_0, iE_0, E_{00}),\\ s_4&=i\rho, \quad e=-i\int s_4 dV,\\ s_5&=\rho_0, \quad e_0=\int s_5 dV, \end{aligned}\right\} \quad (1.5)$$

the integrations proceeding over a given three-dimensional volume. Here $(\mathfrak{G}, W, W_{00})$ denote, respectively, the momentum-, energy-, and rest mass densities of the field, and $(\mathbf{G}, E, E_0)$ the total momentum, energy, and rest mass within the given volume. $\mathbf{G}_0$ is the "rest momentum," i.e., that part of the momentum which arises from the motion of rest mass (e.g., $\kappa\mathbf{v}$ for a particle of rest mass κ). For an assembly of identical particles it is proportional to the current.

We call s_5, the fifth component of the current density, the "rest charge density." For an assembly of identical particles for which $L=0$, s_5 is proportional to the rest mass density.[7]

From the conservation laws (1.4) we now have

$$\left.\begin{aligned} \nabla\cdot\mathfrak{G}+\partial W/\partial t+\partial W_0/\partial t'&=0,\\ \nabla\cdot\mathfrak{G}_0+\partial W_0/\partial t+\partial W_{00}/\partial t'&=0,\\ \nabla\cdot\mathbf{s}+\partial\rho/\partial t+\partial\rho_0/\partial t'&=0. \end{aligned}\right\} \quad (1.4')$$

The extra terms correspond to sinks of energy, rest energy, and charge, respectively. For an isolated region, these equations yield the result that the rates at which the total energy, intrinsic energy, and charge inside the region are increasing are equal to the rates at which these quantities are being created. Allowance is, therefore, made for the creation of annihilation of matter, a process which may be pictured as the appearance of matter from, or its disappearance into, the extra dimension. For the theories discussed in this paper, the extra term in the charge conservation law vanishes identically.

II. PARTICLES OF DEFINITE REST MASS

The fields described by the formulation of Section I do not in general have associated with them arbitrary parameters which may be identified as the rest masses of the corresponding particles. The rest mass, as the momentum and energy, now appears as an operator, and for a particle of charge ϵ, definite rest mass κ, we have

$$\partial_5 U^{(r)}=i\kappa U^{(r)}, \quad \partial_5 U^{*(r)}=-i\kappa U^{*(r)}. \quad (2.1)$$

A complete theory would have to account for

[6] W. Pauli, Rev. Mod. Phys. 13, 203 (1941).

[7] The direct identification of s_5 with the rest mass density (cf. reference 3) is inconsistent with the general theory of this paper.

the fact that, for particles of spin $\frac{1}{2}$, the field variables satisfy (2.1) with two different eigenvalues κ associated with the two signs of the charge. On the other hand, there appears to be some evidence that the rest mass of the mesotron is not definite.[8] The present formulation allows for this possibility in a natural manner.

In this section we consider only field variables describing an assembly of identical particles of charge ϵ, rest mass κ. In the absence of electromagnetic or other real fields, it follows from (1.2), (1.3) that

$$\epsilon T_{5k}=\kappa s_k; \quad \epsilon T_{55}=\kappa s_5-\epsilon L. \tag{2.2}$$

The first of these equations confirms the identification made in (1.1) of

$$E_0=-i\int T_{54}dV$$

with the total rest energy within a given volume. The fifth component of the current vector becomes

$$s_5=(\epsilon/\kappa)[(\partial L/\partial U^{(r)})U^{(r)} + U^{*(r)}(\partial L/\partial U^{*(r)}]. \tag{2.3}$$

From (2.2) and the conservation laws we have

$$\partial_5 L=0, \tag{2.4}$$

so that the Lagrangian does not depend explicitly upon the extra coordinate. This is in any case obvious from (2.1), as the phase factors $\exp(\pm i\kappa x_5)$ in $U^{(r)}$, $U^{*(r)}$ cancel in the Lagrangian. Under these conditions both s_5 and T_{55} are also independent of x_5, and the theory reduces to its usual four-dimensional form.

III. PARTICLES OF SPIN $\frac{1}{2}$

Here it is convenient to define a pentad of anticommuting matrices

$$\epsilon_\mu=(-\rho_3\boldsymbol{\sigma},\ \rho_2,\ \rho_1) \tag{3.1}$$

and write

$$u^\dagger=u^*\epsilon_4.$$

Then the Lagrangian may be written

$$L=\tfrac{1}{2}(u^\dagger\epsilon_\mu(\partial_\mu u)-(\partial_\mu u^\dagger)\epsilon_\mu u)$$
$$=-\frac{i}{2}[(u^*\,\partial u/\partial x_0-\partial u^*/\partial x_0\,u)+(u^*\boldsymbol{\alpha}\cdot\partial u/\partial\mathbf{x}-\partial u^*/\partial\mathbf{x}\cdot\boldsymbol{\alpha}u)+(u^*\rho_3\,\partial u/\partial x_5-\partial u^*/\partial x_5\,\rho_3 u)]. \tag{3.2}$$

The equations for u, $u^\dagger$ are as follows:

$$\epsilon_\mu\partial_\mu u=0; \quad (\partial_\mu u^\dagger)\epsilon_\mu=0. \tag{3.3}$$

These equations may be written

$$\partial u/\partial x_5=-i\rho_2\boldsymbol{\sigma}\cdot\partial u/\partial\mathbf{x}-\rho_3\partial u/\partial x_0,$$
$$\partial u^*/\partial x_5=i\partial u^*/\partial\mathbf{x}\cdot\rho_2\boldsymbol{\sigma}-\partial u^*/\partial x_0\rho_3. \tag{3.3'}$$

They are identical with Dirac's equations if

$$\partial u/\partial x_5=i\kappa u, \quad \partial u^*/\partial x_5=-i\kappa u^*. \tag{3.4}$$

In general

$$s_\mu=\epsilon iu^\dagger\epsilon_\mu u, \tag{3.5}$$

i.e.,

$$s_0=\epsilon u^*u, \quad \mathbf{s}=\epsilon u^*\boldsymbol{\alpha}u, \quad s_5=\epsilon u^*\rho_3 u \tag{3.5'}$$

and

$$T_{\mu\nu}=\tfrac{1}{2}[u^\dagger\epsilon_\nu\partial_\mu u-(\partial_\mu u^\dagger)\epsilon_\nu u] \tag{3.6}$$

with

$$\theta_{\mu\nu}=\tfrac{1}{2}[T_{\mu\nu}+T_{\nu\mu}].$$

Hence,

$$\mathfrak{G}=-iT_{k4}=-\frac{i}{2}[u^*(\partial u/\partial\mathbf{x})-(\partial u^*/\partial\mathbf{x})u],$$
$$W=-T_{44}=-\frac{i}{2}[-u^*(\partial u/\partial x_0)+(\partial u^*/\partial x_0)u], \tag{3.7}$$
$$W_{00}=T_{55}=-\frac{i}{2}[u^*\rho_3(\partial u/\partial x_5)-(\partial u^*/\partial x_5)\rho_3 u]$$

are the momentum-, energy-, and rest mass densities, respectively. The total rest mass in a given volume is

$$E_0=-i\int T_{54}dV=-\frac{i}{2}\int[u^*\partial_5 u-(\partial_5 u^*)u]dV.$$

If Eqs. (3.4) apply, these become

$$E_0=\kappa\int u^*u\,dV,$$
$$W_{00}=T_{55}=\kappa u^*\rho_3 u; \quad \partial_5 s_5=0.$$

[8] E.g., G. Groetzinger and L. Smith, Phys. Rev. **68**, 55 (1945).

The first of these equations gives the total rest energy as the rest mass multiplied by the integrated probability density; the second gives the familiar expression for the rest mass density,[9] the third leads to the usual conservation law.

From (3.6) we have

$$\partial_5 T_{54}=\frac{i}{2}[u^*\partial_5\partial_5 u-(\partial_5\partial_5 u^*)u],$$

$$\partial_5 T_{55}=-\frac{i}{2}[u^*\rho_3\partial_5\partial_5 u-(\partial_5\partial_5 u^*)\rho_3 u].$$

For a field consisting of particles, of either sign of the charge, but of identical rest masses, the conditions

$$\partial_5\partial_5 u=-\kappa^2 u;\quad \partial_5\partial_5 u^*=-\kappa^2 u^*,$$

less stringent than (3.4), cause both of these expressions to vanish.

As usual, we may write[10]

$$u_l(x_\nu)=V^{-\frac{1}{2}}\sum_{\mathbf{k},\kappa}\sum_{r=1,2}[u_+^{(r)}(\mathbf{k},\kappa)a_l^{(r)}(\mathbf{k},\kappa)$$

$$\times\exp(ik_\mu x_\mu)+u_-^{*(r)}(\mathbf{k},\kappa)b_l^{(r)}(\mathbf{k},\kappa)\exp(-ik_\mu x_\mu)],$$

and with

$$N_r^+(\mathbf{k},\kappa)=u_+^{*(r)}(\mathbf{k},\kappa)u_+^{(r)}(\mathbf{k},\kappa),$$

$$N_r^-(\mathbf{k},\kappa)=u_-^{*(r)}(\mathbf{k},\kappa)u_-^{(r)}(\mathbf{k},\kappa),$$

we obtain

$$(\mathbf{G},iE,E_0)=\sum_{\mathbf{k},k}k_\mu\sum_{r=1,2}[N_r^+(\mathbf{k},\kappa)+N_r^-(\mathbf{k},\kappa)-1.]$$

Thus, in particular, if the field consists of n_+ positively charged particles of rest mass m_+, n_- negatively charged particles of rest mass m_-,

$$E_0=m_+n_++m_-n_-$$

apart from the zero-point energy. The expressions for e_0, E_{00}, $\mathbf{G}_0$, $\mathbf{j}$ for this case are more complicated and we do not write them down here.

IV. SCALAR AND VECTOR PARTICLES

(a) Scalar Particles

For this case we derive the field equations from the variational principle

$$\delta\int L d^5x=0$$

with

$$L=(\partial_\mu U^*)(\partial_\mu U). \tag{4.1}$$

Hence,

$$\partial_\mu\partial_\mu U=\square U=0;\quad \square U^*=0, \tag{4.2}$$

$$T_{\mu\nu}=(\partial_\mu U^*)(\partial_\nu U)+(\partial_\nu U^*)(\partial_\mu U)-L\delta_{\mu\nu}, \tag{4.3}$$

$$s_\mu=ei[(\partial_\mu U^*)U-U^*\partial_\mu U]. \tag{4.4}$$

(Alternatively we may write

$$L=(\partial_\mu U^*)U_\mu+U_\mu^*\partial_\mu U-U_\mu^*U_\mu, \tag{4.1*}$$

so that

$$\partial_\mu U=U_\mu;\quad \partial_\mu U_\mu=0, \tag{4.2*}$$

but we do not employ this formalism here.)

As usual, we may break up the field into two real fields; thus,

$$U=2^{-\frac{1}{2}}[V+iW],\quad U^*=2^{-\frac{1}{2}}[V-iW], \tag{4.5}$$

so that

$$L=\tfrac{1}{2}[(\partial_\mu V)(\partial_\mu V)+(\partial_\mu W)(\partial_\mu W)], \tag{4.1'}$$

$$\partial_\mu\partial_\mu V=0;\quad \partial_\mu\partial_\mu W=0, \tag{4.2'}$$

$$T_{\mu\nu}=(\partial_\mu V)(\partial_\nu V)+(\partial_\mu W)(\partial_\nu W)-L\delta_{\mu\nu}, \tag{4.3'}$$

$$s_\mu=e[V\partial_\mu W-W\partial_\mu V]. \tag{4.4'}$$

In addition to the usual expressions for the energy-, momentum- and current densities, these equations yield

$$W_{00}=T_{55}=(\partial_0 U^*)(\partial_0 U)-(\nabla U^*)\cdot(\nabla U)+(\partial_5 U^*)(\partial_5 U), \tag{4.6}$$

$$\mathfrak{G}_0=-iT_{k5}=-i[(\nabla U^*)\partial_5 U+(\partial_5 U^*)\nabla U]_{(k=1,2,3)}, \tag{4.7}$$

$$s_5=ei[(\partial_5 U^*)U-U^*\partial_5 U], \tag{4.8}$$

$$E_0=-i\int T_{45}dV$$

$$=-\int[(\partial_0 U^*)(\partial_5 U)+(\partial_5 U^*)(\partial_0 U)]dV$$

$$=-\int[(\partial_0 V)(\partial_5 V)+(\partial_0 W)(\partial_5 W)]dV, \tag{4.9}$$

[9] L. de Broglie, *L'Electron Magnetique*, p. 225. E. L. Hill and R. Landshoff, Rev. Mod. Phys. 10, 118 (1938).

[10] Cf. reference 6, p. 224.

for the rest mass, momentum- and rest charge density, and for the total rest mass within a given volume.

(b) Five-Vector Particles

The simplest formulation of this theory arises from the Lagrangian

$$L=(\partial_\mu U_\nu^*)(\partial_\mu U_\nu), \tag{4.10}$$

if we postulate the auxiliary condition

$$\partial_\nu U_\nu=0. \tag{4.11}$$

Apart from the complex character of the field functions, this case is similar to ordinary electromagnetic theory in that the absence of κ from the Lagrangian prevents the deduction of (4.11) from the Lagrangian equations. As is well known, the Lagrangian (4.10) is not invariant under a gauge transformation of the second kind

$$U_\mu^*\rightarrow U_\mu^*+\partial_\mu\chi^*, \quad U_\mu\rightarrow U_\mu+\partial_\mu\chi,$$

although if

$$\square\chi=0,$$

the transformed Lagrangian differs from the original by a gradient.

Defining

$$U_{\mu\nu}=\partial_\mu U_\nu-\partial_\nu U_\mu, \tag{4.12}$$

we have from (4.10), (4.11)

$$\partial_\nu\partial_\nu U_\mu=0 \tag{4.13}$$

or

$$\partial_\nu U_{\mu\nu}=0. \tag{4.14}$$

Hence,

$$T_{\mu\nu}=(\partial_\mu U_\sigma^*)(\partial_\nu U_\sigma)+(\partial_\nu U_\sigma^*)(\partial_\mu U_\sigma)-L\delta_{\mu\nu}, \tag{4.15}$$

$$s_\mu=ei[(\partial_\mu U_\sigma^*)U_\sigma-U_\sigma^*(\partial_\mu U_\sigma)], \tag{4.16}$$

giving a generalization of the theory for particles of zero magnetic moment.

For both (4.16) and the scalar current density (4.4) it is clear that the relations

$$\partial_5^2 U_\mu=-\kappa^2 U_\mu; \quad \partial_5^2 U=-\kappa^2 U$$

imply $\partial_5 s_5=0$, so that the current is conserved if the rest energies of the associated particles are identical.

Despite its artificiality, however, we here adopt the Lagrangian

$$L=-\tfrac{1}{2}U_{\mu\nu}^*U_{\mu\nu}+\tfrac{1}{2}U_{\mu\nu}^*(\partial_\mu U_\nu-\partial_\nu U_\mu)+\tfrac{1}{2}(\partial_\mu U_\nu^*-\partial_\nu U_\mu^*)U_{\mu\nu}, \tag{4.10}$$

from which (4.12), (4.14) may be derived. However, (4.11) must again be postulated separately.

We have

$$T_{\mu\nu}=U_{\nu\sigma}^*(\partial_\mu U_\sigma)+(\partial_\mu U_\sigma^*)U_{\nu\sigma}-L\delta_{\mu\nu}, \tag{4.15}$$

$$s_\mu=ei[U_{\mu\sigma}^*U_\sigma-U_\sigma^*U_{\mu\sigma}] \tag{4.16}$$

and for the symmetrized energy momentum tensor we may write

$$\theta_{\mu\nu}=U_{\mu\sigma}^*U_{\nu\sigma}+U_{\nu\sigma}^*U_{\mu\sigma}-L\delta_{\mu\nu}. \tag{4.17}$$

(c) Eigenstates in Momentum Space

It is convenient to define a five vector in momentum space

$$k_\mu=(\mathbf{k}, ik_0, \kappa), \tag{4.18}$$

where the k_μ are the propagation constants of the waves in terms of which we represent the solutions of (4.2) and (4.13). Then k_μ is a null vector

$$k_\mu k_\mu=0. \tag{4.19}$$

For the scalar case we write

$$\begin{aligned} U^*(\mathbf{x}, x_4, x_5)&=V^{-\frac{1}{2}}\sum_{\mathbf{k},\kappa}(2k_0)^{-\frac{1}{2}}\\ &\quad\times[U_+^*(\mathbf{k},\kappa)\exp(-ik_\mu x_\mu)\\ &\quad+U_-(\mathbf{k},\kappa)\exp(ik_\mu x_\mu)],\\ U(\mathbf{x}, x_4, x_5)&=V^{-\frac{1}{2}}\sum_{\mathbf{k},\kappa}(2k_0)^{-\frac{1}{2}}\\ &\quad\times[U_+(\mathbf{k},\kappa)\exp(ik_\mu x_\mu)\\ &\quad+U_-^*(\mathbf{k},\kappa)\exp(-ik_\mu x_\mu)], \end{aligned} \tag{4.20}$$

and we have

$$\left.\begin{aligned} U_+^*(\mathbf{k},\kappa)U_+(\mathbf{k},\kappa)&=N_+(\mathbf{k},\kappa),\\ U_-^*(\mathbf{k},\kappa)U_-(\mathbf{k},\kappa)&=N_-(\mathbf{k},\kappa). \end{aligned}\right\} \tag{4.21}$$

For the five-vector case we write

$$\begin{aligned} U_\mu^*(\mathbf{x}, x_4, x_5)&=V^{-\frac{1}{2}}\sum_{\mathbf{k},\kappa}2^{-\frac{1}{2}}\\ &\quad\times[U_{\mu+}^*(\mathbf{k},\kappa)\exp(-ik_\sigma x_\sigma)\\ &\quad+U_{\mu-}(\mathbf{k},\kappa)\exp(ik_\sigma x_\sigma)],\\ U_\mu(\mathbf{x}, x_4, x_5)&=V^{-\frac{1}{2}}\sum_{\mathbf{k},\kappa}2^{-\frac{1}{2}}\\ &\quad\times[U_{\mu+}(\mathbf{k},\kappa)\exp(ik_\sigma x_\sigma)\\ &\quad+U_{\mu-}^*(\mathbf{k},\kappa)\exp(-ik_\sigma x_\sigma)]. \end{aligned} \tag{4.20'}$$

In virtue of (4.11) it follows that

$$k_\mu U_{\mu\pm}^*(\mathbf{k},\kappa)=0, \quad k_\mu U_{\mu\pm}(\mathbf{k},\kappa)=0 \tag{4.22}$$

or

$$U_{5\pm}(\mathbf{k},\kappa)=\kappa^{-1}(k_0 U_{0\pm}(\mathbf{k},\kappa)-\mathbf{k}\cdot\mathbf{U}_\pm(\mathbf{k},\kappa))$$
$$(\mathbf{U}_\pm(\mathbf{k},\kappa)=U_{i\pm}(\mathbf{k},\kappa), \quad i=1,2,3). \tag{4.23}$$

Here we have

$$N_+(\mathbf{k},\kappa)=k_0 U_{\mu+}^*(\mathbf{k},\kappa)U_{\mu+}(\mathbf{k},\kappa),$$
$$N_-(\mathbf{k},\kappa)=k_0 U_{\mu-}^*(\mathbf{k},\kappa)U_{\mu-}(\mathbf{k},\kappa). \tag{4.21'}$$

It then follows that for both scalar and vector cases the total momentum, energy, and rest energy are given by

$$(\mathbf{G}, iE, E_0)=-i\int T_{\mu 4}dV$$
$$=\sum_{\mathbf{k},\kappa} k_\mu[N_+(\mathbf{k},\kappa)+N_-(\mathbf{k},\kappa)] \tag{4.24}$$

and the integrated current vector is

$$j_\mu=\int s_\mu dV=(\mathbf{j}, ie, e_0)$$
$$=\epsilon\sum_{\mathbf{k},\kappa}\left[\frac{k_\mu}{k_0}(N_+(\mathbf{k},\kappa)-N_-(\mathbf{k},\kappa))\right]. \tag{4.25}$$

Further,

$$(\mathbf{G}_0, iE_0, E_{00})=\int T_{\mu 5}dV$$
$$=\sum_{\mathbf{k},\kappa}\frac{\kappa k_\mu}{k_0}[N_+(\mathbf{k},\kappa)+N_-(\mathbf{k},\kappa)]. \tag{4.26}$$

These relations exhibit the physical significance of the components of the current and energy-momentum tensor involving the suffix 5. Thus $E_0=\sum\kappa(N_++N_-)$ is obtained for the sum of the rest masses of the particles within the volume, i.e., the total intrinsic energy of the particles composing the field. For a field consisting of quanta with zero rest mass, all of these extra components are zero on integration throughout the volume.

We may see more clearly the significance of $T_{\mu 5}$, s_5 if we apply Eqs. (4.24), (4.26) to the classical case of a single particle of charge ϵ, definite rest mass κ, moving with velocity v. Then

$$v_\mu=k_\mu/k_0=[\mathbf{v}, i, (1-v^2)^{\frac{1}{2}}],$$

so that

$$v_\mu v_\mu=0.$$

This is equivalent to the postulate that the particle moves on a null geodesic in the five-dimensional continuum[11]

$$dx_\mu dx_\mu=0,$$

comparison of which with the familiar interval of special relativity theory

$$dx_k dx_k=-ds^2$$

allows us to write

$$dx_5=ds.$$

In this sense the theory treats the proper time on the same basis as the space and time coordinates, and the postulate of five-invariance implies that in the five-dimensional continuum no one particular direction is to be chosen as that of the proper time.

The rest mass and the proper time thus appear as conjugate variables, with the corresponding uncertainty principle[12] $\Delta\kappa\Delta s\gtrsim 1$.

We have, now, for one particle under the influence of no forces

$$\mathcal{T}_{\mu 4}=i\kappa v_\mu(1-v^2)^{-\frac{1}{2}},$$
$$\mathcal{T}_{\mu 5}=\kappa v_\mu,$$
$$j_\mu=\int s_\mu dV=\epsilon v_\mu,$$
$$W_{00}=T_{55}=W(1-v^2),$$
$$\rho_0=s_5=\rho(1-v^2)^{\frac{1}{2}},$$

justifying the nomenclature "rest mass density" and "rest charge density" for W_{00}, ρ_0, respectively. We also have

$$E_{00}=\kappa(1-v^2)^{\frac{1}{2}}, \quad E=\kappa(1-v^2)^{-\frac{1}{2}}, \quad E_0=\kappa,$$

so that E_{00} is the relativistically decreased mass of the particle, j_5 the relativistically decreased charge $\epsilon(1-v^2)^{\frac{1}{2}}$. They are, of course, the volume integrals of W_{00}, ρ_0, respectively.

If all particles have the same rest-mass, the factor κ may be taken outside the summation

[11] Cf. J. Cattermole, Phil. Mag. [7] **33**, 215 (1942).

[12] This result appears also on Flint's theory (ref. 2). It is also a consequence of Mimura, "Wave geometry," J. Sci. Hiroshima, **A5**, No. 2, 99 (1935).

sign in (4.24)–(4.26), and if addition all particles have the same charge (say +) it follows as in section II that

$$\epsilon \mathcal{T}_{\mu 5} = \kappa j_\mu.$$

It also follows for both theories that $\partial_5 s_\mu = 0$ and in particular that $\partial_5 s_5 = 0$, so that the ordinary charge conservation law

$$\partial_k s_k = 0$$

is applicable. If the rest mass of all particles is identically zero we have for the scalar case

$$T_{5k} = 0, \quad W_{00} = T_{55} = -L, \quad s_5 = 0,$$

so that in general the rest mass density of the field is different from zero. The total rest mass in a given volume is of course zero, however. For the vector case with zero rest mass the fifth component of the current becomes, from (4.16),

$$s_5 = ei[U_\sigma^* \partial_\sigma U_5 - (\partial_\sigma U_5^*) U_\sigma],$$

which is in general zero only for real fields.

V. THE ELECTROMAGNETIC FIELD

The Lagrangian and symmetrical energy-momentum tensor for a real five-vector field are obtained from (4.10), (4.17) by writing

$$U_{\mu\nu}^* = U_{\mu\nu} = 2^{-\frac{1}{2}} f_{\mu\nu}; \quad U_\mu^* = U_\mu = 2^{-\frac{1}{2}} \varphi_\mu,$$

i.e.,

$$L = -\tfrac{1}{4} f_{\mu\nu} f_{\mu\nu} + \tfrac{1}{2} f_{\mu\nu} (\partial_\mu \varphi_\nu - \partial_\nu \varphi_\mu), \tag{5.1}$$

$$S_{\mu\nu} = f_{\mu\sigma} f_{\nu\sigma} - \tfrac{1}{4} f_{\sigma\tau} f_{\sigma\tau} \delta_{\mu\nu}. \tag{5.2}$$

Thus

$$f_{\mu\nu} = \partial_\mu \varphi_\nu - \partial_\nu \varphi_\mu, \tag{5.3}$$

$$\partial_\nu f_{\mu\nu} = 0. \tag{5.4}$$

We further postulate

$$\partial_\mu \varphi_\mu = 0. \tag{5.5}$$

We discuss here the particular case in which the particles associated with this field have zero rest mass. From (4.20′) it follows that the derivatives of all field functions with respect to x_5 are zero. Hence we may write

$$-\nabla \varphi_5 = \mathbf{F}, \quad \dot{\varphi}_5 = \theta$$

with

$$\nabla \cdot \mathbf{F} + \dot{\theta} = 0.$$

With the usual identifications of f_{kl} with the electromagnetic field strengths, we have associated with the field

energy density

$$W = -s_{44} = \tfrac{1}{2}(E^2 + H^2 + F^2 + \theta^2),$$

momentum density

$$\mathfrak{G} = -i s_{k4} = \mathbf{E} \times \mathbf{H} + \theta \mathbf{F},$$

rest energy density

$$W_{00} = s_{55} = \tfrac{1}{2}[E^2 - H^2 + F^2 - \theta^2], \tag{5.6}$$

rest momentum density

$$\mathfrak{G}_0 = s_{k5} = \mathbf{F} \times \mathbf{H} + \theta \mathbf{E},$$

total rest mass

$$E_0 = -i \int s_{54} dV = \int \mathbf{E} \cdot \mathbf{F} dV.$$

Without using (5.4), i.e., even if the field under consideration is not composed purely of vector and pseudoscalar photons, we may write, instead

$$\mathfrak{G}_0 = \varphi_5 (\nabla \times \mathbf{H} - \partial \mathbf{E} / \partial t),$$
$$W_0 = -i s_{54} = \varphi_5 \operatorname{div} \mathbf{E}. \tag{5.7}$$

For a pure field, of course, these vanish, but if we assume that $\mathbf{H}, \mathbf{E}$ satisfy the familiar Maxwell equations it follows that the total rest momentum and rest energy within a volume is

$$\mathbf{G}_0 = \int \varphi_5 \mathbf{j} dV, \quad E_0 = \int \rho \varphi_5 dV.$$

Thus in general charge and current distributions cannot exist unless there is associated with them intrinsic energy. In particular, a particle of charge e in a pseudoscalar field φ_5 has associated with it an extra rest mass $e\varphi_5$. The potential φ_5 is thus seen to modify the intrinsic energy of a particle, which according to this theory is not constant under all conditions. It does not appear possible, however, to use φ_5 to describe gravitational potential even approximately.

We discuss the interaction between fields described in this manner in a later paper.

My thanks are due the Melbourne "Herald" for financial assistance during the preparation of this paper.

PHYSICAL REVIEW VOLUME 70, NUMBERS 11 AND 12 DECEMBER 1 AND 15, 1946

Theory of Dipole Interaction in Crystals *

J. M. LUTTINGER AND L. TISZA
Research Laboratory of Electronics, Massachusets Institute of Technology, Cambridge, Massachusetts

(Received July 17, 1946)

It is shown that dipole arrays may be represented as vectors in a many-dimensional vector space. The classical dipole interaction energy is a quadratic form in the components of the dipole moments. Its calculation is reduced to the diagonalization of this form. The characteristic vectors are so called basic arrays. An arbitrary array may be decomposed into a linear combination of basic arrays, the energies are additive and may be obtained from the characteristic values of the quadratic form. The method is demonstrated by the complete solution of the characteristic value problem of a highly symmetric class of cubic arrays. The minimum energy arrays are obtained without and with an external magnetic field for the simple cubic, body-centered cubic, and face-centered cubic lattices. The results are in good qualitative agreement with the experiments of de Haas and Wiersma on Cs Ti alum. Some discrepancies are attributed to quantum effects and to incomplete saturation (entropy $S>0$). The extension to these more general cases will be considered in a following paper.

I. INTRODUCTION

VARIOUS problems in the theory of solids lead to the consideration of interaction among dipoles. Typical examples are the dielectric and thermal behavior of certain crystals containing polar molecules and of most of the substances used in experiments on adiabatic demagnetization.

The paramagnetic substances which are suitable for these experiments contain magnetic moments whose freedom of orientation is restricted by the weakest possible interaction. This requirement is satisfied by magnetic ions containing an odd number of electrons. In fact, a theorem of Kramers[1] states that magnetic ions consisting of an odd number of electrons maintain a double degeneracy in any electrostatic field, and therefore the usually important crystalline Stark effect is ineffective in this case. However, Nernst's theorem requires that some mechanism should exist for removing this degeneracy and the splitting actually is a result only of the weaker forces from the direct coupling between spins. This coupling arises from the magnetic (dipole) forces, or to some extent from exchange forces. The dipole coupling is certainly more important. Moreover, in contrast to most types of interaction, it contains no unknown constants relating to atomic or crystalline structure. Thus the calculation of the magnetic interaction energies and of the partition sum is of added interest.

The present state of the theory of the dipole interaction is rather unsatisfactory. The simplest approach is the Lorentz field method whose shortcomings are well known.[2] That the magnetization is not the only factor in determining the internal field is most clearly visible from the calculations of Sauer[3] who computed the energies of certain intuitively selected dipole arrays and found that ordered arrays of zero magnetization may have widely different energies, some of them lower than that due to the Lorentz field. Sauer's calculation is valid only for absolute zero and vanishing external field.

A consistent theory has been developed by Van Vleck[2] who expands the partition sum of the crystal in decreasing powers of the temperature. This calculation fails at low temperatures where the interaction becomes really important.

Other attempts have been made to develop a theory for all values of the field and temperature[4] with no satisfactory results. The reason seems to be that all attempts were based on some kind of "nearest neighbor" method. However, the

* This paper is based in part on work done for the Office of Scientific Research and Development under contract OEMsr-262 with the Massachusetts Institute of Technology.

[1] H. A. Kramers, Proc. Amsterdam Acad. **33**, 959 (1930).

[2] Cf. J. H. Van Vleck, J. Chem. Phys. **5**, 320 (1937) and Ann. N. Y. Acad. Sci. **40**, 293 (1940).

[3] J. A. Sauer, Phys. Rev. **57**, 142 (1940).

[4] E.g. J. A. Sauer—A. N. V. Temperley, Proc. Roy. Soc. **176**, 203 (1940).

dipole interaction lends itself particularly badly to such kind of treatment. In the first place, the forces are of comparatively long range and even more important, their peculiar directional dependence makes the averaging over the directions inadequate.

The main point of the present paper is the use of a simple and rigorous "normal coordinate" method rather than the clearly inadequate "nearest neighbor" treatment of dipole interactions.

It will be shown in Section II that dipole arrays can be represented as vectors in a many dimensional space $\mathfrak{R}$. The dipole interaction energy appears as a quadratic form in the vector components of the dipole moments.

Thus the whole calculation is reduced to a characteristic value problem, the solution of which is greatly facilitated if the symmetry of the problem allows the application of group theory. The characteristic vectors will be called basic arrays (B.A.), their energies are the characteristic values of the quadratic form. The energy of any arbitrary array can be obtained by means of decomposition into a linear combination of basic arrays, as the energies of the arrays are additive. The arrays of minimum energy may also be obtained in a systematic manner.

The method is demonstrated by the complete solution of the problem for a very symmetrical class of simple cubic (S.C.) arrays (Section II). The results are extended to the body-centered (B.C.) and face-centered (F.C.) cubic arrays in Section IV. The numerical calculations are indicated and their results tabulated in Section III.

As the class of arrays considered in this paper is highly ordered, the results can be applied for real crystals only in case of vanishing entropy. These conditions are approximately realized for demagnetization experiments from high initial fields. Comparison with experiment is discussed in VI. Quantum effects and the extension to more general arrays will be discussed in a following paper.

II. VECTOR SPACE REPRESENTATION OF DIPOLE ARRAYS

Let us first consider S.C. dipole arrays obtained from S.C. lattices by placing a dipole of definite moment and direction at every lattice point (l.p.).

Dimensionless quantities will be used throughout this paper. Dipole moments will be measured in terms of an arbitrary dipole moment μ, length in terms of the lattice constant a. All magnetic (or electric) fields will be expressed in units of μ/a^3 and energies per unit volume in terms of $N^2\mu^2$ where N is the number of dipoles per unit volume. In the S.C., B.C., and F.C. cases one has $N=1/a^3$, $2/a^3$, $4/a^3$, respectively.

As indicated in the introduction, only ordered arrays will be considered in the present paper. A precise definition of an "ordered array" can be given by making use of the symmetry of the array. Let Γ be the group of cubic translations $l_1\mathbf{i}+l_2\mathbf{j}+l_3\mathbf{k}$ (l_1, l_2, l_3 are integers, $\mathbf{i}, \mathbf{j}, \mathbf{k}$, are unit vectors in the x, y, z direction).

The most completely ordered array is invariant under the same group, i.e., all its dipoles are equal and parallel. This array is of importance in building up others and will be called an S array. The dipole interaction energy of an S array is $-\frac{1}{2}(4\pi/3-l)$ where l is the demagnetization coefficient. For a spherical sample $l=4\pi/3$ and the energy vanishes.

A more general class of ordered arrays is obtained if invariance is required only under the subgroup Γ^2 of Γ consisting of the translations of the form $l_1(2\mathbf{i})+l_2(2\mathbf{j})+l_3(2\mathbf{k})$. Such arrays are said to be of the class Γ^2 and will be the only ones considered in this paper.[5]

To generate such arrays we have to specify 8 dipoles $\mathbf{p}^\nu$ ($\nu=1, 2, \cdots 8$), where ν is associated in some definite manner with corners of the unit cube having the coordinates $l_1, l_2, l_3=0, 1$. The whole array is constructed by the translations Γ^2.

The resulting array may be considered as a superposition of eight arrays each of which consists of parallel dipoles. These arrays are geometrically similar to the S arrays previously introduced, but have a lattice constant two (in units of a). These shall also be called S arrays;

[5] There are very good reasons to believe that the configurations of lowest (and highest) energy are of the class Γ^2. All arrays calculated previously[3] are of this class. No rigorous proof of this statement seems to be possible, however, before the investigation of the more general arrays has been carried out. We hope to come back to this question in a sequel to this paper.

in case of ambiguity the lattice constant will be specified. This point of view will be useful for the numerical calculations of Section III.

It is seen that every array of class Γ^2 can be specified by a set of 24 numbers, e.g., the three rectangular components of the 8 dipole moments p_x^ν, p_y^ν, p_z^ν $\nu=1, 2, \cdots 8$. Also, in a more concise notation p_i, $i=1, 2, \cdots 24$.

In the cases of practical interest the dipoles placed at the 8 cube corners will have moments of the same absolute value which will be denoted by p. For such an array the 24 numbers satisfy the 8 conditions:

$$(p_x^\nu)^2+(p_y^\nu)^2+(p_z^\nu)^2=p^2, \quad \nu=1, 2, \cdots 8. \quad (1)$$

It will, however, prove advantageous to temporarily disregard these conditions and admit arrays of unequal dipole moments into the class Γ^2. In this case every set of 24 real numbers defines a Γ^2 array and there is a one to one correspondence between these arrays and the points of a 24-dimensional vector space $\mathfrak{R}$. The arrays satisfying the conditions (1) will be called arrays of constant (dipole) strength p.[6] The corresponding points form a 16-dimensional hypersurface in $\mathfrak{R}$. This will be frequently used in what follows and will be briefly called the "constant dipole surface."

The operations of addition, multiplication with a scalar and taking the scalar product are defined in the usual manner.[7]

$$\begin{aligned} &\text{(a)} \quad \mathbf{P}+\mathbf{Q}=\{\mathbf{p}^\nu+\mathbf{q}^\nu\}, \\ &\text{(b)} \quad c\mathbf{P}=\{c\mathbf{p}^\nu\}, \\ &\text{(c)} \quad \mathbf{P}\cdot\mathbf{Q}=\sum_{\nu=1}^{8}\mathbf{p}^\nu\cdot\mathbf{q}^\nu. \end{aligned} \quad (2)$$

The square of the *norm* of an array $\mathbf{P}$ is defined as

$$\mathbf{P}\cdot\mathbf{P}=\sum_{\nu=1}^{8}(\mathbf{p}^\nu)^2. \quad (3)$$

If the array $\mathbf{P}$ is of constant strength p, its norm is $8^{\frac{1}{2}}p$.

In order to compute the energy of an array $\mathbf{P}$ it is necessary to know the field generated by $\mathbf{P}$ at all the lattice points. Obviously, the field will have the same symmetry (Γ^2) as the array. Hence the set of vectors representing the field *at the lattice points* will again correspond to a vector in the space $\mathfrak{R}$, and will be denoted by $\mathbf{F}$.

The operation leading from any array $\mathbf{P}$ to its field $\mathbf{F}$ can be regarded as a mapping of the space $\mathfrak{R}$ on itself. One may write symbolically

$$\mathbf{F}=\mathfrak{F}\mathbf{P} \quad (4)$$

where $\mathfrak{F}$ is the "field operator." It is linear, as follows at once from the well-known expression for the field $\mathbf{f}$ of a dipole $\mathbf{p}$ at a point $\mathbf{r}$:

$$\mathbf{f}=(3\mathbf{r}(\mathbf{p}\cdot\mathbf{r})-\mathbf{p}r^2)/r^5. \quad (5)$$

The dipole interaction energy per unit volume is[8]

$$U=-(1/16)\mathbf{P}\cdot\mathbf{F}=-(1/16)\mathbf{P}\cdot\mathfrak{F}\mathbf{P}. \quad (6)$$

Equation (6) is an invariant relation independent of the choice of coordinate system. If, as above, we choose a coordinate system in which the array is represented by the rectangular components of the 8 dipole moments then one may rewrite Eq. (6) in matrix form:

$$U=-(1/16)\sum_{\mu,\nu=1}^{8}\sum_{x,y}\mathfrak{F}_{\mu\nu}{}^{xy}p_x p_y. \quad (7)$$

The matrix $\mathfrak{F}_{\mu\nu}{}^{xy}$ satisfies the symmetry relation

$$\mathfrak{F}_{\mu\nu}{}^{xy}=\mathfrak{F}_{\nu\mu}{}^{yx}. \quad (8)$$

This is a direct consequence of the existence of a potential energy for two dipoles; the energy can be considered as scalar product of the first dipole moment with the field due to the second, or *vice versa*.

It is sometimes convenient to write (7) and (8) in a more concise form by replacing the index couple μ, x by a single index i running from 1 to 24.

One has[9]

$$U=-(1/16)\sum_{i,j=1}^{24}\mathfrak{F}_{ij}p^i p^j. \quad (7a)$$

[6] The dipole strength of our array should be distinguished from its resultant dipole moment. The latter is proportional to the vector sum of the moments of the 8 cube corners.

[7] Boldfaced small letters will denote ordinary 3-dimensional vectors and boldfaced capital letters vectors in the 24-dimensional vector space.

[8] The numerical factor in this expression is explained as follows: the energy per unit volume is in our units the energy of one dipole, while (6) involves 8 dipoles. The additional factor $\frac{1}{2}$ corrects in the usual manner the fact that the interaction of every pair of dipoles is counted twice.

[9] In case of vectors in the space $\mathfrak{R}$ superscripts describe components and subscripts distinguish between different vectors.

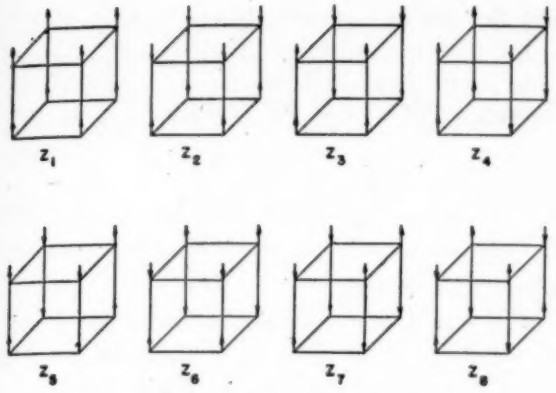

FIG. 1. The eight basic arrays. Interchange the labels Z_3 and Z_4.

The quadratic form (7) can be transformed into a sum of squares by means of an orthogonal transformation of the coordinate system in $\mathfrak{R}$ which leaves (3) invariant (rotation). The new coordinate system will be given by an orthogonal set of vectors $\mathbf{A}_i$, $i=1, 2, \cdots 24$, which will be called basic arrays (B.A.). These are closely analogous to the normal coordinates introduced for the description of vibrating systems. The calculation of the energy of an arbitrary array can then be reduced to finding the characteristic values of the operator $\mathfrak{F}$. This problem is greatly facilitated by group theoretical methods, based on the remark that the operator $\mathfrak{F}$ is invariant under the group $\mathbf{\Gamma}$.[10]

$$\Gamma\mathfrak{F}=\mathfrak{F}\Gamma. \tag{9}$$

This relation is intuitively evident, as it is immaterial whether a translation $\mathbf{\Gamma}$ is carried out on a field $\mathbf{F}$, or on a corresponding array $\mathbf{P}$ and the mapping leading to the field is carried out afterwards.

It follows from (9) by standard methods used in case of other linear operators (Schroedinger operator, vibrating systems) that the eigenvectors can be so chosen as to transform according to irreducible representations of the group $\mathbf{\Gamma}$.[11]

It may be remarked that so far no essential use has been made of the fact that the arrays $\mathbf{P}$ are of the class $\mathbf{\Gamma}^2$. If instead of $\mathbf{\Gamma}^2$ another sub-group of $\mathbf{\Gamma}$ had been chosen, the only difference in the above considerations would be that the number of dimensions of the space $\mathfrak{R}$ would be larger than 24. The formulae (1)–(9) will form the basis for a second paper, in which more general arrays will be discussed.

The actual solution of the eigenvalue problem is considerably simpler, however, for the class $\mathbf{\Gamma}^2$ than for the general classes.

A $\mathbf{\Gamma}^2$ array consisting of dipoles all pointing in, say, the x direction gives rise to fields at the l.p. pointing in the same direction, i.e.,

$$\mathfrak{F}_{\mu\nu}{}^{xy}=0 \text{ unless } x=y. \tag{10}$$

This is caused by the fact that a $\mathbf{\Gamma}^2$ array is invariant under a mirroring $y\rightarrow -y$, while the expression of the y component of the field consists of terms proportional to xy and thus changes sign.

In addition, because of the cubic rotational symmetry

$$\mathfrak{F}_{\mu\nu}{}^{zz}=\mathfrak{F}_{\mu\nu}{}^{yy}=\mathfrak{F}_{\mu\nu}{}^{xx}. \tag{11}$$

Thus the 24-dimensional matrix is reduced to three identical 8×8 matrices.

It is well known that the representations of the group $\mathbf{\Gamma}$ are the roots of unity. In the case of $\mathbf{\Gamma}^2$ arrays the relevant roots are the square roots $+1$ and -1. One is thus led uniquely to a definition of the B.A. which will be given now. The fact that they are B.A., i.e., characteristic vectors of the operator $\mathfrak{F}$ can be easily verified without any reference to group theory.

Corresponding to the reduction of the matrix $\mathfrak{F}$ into 3 identical 8 row matrices, the 24, B.A. fall into 3 groups, $\mathbf{X}_i$, $\mathbf{Y}_i$, $\mathbf{Z}_i$, $i=1, 2, \cdots 8$ consisting of dipoles pointing in the x, y, z directions, respectively.

The 8 non-vanishing components of the $\mathbf{Z}_i$ arrays are given by

$$Z_i=(-1)_{\alpha_i l_1+\beta_i l_2+\gamma_i l_3}, \quad i=1, 2, \cdots 8, \tag{12}$$

where α_i, β_i, $\gamma_i=0$, 1. It may be recalled that the superscripts are associated with the 8 cube corners l_1, l_2, $l_3=0$, 1. One has the following 8 possibilities:

	α	β	γ		α	β	γ
Z_1	0	0	0	Z_5	1	1	0
Z_2	0	0	1	Z_6	0	1	1
Z_3	1	0	0	Z_7	1	0	1
Z_4	0	1	0	Z_8	1	1	1

[10] In fact, it is invariant also under the group including the cubic rotations. However, this will be of no importance in the special case considered in the present paper.

[11] Cf. for instance B. L. van der Waerden, *Die Gruppentheoretische Methode in der Quanten Mechanik* (Edwards Brothers, New York, 1944). E. Wigner, Goettinger Nachrichten, p. 133 (1930).

These arrays are explicitly given in Fig. 1. $\mathbf{X}_i$ and $\mathbf{Y}_i$ are obtained from $\mathbf{Z}_i$ through cubic rotations, so that identical subscripts refer to identical geometric arrangements. Being basic arrays the $\mathbf{Z}_1 \cdots \mathbf{Z}_8$ are orthogonal. They obey the relations:

$$\mathbf{Z}_i \cdot \mathbf{Z}_j = 8\delta_{ij}, \tag{13}$$

and similarly the $\mathbf{X}_i$ and $\mathbf{Y}_i$.

Equation (13) can be verified either by means of Fig. 1 or algebraically as follows:

$$\mathbf{Z}_i \cdot \mathbf{Z}_j = \sum_{\nu=1}^{8} Z_i^{\nu} Z_j^{\nu}$$

$$= \sum (l_1, l_2, l_3 = 0, 1)(-)^{(\alpha_i+\alpha_j) l_1 + (\beta_i+\beta_j) l_2 + (\gamma_i+\gamma_j) l_3}.$$

If $i \neq j$, then at least one of the inequalities holds: $\alpha_i \neq \alpha_j$, $\beta_i \neq \beta_j$, $\gamma_i \neq \gamma_j$. Say $\alpha_i \neq \alpha_j$, then $\alpha_i + \alpha_j = 1$ and $\mathbf{Z}_i \cdot \mathbf{Z}_j = 0$, because of the summation over l_1.

$\mathbf{X}_i$, $\mathbf{Y}_i$, $\mathbf{Z}_i$ form a complete set of 24 orthogonal vectors and are the only ones which have the correct transformation properties. Hence they solve the eigenvalue problem:[12]

$$\mathfrak{F}\mathbf{X}_i = f_i \mathbf{X}_i, \quad \mathfrak{F}\mathbf{Y}_i = f_i \mathbf{Y}_i, \quad \mathfrak{F}\mathbf{Z}_i = f_i \mathbf{Z}_i. \tag{14}$$

Because of the completeness, every Γ^2 array $\mathbf{P}$ can be represented as

$$\mathbf{P} = \sum_{i=1}^{8} (a_i \mathbf{X}_i + b_i \mathbf{Y}_i + c_i \mathbf{Z}_i) \tag{15}$$

with $a_i = \frac{1}{8}\mathbf{P} \cdot \mathbf{X}_i$, $b_i = \frac{1}{8}\mathbf{P} \cdot \mathbf{Y}_i$, $c_i = \frac{1}{8}\mathbf{P} \cdot \mathbf{Z}_i$. The square of the norm of $\mathbf{P}$ is obtained in terms of the new coordinates from (3), (15) and the orthogonality relations:

$$\mathbf{P} \cdot \mathbf{P} = 8 \sum_{i=1}^{8} (a_i^2 + b_i^2 + c_i^2). \tag{16}$$

The factor 8 arises because the B.A. are normalized to have the dipole strength unity, and hence have the norm $8^{\frac{1}{2}}$. The field corresponding to $\mathbf{P}$ is

$$\mathbf{F} = \sum_{i=1}^{8} (a_i f_i \mathbf{X}_i + b_i f_i \mathbf{Y}_i + c_i f_i \mathbf{Z}_i), \tag{17}$$

and the energy per unit volume

$$U = -\tfrac{1}{2} \sum_{i=1}^{8} (a_i^2 + b_i^2 + c_i^2) f_i$$

$$= \sum_{i=1}^{8} (a_i^2 + b_i^2 + c_i^2) U_i, \tag{18}$$

where $U_i = -f_i/2$.

It is seen that the computation of the energy of any Γ^2 array is reduced to the knowledge of the characteristic values f_i. These have been computed by a method outlined in the next section and the values are to be found in Table II.

From the point of view of practical application there is also a somewhat different problem to be considered: given a S.C. crystal with dipoles of constant moment (taken as unity), but undetermined orientation, what is the Γ^2 array of lowest energy? Or, in the terminology introduced above: find the minimum value of the energy (18) for arrays lying on a given constant dipole surface. These arrays satisfy the 8 auxiliary conditions (1) which can be rewritten in terms of B.A. as follows:

$$\left(\sum_{i=1}^{8} a_i \mathbf{X}_i^{\nu}\right)^2 + \left(\sum_{i=1}^{8} b_i \mathbf{Y}_i^{\nu}\right)^2 + \left(\sum_{i=1}^{8} c_i \mathbf{Z}_i^{\nu}\right)^2 = 1, \tag{19}$$

$$\nu = 1, 2, \cdots 8.$$

The standard procedure accounting for the auxiliary conditions by the method of Lagrange multipliers proves to be very cumbersome. The following artifice yields the desired result without any further calculation, not only in the simple case considered here, but also in some of the more complicated cases discussed in Sections IV and V: The condition of constant dipole strength unity implies that the norm of the array is $8^{\frac{1}{2}}$, or, using (16),

$$\sum_{i=1}^{8} (a_i^2 + b_i^2 + c_i^2) = 1. \tag{20}$$

The conditions (19) imply (20), but not *vice versa*. Therefore they will be called briefly the strong and the weak conditions, respectively.

[12] Equation (14) could be easily verified directly using the explicit expressions of Section III.

The procedure consists in minimizing the energy (18) under the weak condition alone. This can be done at once by means of the well-known extremum property of the characteristic values.[13]

The lowest value of the energy is $-f_m/2$ where f_m is the greatest characteristic value of the operator $\mathfrak{F}$. The array is a linear combination of the B.A. corresponding to f_m. If some of these linear combinations satisfy the strong conditions, then the original problem is solved.

It is seen from Table II that the lowest energy for the S.C. lattice is $-f_5/2=-2.676$. The corresponding array is $a_5\mathbf{X}_5+b_5\mathbf{Y}_5+c_5\mathbf{Z}_5$ with $a_5^2+b_5^2+c_5^2=1$. It is easily seen that this array satisfies the strong condition and represents the correct solution of the problem.

III. CALCULATION OF THE FIELDS

The object of this section is the computation of the characteristic values f_i defined in the preceding section. According to its definition f is the value of the field of the ith B.A. say $\mathbf{Z}_i$ at a lattice point. It was pointed out at the beginning of Section II that any $\mathbf{\Gamma}^2$ array (and thus in particular $\mathbf{Z}_i$) can be considered as a superposition of eight S arrays of lattice constant two. Hence, the field at any point of a B.A. will be known as soon as the field of an S array is known at every point. We shall denote the field of a z directed S array as[14] $\mathbf{S}(\mathbf{r})$, $\mathbf{r}$ being the location of the point in question.

Using the expression (5) for the field of a dipole we arrive at the following equations for the x, y, and z components

$$S_x(\mathbf{r})=\sum_{-\infty}^{\infty}{}_{\{l_1,l_2,l_3\}}\frac{3(l_1-x)(l_3-z)}{[(l_1-x)^2+(l_2-y)^2+(l_3-z)^2]^{5/2}},$$

$$S_y(\mathbf{r})=\sum_{-\infty}^{\infty}{}_{\{l_1,l_2,l_3\}}\frac{3(l_2-y)(l_3-z)}{[(l_1-x)^2+(l_2-y)^2+(l_3-z)^2]^{5/2}}, \tag{21}$$

$$S_z(\mathbf{r})=\sum_{-\infty}^{\infty}{}_{\{l_1,l_2,l_3\}}\frac{2(l_3-z)^2-(l_1-x)^2-(l_2-y)^2}{[(l_1-x)^2+(l_2-y)^2+(l_3-z)^2]^{5/2}}.$$

Using the function $\mathbf{S}(\mathbf{r})$ (which we shall call the "characteristic function"), we may write the field $\mathbf{H}_i$ at any point $\mathbf{r}$ of $\mathbf{Z}_i$ explicitly as

$$\mathbf{H}_i(\mathbf{r})=\tfrac{1}{8}\sum_{\{l_1,l_2,l_3=0,1\}}(-)^{\alpha_i l_1+\beta_i l_2+\gamma_i l_3}\times\mathbf{S}\left(\frac{l_1-x}{2},\frac{l_2-y}{2},\frac{l_3-z}{2}\right), \tag{22}$$

where α_i, β_i, γ_i correspond to the B.A. $\mathbf{Z}_i$. The $\frac{1}{2}$ in the argument of the characteristic function and the $\frac{1}{8}$ multiplying the entire expression arise from the fact that the characteristic function is defined for an S array with lattice constant unity, while the component S arrays of a B.A. have lattice constant equal to two. Thus the question of finding the characteristic values is reduced to the knowledge of the values of the function S at the points with coordinates having half integral values.

It will be seen in the next section that the solution of the characteristic value problem for the B.C. and F.C. lattices necessitates the knowledge of the field in the body centers and face centers. These may also be obtained provided a few more values of the function $\mathbf{S}(\mathbf{r})$ are computed.

In the actual computation of the fields full use is made of symmetry considerations, which show that at many points the field is zero, or is simply related to the field at other points. As a typical example, we shall show that the field of $\mathbf{Z}_6$ at a lattice point is minus one-half the field of $\mathbf{Z}_5$ at a lattice point. From the expression for the dipole interaction (5) and the definition of the

[13] C.f. for example, Courant-Hilbert, *Methoden d. Mathematischen Physik* (Verlagsbuchhandlung Julius Springer, Berlin, 1931), Vol. I, p. 26.

[14] $\mathbf{S}(\mathbf{r})$ is a spatial vector point function of the points r within the unit cell, and should not be confused with the 24 dimensional vectors representing the field *at the lattice points*.

TABLE I. Values of the fields. The values given for Z_1 are valid for spherical samples. Otherwise $((4\pi/3)-l)Z_1$ should be added to every term in the first line. l is the demagnetization coefficient. The numerical values of f_i, g, h_i are to be found in Table II.

Array	Field at l.p.	Field at B.C.	Fields at F.C. *XY* Face	*YZ* Face	*ZX* Face
Z_1	0	0	$-2h_1Z_1$	h_1Z_1	h_1Z_1
Z_2	f_2Z_2	0	$-2h_2Z_2$	0	0
Z_3	f_3Z_3	0	0	h_2Z_3	0
Z_4	f_4Z_4	0	0	0	h_2Z_4
Z_5	f_5Z_5	0	0	0	0
Z_6	f_6Z_6	gY_7	0	h_3Y_7	0
Z_7	f_7Z_7	gX_6	0	0	h_3X_6
Z_8	0	0	0	h_4Y_8	h_4X_8

basic arrays one easily finds

$$H_{5z}(0,0,0)=\sum'\frac{2l_3^2-l_1^2-l_2^2}{(l_1^2+l_2^2+l_3^2)^{5/2}}(-)^{l_1+l_2}, \quad (23)$$

$$H_{6z}(0,0,0)=\sum'\frac{2l_3^2-l_1^2-l_2^2}{(l_1^2+l_2^2+l_3^2)^{5/2}}(-)^{l_1+l_2}; \quad (24)$$

noticing that l_1 and l_2 enter into (23) in the same manner, we get

$$H_{5z}=2\sum'\frac{l_3^2-l_2^2}{(l_1^2+l_2^2+l_3^2)^{5/2}}(-)^{l_1+l_2}.$$

Interchanging[15] l_1 and l_3 in (24) we get

$$H_{6z}=\sum'\frac{2l_1^2-l_3^2-l_2^2}{(l_1^2+l_2^2+l_3^2)^{5/2}}(-)^{l_1+l_2}$$

$$=\sum'\frac{l_2^2-l_3^2}{l_1^2+l_2^2+l_3^2}(-)^{l_1+l_2}=-\tfrac{1}{2}H_{5z}$$

which is the required result.

Many other relationships exist, connecting the different fields at the body centers with each other, connecting different lattice point fields, different face-center fields, etc. By means of these relationships it is possible to calculate the fields at the lattice points, body centers, and face centers of a B.A. by computing only six different values of the characteristic function $\mathbf{S}(\mathbf{r})$. These are $S_z(\frac{1}{2},0,0)$, $S_z(0,\frac{1}{2},\frac{1}{2})$, $S_y(\frac{1}{4},\frac{1}{4},\frac{1}{4})$, $S_z(0,\frac{1}{4},\frac{1}{4})$, $S_y(0,\frac{1}{4},\frac{1}{4})$, $S_y(\frac{1}{2},\frac{1}{4},\frac{1}{4})$. It is clear that others could have been chosen, but these turn out to be convenient. Table I gives all the fields expressed in terms of these fields. The numerical values of the first three have been taken from a paper of McKeehan,[16] while the others have been calculated using the Ewald[17] method. A check on our values may be obtained from McKeehan since it is possible to evaluate $S_y(0,\frac{1}{4},\frac{1}{4})-S_y(\frac{1}{2},\frac{1}{4},\frac{1}{4})$ from his tables. The agreement is excellent. The values of these fields are:

$$S_z(\tfrac{1}{2},0,0)=15.040, \quad S_z(0,\tfrac{1}{4},\tfrac{1}{4})=31.521,$$
$$S_z(0,\tfrac{1}{2},1)=4.334, \quad S_y(0,\tfrac{1}{4},\tfrac{1}{4})=2.599,$$
$$S_y(\tfrac{1}{4},\tfrac{1}{4},\tfrac{1}{4})=10.620, \quad S_y(\tfrac{1}{2},\tfrac{1}{4},\tfrac{1}{4})=12.329.$$

Tables I and II give the resulting values of all the fields.

TABLE II. Characteristic values f, g, and h.

$f_2=$	$\frac{1}{2}[S_z(0,\frac{1}{2},\frac{1}{2})-S_z(\frac{1}{2},0,0)]$	$=-9.687$
$f_3=-\frac{1}{2}[S_z(0,\frac{1}{2},\frac{1}{2})-S_z(\frac{1}{2},0,0)]$		$=4.844$
$f_4=-\frac{1}{2}[S_z(0,\frac{1}{2},\frac{1}{2})-S_z(\frac{1}{2},0,0)]$		$=4.844$
$f_5=-\frac{1}{2}[S_z(0,\frac{1}{2},\frac{1}{2})+S_z(\frac{1}{2},0,0)]$		$=5.351$
$f_6=\frac{1}{2}[S_z(0,\frac{1}{2},\frac{1}{2})+S_z(\frac{1}{2},0,0)]$		$=-2.676$
$f_7=\frac{1}{2}[S_z(0,\frac{1}{2},\frac{1}{2})+S_z(\frac{1}{2},0,0)]$		$=-2.676$
$g=$	$S_y(\frac{1}{4},\frac{1}{4},\frac{1}{4})$	$=10.620$
$h_1=$	$S_z(0,\frac{1}{2},\frac{1}{2})$	$=4.334$
$h_2=$	$S_z(0,\frac{1}{4},\frac{1}{4})-S_z(0,\frac{1}{2},\frac{1}{2})$	$=7.992$
$h_3=$	$\frac{1}{2}[S_y(0,\frac{1}{4},\frac{1}{4})+S_y(\frac{1}{2},\frac{1}{4},\frac{1}{4})]$	$=17.065$
$h_4=$	$\frac{1}{2}[S_y(0,\frac{1}{4},\frac{1}{4})-S_y(\frac{1}{2},\frac{1}{4},\frac{1}{4})]$	$=14.461$

IV. BODY-CENTERED AND FACE-CENTERED ARRAYS

It is convenient to consider the B.C. and F.C. arrays as consisting of two and four S.C. arrays, respectively, which can be resolved into B.A. In this representation the field matrix contains diagonal elements corresponding to the energies of the constituent S.C. arrays and off-diagonal elements giving the interaction of B.A. at different points. The interaction terms are listed in Tables I and II. It is apparent that most of the off-diagonal terms vanish and the energy of any B.C. or F.C. array can be readily computed. As an example, we have considered a set of

[15] Such procedures may be justified by transforming these series to absolutely convergent ones by means of the Ewald method. For details see J. Bouman, Archives Neerlandaises [3A], **13**, 1–28 (1931).

[16] L. W. McKeehan, Phys. Rev. **43**, 913 (1933). McKeehan gives values to five decimal places. However, by means of our symmetry relations we can check some of his values. While the agreement is generally very good, sometimes it does not extend beyond the third decimal place. The uncertain digits have been omitted.

[17] P. P. Ewald, Ann. d. Physik **64**, 253 (1921). See also H. Mueller, Phys. Rev. **50**, 547 (1936); M. Born and H. Kornfeld, Physik. Zeits. **24**, 121 (1923); and H. Kornfeld, Zeits. f. Physik **22**, 27 (1924).

arrays previously computed by Sauer.[3] Table III compares the energies resulting from the decomposition into B.A. with the values obtained by Sauer through direct summation.

This representation does not lead in any systematic way to the minimum energy configuration of an array of given dipole strength. The latter problem can be solved by completing the diagonalization of the field matrix and introducing B.A. in the 48- and 96-dimensional vector spaces corresponding to B.C. and F.C. arrays, respectively. Since most of the off-diagonal terms vanished in the above representation, this can be easily carried out. The procedure will be explained in detail for the B.C. case.

It is seen from Table II that if one of the B.A. $\mathbf{X}_i$, $\mathbf{Y}_i$, $\mathbf{Z}_i$ ($i \neq 6, 7$) is placed at the lattice points it gives rise to no field at the body center. Similarly, one of these arrays placed at the body centers will give rise to no field at the lattice points, as the lattice points and body centers are inter-changeable. Thus by placing $\mathbf{X}_i$ at the lattice points and nothing at the body centers, we obtain a B.A. and similarly placing $\mathbf{X}_i$ at the body centers and nothing at the lattice points will also give B.A. We now introduce the notation $[\mathbf{P}, \mathbf{Q}]$ to denote a B.C. array with $\mathbf{P}$ at the lattice points and $\mathbf{Q}$ at the body centers. The above B.A. will then be written as $[\mathbf{X}_i, \mathbf{O}]$ and $[\mathbf{O}, \mathbf{X}_i]$, respectively. Using the same process on $\mathbf{Y}_i$, $\mathbf{Z}_i$, we obtain four more B.A. $[\mathbf{Y}_i, \mathbf{O}]$, $[\mathbf{O}, \mathbf{Y}_i]$, $[\mathbf{Z}_i, \mathbf{O}]$, $[\mathbf{O}, \mathbf{Z}_i]$. These six B.A. all correspond to the same characteristic value f_i of the field operators $\mathfrak{F}$, therefore any set of six orthogonal linear combinations of these B.A. will also be B.A. In view of the considerations at the end of II, it is convenient to choose B.A. having constant dipole strength. Such a choice would be $[\mathbf{Z}_i, \mathbf{Z}_i]$ and $[\mathbf{Z}_i, -\mathbf{Z}_i]$ and similarly for $\mathbf{X}_i$, $\mathbf{Y}_i$.

The number 6 and 7 arrays require special consideration as they give rise to off-diagonal terms in the field matrix. In other words, there is an interaction between, for example, a $\mathbf{Z}_6$ array at the lattice points and a $\mathbf{Y}_7$ array at the body centers. The diagonalization is easily completed by choosing $[\mathbf{Z}_6, \mathbf{Y}_7]$ and $[\mathbf{Z}_6, -\mathbf{Y}_7]$ as B.A. The corresponding characteristic values are f_6+g and f_6-g. Similar B.A. are constructed from the other 6 and 7 arrays.

These results are summed up in Table IV.

The F.C. case can be discussed in exactly the same manner. The treatment is somewhat more complicated because of the presence of many more interaction terms. Only the results are given (Table V). In order to obtain the energy values in units of $N^2\mu^2$ one has to multiply the characteristic values of $\mathfrak{F}$ by $(-\frac{1}{4})$ in the B.C. case and $(-\frac{1}{8})$ in the F.C. case.

Since all the B.A. are defined so as to have a constant dipole strength, the minimum energy configurations are simply obtained by choosing the highest characteristic values from Tables IV and V. Hence, the minimum energy for the B.C. case is $-\frac{1}{4}(g+f_6)N^2\mu^2 = 1.986N^2\mu^2$ and for the F.C. case $-(h_4/8)N^2\mu^2 = -1.808N^2\mu^2$.

It may be noted that Sauer correctly guessed one of the minimum energy arrays in the S.C. and F.C. case, but not in the B.C. case.

Finally, the possibility of "ferromagnetism" for these arrays should be discussed. Summing up our results, we notice that in all cases the minimum energy configuration has been non-

TABLE III. Arrays calculated by Sauer. (Sauer's symbols are in the first column.)

Type	Resolution into basic arrays	Energy constants: Sauer	Energy constants: Present paper
"A"			
a	Z_5	−2.7	−2.676
b	Z_1 at l.p., $-Z_1$ at b.c.	0	0
c	$Z_5+X_7+Y_8$ at l.p. and b.c.	−1.75	−1.770
d	Z_1 at l.p. and XY f.c. $-Z_1$ at YZ and ZX f.c.	2.2	2.167
e	Z_1+Y_1 at l.p. and YZ f.c. $-Z_1-Y_1$ at XY and XZ f.c.	−1.1	−1.084
"B"			
a	Z_5	−2.7	−2.676
b	Z_5 at l.p., $-Z_5$ at b.c.	−1.35	−1.338
c	$Z_5+X_7+Y_8$ at l.p. and b.c.	−1.75	−1.770
d	Z_1 at l.p. and YZ f.c. $-Z_1$ at XY and XZ f.c.	−1.1	−1.084
e	Z_8+Y_8 at l.p., XY and YZ f.c. $-Z_8-Y_8$ at ZX f.c.	−1.8	−1.808

a is S.C., dipole direction 001
b is B.C., dipole direction 001
c is B.C., dipole direction 111
d is F.C., dipole direction 001
e is F.C., dipole direction 011
"A" is an array which has nearest neighbor strings of antiparallel dipoles
"B" is an array which has nearest neighbor strings of antiparallel dipoles if the dipoles are contained in a plane perpendicular to the dipole direction, and passing through the dipole.

polarized. This result, however, is true only for spherical samples. Otherwise one has to add a term $-\frac{1}{2}(4\pi/3-l)N^2\mu^2$ to the energy of the polarized number 1 arrays, for all three cubic types. In the extreme case of a very long thin needle $l=0$, and the energy constant becomes $-2\pi/3=-2.094$, while the energy constants of the lowest non-polarized arrays are for S.C. -2.675, for B.C. -1.986, and for F.C. -1.808. Thus the S.C. array is always non-ferromagnetic, while the other cases should exhibit ferromagnetism for long thin needles. In the case of a F.C. lattice cut in the form of a prolate spheroid the ferromagnetic state is favored above an axis ratio of 6:1. This result has been found before by Sauer.[3] Whether this ferromagnetic state has a physical reality is, however, subject to some doubt. This question is taken up once more in VI.

V. DIPOLE ARRAYS IN A MAGNETIC FIELD

The energy of a given Γ^2 array in a magnetic field is easily calculated. Considering first the S.C. case, one has:

$$U=-\tfrac{1}{2}\sum_{i=1}^{8} f_i(a_i^2+b_i^2+c_i^2)-(a_1H_x+b_1H_y+C_1H_z) -(4\pi/3-l)(a_1^2+b_1^2+c_1^2)/2, \quad (25)$$

since only the number 1 arrays have a resultant magnetic moment. Let us introduce the notation $a_1^2+b_1^2+c_1^2=q^2$, q being the magnetization of the array in units of $N\mu$. Denoting the angle between magnetization and external field by ϑ (25) becomes

$$U=-\tfrac{1}{2}\textstyle\sum_i f_i(a_i^2+b_i^2+c_i^2) -qH\cos\vartheta-(4\pi/3-l)q^2/2. \quad (26)$$

TABLE IV. Characteristic values and typical basic arrays in the B.C. case. Valid for spherical sample, otherwise, cf. Table I.

Characteristic value of $\mathfrak{F}$	Degree of degeneracy	Typical B.A. At lattice points	Typical B.A. At body centers
$f_1=f_8=$ 0	6	Z_1	Z_1
	6	Z_8	Z_8
$f_2=-$ 9.687	6	Z_2	Z_2
$f_3=f_4=$ 4.844	12	Z_3	Z_3
$f_5=$ 5.351	6	Z_5	Z_5
$f_6+g=$ 7.944	6	Z_6	Y_7
$f_6-g=-13.296$	6	Z_6	$-Y_7$

This expression should be minimized under the strong condition (19), which we again replace temporarily by the weak condition (20). In our present notation (20) takes the form:

$$\sum_{i=2}^{8}(a_i^2+b_i^2+c_i^2)+q^2=1 \quad (27)$$

We now minimize the energy at fixed q. From (26) we see that $\cos\vartheta=1$, i.e., the magnetization is parallel to the magnetic field. The minimization of the first term is exactly the problem solved at the end of II since $f_1=0$. The solution is

$$\mathbf{P}=a_1\mathbf{X}_1+b_1\mathbf{Y}_1+c_1\mathbf{Z}_1+a_5\mathbf{X}_5+b_5\mathbf{Y}_5+c_5\mathbf{Z}_5, \quad (28)$$

with $a_5^2+b_5^2+c_5^2=1-q^2$.

The energy becomes

$$U=-\tfrac{1}{2}(1-q^2)f_5-qH-(4\pi/3-l)q^2/2. \quad (29)$$

Equation (29) may now be minimized with respect to q: $\partial U/\partial q=0$ leads to

$$q=\frac{H}{f_5-(4\pi/3-l)}.$$

Defining a critical field H_c as

$$H_c=f_5-(4\pi/3-l) \quad (30)$$

and remembering that $q\leqq 1$, we have

$$q=\begin{cases} H/H_c & \text{for } H\leq H_c \\ 1 & \text{for } H\geq H_c. \end{cases} \quad (31)$$

In other words there exists a magnetic field H_c above which the magnetization is constant (saturation) and below which it drops to zero linearly with the field. It is recalled that the magnetization is given in units of $N\mu$.

Whether or not (28) is the correct solution is still dependent on whether it satisfies the strong conditions. This is generally not the case for an arbitrary direction of the magnetic field ($a_1\neq 0$, $b_1\neq 0$, $c_1\neq 0$). If, however, the magnetic field is along one of the cubic axis or in one of cubic planes, then the resulting array can be chosen to have constant dipole strength. For example, if the field is along the cubic axis, say in the Z direction, then the array

$$\mathbf{P}=a_5\mathbf{X}_5+b_5\mathbf{Y}_5+c_1\mathbf{Z}_1$$

satisfies all the requirements.

TABLE V. Characteristic values and typical basic arrays in the F.C. case. Valid for spherical samples, otherwise, cf. Table I.

Characteristic value of $\mathfrak{F}$	Degree of degeneracy	Typical B.A. with this characteristic value			
		At l.p.	At XY face	At YZ face	At ZX face
0	3	Z_1	Z_1	Z_1	Z_1
$-4h_1=-17.336$	3	Z_1	Z_1	$-Z_1$	$-Z_1$
$2h_1=8.668$	6	Z_1	$-Z_1$	Z_1	$-Z_1$
$f_2-2h_2=-25.671$	6	Z_2	Z_2	Z_2	$-Z_2$
$f_2+2h_2=6.297$	6	Z_2	$-Z_2$	Z_2	Z_2
$f_3+h_2=12.836$	12	Z_3	Z_3	Z_3	Z_3
$f_3-h_2=-3.148$	12	Z_3	Z_3	$-Z_3$	$-Z_3$
$f_5=5.351$	12	Z_5	Z_5	Z_5	Z_5
$f_6+h_3=14.389$	12	Z_6	Z_6	Y_7	$-Y_7$
$f_6-h_3=-19.741$	12	Z_6	Z_6	$-Y_7$	Y_7
$h_4=14.461$	4	Z_8	Z_8	Y_8	$-Y_8$
$h_4=14.461$	4	$2X_8+Y_8-Z_8$	$2X_8+Y_8-Z_8$	$2X_8+Y_8-Z_8$	$2X_8-Y_8+Z_8$
$-2h_4=-28.922$	4	$X_8-Y_8-Z_8$	$X_8-Y_8+Z_8$	$X_8+Y_8+Z_8$	$X_8+Y_8-Z_8$

Since in the general case the simple artifice of first ignoring the strong conditions does not work, one has to introduce (19) at the outset. This can be done by the method of Lagrange multipliers, but the resulting equations are very complicated and have not been solved. The case of physical interest is the F.C. array (paramagnetic alums), and here the simple method works once more.

The above considerations may be repeated for the F.C. case. Equations (25) through (31) are maintained provided the characteristic values and B.A. defined for the S.C. case for the space $\mathfrak{R}$ are replaced by the corresponding quantities in the 96-dimensional space. In particular the energy constant $-f_5/2$ should be replaced by $-h_4/8$. The minimum energy array under the weak condition is a superposition of the polarized B.A. and those belonging to the characteristic value h_4. Here, however, the formal identity ceases. Actually, the situation is more favorable than in the S.C. case as the strong conditions may now be satisfied for an arbitrary magnetic field. The array which satisfies the strong conditions is a superposition of the polarized arrays and those arrays belonging to the second class of h_4 arrays given in Table V. In the case $H_0 \leq 0$ ferromagnetism will exist. Cf. IV.

VI. DISCUSSION

The main purpose of the present paper is to demonstrate the application of the proposed method and to lay the groundwork for generalizations. These would include, first of all, a treatment of the statistical mechanics of dipole arrays which requires the discussion of more general arrays than those of the class Γ^2, and a method of evaluating the partition sum in terms of them. The statistical problem must be solved before the theory may be applied to cases in which the entropy is finite (not equal to zero) such as is found for the hydrogen halide crystals in the neighborhood of their phase transition.

The ordered arrays of class Γ^2 should, however, be expected to give an adequate description of paramagnetic crystals containing ions with one valence electron (Ti, for example) in a state of zero entropy. Such a state is realized to a high degree of approximation for the entire process of adiabatic demagnetization with high initial fields. Although in reality the spin system should be treated quantum mechanically, it may be expected that the present classical method will give the essential features. A rigorous quantum treatment in which the Hamiltonian is set up in terms of the Pauli spin matrices is being planned for a sequel to this paper.

The computation of the magnetization curve in V will now be compared with the measurements of de Haas and Wiersma[18] on Cs–Ti alum. The salient feature of these experiments is that the magnetization stayed constant from $H=24{,}000$ gauss (approximately 90 percent saturation) to a field of about 100 gauss, and then dropped to zero almost linearly with the

[18] W. J. de Haas and E. C. Wiersma, Physica **3**, 491 (1936); cf. also H. B. O. Casimir, *Magnetism and Very Low Temperatures* (Cambridge University Press, England, 1940), p. 74.

field. This behavior is in excellent agreement with the results of Section V. The calculation leads to a critical field of $H_c = 65$ gauss which is the correct order of magnitude. The theory of this experiment has been worked out by Van Vleck[19] as an application of his general method.[2] The resulting magnetization curve is much too smooth. In fact, it is well known that no discontinuity of any kind can be expected on the basis of a "virial coefficients" method.

The magnetization could also be obtained on the basis of a theory of Sauer and Temperley.[4] This leads to a critical field below which the magnetization drops at once to zero. Such a result is an immediate consequence of their assumption that the spins are always parallel or antiparallel to the field. Hence, in this model there is no possibility of a state with vanishing entropy and having a magnetization intermediate between zero and the saturation value. This coupling scheme corresponds to that used in the case of the Paschen-Back effect. Actually for $H < H_c$ one is in the region of anomalous Zeeman effect. The sharpness of the transition arises from the fact that one is dealing with a crystal rather than an atom.

In the case of alums containing magnetic ions with more than one electron the magnetization curve is very much influenced by the crystalline field and the present theory may not be used alone. The dipole interaction, however, should be the decisive factor for the state of the system at absolute zero if the number of electrons in the magnetic ions is odd. The question of main interest is whether or not the state will be polarized (ferromagnetism or anti-ferromagnetism). In IV it was shown that for spherical samples the lowest state was always non-polarized, but that in the important F.C. case (to which the paramagnetic alums belong) a prolate spheroidal sample of axis ratio larger than 6, the polarized state will have the lower energy. This is of interest in connection the "ferromagnetism" observed by Kürti, Lainé, and Simon[20] for iron ammonium alum at low temperatures. That a stable ferromagnetic state really exists is still open to some question. In the first place, the numerical values of the energy constants might be changed by the above mentioned quantum mechanical treatment. In addition, it should be emphasized that pure energy considerations cannot completely decide questions of stability. The forces tending to polarize the crystal originate in distant parts of the sample, while the depolarization forces are due to relatively near neighbors. If the sample is cooled to a temperature below the Curie point by contact with a heat bath, rather than by adiabatic demagnetization, a ferromagnetic state would certainly not be established. This is not to be confused with the situation in true ferromagnetics, where the saturation moment is masked only by the domain structure. The question needs further study, both from the theoretical and the experimental point of view. It may certainly be said, however, that dipole ferromagnetism—if it exists—has a character essentially different from exchange ferromagnetism.

Finally, it may be noted that the more general developments of II are by no means restricted to cubic crystals. The difference in a non-cubic crystal would be in the characteric function $\mathbf{S}(\mathbf{r})$ defined in III, and in the detailed structure of the B.A. The calculations are much more difficult for the non-cubic case, however.

The method is not even restricted to dipole forces, but could be extended to Coulomb, quadrupole or exchange interactions. In fact, the method is applicable to any interaction which is quadratic in a property of the source.

In conclusion, the authors wish to thank Professor John C. Slater for having read and criticized the manuscript.

[19] J. H. Van Vleck, J. Chem. Phys. 6, 81 (1938).

[20] N. Kürti, P. Lainé, and F. Simon, Comptes rendus 204, 675 (1937).

PHYSICAL REVIEW VOLUME 70, NUMBERS 11 AND 12 DECEMBER 1 AND 15, 1946

Theory of the Structure of Ferromagnetic Domains in Films and Small Particles

CHARLES KITTEL*
Research Laboratory of Electronics, Massachusetts Institute of Technology, Cambridge, Massachusetts
(Received October 3, 1946)

The theory is developed of the domain structure of ferromagnetic bodies whose smallest dimension is comparable with the thickness of the Weiss domains as found in crystals of ordinary size. Calculations of the domain boundary, magnetic, and anisotropy energies of various domain configurations are given for thin films, small particles, and long needles of ferromagnetic material. For sufficiently small dimensions the optimum structure consists of a single domain magnetized to saturation in one direction. This result implies unusual magnetic characteristics, such as have in fact been reported by a number of experimenters. The critical dimensions for transition from a configuration with domain structure to a saturated configuration are estimated $\sim 3\times10^{-5}$ cm in films and $\sim 2\times10^{-6}$ cm in particles or grains. These estimates are based on typical values of the relevant material constants, and may be increased or decreased by a factor of ten for other values of the constants.

THE present paper discusses the theory of the domain structure of ferromagnetic bodies whose smallest dimension is comparable with the thickness of the Weiss domains as found in crystals of ordinary size. The problem does not appear to have been considered previously. It will be shown that the normal macroscopic magnetization characteristics of ferromagnetic materials may be expected to alter radically as one or more dimensions of the test specimen are reduced below a critical length which is of the order of 10^{-5} to 10^{-6} cm. A number of experimental results in the literature are in agreement with the theory put forward here.

In the absence of an applied magnetic field it is a matter of common observation that the demagnetized state is the stable state in large ferromagnetic crystals. In the demagnetized state the domains are oriented so that the magnetic flux circuit lies almost entirely within the specimen. Internal flux closure implies a high degree of ordering in the domain configurations —this is contrary to the usual statement that in the demagnetized condition the domains are oriented at random. Geometrical configurations of domains in large crystals were first discussed theoretically in an important and often neglected paper by Landau and Lifshitz[1]; further contributions have been made by Kennard,[2] Lifshitz,[3] and Néel.[4]

As the dimensions of the specimen are diminished, the relative contributions of the various energy terms to the total energy are changed, and surface energies become more important than volume energies. The surface of the boundary (Bloch wall) between domains is a surface energy, while the energy in the magnetic field (magnetostatic self-energy) is a volume energy. When very small dimensions are reached, *there will be a point at which it is favorable energetically to do away with the domain boundaries, so that the whole specimen becomes one domain and acts as a permanent magnet.* This was first predicted by Frenkel and Dorfman.[5] Experimental evidence of permanent magnetization in small ferromagnetic particles was discovered by Elmore,[6] who worked with magnetite particles with a diameter of the order of 2×10^{-6} cm.

The conditions in which the lowest energy state of a specimen represents a structure with a single domain are expected to differ somewhat in films, needles, and powders. In a film one dimension is small; in a needle or wire two dimensions are small, while in a powder particle of the material all three dimensions are small.

* Fellow of the John Simon Guggenheim Memorial Foundation.

[1] L. Landau and E. Lifshitz, Physik. Zeits. Sowjetunion **8**, 153 (1935).

[2] E. H. Kennard, Phys. Rev. **55**, 312 (1939).

[3] E. Lifshitz, J. Phys. U.S.S.R. **8**, 337 (1944).

[4] L. Néel, J. de Physique [8] **5**, 241, 265 (1944).

[5] J. Frenkel and J. Dorfman, Nature **126**, 274 (1930); in this note the surface energy of the boundary between domains is overestimated by a factor of the order of 50, so that a critical length L_c for particles $\sim 10^{-4}$ cm is obtained, instead of $\sim 2\times10^{-6}$ cm which we find. A correct method for treating the boundary surface energy was given first by F. Bloch, Zeits. f. Physik **74**, 295 (1932).

[6] W. C. Elmore, Phys. Rev. **54**, 1092 (1938); **60**, 593 (1941).

ENERGY RELATIONS

The energy relationships in ferromagnetic single crystals have been discussed by Landau and Lifshitz,[1,3] and Brown.[7] The results of these papers are used as a starting point for the present treatment. We shall assume that no applied magnetic field is acting, and that the specimens are each composed of an ideal crystal lattice. The effect of lattice distortions at the surface of the specimen is not considered. We shall make other simplifications which are pointed out below. These simplifications appear to be justified in a first approach to the subject and can be eliminated in favor of a more detailed treatment when adequate experimental data become available on the crystal orientation and mechanical structure of the specimens.

The terms in the free energy of the specimen which are relevant to the present problem may be represented as the sum

$$F=F_w+F_m+F_a, \tag{1}$$

where

F_w = surface energy of the boundary surfaces between domains;
F_m = magnetic field energy of the configuration;
F_a = anisotropy energy of spin orientation.

The free energy is a minimum for a stable configuration* in the absence of external forces. The essential theoretical problem is to determine the balance between the three components of the free energy which will minimize the sum F. The determination of the configuration of domains which will minimize the free energy is a problem in the calculus of variations for which an exact solution has been found only in a few special cases. In other cases of interest we assume a solution which appears plausible on physical grounds and which contains one or more arbitrary parameters. The free energy is then minimized with respect to the parameters.

Wall Energy F_w

In discussing the surface energy of the domain boundaries it is convenient to introduce the surface energy per unit area denoted by σ_w. Naturally σ_w will be a function of the crystallographic direction of the boundary plane and of the total change in spin direction across the boundary. Calculations by Lifshitz and others suggest values of σ_w of the order of 1 to 5 ergs/cm^2. In the present paper the arbitrary value $\sigma_w=3$ ergs/cm^2 will be used for the sake of concreteness in all cases. We may, therefore, write

$$F_w=\sigma_w S, \tag{2}$$

where S is the total area of the domain boundaries within the body.

No account is taken of the special situation at boundary junctions, where there is a small additional energy caused by the finite limiting radius of curvature of the Bloch walls. This situation is probably responsible for the existence of narrow lines of free poles on the surface of magnetic specimens as revealed by colloid powder patterns.

Magnetic Energy F_m

The magnetic field energy F_m represents the work necessary to assemble the distribution of effective magnetic poles within and on the surface of the specimen, starting from a configuration with $\mathbf{H}$ everywhere zero. This energy is given by

$$F_m=-\tfrac{1}{2}\int(\mathbf{H}\cdot\mathbf{M})dV, \tag{3}$$

where $\mathbf{M}$ is the magnetization or magnetic moment per unit volume and $\mathbf{H}$ is the magnetic field arising from the magnetization. The integral is to be carried out over the volume of the specimen. It should be emphasized that this relation supposes that there is no external applied magnetic field. A careful discussion of Eq. (3) has been given by Jeans and also by Guggenheim.[8]

The special case of a uniformly magnetized ellipsoid is of particular importance. Here a demagnetizing factor N may be defined such that in the absence of an applied field the internal field is given by $H=-NM$, giving

$$F_m=NM^2V/2, \tag{4}$$

[7] W. F. Brown, Jr., Phys. Rev. **58**, 736 (1940).

* It is supposed that the stable configuration may be attained by carrying the specimen through a suitable "demagnetization" process, as by cooling in field-free space from above the Curie point.

[8] J. H. Jeans *Electricity and Magnetism* (Cambridge University Press, Cambridge, 1933), fifth edition, p. 398; E. A. Guggenheim, Proc. Roy. Soc. **A155**, 49 (1936). Guggenheim takes $\mathbf{B}=0$ as his standard zero energy state; this convention is somewhat clumsy and for our purposes may be replaced by $\mathbf{H}=0$, so that the standard state is represented by a flux-closure configuration.

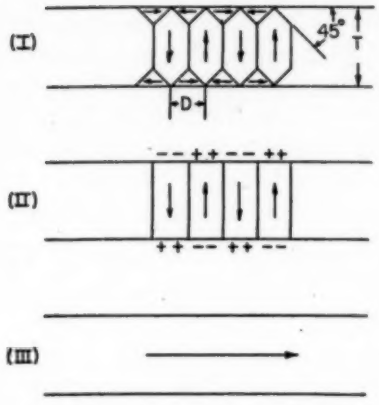

FIG. 1. Domain configurations in films.

where V is the volume. Numerical values of the demagnetizing factors for the general ellipsoid have been tabulated by Osborn.[9]

In other cases of interest the magnetic energy is computed using

$$F_m=(1/8\pi)\int H^2 dV, \tag{5}$$

where now the integral is extended over all space. For parallel coplanar strips of width D with magnetic pole densities alternately $+M$ and $-M$ per unit area the magnetic energy density per unit area σ_m is given by

$$\sigma_m=0.85M^2D. \tag{6}$$

This formula will be used later and is derived in Appendix A.

It is possible to devise domain configurations such that there are no magnetic poles within or on the surface of the specimen. An obvious example would be ring-shaped "domains" in a toroidal specimen. It is also possible to have sudden changes in spin direction between adjacent domains without giving rise to "free" magnetic poles. To have this requires only the continuity of the normal component of the magnetization across the boundary.

Anisotropy Energy F_a

The anisotropy energy arises from the existence of preferred axes of easiest magnetization in ferromagnetic crystals. The interactions responsible for anisotropy have been treated by Van Vleck,[10] Brooks,[11] and others. It will suffice for the present purpose to suppose that there is an anisotropy energy density ρ_a associated with domains oriented in directions away from an axis of easy magnetization, so that

$$F_a=\rho_a V_a, \tag{7}$$

where V_a is the total volume of the domains in the specimen *not* oriented near an easy direction. Values[12] of ρ_a are of the order of 10^5 and 10^6 ergs/cm^3. For the sake of concreteness we shall use the arbitrary value $\rho_a=5\times10^5$ ergs/cm^3. Following Landau and Lifshitz we shall usually assume that the crystal is *uniaxial*, as in cobalt or in iron under tension. In general, as Lifshitz has shown, this assumption does not change the nature of the results, thanks to contributions from the magnetostrictive energy of the domains of closure. This energy we do not consider explicitly.

In treating thin films we suppose that the preferred axis is normal to the plane of the film: this would lead to erroneous results if there existed one or more other preferred axes in the plane of the film. In the case of iron this would occur if the [100] direction were normal to the film. In actual fact this orientation does not occur.[13]

APPLICATION TO PARTICULAR CONFIGURATIONS

Films

We shall consider the energy of various configurations of the film of thickness T shown in Fig. 1. The surface of the film is assumed to be perpendicular to the preferred direction of magnetization.

Case I. Figure 1-I shows a cross section of a structure which provides flux closure within the film. The domain width is D. The area of the Bloch walls per unit area of film is $2\sqrt{2}+(T-D)/D$, so that

$$F_w=\sigma_w[2\sqrt{2}+(T-D)/D], \tag{8}$$

where σ_w is the surface energy density of the Bloch wall.

The triangular prisms contribute an anisotropy

[9] J. A. Osborn, Phys. Rev. **67**, 351 (1945).
[10] J. H. Van Vleck, Phys. Rev. **52**, 1178 (1937).
[11] H. Brooks, Phys. Rev. **58**, 909 (1940).
[12] R. Becker and W. Döring, *Ferromagnetismus* (Edwards Brothers, Ann Arbor, 1943).
[13] See, for example, O. Beeck, A. Wheeler, and A. E. Smith, Phys. Rev. **55**, 601A (1939); O. Beeck, Rev. Mod. Phys. **17**, 61 (1945).

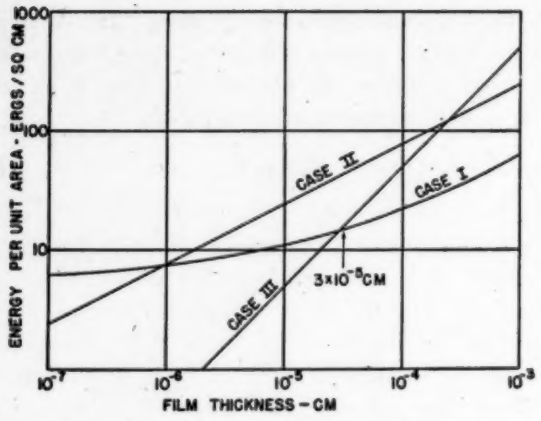

FIG. 2. Energy of various domain configurations in films.

energy given by the product of the anisotropy energy density ρ_a and the volume of the prisms, which is $D/2$ per unit area of film, so that

$$F_a=\rho_a D/2. \tag{9}$$

The magnetic energy F_m is zero for this configuration.

The total energy per unit area is then

$$F=\sigma_w[2\sqrt{2}+(T-D)/D]+\rho_a D/2. \tag{10}$$

This is a minimum with respect to the domain width D when

$$D=(2\sigma_w T/\rho_a)^{\frac{1}{2}}, \tag{11}$$

so that

$$F_{\min}=(2\sqrt{2}-1)\sigma_w+(2\sigma_w T\rho_a)^{\frac{1}{2}}. \tag{12}$$

Case II. Figure 1-II shows a structure for which the flux circuit is open. The magnetic energy per unit area is given by Eq. (6) with M set equal to M_s, the saturation magnetization:

$$F_m=1.7M_s^2D, \tag{13}$$

when it is remembered that the film has two surfaces. It is assumed here that $T>D$. The wall energy is

$$F_w=\sigma_w T/D. \tag{14}$$

The anisotropy energy F_a is zero.

The total energy is a minimum for

$$D=(\sigma_w T/1.7M_s^2)^{\frac{1}{2}}, \tag{15}$$

giving

$$F_{\min}=2(1.7\sigma_w T)^{\frac{1}{2}}M_s. \tag{16}$$

Case III. In Fig. 1-III the film is uniformly magnetized in its own plane. If the film is very long in comparison with the thickness the demagnetization factor and hence the magnetic field energy is small. The principal contribution to the energy comes from the anisotropy, supposing always that the plane of the film does not contain a direction of easy magnetization. We have

$$F=\rho_a T. \tag{17}$$

Numerical values of the energy for cases I, II, and III as a function of film thickness are plotted in Fig. 2, taking $\sigma_w=3$ ergs/cm^2, $\rho_a=5\times10^5$ ergs/cm^3 and $M_s=1700$ gauss. It is seen that for films greater than 3×10^{-5} cm in thickness, case I has the lowest energy of the three cases considered. This is not surprising, as case I is the structure evolved by Landau and Lifshitz in their original study of large uniaxial crystals. It is interesting to note that an experimental demonstration of the existence of "domains of closure" has been given by Shoenberg and Wilson[14] by means of magnetic torque measurements on a Si-Fe crystal.

For thinner films case III has the lowest energy. If the demagnetization factor parallel to the surface is not negligible, because of the finite extent of the film, then the case I structure will persist to smaller dimensions than calculated above. Case II occurs only with very much larger anisotropy.*

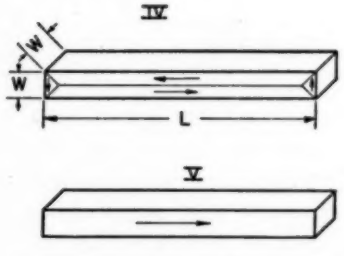

FIG. 3. Domain configurations in needles.

[14] D. Shoenberg and A. J. C. Wilson, Nature **157**, 548 (1946).

* In cobalt the anisotropy is unusually pronounced: $\rho_a=5.1\times10^6$ ergs/cm^3, according to R. Gans and E. Czerlinsky, Ann. d. Physik [5] **16**, 625 (1933). The saturation magnetization at room temperature is $M_s=1400$ gauss, according to K. Honda and H. Masumoto, Sci. Rep. Tôhoku Univ. **20**, 323 (1931). In the limit of large crystals we have for case I the value $F(I)=3.2(\sigma_w T)^{\frac{1}{2}}\times10^3$ ergs, and for case II the value $F(II)=3.6(\sigma_w T)^{\frac{1}{2}}\times10^3$ ergs, so that there is not much difference energetically between the two configurations. If the constants are varied slightly so that $F(\mathrm{I})=F(\mathrm{II})$, it may be shown that the most favorable configuration is somewhat intermediate between these two cases, with part of the unit flux circuit completed internally and part giving rise to a free pole distri-

At the critical thickness of 3×10^{-5} cm the domain width for case I is 2×10^{-5} cm.

Needles and Wires

The general relationship between the energies of structures I, II, and III may be expected to hold also in long wires, provided that small adjustments are made in numerical factors.

The relations for needles are of somewhat greater interest. For the sake of example the anisotropy energy is omitted.

Case IV. The needle (Fig. 3-IV) of dimensions $L\times W\times W$ consists of two long domains with the flux circuit closed internally by triangular caps. The energy is largely in the wall separating the long domains, and is given approximately by

$$F=\sigma_w LW. \tag{18}$$

Case V. The needle (Fig. 3-V) consists of one domain magnetized along the length of the needle. The energy is entirely magnetic and is given by

$$F=NM_s^2LW^2/2, \tag{19}$$

following Eq. (4).

The critical dimension below which case V is the probable state is given by $W_c=2\sigma_w/NM_s^2$. Values of W_c and the associated L_c are given in Table I, which is calculated for $\sigma_w=3$ ergs/cm^2, $M_s=1700$ gauss.

The values of the demagnetizing factor were taken to be equal to the values for a prolate spheroid with the same axial ratio.

Particles

Case VI. Figure 4-VI represents a cube of side L. The particle consists of one domain. The

TABLE I.

L/W	N	W_c (cm)	L_c (cm)
5	0.702	2.8×10^{-6}	1.4×10^{-5}
10	0.255	7.9×10^{-6}	7.9×10^{-5}
15	0.135	1.5×10^{-5}	2.2×10^{-4}
20	0.085	2.4×10^{-5}	4.7×10^{-4}

bution. The domains of partial flux closure occupy the fraction P of the surface, where $\sin(\pi P/2)\approx 4P/\pi$; the root is $P\cong 0.7$. L. H. Germer, Phys. Rev. 62, 295A (1942) has studied by electron beams the magnetic fields at the hexagonal surface of a "demagnetized" cobalt crystal, and finds indication of a non-closure or type II configuration. The possibility of non-closure configurations was apparently overlooked by Landau and Lifshitz. I wish to thank Dr. Germer for a discussion of the results on which his published abstract is based.

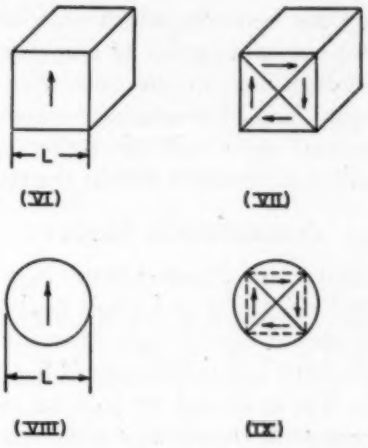

FIG. 4. Domain configurations in small particles.

energy is entirely magnetic and is given by

$$F\cong(2\pi/3)M_s^2L^3, \tag{20}$$

where the effective demagnetization factor has been taken as $4\pi/3$, the value for a sphere.

Case VII. Figure 4-VII shows a cube with domains arranged to give internal flux closure. The magnetic energy is zero. The wall energy is

$$F_w=\sigma_w 2\sqrt{2}L^2. \tag{21}$$

The anisotropy energy is approximately

$$F_a=\rho_a L^3/2 \tag{22}$$

and is relatively small.

The critical diameter below which case VI becomes the probable configuration is given by

$$L_c=\frac{2\sqrt{2}\sigma_w}{(2\pi/3)M_s^2-\rho_a/2}\cong 1.5\times10^{-6}\text{ cm}, \tag{23}$$

using the numerical values previously assumed.

The relations for the small sphere pictured in Figs. 4-VIII and 4-IX are similar to the relations for cubes. The energy in case VIII is magnetic and equal to $L^3/9$. In case IX most of the energy is in the walls, and $F_w=\pi\sigma_w L^2/2$. The flux closure in case IX is not complete. Fields of octopole symmetry arise from the volume between the surface of the sphere and the boundary of an inscribed cube. The critical dimension for a sphere is close to that for a cube.

For particles just larger than the critical dimension the domain structure shown in Figs. 4-VII and 4-IX should not be interpreted too

literally, since here the width of a Bloch wall may be of the same order of magnitude as the domain dimensions. In this case there will not be a sharply defined boundary between discrete domains, but there will be rather a gradual rotation of spin direction within the particle.

EXPERIMENTAL RESULTS

The theory developed above suggests that films $\sim 10^{-5}$ cm thick and small particles $\sim 10^{-6}$ cm across should exhibit quite different magnetic properties from bulk specimens of ferromagnetic materials. The evidences we look for include:

(*A*) *Permanent saturation magnetization.* Specimens consisting of a single domain should behave as if magnetized to saturation in one direction. It is supposed that ordinary remanent effects have been distinguished by carrying the material through a demagnetization process, as by cooling from above the Curie point in field-free space.

(*B*) *High coercive force.* If no domain boundaries are formed the only magnetization changes in a specimen occur through spin rotation. Spin rotation is opposed by the anisotropy forces, which are usually much greater than the local forces opposing movement of a domain boundary. With decreasing particle size it may therefore be expected that the coercive force will increase and approach the anisotropy force in value.

(*C*) *Low initial permeability.* If there are no domain boundaries the magnetization changes in weak fields must come from reversible spin rotations. The associated permeabilities are quite low.

Relevant experimental results are reviewed briefly below. The results as a whole are in very good agreement with theory.

(1) Elmore[6] has obtained positive evidence that small particles behave as permanent magnets. He studied the susceptibility of colloidal suspensions of iron oxides. On the assumption[15] that the particles behave as the molecules of a classical paramagnetic gas he is able to fit the experimental susceptibility curve. Magnetite (Fe_3O_4) particles of mean diameter 1.7×10^{-6} cm show an average permanent magnetization equal to 44 percent of the saturation value. Siderac (γ-Fe_2O_3) particles of mean diameter 2.1×10^{-6} show 38 percent of the saturation value. The discrepancy between the observed and the saturation values has been attributed to the presence of non-ferromagnetic oxides of iron in the colloid. Heaps[16] has also detected a tendency of particles to agglomerate in groups which were only partly magnetic. Consideration shows that group formation is likely to occur when the magnetic bond energy between particles is large in comparison with kT. This is satisfied in the conditions of Elmore's experiments.

(2) Montgomery,[15] Heaps,[16] Benedikt,[17] and Mueller and Shamos[18] have made measurements by various methods using particles larger than those used by Elmore. The particles averaged between 10^{-3} and 10^{-5} cm. The interpretation of some of the results is complicated. In general there is an indication of permanent magnetism, but less than in Elmore's measurements. The theory predicts a critical dimension $\sim 2\times10^{-6}$ cm for particles, so that the measurements fit into the expected pattern when allowance is made for dispersion in particle size and for the unavoidable presence of some remanent magnetization in the larger particles.

(3) In the older literature[19–22] a considerable amount of work is reported on the properties of iron and nickel films deposited under the influence of weak magnetic fields in the plane of the film. The effects observed, such as quadrilateral hysteresis loops, are generally compatible with the concept that thin films consist of a single domain. It would be valuable to repeat some of the early work using electron diffraction methods[23] to give some control of the quality of the film deposited.

(4) High values of the coercive force ($\sim$300 gauss) in small particles and thin films have been measured by Sappa,[24] Gottschalk,[25] Procopiu,[26]

[15] C. G. Montgomery, Phys. Rev. **38**, 1782 (1931); **39**, 162 (1931).

[16] C. W. Heaps, Phys. Rev. **57**, 528 (1940).
[17] E. T. Benedikt, J. App. Phys. **13**, 105 (1942).
[18] H. Mueller and M. Shamos, Phys. Rev. **61**, 631 (1942).
[19] C. Maurain, J. de phys. et rad. [3] **10**, 123 (1901); [4] **1**, 90, 151 (1902).
[20] W. Leick, Wied. Ann. **58**, 691 (1896).
[21] K. Schild, Ann. d. Physik [4] **25**, 586 (1908).
[22] W. Kaufmann and W. Meyer, Physik. Zeits. **12**, 513 (1911).
[23] L. Germer, Phys. Rev. **55**, 605 (1939); **56**, 58 (1939).
[24] O. Sappa, Ricerca Scient. **8**, 413 (1937).
[25] V. H. Gottschalk, Physics **6**, 127 (1935).
[26] S. Procopiu, J. de phys. et rad. [7] **5**, 199 (1934).

and Maurain.[19] The result that small grains of a material show high values of the coercive force has been applied to the selection of materials for permanent magnets.

(5) Low values of the initial permeability have been reported for thin films by Florescu[27] and for small particles by Gottschalk and Wartman,[28] and Chevalier and Mathieu.[29] Florescu finds $\mu=3.5$ for an iron film 8×10^{-6} cm thick at a frequency near 100 kc/sec. An iron wire 5×10^{-3} cm in diameter at the same frequency gave $\mu=69.2$. Gottschalk and Wartman find $\mu=4.62$ for Ural Mountain magnetite of grain size 180×10^{-4} cm, and $\mu=2.53$ for grain size 3.5×10^{-4} cm.

CONCLUDING REMARKS

The study of the magnetic behavior of thin films and small particles appears to offer considerable promise of elucidating some of the problems of domain theory. It would be of particular interest to study magnetization processes in films using a number of different techniques, including magnetometer measurements, electron diffraction studies of the surface structure, and magneto-optic and colloid pattern studies of the domain structure. In this way we might hope to establish quantitative relationships between domain displacements and magnetization in configurations which may be amenable to theoretical treatment. It must be emphasized, however, that the film technique will only be useful if a reasonably homogeneous film can be prepared, and one which is tolerably free from internal stresses.

Measurements of the transmission of microwaves through thin films are of particular interest in the study[30] of the dispersion of ferromagnetism at high frequencies.

I am indebted to Dr. R. M. Bozorth of the Bell Telephone Laboratories for discussion on the subject of this paper.

APPENDIX A

Magnetic Field Energy of Coplanar Strips of Alternate Sign

Let the plane of the strips be the (x, y) plane with the y axis parallel to the axis of the strips; the width of a single strip is D, and the pole strength per unit area of a strip is $\pm M$. The vertical or z component of the magnetic field directly above the plane of the strips is given by the Fourier expansion of a square-wave of amplitude $2\pi M$. The appropriate solution of the Laplace equation is

$$H_z=2\pi M[(4/\pi)\sin kxe^{-kz}+\text{terms in odd multiples of } k],$$

where $k=\pi/D$. For the present the harmonic terms in the expansion will be neglected. To satisfy $\operatorname{div}\mathbf{H}=0$ we must have

$$H_z=-2\pi M[(4/\pi)\cos kxe^{-kz}].$$

The energy per unit area above the strips is given, using Eq. (5), by $(1/8\pi)\int_0^\infty H^2dz$, so that the surface energy density σ_m is given by

$$\sigma_m=(1/4\pi)(2\pi M)^2(4/\pi)^2\int_0^\infty e^{-2kz}dz,$$

when both faces of the plane of the strips are taken into account. This gives $\sigma_m=(8/\pi^2)M^2D$, which is the contribution from the first order term alone. The complete expression including the effect of the harmonic terms is obtained by multiplying by Σn^{-2}, where the sum is over odd integers and is approximately equal to 1.05. We have finally

$$\sigma_m\leqq 0.85M^2D,$$

as given in Eq. (6), and in agreement with Néel.[4]

The treatment of double layers of charged strips proceeds similarly, but is somewhat more complicated.

---

[27] N. A. Florescu, Comptes rendus (Paris) **208**, 1717 (1939).

[28] V. H. Gottschalk and F. S. Wartman, U. S. Bureau of Mines Report of Investigations **3268**, 67 (1935).

[29] R. Chevalier and S. Mathieu, Comptes rendus (Paris) **204**, 854 (1937).

[30] C. Kittel, Phys. Rev. **70**, 281 (1946). An interesting dispersion calculation by G. Heller is referred to by M. J. O. Strutt and K. S. Knol, Physica **7**, 635 (1940).

Neutron Polarization and Ferromagnetic Saturation

F. BLOCH, R. I. CONDIT, AND H. H. STAUB
Department of Physics, Stanford University, Stanford University, California
(Received December 2, 1946)

IN a previous paper[1] (referred to as I we have shown that the relative intensity change $\Delta I/I$ observed when slow neutrons pass through a magnetized piece of iron, can be well represented by a theoretical expression given by Halpern and Holstein,[2] *viz.*:

$$\Delta I/I = \tfrac{1}{4}n^2p^2d^2f(\lambda/\epsilon d)$$
$$f(x) = 2x^2(l^{-1/x}+1/x-1). \qquad (1)$$

In this formula n represents the number of iron atoms per cc, p the change of the cross section arising from magnetic scattering, ϵ the percentage deviation of the magnetization from complete saturation, and λ a quantity related to the linear dimension of the iron microcrystals.

We have extended these measurements to a much closer approach to saturation by using a rather powerful electromagnet, which produces magnetizing fields up to about 10,000 gauss in steel samples $1\frac{1}{2}''$ long, $2''$ high, and $\frac{3}{4}''$ or $1\frac{1}{2}''$ thick. Except for minor changes, the experimental arrangement for these measurements was otherwise identical to that used in I. A slow neutron beam from the target of the cyclotron was collimated through a $3''\times3''$ opening in the hydrogenous shield around the target and directed through a cadmium canal of $1\frac{1}{2}''\times2''$ opening and $6''$ length, mounted on the steel sample in the gap of the magnet. The sample was located at a distance of $4'$ from the cyclotron target. After passing through the sample the beam emerged through a similar cadmium canal on the rear side of the magnet and finally entered the neutron detector through a cadmium tube $30''$ long with a diameter of $2\frac{1}{4}''$. The distance of the detector from the target was $8'$, resulting in a collimation of the arrangement to within 1.5°. The new detector, a boron trifluoride proportional counter, is considerably shallower than the one previously used. Its active length is $10''$ and it was filled with purified commercial boron trifluoride to a pressure of one-half atmosphere. As in I, the primary intensity of the neutron beam was monitored by a small auxiliary integrating boron trifluoride ionization chamber.

The magnetic fields in the iron samples were determined in the same manner as described in I by placing a thin rectangular search coil close to the surface of the iron plates. From the value of H thus found, the value of $1/\epsilon$ was deduced by using our previous measurements with the isthmus method. This procedure seemed to be permissible since the steel samples were of the same type as those used in I. For sufficiently large values of H proportionality of $1/\epsilon$ and H^2 was assumed.

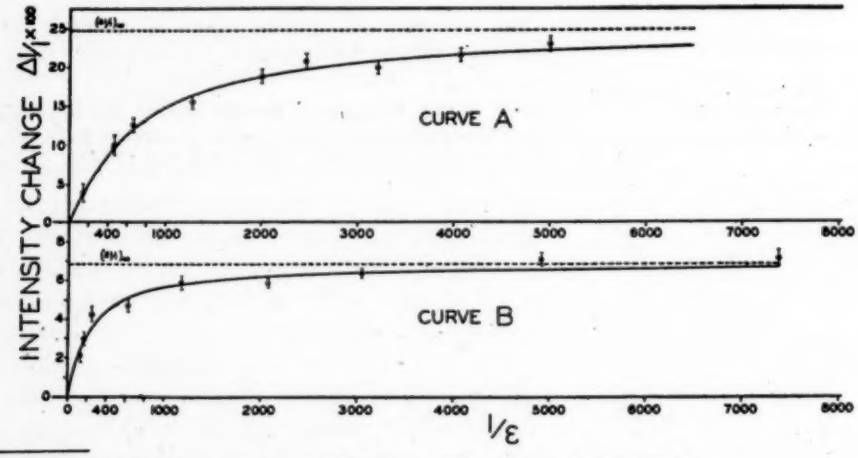

FIG. 1. Relative intensity change of transmitted neutrons. A—$1\frac{1}{2}''$ Sample; B—$\frac{3}{4}''$ Sample.

[1] F. Bloch, M. Hamermesh, and H. Staub, Phys. Rev. **64**, 47 (1943).
[2] O. Halpern and T. Holstein, Phys. Rev. **59**, 960 (1941).

Figure 1 shows the results of the measurements for samples of $1\frac{1}{2}''$ (curve A) and $\frac{3}{4}''$ (curve B) thickness, together with the best fitting theoretical curves computed from I by using the following values of the parameters.

$d=1\frac{1}{2}''$: $(\Delta I/I)_\infty=24.8\pm.9\%$;
$p=2.20\pm.04\times10^{-24}$ cm^2;
$\lambda=2.1\pm.3\times10^{-3}$ cm.

$d=\frac{3}{4}''$: $(\Delta I/I)_\infty=6.82\pm.2\%$;
$p=2.3\pm.03\times10^{-24}$ cm^2;
$\lambda=3.2\pm.5\times10^{-3}$ cm.

The errors shown with the experimental points as well as those given with the above numerical values are standard mean square deviations.

These results show firstly that the saturation values $(\Delta I/I)_\infty$ of the polarization effect are considerably larger than those reported in I, which were 4.75 percent for $d=\frac{3}{4}''$ and 19 percent for $d=1\frac{1}{2}''$. The fact that the previous saturation values seemed lower was probably caused by the lack of data at higher values of $1/\epsilon$. As a consequence, the saturation value had to be obtained by a rather large extrapolation, strongly influenced by the last two points measured with $d=\frac{3}{4}''$, which happened to be considerably lower than the values obtained at present. It should be pointed out, however, that in the old arrangement the effective neutron velocity (arising from differences in the paraffin arrangement and also from the different sensitivity of the detector) might have caused a lowering of the observed saturation values. It also appears that with the two rather different values of λ, the two sets of data cannot very well be represented by the same curve through a mere scaling of the abscissa by a factor two and of the ordinate by a factor four, as required by Eq. (1).

If the discrepancy in the values of λ for the two different thicknesses is significant, it is somewhat difficult to explain why. A possible explanation might be found in a rather large change of the average neutron velocity caused by the passage of the neutrons through iron. Since λ is proportional to the square of the neutron velocity, the observed change in λ would mean that the average neutron velocity is about 25 percent larger after passage through 3.8 cm of iron than after passage through 1.9 cm. This velocity change might also be responsible for the observed change of p for the two values of d. The quantitative evaluation of this effect is rather complicated and has so far not been undertaken. The change in the average velocity of the neutrons is obviously not only caused by capture which is inversely proportional to the velocity but also by crystalline scattering.

In order to facilitate such a calculation, we have made a rough determination of the average energy of the neutron beam upon its emergence from the paraffin by measuring its absorption in boron. The fraction of neutrons transmitted through a cell of 21 cm length, filled with boron trifluoride, to a pressure of 790 mm was found to be 71.9 ± 1.2 percent. Previously Fryer[3] determined the shape of the neutron spectrum for a similar paraffin arrangement by the velocity selector method. Computing the transmission through a boron absorber with our dimensions, and using Fryer's spectrum, one finds the transmitted fraction to be 70.9 percent. This indicates that the spectrum of the neutrons used in the present measurements was very similar to the one determined by Fryer. His results might serve, therefore, as a basis for the evaluation of the velocity effect.

Hamermesh[4] has estimated the effect of the variation of the velocity on $(\Delta I/I)_\infty$ considering only the capture of the neutrons. For the two thicknesses $d=1.95$ cm and 4.0 cm, which are close to the values used by us, he finds that owing to velocity change the ratio of $(\Delta I/I)_\infty$ is about 14 percent smaller than the expected value, which should be proportional to d^2. Applying this correction to our value of $(\Delta I/I)_\infty=6.82$ percent for $d=1.9$ cm, one should thus expect, for $d=3.8$ cm thickness, a value of $(\Delta I/I)_\infty=24.2$ which agrees very well with our observation, although the calculation is based upon a spectrum which differs considerably from that of Fryer.

It is satisfactory that the very substantial increase of polarization effect which we expected from our previous data can actually be materialized by the use of magnetizing fields of the order of 10^4 gauss. This will be very useful for further experiments with polarized neutrons. It might be mentioned that the highest observed polarization effect $\Delta I/I=22.5$ percent corresponds to a degree of polarization of the neutron beam $\eta=|(I^+-I^-)/(I^++I^-)|$ of about 60 percent.

[3] E. M. Fryer, Phys. Rev. 70, 235 (1946).
[4] M. Hamermesh, Phys. Rev. 61, 17 (1942).

Letters to the Editor

PROMPT publication of brief reports of important discoveries in physics may be secured by addressing them to this department. The closing date for this department is the third of the month. Because of the late closing date for the section no proof can be shown to authors. The Board of Editors does not hold itself responsible for the opinions expressed by the correspondents. Communications should not in general exceed 600 words in length.

Pairs of Fission Fragments from U^{235}

PIERRE DEMERS
Division of Atomic Energy, National Research Council, Chalk River, Ontario, Canada
November 5, 1946

EIGHT complete and fourteen incomplete pairs of heavy fission tracks were obtained by Bøggild, Brostrom, and Lauritsen,[1] which sufficed to indicate two groups of different ranges. Using a new emulsion (Formula II),[2] the writer obtained numerous pairs of complete tracks in the photographic emulsion in which the origin of each pair can be recognized. The technique used was to superpose on a glass slide three coatings: emulsion, uranium compound, and emulsion, the second one being very thin and made from a suspension of ammonium uranate. If a fission occurs, it is not recorded in the insensitive layer where it originates, but only above and below the layer. Thus a dark line with a blank gap is visible after processing (Fig. 1). About 1500 such pairs have been sighted and 129 measured. Irradiation was performed with the low power heavy water pile at Chalk River.

(1) The tracks associated in a pair were of unequal length in 127 cases out of 129 and clearly belong to two range groups. The central gap was about 0.7μ or 0.1 cm of air on the average. The mean range of the short (S) and of the long (L) track, their sum (T), and mean difference (D) are as follows. Equivalent ranges were calculated by assuming the same stopping power (1675) as for the $N^{14}(n, p)C^{14}$ protons (P) visible in the same plate. The range of P was previously compared with that of UI (2.63 cm) and of UII (3.18) in a soaked plate (see Fig. 2).

	L	S	T	D	P
Microns	14.4	11.2	25.5	3.2	6.34
cm of air	2.39	1.87	4.27	0.53	1.06
B_r, B and L^1	2.5	1.9	4.5	0.6	—

(2) In the first 5 or 6μ of its range L appears darker than S on the average and therefore is quite probably more ionizing (Fig. 1). A rough estimate of the difference in ionization is 10 percent on the average and 30 percent in some pairs. The fragment producing L is more ionizing, carries more energy, and must be the lighter particle.

(3) There is a maximum of blackening, and presumably of ionization, some 3μ from the beginning of L, in about $\frac{1}{3}$ of the cases. On the average there is a minimum of blackening about 0.5–1μ from the end of L and of S, in agreement with known ionization properties.

(4) In general agreement with work done elsewhere, examples of an α-ray accompanying fission have been observed. So far, six α-ray tracks have been seen, one was longer than 28 cm. In one case (Fig. 1), the origin of the two heavy tracks and of the α-ray track were found to coincide within 0.2μ. As the velocity of the fragments when emitted was about 10^9 cm/sec., the α-particle was emitted less than $0.2\ 10^{-4}/10^9 = 2.10^{-14}$ sec. after fission. This is an upper limit for this quantity.

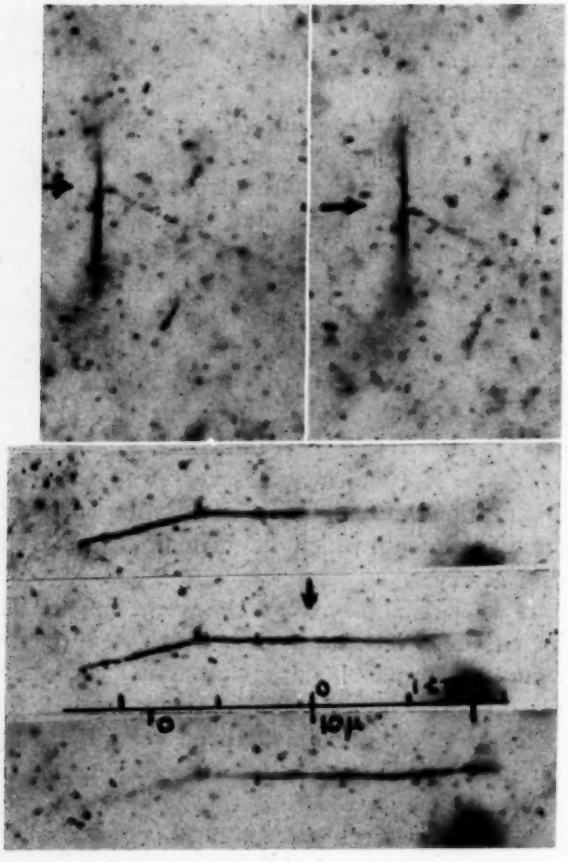

FIG. 1. Photographs of tracks of fission fragments. The point of common origin is indicated by the arrow. At top are two focusings of a fission accompanied by an alpha-particle. At bottom are three focusings of two heavy tracks.

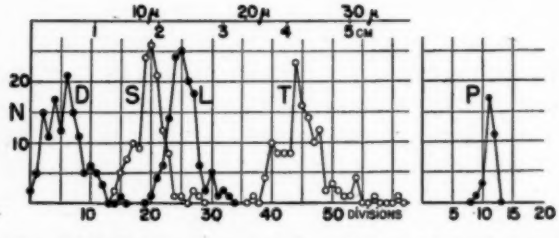

FIG. 2. Distribution of observed ranges of pairs of fission fragments. S is for the fragment of shorter range, L for the fragment of longer range, D is the difference and T the sum of the ranges. P is for protons from the $N^{14}(n, p)C^{14}$ reaction and is included for calibration purposes.

(5) Three main kinds of collisions occur: protons (mass 1), C, N, O (12 to 16); Br, Ag (80 to 108). The last kind gives rise to forks with the two branches at nearly right angles and equally ionizing. Small bumps along the fission tracks are probably owing mostly to the second kind, as well as the occasional blooming near the end. About 30 recoil protons have been seen. When the range and angle of deflection of the proton are suitable for measurement, the velocity of the fragment can be derived at the point of collision. As the group to which the fragment belongs is evident, the writer intends to obtain independent range-velocity curves for each group of fragments.

[1] J. K. Bøggild, K. J. Brostrom, and T. Lauritsen, Kgl. Danske Vid. Sels. Math.-Fys. Medd. 18, No. 4, 1–32 (1940).
[2] P. Demers, Phys. Rev. 70, 86 (1946); Can. J. Research, to be published.

The Density Spectrum and the Origin of Extensive Atmospheric Cosmic-Ray Showers

GIUSEPPE COCCONI
Institute of Physics, University of Catania, Catania, Italy
June 17, 1946

RECENTLY Wolfenstein[1] calculated the density spectrum of extensive cosmic-ray showers (relation between frequency and density of the showers) at various altitudes on the basis of the multiplicative cascade theory of electrons and photons. He compared his results with the density spectra deduced from the measurements with ionization chambers of Lewis[2] and others.[3] Wolfenstein concluded that the extensive showers were not generated by cascade multiplication of very energetic primary electrons because the experimental frequencies are more than ten times greater than the theoretical, and also because the character of the theoretical and experimental spectra are quite different.

The same problem was studied by the writer and coworkers during 1942, 1943, and 1944. The theoretical calculation of the density spectra at various altitudes was carried out[4] by employing Heisenberg's and Molière's equations for cascade multiplication.[5] Our results are in good agreement with Wolfenstein's which indicates the equivalence of the approximations introduced in the calculations of various authors. The experimental spectra were determined at sea level and at 2200 m with coincident counters.[6] The agreement between theory and experiment was excellent, the character of the spectra is the same, and the experimental frequencies exceed the theoretical by a factor of about 1.7 which is within the uncertainty of the calculations. We therefore conclude in contradiction to Wolfenstein that the cascade theory explains quite satisfactorily the origin of extensive showers.

The reason for the disagreement between Wolfenstein's conclusion and ours lies in the diversity of the experimental data with which the theory is compared, a diversity which we believe is caused by the different experimental methods employed to measure the density of showers. We think our data on the density obtained from the measurements are more reliable than those used by Wolfenstein because with the ionization chamber the total ionization is recorded, hence the deduced densities may be influenced by secondary radiations of all types (multiplicative electrons, nuclear fragments, etc.) generated in the walls of the chamber. The counter-measurements obviously are not invalidated by such local phenomena because G.M. counters record the "events" and not the related secondary processes.

In support of our thesis we draw attention to the circumstance that other counter data may be well explained by the cascade theory. This is the case for the frequency-height measurements of Hilberry[7] and the frequency-shower measurements of Auger (see Molière[6]). On the contrary, the frequency-burst size measurements of Lewis with the ionization chamber, as was also pointed out by Wolfenstein, do not agree with the theory.

[1] L. Wolfenstein, Phys. Rev. 67, 238 (1945).
[2] L. G. Lewis, Phys. Rev. 67, 228 (1945).
[3] H. Carmichael, Nature 144, 325 (1939).
[4] G. Cocconi, A. Loverdo, and V. Tongiorgi, Nuovo Cimento 4 (1946).
[5] W. Heisenberg and G. Molière, *Vorträge über Kosmische Strahlung* (Berlin, 1943).
[6] G. Cocconi, A. Loverdo, and V. Tongiorgi, Nuovo Cimento 2, 28 (1944).
[7] N. Hilberry, Phys. Rev. 60, 1 (1941).

A Note on the Proton Hypothesis of the Primary Component of Cosmic Rays

NIELS ARLEY
Institute of Theoretical Physics, Copenhagen and Palmer Physical Laboratory, Princeton, New Jersey
November 14, 1946

FROM the results of Schein and collaborators[1] it has been concluded[2] that the primary component of cosmic rays may consist exclusively of protons. We want to point out, firstly, that this conclusion is not yet certain, because at the maximum altitude used by Schein and his collaborators, *viz.* 2 cm Hg, the total radiation, soft and hard, still contains about 50 percent electrons, as is shown by a comparison between the curves of Pfotzer and of Schein.[1] Whether or not these curves coincide at the top of the atmosphere cannot be decided, however, by extrapolation from the experiments of Schein *et al.*, but only from the results of the V-2 rocket flights. Apart from this, in order to compare the two curves safely they must be measured with the same apparatus and at the same place. In order to obtain information on the energies of the large number of electrons certainly present up to the highest altitudes investigated in balloon flights, it would also be extremely important to obtain the transition between the Schein and the Pfotzer curve, i.e., to measure the intensity *vs.* altitude curve for lead absorbers with thickness *between* 0 and 4 cm, and not only for lead absorbers *above* 4 cm. (We also note that the 4-cm and 6-cm absorbers are only represented by *one* point each on the Schein curve, *viz.*, at the maximum altitude.)

Next we want to remark that the proton hypothesis of the primary cosmic rays leads to difficulties in the interpretation of other experiments. First of all, it would give a high positive east-west asymmetry at the top of the atmosphere for *both* the hard and the soft component (and thus for the total). Experimentally Johnson and Barry[3]

found, however, for the *total* radiation averaged over altitudes from 3–10 cm Hg only an east-west asymmetry of +7 percent (at geomagnetic latitude 20°N and for zenith angle 60°). It is to be hoped that this very important result will be checked in further experiments. The author has previously suggested[4] that this small east-west asymmetry of the *total* radiation at high altitudes may perhaps be interpreted as being the result of the combination of a high *positive* east-west asymmetry for the hard component, assumed to be produced mainly from primary positive protons, and a high *negative* east-west asymmetry for the soft component, assumed to be produced mainly from primary *negative* protons. Direct measurements at high altitudes of the east-west asymmetry of the soft and hard components *separately* are, therefore, highly desirable.

Apart from the problem of the east-west asymmetry it is also very difficult to interpret from the proton hypothesis the conspicuous difference between the latitude effect of the soft and that of the hard component, the first increasing strongly with increasing altitude, reaching values about 70–80 percent at the Pfotzer maximum,[5] the latter increasing only slowly with altitudes from about 12 percent at sea level to about 18 percent at an altitude of 21 cm.[6]

From the earlier hypothesis assuming the soft component to be created by cascade multiplication of primary electrons from the top of the atmosphere and down, the latitude effect could be satisfactorily accounted for, as shown by Heitler,[7] assuming a primary energy spectrum of approximately the well-known inverse power type. If, now, as in the proton hypothesis, the soft component is to be produced not as a secondary, but as a *tertiary* radiation, but still from the same primary energy spectrum and still practically at the top of the atmosphere, as in the form of the proton hypothesis given by Heitler *et al.*[3] (i.e., protons being transformed in single processes into long-lived pseudoscalar and short-lived vector mesons, the latter decaying at once into electrons and neutrinos), energy is lost in the transformation of the primary radiation into the soft component. Consequently the primary energy necessary to produce the same primary electron energies at the top of the atmosphere as before is much higher. As the primary energy spectrum decreases with increasing energies and as the field sensitive region is only 2–15 Bev, this energy decrease means that the latitude effect becomes smaller than that calculated from the earlier electron hypothesis which agreed with experiments. (Unfortunately Heitler and Walsh do not give the intensity *vs.* altitude curves of the soft component at equator and at 50°N, which would follow from their theory.)

In the Feynman-Bethe form of the proton hypothesis,[3] the protons produce in multiple processes only the long-lived pseudoscalar mesons ($\tau \sim 2\times10^{-6}$ sec.) decaying into electrons and neutrinos all the way down through the atmosphere and not only at the top of the atmosphere as in Heitler's form of the theory. In this form the difference between the latitude effect of the soft and that of the hard component would be even more difficult to interpret than in Heitler's form, partly because the energy decrease in the transformation of the primary radiation into the soft component is here much larger owing to the multiple processes, partly because after a few radiation units the soft component will be in equilibrium with the mesons, as is known from the calculations of Euler and Heisenberg.[8] All through the lower part of the atmosphere the latitude effect of both components should consequently increase approximately in the same way, in contrast to the difference observed.[5,6] Another difficulty for this form of the proton hypothesis is to explain the increase of the ratio of soft to hard intensity in the lower part of the atmosphere. A further consequence is that the electrons of the soft component produced in this way would be expected to be less energetic than those produced in the Heitler theory. Not only the intensity of the soft component but also the electron spectra at different altitudes would, therefore, be interesting to have worked out and compared with the spectra found experimentally.

We thus conclude from the experimental evidence as it stands at present that it seems necessary to assume at least one more component in the primary radiation, in addition to the protons which seem to be the primaries of most of the hard component. Whether this second component consists of electrons, negative protons[4] or perhaps higher charged nuclei as suggested by Swann[9] can, of course, only be decided by further experiments. *Especially a more systematic investigation of the intensity, latitude effect, and east-west asymmetry* of the soft and hard component *separately* at high altitudes is highly desirable.

[1] M. Schein, W. Jesse and E. Wollan, Phys. Rev. **59**, 615 (1941).
[2] J. Hamilton, W. Heitler, and H. Peng, Phys. Rev. **64**, 78 (1943); W. Heitler and P. Walsh, Rev. Mod. Phys. **17**, 252 (1945); R. P. Feynman and H. Bethe, Bull. Am. Phys. Soc. **21**, No. 5, 5 (1946).
[3] T. Johnson and J. Barry, Phys. Rev. **56**, 219 (1939).
[4] N. Arley, Kgl. Danske Vid. Sels. Math.-Fys. Medd. **23**, No. 7 (1945); Physica **12**, 177 (1946).
[5] I. Bowen, R. A. Millikan, and H. V. Neher, Phys. Rev. **53**, 855 (1938).
[6] H. Bhabha, S. Chandrashekhar, H. Hoteko, and R. Saxena, Phys. Rev. **68**, 147 (1945).
[7] W. Heitler, Proc. Roy. Soc. **161**, 261 (1937).
[8] H. Euler and W. Heisenberg, Ergeb. d. exact. Naturwiss. **17**, 1 (1938).
[9] W. F. G. Swann, J. Frank. Inst. **236**, 1 and 111 (1943).

On the Possible Use of Brownian Motion for Low Temperature Thermometry

JAMES B. BROWN AND D. K. C. MACDONALD
Clarendon Laboratory, Oxford, England
October 26, 1946

In a recent communication,[1] Lawson and Long proposed two interesting methods for low temperature thermometry using spontaneous electrical fluctuations. In the present note it is desired to point out that a drastic modification of the first method would be required, and that a fundamental principle, apparently overlooked, invalidates the conclusions in favor of the second method proposed.

Their first method consists in measuring the thermal voltage fluctuations generated in a resistance of large value at the grid of an amplifier valve. The arrangement suggested is one of an ohmic resistor $R(\sim10^9\Omega)$ in parallel with inevitable circuit capacity ($\sim30\mu\mu f$) resulting in a frequency response 0–5 c/sec. Concomitantly, the shot noise in the amplifier valve is assessed by the familiar expression,[2] $3/g$, for a valve operating in the space charge region. This

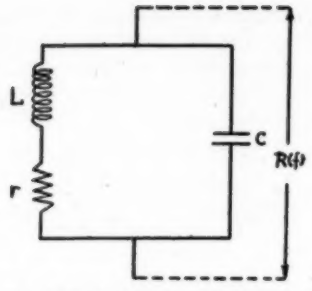

FIG. 1. Equivalent circuit of a crystal.

formula, however, is not valid except for frequencies sufficiently high to exclude the incidence of "flicker effect."[3,4] Indeed, below a few hundred cycles/sec., flicker effect becomes entirely dominant and the fluctuations may rise to the order of 10^2–10^3 times the theoretical value of "true" shot noise as predicted by the formula above. For this reason all modern fluctuations experiments, apart from those designed expressly to examine "flicker" effect, are carried out at frequencies of the order of 10^5 c/sec. or higher to exclude the relatively slow, gross variations characteristic of "flicker" phenomena.

Since the high resistance required must now be *dynamic* in character the question arises whether such a resistance can be provided and utilized. Fortunately, the high conductivity of pure metals near absolute zero favors the provision of a coil of low ohmic resistance and hence a tuned circuit of very high dynamic impedance. Indeed, one might visualize the use of a super-conductor for this purpose.

The next difficulty that arises is the effect of the dynamic input resistance of the valve amplifier itself resulting from reaction. This can be estimated from the expression for the input admittance to the valve

$$Y_i = i\omega\{C_{go} + C_{gp}(1-m_a)\}, \qquad (1)$$

where m_a is the complex amplification of the amplifier stage. It appears very unlikely that it would be possible to maintain the real part of Y_i (i.e., the dynamic input conductance) sufficiently small; (in this connection, however, a cathode follower might prove feasible, the input admittance being very low). In addition, it would of course be essential to ensure that the over-all ohmic leakage between grid and earth was also large compared with the dynamic resistance of the tuned circuit.

A rather more fundamental criticism must be directed against the second part of Lawson and Long's letter. They suggest that effectively increased Brownian voltage might be derived from the piezoelectric fluctuations of a quartz crystal arising primarily from the random energy of mechanical vibration. They make a detailed numerical estimate of the voltage generated, namely

$$\langle V^2\rangle_{Av} = 1.4\times 10^{-12}\cdot T, \qquad (2)$$

(reference 1, Eq. (5)) and suggest that the internal resistance of the quartz is only a few thousand ohms, so that an input resistance of 10^8 ohms is adequate.

It must be pointed out that for *any* system in complete thermal equilibrium, *irrespective of the particular electrical or electromechanical mechanisms involved or of the number of causes of the irregular movement*, the Brownian voltage generated between any two terminals is given by Nyquist's formula

$$\langle V^2\rangle_{Av} = 4R(f)kT\Delta f, \qquad (3)$$

(reference 1, Eq. (1)) where $R(f)$ is the resistance (at frequency f) measured between the two terminals concerned. The classical example of the galvanometer has been analyzed in detail by Ornstein,[5] and Professor M. H. L. Pryce kindly informs us that similar conclusions can be drawn for the more general case of a linear inter-connected system of n degrees of freedom.

It must, therefore, be possible to calculate Eq. (2) directly from the crystal impedance as viewed from its (electrical) terminals. It is evident, however, that this step cannot be reconciled with Eq. (3), (bearing in mind that the bandwidth ($\Delta f \doteqdot f/Q$) is only of the order of one cycle/sec.) unless the crystal impedance is in fact very high. The paradox is resolved by considering the equivalent electrical circuit of the crystal; to a sufficient approximation this may be represented as in Fig. 1.

It is true that r is only of the order of $10^3\Omega$, but at resonance $R(f) = Q^2\cdot r$ and Q is in the order of 10^3–10^4, so immediately showing that the relevant impedance is exceedingly high. Thus taking $R(f) \doteqdot 2.5\times 10^{10}\Omega$ (clearly a reasonable value on the quoted figures) and $\Delta f \sim 1$ c/sec., we immediately arrive at (our) Eq. (2) from the fundamental formula (3) without further ado.

It therefore appears that, contrary to Lawson and Long's conclusion, the electrical fluctuations of a crystal, despite its mechanical Brownian movement, do not differ fundamentally from those of any other electrical network and can offer no inherent superiority as a low temperature thermometer. The only possible advantage is of a practical nature, since the crystal may more readily provide a very high electrical dynamic resistance, in the use of which, however, all the difficulties mentioned above would still have to be overcome.

Similar conclusions must of course apply to any other physical system of coupled elements in thermal equilibrium.

[1] A. W. Lawson and E. A. Long, Phys. Rev. **70**, 220 (1946).
[2] D. O. North, *et al.* R. C. A. Rev. **4**, 471 (1940).
[3] J. B. Johnson, Phys. Rev. **26**, 71 (1925).
[4] W. Schottky, Phys. Rev. **28**, 74 (1926).
[5] L. S. Ornstein, *et al.* Proc. Roy. Soc. **A115**, 391 (1927).

Further Remarks on the Possible Use of Brownian Motion in Low Temperature Thermometry

A. W. LAWSON AND EARL A. LONG
Institute for the Study of Metals, University of Chicago, Chicago, Illinois
November 13, 1946

IN a recent letter, Brown and MacDonald[1] have reviewed our discussion concerning the possibility of using Brownian motion for low temperature thermometry and have raised a number of objections concerning which we would like to make some additional remarks.

Brown and MacDonald point out that the estimates made by us of the lowest temperatures measurable with the thermal noise generated by a large resistance at the control grid of an electrometer tube neglect the flicker effect. For this reason, they believe that such a device would only be practical after a "drastic modification." The effect mentioned was omitted from our previous discussion because it appears likely that with an electrometer tube such as the Western Electric D-96475 operating at the necessarily low frequency of 5 cycles/second, the flicker noise can be substantially cancelled out by utilizing the screen grid, as in the familiar balanced circuit of Dubridge and Brown.[2]

The belief entertained by Brown and MacDonald that we have "apparently overlooked" a fundamental principle, namely the universal applicability of Nyquist's theorem, we can only attribute to the occurrence of an erroneous statement in our previous note, namely that an input resistance of 10^6 ohms is adequate for the successful operation of a piezoelectric thermometer. The statement in question should read that an input resistance of 10^{12} ohms should be adequate for such operation. Except for this error, we believe that there is no basis for drawing the conclusion of Brown and MacDonald that we claim any fundamental difference in the behavior of a piezoelectric thermometer from that of a resistance thermometer; the advantage is that of practicability. Although it is certainly more expeditious to make numerical estimates by applying Nyquist's theorem to experimentally determined dynamic resistances, it appeared worth while to derive our formula (4) expressing the noise voltage directly in terms of crystal constants, since this expression not only permits estimates of optimum crystal dimensions, but also reveals the inherent frequency limitation in such devices in a manner not immediately apparent from a consideration of Nyquist's formula itself.

The fact that the advantages of a piezoelectric thermometer are merely of a practical nature is not unimportant. Thus the piezoelectric thermometer avoids the following intrinsic difficulties associated with the first device described: (1) the long measurement time associated with low frequencies, owing to limitations imposed on band width by input capacities, (2) the necessity of minimizing microphonics, low frequency power supply variations, and flicker effects, and (3) the temperature-independence of the resistance, since the equivalent dynamic resistance of the piezoelectric crystal may be controlled by temperature-independent mechanical loading.

The principal disadvantage associated with a piezoelectric thermometer is the increased difficulty of obtaining a sufficiently high input resistance at the higher frequencies involved. However, recent developments in miniature tubes with small electron transit times (e.g., the RCA 6AK5) appear to offer some promise of meeting the required specifications.

In conclusion, it appears worth while to mention that Professor W. W. Hansen[3] has kindly pointed out to us that it may be advantageous to consider the use of a modification of the ingenious method recently described by Dicke[4] for the determination of temperature by the measurement of microwave radiation. A preliminary study by us of the design factors involved indicates that it should be possible to measure temperatures of the order of 0.1°K to 0.01°K using ordinary vacuum tubes with a noise generating resistance as low as 10^6 ohms.

[1] James B. Brown and D. K. C. MacDonald, Phys. Rev. **70**, 976 (1946).
[2] L. A. Dubridge and H. Brown, Rev. Sci. Inst. **4**, 532 (1933).
[3] Private communication.
[4] R. H. Dicke, Rev. Sci. Inst. **17**, 268 (1946).

The Angular Distribution of Gamma-Rays in Na^{24}, Co^{60}, Y^{88}*

WILFRED M. GOOD**
Massachusetts Institute of Technology, Cambridge, Massachusetts
October 25, 1946

WHEN two gamma-rays are emitted successively in the process of nuclear de-excitation, a distribution in angle is expected for the second gamma-ray relative to the first.[1,2] Coincidence studies to observe this angular correlation have been largely unsuccessful in showing any distribution apart from isotropy.[3,4]

The radioactive nuclei Na^{24}, Co^{60}, Y^{88} are particularly suited for deciding whether or not the above effect can be observed for the following reasons: (i) each of the radioactive transformations is followed by two successive gamma-ray transitions; (ii) the gamma-ray transitions occur, respectively, in the nuclei Mg^{24}, Ni^{60}, Sr^{88}. These nuclei are of the even-even type, and hence possess in their ground state no angular momentum. Zero to zero transitions are forbidden for gamma-ray transitions, hence the intermediate state cannot have an angular momentum zero. But theory shows that in the cases of these nuclei, only an intermediate state with an angular momentum of zero can give rise to an isotropic distribution. It follows, therefore, that in the cases of these nuclei, a distribution apart from isotropy is known to exist. It can further be said that as far as theory goes, the minimum asymmetry to be expected from all permissible angular momentum and parity assignments is seven percent; (iii) the respective half-lives of 14.8 hr., 5 yr., and 105 days are sufficiently long so that complications do not arise due to short half-lives.

The expected distribution is a power series in $\cos^2\theta$. The instrument used in the investigation subtended a solid angle of 0.3 steradian at the source. Analysis showed that an observed distribution would differ, because of finite solid angles, from the real distribution by only a couple of percent. Because of the low coincidence rates, and because the distribution has its extremes at the angles 90° and 180°, counting was restricted to these angles. The results are tabulated in Table I.

TABLE I. Observations of γ-ray emission at 90° and 180°.

Nucleus	180°	90°	Difference	Net rate at 90°	Percent asymmetry
Y^{88}	1.12±0.02 c.p.m.	1.08±0.02 c.p.m.	0.04±0.03 c.p.m.	0.78 c.p.m.	5.1±3.9
Co^{60}	1.67±0.04	1.63±0.04	0.04±0.06	0.56	7.1±10.
Na^{24}	3671±60*	3613±60*	58±84*	1800*	3.2±4.7

* Total coincidence

TABLE II. Estimated line widths for electric quadripole radiation.

Nucleus	γ-ray	τ	ΔE line width	ΔE hyperfine
Mg^{24}	2.75 Mev	1.4×10^{-12} sec.	2.8×10^{-3} ev	0.01×10^{-3} ev
	1.38	22.	0.18	
Ni^{59}	1.30	19.	0.21	0.08
	1.10	38.	0.11	
Sr^{38}	1.90	35.	0.11	0.12
	0.91	680.	0.006	

It is improbable from these data that an asymmetry can exist, though one as large as the minimum expected is not completely excluded. Until it can be demonstrated otherwise, magnetic coupling between the nucleus and the atomic electrons seems the most plausible reason for the distribution not being observed. Such a coupling will interfere with the distribution unless the lifetime of the nuclear state is very small compared with the precession times of the nuclear moment in the magnetic field of the electrons; that is, the width of the gamma-state must be large compared with the hyperfine splitting. Table II gives a summary of the estimated line widths for electric quadripole radiation, based upon a calculation of Lowen.[5] The right-hand column which is this coupling with a penetrating electron is not too significant because the materials were all in the solid state. However, consideration must be taken of the fact that when the gamma-rays are emitted, the atoms are most probably in deeper than optical degree of excitation due to the initial radioactive transformations. The right-hand column represents then a reasonable lower limit of coupling energy, and it is seen that the conditions for observing the distribution may not be met, in the case of quadra—or higher pole radiation.

A limited attempt was made to de-couple nucleus and electrons by the use of strong magnetic fields. The argument is that according to the assumptions of the theory, the components of angular momentum in the direction of the first gamma-rays are constants of motion. In the limit of an infinitely strong magnetic field parallel to the first gamma-ray, the nucleus and the atom become de-coupled, with their components along the magnetic field constant, thus satisfying the condition assumed by theory. Since this is true for strong fields, it should be true to lesser degree for finite fields. The experiment was attempted with a magnetic field of about 17,000 gauss. Counters were placed in the pole pieces of the magnet, 180° apart, and a difference was sought in the coincidence rate with the field on and the field off. No effect was observed outside the error of the data which was only sufficient to detect asymmetries of forty percent or greater in the form of the distribution. It is regretted that this work was terminated by the war and in the light of the paper of G. Goertzel in this issue of *The Physical Review* it is desirable to pursue the investigation further.

* Part of a thesis submitted to the faculty of Massachusetts Institute of Technology in partial fulfillment of the requirements of the Degree of Doctor of Philosophy, February, 1944.
** Now at Clinton Laboratories, Oak Ridge, Tennessee.
[1] D. R. Hamilton, Phys. Rev. **58**, 122 (1940).
[2] G. Goertzel and I. S. Lowen, Phys. Rev. **69**, 533 (1946).
[3] Kituchi, Watuse, and Itoh, Zeits. f. Physik **119**, 185 (1942).
[4] R. Beringer, Phys. Rev. **63**, 23 (1943).
[5] I. S. Lowen, Phys. Rev. **59**, 835 (1941).

Stark and Zeeman Effects in the Inversion Spectrum of Ammonia

DONALD K. COLES AND WILLIAM E. GOOD
Westinghouse Research Laboratories, East Pittsburgh, Pennsylvania
November 2, 1946

WE have observed Stark and Zeeman effects in the microwave absorption spectrum of NH_3 in the 1.25-cm region, using ammonia containing both N^{14} and N^{15}.

Ordinarily a rotational level of a symmetric top molecule is split by an electric field into $2J+1$ components, corresponding to the different values of M where $-J \leqslant M \leqslant J$. Because of the high frequency of inversion of the NH_3 molecule, however, there is no first-order Stark effect. The second-order effect is proportional to the square of the electric field E, and to M^2. Thus there are only $J+1$ levels corresponding to the different values of M^2.

Our d.c. electric field was parallel to the high frequency field as described previously,[1] so that only transitions corresponding to $\Delta M=0$ could be observed, with the transition $M=0$ to $M=0$ forbidden.

The increase in frequency produced by the electric field E is described approximately by the equation

$$\Delta\nu(\text{cm}^{-1})=1.5\times10^{-4}\cdot[MK/J(J+1)]^2\cdot E^2,$$

where E is given in e.s.u. This equation applies to ammonia made with either N^{14} or N^{15}.

A shift of this amount corresponds roughly to a semi-permanent dipole moment of 1.5×10^{-18} e.s.u.

A magnetic field of 6600 oersteds perpendicular to the high frequency field splits a rotational line into a doublet with a separation of approximately 2.0×10^{-4} cm^{-1}, independent of J and K within experimental error. A magnetic field parallel to the high frequency electric field produced no observable effect.

Good,[2] working with ordinary ammonia, has reported that several of the rotational lines exhibit a hyperfine structure. We have now resolved a hyperfine structure in most of the rotational lines of $N^{14}H_3$. We interpret the structure as a splitting of the rotational energy levels by a coupling between the angular momentum of the molecule as a whole and the spin of the nitrogen nucleus. This interaction appears to result from an electric quadrupole moment of the N^{14} nucleus, and is described by the equation

$$\Delta\nu=[e^2qQ]\cdot\left(\frac{3K^2}{2J(J+1)}-\frac{1}{2}\right)\cdot\left[\frac{(\tfrac{3}{4})C(C+1)-2J(J+1)I(I+1)}{(2J-1)(2J+3)(2I-1)(2I+3)}\right],$$

where

$$C=F(F+1)-I(I+1)-J(J+1),$$
$$I=1,$$
$$F=J+0,\ \pm1,$$
$$[e^2qQ]=3.4\times10^{-4}\ \text{cm}^{-1}.$$

$N^{15}H_3$ shows no trace of hyperfine structure. This is to be expected since N^{15} has a spin of $\frac{1}{2}$. The frequencies of the rotational lines of $N^{15}H_3$ are given approximately by the equation

$$\nu(\text{cm}^{-1})=0.7575-0.0047(J^2+J-K^2)+0.0019K^2.$$

[1] T. W. Dakin, W. E. Good, and D. K. Coles, Phys. Rev. **70**, 560 (1946).
[2] W. E. Good, Phys. Rev. **70**, 213 (1946).

β-Ray Spectrum of K^{40} and Theory of β-Decay

R. E. MARSHAK
University of Rochester, Rochester, New York
October 27, 1946

IN principle, the highly forbidden β-ray transition $K^{40} \rightarrow Ca^{40} + \beta^-$, associated with a spin change of four units, should provide a sensitive test of the possible theories of β-decay. At first it was thought[1] that the known lifetime of K^{40} was best explained by the tensor or pseudo-vector interactions. It was argued that the other three interactions, in particular the vector interaction, led to *minimum* lifetimes comparable to the observed lifetime and could therefore be ruled out on the supposition that the nuclear matrix element is small compared to unity. Implicit in this argument, however, was an estimate of the magnitude of the Dirac α-operator.[2] Grueling[3] has shown that this estimate may be in error by a rather large factor and thereupon pointed out that the vector interaction could also explain the observed lifetime of K^{40}.

Since the lifetime calculations are inconclusive, it is of interest to consider the evidence on the energy spectrum. Recently, Dželepow, Kopjova, and Vorobjov[4] published a measurement of the β-ray spectrum of K^{40}. It seems worth while to compare the predictions of the theory with this admittedly crude measurement. The results are given in Fig. 1, taking $W_0 = 3.64$ (the total energy in units of mc^2) as the upper limit of the spectrum. Curves I–IV represent the ratios of D_i to D where D is the allowed energy distribution function and is plotted as Curve V. The circles represent the ratio of the experimental points to D. The D_i's are defined as follows (cf. Eq. (11) of Greuling's paper[3]):

$$C_{3T} = D_2 |Q_4(\beta\sigma, r)|^2;\ C_{3A} = D_2 |Q_4(\sigma, r)|^2$$
$$C_{4S} = D_1' |Q_4(\beta r, r)|^2;\ C_{4P} = D_1' |Q_4(\beta\gamma_5 r, r)|^2$$
$$C_{4V} = D_1'' |Q_4(r, r)|^2 + D_2 |Q_4(\alpha, r)|^2 + D_{23}[Q_4(\alpha, r) Q_4^*(r, r) - \text{c.c.}]$$
$$C_{4T} = D_1 |Q_4(\beta\sigma \times r, r)|^2 + D_2 |Q_4(\beta\alpha, r)|^2 - D_3[Q_4(\beta\sigma \times r, r) Q_4^*(\beta\alpha, r) + \text{c.c.}]$$
$$C_{4A} = D_4 |Q_4(\sigma \times r, r)|^2$$

The quantities D_1' and D_1'' are not identical with D_1 but are so closely represented by D_1 over the entire range of W (within a few percent) that Curve I may be used. Curves I–IV are all fitted at $W = 2$, the maximum of D.

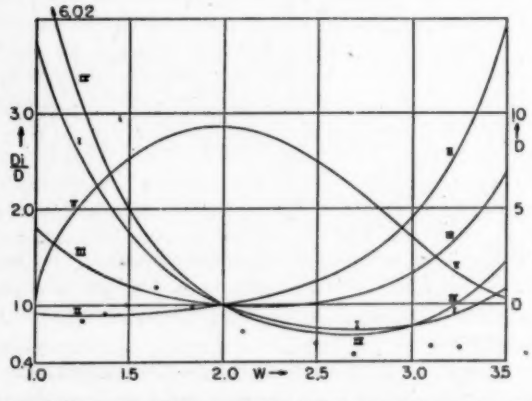

FIG. 1. Comparison of the predictions of theory and experiment for the β-ray spectrum of K^{40}.

The third forbidden transitions C_{3T} and C_{3A} require a parity change. Hence, if the parities of K^{40} and Ca^{40} were different, the energy dependence would be unique and given by Curve II. The disagreement is so striking in the high energy region—where the experimental results are supposedly most accurate[4]—that C_{3T} and C_{3A} may be excluded. If the parities of K^{40} and Ca^{40} are the same, the transition must be fourth forbidden. C_{4S}, C_{4P}, and C_{4A} lead to unique energy spectra—expressed by Curves I and IV—which deviate sharply from the experimental points in the low energy region. C_{4V} and C_{4T} are more flexible because one may choose the two matrix elements arbitrarily, but here too a satisfactory fit is impossible to achieve if one takes seriously the "peaked" character of the measured spectrum. Since the low energy experimental points are poor and the entire spectrum is preliminary, the question of which fourth forbidden transition is correct—if any—is still undecided. The most impressive feature of Fig. 1 is the sensitivity of the energy spectrum to the different interactions. A good measurement of the β-ray spectrum of K^{40}—using enriched K^{40}—would thus be extremely valuable. In particular, if it turned out that the clustering of the experimental points about the allowed spectrum is real (cf. Fig. 1), a satisfactory fit could only be obtained with C_{4V} or C_{4T}.

Figure 1 was prepared for the author by Messrs. B. Carlson and A. Wightman while all three were at the Research Laboratories of the General Electric Company last summer.

[1] R. E. Marshak, Phys. Rev. **61**, 431 (1942).
[2] E. J. Konopinski and G. E. Uhlenbeck, Phys. Rev. **60**, 308 (1941).
[3] E. Grueling, Phys. Rev. **61**, 568 (1942).
[4] B. Dželepow, M. Kopjova, and E. Vorobjov, Phys. Rev. **69**, 538 (1946).

Possibility of "Conditional" Saturation in Nuclei

E. FEENBERG AND H. PRIMAKOFF
Washington University, St. Louis, Missouri
November 20, 1946

NUCLEAR forces are commonly supposed to possess a saturation property in the sense that, within a given nucleus, one nucleon is presumed, under all circumstances, to interact effectively only with a limited number of other nucleons.[1] Actually the empirical uniformities in binding energy, spin, isotopic number, size, etc., do not require saturation in such an absolute sense, but only that this property holds for all nuclear states not too far different (in energy, etc.) from those heretofore found.

A physical analogy may be helpful in making the situation clear. Consider, for example, a microcrystal of solid deuterium consisting of 90 atoms. There is a theoretical possibility for this crystal to make a transition to the state of a single Th atom ($Z = 90$, $A = 180$) with release of nearly 10^9 ev of energy. The corresponding transition probability is, of course, immeasurably small, because the individual deuterons in the crystal are separated by distances large

compared to the range of the nuclear forces and because an electronic transition of very high order is required. However, the essential point for our discussion is that this probability does not entirely vanish.

This example demonstrates the existence of a property which may be called "conditional" saturation. Thus, the system under consideration (the microcrystal) exists in a metastable state of extremely long life with binding energy and volume proportional to the number of a certain type of structural unit (the deuterium molecule) while another state of the same system is possible (the single heavy atom) with far greater binding energy, greatly reduced volume, and without the saturation property with respect to the previously defined unit. It is evident that such "conditional" saturation is not an uncommon occurrence in ordinary matter.

We now wish to suggest that perhaps a similar phenomenon may occur entirely on the nuclear level. Wigner and Eisenbud,[2] Bethe,[3] and particularly Volkoff[4] have discussed the possibility of the nuclear tensor force causing the failure of saturation and have pointed out some of the restrictions to be placed on the tensor force if this failure is not to occur. Let us here suppose, however, that the conditions required for the breakdown of "absolute" saturation in nuclei are actually present in nature, i.e., the ratio of the magnitudes of the tensor and central forces exceeds a certain critical value. Then the observed nuclear saturation (with its attendant properties of small and fairly uniform binding energy per particle, spherical shape, small spin, and isotopic number, etc.) is of the "conditional" type, and some nuclei (presumably the heavier ones) can exist in much lower energy states associated with a (average) total potential energy more or less proportional to the square of the mass number, a total binding energy comparable with the sum of the rest masses of the original nucleons, greatly reduced dimensions, shape highly distorted from the spherical, very large spin, and possibly very large isotopic number. If this supposition is correct, transitions may occur from the comparatively loosely bound "saturation" states to the much more tightly bound "collapsed" states with the emission of (a) γ-radiation or (b) one or more (but not too many) nucleons. The product "collapsed" nucleus will then undergo a certain number of $\beta^{\pm}$-transitions until it attains an equilibrium value of charge.[5] Because of the large spin difference between the original and product nuclei, the transition via (b) is perhaps more likely than (a), particularly in view of the strength of the nucleon-nucleon interaction, the order of magnitude equality of the nuclear force range and the nuclear dimensions, and the comparatively large statistical weight associated with the emission of several nucleons. Finally it should be mentioned that nucleons released in the transitions under consideration would have energies of the order 10^{9}–10^{10} ev and so could play a role as cosmic-ray primaries.

As a test of these ideas one could search for "collapsed" nuclei constituting extremely rare isotopes of known elements. Of course, the terrestrial concentrations of the collapsed nuclei might be much greater than the value expected from the above described transition probability and the age of the earth, since it is quite possible that some collapsed nuclei were formed at the time of formation of ordinary saturated nuclei. The extremely large binding energy of the collapsed nuclei would probably make it difficult to establish the exact number of neutrons in them; on the other hand, distinguishing features of these nuclei (in addition to their characteristic charge mass ratios) would be their completely non-integral mass values, and a tremendous hyperfine structure.

If the collapsed nuclei exist it is to be expected that their relative concentration is greatest in (terrestrially) rare elements since the final product of the above mentioned series of $\beta^{\pm}$-transitions is just as likely to have a value of Z associated with a rare as with a common element. The possibility of collapsed transuranic nuclei should also be considered.

Emphasis has here been placed on the possible role of the tensor force in breaking down "absolute" saturation, but other causes of "conditional" saturation can be found within the bounds of current field theories of nuclear forces; for example, in the existence of short range, attractive many body forces[6] which become fully effective only in collapsed nuclei.

[1] G. Breit and E. Wigner, Phys. Rev. **53**, 998 (1938).
[2] E. Wigner and L. Eisenbud, Phys. Rev. **56**, 214 (1939).
[3] H. A. Bethe, Phys. Rev. **57**, 260 (1940).
[4] G. M. Volkoff, Phys. Rev. **62**, 126, 134 (1942).
[5] The equilibrium value of charge appropriate to a collapsed nucleus possibility corresponds to a much greater neutron excess than is found in ordinary conditionally saturated nuclei, so that the $\beta^{\pm}$-transitions are largely β^{+}. This conclusion is a consequence of the fact that in collapsed nuclei an exchange type tensor force will have a potential energy which decreases (algebraically) more rapidly with increasing isotopic number than the kinetic energy increases; the Coulomb energy then favors a large neutron excess.
[6] H. Primakoff and T. Holstein, Phys. Rev. **55**, 1218 (1939).

On the Dynamics of the RbI Crystal

T. A. Hoffmann
Physical Institute of the University for Technical and Economic Sciences, Budapest, Hungary
October 8, 1946

THE alkali halogenide ionic crystals can be dealt with by the statistical atomic model without the aid of empirical or semi-empirical parameters, especially in the case of ions containing many electrons. Jensen has made calculations on the whole alkali halogenide series by a combination of the Thomas-Fermi-Dirac and the Fermi-Amaldi models, called in the following the Jensen model.[1] Jensen took into account the van der Waals correction also, using the approximating formula $-1330\times10^{-60}/\delta^{6}$ erg of Mayer.[2] His results can be improved essentially by using the Gombás model, which takes into account the correlation effect.[3] Jensen's calculations must be extended at two points. First, we must introduce the electron densities of Gombás instead of those of Jensen, and secondly we must take into account the energy term resulting from the correlation. This last can be done by taking $\kappa_a' = 1.13\kappa_a$ for Jensen's κ_a in the exchange energy term, since the correlation gives a term proportional to the exchange energy. I have performed the calculations for the face-centered lattice of the RbI crystal.

TABLE I. Comparison of theory and experiment.

		Lattice constant (10^{-8} cm)		Compressibility at $T=0°$ (10^{-12} cm²/dyne)		Infra-red wave-length (10^{-4} cm)		Tensile strength at $T=0°$ (10^{10} dyne/cm²)
Without van der Waals correction	Calc. by Jensen	3.96	8.0%	15.5	82.4%	215	66.6%	—
	Calc. here	3.79	3.4%	9.57	12.6%	82	36.4%	2.63
With van der Waals correction	Calc. by Jensen	3.84	3.5%	13.0	52.9%	195	51.2%	—
	Calc. here	3.69	0.7%	8.47	0.4%	124	3.9%	1.52
Experimental values		3.67		extrapol. to $T=273°$: 9.4. lin. extr. to $T=0°$: 7.6. mean value: 8.5		129		—

The whole calculation was not performed according to the Gombás model, but the results were obtained with the aid of a perturbation method from Jensen's results, leading to great simplifications in the numerical evaluations. The two corrections mentioned above give a perturbation term in each of Jensen's second and third energy terms. The new state of equilibrium is given by the vanishing of the derivative of the total lattice energy obtained in this way. Supposing the correction in the lattice constant to be small, which is verified by the results, the new lattice constant can be written as $\delta_0'=\delta_0+\Delta\delta_0$, where δ_0 is Jensen's lattice constant. Neglecting terms of the second or higher order in $\Delta\delta_0$ we get

$$\Delta\delta_0=-\frac{(d\Delta E/d\delta)_{\delta=\delta_0}}{(d^2E/d\delta^2)_{\delta=\delta_0}+(d^2\Delta E/d\delta^2)_{\delta=\delta_0}},$$

where E is Jensen's lattice energy and $\Delta E=E'-E$ is the energy change, E' being the new lattice energy. We get the value of $(d^2E/d\delta^2)_{\delta=\delta_0}$ in this expression from the compressibility calculated by Jensen (see Table I), since

$$(d^2E/d\delta^2)_{\delta=\delta_0}=18\delta_0/\kappa,$$

κ being the compressibility at zero absolute temperature. Detailed calculations must be made to evaluate $(d\Delta E/d\delta)_{\delta=\delta_0}$ and $(d^2\Delta E/d\delta^2)_{\delta=\delta_0}$. This can be done as follows. Gombás' ν' can be introduced by an additive term $\delta\nu=\nu'-\nu$ to the electron density, ν, of Jensen. $\delta\nu$ can be approximated very well as a linear function of r in the range important here, i.e., in the outer parts of the ions, and the Jensen densities also can be approximated well by analytical functions in the same region. So the integrals concerned can be evaluated in closed form, which in the present case is more advantageous than numerical evaluation.

In the accompanying table my results are compared with those of Jensen and with the experimental values. For each theoretical value the percentage deviation from the experimental value is given. Taking into account the expression for the van der Waals energy given above, the results are in excellent agreement with the experimental values even for such sensitive properties as the compressibility or the infra-red frequencies. This good agreement would not be disturbed even by a smaller change in the approximating expression used for the van der Waals energy. I have calculated the tensile strength of the crystal with respect to a uniform dilatation also, but these results cannot be compared with the observed value, since the last is a structure-sensitive property, while the former was calculated on the basis of a structure-insensitive model.[4]

Detailed calculations will be published elsewhere.

[1] H. Jensen, Zeits. f. Physik 101, 164 (1936).
[2] E. J. Mayer, J. Chem. Phys. 1, 270 (1933).
[3] P. Gombás, Zeits. f. Physik 121, 523 (1943).
[4] See e.g., A. Joffé, Internat. Conference on Physics, Papers and Discussions, London, 1934. Vol. II, page 72.

Isotopic Assignment of Cd and Ag Activities

A. C. HELMHOLZ
Radiation Laboratory, Department of Physics, University of California, Berkeley, California
July 15, 1946

THE author has reported[1] that the 6.7 hr. Cd and the long-lived Cd of 158-day half-life, K-capture activities formed by the reaction Ag(d, $2n$)Cd, both decay to isomeric states of Ag, both of which have half-lives of 40 sec. and decay by the emission of γ-rays of 93 kev and 87 kev, respectively. The fact that the γ-rays are distinct was checked by observing the K and L conversion lines of both on a single photograph in a β-ray spectrograph[2] and noting that on successive photographs the 93-kev lines disappeared with the 6.7 hr. half-life. Bradt, Gugelot, Huber, Medicus, Preiswerk, and Scherrer[3] confirmed this result and in addition report that the 93-kev isomeric state has a half-life of 44.3 sec., the 87-kev. state of 40.5 sec.

The purpose of this letter is to report the isotopic assignment of these activities. In this laboratory a group under the direction of Dr. Burton Moyer has prepared approximately 100 mg. samples enriched in Cd^{106} and Cd^{108}. Mass spectrographic analysis showed the former to be 58.3 percent Cd^{106}, 0.6 percent Cd^{108}, and the latter to be 0.7 percent Cd^{106}, 45.4 percent Cd^{108}. The remaining percentages of each sample contained the other Cd isotopes in approximately their normal ratio. Through the kindness of Dr. Moyer the author was able to bombard these samples with slow neutrons from the 60″ cyclotron. The 6.7-hr. period was the predominant activity in the 106 sample after a few hours bombardment. A three-week bombardment produced in the 108 sample a weak, long-lived activity with absorption curve characteristic of the 158-day Cd. These two activities are easily identified by absorption curves of their electrons since the only electrons emitted (except for the rare positrons found by Bradt *et al.*) are the conversion lines with range about 10 mg/cm². The results then assign the 6.7 hr. Cd to Cd^{107}, the 93-kev isomer to Ag^{107}; the 158-day Cd to Cd^{109}, and the 87-kev isomer to Ag^{109}. A deuteron bombardment of normal Ag showed that the Cd isotopes are formed in roughly equal numbers as would be expected from the roughly equal abundances of the Ag isotopes. The Cd^{109} assignment was further checked in the following way. If Ag is bombarded with α-particles, Cd^{107} is formed only by the reaction (α, $p3n$), while Cd^{109}

is formed both by this reaction and the more probable (α, pn). Bombardment of Ag with approximately 40 Mev α-particles produced a good yield of the long-lived Cd, a small or possibly zero yield of the 6.7 hr. Cd. This latter yield will be further checked.

The bombardment of Ag with approximately 20-Mev deuterons also produced in the surface layers of the target a Pd activity of 13 hr. half-life. Rall[4] has assigned this activity to Pd^{109}, so in this case it is formed by the reaction $Ag(d, 2p)Pd$. An absorption measurement gave 1.0 Mev as the upper limit of the β-spectrum, in satisfactory agreement with the 1.08 Mev reported by Kraus and Cork.[5] The threshold of the reaction is $E_{max}+2M_H-M_D$ or about 2.5 Mev. However, the low probability that protons be ejected through the barrier with low energy explains the fact that Krishnan[6] with 9-Mev deuterons observed no Pd activity, and that the yield here was observable only at high bombarding energies. No other Pd activity was found. Pd^{107} must have a very short half-life to have escaped detection in other investigations, or a half-life greater than 25 years to be undetected in this case.

I wish to thank Dr. Moyer for the use of the enriched samples and Dr. J. G. Hamilton and the members of the 60″ cyclotron crew for the bombardments.

This work was done under the auspices of the Manhattan District, Contract No. W-7405-ENG-48.

[1] A. C. Helmholz, Phys. Rev. **60**, 160 (1941).
[2] A. C. Helmholz, Phys. Rev. **60**, 415 (1941).
[3] H. Bradt, P. C. Gugelot, O. Huber, H. Medicus, P. Preiswerk, and P. Scherrer, Helv. Phys. Acta **18**, 256 (1945).
[4] W. Rall, Bull. Am. Phys. Soc. **21**, 3, 18 (1946).
[5] J. D. Kraus and J. M. Cork, Phys. Rev. **52**, 763 (1937).
[6] R. S. Krishnan, Proc. Camb. Phil. Soc. **36**, 500 (1940).

Beta- and Gamma-Ray Energies of Several Radioactive Isotopes*

L. C. Miller and L. F. Curtiss
Clinton Laboratories, Oak Ridge, Tennessee
October 24, 1946

THE thin magnetic lens spectrometer constructed by Wilkinson and Rall at the Metallurgical Laboratory and now in use at Clinton Laboratories has been used to obtain data on the beta- and gamma-ray energies of several additional radioactive isotopes.

All activities were produced by slow neutron irradiation of the elements or their compounds in the Clinton pile. All samples, with the exception of the dysprosium compound, were spectroscopically analyzed for impurities. In no cases did the combination of factors, such as amount of impurity, cross section of impurity for slow neutron capture, and period of any activity due to the impurity, appear to be such that the impurity could be responsible for any observed gamma-rays.

Table I summarizes the results obtained. The gamma-ray energies are probably correct within 2 percent except where the approximation sign indicates less reliable data. The last column gives rough estimates on the relative intensities of gamma-rays from most of the isotopes. These may be in error by as much as 50 percent.

Table I. Energies of beta- and gamma-rays.

Isotopes	Beta-ray End points (Mev)	Gamma-rays (Mev)	Rel. intensities of gamma-rays
26.8 hr. As^{76}		0.57	5
		1.25	2
		1.84	very weak
		2.15	very weak
24.1 hr. W^{187}	0.6 and 1.3	0.48	3
		0.69	2
14.1 hr. Ga^{72}		0.64	1
		0.84	6
		2.25	6
26.5 d. Cr^{51}		0.32	
18 hr. Re^{188}		0.16	4
		0.48	1
		0.64	2
		0.94	2
		1.43	1
51.5 d. Hg^{203} or ^{205}	<0.3	0.28	
40 hr. La^{140}		0.335	1
		0.49	10
		0.83	20
		1.63	100
		~2.3	5
46 hr. Sm		0.11	
		~0.6	
60 d. Sb^{124}	0.53 and 2.25		
2.8 d. Sb^{122}	1.36 and 1.94		
11 d. Ge^{71}	~0.6[a]	~0.5[b]	
67 hr. Mo^{99}		0.24[c]	
		0.75	
2.5 hr. Dy^{165}		0.37[d]	
		~1.0	

[a] Probably positrons.
[b] Possibly annihilation radiation.
[c] Preliminary data; no chemical separation, but these gamma-rays are probably not from 6.1-hr. activity of element 43. Data indicate that other gamma-rays may also be present.
[d] Preliminary data; other gamma-rays may also be present.

Details of these studies will appear in the *Volume of Collected Papers on Nuclear Physics of the Plutonium Project Record.*

* This document is based on work performed under Contract No. W-7405-eng-39 with the Manhattan Project at Clinton Laboratories.

The Abundance of He^3 in Atmospheric and Well Helium

L. T. Aldrich and Alfred O. Nier
University of Minnesota, Minneapolis, Minnesota
December 2, 1946

BY means of a 60° mass spectrometer we have just completed an investigation of the relative abundances of the helium isotopes. The average value for the He^4/He^3 ratio in two samples of atmospheric helium from the Air Reduction Sales Company was found to be 9×10^5,[1] and that for two samples of well helium 7×10^6. These values should not be in absolute error by more than 25 percent. The relative He^3 concentrations are within 10 percent. The He^3 peak was completely resolved from HD. In all cases the He^4/He^3 ratio was independent of pressure and amount of hydrogen impurity. The ionization efficiency curve for the He^3 peak agreed within experimental error with that for He^4 and was distinctly different from that for HD.

Alvarez and Cornog[2] have reported the existence of He^3 as a result of observation of a mass three beam in the Berkeley 60″ cyclotron and gave He^4/He^3 ratios of 10^8

and 10^7 for well and atmospheric helium, respectively. In a private communication Dr. Alvarez has indicated that owing to difficulties in shimming the cyclotron and to the fact that different detecting devices were used for He^3 and He^4 in their work, it is possible that their absolute determination of the He^3 abundance might be in error. However, since the same experimental arrangements were used for air and well helium, their relative He^3 concentrations should be correct. Our relative concentrations are in good agreement with their values, and since at present we see no reason to doubt our absolute determinations, it appears that He^3 is approximately ten times as abundant as has been assumed heretofore.

Helium from different geological sources including radioactive minerals will be investigated in further studies.

While the problem of concentrating He^3 from natural sources remains a formidable one, the higher value for the abundance brings it closer to reality. Also since measurements are in the range of a good mass spectrometer, the results of concentration processes can be evaluated.

The mass spectrometer used in this investigation was built from a grant from the Graduate School. This research was made possible through a grant from the Research Corporation.

[1] In a preliminary report in the Bulletin of the American Physical Society, Vol. 21, No. 6, November 29, 1946 we gave 6×10^6 for this ratio.
[2] L. W. Alvarez and R. Cornog, Phys. Rev. 56, 613 (1939); 56, 379 (1939).

The Hyperfine Structure of the Microwave Spectrum of Ammonia and the Existence of a Quadrupole Moment in N^{14} *

B. P. Dailey, R. L. Kyhl, M. W. P. Strandberg, J. H. Van Vleck, and E. B. Wilson, Jr.
Massachusetts Institute of Technology and Harvard University, Cambridge, Massachusetts
November 29, 1946

Good[1] has reported the existence of a hyperfine structure for many of the lines of the inversion spectrum of ammonia, $N^{14}H_3$, which falls in the microwave region near 1.25 cm. This feature had not been predicted theoretically. Of the possible explanations, the interaction of a quadrupole moment of the N^{14} nucleus with the electrical field of the other charges in the molecule seems the most likely and has been widely discussed. Another possibility, magnetic spin-spin interaction of the nuclei, is theoretically of too small a magnitude and does not fit in other ways.

In order to test the quadrupole hypothesis, a quantum-mechanical treatment of the interaction has been carried out and the results compared with accurate measurements of the hyperfine structure spacings.

The equations, the derivation of which will be published separately, are as follows for the frequency difference between the central line and each of the four satellites:

$$h\Delta\nu = \pm(\tfrac{3}{16})Q(\partial^2V/\partial z^2)\{1-[3K^2/J(J+1)]\}[(J+1)/(2J+3)],$$

$$h\Delta\nu' = \pm(\tfrac{3}{16})Q(\partial^2V/\partial z^2)\{1-[3K^2/J(J+1)]\}[J/(2J-1)],$$

in which Q is the so-called nuclear quadrupole moment[2] $\langle\rho(3z^2-r^2)\rangle_{Av}$ and J and K are the total angular momentum and axial angular momentum quantum numbers for the rotation of the molecule. V is the electrostatic potential at the nitrogen nucleus owing to the charges outside that nucleus. Z is along the symmetry axis. These formulas assume that the molecule is of the symmetrical top type, that the spin of the N nucleus is unity, and that the magnetic couplings of the nuclei are negligible.

The hyperfine structure for the (J, K) 11, 22, 33, and 44 lines of $N^{14}H_3$ was measured with an apparatus using a wave guide absorption cell and a sweeping technique in which the carrier was frequency modulated, so that sidebands are produced which cause images of the central absorption line to be displayed. These are compared in frequency with the satellite lines. The results are given in the Tables I and II. Since the absolute values of Q and $\partial^2V/\partial z^2$ are not known, only ratios of splittings can be predicted theoretically.

It is seen that the agreement is excellent. Furthermore no hyperfine structure has been detected for $J=3$, $K=2$, for which the theory predicts zero splitting, or for higher J values, for which a further theoretical treatment predicts a lower relative intensity for the satellites.

Since N^{15} is reported[2] to have a nuclear spin of $\frac{1}{2}$ units, it should not show this effect. Therefore a sample of ammonia containing 60 percent N^{15} was prepared from ammonium nitrate procured from the Eastman Kodak Laboratory and its inversion spectrum examined in a simple wave guide absorption apparatus similar to that used by Hershberger.[3] Lines ascribed to $N^{15}H_3$ were found at 24560(77), 23928(66), 23686(11, 10), 23406(55), 23049(44), 22769(33), 22640(22) megacycles, the probable quantum numbers being given in parenthesis. Although the hyperfine structure of the $N^{14}H_3$ lines 11, 22, 33, and 44 was clearly observed with the same sample of ammonia, no hyperfine structure was seen on the $N^{15}H_3$ lines.

We therefore conclude that the hypothesis that the hyperfine structure of $N^{14}H_3$ is caused by a quadrupole interaction is strongly supported by several types of observations.

Table I. Hyperfine structure spacings in $N^{14}H_3$ in megacycles/sec. from the central line.

JK	$\Delta\nu$	$\Delta\nu'$	JK	$\Delta\nu$	$\Delta\nu'$
11	0.60	1.57	33	1.72	2.34
22	1.30	2.05	44	1.91	2.48
		(all values ±0.05)			

Table II. Calculated and observed ratios.

JK	$\Delta\nu JK/\Delta\nu 11$ obs.	calc.	$\Delta\nu' JK/\Delta\nu' 11$ obs.	calc.	$\Delta\nu' JK/\Delta\nu JK$ obs.	calc.
11					2.62	2.50
22	2.17	2.14	1.31	1.33	1.58	1.56
33	2.87	2.78	1.49	1.50	1.36	1.35
44	3.18	3.18	1.58	1.60	1.30	1.26

* Part of this work was supported by the Office of Naval Research under Task Order V of Contract N5ori-76 with Harvard University.
[1] W. E. Good, Phys. Rev. 70, 213 (1946).
[2] R. W. Wood and G. H. Dieke, J. Chem. Phys. 6, 908 (1938).
[3] W. D. Hershberger, J. App. Phys. 17, 495 (1946). J. E. Walter and W. D. Hershberger, J. App. Phys. 17, 814 (1946).

Pressure and Temperature Measurements in the Upper Atmosphere

NOLAN R. BEST, ERIC DURAND, DONALD I. GALE, AND RALPH J. HAVENS
Naval Research Laboratory, Washington, D. C.
November 29, 1946

THE October 10 V-2 firing at White Sands, New Mexico, gave interesting atmospheric pressure data in the region from 50 to 90 km above sea level.

The nose-tip of this rocket was made in the form of a cone of 13° apex angle. A ring of holes around the cone afforded connection between the exterior surface and the interior instrument compartment. Additional pressure measurements were made at a point near the tail of the rocket. Experiments by Taylor and Maccoll[1] show that the pressure on the side of a 13° nose cone should be about 1.8 times ambient when the rocket velocity is about 1 mile per second. German wind-tunnel measurements indicate that the tail section gauges should read ambient pressure to within about 10 percent.

Two different types of gauges gave usable data, their readings being transmitted by radio to a telemetering ground station.[2]

Pressures in the lower atmosphere were measured by a sylphon bellows gauge at the tail position. Bellows displacement was transformed into shaft-rotation of a Microtorque potentiometer. This gauge was designed to cover the range from 760 to 15 mm Hg, but broke at a pressure of 150 mm evidently from vibration. Figure 1 A shows the correlation with data computed from Weather Bureau temperature measurements taken over El Paso, Texas, (80 miles distant) at 8:00 A.M. the morning of the flight. Note the deviation when the rocket reached the speed of sound (Mach number =1).

Tungsten wire Pirani gauges in nose and tail gave satisfactory data. These consisted of 6-watt, 110-volt Mazda pilot lamps with a hole in the bulb tip. The tail gauge measurements are plotted in Fig. 1B. The points determined from the nose gauge lie almost exactly on the same curve. The twofold increase in pressure predicted by Taylor and Maccoll is absent. The discrepancy is unexplained to date, and is most surprising, since on the one hand, some pressure build-up can be predicted from elementary considerations, while on the other hand, a factor of 2 difference in gauge performance is hard to believe. Further studies should clarify the matter.

For comparison with the present observations NACA atmospheric pressure values based on assumed standard temperature[3] are shown by the dashed line in Fig. 1B. The good agreement obtained confirms the essential validity of the assumptions underlying the NACA curve, which is based entirely on indirect evidence. The bend in the solid curve between 60 and 80 km confirms the existence of the negative temperature gradient predicted by the NACA.

Because of the high V-2 velocity and the rapid rate of change of pressure with altitude, it was possible to fix within ±2 sec. the time of maximum altitude by noting the times on the ascent and the descent at which the pressure had a certain value; namely, 0.05 mm Hg. From this, a peak altitude of 108±2 miles was computed.

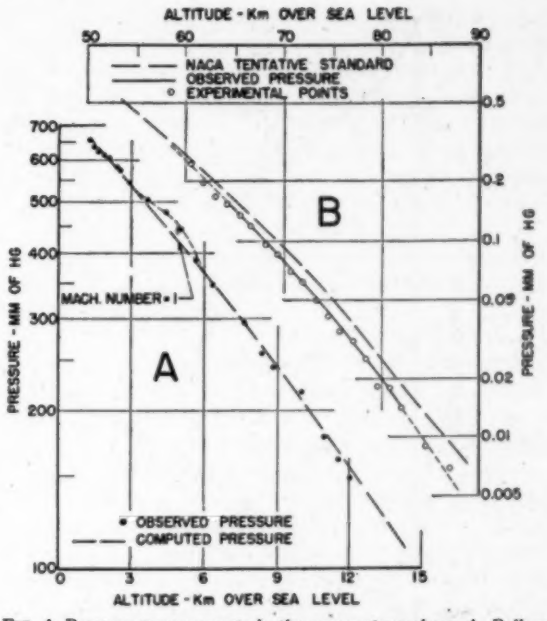

FIG. 1. Pressure measurements in the upper atmosphere. A. Bellows gauge. Use lower and left-hand scales. B. Platinum Pirani gauge. Use upper and right-hand scales.

Eleven platinum resistance and thermistor temperature gauges were installed to measure the adiabatic air temperature and the skin heating. The highest skin temperature observed was 180° C on a 0.3-mm wall section in the control chamber. Further results will not be published at the present time, pending a more complete analysis.

[1] G. I. Taylor and J. W. Maccoll, Proc. Roy Soc. 139, 278 (1933).
[2] Naval Research Laboratory Report R-2955, Chapter II, Section C, (October 1, 1946).
[3] National Advisory Committee for Aeronautics, *Tentative Tables for the Properties of the Upper Atmosphere* (Prepared by Calvin N. Warfield), Table III—(Sept. 1946).

On the Disintegration Scheme of Na^{24}

C. S. COOK, E. JURNEY, AND L. M. LANGER
Indiana University, Bloomington, Indiana
December 1, 1946

WHAT appear to be the most reliable measurements on the disintegration of Na^{24} suggest a simple beta-particle spectrum with an end point of 1.39 Mev and two gamma-rays of about equal intensity with energies of 1.38 Mev and 2.76 Mev.[1]

Experiments on the inelastic scattering of protons and neutrons[2] by the Mg nucleus indicate excited levels at 1.3 Mev, 2.74 Mev, and 3.88 Mev.

The existence of γ-γ coincidences[3] and the fact that their intensities are equal suggests that the 2.76-Mev and 1.38-Mev rays are in cascade. However, Sachs[4] in a recent letter, has called attention to the fact that such a level system would yield a mass for Na^{24} which would be in disagreement with the value predicted by Barkas.[5] He has, therefore, proposed an alternative scheme, whereby the 1.39

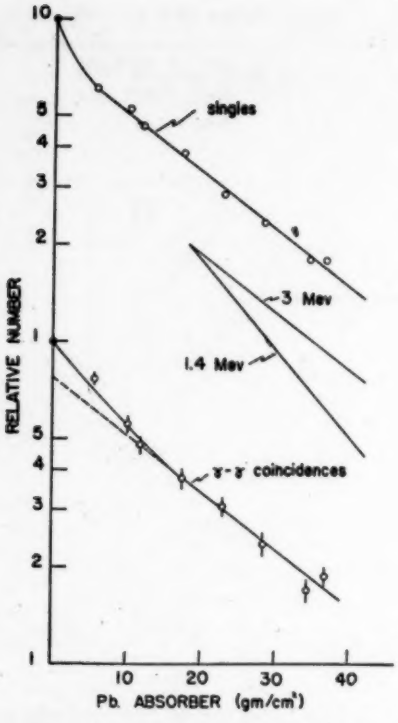

FIG. 1. Coincidence and single absorption in Pb of the gamma-rays of Na^{24}.

Mev β-ray is followed by *either* two 1.38-Mev γ-rays in cascade *or* by a 2.76-Mev γ-ray going directly to the ground state of Mg^{24}. The fact that the intensity ratio is 1, could be accounted for by assuming a branching ratio of 1:2. Both of these level schemes are consistent with the excited levels found in Mg^{24}.

It would be helpful in deciding between these two proposed level systems to know whether the γ-γ coincidences arise from two γ-rays each of 1.38 Mev or from one γ-ray of 1.38 Mev and one of 2.76 Mev.

In order to test this point, γ-γ coincidences were measured as a function of the thickness of Pb absorber interposed between the source and one of a pair of G-M counters. The absorption curve so obtained is to be compared with the absorption of all γ-rays in a single counter, taken at the same time with identical geometry. The results of such an experiment are shown in Fig. 1. Chemically pure NaCl was bombarded by 11-Mev deuterons in the external beam of the cyclotron. After all short periods had disappeared, the source, decaying with the proper 14.8-hr. period, was mounted approximately midway between two counters spaced 11 cm apart. Sufficient aluminum to remove all β-rays was placed on both sides of the source. The data in Fig. 1 have been corrected for decay, background, and chance. The errors indicated are statistical.

Because of the poor geometry (which must be tolerated in such coincidence measurements in order to minimize the statistical errors) no real significance should be attached to the absolute values of the absorption coefficients. However, it does appear significant that both the singles and coincidence curves have the same slope at higher absorber thicknesses. If the coincidences were caused by two 1.38-Mev rays in cascade, one should expect a slope quite different from that which one gets for the mixture of 1.38-Mev and 2.76-Mev rays. The experimental slopes yield absorption coefficients which correspond theoretically to a γ-ray energy of 3 Mev. The slope corresponding to 1.4 Mev is shown for comparison. Since the 1.38-Mev and 2.76-Mev γ-rays have equal intensities and since their absorption coefficients in Pb are considerably different, one concludes from the curves that both the singles and coincident measurements involve the 2.76-Mev γ-ray as a component, i.e., the 2.76-Mev ray is in cascade with another γ-ray. The data do not warrant further resolution of the curves into components. Coincidence measurements in conjunction with a spectrometer should yield more decisive data.

[1] K. Siegbahn, Phys. Rev. **70**, 127 (1946). L. G. Elliot, M. Deutsch, and A. Roberts, Phys. Rev. **63**, 386 (1943). J. Itoh, Proc. Phys. Math. Soc. Japan **23**, 605 (1941). C. E. Mandeville, Phys. Rev. **63**, 387 (1943).
[2] R. H. Dicke and J. Marshall, Jr., Phys. Rev. **63**, 86 (1943). R. N. Little, R. W. Long, and C. E. Mandeville, Phys. Rev. **69**, 414 (1946).
[3] L. M. Langer, A. C. G. Mitchell, and P. W. McDaniel, Phys. Rev. **56**, 962 (1939). N. Feather and J. V. Dunworth, Proc. Camb. Phil. Soc. **34**, 442 (1938).
[4] R. G. Sachs, Phys. Rev. **70**, 572 (1946).
[5] W. H. Barkas, Phys. Rev. **55**, 691 (1939).

Nuclear Magnetic Resonance Absorption in Hydrogen Gas

E. M. PURCELL, R. V. POUND,* AND N. BLOEMBERGEN
Harvard University, Cambridge, Massachusetts
December 1, 1946

WE have recently observed nuclear magnetic resonance absorption[1] in hydrogen gas, at room temperature, and at pressures ranging from 10 to 30 atmospheres. The resonance occurs at the frequency and magnetic field strength corresponding to the g value for the proton, but the process of course involves both protons, in the orthohydrogen molecule only. The r-f coil, excited at 29.1 mc/sec., was enclosed in a small brass cylinder which was filled with tank hydrogen to the desired pressure. The volume of the coil itself was 0.5 cm^3, and the volume of gas contributing to the observed effect was perhaps 0.8 cm^3.

A single extremely sharp resonance line was observed, the width of which remained constant at 0.25 gauss, over the whole pressure range. This width may well be caused by field inhomogeneity and is to be regarded as an upper limit on the true width. The intensity of the line was directly proportional to the gas pressure. The sensitivity of our apparatus was such that at 10 atmospheres pressure the observed signal arising from nuclear resonance in the gas was roughly 15 times background noise on a voltage basis.

In molecular beam experiments[2] on H_2 the proton resonance is split into six peaks spaced over a region some 90 gauss wide, because of the interaction of the protons in the ortho-H_2 molecule with each other and with the field owing to the molecular rotation. In our experiment, however, a molecule suffers collisions at a rate much higher

than the radiofrequency itself, with the result that these local fields fluctuate rapidly and very nearly average out. The residual mean-square components of these internal fields, in a frequency band $\Delta\nu$, should be inversely proportional to the collision frequency, and the line width hence *inversely* proportional to pressure. A rough calculation of the line width on this basis yields the value 0.04 gauss, considerably smaller than the upper limit found experimentally.

On the other hand the process described is a potent one for thermal relaxation. It should lead to a relaxation time proportional to the pressure. We have measured the relaxation time by observing the onset of saturation as the r-f voltage is increased and find that the relaxation time does in fact *increase* with *increasing* pressure, and in a proportional manner within the accuracy of our measurement, which is not great. At 10 atmospheres the relaxation time is of the order of 10^{-2} sec., which is in fact the order of magnitude to be expected as a result of the process described.

We suggest that a related process may be important in liquids, and perhaps also in non-crystalline solids. The unexpectedly short relaxation time of protons in paraffin, for example, is well established.[3,4] If this view is correct, the rate of local rearrangements and rotations of the molecule and its neighbors may control the relaxation time in such substances, and in such a way that a slow rate, so long as it is greater than the radiofrequency, leads to a short relaxation time.

In any case the extreme sharpness of the H_2 resonance is of interest in connection with precise g value determinations. As was suggested by J. S. Schwinger at the beginning of this investigation, the H_2 absorption might be useful in measuring orthohydrogen concentration. We are interested in the eventual application of the method to He^3; in that case, however, thermal relaxation will presumably have to be brought about by other means, e.g., by admixture of oxygen.

This work was supported by a grant from the Research Corporation.

* Society of Fellows.
[1] E. M. Purcell, H. C. Torrey, and R. V. Pound, Phys. Rev. **69**, 37 (1946).
[2] J. M. B. Kellogg, I. I. Rabi, N. F. Ramsey, and J. R. Zacharias, Phys. Rev. **56**, 728 (1939).
[3] F. Bloch, W. W. Hansen, and M. Packard, Phys. Rev. **70**, 484 (1946).
[4] B. V. Rollin, Nature **158**, 669 (1946).

Long-Life Radio-Iodine *

ALLEN F. REID[1]
Columbia University, New York, New York
AND ALBERT S. KESTON[2]
Departments of Psychiatry and Chemistry, College of Medicine, New York University, New York, New York
November 25, 1946

A Te target bombarded for 40 hr. with 14.5-Mev deuterons by the MIT cyclotron was received. The radio-iodine was separated in substantially quantitative yield without addition of carrier by oxidizing (heating to 200°C) the target with excess chromic and sulfuric acids, adding water, and reducing to free iodine by heating with phosphorous acid. Addition of a small amount of oxalic acid after the reduction by phosphorous acid served to complete the reduction, but without the usual frothing experienced when oxalic acid is used alone in large quantity. During the reduction, the iodine was distilled in a brisk stream of air into a dilute solution of sodium carbonate and sodium sulfite.

An aliquot of the solution showed considerable activity 6 months later, which was incompatible with the known radio-isotopes.

On addition of iodide as carrier, the bulk of the activity was found to precipitate with silver iodide, and was extractable into carbon tetrachloride after oxidation with iodate Upon injection into rats, large fractions of the carrier free material injected could be found in the excised thyroid glands

The emission of material freshly reseparated by CCl_4 extraction was studied using a mica-window Geiger-counter tube Aluminum, copper, and silver foils were used to determine absorption characteristics, with corrections made for obliquity of the paths through the foils. An x-ray with $\mu = 22.7$ cm²/g Ag, 15.1 cm²/g Cu, and 1.51 cm²/g Al was found. This is equivalent to an energy of 27.0 kev and corresponds to the $K\alpha$-radiation from tellurium, indicating K-electron capture by iodine.

A particle emission of weak energy having an absorption coefficient of about 270 cm²/g Al, corresponding to a maximum energy of *ca.* 0.1 Mev ocurred once to about every forty K-electron captures. No γ-ray was found.

A half-life of about 56 days was found for the I_3. The total long-life iodine activity of the target 235 days after bombardment was about 930 μCuries. That would amount to the order of 10 milliCuries at bombardment end.

Another activity was found in the iodine solution. It was not removable by boiling. Sodium tellurite was added as a carrier to the mixture, and the tellurium precipitated with SO_2. This was redissolved in KCN, a sample made and counted. The foreign activity was found to have quantitatively followed the tellurium. It decayed with a long half-life (>200 days) by particle emission (no γ-rays observed) with an absorption coefficient of 5.1 cm²/g Al (*ca.* 1.6 Mev). Its maximum activity was only about 1 disintegration per 1000 K-electron captures.

Two other targets we have examined have furnished radio-iodine with the same properties. It seems probable that the new iodine is the missing I^{129} formed by a (d, n) reaction on the abundant Te^{128} (32.8 percent)[3] or by β-decay of a (d, p) produced Te^{129}. If the I^{129} is the isotope produced as a decay product of the 72-minute half-life Te^{129}, there is present the unique case of isomeric transition through β-decay and subsequent K-electron capture.

The position of the Te^* in the scheme is not clear. It may be an impurity; however no such long-lived Te isotope is listed in Seaborg's table.[4] If it were a daughter of the I^* which had been building up after the last I_3 separation, it would then have a half-life of about 10 or 400 years depending on the channel responsible for its production. With the activities available, no estimation as to

whether growth was occurring could be made in the time of observation.

A possible transformation scheme would be

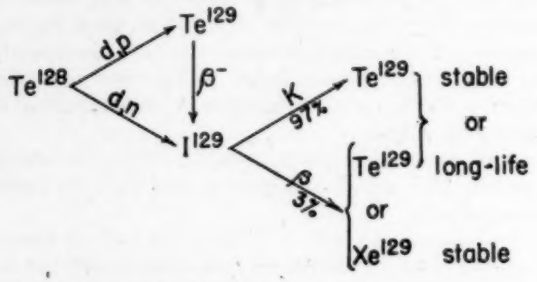

The authors wish to thank Dr. Robley Evans and the MIT cyclotron group for furnishing the irradiated targets; and Professor J. R. Dunning and the Columbia University radioactivity group for their interest and cooperation in the measurements.

* Publication assisted by the Ernest Kempton Adams Fund for Physical Research of Columbia University, New York, New York.
[1] Present address: Sun Oil Company, Marcus Hook, Pennsylvania.
[2] Aided by a grant from the John and Mary Markle Foundation.
[3] Aston, *Mass Spectra and Isotopes* (E. Arnold and Company, London, 1942).
[4] G. T. Seaborg, Rev. Mod. Phys. 16, 1 (1944).

Resonance Absorption by Nuclear Magnetic Moments in a Single Crystal of CaF_2

E. M. PURCELL, N. BLOEMBERGEN, AND R. V. POUND*
Harvard University, Cambridge, Massachusetts
December 1, 1946

THE magnetic dipole-dipole interaction between nuclei arranged on a cubic lattice in the presence of a strong external field H_0 depends markedly on the direction of H_0 with respect to the lattice axes. If the width of the radiofrequency absorption[1] line at $\nu=\mu H_0/Ih$ arises mainly from this interaction, the width and also the peak intensity of the resonance absorption observed in a suitable single crystal should vary as the crystal is rotated in the field H_0. We have observed such an effect in a single crystal of fluorite, CaF_2, in which the magnetic nuclei (F^{19}) occupy a simple cubic lattice.

A cylindrical specimen, 6-mm diam. by 15 mm long, was cut from a fluorite crystal, the axis of the cylinder lying in the *110*-direction. The axis of the r-f coil into which the specimen was inserted was perpendicular to the strong field H_0, and the specimen could be rotated within the coil to align any vector in the *110*-plane with H_0. The fluorine resonance was observed at 29.1 mc/sec. by our modulation method.[2] Quantities related to line width and peak intensity were measured as functions of crystal orientation. The "line width" measured (expressed in gauss) is the width between points of maximum slope of the curve of absorption *vs.* H_0 at constant frequency. The maximum slope multiplied by this line width is taken as a measure of the peak intensity; it would be strictly that for lines of similar shape, for which in addition, the product of line width and peak intensity should be constant in our experiment.

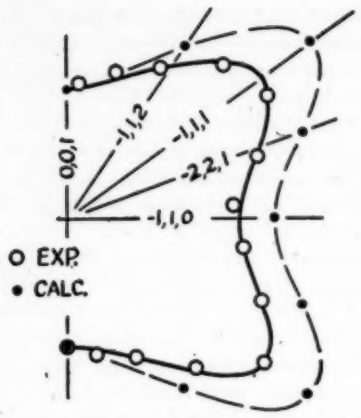

FIG. 1. Polar plot of the dependence of the intensity of magnetic resonance absorption in CaF_2 with the direction of H_0 with respect to the crystal. Absorption is maximum, for example, when H_0 lies along the $(-1, 1, 1)$ direction.

The variation of the product of measured width and measured intensity was in fact no more than ± 5 percent, while each of these quantities individually displayed a pronounced anisotropy of the expected type. Figure 1 is a polar plot of the relative intensity observed with H_0 in various directions. The solid points are located on radii inversely proportional to the r.m.s. line width from dipole-dipole interaction, calculated for certain crystal directions. That the observed anisotropy is somewhat less pronounced that that calculated may be ascribable to variation of line shape with orientation or to broadening influences other than the dipole-dipole interaction.

In absolute magnitude, the measured line width for the *001*-direction was 8.5 gauss. The theoretical r.m.s. width, computed from a rigorous formula kindly provided by Professor Van Vleck, is 5.4 gauss in this case. The quantities are not strictly comparable, but one would expect rough agreement.

The spin-lattice relaxation time was of the order of 5 sec., and no variation with crystal orientation was found. All line width measurements were made at low signal power to avoid saturation. In all these experiments, moreover, the r-f field is so weak ($<10^{-2}$ gauss) as to have no direct influence on the line width.

This work was supported by a grant from the Research Corporation.

* Society of Fellows.
[1] E. M. Purcel, H. C. Torrey, and R. V. Pound, Phys. Rev. 69, 37 (1946).
[2] R. V. Pound, E. M. Purcell, and H. C. Torrey, Phys. Rev. 69, 681 (1946).

PHYSICAL REVIEW VOLUME 70, NUMBERS 11 AND 12 DECEMBER 1 AND 15, 1946

Proceedings of the American Physical Society

Minutes of the Fall Meeting of the New York State Section at Saratoga Springs, New York, November 2, 1946

THE 1946 Fall Meeting of the New York State Section of the American Physical Society was held at the Little Theatre, Skidmore College, on Saturday, November 2, 1946. The meeting was sponsored jointly by the section and the New York State Science Teachers Association. The following program of invited papers was presented.

Morning Session

Address of Welcome, President Henry T. Moore, *Skidmore College.*

Spectrographic Analysis: Its Principles and Application, Lester W. Strock, *Geochemist and Spectrochemist at Saratoga Spa.*

Optical Tools in the Color Pigment Industry, H. S. Davidson, *Imperial Paper and Color Corporation, Glens Falls, New York.*

Afternoon Session

The Physics of Jet Propulsion, J. S. Alford, *Aircraft Gas Turbine Engineering Division, General Electric Company*

Description of the Spier Falls Plant of the New York Power and Light Company, John L. Harvey, *Spier Falls Plant.*

An inspection trip to the Spier Falls Plant followed the last paper.

W. R. Fredrickson
Secretary

Author Index to Volume 70

References with (A) are to abstracts of papers presented at meetings of the American Physical Society. References with (L) are to Letters to the Editor, and those with (T) designate title only.

Abelson, P. H., A. V. Masket, and Nathan Rosen. Possibility of observing a transverse Doppler effect—227(L)

Agnew, H. M. (see Manley, J. H.)—602

——, **W. C. Bright, and D. K. Froman.** Distribution of neutrons in the atmosphere—102(A)

Akeley, E. S. (see Haxby, R. O.)—797(A)

Aldrich, L. T. and Alfred O. Nier. Abundance of He^3 in atmospheric and well helium—983(L)

Alford, J. S. Physics of jet propulsion—989(T)

Allessandrini, E. I. Oxide films on chromium—575(T)

Almy, G. M. (see Skaggs, L. S.)—95(L)

Alvarez, Luis W. Design of a linear accelerator for protons—784(T)

—— Design of a proton linear accelerator—799(A)

Amaldi, E., D. Bocciarelli, and G. C. Trabacchi. Diffraction phenomena in angular distribution of fast neutrons scattered by Pb-nuclei—103(A)

Anderson, C. B. Cosmic-ray effects at high altitudes—788(A)

Anderson, Herbert L., Enrico Fermi, and Leona Marshall. Production of low energy neutrons by filtering through graphite—102(A), 815

Anderson, L. J., C. H. Freres, J. P. Day, and A. P. D. Stokes. Attenuation of 1.24-centimeter radiation through rain—449(A)

Argo, Harold, Arthur Hemmendinger, Howard Kratz, Rolland Perry, Rubby Sherr, Richard Taschek, and Dudley Williams. Reaction constants of Li^7 (pn) Be^7—102(A)

Arley, Niels. Note on the proton hypothesis of the primary component of cosmic rays—975(L)

Armstrong, E. J. Application of the Barrett technique to some problems concerning non-metallic crystals—575(T)

Arnold, Wayne R. and Arthur Roberts. Magnetic moments of the neutron and the deuteron—766(L)

Autler, Stanley H. (see Becker, Gordon E.)—300

Badger, A. E. (see Collin, R. L.)—437(L)

—— (see Graaff, W. A.)—220(L)

Bailey, C. L., William E. Bennett, T. Bergstralh, Richard G. Nuckolls, H. T. Richards, and J. H. Williams. Neutron-proton and neutron-carbon scattering cross sections for fast neutrons—118(A)

Bailey, Carl L. (see Nuckolls, Richard G.)—805

——, **William E. Bennett, T. Bergstralh, Richard G. Nuckolls, Hugh T. Richards, and John H. Williams.** Neutron-proton and neutron-carbon scattering cross sections for fast neutrons—583

Baldwin, G. C. (see Klaiber, G. S.)—789(A)

—— **and G. Stanley Klaiber.** Multiple nuclear disintegration induced by 100-Mev x-rays—259

Banos, Alfredo, Jr. Application of the dynamical theory of currents to cavity resonators—448(A)

Bardeen, J., W. H. Brittain, and W. Shockley. Investigation of oxidation of copper by use of radioactive Cu tracer—105(A)

Barker, Edgar C. Thick target yields with deuteron-proton reactions—101(A)

Barschall, H. H. (see Coon, J. H.)—104(A), 592

—— (see Manley, J. H.)—602

—— **and M. E. Battat.** On the disintegration of nitrogen by fast neutrons—245

——, **M. E. Battat, and W. C. Bright.** Scattering of fast neutrons by boron—458

Barss, W. M. (see Yearian, H. J.)—108(A)

—— **and H. J. Yearian.** Electron diffraction study of CCl_2NO_2—108(A)

Battat, M. E. (see Barschall, H. H.)—245, 458

Baum, W. A., F. S. Johnson, J. J. Oberly, C. C. Rockwood, C. V. Strain, and R. Tousey. Solar ultraviolet spectrum to 88 kilometers—781(L)

Becker, Gordon E. and Stanley H. Autler. Water vapor absorption of electromagnetic radiation in the centimeter wave-length range—300

Beers, Yardley. (see Roberts, Arthur)—112(A)

Belenky, S. (see Tamm, I.)—660

Benade, J. M. (see Lewis, Lloyd G.)—792(A)

Bendigo, C. W. Tricot—802(T)

Benedetto, F. A. Some mesotron observations by simultaneous registration at two stations—817

Bennett, W. E., T. W. Bonner, C. E. Mandeville, and B. E. Watt. Resonances in the disintegration of flourine by protons—882

——, **C. E. Mandeville, and H. T. Richards.** Yield function and angular distribution of the D+D neutrons—101(A)

—— **and H. T. Richards.** Neutrons from C^{12}+D—118(A)

Bennett, William E. (see Bailey, C. L.)—118(A)

—— (see Bailey, Carl L.)—583

—— (see Nuckolls, Richard G.)—805

Benzer, S. Photo-diode and photo-peak characteristics in germanium—105(A)

Bergmann, Peter G. Propagation of radiation in a medium with random inhomogeneities—486

Bergstralh, T. (see Bailey, C. L.)—118(A)

Bergstralh, Thor (see Bailey, Carl L.)—583

—— (see Nuckolls, Richard G.)—805

Beringer, Robert. Absorption of one-half centimeter electromagnetic waves in oxygen—53

—— (see Dicke, Robert H.)—340

Berlin, T. (see Dennison, D. M.)—764

—— (see Dennison, David M.)—58

Bernstein, S. On the existence of a resonance absorption of neutrons in graphite—107(A)

—— (see Sawyer, R. B.)—791(A)

Berry, Clifford E. (see Washburn, Harold W.)—559(L)

Best, Nolan R., Eric Durand, Donald I. Gale, and Ralph J. Havens. Pressure and temperature measurements in the upper atmosphere—985(L)
Bethe, H. A. Multiple production of mesons by protons—787(A)
—— Multiple scattering and the mass of the meson—821
—— (see Courant, E. D.)—798(A)
—— (see Feynman, R. P.)—786(A)
—— (see Oppenheimer, J. R.)—796(A)
—— **and J. Robert Oppenheimer.** Reaction of radiation on electron scattering and Heitler's theory of radiation damping—451
Bhabha, H. J. On the expansibility of solutions in powers of the interaction constants—759
—— Relativistic wave equations—794(A)
Bittencourt, P. T. (see Burson, S. B.)—566(L)
—— **and M. Goldhaber.** "Two-step" isomeric transition in Te^{121}—780(L)
Bitter, F., J. B. Garrison, J. Halpern, E. Maxwell, J. C. Slater, and C. F. Squire. Superconductivity of lead at 3-cm wave-length—97(L)
Blachman, Nelson M. System of microstresses in cold-worked metal—698
Blandford, Josephine M. (see Schiefer, Herbert F.)—803(A)
Bleaney, B. and R. P. Penrose. Inversion spectrum of ammonia—775(L)
Blewett, J. P. Transition from betatron to synchrotron operation—798(A)
—— (see Pollock, H. D.)—798(A)
——, **D. A. Wilbur, and L. D. Roberts.** Split anode magnetrons for the 100–800 megacycle range—118(A)
Bloch, F. Nuclear induction—460
——, **R. I. Condit, and H. Staub.** Neutron polarization and ferromagnetic saturation—972
——, **W. W. Hansen and M. Packard.** Nuclear induction experiment—474
Bloembergen, N. (see Purcell, E. M.)—986(L), 988(L)
Bloomenthal, S. Instrument lubricant having a low hardy coefficient—104(A)
Bocciarelli, D. (see Amaldi, E.)—103(A)
Bohm, D. Excitation of plasma oscillations—448(A)
—— (see Foldy, Leslie)—445(A)
—— **and L. Foldy.** Theory of the synchrotron—249
Bohm, David. Relations of Dirac's new method of field quantization to older theories—795(A)
Bol, K. (see Marton, L.)—447(A)
Bonner, T. W. (see Bennett, W. E.)—882
Boorse, H. A., D. B. Cook, R. B. Pontius, and M. W. Zemansky. Electrical conductivity of rapidly frozen solutions of sodium in liquid ammonia—92(L)
Booth, A. D. Fourier methods and machines in England 1940–1946—575(T)
Borst, L. B. and J. J. Floyd. Fissionability studies—107(A)
——, **A. J. Ulrich, C. L. Osborne, and B. Hasbrouck.** Diffraction of neutrons and neutron absorption spectra—108(A)
——, **A. J. Ulrich, C. L. Osborne, and B. Hasbrouck.** Neutron diffraction and nuclear resonance structure—557(L)
Boyd, G. E. (see Swartout, J. A.)—232(L)
Bozorth, R. M. Magneto-resistance and domain theory—106(A)
—— Magneto-resistance and domain theory of iron-nickel alloys—923
Brattain, W. H. (see Bardeen, J.)—105(A)
Breazeale, Francis B. Apparatus for determining the coefficient of friction of running yarn—803(A)
Breit, Gregory. Theory of nuclear reactions—100(T)
Bridgman, P. W. On higher order transitions—425
Bright, W. C. (see Agnew, H. M.)—102(A)
—— (see Barschall, H. H.)—458
—— (see Manley, J. H.)—602
Brillouin, L. Influence of space charge on the bunching of electron beams—187
Brode, R. B. (see Fretter, W. B.)—791(A)
Brody, S. B. (see Nierenberg, W. A.)—773(L)
Brosi, A. R. (see Conn, E. E.)—768(L)
Brown, F. W. III (see Pierce, A. K.)—779(L)
Brown, James B. and D. K. C. MacDonald. On the possible use of Brownian motion for low temperature thermometry—976(L)
Broxon, James W. Recurrence phenomena in small cosmic-ray bursts—494
Buechner, W. W. (see Van de Graaff, R. J.)—797(A)
—— **and R. J. Van de Graaff.** Calorimetric experiment on the radiation losses of 2-Mev electrons—174
Buerger, M. J. Derivative crystal structures—575(T)
—— Interpretation of Harker syntheses—575(T).
——, **G. Klein, and G. Hamburger.** Structure of nepheline—575(T)
deBretteville, A., Jr. Oscillographic study of the dielectric properties of barium titanate—575(T)
Burgess, J. S. (see Koller, L. R.)—571(L)
Burgy, Merle, L. A. Pardue, H. B. Willard, and E. O. Wollan. Energy of delayed neutrons from U^{238} fissions—104(A)
Burrill, E. A. (see Van de Graaff, R. J.)—797(A)
Burson, S. B., P. T. Bittencourt, R. B. Duffield, and M. Goldhaber. Decay scheme for Te^{121}—566(L)

Cameron, A. E. (see Conn, E. E.)—768(L)
—— (see Swartout, J. A.)—232(L)
Carmichael, H. and C. N. Chou. Cosmic-ray bursts in a large and in a small ion chamber at sea level and in a small ion chamber under 30 meters of clay—792(A)
Carter, R. L. (see Conn, E. E.)—768(L)
Chamberlain, Owen, Dudley Williams, and Philip Yuster. Half-life of uranium (234)—580
Chandrasekhar, S. Continuous absorption coefficient of the negative hydrogen ion—109(A)
Chang, W. Y. Low energy alpha-particles from radium—632
Cheng, K. C. (see Wang, K. C.)—516
Chesley, F. G. Design and construction of an electron diffraction camera and its application to the selenium rectifier problem—575(T)
Chou, C. N. (see Carmichael, H.)—792(A)
Christy, R. R. Small enriched reactor at Los Alamos—100(T)

Cisney, E. (see Parrish, W.)—575(T)
Clark, Arnold F. Magnetic field due to dee structures in a synchrotron—444(A)
Clark, J. S., I. A. Getting, and J. E. Thomas, Jr. New method for displaying the electron beam in a synchrotron—562(L)
Clarke, E. T. and John W. Irvine, Jr. Experimental yields with 14-Mev deuterons—893
Cobine, J. D. (see Gallagher, C. J.)—113(A)
—— **and C. J. Gallagher.** High level electronic noise source—119(A)
—— **and C. J. Gallagher.** Noise and oscillations in hot-cathode arcs—113(A)
Cocconi, G., A. Loverdo, and V. Tongiorgi. Density spectrum of the extensive cosmic-ray showers of the air—841
——, **A. Loverdo, and V. Tongiorgi.** Experimental and theoretical evaluation of the density spectrum of extensive cosmic-ray showers—846
——, **A. Loverdo, and V. Tongiorgi.** Penetrating particles in air showers—852
—— **and V. Tongiorgi.** Mean lifetime of the meson—855
—— **and V. Tongiorgi.** On the fine structure of zenithal curves of the cosmic radiation—850
Cocconi, Giuseppe. Density spectrum and the origin of extensive atmospheric cosmic-ray showers—975(L)
Coggeshall, Norman D. Paths of ions and electrons in nonuniform crossed electric and magnetic fields—270
Colby, M. Y. and R. N. Little, Jr. Possible results of a new reaction—437(L)
Coles, D. K. (see Dakin, T. W.)—560(L)
—— **and William E. Good.** Stark and Zeeman effects in the inversion spectrum of ammonia—979(L)
Collin, R. L. and A. E. Badger. Solarization of manganese-bearing glass at higher temperatures—437(L)
Collins, S. C. Helium cryostat—98(L)
Compton, A. H. Physics research and release of nuclear energy—100(T)
Condit, R. I. (see Bloch, F.)—972
Conn, E. E., A. R. Brosi, J. A. Swartout, A. E. Cameron, R. L. Carter, and Douglas G. Hill. Confirmation of assignment of 2.6 *h* Ni to a mass number of 65—768(L)
Conversi, M. and O. Piccioni. On the disintegration of slow mesons—874
—— **and O. Piccioni.** On the mean life of slow mesons—859
Cook, C. S., E. Jurney, and L. M. Langer. On the disintegration scheme of Na^{24}—985(L)
Cook, D. B. (see Boorse, H. A.)—92(L)
Coon, J. H. (see Graves, A. C.)—101(A)
—— (see Manley, J. H.)—101(A), 602
—— **and H. H. Barschall.** Angular distribution of 2.5-Mev neutrons scattered by deuterium—592
——, **R. W. Davis, and H. H. Barschall.** Angular distribution of *n-d* scattering for 2.5-Mev neutrons—104(A)
Corben, H. C. Special relativistic field theories in five dimensions—947
Cork, J. M. Relative probability of the (d,p) and the (d,n) reactions in bombarded bismuth—563(L)
Corson, E. M. Second quantization and representation theory—728
—— Theory of the fine structure of x-ray absorption limits in polyatomic molecules—645
Courant, E. D. and H. A. Bethe. Theoretical considerations on bringing the beam out of a betatron—798(A)
Crane, H. R. Racetrack—800(A)
Critchfield, Charles L. Electron waves in the magnetic dipole field of a neutron—793(A)
Cross, Paul C. (see Hainer, R. M.)—108(A)
Cummerow, Robert L. and David Halliday. Paramagnetic losses in two manganous salts—433(L)
Curtiss, L. F. (see Miller, L. C.)—983(L)

Dailey, E. P., R. L. Kyhl, M. W. P. Strandberg, J. H. Van Vleck, and E. B. Wilson, Jr. Hyperfine structure of the microwave spectrum of ammonia and the existence of a quadrupole moment in N^{14}—984(L)
Dakin, T. W., W. E. Good, and D. K. Coles. Resolution of a rotational line of the OCS molecule and its stark effect—560(L)
Dancoff, S. M. Short range alphas in natural radioactivity —116(A)
Daniels, Farrington. Problems and plans of nucleonics research—100(T)
Darrow, Karl K. Local secretaryship for the Pacific coast —446(A)
Daunt, J. G., M. Désirant, and K. Mendelssohn. Conductivity of sodium-ammonia solutions—219(L)
Davidson, H. S. Optical tools in the color pigment industry —989(T)
Davidson, N. and J. Hillier. Single crystal electron diffraction by microcrystalline materials—575(T)
Davis, R. W. (see Coon, J. H.)—104(A)
Davisson, J. W. Orientation of electrical breakdown paths in single crystals—685
Day, J. P. (see Anderson, L. J.)—449(A)
Dearnley, I. H. (see Margenau, H.)—349
DeBennedetti, S. and F. K. McGowan. Metastable state of 22 microseconds in Ta^{181}—569(L)
Demers, Pierre. New photographic emulsions showing improved tracks of ionizing particles—86(L)
—— Pairs of fission fragments from U^{235}—974(L)
Dempster, A. J. (see Lapp, R. E.)—104(A)
Dennison, D. M. (see Hadley, Lawrence N.)—780(L)
—— **and T. Berlin.** Racetrack stability—764
Dennison, David M. and T. H. Berlin. Stability of synchrotron orbits—58
De Oyarzabal, J. (see Vallarta, M. S.)—785(A)
Désirant, M. (see Daunt, J. G.)—219(L)
D'Eustachio, D. Note on thickness of quartz wafers for observed surface phenomena—229(L)
—— Surface layers and mosaic structure in some valence crystals—575(T)
—— Surface layers on quartz and topaz—522
Dicke, Robert H., Robert Beringer, Robert L. Kyhl, and A. B. Vane. Atmospheric absorption measurements with a microwave radiometer—340
Dickey, Fred P. and Harald H. Nielsen. Infra-red spectrum of heavy water—109(A)
Duffield, R. B. (see Burson, S. B.)—566(L)
Dunning, J. R. Neutron spectroscopy—100(T)
—— (see Reid, Allen F.)—431(L)
Durand, Eric (see Best, Nolan R.)—985(L)

Eggen, D. T. and M. L. Pool. X-radiation and internal conversion from Ru+d—446(A)
Ehrenhaft, Felix. Rotational movements of matter in the homogeneous fields of magnets or of radiation—119(A)
—— Unipolar magnetic charges—114(A)
Ekstein, H. Forced vibrations of piezoelectric crystals—76
—— Force on a conducting tube moving through a magnetic field—450(A)
Elder, F. R. (see Pollock, H. D.)—798(A)
Eliezer, C. Jayaratnam. On the theory of the electron—793(A)
Elsasser, Walter M. Electric quadrupole of the earth—438(L)
—— Induction effects in terrestrial magnetism. Part II. Secular variation—202
Ellickson, R. T. and W. L. Parker. Decay in brightness of infra-red sensitive phosphors—290
Engle, A. Wendell (see Fearon, R. E.)—564(L)
Epstein, Paul S. On the elastic properties of lattices—915
Evans, W. E., Jr. (see Manning, L. A.)—767(L)

Fairbank, Henry (see Lane, C. T.)—431(L)
Fairbank, William (see Lane, C. T.)—431(L)
Fankuchen, I. (see Schneider, M.)—575(T)
Fano, U. On the theory of ionization yield of radiations in different substances—44
Fearon, R. E. (see Scherbatskoy, S. A.)—96(L)
——, **A. Wendell Engle, Jean Thayer, Gilbert Swift, and Irving Johnson.** Results of atmosphere analyses done at Tulsa, Oklahoma, during the period neighboring the time of the second Bikini atomic bomb test—564(L)
Feather, N. Probability of excitation of the nucleus^{206} Pb in the α-disintegration of polonium—88(L)
Fein, Elihu. Comparison of the stopping power of lead and aluminum for cosmic-ray mesotrons—567(L)
Feenberg, E. and G. Goertzel. Theory of nuclear coulomb energy—597
—— **and N. Primakoff.** Possibility of "conditional" saturation in nuclei—980(L)
Feenberg, Eugene. Representation of single particle operators in two-particle form—768(L)
Feld, Bernard T. Nuclear electric quadrupole moment and the radiofrequency spectra of homonuclear diatomic molecules—112(A)
—— Proposed neutron spectrometer in the 10–100 kev range—429(L)
Fermi, E. Elementary pile theory—100(T)
—— (see Anderson, Herbert L.)—102(A), 815
—— **and L. Marshall.** Phase of neutron scattering—103(A)
—— **and W. N. Zinn.** Reflection of neutrons on mirrors—103(A)
Feynman, R. P. and H. A. Bethe. Attempt of an analysis of some cosmic-ray phenomena—786(A)
Floyd, J. J. (see Borst, L. B.)—107(A)
Foldy, L. (see Bohm, D.)—249
—— **and D. Bohm.** Efficiency of frequency modulated cyclotron—445(A)
Forbush, Scott E. Three unusual cosmic-ray increases possibly due to charged particles from the sun—771(L)
Fox, Francis E., Karl F. Herzfeld, and George D. Rock. Effect of ultrasonic waves on the conductivity of salt solutions—329
—— **and George D. Rock.** Compressional viscosity and sound absorption in water at different temperatures—68
Franck, J. V. (see Helmholz, A. C.)—448(A)
Franck, James. Proposal of a method for the separation of He^3 from He^4—561(L)
Frank, N. H. Stability of electron orbits in the synchrotron—177
Freres, C. H. (see Anderson, L. J.)—449(A)
Fretter, W. B. Range-momentum relationship for cosmic-ray mesotrons—444(A)
—— **and R. B. Brode.** Mass of cosmic-ray mesotrons—791(A)
—— **and W. E. Hazen.** Successive multiple production of penetrating particles—230(L)
Fretter, William B. Mass of cosmic-ray mesotrons—625
Friedlander, G., M. Perlman, and L. Pepkowitz. Radiochemical search for gamma-meson reactions induced by 100-Mev x-rays—790(A)
Frisch, D. H. (see McKibben, J. L.)—117(A)
Frisch, David H. Total cross section of hydrogen for neutrons of energies from 35 to 490 kev—792(A)
—— Total cross sections of carbon and hydrogen for neutrons of energies from 35 to 490 kev—589
Froman, D. K. (see Agnew, H. M.)—102(A)
Fryer, Edward M. Transmission of velocity-selected neutrons through magnetized iron—235

Gale, Donald I. (see Best, Nolan R.)—985(L)
Gallagher, C. J. (see Cobine, J. D.)—113(A), 119(A)
—— **and J. D. Cobine.** Effect of magnetic field on noise and oscillations in hot-cathode arcs—113(A)
Gamow, G. Expanding universe and the origin of elements—572(L)
Garrison, J. B. (see Bitter, F.)—97(L)
George, E. P. and L. Janossy. Penetrating cosmic-ray bursts—773(L)
Gerö, L. (see Schmid, R. F.)—226(L)
Getting, I. A. (see Clark, J. S.)—562(L)
Ginzbarg, A. (see Haxby, R. O.)—797(A)
Gladrow, E. M. (see Sullivan, W. H.)—778(L)
Goertzel, G. Angular correlation of gamma-rays—897
—— (see Feenberg, E.)—597
Golay, M. J. E. (see Zahl, Harold A.)—450(A)
Goldberg, H. and O. Sandvik. Simple instrument for measuring the rheological properties of elastic fluids—110(A)
Goldberger, M. L. and Frederick Seitz. Refraction and diffraction of neutrons by crystals—116(A)
Goldhaber, M. Activation of Ag (225 d.) by resonance neutrons—89(L)
—— (see Bittencourt, P. T.)—780(L)
—— (see Burson, S. B.)—566(L)
—— (see Muelhause, C. O.)—85(L)
—— **and W. J. Sturm.** Decay of Cb^{94} (6.6 min.)—111(A)
Goldsmith, H. H. Critical survey of neutron cross sections—100(T)

Goldstein, Herbert. Frequency dependence of the properties of sea echo—938
—— Properties of radar echoes from shell splashes—232(L)
Golian, S. E., E. H. Krause, and G. J. Perlow. Additional cosmic-ray measurements with the V-2 rocket—776(L)
——, **E. H. Krause, and G. J. Perlow.** Cosmic radiation above 40 miles—223(L)
Good, W. E. (see Dakin, T. W.)—560(L)
Good, Wilfred M. Angular distribution of gamma-rays in Na^{24}, Co^{60}, Y^{88}—978(L)
Good, William E. Inversion spectrum of ammonia—109(A), 213
—— (see Coles, Donald K.)—979(L)
Goodman, B. (see Miller, P. H., Jr.)—110(A)
Goodman, J. Leon and M. L. Pool. Radioactive isotopes in the osmium region—112(A)
Graaff, W. A. and A. E. Badger. Viscosity of glass as affected by dissolved gases—220(L)
Graef-Fernández, Carlos. Periodic orbits of cosmic-ray particles at high magnetic latitudes—786(A)
Graves, A. C., E. R. Graves, J. H. Coon, and J. H. Manley. Cross section of D(d,p) He^3 reaction—101(A)
Graves, E. R. (see Graves, A. C.)—101(A)
—— (see Manley, J. H.)—101(A), 602
—— **and J. H. Coon.** Disintegrations of neon and argon by d-d neutrons—101(A)
Greanias, E. C. (see Kaiser, H. F.)—797(A)
—— **and E. O. Wukasch.** Electron injection technique for betatrons—797(A)
Greenblatt, M. H., P. H. Miller, Jr., and L. I. Schiff. Electrical contact noise—113(A)
Grenchik, Raymond (see Palevsky, Harry)—117(A)
Groetzinger, Gerhart (see Smith, Lloyd)—96(L), 102(A)
Groshev, L. (see Veksler, V.)—440(L)
Grosse, Aristid V. (see Reid, Allen F.)—431(L)
Gulbransen, E. A. Deviation of lattice parameters of thin oxide films by electron diffraction analysis—575(T)
Gurewitsch, A. M. (see Pollock, H. D.)—798(A)

ter Haar, D. Vibrational levels of an anharmonic oscillator—222(L)
Hadley, Lawrence N. and D. M. Dennison. Microwave spectrum of ammonia—780(L)
Hainer, R. M., Gilbert W. King, and Paul C. Cross. Expected absorption in the microwave region by water vapor and similar molecules—108(A)
Halliday, David (see Cummerow, Robert L.)—433(L)
Halpern, J. (see Bitter, F.)—97(L)
Hamburger, G. (see Buerger, M. J.)—575(T)
Hamilton, J. G. (see York, Herbert)—446(A)
Hammermesh, B. (see Korff, S. A.)—429(L)
Hansen, W. W. (see Bloch, F.)—474
Harker, D. Microwaves (short wave radio) and scale models in determining crystal structures—575(T)
Hartzler, A. J. (see Schein, Marcel)—435(L)
Harvey, John L. Description of the Spier Falls plant of the New York Power and Light Company—989(T)
Hasbrouck, B. (see Borst, L. B.)—108(A), 557(L)
Havens, Ralph J. (see Best, Nolan R.)—985(L)
Havens, William W., Jr. (see Rainwater, James)—107(A), 136
—— **and James Rainwater.** Slow neutron cross sections of indium, gold, silver, antimony, lithium, and mercury as measured with a neutron beam spectrometer—107(A), 154
Haxby, R. O., E. S. Akeley, A. Ginzbarg, R. N. Smith, H. W. Welch, and R. M. Whaley. Preliminary studies on the Purdue microwave electron accelerator—797(A)
Hayden, Richard J. (see Lewis, Lloyd, G.)—111(A)
—— **and Mark G. Inghram.** Assignment of mass to 46-hr. samarium and 9.2-hr. europium by a mass spectrograph—89(L)
—— **and Lloyd G. Lewis.** Assignments of mass to fission isotopes by mass spectrograph—111(A)
Hayes, Albert E., Jr. R-F heating cyclotron filaments—220(L)
Hazen, W. E. (see Fretter, W. B.)—230(L)
Hazen, Wayne. Recent cloud-chamber observations of the soft component of cosmic-rays—789(A)
Hazen, Wayne E. Cloud chamber for airborne cosmic-ray observations—445(A)
Heitler, W. Quantum theory of damping—795(A)
Helliwell, R. A. (see Manning, L. A.)—767(L)
Helmholz, A. C. Isotopic assignment of Cd and Ag activities—982(L)
——, **J. V. Franck, and J. M. Peterson.** Synchrotron radiofrequency system—448(A)
Hemmendinger, Arthur. (see Argo, Harold)—102(A)
Herzberg, G. On the high pressure bands of carbon and the formation of C_2 molecules—762
Herzfeld, Karl F. (see Fox, Francis E.)—329
Herzog, G. Gamma-ray anomaly following the atomic bomb test of July 1, 1946—227(L)
Hess, Victor F. and Paul Luger. Ionization of the atmosphere in the New York area before and after the Bikini atom bomb test—564(L)
Hickman, J. W. Electron diffraction studies of oxide film formation on W, Mo, and W, Mo, Ni, and Cr alloys—575(T)
Hildebrand, Roger (see York, Herbert)—446(A)
Hill, A. G. (see Roberts, Arthur)—112(A)
Hill, Douglas G. (see Conn, E. E.)—768(L)
Hillier, J. (see Davidson, N.)—575(T)
—— **and Edward G. Ramberg.** Contour fringes and asymmetries of electron microscope objectives—113(A)
Hincks, E. P. Evidence for the reaction $O^{17}(n,a)$ C^{14}—770(L)
Ho, Zah-Wei. Disintegration of $_{17}Cl^{34}$—782(L)
—— Single scattering and annihilation of positrons—224(L)
Hock, Charles W. (see Kinsinger, William G.)—802(A)
Hodgins, J. W. Persistent currents in frozen metal-ammonia solutions—568(L)
Hoffman, T. A. On the dynamics of the Rb I crystal—981(L)
Hofstadter, Robert. Mechanical-electronic control system—113(A)
Hole, Njål (see Siegbahn, Kai)—133

Holloman, J. H. and J. D. Lubahn. Plastic flow of metals—775(L)
Holstein, T. Energy distribution of electrons in high frequency gas discharges—367
Huang, Kun. Wave function for the ground state of lithium—197
Huggins, M. L. Equations for various types of summations—575(T)
Hughes, D. J. Radiative capture cross sections for fast neutrons—106(A)
Hughes, Donald. Mass of the mesotron as determined by cosmic-ray measurements—791(A)
—— Mass of the neutron—219(L)
Hughes, E. W. Punched card methods in x-ray and electron diffraction calculations—575(T)
—— X-ray examinations of some synthetic oxygen-carrying chelate compounds—575(T)
—— **and W. N. Lipscomb, Jr.** Structure of methyl ammonium chloride—575(T)
Hughes, Harold Kenneth. New method of measuring the electric dipole moment, moment of inertia, and internuclear distance of diatomic polar molecules—570(L)
—— Errata: New method of measuring the electric dipole moment of inertia of diatomic polar molecules—909
Hush, J. M. (see McKibben, J. L.)—117(A)

Infeld, L. and A. E. Schild. New approach to kinematic cosmology—(B)—410
Inghram, M. G. (see Norris, L. D.)—772(L)
Inghram, Mark G. Isotopic composition of tungsten, silicon, and boron—119(A), 653
—— Mass spectrometric observation of radioactive C^{14}—111(A)
—— (see Hayden, Richard J.)—89(L)
—— (see Nier, Alfred O.)—116(A)
Iona, Mario, Jr. High particle density in cosmic-ray air showers—114(A)
Irvine, John W., Jr. (see Clarke, E. T.)—893

Jacobsen, J. C. On the recoil of the nucleus in beta-decay—789(A)
Janossy, L. (see George, E. P.)—773(L)
Jarvis, G. A. Positive ions from thoriated tungsten—106(A)
Jehle, Herbert. Statistical hypotheses in stellar dynamics—538
Jnanananda, Swami. Radioactive isotope of gold $_{79}Au^{198}$ and low energy range of its spectrum—812
Joffe, Joseph. Maximum inversion temperatures of helium, hydrogen, and neon—766(L)
Johnson, F. S. (see Baum, W. A.)—781(L)
Johnson, Irving (see Fearon, R. E.)—564(L)
Johnston, Lawrence H. (see Oppenheimer, Frank)—447(A)
Jones, Stanley B. Strengths of some model magnets—450(A)
Jorgensen, T. (see Manley, J. H.)—602
Jurney, E. (see Cook, C. S.)—985(L)

Kac, M. and A. F. J. Siegert. Note on the theory of noise in receivers with square law detector—449(A)
Kaiser, H. F. and E. C. Greanias. Synchro-betatron electron accelerator guide fields—797(A)
Kaplan, Joseph. Afterglows and the upper atmosphere—448(A)
Karle, J. Theory of electron scattering by oriented long chain molecules—575(T)
Karrer, Enoch and R. S. Orr. Measurement of irregular distances and its use in studying the swelling of cotton fibers—803(T)
Kaswell, E. R. Design of parachute shroud lines as influenced by fundamental energy absorption properties—803(T)
Kê, T'ing-Sui. High temperature anelastic effects in polycrystalline aluminum—105(A)
Keim, C. P. (see Swartout, J. A.)—232(L)
Kennedy, J. W., G. T. Seaborg, E. Segrè, and A. C. Wahl. Properties of 94 (239)—555
Kerst, D. W. (see Skaggs, L. S.)—95(L)
Keston, Albert S. (see Reid, Allen F.)—987(L)
Kidnapillai, M. and A. W. Mailvaganam. Solar and lunar effects on cosmic-rays—94(L)
King, Gilbert W. Calculation of the higher energy levels of the asymmetric rotor by means of the correspondence principle—108(A)
—— (see Hainer, R. M.)—108(A)
Kingshill, Konrad L. (see Lewis, Lloyd G.)—792(A)
Kinsinger, William G. and Charles W. Hock. Electron microscopical studies of natural cellulose fibers—802(A)
Kirkpatrick, Paul. Theory of continuous x-ray spectra from thick targets—446(A)
Kittel, Charles. Theory of the dispersion of magnetic permeability in ferromagnetic materials at microwave frequencies—281
—— Theory of the structure of ferromagnetic domains in films and small particles—965
Klaiber, G. S. (see Scharff-Goldhaber, G.)—229(L)
—— (see Schein, Marcel)—435(L)
——, **A. E. Luebke, and G. C. Baldwin.** Range-momentum measurements of particles emitted in nuclear disintegrations induced by 100-Mev x-rays—789(A)
Klaiber, G. Stanley (see Baldwin, George C.)—259
Klein, G. (see Buerger, M. J.)—575(T)
Knipp, J. K. (see Present, R. D.)—557(L)
Koller, L. R. and J. S. Burgess. Secondary emission from germanium, boron, and silicon—571(L)
Korff, S. A. and B. Hammermesh. Multiple production of neutrons by cosmic radiation—429(L)
Kovacs, Magdalene. Excitation-function of the γ-radiation generated by Po-α bombardment of Na—895
Kratz, Howard (see Argo, Harold)—102(A)
Krause, E. H. (see Golian, S. E.)—223(L), 776(L)
Kundu, D. N. and M. L. Pool. Mo^{93} and Cb^{94} from columbium—111(A)
Kusaka, Shuichi. Difficulties of the meson theories of nuclear forces—794(A)
Kyhl, R. L. (see Dailey, E. P.)—984(L)
Kyhl, Robert L. (see Dicke, Robert H.)—340

Lamb, William E., Jr. Theory of a microwave spectroscope—308

LaMer, Victor K. (see Rosenblatt, Philip)—385
Lane, C. T., Henry Fairbank, Howard Schultz, and William Fairbank. "Second sound" in liquid helium II—431(L)
Langer, L. M. (see Cook, C. S.)—985(L)
Langmuir, R. V. (see Pollock, H. D.)—798(A)
—— **and R. B. Nelson.** A 10-kilowatt magnetron with water-cooled cathode—118(A)
Lanz, L. H. (see Skaggs, L. S.)—95(L)
Lapp, R. E., J. R. Van Horn, and A. J. Dempster. Neutron absorbing isotopes in samarium and gadolinium—104(A)
Larson, C. E. (see Swartout, J. A.)—232(L)
Larson, L. L. Spun Nylon—803(T)
Lassen, N. O. Specific ionization by fission fragments—577
Lawrence, Ernest O. Experimental problem of accelerating charged particles—784(T)
Lawson, A. W. and Earl A. Long. Further remarks on the possible use of Brownian motion in low temperature thermometry—977(L)
—— **and Earl A. Long.** On the possible use of Brownian motion for low temperature thermometry—220(L)
Lazareva, L. Investigation of auger showers by the proportional counted method—439(L)
—— (see Veksler, V.)—440(L)
Leaf, Boris. Phenomenological theory of transport processes in fluids—748
LePrince-Ringuet, L. Measurement of meson masses by the method of elastic collision. Probable existence of a heavy meson (1000 M_0) in the cosmic radiation—791(A)
Levinger, J. S. (see Snell, A. H.)—111(A)
Lewis, Lloyd G. (see Hayden, Richard J.)—111(A)
—— **and Richard J. Hayden.** Mass spectrograph for the study of fission product mixtures—111(A)
——, **Konrad L. Kingshill, and J. M. Benade.** Ionization chamber measurements on cosmic-ray air showers—792(A)
Lipscomb, W. N., Jr. (see Hughes, E. W.)—575(T)
Little, R. N., Jr. (see Colby, M. Y.)—437(L)
Livingston, M. R. (see Work, R. W.)—803(A)
Lofgren, E. J. and B. Peters. Description of a frequency modulated cyclotron and a discussion of the deflector problem—444(A)
Long, Earl A. (see Lawson, A. W.)—220(L), 977(L)
Lopes, J. Leite. High energy neutron-proton scattering and the meson theory of nuclear forces with strong coupling—5
Loverdo, A. (see Cocconi, G.)—841, 846, 852
Lubahn, J. D. (see Hollomon, J. H.)—775(L)
Lucht, C. M. (see Smoluchowski, R.)—318
Luebke, A. E. (see Klaiber, G. S.)—789(A)
Luger, Paul (see Hess, Victor F.)—564(L)
Luttinger, J. M. and L. Tisza. Theory of dipole interaction in crystals—954
Lyons, W. James, Hilda M. Ziifle, Mary L. Nelson, and Trinidad Mares. Moisture transfer to and from tire cords encased in GR-S—802(A)

MacDonald, D. K. C. (see Brown, James B.)—976(L)
Machlin, E. S. (see Nowick, A. S.)—104(A)
MacKenzie, K. R. and F. H. Schmidt. Frequency modulation for Berkeley 37″ cyclotron—445(A)
Mailvaganam, A. W. (see Kidnapillai, M.)—94(L)
Mandeville, C. E. (see Bennett, W. E.)—101(A), 882
Manley, J. H. (see Graves, A. C.)—101(A)
——, **H. M. Agnew, H. H. Barschall, W. C. Bright, J. H. Coon, E. R. Graves, T. Jorgensen, and B. Waldman.** Elastic backscattering of *d-d* neutrons—602
——, **J. H. Coon, and E. R. Graves.** Cross section of D(d,n)He^3 reaction—101(A)
Mann, M. (see Smoluchowski, R.)—318
Manning, L. A., R. A. Helliwell, O. G. Villard, Jr., and W. E. Evans, Jr. On the detection of meteors by radio—767(L)
Many, Abraham. On the deep configurations of Ti I, Ti II, V II, V III—511
Marais, E. J. Perturbations in the ultraviolet band spectrum of P_2—499
Mares, Trinidad (see Lyons, W. James)—802(A)
Margenau, H., F. L. McMillan, Jr., I. H. Dearnley, C. S. Pearsall, and C. G. Montgomery. Physical processes in the recovery of TR tubes—349
Marshak, R. E. β-ray spectrum of K^{40} and theory of β-decay—980(L)
Marshall, Fitz-Hugh. Microsecond phosphorescent decay periods of x-ray fluorescent screens—114(A)
Marshall, John. Total cross sections of various materials for indium resonance neutrons—107(A)
Marshall, L. (see Fermi, E.)—103(A)
Marshall, Leona (see Anderson, Herbert L.)—102(A), 815
Martinelli, E. A. (see Woodyard, J. R.)—447(A)
Marton, L. and K. Bol. Reduction of spherical aberration in strong magnetic lenses—447(A)
Masket, A. V. (see Abelson, P. H.)—227(L)
Mason, W. P. Elastic, piezoelectric, and dielectric properties of sodium chlorate and sodium bromate—529
—— Properties of monoclinic crystals—705
—— Variations of the viscosity of polyatomic gases with frequency—110(A)
Mattoon, Richard W. X-ray long spacing diffraction from lauryl amine hydrochloride and sodium laurate—116(A)
Maxwell, E. (see Bitter, F.)—97(L)
McDaniel, Boyce D. Slow neutron resonances in indium—832
McGowan, F. K. (see DeBennedetti, S.)—569(L)
McIntosh, L. R. (see Van de Graaff, R. J.)—797(A)
McKibben, J. L. Nomographic charts for nuclear reactions—101(A)
——, **D. H. Frisch, and J. M. Hush.** Control equipment for 2.5-Mev Van de Graaff giving an ion beam constant to ±1.5 kev—117(A)
McLachlan, D., Jr. New numbered strip method for summing Fourier series—575(T)
McManus, H. (see Peierls, R. E.)—795(A)
McMillan, Edwin M. Resonance acceleration of charged particles—800(A)
—— Synchrotron—784(T)
—— **and Samuel Ruben.** Radioactivity of Be^{10}—123
McMillan, F. L., Jr. (see Margenau, H.)—349
Meiners, E. P. (see Snell, A. H.)—111(A)
Meiners, E. P., Jr. (see Norris, L. D.)—110(A)
Mendelssohn, K. (see Daunt, J. G.)—219(L)

Merritt, F. R. (see Towns, C. H.)—558(L)
Meyerhof, W. E. Contact potential difference in crystal rectifiers—106(A)
Meyerott, Roland. Helium molecular energy states as detected by collisions of the second kind in helium—671
Miller, L. C. and L. F. Curtiss. Beta- and gamma-ray energies of several radioactive isotopes—983(L)
Miller, P. H., Jr. (see Greenblatt, M. H.)—113(A)
—— **and B. Goodman.** Optical microwave detector—110(A)
Montgomery, C. G. (see Margenau, H.)—349
Moore, Henry T. Address of welcome—989(T)
Morton, Paul L. Ionization currents in non-uniform electric fields—358
Moyer, B. J., B. Peters, and F. H. Schmidt. Isotopic absorption of slow neutrons in cadmium—446(A)
Moyer, W. E. (see Seren, Leo)—561(L)
Muelhause, C. O. and M. Goldhaber. Capture cross sections for slow neutrons. II. Small capture cross sections—85(L)
Mullin, Charles J. Initiation of discharge in arcs of the thyratron type—401

Nelson, Mary L. (see Lyons, W. James)—802(A)
Nelson, R. B. Methods of tuning multiple-cavity magnetrons—118(A)
—— (see Langmuir, R. V.)—118(A)
Nestmann, A. L. (see Rainard, L. W.)—802(T)
Newman, Brownie (see Rosen, Nathan)—656(L)
Ney, Edward P. Power spectrum of the cosmic-ray cascade component—221(L)
—— (see Nier, Alfred O.)—116(A)
Nielsen, Carl E. Magnetic field with small axial variation—450(A)
—— Momentum and specific ionization of 25–100 Kv electrons—444(A)
Nielsen, Harald H. Note concerning the coriolis contribution to the energy of a symmetric polyatomic molecule—184
—— (see Dickey, Fred P.)—109(A)
Nier, Alfred O. (see Aldrich, L. T.)—983(L)
——, **Edward P. Ney, and Mark G. Inghram.** Null method for the comparison of two ion currents in a mass spectrometer—116(A)
Nierenberg, W. A., N. F. Ramsey, and S. B. Brody. Measurements of nuclear quadrupole moment interactions—773(L)
Nordheim, L. W. Pile kinetics—115(A)
—— (see Scalettar, R.)—115(A)
Norris, L. D. and M. G. Inghram. Half-life determination of carbon (14) with a mass spectrometer and low absorption counter—772(L)
——, **A. H. Snell, E. P. Meiners, Jr., and L. Slotin.** Manufacture of carbon 14 in the chain-reacting pile—110(A)
Nowick, A. S. and E. S. Machlin. Dislocation theory of the creep of metals—104(A)
Nuckolls, Richard G. (see Bailey, C. L.)—118(A)
—— (see Bailey, Carl L.)—583
——, **Carl L. Bailey, William E. Bennett, Thor Bergstralh, Hugh T. Richards, and John H. Williams.** Total scattering cross sections of deuterium and oxygen for fast neutrons—805

Oberly, J. J. (see Baum, W. A.)—781(L)
Ogg, Richard A., Jr. Experimental demonstration of electrical superconductivity in metal-ammonia solutions—446(A)
—— Superconductivity in solid metal-ammonia solutions—93(L)
Oldenburger, Rufus. Thermodynamic equilibria of higher order—433(L)
O'Neal, R. D. Slowing down of low energy neutrons in water. II. Determination of photo-neutron energies—1
Opatowski, I. On the irradiation of microorganisms with variable sensitivity—114(A)
Opechowski, W. Remarks on Dr. Ma's "Redundant zeros in the discrete energy spectra in Heisenberg's theory of characteristic matrix"—772(L)
Oppenheimer, Frank, Lawrence H. Johnston, and Chaim Richman. Drift tubes for linear proton accelerator—447(A)
Oppenheimer, J. R. and H. A. Bethe. Reaction of radiation on electron scattering, and Heitler's theory of radiation damping—796(A)
Oppenheimer, J. Robert. Why are we interested in high energy particles?—784(T)
—— (see Bethe, H. A.)—451
Ore, Aadne. Binding energy of polyelectrons—90(L)
Orr, R. S. (see Karrer, Enoch)—803(T)
Osborne, C. L. (see Borst, L. B.)—108(A), 557(L)
Osborne, M. F. M. and A. H. Taylor. Non-linear propagation of underwater shock waves—322
O'Shaughnessy, M. T. Creep behavior of textile fibers—802(A)

Packard, M. (see Bloch, F.)—474
Pais, A. Some general aspects of the self-energy problem—796(A)
Palevsky, Harry, Robert K. Swank, and Raymond Grenchik. Dynamic condenser electrometer—117(A)
Panofsky, Wolfgang K. H. Measurement of electric field strength in a cavity resonant at 200 mc—447(A)
—— (see Woodyard, J. R.)—447(A)
Pardue, L. A. (see Burgy, Merle)—104(A)
Parker, W. L. (see Ellickson, R. T.)—290
Parrish, W. and E. Cisney. Collimator systems and filter techniques for x-ray powder cameras—575(T)
Peacock, M. A. Structure of rickardite, $Cu_{4-x}Te_2$—575(T)
Pearsall, C. S. (see Margenau, H.)—349
Peierls, R. E. and H. McManus. Electrodynamics without point singularities—795(A)
Pekeris, C. L. Accuracy of the earth-flattening approximation in the theory of microwave propagation—518
Penrose, R. P. (see Bleaney, B.)—775(L)
Pepinsky, R. Some aspects of electronic instrumentation in x-ray diffraction studies—575(T)
—— Summation of two-dimensional Fourier series by electronic means—575(T)

Pepkowitz, L. (see Friedlander, G.)—790(A)
Perlman, I. H. (see Richards, H. T.)—118(A)
Perlman, M. (see Friedlander, G.)—790(A)
Perlow, G. J. (see Golian, S. E.)—223(L), 776(L)
Perry, Rolland (see Argo, Harold)—102(A)
Perusquía, M. L. (see Vallarta, M. S.)—785(A)
Peters, B. (see Lofgren, E. J.)—444(A)
—— (see Moyer, B. J.)—446(A)
Peterson, J. M. (see Helmholz, A. C.)—448(A)
Peterson, K. C. (see Sawyer, R. B.)—791(A)
Phillips, M. Lindeman. Ionosphere as a measure of solar activity—119(A)
Piccioni, O. (see Conversi, M.)—859, 874
Pierce, A. K. and F. W. Brown, III. Mass spectrographic confirmation of the isotopic assignment for the long-lived radioactivity in beryllium—779(L)
Plass, Gilbert N. and John A. Wheeler. Blackbody radiation in the theory of action at a distance—793(A)
Platt, John R. Suggestion concerning fundamental particles—110(A)
Pollock, H. D., R. V. Langmuir, F. R. Elder, J. P. Blewett, A. M. Gurewitsch, and R. L. Watters. Design of a 70-Mev synchrotron—798(A)
Pomerantz, Martin A. Temperature dependence of secondary electron emission from oxide-coated cathodes—33
Pontius, R. B. (see Boorse, H. A.)—92(L)
Pool, M. L. (see Eggen, D. T.)—446(A)
—— (see Goodman, Leon J.)—112(A)
—— (see Kundu, D. N.)—111(A)
—— (see Schwarz, W. M.)—102(A)
Pound, R. V. (see Purcell, E. M.)—986(L), 988(L)
Powell, Wilson M. Method for measuring small changes in alternating magnetic fields—444(A)
Present, R. D., F. Reines, and J. K. Knipp. Liquid drop model for nuclear fission—557(L)
Primakoff, N. (see Feenberg, E.)—980(L)
Purcell, E. M., N. Bloembergen, and R. V. Pound. Resonance absorption by nuclear magnetic moments in a single crystal of CaF_2—988(L)
——, **R. V. Pound, and N. Bloembergen.** Nuclear magnetic resonance absorption in hydrogen gas—986(L)
Putnam, Thomas (see York, Herbert)—446(A)

Racah, Giulio. On the self-energy of the electron—406
Rainard, L. W., E. L. Wilson, and A. L. Nestmann. Air and water vapor permeability of fabrics—802(T)
Rainwater, James (see Havens, William W., Jr.)—107(A), 154
—— **and William W. Havens, Jr.** Neutron beam spectrometer studies of boron, cadmium, and the energy distribution from paraffin—107(A), 136
Rall, W. (see Shaw, A. E.)—117(A)
Rall, Wilfred. Mass assignments of some radioactive isotopes of Pd and Ir—112(A)
Ramberg, Edward G. (see Hillier, James)—113(A)
Ramsey, N. F. (see Nierenberg, W. A.)—773(L)
Rasetti, F. Disintegration of mesons at rest—790(A)
Ray, L. G., Jr. Tensile and torsional properties of textile fibers—802(A)
Raymond, Richard C. and Wayne Webb. Radiation resistance of loaded antennas—114(A)
Rayski, George. Problem of quantization of higher order equations—573(L)
Regener, Victor H. Multiple master-coincidence method for cosmic-ray studies—449(A)
Reid, Allen F., John R. Dunning, Sidney Weinhouse, and Aristid V. Grosse. Half-life of C^{14}—431(L)
—— **and Albert S. Keston.** Long-life radio-iodine—987(L)
Reines, F. (see Present, R. D.)—557(L)
Rhines, F. N. Thesis that order-disorder changes are ordinary phase changes—575(T)
Rhodes, J. Elmer, Jr. Dispersion of the velocity of sound in normal and para-hydrogen—91(L)
—— Velocity of sound in hydrogen when rotational degrees of freedom fail to be excited—932
Rice, Chester W. Volt-ampere characteristics for the flow of ions or electrons between concentric cylinders in gases at atmospheric pressure—228(L)
Richards, H. T. (see Bailey, C. L.)—118(A)
—— (see Bennett, W. E.)—101(A), 118(A)
——, **Lyda Speck, and I. H. Perlman.** Neutron spectra—118(A)
Richards, Hugh T. (see Bailey, Carl L.)—583
—— (see Nuckolls, Richard G.)—805
Richardson, J. M. and W. Shockley. Electrostatic potentials and fields in ionic lattices—105(A)
Richardson, J. Reginald (see Wright, Byron T.)—445(A)
—— **and Byron T. Wright.** Nuclear reaction (p,pn)—445(A)
Richman, Chaim (see Oppenheimer, Frank)—447(A)
Roberts, Arthur (see Arnold, Wayne R.)—766(L)
——, **Yardley Beers, and A. G. Hill.** Measurement of nuclear spin, magnetic moment, and hyperfine structure separation by a microwave frequency-modulation method—112(A)
Roberts, L. D. (see Blewett, J. P.)—118(A)
Rock, George D. (see Fox, Francis E.)—68, 329
Rockwood, C. C. (see Baum, W. A.)—781(L)
Rosen, Nathan. Note on the problem of uniform rotation—93(L)
—— (see Abelsen, P. H.)—227(L)
—— **and Brownie Newman.** Schwarzschild interior solution—565(L)
Rosenblatt, Philip and Victor K. LaMer. Motion of a particle in a temperature gradient; thermal repulsion as a radiometer phenomenon—385
Rosenfeld, L. Conservation theorems and invariance properties of the Lagrangian—794(A)
Rossi, Bruno. Some problems in the study of cosmic-ray mesons—788(A)
Ruben, Samuel (see McMillan, Edwin M.)—123
Rubin, S. Particle scattering camera—447(A)
Ruthberg, Stanley. Cold-cathode gas tubes as noise generators—112(A)

Sachs, R. G. On the level scheme of Mg^{24} and the mass of Na^{24}—572(L)
—— **and Julian Schwinger.** Magnetic moments of H^3 and He^3—41

Saibel, Edward. Thermodynamic criterion for the fracture of metals—Reply to a criticism—779(L)
Sala, O. and G. Wataghin. Showers of penetrating particles at altitude of 22,000 feet—430(L)
Sampson, M. B. (see Snell, A. H.)—111(A)
Sandvik, O. (see Goldberg, H.)—110(A)
Sawyer, R. B., E. O. Woolan, K. C. Peterson, and S. Bernstein. Application of a bent crystal neutron spectrometer to measurements of resonance absorption—791(A)
Saxon, D. (see Shrader, E. F. O.)—791(A)
Scalettar, R. and L. W. Nordheim. Theory of pile control rods—115(A)
Scharff-Goldhaber, G. and G. S. Klaiber. Spontaneous emission of neutrons from uranium—229(L)
Schein, Marcel. Origin of cosmic-ray mesons—788(A)
——, **A. J. Hartzler, and G. S. Klaiber.** Production of heavily ionizing particles by x-rays generated by a 100-Mev betatron—435(L)
Scherbatskoy, S. A. and R. E. Fearon. Electrostatic generating voltmeter for measurement of very small e.m.f.'s—96(L)
Schiefer, Herbert F. and Josephine M. Blandford. Performance of tensile testing machines—803(A)
Schiff, L. I. Discussion of the fluorine-proton resonances—891
—— Energy-angle distribution of betatron target radiation—87(L)
—— Resonance fluorescence of nuclei—761, 794(A)
—— Thresholds for slow neutron induced reactions—106(A), 562(L)
—— (see Greenblatt, M. H.)—113(A)
Schild, A. E. (see Infeld, L.)—410
Schmid, R. F. and L. Gerö. Homogeneous perturbations in band spectrum of AgH molecule—226(L)
Schmidt, F. H. (see MacKenzie, K. R.)—445(A)
—— (see Moyer, B. J.)—446(A)
Schneider, M. and I. Frankuchen. Some D.D.T. analogues—575(T)
Schultz, Howard (see Lane, C. T.)—431(L)
Schwarz, W. M. and M. L. Pool. Gamma-rays from tungsten—102(A)
Schwinger, Julian. Electron radiation in high energy accelerators—798(A)
—— (see Sachs, R. G.)—41
Seaborg, G. T. Transuranium elements—100(T)
—— (see Kennedy, J. W.)—555
Segrè, E. (see Kennedy, J. W.)—555
—— **and C. Wiegand.** Stopping power of various substances for fission fragments—808
Segrè, Emilio. Paradox on nuclear isomerism—445(A)
—— (see Tobias, Cornelius)—89(L)
Seitz, Frederick (see Goldberger, M. L.)—116(A)
Serber, Robert. Orbits of particles in the racetrack—434(L)
Seren, Leo, W. E. Moyer, and W. Sturm. Absorption curve of 31-second $_8O^{19}$ beta-rays and cross section for production by thermal neutrons—561(L)
Serin, B. Energy of impurity levels in semi-conductors—104(A)
Shaw, A. E. and W. Rall. An a.c. operated Mattauch type mass spectrograph—117(A)
Shaw, C. H. Secondary structure in the *K* absorption limit of germanium tetrachloride—643
Sherr, Rubby. Electron collection in ionization chamber—450(A)
—— (see Argo, Harold)—102(A)
Shockley, W. Atomic polarizabilities and the local field in alkali-halide crystals—105(A)
—— (see Bardeen, J.)—105(A)
—— (see Richardson, J. M.)—105(A)
Shrader, E. F., D. Saxon, and A. H. Snell. An attempt to observe the radioactivity of the neutron—791(A)
Shull, C. G. Determination of x-ray diffraction line widths—679
Siegbahn, Kai. Disintegration of Na^{24} and P^{32}—127
—— **and Njål Hole.** Disintegration of I^{128}—133
Siegert, A. J. F. On the first passage time problem for a one-dimensional Markoffian gaussian random function—449(A)
—— (see Kac, M.)—449(A)
Simpson, John A., Jr. Precision alpha-proportional counter—117(A)
Skaggs, L. S., G. M. Almy, D. W. Kerst, and L. H. Lanzl. Removal of the electron beam from the betatron—95(L)
Skobeltzyn, D. Atmospheric showers and bursts—441(L)
Skolil, Lester L. Average specific ionization of cosmic-ray mesons in hydrogen, helium, and argon—619
Slater, J. C. Design of linear accelerators—799(A)
—— (see Bitter, F.)—97(L)
Sleight, N. R. (see Sullivan, W. H.)—778(L)
Slotin, L. (see Norris, L. D.)—110(A)
Smith, Lloyd, and Gerhart Groetzinger. On the positive particles appearing near beta-ray emitters—96(L)
—— **and Gerhart Groetzinger.** On the positive particles emitted by radioactive electron sources—102(A)
Smith, R. N. (see Haxby, R. O.)—797(A)
Smoluchowski, R., C. M. Lucht, and M. Mann. X-ray microradiography of distorted crystals—318
Smyth, J. B. and L. G. Trolese. Reflection of radio waves from tropospheric layers—449(A)
Snell, A. H. (see Norris, L. D.)—110(A)
—— (see Shrader, E. F.)—791(A)
——, **J. S. Levinger, R. G. Wilkinson, E. P. Meiners, and M. B. Sampson.** Chemical isolation of two of the delayed neutron activities; resolution of delayed neutron periods—111(A)
Soodak, Harry. Pile perturbation theory—115(A)
Speck, Lyda (see Richards, H. T.)—118(A)
Sperduto, A. (see Van de Graaff, R. J.)—797(A)
Spitzer, Lyman, Jr. Magnetic field of the galaxy—777(L)
Squire, C. F. (see Bitter, F.)—97(L)
Staub, H. (see Bloch, F.)—972
Stokes, A. P. D. (see Anderson, L. J.)—449(A)
Strandberg, M. W. P. (see Dailey, E. P.)—984(L)
Strain, C. V. (see Baum, W. A.)—781(L)
Strock, Lester W. Spectrographic analysis: its principles and application—989(T)
Sturkey, L. Refraction and absorption effects in electron diffraction—575(T)

Sturm, W. (see Seren, Leo)—561(L)
—— (see Goldhaber, M.)—111(A)
—— **and Solomon Turkel.** Studies of neutron resonances with a crystal spectrometer—103(A)
Sullivan, W. H., N. R. Sleight, and E. M. Gladrow. Discovery, identification, and characterization of 2.8*d* Ru^{97}—778(L)
Swank, Robert K. (see Palevsky, Harry)—117(A)
Swartout, J. A. (see Conn, E. E.)—768(L)
——, **G. E. Boyd, A. E. Cameron, C. P. Keim, and C. E. Larson.** Mass assignment of 2.6 *h* Ni^{65}—232(L)
Swift, Gilbert (see Fearon, R. E.)—564(L)

Tamm, I. and S. Belenky. Energy spectrum of cascade electrons—660
Taschek, Richard (see Argo, Harold)—102(A)
Tawde, N. R. Effective temperatures of molecules in relation to the temperatures of sources—432(L)
Taylor, A. H. (see Osborne, M. F. M.)—322
Thayer, Jean (see Fearon, R. E.)—564(L)
Thomas, J. E., Jr. (see Clark, J. S.)—562(L)
Thorne, A. M. (see Work, R. W.)—803(A)
Thornton, R. L. The 184″ cyclotron—784(T)
Tisza, L. (see Luttinger, J. M.)—954
Tobias, Cornelius and Emilio Segrè. High energy carbon nuclei—89(L)
du Toit, S. J. (see de Vos, P. J. G.)—229(L)
Tongiorgi, V. (see Cocconi, G.)—841, 846, 850, 852, 855
Toulis, William (see Woodyard, J. R.)—447(A)
Tousey, R. (see Baum, W. A.)—781(L)
Townes, C. H. and F. R. Merritt. Water spectrum near one centimeter wave-length—558(L)
Townes, Charles Hard. Ammonia spectrum and line shapes near 1.25-cm wave-length—665
—— Resolution and pressure broadening of the ammonia spectrum near one-cm wave-length—109(A)
Trabacchi, G. C. (see Amaldi, E.)—103(A)
Trolese, L. G. (see Smyth, J. B.)—449(A)
Turkel, Solomon (see Sturm, William J.)—103(A)

Ufford, C. W. Internal waves in the ocean—448(A)
Ulrich, A. J. (see Borst, L. B.)—108(A), 557(L)

Vallarta, M. S., M. L. Perusquía and J. De Oyarzabal. On the determination of the energy spectrum and sign of primary cosmic radiation—785(A)
Van de Graaff, R. J. (see Buechner, W. W.)—174
——, **W. W. Buechner, W. M. Woodward, L. R. McIntosh, E. A. Burrill, and A. Sperduto.** Electrostatic generator for nuclear research—797(A)
Vane, A. B. (see Dicke, Robert H.)—340
Van Horn, J. R. (see Lapp, R. E.)—104(A)
Van Vleck, J. H. (see Dailey, E. P.)—984(L)
Vavilov, O. N. (see Vernov, S. N.)—769(L)
Veksler, V., L. Groshev, and L. Lazareva. Penetrating (atmospheric) showers in cosmic rays—440(L)
Vernov, S. N. and O. N. Vavilov. Transition effects of the soft component of cosmic rays—769(L)
Villard, O. G., Jr. (see Manning, L. A.)—767(L)
de Vos, P. J. G. and S. J. du Toit. On the production of penetrating ionizing particles by the non-ionizing component of cosmic radiation—229(L)
Vought, R. H. Dissociation of $SiCl_4$ by electron bombardment—109(A)

Wahl, A. C. (see Kennedy, J. W.)—555
Waldman, B. (see Manley, J. H.)—602
Wang, K. C. and K. C. Cheng. Five-dimensional field theory—516
Wang, Mu-Hsien. Calculation of the binding energies of H^3 and He^4 with a new potential—492
Warburton, F. W. Advance of the perihelion of mercury—86(L)
Washburn, Harold W. and Clifford E. Berry. Effects of high initial energies on mass spectra—559(L)
Wataghin, G. On the abundance of nuclei in the universe—430(L)
—— (see Sala, O.)—430(L)
Wataghin, Gleb. On the production of groups of mesons and nucleons—787(A)
Watt, B. E. (see Bennett, W. E.)—882
Watters, R. L. (see Pollock, H. D.)—798(A)
Watts, Richard J. and Dudley Williams. Beta-rays from H^3—640
Way, Katherine and E. P. Wigner. Radiation from fission products—115(A)
Webb, Wayne (see Raymond, Richard C.)—114(A)
Webster, D. L. Forces on ferromagnets through which electrons are moving—446(A)
Weekes, Donald F. (see Weekes, E. Dorothy)—565(L)
Weekes, E. Dorothy and Donald F. Weekes. Effort to observe anomalous gamma-rays connected with atomic bomb test of July 1, 1946—565(L)
Weinberg, A. M. Calculation of critical size of heterogeneous slow neutron chain reactors—115(A)
Weinhouse, Sidney (see Reid, Allen F.)—431(L)
Weissman, S. I. Conductivity of metal-amine solutions—571(L)
Weisz, Paul B. Particle accelerators as mass analyzers—91(L)
Welch, H. W. (see Haxby, R. O.)—797(A)
Welton, Theodore A. Convergent quantum electrodynamics—793(A)
Wexler, Aaron. Transmission of light by superconducting lead films—219(L)
Whaley, R. M. (see Haxby, R. O.)—797(A)
Wheeler, John A. Two-particles problem in the theory of action at a distance—793(A)
—— (see Plass, Gilbert N.)—793(A)
Whitman, Ross. Curl in woven textile fabrics—802(A)
Wick, G. C. Application of the Fokker-Planck equation of the energy spectrum of thermal neutrons—103(A)
Weidenbeck, M. L. Radioactive isotopes in the columbium region—435(L)
Wiegand, C. (see Segrè, E.)—808
Wiens, Jacob H. Production of Hg^{198} as a possible source of an improved wave-length standard—910
Wigner, E. P. Introduction to the theoretical papers from Princeton—100(T)

Wigner, E. P. Relativistic wave equations—794(A)
—— (see Way, Katherine)—115(A)
Wigner, Eugene P. Resonance reactions—606
—— Resonance reactions and anomalous scattering—15
Wilbur, D. A. New magnetron designs for continuous operation in the decimeter wave range—118(A)
—— (see Blewett, J. P.)—118(A)
Wilkinson, R. G. (see Snell, A. H.)—111(A)
Willard, H. B. (see Burgy, Merle)—104(A)
Williams, Dudley (see Argo, Harold)—102(A)
—— (see Chamberlain, Owen)—580
—— (see Watts, Richard J.)—640
—— **and Philip Yuster.** Isotopic constitution of tellurium and tungsten—118(A)
Williams, J. H. Magnetic domain patterns on silicon-iron crystals—106(A)
—— (see Bailey, C. L.)—118(A)
Williams, John H. (see Bailey, Carl L.)—583
—— (see Nuckolls, Richard G.)—805
Wilson, E. B., Jr. (see Dailey, E. P.)—984(L)
Wilson, E. L. (see Rainard, L. W.)—802(T)
Winchester, George. Influence of intercrystalline forces on β-ray absorption—437(L)
Wollan, E. O. (see Burgy, Merle)—104(A)
Woodward, W. M. (see Van de Graaff, R. J.)—797(A)
Woodyard, J. R., E. A. Martinelli, William Toulis, and Wolfgang K. H. Panofsky. Methods of driving a high Q cavity with many self-excited oscillators—447(A)
Woolan, E. O. (see Sawyer, R. B.)—791(A)
Work, R. W., A. M. Thorne, and M. R. Livingston. Investigation of the load-deformation characteristics of celanese and wool with particular reference to the use of these materials in carpet pile—803(A)
Wright, Byron T. (see Richardson, J. Reginald)—445(A)
—— **and J. Reginald Richardson.** Frequency modulated cyclotron characteristics—445(A)
Wrinch, D. Fourier transforms and complex organic crystals—575(T)
Wukasch, E. O. (see Greanias, E. C.)—797(A)
Wyckoff, R. W. G. Structure of macro molecular crystals by use of the electron microscope—575(T)
Wyman, Max. Equations of state for radially symmetric distributions of matter—396
—— Schwarzschild interior solution in an isotropic coordinate system—74

Yearin, H. J. (see Barss, W. M.)—108(A)
—— **and W. M. Barss.** Mechanical synthesizer for gas diffraction patterns—108(A)
York, Herbert, Roger Hildebrand, Thomas Putnam, and J. G. Hamilton. Acceleration of stripped light nuclei in the cyclotron—446(A)
Yuster, Philip (see Chamberlain, Owen)—580
—— (see Williams, Dudley)—118(A)

Zachariasen, W. H. Crystal structure studies of plutonium and neptunium compounds—116(A)
Zahl, Harold A. and M. J. E. Golay. Pneumatic heat detector—450(A)
Zemansky, M. W. (see Boorse, H. A.)—92(L)
Zener, Clarence. Thermodynamic criterion for the fracture of metals—A criticism—225(L)
Ziifle, Hilda M. (see Lyons, W. James)—802(A)
Zinn, W. H. Bragg reflection of neutrons by a single crystal—102(A)
—— (see Fermi, E.)—103(A)

Analytic Subject Index to Volume 70

References with (A) are to abstracts of papers presented at meetings of the American Physical Society. References with (L) are to Letters to the Editor.

Absorption (see also **Spectra, absorption**)
- Atmospheric absorption, microwave radiometer, R. H. Dicke, R. Beringer, R. L. Kyhl, and A. B. Vane—340
- Of moisture in tire cords, W. J. Lyons, H. M. Ziifle, M. L. Nelson, and T. Mares—802(A)
- Of one-half cm waves in oxygen, R. Beringer—53
- Of 1.24-centimeter radiation through rain, L. J. Anderson, C. H. Freres, J. P. Day, and A. P. D. Stokes—449(A)
- Sound absorption in water at different temperatures, F. E. Fox and G. D. Rock—68
- Of water vapor in centimeter wave-length range, G. E. Becker and S. H. Autler—300; R. M. Hainer, G. W. King, and P. C. Cross—108(A)

Acoustics
- "Second sound," liquid helium II, C. T. Lane, H. Fairbank, H. Schultz, and W. Fairbank—431(L)
- Sound absorption in water at different temperatures, F. E. Fox and G. D. Rock—68
- Ultrasonic waves and conductivity of salt solutions, F. E. Fox, K. F. Herzfeld, and G. D. Rock—329
- Velocity of sound in H_2, J. E. Rhodes, Jr.—932
- Velocity of sound in normal and parahydrogen, dispersion, J. E. Rhodes, Jr.—91(L)

Afterglow
- In upper atmosphere, J. Kaplan—448(A)

Astrophysics
- Abundance of nuclei in universe, G. Wataghin—430(L)
- Advance of perihelion of mercury, F. W. Warburton—86(L)
- Detection of meteors by radio, L. A. Manning, R. A. Helliwell, O. G. Villard, Jr., and W. E. Evans, Jr.—767(L)
- Equations of state, symmetric distribution of matter, M. Wyman—396
- Expanding universe and origin of elements, G. Gamow—572(L)
- Ionosphere as a measure of solar activity, M. L. Phillips—119(A)
- Kinematic cosmology, L. Infeld and A. E. Schild—410
- Magnetic field of galaxy, L. Spitzer, Jr.—777(L)
- Statistical hypotheses in stellar dynamics, H. Jehle—538

Atmosphere (see **Meteorology**)

Atomic mass (see **Isotopes**)

Atomic structure (see also **Energy states of atoms; Spectra, atomic**)

Biophysics
- Irradiation of microorganisms, I. Opatowski—114(A)

Brownian movement
- Brownian motion and low temperature thermometry, A. W. Lawson and E. A. Long—220(L), 977(L); J. B. Brown and D. K. C. MacDonald—976(L)

Chemical reactions
- Oxidation of Cu, use of radioactive Cu tracer, J. Bardeen, W. H. Brattain, and W. Shockley—105(A)

Cosmic radiation
- Above 40 miles, S. E. Golian, E. H. Krause, and G. J. Perlow—223(L)
- Analysis of cosmic-ray phenomena, R. P. Feynman and H. A. Bethe—786(A)
- Auger showers, proportional counter, L. Lazareva—439 (L)
- Bursts in large and in small ion chambers, H. Carmichael and C. N. Chou—792(A); L. G. Lewis, Konrad L. Kingshill, and J. M. Benade—792 (A)
- Cloud-chamber observations of soft component, W. Hazen—789(A)
- Cloud chamber for airborne observations, W. E. Hazen—445(A)
- Cosmic-ray mesons, B. Rossi—788(A)
- Density spectrum of extensive showers, G. Cocconi, A. Loverso and V. Tongiorgi—840, 846, 852
- Disintegration of, M. Conversi and O. Piccioni—874
- Effects at high altitudes, C. B. Anderson—788(A)
- Fine structure of zenithal curves, G. Cocconi and V. Tongiorgi—850
- High particle density in showers, M. Iona, Jr.—114(A)
- Magnets for airplane flights, S. B. Jones—450(A)
- Mass of mesotron W. B. Fretter—625; W. B. Fretter and R. B. Brode—791(A); D. J. Hughes—791(A)
- Mean lifetime of meson, G. Cocconi and V. Tongiorgi—855
- Measurements with V-2 rocket, S. E. Golian, E. H. Krause, and G. J. Perlow—223(L); 776(L)
- Meson masses by method of elastic collision, L. Leprince-Ringuet—791(A)
- Multiple master-coincidence method, V. H. Regener—449(A)
- Multiple production of mesons, H. A. Bethe—787(A)
- Multiple production of penetrating particles, W. B. Fretter and W. E. Hazen—230(L)
- Neutrons in the atmosphere, H. M. Agnew, W. C. Bright, and D. K. Froman—102(A)
- Neutrons, production of, S. A. Korff and B. Hamermesh—429(L)
- Origin of extensive showers, G. Cocconi—975(L)
- Origin of mesons, M. Schein—788(A)
- Penetrating bursts, E. P. George and L. Janossy—773(L)
- Penetrating ionizing particles, P. J. G. de Vos and S. J. du Toit—229 (L)

Penetrating particles in showers, G. Cocconi, A. Loverdo, and V. Tongiorgi—852
Penetrating particles at 22,000 feet, O. Sala and G. Wataghin—430(L)
Penetrating showers, D. Skobeltzyn—411(L); V. Veksler, L. Groshev, and L. Lazareva—440(L)
Periodic orbits at high magnetic latitudes, C. Graef-Fernandez—786(A)
Production of groups of mesons and nucleons, G. Wataghin—787(A)
Proton hypothesis of primary component, N. Arley—975(L)
Range-momentum relationship for mesotrons, W. B. Fretter—444(A)
Recurrence phenomena, J. W. Broxon—494
Sign of primary radiation, M. S. Vallarta, M. L. Perusquia, and J. De Oyarzabal—785(A)
Simultaneous registration at two stations of mesons, F. A. Benedetto—817
Solar and lunar effects, M. Kidnapillai and A. W. Mailvaganam—94(L)
Specific ionization of mesons in H_2, He, and A, L. L. Skolil—619
Spectrum of cascade component, E. P. Ney—221(L)
Spectrum of cascade electrons, I. Tamm and S. Belenky—660
Stopping power of Pb and Al for mesotrons, E. Fein—567(L)
Three unusual increases, S. E. Forbush—771(L)
Transition effects of soft component, S. N. Vernov and O. N. Vavilov—769(L)

Cosmology
Equations of state, symmetric distribution of matter, M. Wyman—396
Kinematic cosmology, L. Infeld and A. E. Schild—410

Crystal structure
Of plutonium and neptunium compounds, W. H. Zachariasen—116(A)
X-ray microradiography of distorted crystals, R. Smoluchowski, C. M. Lucht, and M. Mann—318

Crystalline state
Atomic polarizabilities in alkali-halide crystals, W. Shockley—105(A)
Dipole interaction in crystals, J. M. Luttinger and L. Tisza—954
Dynamics of RbI crystal, T. A. Hoffmann—981(L)
Elastic, piezoelectric, and dielectric properties of $NaClO_3$ and $NaBrO_3$, W. P. Mason—529
Elastic properties of lattices, P. S. Epstein—915
Electrical breakdown paths in single crystals, J. W. Davisson—685
Intercrystalline forces and β-ray absorption, G. Winchester—437(L)
Microstresses in cold-worked metal, N. M. Blachman—698
Oxidation of Cu, use of radioactive Cu tracer, J. Bardeen, W. H. Brattain, W. Shockley—105(A)
Photo-diode and photo-peak characteristics in Ge, S. Benzer—105(A)
Potentials and fields in ionic lattices, J. M. Richardson and W. Shockley—105(A)
Properties of (DKT) crystals, W. P. Mason—705
Structure of ferromagnetic domains, C. Kittel—965
Surface layers on quartz and topaz, D. D'Eustachio—229(L), 522

Dielectrics and dielectric properties
Of (DKT) crystals, W. P. Mason—705
Of $NaClO_3$ and $NaBrO_3$, W. P. Mason—529

Discharge of electricity in gases
Effect of magnetic field on oscillations in hot-cathode arcs, C. J. Gallagher and J. D. Cobine—113(A)
Energy distribution of electrons in high frequency discharges, T. Holstein—367
Excitation of plasma oscillations, D. Bohm—448(A)
Flow of ions between concentric cylinders, C. W. Rice—228(L)
Gas tubes as noise generators, S. Ruthberg—112(A)
He_2 ions, R. Meyerott—671
High level electronic noise source, J. D. Cobine and C. J. Gallagher—119(A)
Initiation of discharge in the thyratron, C. J. Mullin—401
Ionization currents in non-uniform fields, P. L. Morton—358
Oscillations in hot-cathode arcs, J. D. Cobine and C. J. Gallagher—113(A)
Recovery of switching tubes, H. Margenau, F. L. McMillan, Jr., I. H. Dearnley, C. S. Pearsall, and C. G. Montgomery—349

Discharge of electricity in high vacua (see also **Thermionic emission; High voltage tubes and machines**)
Influence of space charge on bunching, L. Brillouin—187

Disintegration and excitation of nucleus (see also **Radioactivity**)
Angular correlation of gamma-rays, G. Goertzel—897
Cross section of $D(d,n)$ He^3 reaction, J. H. Manley, J. H. Coon, and E. R. Graves—101(A)
Cross section of $D(d,p)$ H^3 reaction, A. C. Graves, E. R. Graves, J. H. Coon, and J. H. Manley—101(A)
Disintegrations induced by 100-Mev x-rays, G. C. Baldwin and G. S. Klaiber—259
Excitation-function of γ-radiation, M. Kovacs—895
Excitation of the nucleus ^{255}Pb in α-disintegration of Po, N. Feather—88(L)
Fluorine-proton resonances, L. I. Schiff—891
Of F by protons, resonances, W. E. Bennett, T. W. Bonner, C. E. Mandeville, and B. E. Watt—882
By high energy carbon nuclei, C. Tobias and E. Segrè—89(L)
Of I^{128}, K. Siegbahn and N. Hole—133
Of Ne and A by *d-d* neutrons, E. R. Graves and J. H. Coon—101(A)
Neutrons from a new reaction, M. Y. Colby and R. N. Little, Jr.—437(L)

Of N by neutrons, H. H. Barschall and M. E. Battat—245
Nomographic charts for nuclear reactions, J. L. McKibben—101(A)
Nuclear reaction (p,pn), J. R. Richardson and B. T. Wright—445(A)
Particles emitted in disintegrations induced by x-rays, G. S. Klaiber, A. E. Luebke, and G. C. Baldwin—789(A)
Radiochemical search for gamma-meson reactions, G. Friedlander, M. Perlman, and L. Pepkowitz—790(A)
Reaction constants of Li^7 (pn) Be^7, H. Argo, A. Hemmendinger, H. Kratz, R. Perry, R. Sherr, R. Taschek, D. Williams—102(A)
Reaction O^{17} $(n, \alpha)C^{14}$, evidence for, E. P. Hincks—770(L)
Relative probability of (d,p) and the (d,n) reactions in Bi, J. M. Cork—563(L)
Resonance fluorescence of nuclei, L. I. Schiff—794(A)
Resonance reactions, E. P. Wigner—606
Resonances in indium, B. D. McDaniel—832
Of Na^{24} and P^{32}, K. Siegbahn—127
Thick target yields with deuteron-proton reactions, E. C. Barker—101(A)
Thresholds for slow neutron induced reactions, L. I. Schiff—562(L); 106(A)
X-radiation and internal conversion from Ru+d, D. T. Eggen and M. L. Pool—446(A)
Yield function and angular distribution of D+D neutrons, W. E. Bennett, C. E. Mandeville, H. T. Richards—101(A)

Dissociation
Of $SiCl_4$ by electron bombardment, R. H. Vought—109(A)

Dynamics
Single particle operators in two-particle form, E. Feenberg—768(L)

Elasticity
Anelastic effects in polycrystalline aluminum, T'ing-Sui Kê—105(A)
Compressional viscosity and sound absorption, F. E. Fox and G. D. Rock—68
Creep behavior of fibers, M. T. O'Shaughnessy—802(A)
Curl in woven fabrics, R. Whitman—802(A)
Of (DKT) crystals, W. P. Mason—705
Dislocation theory of creep, A. S. Nowick and E. S. Machlin—104(A)
Forced vibrations of piezoelectric crystals, H. Ekstein—76
Load-deformation characteristics of celanese and wool, R. W. Work, A. M. Thorne, and M. R. Livingston—803(A)
Microstresses in cold-worked metal, N. M. Blachman—698
Performance of tensile testing machines, H. F. Schiefer and J. M. Blandford—803(A)
Plastic flow of metals, J. H. Hollomon and J. D. Lubahn—775(L)
Propagation of underwater shock waves, M. F. M. Osborne and A. H. Taylor—322
Properties of lattices, P. S. Epstein—915
Of $NaClO_3$ and $NaBrO_3$, W. P. Mason—529
Tensile and torsional properties of textile fibers, L. G. Ray, Jr.—802(A)
Thermodynamic criterion for fracture, E. Saibel—779(L), C. Zener—225(L)

Electrical circuits
Noise in receivers, M. Kac and A. F. J. Siegert—449(A)

Electrical conductivity and resistance
Contact potential difference in crystal rectifiers, W. E. Meyerhof—106(A)
Electrical breakdown paths in single crystals, J. W. Davisson—685
Electrical contact noise, M. H. Greenblatt, P. H. Miller, Jr., and L. I. Schiff—113(A)
Energy of impurity levels in semi-conductors, B. Serin——104(A)
Of metal-amine solutions, low temperatures, S. I. Weissman—571(L)
Persistent currents in metal-ammonia solutions, J. W. Hodgins—568(L)
Photo-diode and photo-peak characteristics in Ge, S. Benzer—105(A)
Of rapidly frozen solutions of Na in liquid ammonia, H. A. Boorse, D. B. Cook, R. B. Pontius, and M. W. Zemansky—92(L); J. G. Daunt, M. Desirant, and K. Mendelssohn—219(L); R. A. Ogg Jr.—93(L), 446(A)
Superconductivity of Pb at 3-cm wave-length, F. Bitter, J. B. Garrison, J. Halpern, E. Maxwell, J. C. Slater, and C. F. Squire—97(L)
Ultrasonic waves and conductivity of salt solutions, F. E. Fox, K. F. Herzfeld, and G. D. Rock—329

Electromagnetic theory
Blackbody radiation, action at a distance, G. N. Plass and J. A. Wheeler—793(A)
Conservation theorems and invariance of the Lagrangian, L. Rosenfeld—794(A)
Convergent quantum electrodynamics, T. A. Welton—793(A)
Dynamical theory of currents in cavity resonators, A. Banos, Jr.—448(A)
Earth-flattening, theory of microwave propagation, C. L. Pekeris—518
Electric field strength in cavity resonant, W. K. H. Panofsky—447(A)
Electrodynamics without point singularities, R. E. Peierls and H. McManus—795(A)
Electron radiation in high energy accelerators, J. Schwinger—798(A)
Energy-angle distribution of radiation, L. I. Schiff—87(L)
Force on conducting tube moving through magnetic field, H. Ekstein—450(A)

Forces on ferromagnets moving electrons, D. L. Webster—446(A)
Quantum theory of damping, W. Heitler—795(A)
Radar echoes from shell splashes, H. Goldstein—232(L)
Reaction of radiation on electron scattering, J. R. Oppenheimer and H. A. Bethe—784(A)
Two-particle problem, action at a distance, J. A. Wheeler—793(A)

Electron diffraction (see also **Electron optics**)
Of C Cl_3NO_2, W. M. Barss and H. J. Yearian—108(A)

Electron optics
Asymmetries of electron microscope objectives, J. Hillier and E. G. Ramberg—113(A)
Spherical aberration in magnetic lenses, L. Marton and K. Bol—447(A)

Electronic tubes
Influence of space charge on bunching, L. Brillouin—187
Initiation of discharge in the thyratron, C. J. Mullin—401

Electrons
Binding energy of polyelectrons, A. Ore—90(L)
Self-energy of the electron, G. Racha—406
Self-energy problem, A. Pais—796(A)
Theory of, C. J. Eliezer—793(A)

Electrons, secondary
Temperature dependence of emission from oxide-coated cathodes, M. A. Pomerantz—33

Energy states of atoms (see also **Spectra, atomic**)
Ground state of Li, Kun Huang—197

Errata
Method of measuring the electric dipole moment, H. K. Hughes—909

Field theory
Five-dimensional theory, K. C. Wang and K. C. Cheng—516

Fission of nucleus
Chemical isolation of delayed neutron activities, A. H. Sneel, J. S. Levinger, R. G. Wilkinson, E. P. Meiners and M. B. Sampson—111(A)
Critical size of slow neutron chain reactors, A. M. Weinberg—115(A)
Energy of delayed neutrons, M. Burgy, L. A. Pardue, H. B. Willard and E. O. Wollan—104(A)
Fission products detected photographically, L. B. Borst and J. J. Floyd—107(A)
Fragments from U^{235}, P. Demers—974(L)
Liquid drop model, R. D. Present, F. Reines, and J. K. Knipp—557(L)
Mass of fission isotopes, R. J. Hayden and L. G. Lewis—111(A)
Pile kinetics, L. W. Nordheim—115(A)
Pile perturbation theory, H. Soodak—115(A)
Properties of 94(239), J. W. Kennedy, G. T. Seaborg, E. Segrè, and A. C. Wahl—555
Radiation from fission products, K. Way and E. P. Wigner—115(A)
Specific ionization by fragments, N. O. Lassen—577
Spontaneous emission of neutrons, G. Scharff-Goldhaber and G. S. Klaiber—229(L)
Stopping power of substances for fission fragments, E. Segrè and C. Wiegand—808
Theory of pile control rods, R. Scalettar and L. W. Nordheim—115(A)
Thresholds for slow neutron induced reactions, L. I. Schiff—106(A); 562(L)

Friction
Coefficient of friction of running yarn, F. B. Breazeale—803(A)

Gases (see also **Kinetic theory**)
Inversion temperatures of He, H_2, and Ne, J. Joffe—766(L)
Variations of viscosity of polyatomic gases with frequency, W. P. Mason—110(A)

Geophysics
Electric quadrupole of earth, W. M. Elsasser—438(L)
Schwarzschild interior solution, N. Rosen and B. Newman—565(L)
Terrestrial magnetism, secular variation. Data on earth's core, W. M. Elsasser—202

High voltage tubes and machines (see also **Methods and instruments**)
Electrostatic generator, R. J. Van de Graaff, W. W. Buechner, W. M. Woodward, L. R. McIntosh, E. A. Burrill, and A. Sperduto—797(A)
Removal of beam from betatron, L. S. Skaggs, G. M. Almy, D. W. Kerst, and L. H. Lanzl—95(L)
Theory of synchrotron, D. Bohm and L. Foldy—249

Humidity
Moisture in tire cords, W. J. Lyons, H. M. Ziifle, M. L. Nelson, and T. Mares—802(A)

Hydrodynamics
Internal waves in the ocean, C. W. Ufford—448(A)
Phenomenological theory of transport processes, B. Leaf—748
Propagation of underwater shock waves, M. F. M. Osborne and A. H. Taylor—322

Ionization by collision
By fission fragments, N. O. Lassen—577
Specific ionization of cosmic-ray mesons in H_2, He, and A, L. I. Skolil—619
Of 25–100 Kv electrons, C. E. Nielsen—444(A)

Ionization by radiation
Theory of ionization yield, U. Fano—44

Ionosphere
Detection of meteors by radio, L. A. Manning, R. A. Helliwell, O. G. Villard, Jr., and W. E. Evans, Jr.—767(L)
Measure of solar activity, M. L. Phillips—119(A)

Ions
Paths of ions in non-uniform crossed fields, N. D. Coggeshall—270

Ions, mobility
Of He ions, R. Meyerott—671

Isotopes
Abundance of He^3, L. T. Aldrich and A. O. Nier—983(L)
Composition of W, Si, and B, M. G. Inghram—119(A); 653
Constitution of Te and W, D. Williams and P. Yuster—118(A)
Effects of initial energies on mass spectra, H. W. Washburn and C. E. Berry—559(L)
Of $_{79}Au^{198}$, S. Jnanananda—812
Manufacture of C^{14}, L. D. Norris, A. H. Snell, E. P. Meiners, Jr., and L. Slotin—110(A)
Mass assignment by resonance neutrons, M. Goldhaber—89(L)
Mass assignment of 2.6 h Ni^{65}, J. A. Swartout, G. E. Boyd, A. E. Cameron, C. P. Keim, and C. E. Larson—232(L)
Mass of fission isotopes, R. J. Hayden and L. G. Lewis—111(A)
Mass of 46-hr. Sm and 9.2-hr. Eu, R. J. Hayden and M. G. Inghram—89(L)
Hg^{198} as source of wave-length standard, J. H. Wiens—910
Particle accelerators as mass analyzers, P. B. Weisz—91(L)
Radioactive isotopes in Os region, L. J. Goodman and M. L. Pool—112(A)
Radioactive isotopes of Pd and Ir, mass assignments, W. Rall—112(A)
Separation of He^3 from He^4, J. Franck—561(L)

Isomers, nuclear (see also **Nuclear structure** and **Radioactivity**)
Paradox on nuclear isomerism, E. Segrè—445(A)

Kinetic theory
Inversion temperatures of He, H_2, and Ne, J. Joffe—766(L)
Motion of particle in temperature gradient, radiometer phenomenon, P. Rosenblatt and V. K. LaMer—385
Phenomenological theory of transport processes, B. Leaf—748

Liquids (see also **Hydrodynamics**)
Instrument lubricant, low hardy coefficient, S. Bloomenthal—104(A)
Liquid helium II, "second sound," C. T. Lane, H. Fairbank, H. Schultz, and W. Fairbank—431(L)
Rheological properties of elastic fluids, H. Goldberg and O. Sandvik—110(A)

Low temperature phenomena (see **Electrical conductivity and resistance**)

Magnetic fields
With small axial variation, C. E. Nielsen—450(A)

Magnetic properties (see also **Nuclear moments and spin**)
Domain patterns on silicon-iron crystals, H. J. Williams—106(A)
Magneto-resistance and domain theory, Fe-Ni alloys, R. M. Bozorth—106(A), 923
Nuclear resonance absorption in hydrogen, E. M. Purcell, R. V. Pound, and N. Bloembergen—986(L)
Paramagnetic losses in manganous salts, R. L. Cummerow and D. Halliday—433(L)
Permeability in ferromagnetic materials at microwave frequencies, C. Kittel—281
Resonance absorption in a single crystal of CaF_2, E. M. Purcell, N. Bloembergen, and R. V. Pound—988(L)
Rotational movements of matter in homogeneous fields, F. Ehrenhaft—119(A)
Structure of ferromagnetic domains, C. Kittel—965
Terrestrial magnetism, secular variation, W. M. Elsasser—202
Unipolar magnetic charges, F. Ehrenhaft—114(A)

Mechanics, quantum—general
Convergent quantum electrodynamics, T. A. Welton—793(A)
Dirac's method of field quantization and older theories, D. Bohm—795(A)
Energy levels of asymmetric rotor, G. W. King—108(A)
Expansibility of solutions in powers of constants, H. J. Bhabha—759
Nuclear coulomb energy, E. Feenberg and G. Goertzel—597
Quantization of higher order equations, G. Rayski—573(L)
Quantum theory of damping; processes involving mesons, W. Heitler—795(A)
Reaction of radiation on electron scattering; theory of damping, J. R. Oppenheimer and H. A. Bethe—796(A)
Redundant zeros in the discrete energy spectra, W. Opechowski—772(L)
Relativistic wave equations, H. J. Bhabha—794(A)
Relativistic wave equations, E. P. Wigner—794(A)
Second quantization and representation theory, E. M. Corson—728
Self-energy of the electron, G. Racha—406
Self-energy problem, A. Pais—796(A)
Statistical hypotheses in stellar dynamics, H. Jehle—538
Suggestion concerning fundamental particles, J. R. Platt—110(A)
Two-particle problem, action at a distance, J. A. Wheeler—793(A)

Mesons (see also **Cosmic radiation**)
Cosmic-ray mesons, B. Rossi—788(A); M. Schein—788(A)
Difficulties of meson theories, S. Kusaka—794(A)
Disintegration of mesons at rest, F. Rasetti—790(A)
Disintegration of slow mesons, M. Conversi and O. Piccioni—874
Mass of mesotron from cosmic-ray measurements, W. B. Fretter—625; W. B. Fretter and R. B. Brode—791(A); D. J. Hughes—791(A)
Mean life of slow mesons, M. Conversi and O. Piccioni—859
Mean lifetime, G. Cocconi and V. Tongiorgi—855

Meson masses by method of elastic collision, L. Le-Prince-Ringuet—791(A)
Multiple scattering mass of meson, H. A. Bethe—821
Particles emitted in disintegrations induced by x-rays, G. S. Klaiber, A. E. Luebke, and G. C. Baldwin—789(A)
Production of heavily ionizing particles by x-rays, M. Schein, A. J. Hartzler, and G. S. Klaiber—435(L)
Production of mesons by protons, H. A. Bethe—787(A)
Radiochemical search for gamma-meson reactions, G. Friedlander, M. Perlman, and L. Pepkowitz—790(A)
Simultaneous registration at two stations of mesons, F. A. Benedetto—817
Stopping power of Pb and Al, E. Fein—567(L)

Meteorology

Measurements in upper atmosphere, N. R. Best, E. Durand, D. I. Gale and R. J. Havens—985(L)

Methods and instruments

Alpha-proportional counter, J. A. Simpson—117(A)
Atmospheric absorption, microwave radiometer, R. H. Dicke, R. Beringer, R. L. Kyhl, and A. B. Vane—340
Bent crystal neutron spectrometer, R. B. Sawyer, E. O. Wollan, K. C. Peterson, and S. Bernstein—791(A)
Bringing beam out of betatron, E. D. Courant and H. A. Bethe—798(A)
Brownian motion for low temperature thermometry, A. W. Lawson and E. A. Long—220(L), 977(L); J. B. Brown and D. K. C. MacDonald—976(L)
C^{6+} in cyclotron, H. York, R. Hildebrand, T. Putnam, and J. G. Hamilton—446(A)
Cloud chamber for airborne observations, W. E. Hazen—445(A)
Coefficient of friction of running yarn, F. B. Breazeale—803(A)
Control equipment for Van de Graaff generator, J. L. McKibben, D. H. Frisch and J. M. Hush—117(A)
Design of linear accelerators, J. C. Slater—799(A)
Displacing electron beam in a synchrotron, J. S. Clark, I. A. Getting, and J. E. Thomas, Jr.—562(L)
Drift tubes for linear accelerator, F. Oppenheimer, L. H. Johnston, and C. Richman—447(A)
Driving high Q cavity, J. R. Woodyard, E. A. Martinelli, W. Toulis, and W. K. H. Panofsky—447(A)
Dynamic condenser electrometer, H. Palevsky, R. K. Swank, and R. Grenchik—117(A)
Effects of initial energies on mass spectra, H. W. Washburn and C. E. Berry—559(L)
Efficiency of frequency modulated cyclotron, L. Foldy and D. Bohm—445(A)
Electric dipole moment, moment of inertia, and internuclear distance of polar molecules, H. K. Hughes—570(L)
Electric field strength in cavity resonant, W. K. H. Panofsky—447(A)
Electron collection in ionization chamber, R. Sherr—450(A)
Electron microscopical studies of cellulose fibers, W. G. Kinsinger and C. W. Hock—802(A)
Electron radiation in high energy accelerators, J. Schwinger—798(A)
Electrostatic generator, R. J. Van de Graaff, W. W. Buechner, W. M. Woodward, L. R. McIntosh, E. A. Burrill, and A. Sperduto—797(A)
Fission product mixtures; mass spectrograph, L. G. Lewis and R. J. Hayden—111(A)
Fission products detected photographically, L. B. Borst and J. J. Floyd—107(A)
Frequency modulated cyclotron characteristics, B. T. Wright and J. R. Richardson—445(A)
Frequency modulated cyclotron, deflector, E. J. Lofgren and B. Peters—444(A)
Frequency modulated Berkeley cyclotron, K. R. MacKenzie and F. H. Schmidt—445(A)
Guide fields; synchrobetatron electron accelerator, H. F. Kaiser and E. C. Greanias—797(A)
Helium cryostat, S. C. Collins—98(L)
Infra-red sensitive phosphors, R. T. Ellickson and W. L. Parker—290
Initiation of discharge in the thyratron, C. J. Mullin—401
Injection technique for betatrons, E. C. Greanias and E. O. Wukasch—797(A)
Low energy neutrons by filtering through graphite, H. L. Anderson, E. Fermi, and L. Marshall—815
Magnetic fields due to dee structures, A. F. Clark—444(A)
Magnetron with water-cooled cathode, R. V. Langmuir and R. B. Nelson—118(A)
Magnetron designs for continuous operation, D. A. Wilbur—118(A)
Manufacture of C^{14}, L. D. Norris, A. H. Snell, E. P. Meiners, Jr., and L. Slotin—110(A)
Master-coincidence method, V. H. Regener—449(A)
Mattauch type mass spectrograph, A. E. Shaw and W. Rall—117(A)
Measuring sound fields, ultrasonic waves, and conductivity of salt solutions, F. E. Fox, K. F. Hertzfeld and G. D. Rock—329
Mechanical-electronic control system, R. Hofstadter—113(A)
Mechanical synthesizer for gas diffraction patterns, H. J. Yearian and W. M. Barss—108(A)
Hg^{198} as source of wave-length standard, J. H. Wiens—910
Microsecond phosphorescent decay, F.-H. Marshall—114(A)
Neutron spectrometer, B. D. McDaniel—832
Noise in receivers, M. Kac and A. F. J. Siegert—449(A)
Noise source, J. D. Cobine and C. J. Gallagher—119(A)
Null method for comparison of ion currents, A. O. Nier, E. P. Ney, and M. G. Inghram—116(A)
One-dimensional Markoffian gaussian random function, A. T. F. Siegert—449(A)
Optical microwave detector, P. H. Miller, Jr. and B. Goodman—110(A)

Orbits of particles in racetrack synchrotron, R. Serber—434(L)
Particle accelerators as mass analyzers, P. B. Weisz—91(L)
Particle scattering camera, S. Rubin—447(A)
Paths of ions in non-uniform crossed fields, N. D. Coggeshall—270
Photographic emulsions showing tracks of ionizing particles, P. Demers—86(L)
Photo-neutron energies, determination of, R. D. O'Neal—1
Pneumatic heat detector, H. A. Zahl and M. J. E. Golay—450(A)
Proposed neutron spectrometer, B. T. Feld—429(L)
Proton linear accelerator, L. W. Alvarez—799(A)
Purdue microwave electron accelerator, R. O. Haxby, E. S. Akeley, A. Ginzbarg, R. N. Smith, H. W. Welch, and R. M. Whaley—797(A)
Racetrack synchrotron, H. R. Crane—800(A)
R-F heating cyclotron filaments, A. E. Hayes, Jr.—220(L)
Recovery of switching tubes, H. Margenau, F. L. McMillan, Jr., I. H. Dearnley, C. S. Pearsall, and C. G. Montgomery—349
Reflection of neutrons by a single crystal, W. H. Zinn—102(A)
Regulation of electrostatic generator, W. E. Bennett, T. W. Bonner, C. E. Mandeville, and B. E. Watt—882
Removal of beam from betatron, L. S. Skaggs, G. M. Almy, D. W. Kerst, and L. H. Lanzl—95(L)
Resonance acceleration of charged particles, E. M. McMillan—800(A)
Rheological properties of elastic fluids, measurement of, H. Goldberg and O. Sandvik—110(A)
Separaton of He^3 from He^4, J. Franck—561(L)
70-Mev G.E. synchrotron, H. D. Pollock, R. V. Langmuir, F. R. Elder, J. P. Blewett, A. M. Gurewitsch, and R. L. Watters—798(A)
Small changes in alternating magnetic fields, W. M. Powell—444(A)
Split anode magnetrons, J. P. Blewett, D. A. Wilbur, and L. D. Roberts—118(A)
Stability of orbits in the synchrotron, N. H. Frank—177
Stability in "racetrack" synchrotron, D. M. Dennison and T. H. Berlin—764
Stability of synchrotron orbits, D. M. Dennison and T. H. Berlin—58
Stopping power of substances for fission fragments, E. Segrè and C. Wiegand—808
Strengths of some model magnets, S. B. Jones—450(A)
Synchrotron radiofrequency system, A. C. Helmholz, J. V. Franck, and J. M. Peterson—448(A)
Theory of microwave spectroscope, W. E. Lamb, Jr.—308
Theory of pile control rods, R. Scalettar and L. W. Nordheim—115(A)
Theory of synchrotron, D. Bohm and L. Foldy—249
Transition from betatron to synchrotron operation, J. P. Blewett—798(A)
Tuning multiple-cavity magnetrons, R. B. Nelson—118(A)
Voltmeter for measurement of very small e.m.f.'s, S. A. Scherbatskoy and R. E. Fearon—96(L)
X-ray diffraction line widths, C. G. Shull—679
X-ray microradiography of distorted crystals, R. Smoluchowski, C. M. Lucht, and M. Mann—318

Mobility of ions (see **Ions, mobility**)

Molecular structure and constants (see also **Spectra, molecular,** etc.)
Energy levels of asymmetric rotor, G. W. King—108(A)
He molecular energy states, R. Meyerott—671
Molecular arrangements in lauryl amine hydrochloride and sodium laurate, R. W. Mattoon—116(A)
Vibrational levels of anharmonic oscillator, D. ter Haar—222(L)

Neutrino (see also **Radioactivity; Scattering of electrons, neutrons and ions**)
Search for radiation losses of 2-Mev electrons, W. W. Buechner and R. J. Van de Graaff—174

Neutrons
Absorbing isotopes in Sm and Gd, R. E. Lapp, J. R. Van Horn, and A. J. Dempster—104(A)
Bent crystal neutron spectrometer, resonance absorption, R. B. Sawyer, E. O. Wollan, K. C. Peterson, and S. Bernstein—791(A)
Bragg reflection of neutrons by a single crystal, W. H. Zinn—102(A)
From C^{12}+D, W. E. Bennett and H. T. Richards—118(A)
Cross sections of In, Au, Ag, Sb, Li, and Hg, W. W. Havens, Jr. and J. Rainwater—107(A), 154
Cross sections of materials for indium resonance neutrons, J. Marshall—107(A)
Delayed neutrons, M. Burgy, L. A. Pardue, H. B. Willard, and E. O. Wollan—104(A)
Determination of photo-neutron energies, R. D. O'Neal—1
Diffraction and absorption, L. B. Borst, A. J. Ulrich, C. L. Osborne, and B. Hasbrouck—108(A)
Diffraction and nuclear resonance structure, L. B. Borst, A. J. Ulrich, C. L. Osborne, and B. Hasbrouck—557(L)
Electron waves in magnetic dipole field, C. L. Critchfield—793(A)
Isotopic absorption in Cd, B. J. Moyer, B. Peters, and F. H. Schmidt—446(A)
Low energy neutrons by filtering through graphite, H. L. Anderson, E. Fermi and L. Marshall—102(A); 815
Mass of, D. J. Hughes—219(L)
Neutron beam studies on B, Cd, and the energy distribution from paraffin, J. Rainwater and W. W. Havens, Jr.—107(A)
Neutron resonances, W. J. Sturm and S. Turkel—103(A)

Neutron spectra, H. T. Richards, L. Speck, and I. H. Perlman—118(A)
Neutrons in the atmosphere, H. M. Agnew, W. C. Bright, and D. K. Froman—102(A)
From a new reaction, M. Y. Colby and R. N. Little, Jr.—437(L)
Phase of neutron scattering, E. Fermi and L. Marshall—103(A)
Polarization and ferromagnetic saturation, F. Bloch, R. I. Condit, and H. Staub—972
Production by cosmic radiation, S. A. Korff and B. Hamermesh—429(L)
Proposed neutron spectrometer, B. T. Feld—429(L)
Radiative capture cross sections, D. J. Hughes—106(A)
Radioactivity of neutron, E. F. Shrader, D. Saxon, and A. H. Snell—791(A)
Reflection on mirrors, E. Fermi and W. H. Zinn—103(A)
Refraction and diffraction by crystals, M. L. Goldberger and F. Seitz—116(A)
Resonance absorption in graphite, S. Bernstein—107(A)
Scattering, absorption resonance studies, J. Rainwater and W. W. Havens, Jr.—107(A); 136
Small capture cross sections, C. O. Muehlhause and M. Goldhaber—85(L)
Spontaneous emission at fission, G. Scharff-Goldhaber and G. S. Klaiber—229(L)
Transmission through magnetized iron, E. M. Fryer—235
Yield function and angular distribution of D+D neutrons, W. E. Bennett, C. E. Mandeville, and H. T. Richards—101(A)

Nuclear moments and spin
Magnetic moments of H^3 and He^3, R. G. Sachs and J. Schwinger—41
Magnetic moments of neutron and deuteron, W. E. Arnold and A. Roberts—766(L)
Nuclear spin, magnetic moment, and hyperfine structure separation by a microwave frequency-modulation method, A. Roberts, Y. Beers, and A. G. Hill—112(A)
Quadrupole moment and radiofrequency spectra of homonuclear diatomic molecules, B. T. Feld—112(A)

Nuclear structure (see also **Disintegration and excitation of nucleus**)
Binding energies of H^3 and He^4, Mu-Hsien Wang—492
Difficulties of meson theories, S. Kusaka—794(A)
Level scheme of Mg^{24} and mass of Na^{24}, R. G. Sachs—572(L)
Liquid drop model, R. D. Present, F. Reiner, and J. K. Knipp—572(L)
Meson theory of nuclear forces, J. L. Lopes—5
Nuclear coulomb energy, E. Feenberg and G. Goertzel—597
Nuclear induction experiment, F. Bloch, W. W. Hansen, and M. Packard—474
Nuclear induction, theory, F. Bloch—460
Paradox on nuclear isomerism, E. Segrè—445(A)
Quadrupole moment interactions, W. A. Nierenberg, N. F. Ramsey, and S. B. Brody—773(L)
Resonance fluorescence of nuclei, L. I. Schiff—761
Resonance levels, L. B. Borst, A. J. Ulrich, C. L. Osborne, and B. Hasbrouck—557(L)
Resonance reactions, E. P. Wigner—606
Resonance reactions and anomalous scattering, E. P. Wigner—15
Saturation in nuclei, E. Feenberg and H. Primakoff—980(L)

Optical constants and properties
Magnetic permeability in ferromagnetic materials at microwave frequencies, C. Kittel—281
Hg^{198} as source of wave-length standard, J. H. Wiens—910
Solarization of manganese-bearing glass, R. L. Collin and A. E. Badger—437(L)
Transmission of superconducting Pb films, A. Wexler—219(L)

Optical instruments (see **Methods and instruments**)

Optical theory
Propagation of radiation, random inhomogeneities, P. G. Bergmann—486

Phosphorescence
Infra-red sensitive phosphors, R. T. Ellickson and W. L. Parker—290

Photography
Photographic emulsions showing tracks of ionizing particles, P. Demers—86(L)

Piezoelectric effect
In (DKT) crystals, W. P. Mason—705
In $NaClO_3$ and $NaBrO_3$, W. P. Mason—529

Proceedings of the American Physical Society
Chicago, Illinois, Meeting June 20–22, 1946—99
Berkeley, California, Meeting July 12–13, 1946—443; Addendum—784
New York, New York, Meeting September 19–21, 1946—784
Charlottesville, Virginia, Meeting September 26–28, 1946—801
Saratoga Springs, New York, Meeting November 2, 1946—989

Proceedings of the American Society for X-Ray and Electron Diffraction
Spring meeting 1946 (titles only)—575

Radar (see also **Electromagnetic theory; Electronic tubes; Electrical circuits** and **Radio**)
Echoes from shell splashes, H. Goldstein—232(L)
Sea echo frequency dependence, H. Goldstein—938

Radiation
Blackbody radiation, action at a distance, G. N. Plass and J. A. Wheeler—793(A)
Energy-angle distribution of radiation, L. I. Schiff—87(L)

Radio (see also **Ionosphere**)
Earth-flattening, theory of microwave propagation, C. L. Pekeris—518
Radiation resistance of loaded antennas, R. C. Raymond and W. Webb—114(A)

Reflection of waves from tropospheric layers, J. B. Smyth and L. G. Trolese—449(A)

Radioactivity (see also **Disintegration of nucleus**)

Absorption curve of 31 sec. $_8O^{19}$ beta-rays, production by thermal neutrons, L. Seren, W. E. Moyer, and W. Sturm—561(L)

Alpha-particles from Ra, W. Y. Chang—632

Angular correlation of gamma-rays, G. Goertzel—897

Of Be^{10}, E. M. McMillan and S. Ruben—123

Beta- and gamma-ray energies, L. C. Miller and L. F. Curtiss—983(L)

Beta-rays from H^3, R. J. Watts and D. Williams—640

Bikini bomb test; atmosphere analyses at Tulsa, R. E. Fearon, A. W. Engle, J. Thayer, G. Swift, and I. Johnson—564(L); gamma-ray anomaly, G. Herzog—227(L); ionization in New York, V. F. Hess and P. Luger—564(L); anomalous gamma-rays, E. D. Weekes and D. F. Weekes—565(L)

Cd and Ag activities, isotopic assignment, A. C. Helmholz—982(L)

Decay of Cb^{94} (6.6 min.), M. Goldhaber and W. J. Sturm—111(A)

Decay scheme for Te^{121}, S. B. Burson, P. T. Bittencourt, R. B. Duffield, and M. Goldhaber—566(L)

Disintegration of $_{17}Cl^{34}$, Ho Zah-Wei—782(L)

Disintegration scheme of Na^{24}, C. S. Cook, E. Jurney and L. M. Langer—985(L)

Excitation of the nucleus^{206} Pb in α-disintegration of Po, N. Feather—88(L)

Fluorine-proton resonances, L. I. Schiff—891

Gamma-rays from Na^{24}, Co^{60}, Y^{88}, angular distribution, W. M. Good—978(L)

Gamma-rays from W, W. M. Schwarz and M. L. Pool—102(A)

Of $_{79}Au^{198}$, S. Jnanananda—812

Half-life of carbon (14), L. D. Norris and M. G. Inghram—772(L)

Half-life of C^{14}, A. F. Reid, J. R. Dunning, S. Weinhouse, and A. V. Grosse—431(L)

Half-life of U^{234}, O. Chamberlain, D. Williams, and P. Yuster—580

Intercrystalline forces and β-ray absorption, G. Winchester—437(L)

Of I^{128}, K. Siegbahn and N. Hole—133

Isomeric transition in Te^{121}, P. T. Bittencourt and M. Goldhaber—780(L)

Isotopes in Cb region, M. L. Wiedenbeck—435(L)

Isotopes in Os region, L. J. Goodman and M. L. Pool—112(A)

Long-life radio-iodine, A. F. Reid and A. S. Keston—987(L)

Long-lived Be^{10}, A. K. Pierce and F. W. Brown, III—779(L)

Manufacture of C^{14}, L. D. Norris, A. H. Snell, E. P. Meiners, Jr., and L. Slotin—110(A)

Mass of 46-hr. Sm and 9.2-hr. Eu, R. J. Hayden and M. G. Inghram—89(L)

Mass spectrometric observation of C^{14}, M. G. Inghram—111(A)

Metastable state of 22 microseconds in Ta^{181}, S. De-Benedetti and F. K. McGowan—569(L)

Mo^{93} and Cb^{94} from Cb, D. N. Kundu and M. L. Pool—111(A)

Ni^{65}, 2.6 hr., E. E. Conn, A. R. Brosi, J. A. Swartout, A. E. Cameron, R. L. Carter, and D. G. Hill—768(L); J. A. Swartout, G. E. Boyd, A. E. Cameron, C. P. Keim, and C. E. Larson—232(L)

Positive particles appearing near beta-ray emitters, L. Smith and G. Groetzinger—96(L); 102(A)

Properties of 94-239, J. W. Kennedy, G. T. Seaborg, E. Segrè, and A. C. Wahl—555

Of K^{44}, theory of β-decay, R. E. Marshak—980(L)

Of radioactive isotopes by deuteron bombardment, E. T. Clarke and J. W. Irvine, Jr.—893

Radioactive isotopes of Pd and Ir, mass assignments, W. Rall—112(A)

Of neutron radioactivity, E. F. Shrader, D. Saxon, and A. H. Snell—791(A)

Recoil of nucleus in beta-decay, J. C. Jacobsen—789(A)

Resonances in indium, B. D. McDaniel—832

Short range alphas, S. M. Dancoff—116(A)

Of Na^{24} and P^{32}, K. Siegbahn—127

Of 2.8d Ru^{97}, W. H. Sullivan, N. R. Sleight, and E. M. Gladrow—778(L)

Rectifiers (see **Electrical conductivity and resistance**)

Relativity

Advance of perihelion of mercury, F. W. Warburton—86(L)

Field theories in five dimensions, H. C. Corben—947

Note on uniform rotation, N. Rosen—93(L)

Observing transverse Doppler effect, P. H. Abelson, A. V. Masket, and N. Rosen—227(L)

Relativistic wave equations, H. J. Bhabha—794(A); E. P. Wigner—794(A)

Schwarzschild interior solution, N. Rosen and B. Newman—565(L)

Schwarzschild solution in an isotopic coordinate, M. Wyman—74

Scattering of electrons, neutrons, and ions (see also **Electron diffraction**)

Angular distribution of 2.5-Mev neutrons by *d*, J. H. Coon, R. W. Davis and H. H. Barschall—104(A)

Cross section of hydrogen for neutrons, D. H. Frisch—792(A)

Diffraction phenomena in scattering of neutrons, E. Amaldi, D. Bocciarelli, and G. C. Trabacchi—103(A)

Elastic backscattering of *d-d* neutrons, J. H. Manley, H. M. Agnew, H. H. Barschall, W. C. Bright, J. H. Coon, E. R. Graves, T. Jorgensen, and B. Waldman—602

Fokker-Planck equation, energy of thermal neutrons, G. C. Wick—103(A)

High energy neutron-proton scattering, J. L. Lopes—5

Multiple scattering, mass of meson, H. A. Bethe—821
Neutron-proton and neutron-carbon cross sections for fast neutrons, C. L. Bailey, W. E. Bennett, T. Bergstralh, R. G. Nuckolls, H. T. Richards, and J. H. Williams—118(A); 583
Phase of neutron scattering, E. Fermi and L. Marshall—103(A)
Radiation losses of 2-Mev electrons, W. W. Buechner and R. J. Van de Graaff—174
Reaction of radiation on electron scattering, radiation damping, H. A. Bethe and J. R. Oppenheimer—451
Reflection of neutrons on mirrors, E. Fermi and W. H. Zinn—103(A)
Resonance reactions and anomalous scattering, E. P. Wigner—15
Scattering and annihilation of positrons, Ho Zah-Wei—224(L)
Scattering of fast neutrons by boron, H. H. Barschall, M. E. Battat, and W. C. Bright—458
Scattering and mass of meson, H. A. Bethe—821
Total cross sections of C and H for neutrons, 35 to 490 kev, D. H. Frisch—589
Total cross sections of D and O for fast neutrons, R. G. Nuckolls, C. L. Bailey, W. E. Bennett, T. Bergstralh, H. T. Richards, and J. H. Williams—805
Of 2.5-Mev neutrons by deuterium, angular distribution, J. H. Coon and H. H. Barschall—592

Scattering of radiation

Secondary electrons
From Ge, B, and Si, L. R. Koller and J. S. Burgess—571(L)

Semi-conductors (see **Electrical conductivity and resistance**)

Solid state (see **Crystalline state**)

Sound (see **Acoustics**)

Spectra, absorption (see also **Absorption**)
Continuous absorption of negative H ion, S. Chandrasekhar—109(A)
Of water vapor in centimeter wave-length range, G. E. Becker and S. H. Autler—300

Spectra, atomic
Configurations of Ti I, Ti II, V II, V III, A. Many—511
Ground state of Li, Kun Huang—197

Spectra, general
Observing transverse Doppler effect, P. H. Abelson, A. V. Masket, and N. Rosen—227(L)
Resolution and pressure broadening of NH_3 spectrum, C. H. Townes—109(A)
Solarization of manganese-bearing glass, R. L. Collin and A. E. Badger—437(L)
Of sun at 88 km, W. A. Baum, F. S. Johnson, J. J. Oberly, C. C. Rockwood, C. V. Strain, and R. Tousey—781(L)

Spectra, molecular (see also **Molecular structure and constants**)
Of NH_3 in microwave region, L. N. Hadley and D. M. Dennison—780(L)
Bands of C, formation of C_3 molecules, G. Herzberg—762
Coriolis contribution to energy of molecule, H. H. Nielsen—184
Effective temperatures of molecules, N. R. Tawde—432(L)
Hyperfine structure in ammonia quadrupole moment in N^{14}, B. P. Dailey, R. L. Kyhl, M. W. P. Strandberg, J. H. Van Vleck and E. B. Wilson, Jr.—984(L)
Infra-red spectrum of heavy water, F. P. Dickey and H. H. Nielsen—109(A)
Inversion spectrum of NH_3, R. Bleaney and R. P. Penrose—775(L), B. P. Dailey, R. L. Kyhl, M. W. P. Strandberg, J. H. Van Vleck and E. B. Wilson, Jr.—984(L), W. E. Good—109(A), 213
Line shapes of NH_3 near 1.25-cm wave-length, C. H. Townes—665
Perturbations in spectrum of AgH, R. F. Schmid and L. Gerö—226(L)
Rotational line of OCS, Stark effect, T. W. Dakin, W. E. Good, and D. K. Coles—560 (L)
Stark and Zeeman effects in NH_3, D. K. Coles and W. E. Good—979(L)
Ultraviolet band spectrum of P_2, E. J. Marais—499
H_2O spectrum near one-centimeter wave-length, C. H. Townes and F. R. Merritt—558(L)

Spectroscopy, technique
Theory of microwave spectroscope, W. E. Lamb, Jr.—308

Superconductivity (see **Electrical conductivity and resistance**)

Thermionic emission of positive ions
From thoriated tungsten, G. A. Jarvis—106(A)

Thermodynamics
Thermodynamic equilibria of higher order, P. W. Bridgman—425; R. Oldenburger—433(L)

Viscosity
Of glass, dissolved gases, W. A. Graaff and A. E. Badger—220(L)
Phenomenological theory of transport processes, B. Leaf—748

Wave mechanics (see **Mechanics, quantum**, etc.)

Wave motion
Internal waves in the ocean, C. W. Ufford—448(A)
Propagation of radiation, random inhomogeneities, P. G. Bergmann—486
Reflection of waves from tropospheric layers, J. B. Smyth and L. G. Trolese—449(A)
Underwater shock waves, M. F. M. Osborne and A. H. Taylor—322

X-rays, absorption
Fine structure in polyatomic molecules, theory of, E. M. Corson—645
K limit of $GeCl_4$, secondary structure, C. H. Shaw—643
X-rays, diffraction, scattering, reflection, refraction, and polarization
Determination of line widths, C. G. Shull—679
Production of heavily ionizing particles by x-rays, M. Schein, A. J. Hartzler, and G. S. Klaiber—435(L)
X-rays, emission
Spectra from thick targets, theory of, P. Kirkpatrick—446(A)
X-radiation and internal conversion from Ru+*d*, D. T. Eggen and M. L. Pool—446(A)

JAN 2 3 1947

THE PHYSICAL REVIEW

VOLUME [illegible] Second Series NUMBERS 11 AND 12

MBER 1 AND 15, 1946

Published for the

ICAN PHYSICAL SOCIETY

by the

AMERICAN INSTITUTE OF PHYSICS

Lancaster, Pa. and New York, N. Y.

THE AMERICAN INSTITUTE OF PHYSICS

INCORPORATED

[illegible] East 55 Street New York 22, N.Y.

MEMBER SOCIETIES:

American Physical Society
KARL K. DARROW, Secretary, Columbia University, New York 27, New York.

Optical Society of America
ARTHUR C. HARDY, Secretary, Massachusetts Institute of Technology, Cambridge 39, Massachusetts.

Acoustical Society of America
WALLACE WATERFALL, Secretary, 330 Fifth Avenue, 64th floor, New York 1, New York.

Society of Rheology
R. B. DOW, Secretary, Bureau of Ordnance, Navy Department, Washington 25, D. C.

American Association of Physics Teachers
C. J. OVERBECK, Secretary, Northwestern University, Evanston, Illinois.

ASSOCIATED SOCIETIES:

American Society for X-Ray and Electron Diffraction

Electron Microscope Society of America

Physical Society of Philadelphia

Physics Club of Chicago

Physics Club of Philadelphia

ASSOCIATES:

Over seventy-five leading industrial enterprises and other institutions which contribute to the support of the Institute.

JOURNALS:

The Physical Review

Reviews of Modern Physics
JOHN T. TATE, Editor; W. BUCHTA, *Assistant Editor*

Journal of the Optical Society of America
GRANCE R. HARRISON, Editor

The Journal of the Acoustical Society of America
FLOYD A. FIRESTONE, Editor

American Journal of Physics
DUANE ROLLER, Editor; SAMUEL D. ELIOT, *Assistant Editor*

The Review of Scientific Instruments
GAYLORD P. HARNWELL, Editor

The Journal of Chemical Physics
JOSEPH E. MAYER, Editor

Journal of Applied Physics
ELMER HUTCHISSON, Editor

OFFICERS

PAUL E. KLOPSTEG, *Chairman*
Northwestern University

WALLACE WATERFALL, *Secretary*
The Celotex Corporation

GEORGE B. PEGRAM, *Treasurer*
Columbia University

JOHN T. TATE,
Adviser on Publications
University of Minnesota

GOVERNING BOARD

R. B. DOW
L. A. DUBRIDGE
W. F. FAIR, JR.
FLOYD A. FIRESTONE
HARVEY FLETCHER
R. C. GIBBS
K. S. GIBSON
PAUL E. KLOPSTEG
W. H. MARKWOOD, JR.
GEORGE B. PEGRAM
A. H. PFUND
JOHN T. TATE
L. W. TAYLOR
WALLACE WATERFALL
A. G. WORTHING

ADMINISTRATIVE STAFF

HENRY A. BARTON, *Director*

MARGARET S. GRIFFIN,
Publications Manager

THEODORE VORBURGER,
Business Manager

THE American Institute of Physics was founded in 1931 as a federation of leading societies in the field of Physics. It combines into one operating agency those functions on behalf of physics which can best be done by the Societies jointly. Its purpose is the advancement and diffusion of physics and its applications to human welfare. To this end it publishes for itself or the Societies the eight journals listed on this page; promotes unity and effectiveness of effort among all who are interested in physics; renders numerous direct services to physicists and to the public; and cooperates with government agencies, national associations, educational institutions, technical industries, and others in such manner as to realize the opportunities and fulfill the responsibilities of physics as an important and constructive human activity.